universität wien

DISSERTATION / DOCTORAL THESIS

Titel der Dissertation / Title of the Doctoral Thesis

"Heavy Quark Masses from Jets with Effective Field Theory Methods"

verfasst von / submitted by

Christopher Lepenik, BSc MSc

angestrebter akademischer Grad / in partial fulfillment of the requirements for the degree of

Doktor der Naturwissenschaften (Dr. rer. nat.)

Wien, 2022 / Vienna, 2022

Studienkennzahl lt. Studienblatt / degree programme code as it appears on the student record sheet:	A 796 605 411
Dissertationsgebiet lt. Studienblatt / field of study as it appears on the student record sheet:	Physik
Betreut von / Supervisor:	Univ.-Prof. Dr. André H. Hoang

Acknowledgments

First of all, I would like to thank my supervisor André Hoang for giving me the opportunity to work in the particle physics group at the University of Vienna and to write this thesis. He supported me and my work whenever it was needed, but also granted me a lot of freedom such that I could devote time and effort to the topics I thought were interesting and find my own way. The discussions about my ongoing projects have always been incredibly insightful and instructive. I also appreciate the tremendous number of opportunities he gave me to present our work at conferences and workshops, and attend the most inspiring summer schools. In this context, I would also like to thank the DKPI for their generous financial support.

Very, very special thanks also to Vicent Mateu. For the invitation to the University of Salamanca, for all these extremely interesting and fun discussions, for sharing his knowledge and enthusiasm for computational methods and so much more. Vicent always helped and supported me whenever he could and without hesitation, no matter how much time and effort it would take. I will always think back to the months in Salamanca very fondly.

Moreover, I would also like to thank all my other collaborators, especially Maximilian Stahlhofen, for their time and support. It is a great privilege to be able to discuss the most interesting topics with people who share this interest and have such profound insights.

I could not have wished for better colleges and fellow students at the University of Vienna, the DKPI, and the University of Salamanca. I've always learned a lot from my colleges and friends and had a lot of fun with them. Somehow, the atmosphere was always family-like and there was never only just a sense of competitiveness. We always helped each other out. I don't dare to provide a list of names here, as it would always be incomplete. However, I want to specifically mention Moritz Preisser and Daniel Samitz, with whom I shared the office for many years. I deeply enjoyed our numerous conversations, whether it was about physics, philosophy, politics, or just nonsense. Special thanks to Daniel Samitz for reading an early draft of this thesis.

I also want to thank all of my friends who are not directly related to the university and who contributed to my past exciting years. Again, I couldn't come up with a complete list, but I hope the people I am writing about know how much I appreciate their friendship and support.

Furthermore, I would like to thank my parents for always supporting me in every possible way, regardless of the nature of my goals and how I wanted to pursue them. I am not sure if it is possible to find the appropriate words to express my gratitude.

Last but not least, I would like to thank my wife Astrid, who was always there when I needed her. She cheered me up at the points it was necessary and listened to me when I complained about tedious calculations that didn't seem to work out. I hope she knows how much I love her and that she played an important role in completing this thesis.

Abstract

The consideration of heavy quark masses is of crucial importance in many phenomenological applications in quantum chromodynamics, either because they represent important corrections in precision calculations or because they introduce additional conceptual complications. In this thesis, I tackle a wide range of aspects related to quark masses in the theory of strong interactions, including technical calculations as well as theory innovations. Essentially, this work is centered around four main results:

The first is a general formula for NLO massive event-shape cross sections. This formula enables the computation of the NLO cross section with respect to any massive event shape by providing simple analytic formulas for the distributional terms and a general instruction for the algorithmic computation of the non-distributional terms. This represents a big improvement compared to previous approaches, where calculations were performed from the ground up, one type of event shape at a time, and mostly with only numerical results, even for distributional terms.

The second result is the two-loop massive quark SCET jet function. This challenging-to-compute quantity was the last missing piece to perform $\mathrm{N^3LL}$ resummation for some event shapes with massive quarks, including 2-jettiness.

Third, the MSR mass renormalization scheme is introduced, a low-scale generalization of the $\overline{\mathrm{MS}}$ mass with variable intrinsic scale. Together with R-evolution, its associated renormalization group evolution, the MSR mass enables the systematic investigation of issues related to the pole-mass renormalon and the resummation of potentially large logarithms of mass-intrinsic scale ratios. Such logarithms are relevant in the conversion between short-distance mass renormalization schemes and for the comparison of mass values that were extracted at widely separated scales. Additionally, the MSR mass can be extended to include the effects of lighter massive quark flavors, resulting in a systematic and consistent matching and running procedure. That procedure can be used to decouple the momentum modes in the pole-$\overline{\mathrm{MS}}$ mass relation, which allows to systematically study the pole-mass renormalon and its flavor-number dependence. Both the resummation of logarithms of intrinsic scales and the systematic treatment of light massive flavors are unique to the MSR mass scheme.

The fourth main result of this thesis is `REvolver`, a `C++` library with additional `Mathematica` and `Python` interfaces. `REvolver` implements the MSR mass, R-evolution, and the related concepts in a user-friendly way, and is aimed both at theorists and experimentalists. The provided functionalities include exact renormalization group running of the $\overline{\mathrm{MS}}$ and MSR masses as well as the strong coupling, conversions between various mass renormalization schemes (with or without log-resummation via R-evolution), and the extraction of parameters that are related to the pole-mass renormalon such as the pole-mass ambiguity. The interaction with the library is based on the creation of so-called `Core` objects that encode a physical scenario, and the extraction of values from them. This makes the use of `REvolver` especially intuitive and streamlined. `REvolver` is the only public code that fully exploits the features of the MSR mass and R-evolution in mass-scheme and renormalon-related computations.

All results presented in this thesis represent essential contributions to the investigation of quark mass effects, either by providing mass corrections for precision calculations or by introducing new concepts, methods, and tools that lead to a better understanding or facilitate computations.

Zusammenfassung

Die Berücksichtigung schwerer Quarkmassen ist in vielen phänomenologischen Anwendungen der Quantenchromodynamik von entscheidender Bedeutung, entweder weil sie wichtige Korrekturen bei Präzisionsrechnungen darstellen oder weil sie zusätzliche konzeptionelle Komplikationen mit sich bringen. In dieser Arbeit behandle ich eine Vielzahl von Aspekten im Zusammenhang mit Quarkmassen in der Theorie starker Wechselwirkungen, einschließlich technischer Berechnungen sowie theoretischer Innovationen. Im Wesentlichen konzentriert sich diese Arbeit auf vier Hauptergebnisse:

Das erste ist eine allgemeine Formel für massive NLO Event-Shape-Wirkungsquerschnitte. Diese Formel ermöglicht die Berechnung des NLO-Wirkungsquerschnitts in Bezug auf einen beliebigen massiven Event-Shape, indem einfache, analyische Formeln für die distributionellen Terme und eine allgemeine Anleitung zur algorithmischen Berechnung der nicht-distributionellen Terme bereitgestellt werden. Dies stellt eine große Verbesserung im Vergleich zu den vorherigen Ansätzen dar, bei denen Berechnungen von Grund auf für jeden Event-Shape durchgeführt wurden, meist nur mit numerischen Ergebnissen.

Das zweite Ergebnis ist die Zwei-Schleifen-SCET-Jet-Funktion für massive Quarks. Diese schwer zu berechnende Größe war der letzte fehlende Beitrag, um für einige Event-Shapes mit massiven Quarks, einschließlich 2-Jettiness, eine $\mathrm{N}^3\mathrm{LL}$ Resummation zu ermöglichen.

Drittens wird das MSR-Massenrenormierungsschema eingeführt, eine Verallgemeinerung der $\overline{\mathrm{MS}}$-Masse für niedrige Energien mit variabler intrinsischer Skala. Zusammen mit der R-Evolution, der damit verbundenen Renormierungsgruppengleichung, ermöglicht die MSR-Masse die systematische Untersuchung von Problemen in Zusammenhang mit dem Polmassen-Renormalon und die Resummierung potenziell großer Logarithmen von massen-intrinsischen Skalenverhältnissen. Solche Logarithmen sind beispielsweise bei der Konvertierung zwischen Short-Distance-Massenschemata, oder dem Vergleich von Massenwerten relevant, die an weit separierten Energieskalen extrahiert wurden. Darüber hinaus kann die MSR-Masse erweitert werden, um die Auswirkungen von leichteren massiven Quark-Flavors einzubeziehen, was ein systematisches und konsistentes Matching- und Evolutionsverfahren ergibt. Diese Prozedur kann zur Entkopplung von Impulsmoden in der Pol-$\overline{\mathrm{MS}}$ Massenrelation verwendet werden, was wiederum eine systematische Untersuchung des Polmassen-Renormalons und seiner Flavor-Zahl-Abhängigkeit ermöglicht. Sowohl die Resummierung von Logarithmen intrinsischer Skalen als auch die systematische Behandlung von leichten massiven Flavors sind einzigartig für das MSR-Massenschema.

Das vierte Hauptergebnis dieser Arbeit ist `REvolver`, eine `C++`-Bibliothek mit zusätzlichen `Mathematica`- und `Python`-Schnittstellen. `REvolver` implementiert die MSR-Masse, die R-Evolution und die dazugehörigen Konzepte auf benutzerfreundliche Weise und richtet sich sowohl an Theoretiker als auch an Experimentatoren. Die bereitgestellten Funktionen umfassen die exakte Lösung der Renormierungsgruppengleichungen der $\overline{\mathrm{MS}}$- und MSR-Massen sowie der starken Kopplung, Konvertierungen zwischen verschiedenen Massenrenormierungsschemata (mit oder ohne log-Resummierung per R-Evolution) und die Extraktion von Renormalon-bezogenen Parametern wie die Polmassen-Ambiguität. Die Interaktion mit der Bibliothek basiert auf der Erstellung sogenannter `Core`-Objekte, die ein physikalisches Szenario kodieren, und der Extraktion von Werten daraus. `REvolver` ist der einzige öffentliche Code, der die Eigenschaften der MSR-Masse und der R-Evolution bei Massenschema- und Renormalon-bezogenen Berechnungen vollständig ausnutzt.

Alle in dieser Arbeit vorgestellten Ergebnisse stellen wesentliche Beiträge zur Untersuchung von Quarkmasseneffekten dar, entweder weil diese Massenkorrekturen für Präzisionsberechnungen liefern oder durch Einführung neuer Konzepte, Methoden und Werkzeuge, die zu einem besseren Verständnis führen oder Berechnungen erleichtern.

Contents

Preface

This thesis consists of three main parts:

Part I presents a short introduction to the topics covered in this thesis from a bigger-picture point of view, as well as more detailed introductions to some of the relevant topics and tools.

Part II summarizes and discusses the most important results of the publications in this cumulative thesis, including outlooks with possible next steps and future developments.

Part III contains the articles published during my doctoral studies.

Part I

Preamble

Chapter 1

The Golden Thread of this Thesis

The interest in quark masses and their effects on QCD-related observables in high-energy physics is increasing in both the theoretical and experimental domain due to the high level of precision in calculations and measurements. In addition, the prospect of a future linear collider and the associated determinations of heavy quark masses demand further efforts to improve the current understanding of heavy quarks and to provide further corrections to existing results. Effects that until recently were considered insignificant, e.g. power corrections in connection with massive quarks or more subtle issues such as the ambiguity of the pole mass scheme and the meaning of directly reconstructed heavy quark masses, are gaining more and more attention.

This thesis examines a wide range of phenomenological and theoretical aspects related to quark mass effects in quantum chromodynamics. The contained studies and their results will play an important role, not only at the precision frontier of the strong interactions but also in more general considerations, e.g. related to mass renormalization schemes. All results are, however, deeply related.

The main results of this thesis include

- the general computation of NLO massive event-shape cross sections (Chap. 5, summarized in Chap. 3.1),
- the computation of the two-loop massive SCET jet function (Chap. 6, summarized in Chap. 3.2),
- the introduction and extension of the MSR mass renormalization scheme and R-evolution, together with their application to the investigation of the pole mass renormalon (Chaps. 7 and 8, summarized in Chap. 3.3 and 3.4, respectively),
- the development of the `C++` library `REvolver` to precisely and efficiently evolve and convert quark masses renormalization schemes, by utilizing the frameworks developed in the context of the MSR scheme (Chap. 9, summarized in Chap. 3.5).

All of these results are briefly described and contextualized below, with references to the relevant chapters and sections in this work.

General Computation of NLO Event-Shape Cross Sections
The article that is presented in Chap. 5 deals with event shapes, a group of observables with a long history of use in studies of the strong interactions, see Chap. 2.3.2, mainly in the form of differential or cumulative cross sections. Most of the time, these computations are carried out in the approximation that all quark flavors and hadronic final states are massless. This can be a good approximation as long as the center of mass energy of the collision is much larger than the respective particle masses. However, quark mass effects can become important if the precision goal requires the inclusion of quark mass power corrections or if one of the physical scales of the observed process is of the order of the mass. The latter can happen, for example, if the collision energy of interest Q is of the order of the mass, or in the context of the peak region of differential event-shape distributions if the invariant mass of the jets is of the order of the mass, i.e. $Q\sqrt{e} \sim m$, with e the

event-shape value. In Chap. 5, a general and efficient method for the computation of massive event-shape cross sections at next to leading order (NLO) in the strong coupling is presented. The consequences of non-zero quark masses enter at two places: first, the quark mass parameters are kept arbitrary in all matrix-element computations, so that our results incorporate full quark mass dependence; second, we examine the effects of finite masses on the observable definitions themselves, which leads to different "schemes" of event shapes that can be exploited as a tool to suppress or enhance mass effects in the respective observable and that reduce to the standard definitions in the massless limit. So far, analytic results for massive event shapes, even at NLO, have been quite scarce and had to be computed from scratch, one event shape at a time. The new approach presented here introduces a completely general and simple method of obtaining differential and cumulative NLO event-shape cross sections.

Two-Loop Massive SCET Jet Function
At the next perturbative level, NNLO, perturbative fixed-order results that include full mass dependence are even rarer. However, most ingredients are known to determine the distribution of many event shapes in the peak region where a large scale separation enables the application of effective field theory (EFT) methods, see Chaps. 2.2.2 and 2.3.2. The peak of an e^+e^- event-shape distribution refers to phase-space regions with back-to-back pencil-like jets, accompanied by soft radiation, in which the bulk of the collision events is located. Using a combination of two EFTs, boosted Heavy Quark Effective Theory (bHQET) and Soft Collinear Effective Theory (SCET), factorization theorems have been established that divide, up to power corrections, the differential cross section into independent quantities, where each encodes contributions from only one of the characteristic, widely separated scales. The last missing piece to perform next-to-next-to-next-to-leading-log ($\mathrm{N^3LL}$) resummation for some event shapes (e.g. 2-jettiness and jet-mass distributions) was the two-loop contribution to the massive quark SCET jet function. The calculation of this missing piece is presented in Chap. 6. This is a rather challenging computation due to several factors: It is a two-loop computation that involves two scales (the heavy quark mass as well as the invariant mass of the jet). Additionally, the computation involves some specifics related to massive SCET, e.g. eikonal propagators that give rise to rapidity divergences. The article also shows well that a deep understanding of the conceptual backgrounds is of crucial importance even for rather technical calculations by discussing extensively how collinear-soft subtractions in the massive SCET jet function can be viewed from different perspectives and how they have to be treated to obtain correct results.

MSR Mass, R-Evolution, and Renormalons
The fact that quark mass parameters lead to challenging problems in the calculation described in the previous paragraph is not an isolated incident. More often than not, quark masses induce or imply conceptual issues. Some critical examples that concern the mass parameter itself are the pole mass renormalon and the right choice of a quark mass renormalization scheme, see Chap. 2.3.1. Chaps. 7 and 8 address some of these issues. In Chap. 7 the MSR mass scheme, a generalization of the $\overline{\mathrm{MS}}$ mass for low renormalization scales, is introduced in detail. The $\overline{\mathrm{MS}}$ mass is suitable for renormalization scales that are equal to or larger than the mass scale and has an intrinsic scale that is of the order of the mass (i.e. if $\mu \sim m$ there are no large logarithms). On the other hand, the MSR mass scheme is suitable for renormalization scales below the mass scale and has a variable intrinsic scale R. Together with R-evolution, its associated renormalization group evolution, the MSR scheme is a valuable tool to investigate renormalon-related issues and to deal with widely separated kinematic scales in precision physics applications. Using R-evolution, it is possible to resum potentially large logarithms associated with ratios of intrinsic scales such as those involved in the conversion of quark mass parameters between high- and low-scale

short-distance renormalization schemes. At the same time, R-evolution can quantify the asymptotic character of the series that is associated with the pole mass renormalon. This is the first time a renormalization group equation can achieve this. The MSR mass concept is extended in Chap. 8 to include the effects of lighter massive quark flavors, giving a systematic and consistent matching and running procedure: in analogy to the evolution of the strong coupling, light flavors are integrated out by applying flavor-threshold matching at the appropriate scales, with intermediate flavor-number-dependent evolutions. Currently, the MSR mass is the only mass renormalization scheme for which a procedure of this type has been formulated systematically and consistently. In Chap. 8, this new formalism is immediately applied to some interesting problems such as the asymptotic behavior of the pole-$\overline{\text{MS}}$ mass relation with light massive flavor effects, and the determination of the renormalon ambiguity of the pole mass.

REvolver
The MSR mass scheme, together with its renormalization group equation, the R-evolution equation, is one of the main outcomes of this thesis and it is highly desirable that the associated advantages and implications be made readily available to both theorists and experimentalists. For this reason, the library `REvolver` was developed, which is presented in Chap. 9. `REvolver` implements, in an easy-to-use way, all the concepts that are promoted in Chaps. 7 and 8. The library is written in `C++`, with additional interfaces for use in `Mathematica` notebooks and `Python`. Apart from exact renormalization group running of the strong coupling α_s as well as the $\overline{\text{MS}}$ and MSR masses, the library supports conversions between various mass renormalization schemes (with or without log-resummation via R-evolution) and the extraction of parameters that are related to the pole-mass renormalon, always exploiting the full potential of the MSR mass. At the moment, only strong interactions are implemented in `REvolver`. However, the code is easily extendable and electroweak interaction might be implemented in the future. The user interaction with the library is centered around creating so-called `Core` objects. `Core` objects encode physical scenarios, i.e. specific values of the strong coupling, the number of flavors, and a spectrum of quark mass values. In addition, a variety of optional parameters can be set, including the number of perturbative orders of the evolution equations and matching conditions. The user can interact with those objects e.g. by extracting quark masses in any scheme, strong coupling values at any renormalization scale and flavor number scheme, or by adding additional heavier quark flavors to the setup. The features of the MSR mass and R-evolution, which are exploited in almost all routines of the library, have never been implemented in a public code before. Also, the `Core` concept is new in this type of software and makes the use of `REvolver` particularly intuitive and streamlined.

Taken together, the works presented in this thesis offer significant improvements for the study of heavy quark masses on a very broad spectrum: general methods are developed, high-order corrections are calculated, new theoretical concepts are introduced and computational tools are built. All of this will make many precision computations including heavy quark masses more precise, either directly or indirectly, and will improve the overall understanding of quark mass effects.

The following chapters of this thesis are structured as follows: Chap. 2 presents a brief introduction to the relevant topics, including multi-loop computations, effective field theory, and renormalons. Chap. 3 contains summaries of all the articles and results that make up the main part of this thesis and that are collected in Part III. In Chap. 4 I conclude and give an outlook on possible next steps and future developments. Finally, Chaps. 5-9 contain the publications.[1]

[1] In the following, the term "Section" is always used to refer to sections of a reference or publication, while the terms "Part" and "Chapter" are used to refer to parts of this thesis.

Chapter 2

Conceptual Overview

2.1 The Era of Precision Physics

Fundamental particle physics stands at the frontier of human understanding of physics at small length scales and high energy, many orders of magnitude away from our everyday life experiences. Although highly unintuitive at first glance, it has been possible to gain a much deeper understanding of this regime in the past decades, using the mathematical frameworks of relativity, quantum mechanics, and ultimately quantum field theory (QFT).

With the prediction of the positron as a consequence of the Dirac equation in 1928 [1] and the following discovery in 1932 [2], an extraordinary run began: often, following the constraints set by QFT and guided by principles such as symmetry and simplicity, new particles were predicted that were often found with the exact properties as anticipated by the theory. Some famous examples include the pion (prediction 1935 [3], discovery 1947 [4]), the neutrino (prediction 1930 [5], discovery 1956 [6]), quarks (prediction 1964 [7,8], discovery 1969 [9]) and the W and Z bosons (prediction 1968 [10], discovery 1983 [11]).

Since the discovery of the Higgs boson in 2012 [12] (predicted 1964 [13, 14]), all of the basic building blocks of the *standard model* of particle physics have been detected by experiments. Now, theoretical particle physics is in need of new inspirations from unexpected experimental results. Unfortunately, recent experiments at the LHC and other colliders have not shown clear signals from as-yet-unknown particles, despite the presence of many appealing extensions of the standard model such as supersymmetry and other "beyond the standard model" theories.

Basically, there are two directions to push to find signals of "new physics" (whereby it should be noted that categorization always means oversimplification): the *high energy frontier*, i.e. to collide particles with more and more energy to produce heavier field excitations that are visible as signals in the data; and the *precision frontier*, i.e. to carry out more and more precise experiments, paired with ever more precise calculations, in order to find small deviations from standard model predictions.

"Ever more precise calculations" does not just mean "lengthier calculations": it turns out that the demand for precision leads to many conceptual difficulties of various kinds, forcing researchers to examine more subtle details and, consequently, to gain a deeper understanding of the underlying principles and to develop new technical and conceptual innovations. Some of them are briefly discussed in the following section.

2.2 Some Aspects of Precision Calculations in Collider Phenomenology

2.2.1 Multi-Loop Computations

One large subarea in theoretical precision particle physics is concerned with the computation of perturbative corrections that are related to high powers in the coupling, or equivalently,

high numbers of loops in Feynman diagrams (*multi-loop computations*). Most of the time, multi-loop refers to #loops≥ 2. To achieve novelties in this area, it is indeed necessary to do very lengthy, sophisticated computations. However, the field of multi-loop computations gives also rise to many interesting conceptual and technical innovations that contribute to physics and mathematics alike.

In the following, some of the most important techniques are briefly reviewed, many of them are applied in Chap. 6.

In order to deal with the very large number of Feynman integrals (the number of integrals grows exponentially with the number of loops), new techniques and algorithms have been developed to reduce the number of integrals to linearly independent ones (the *master integrals*, MIs). At the same time, master integrals are usually easier to solve than the original ones. The most widely known and used method is integration by parts (IBP) reduction [15, 16] by using the Laporta algorithm [17]. IBP reduction makes use of a fundamental property of dimensionally regularized integrals

$$\int \mathrm{d}^d k_1 \cdots \mathrm{d}^d k_L \, f(k_1, \ldots, k_L) \,, \tag{2.1}$$

where k_i are 4-vectors extended to d dimensions and f is an integrable function (the dependence on variables other than the loop momenta is suppressed): namely, that surface terms always vanish, i.e.

$$\int \mathrm{d}^d k_1 \cdots \mathrm{d}^d k_L \, \frac{\mathrm{d}}{\mathrm{d}k_i^\mu} p^\mu f(k_1, \ldots, k_L) = 0 \qquad \forall i \in \{1, \ldots, L\} \,, \tag{2.2}$$

where p^μ can, but does not have to be, one of the vectors k_i. It is easy to see that, by choosing suitable functions f in Eq. (2.2), it is possible to derive nontrivial relations between the terms that result from an explicit evaluation of the derivative.

When applying this technique in practice, the first step usually is to reduce the number of distinct propagators for each integral, e.g. by employing partial fraction relations and by exploiting relations between linear dependent sets of propagators. The structures that appear in the numerators of the integrands are modified as well to match the propagators in the denominators, by using Passarino-Veltman reduction if necessary. After this procedure, one usually obtains several sets (also called *families* or *topologies*) of integrals. Each topology is characterized by a certain set of linearly independent propagators and consists of the integrals that can be built from these propagators raised to arbitrary integer powers, including zero. To IBP-reduce these sets, all possible IBP relations are derived for arbitrary powers of the propagators in the individual families, and systematically applied until all integrals can be expressed as a linear combination of a small set of MIs, usually by using the Laporta algorithm mentioned above. The coefficients in these linear combinations generally depend on the number of dimensions d and kinematic invariants. In modern calculations around $\mathcal{O}(10^5) - \mathcal{O}(10^6)$ equations are processed, leading to $\mathcal{O}(10) - \mathcal{O}(100)$ master integrals, even at two loops.

Automation plays an important role here, and most steps that are described in the previous paragraph are indeed automated and implemented very efficiently in computer programs such as AIR [18], FIRE [19], Kira [20], and Reduze [21]. It should also be mentioned that there are alternatives to the Laporta algorithm, with individual advantages and disadvantages, such as using symbolic reduction rules as employed in LiteRed [22].

Even after reducing the number of integrals to be solved and the powers of their propagators, the solution of those integrals is not trivial. The development of useful techniques for the solution of multi-loop integrals is a very active field of research and new methods

are constantly developed. However, there are some standard techniques that are shortly described in the following.

Feynman parametrization is one of the most popular methods due to its simplicity, broad applicability in the one- and multi-loop context, and capability to be automatized. Let's consider a general dimensionally regularized Feynman integral

$$F(a_1,\dots,a_N) = \int \frac{\mathrm{d}^d k_1 \cdots \mathrm{d}^d k_L}{E_1^{a_1}\cdots E_N^{a_N}}\,, \tag{2.3}$$

where

$$E_k \equiv \sum_{i\geq j\geq 1} A_k^{ij} r_i r_j - m_k^2 + i0^+\,, \tag{2.4}$$

are propagators that contain loop momenta k_i, external momenta p_i and masses m_i, with $r = \{k_1,\dots,k_L,p_1,\dots\}$. A_k are coefficient matrices. It can be shown that, see e.g. Secs. 2.2, 2.3 and 3.4 of Ref. [23], the integral in Eq. (2.3) can be expressed as an integral over Feynman parameters x_i of the form

$$\begin{aligned} &F(a_1,\dots,a_N) = \\ &(i\pi^{d/2})^L \frac{\Gamma(\sum_i a_i - Ld/2)}{\prod_i \Gamma(a_i)} \int_0^\infty \mathrm{d}x_1\cdots\mathrm{d}x_N\,\delta(1-\sum_i x_i)\, x_1^{a_1-1}\cdots x_N^{a_n-1} \frac{\mathcal{U}^{\sum_i a_i-(L+1)d/2}}{\mathcal{F}^{\sum_i a_i - Ld/2}}\,, \end{aligned} \tag{2.5}$$

where the integral boundaries of the Feynman parameters x_i are set to zero and infinity for later convenience, and with $\mathcal{U}$ and $\mathcal{F}$ the *Symanzik-* or *graph polynomials* in x_i

$$\begin{aligned} \mathcal{U} &= \det M\,, \\ \mathcal{F} &= \det M(QM^{-1}Q - J)\,. \end{aligned} \tag{2.6}$$

The matrix M, the vector Q, and the scalar J are independent of the loop-momenta k_i and defined via the equation

$$x_i E_i = -k_i M_{ij} k_j + 2Q_j k_j - J\,. \tag{2.7}$$

The proof of Eq. (2.5) is relatively straightforward, but interesting: First, the identity

$$\frac{1}{E_1^{a_1}\cdots E_N^{a_N}} = \frac{\Gamma(\sum_i a_i)}{\prod_i \Gamma(a_i)} \int_0^\infty \mathrm{d}x_1\cdots\mathrm{d}x_N\, x_1^{a_1-1}\cdots x_N^{a_N-1} \frac{\delta(1-\sum_i x_i)}{(\sum_k x_k E_k)^{\sum_i a_i}}\,, \tag{2.8}$$

is applied to the integrand in Eq. (2.3). Subsequently, the denominator of the integrand in Eq. (2.8) can be transformed such that

$$\begin{aligned} x_i E_i &= -k_i M_{ij} k_j + 2Q_J k_j - J \\ &= -\ell_i M_{ij} \ell_j + Q_i M_{ij}^{-1} Q_j - J \\ &= -\alpha_i \ell_i' \ell_i' + Q_i M_{ij}^{-1} Q_j - J \end{aligned} \tag{2.9}$$

where the Einstein sum convention is used. In the second line, the integration variables k are changed to $\ell = k - M^{-1}Q$ to remove the integration variables from the second term. In the last line, another variable $\ell' = P^{\mathrm{T}}\ell$ is introduced to diagonalize M in the first term via $P^{\mathrm{T}}MP = A$, where P is an orthogonal matrix and A is a diagonal matrix with diagonal entries α_i. Remarkably, these transformations of the integration variables do not lead to additional factors in the integrand, as the transformation to ℓ is a simple shift and P is an orthogonal matrix and therefore $|\det P| = 1$.

After these transformations, the final result of Eq. (2.5) can be obtained by solving the d-dimensional integrals one after another by using the standard formula

$$\int \frac{\mathrm{d}^d k}{(-k^2+M^2)^a} = i\pi^{d/2}\frac{\Gamma(a-d/2)}{\Gamma(a)}(M^2)^{d/2-a}\,. \tag{2.10}$$

The determinant of M comes into equation Eq. (2.6) when the integration variables ℓ_i' are rescaled to remove the factors α_i before applying Eq. (2.10).

It is straight-forward to compute the Symanzik polynomials automatically and in further consequence to automatically derive a standard integral form as shown in Eq. (2.5) from a d-dimensional Feynman integral. It should be mentioned that, although the propagator powers a_i are assumed to be positive in most derivations, the formula can be analytically continued to negative values such that propagators in the numerators can be treated without further manipulations.

Let's demonstrate the application of Eq. (2.5) with a simple example. Considering Eq. (2.7) for the 1-loop Feynman integral

$$F(\lambda_1,\lambda_2) = \int \frac{\mathrm{d}^d k}{(k^2-m_1^2)^{\lambda_1}[(q-k)^2-m_2^2]^{\lambda_2}}\,, \tag{2.11}$$

with positive integer propagator powers λ_i leads to

$$x_1(k^2-m_1^2)+x_2[(q-k)^2-m_2^2] = -k^2(-x_1-x_2)+2(-x_2q)\cdot k-(m_1^2x_1+m_2^2x_2-q^2x_2)\,, \tag{2.12}$$

and consequently, according to Eq. (2.6),

$$\mathcal{U} = \det M = -x_1-x_2\,, \tag{2.13}$$

$$J = m_1^2x_1+m_2^2x_2-q^2x_2\,, \tag{2.14}$$

$$QM^{-1}Q = \frac{x_2^2q^2}{(-x_1-x_2)}\,, \tag{2.15}$$

$$\Rightarrow \quad \mathcal{F} = (x_1+x_2)(m_1^2x_1+m_2^2x_2)-q^2x_1x_2\,. \tag{2.16}$$

Inserting everything into Eq. (2.5) gives the Feynman parameter integral

$$F(\lambda_1,\lambda_2) = \\ i\pi^{d/2}\frac{\Gamma(\lambda_1+\lambda_2-2+\varepsilon)}{\Gamma(\lambda_1)\Gamma(\lambda_2)}\int_0^\infty \mathrm{d}x_1\,\mathrm{d}x_2\,\frac{\delta(1-x_1-x_2)x_1^{\lambda_1-1}x_2^{\lambda_2-1}(-x_1-x_2)^{\lambda_1+\lambda_2-4+2\varepsilon}}{[(x_1+x_2)(m_1^2x_1+m_2^2x_2)-q^2x_1x_2]^{\lambda_1+\lambda_2-2+\varepsilon}}\,. \tag{2.17}$$

When solving Feynman parameter integrals in the form of Eq. (2.5), the *Cheng-Wu theorem* [24] is especially useful. It says that the delta function $\delta(1-\sum_{i=1}^N x_i)$ in Eq. (2.5) can be exchanged with $\delta(1-\sum_{i\in\nu} x_i)$, where ν is an arbitrary non-empty subset of $\{1,\ldots,N\}$. The parameters that are not present in the delta functions are then integrated over $\mathbb{R}^+$ as already suggested by the integration boundaries in Eq. (2.5).

The Cheng-Wu theorem is a remarkable fact that is easy to show: In the derivation of the formula in Eq. (2.5), instead of using Eq. (2.8) for all propagators in the denominator, the identity

$$\frac{1}{E_i^{a_i}E_j^{a_j}} = \frac{\Gamma(a_i+a_j)}{\Gamma(a_i)\Gamma(a_j)}\int_0^\infty \mathrm{d}x_i\,x_i^{a_i-1}\frac{1}{(x_iE_i+E_j)^{a_i+a_j}}\,, \tag{2.18}$$

is applied iteratively for a chosen subset of propagators that are previously left out of Eq. (2.8). It is easy to see that this subset corresponds to the Feynman parameters that are removed from the delta function in the final result.

Coming back to the example with the Feynman parameter integral in Eq. (2.17), it is interesting to consider two options of the delta function according to the Cheng-Wu theorem: When $\delta(1-x_1-x_2)$ is chosen, the factors (x_1+x_2) in the integrand can be eliminated. On the other hand, choosing $\delta(1-x_2)$ instead of $\delta(1-x_1-x_2)$ allows setting $x_2 \to 1$ which eliminates a different factor in the numerator and simplifies the denominator. The two equivalent forms of Eq. (2.17) are

$$\begin{aligned} &F(\lambda_1,\lambda_2) \\ &\overset{\delta(1-x_1-x_2)}{=} i\pi^{d/2}\frac{\Gamma(\lambda_1+\lambda_2-2+\varepsilon)}{\Gamma(\lambda_1)\Gamma(\lambda_2)}\int_0^1 \mathrm{d}x_1\, \frac{x_1^{\lambda_1-1}(1-x_1)^{\lambda_2-1}}{[m_1^2x_1+m_2^2(1-x_1)-q^2x_1(1-x_1)]^{\lambda_1+\lambda_2-2+\varepsilon}} \\ &\overset{\delta(1-x_2)}{=} i\pi^{d/2}\frac{\Gamma(\lambda_1+\lambda_2-2+\varepsilon)}{\Gamma(\lambda_1)\Gamma(\lambda_2)}\int_0^\infty \mathrm{d}x_1\, \frac{x_1^{\lambda_1-1}(-1-x_1)^{\lambda_1+\lambda_2-4+2\varepsilon}}{[(1+x_1)(m_1^2x_1+m_2^2)-q^2x_1]^{\lambda_1+\lambda_2-2+\varepsilon}}\,. \end{aligned} \tag{2.19}$$

Another technique for solving loop integrals that is, in many variants, the one most frequently used for non-trivial cases is *evaluation by differential equations* [25–27]. This method is tailored on top of IBP reduction and exploits the fact that after differentiation w.r.t. a kinematic invariant (masses, squared external momenta, etc.), the resulting integrals are always elements of the same family as the original one and can therefore be re-reduced by utilizing the same IBP relations. Consequently, having reduced a family of Feynman integrals to a set of MIs M_i, $i \in \{1,\dots,N\}$, one can take the derivative w.r.t. a kinematic invariant q of each M_i, apply IBP reduction to the outcome, and arrive at a system of coupled differential equations

$$\frac{\mathrm{d}\vec{M}}{\mathrm{d}q} = C^{(q)}(q,\varepsilon)\vec{M}\,, \tag{2.20}$$

with the coefficient matrix $C^{(q)}$. Analogous to the usual IBP reduction, the elements of the coefficient matrix generally depend on the number of dimensions $d = 4-2\varepsilon$ and the kinematic invariants (dependencies on invariants other than q itself are suppressed in Eq. (2.20) for simplicity).

One of the advantages of this method is that the resulting differential equations can be solved order by order in ε without any previous manipulations, given appropriate boundary conditions. Usually, the MIs M_i are formally expanded in ε (in many cases the minimal power n of ε^n is known from general considerations) and then solved up to the required order in the computation of interest. This can make the procedure of solving the MIs much easier since other methods (like Feynman parameters) do not immediately permit such an expansion.

To fully determine the solution of the differential equations, boundary conditions at certain points in the space of kinematic variables must be known. In the case of massive particles this can be the solution of the massless variant (assuming the massless limit exists). Other popular boundary values are $p^2 \to 0$ and $p^2 \to \infty$, respectively, where p is an external momentum. In some cases, no additional boundary condition is needed due to consistency arguments, e.g. the finiteness of the solution at specific points.

If solving the original system of differential equations in Eq. (2.20) is not possible in practice, a common strategy is to try to bring the system to *epsilon form* [28]. Essentially, this means to look for a system equivalent to Eq. (2.20) (by finding a different basis of MIs M_i') of the form

$$\frac{\mathrm{d}\vec{M}'(q)}{\mathrm{d}q} = \varepsilon\, C'^{(q)}(q)\vec{M}'(q)\,, \tag{2.21}$$

with q the kinematic variable as in Eq. (2.20), and $C'^{(q)}(q)$ the new coefficient matrix, independent of ε and Fuchsian. Fuchsian means that the expansion of $C'^{(q)}(q)$, in all its singular points q_j, has the form

$$C'^{(q)}(q \to q_j) = \begin{cases} \frac{1}{q-q_j}\left(C'^{(q)}_{j,0} + C'^{(q)}_{j,1}(q-q_j) + \dots\right) & (q_j \neq \infty)\,, \\ \frac{1}{q}\left(C'^{(q)}_{j,0} + C'^{(q)}_{j,1} q^{-1} + \dots\right) & (q_j = \infty)\,. \end{cases} \tag{2.22}$$

In this special form, the system in Eq. (2.21) can be solved trivially as a Laurent series. However, up to now no generally applicable strategy to find the epsilon form as shown in Eq. (2.21) is known. In general, not even the criteria for the existence of such a basis are known, and for processes involving several legs or masses, the functions that make up the analytic solutions (iterative integral functions) might not be known yet. There are codes available that can automatically find the transformation to epsilon form in many cases [29–31], as long as only one kinematic variable is involved.

The question of what classes of functions can appear in the analytic solutions of arbitrary Feynman integrals is a heavily discussed topic on its own with many insights and innovations in the past years, see e.g. Secs. 5.3–5.6 of Ref. [32] for a short overview.

In many cases, an analytic solution of multi-loop Feynman integrals is not feasible (or necessary) and a numerical method can be used to evaluate them. The by far most popular technique is *sector decomposition* [33–35]. This method starts with a Feynman integral as shown in Eq. (2.5), i.e. expressed in terms of Feynman parameters, and, through clever reparametrizations and splittings of the integrals, achieves a form where the poles in ε are explicit. Consequently, subtraction methods can be used to achieve a series in ε with finite ε-independent integrals as coefficient functions. These integrals can then be solved numerically up to, in principle, arbitrary precision. Popular implementations of sector decomposition are FIESTA [36] and pySecDec [37]. Obviously, sector decomposition is also a valuable tool to check analytic solutions.

The obvious disadvantage of sector decomposition is that it does not provide any information about the analytical structure of integral solutions. That fact is e.g. especially limiting if distributional structures are involved (delta functions can obliviously not be resolved). Also, if integrals depends on more than one kinematic variable, e.g. masses, those integrals have to be evaluated at all parameter values separately since in general no functional form can be extracted. Of course, a fit can be generated if the numeric evaluation at many points is feasible.

For more details on the most important techniques in multi-loop computations and many pedagogic examples, Ref. [23] is highly recommended.

Finally, it should be mentioned that, although the tools described above are extremely useful, due to the unique structure of most multi-loop computations one can not fully rely on standard recipes. In most cases, it is necessary to modify existing techniques, or even to develop new ones.

2.2.2 Effective Field Theory and Renormalization

Effective field theory is a very rich and interesting field, with an abundance of good articles and books. Any brief introduction must necessarily focus on a few aspects that will hopefully give an interesting first overview and arouse interest in the subject. Some particularly useful and interesting introductions to study after reading this section are Refs. [38–40] and the references therein.

The idea of effective theories is to construct theories that are tailored to a specific energy scale or kinematic setup, where only the relevant degrees of freedom that are dynamical in the considered setup are explicitly included in the theory.

This is a very natural thing to do. Basically, all subfields of physics, and all natural sciences, are effective theories at a certain length scale: Fundamental particle physics describes the dynamics of fundamental particles and therefore deals with length scales that are much larger than the Planck length. Dynamics at the Planck length is therefore not relevant and not part of the standard model. Atomic physics describes the dynamics of atoms. Therefore, instead of quarks, whose dynamics take place at a much smaller length scale, atomic nuclei are the relevant degrees of freedom. Thermodynamics describes the dynamics at length scales much larger than individual molecules. Consequently, the dynamics of individual molecules are not the relevant degrees of freedom, but instead, temperature, pressure, etc. are.

Every length scale has its own distinct phenomena that can best be studied at their characteristic length scales. Obviously, this approach works best if there is a *large hierarchy* between scales.

Effective field theory, as used in many areas of physics, is a particularly systematic approach to the principle described in the previous paragraphs. In particle physics, one mostly uses Lagrangians to encode degrees of freedom and their interactions as quantum field operators, i.e. as a Quantum Field Theory (QFT). Consequently, effective field theories in particle physics are usually constructed by building quantum theoretic Lagrangians with the appropriate symmetries and operators.

Schematically, the Lagrangian of an EFT has the form

$$\mathcal{L}_{\text{EFT}} = \sum_{D\geq 0,i} \frac{c_i^{(D)} \mathcal{O}_i^{(D)}}{\Lambda^{D-d}} \,, \tag{2.23}$$

where d is the number of spacetime dimensions, $\mathcal{O}_i^{(D)}$ are local operators of mass dimension D, $c_i^{(D)}$ are their dimensionless coefficients and Λ is the scale[1] of "new physics", i.e. the scale at which the theory is not applicable anymore due to the appearance of new dynamical degrees of freedom.

The sum over D in Eq. (2.23) has, in principle, infinitely many terms[2] and can be seen as an expansion in Λ^{-1}. The number of terms in the sum over i on the other hand, i.e. the sum of operators of the same mass dimension, is finite. In practice, the sum in D is truncated depending on the demanded precision of the calculation and the physical scales of the considered process. In general, matrix elements of an operator $\mathcal{O}_i^{(D)}$ scale like $\langle \mathcal{O}_i^{(D)} \rangle \sim m^D$, where m is the typical scale of the considered process. This is called *power counting*, and determines which operator dimensions have to be included in the computation of an observable to achieve a certain precision. It is of utter importance to be consistent in the choice of operators that are included in the effective Lagrangian of Eq. (2.23), i.e. after a certain maximal order in the power counting is chosen, it is required to include *all* operators of that order. Otherwise, necessary cancellations can not happen, including the cancellation of UV divergences with renormalization constants.

There exist two distinct approaches to constructing an effective Lagrangian as shown in Eq. (2.23): *top down* and *bottom up*.

[1] In the following, "scale" refers to mass or energy scales.

[2] This means that EFT Lagrangians are in general "non-renormalizable". However, an EFT can be renormalized (i.e. there is a finite number of counterterms) at any fixed order in the power counting parameter.

The bottom-up approach is usually employed if the underlying theory is not known or a systematic expansion is not feasible. To achieve the bottom-up construction of an EFT, the appropriate symmetries and degrees of freedom of a system are specified and a Lagrangian of the form of Eq. (2.23) that contains all terms consistent with these symmetries and other fundamental properties of the theory (Lorentz invariance, unitarity, locality, etc.) is written down. The values of the couplings can then be extracted from experiments or from other methods that are capable to derive them from the underlying theory. One prominent example of an EFT that is constructed in this way is chiral perturbation theory (χPT) [41, 42]. χPT describes the low energy dynamics of QCD where usual perturbation theory can not be applied and the appropriate degrees of freedom are hadrons instead of quarks and gluons. In that context, $\Lambda = \Lambda_\chi \sim 1\,\text{GeV}$. The couplings can be fixed by experiment or by Lattice QCD. χPT is an especially interesting example as it demonstrates the emergence of distinct appropriate degrees of freedom compared to the underlying theory.

In the top-down approach, one obtains the effective Lagrangian by starting from the underlying theory from which the non-dynamical degrees of freedom are integrated out (by formally evaluating the path integral in the generating functional over the heavy fields). After that procedure, the resulting non-local Lagrangian is expanded in terms of local operators[3]. In the following, I will focus on that approach as this is the appropriate way for most EFT-related concepts in this thesis.

Before going into more detail, the close connection between EFT construction and renormalization should be elaborated: due to the presence of UV divergences (i.e. divergences that emerge from high energies) in quantum corrections in QFTs, regularization and renormalization is required to obtain quantitative predictions. Essentially this means that physics at high scales is modified in a way such that the related computations can be performed without encountering ill-defined expressions (*regularization*) with a subsequent redefinition of the theory parameters to absorb the divergences (and possibly finite contributions) that arise when taking the limit back to the physical theory (*renormalization*).

This is very similar to what happens when an EFT is constructed: there is physics at high energies that can not (or should not) be resolved, so the (non-dynamical) effects that come from these scales are absorbed into the low-energy theory parameters. The similarity is no coincidence: it is known that the standard model of particle physics is an effective field theory and that there must be "new physics" at a certain "new physics scale" whose exact value is not yet known[4].

In the following, some fundamental concepts of renormalization and the construction of EFTs are described on the same footing.

An intuitive approach to renormalization and EFT construction is to implement explicitly a finite cutoff energy scale Λ, in analogy to the new physics scale in Eq. (2.23). Modes that are related to degrees of freedom above Λ are integrated out and loop integrals are cut off there, which renders them finite and introduces a dependence on the cutoff scale. The effects of physics beyond the UV scale (after expanding in powers of Λ^{-1}) can then be absorbed into the remaining low-energy theory parameters e.g. by using a momentum subtraction scheme. In a momentum subtraction scheme, the considered loop integral

[3] Under some conditions, non-local operators can appear in effective Lagrangians. One prominent example is the SCET Lagrangian, where a non-local operator along a specific light-cone direction emerges as a consequence of the non-local nature of collinear-soft interactions. However, the non-locality is of the order of the hard scale in power counting.

[4] Standard Model Effective Theory (SMEFT) [43, 44] takes this approach seriously and enables to study composite operators of standard model fields with higher mass dimensions that encode traces of physics beyond the standard model.

is subtracted at a certain euclidean momentum value $p^2 = -\mu_M^2$, where p is an external momentum[5]. The momentum subtraction scheme is an example of a *mass dependent* renormalization scheme.

The dependence of renormalized quantities on the renormalization scale μ_M that is introduced through the renormalization scheme gives rise to the *renormalization group equation* (RGE) and *renormalization group evolution*, which allow evolving the respective quantities between renormalization scales through coupled differential equations. Given a renormalized coefficient (e.g. a coupling or mass) $c(\mu_M)$, and ignoring the subtlety of operator mixing for simplicity, the RGE is given by

$$\frac{\mathrm{d}}{\mathrm{d}\log\mu_M} c(\mu_M) = \gamma_c(\mu_M)\, c(\mu_M)\,, \tag{2.24}$$

where $\gamma_c(\mu_M)$ is called the *anomalous dimension* of $c(\mu_M)$ and is usually expanded perturbatively. The RGE can be derived from the requirement that the theory is independent of μ_M and its solution can be used to evolve the parameter c between different values of μ_M (while keeping observables the same). This is a very important technique to sum up large logarithms, see below. Quantities that depend on a renormalization scale and satisfy an RGE are called *running* quantities, e.g. a mass parameter $m(\mu_M)$ would be called a running mass.

Before discussing the severe disadvantages of cutoff regularization and mass-dependent regularization schemes, let's look at the advantages: besides the fact that a cutoff and momentum subtraction are intuitive concepts and seem to reflect the philosophy of EFTs, the *decoupling theorem* [45] holds for mass-dependent renormalization schemes. This means that the contribution of a particle with mass m vanishes automatically ("decouples") if $m \gg \mu_M$, e.g. in the β-function coefficients that govern the renormalization group running of a coupling. This is only possible due to the explicit dependence of the anomalous dimension coefficients on the mass m, which gives renormalization schemes of this type their name.

However, although intuitive, cutoffs and momentum subtractions introduce various severe issues. Apart from the fact that an explicit cutoff breaks Lorentz and gauge invariance, which must be restored tediously at the end of the computation, this approach to renormalization is useless for EFT computations since the explicit introduction of the cutoff scale Λ in loop integrals breaks the power counting of the EFT. Since, as argued above, the standard model itself can be interpreted as an effective theory, a cutoff should not be used at all. In addition, computations that utilize mass-dependent schemes and cutoffs are much harder to do, which makes computations beyond one loop extremely demanding or even unfeasible.

To circumvent these problems, one should use regularization and renormalization schemes that are easy to apply and that conserve symmetries and power counting. The de-facto standard regularization+renormalization approach that is employed in high energy physics today is *dimensional regularization* (DimReg) in combination with the (modified) *minimal subtraction* ($\overline{\text{MS}}$) scheme. The idea behind dimensional regularization is to analytically continue the usual four spacetime dimensions to an in general arbitrary complex number of $d = 4 - 2\varepsilon$ dimensions in loop integrals, i.e.

$$\int \frac{\mathrm{d}^4 p}{(2\pi)^4} \;\to\; \mu^{2\varepsilon} \int \frac{\mathrm{d}^d p}{(2\pi)^d}\,, \tag{2.25}$$

[5] The momentum subtraction scheme and most other schemes can also be applied if regularization schemes other than a cutoff are used. However, for simplicity, and since they both are considered to be "physical" schemes, they are treated together here.

where the *renormalization scale* μ is introduced to maintain the total dimensionality of the expression. At the end of the computation, ε is expanded around zero, and, applying the minimal subtraction scheme, the poles in ε are absorbed into the theory parameters.

Considering the great success and wide usage of DimReg+$\overline{\text{MS}}$ renormalization, it is rarely discussed why DimReg works and how the scale μ can be interpreted, although it is always stated, mostly vaguely, that μ can be seen as a "separation of high and low energy physics". An especially simple and vivid way to make many properties of DimReg+$\overline{\text{MS}}$ explicit (although not a strict or general study) is e.g. illustrated in Sec. 2.4 of Ref. [46], which I will briefly summarize in the following. Starting with the simple euclidean loop integral

$$I \equiv \int \frac{\mathrm{d}^4 k}{(2\pi)^4} \frac{1}{(k^2 + A^2)^\alpha} \,, \tag{2.26}$$

with some integer α and a kinematics-type variable A, potentially containing external momenta and masses, the dimensionally regularized version is

$$I_\varepsilon = c(\varepsilon) \int \frac{\mathrm{d}^{4-2\varepsilon} k}{\mu^{-2\varepsilon}(2\pi)^{4-2\varepsilon}} \frac{1}{(k_\varepsilon^2 + k^2 + A^2)^\alpha} \,, \tag{2.27}$$

with $c(\varepsilon) \to 1$ ($\varepsilon \to 0$) and with the squared loop momentum explicitly separated into the usual 4-dimensional part k^2 and a term k_ε^2 that originates from the additional -2ε dimensions. Solving only the integral over the extra dimensions gives

$$I_\varepsilon = r(\varepsilon) \int \frac{\mathrm{d}^4 k}{(2\pi)^4} \frac{1}{(k^2 + A^2)^\alpha} \left(\frac{k^2 + A^2}{4\pi\mu^2} \right)^{-\varepsilon} \,, \tag{2.28}$$

where $r(\varepsilon) = c(\varepsilon)\Gamma(\alpha + \varepsilon)/\Gamma(\alpha) \to 1$ ($\varepsilon \to 0$). Evidently, the integral over the additional dimensions gives rise to a convergence factor

$$\left(\frac{k^2 + A^2}{4\pi\mu^2} \right)^{-\varepsilon} \equiv \rho^{-\varepsilon} = \mathrm{e}^{-\varepsilon \log \rho} \,. \tag{2.29}$$

This additional factor illustrates several properties of DimReg: physics is not changed for $|\log \rho| \ll 1/\varepsilon$, i.e. if the loop momentum k and the kinematic variable A are of the order of μ. On the other hand, physics is changed if either k or A are significantly larger than μ or if both variables are significantly smaller than μ. This illustrates that DimReg acts as an UV as well as an IR regulator and that the renormalization scale μ controls what is considered to be IR or UV. In other words, the choice of the renormalization scale μ determines which physical scale is faithfully resolved.

$\overline{\text{MS}}$ is a *mass-independent* renormalization scheme, which means that the anomalous dimension coefficients are independent of the heavy mass or the renormalization scale μ, i.e. no unphysical scales appear. Consequently, however, the decoupling theorem does not hold for mass-independent schemes (anomalous dimensions are the same at all scales without further doings) such that heavy degrees of freedom have to be removed "by hand". This results in so-called *matching* corrections that guarantee that the effective theory (with the heavy degree of freedom removed), and the underlying theory (that includes the heavy degree of freedom) agree at the scale where the degree of freedom is removed, the *matching scale*. If this is ignored, large (and wrong) logarithmic corrections appear in the calculation, e.g. when running theory parameters to scales much smaller than the heavy mass.

In the matching procedure, one basically first integrates out the heavy degree of freedom, which results in a new low-energy theory. Afterward, the dimensionally regularized Lagrangians of the two theories are evaluated at the same renormalization scale (usually

near the scale of the particle to be integrated out) and the effects of the heavy particle are absorbed into the theory parameters of the low energy theory (order by order in perturbation theory). The resulting matching corrections, which are independent of the physics at low scales, make sure that high and low energy physics are the same at and below the matching scale. This procedure is performed for all couplings that multiply EFT operators.

The presence of the unphysical renormalization scale μ in the results of perturbative calculations that use DimReg+$\overline{\text{MS}}$ (or μ_M in the momentum subtraction scheme) is a feature rather than a bug: first of all, since all-order physical predictions can not depend on μ, but results at a finite order in perturbation theory do, the variation of an observable with the variation of μ is a measure of the remaining uncertainty due to higher-order corrections. However, much more important and extremely valuable is the ability to *resum large logarithms* by employing renormalization group evolutions.

The issue of large logarithms is a very common one. If the problem of interest depends on several widely separated physical scales, this might lead to large logarithms of ratios of these scales. In case these logarithms become too large in comparison to the coupling that serves as the perturbative expansion parameter (i.e. $\alpha \log = \mathcal{O}(1)$), the expansion breaks down. As described earlier in this section, however, a large scale hierarchy gives rise to the applicability of EFT methods: often it is possible to construct an EFT (or a tower of EFTs), that allows to effectively separate the physics at the widely separated scales such that perturbative predictions *factorize*. Factorization means that the mathematical expressions that describe an observable decay into several factors, where each contains the contribution from only one specific scale. Each of these factors then contains logs of ratios of the respective characteristic scale and the renormalization scale μ, such that each factor can be evaluated at a scale for which the logarithms are small. Subsequently, renormalization group evolution is used to evolve each factor to a common scale. An example of a factorization formula is discussed in Chap. 2.3.2 in the context of SCET and event shapes.

It should be mentioned that some renormalization schemes have an intrinsic physical scale themselves, which is especially pronounced e.g. in mass renormalization schemes. Consequently, depending on the observable and characteristic scales of interest, the choice of the renormalization scheme can already have a considerable impact on the precision of the calculation, see Chap. 2.3.1 for more details.

The EFT approach will be applied to quark masses in the publications presented in Chaps. 7 and 8. In the latter, especially the process of integrating out light massive flavors can be seen to follow the elaborations above. See also Chap. 2.3.1 for more details regarding the renormalization of heavy quark masses.

2.3 Heavy Quark Masses in Precision Calculations

Quark masses are interesting for several reasons:

First of all, they are interesting on their own. The values of the mass parameters (or equivalently the values of the respective Higgs Yukawa couplings) are fundamental parameters of the standard model Lagrangian. Therefore, a deep understanding of the meaning and consequences of the theory requires a deep understanding of these parameters.

Secondly, mass effects become more and more important due to the high precision of calculations and experiments in recent years. In many phenomenological high-energy computations, quark masses are set to zero. With the availability of more and more precise

data and loop corrections, however, the finiteness of the heavy quark mass values can not be neglected anymore, e.g. for precise determinations of the strong coupling by using differential event-shape cross sections [47,48]. In the context of mass effects, it is important to understand that these do not only refer to correction terms but that there exists a broad range of aspects related to them.

Thirdly, one of the quark masses happens to be by far the largest mass value of all particles that are considered fundamental in the standard model: the top quark, which has roughly the mass of a gold atom. Consequently, the top quark has a special status among all standard model particles and heavily contributes to electroweak and Higgs physics, with a Yukawa coupling of order unity. Also, in many theories beyond the standard model, the top quark plays a special role, either as a door to new phenomena or as an element of the standard model that has to be modified, see Sec. 60.3.3 of Ref. [49] for a short review. In the context of electroweak physics, especially the strong impact on the electroweak vacuum stability [50–52], and electroweak fits of the Higgs boson should be mentioned. These fits also serve as a consistency check of the standard model [53,54].

In many scenarios, it is useful to divide the six quark flavors into "heavy" and "light" ones, depending on the size of their mass parameters in relation to the chiral symmetry breaking scale $\Lambda_\chi \sim 1\,\text{GeV}$ [55]. Consequently, the charm, bottom, and top quarks are considered to be "heavy", while the down, up, and strange quarks are "light". Light quark mass values are usually determined within the frameworks of chiral perturbation theory [41,42,56], lattice QCD [57], and QCD sum rules [58]. For the heavy flavors, the usual perturbative techniques can be applied in many cases. In addition, the wide separation between the mass values and the non-perturbative scale allows to construct effective field theories [59–61] within which non-perturbative corrections can be examined systematically. However, also in the case of heavy quarks, lattice approaches [57] or relativistic sum rules [62] can be used, e.g. to study charm and bottom quark masses.

The following subsection 2.3.1 deals with quark mass renormalization schemes and the associated conceptual issues. Due to confinement in QCD, quark masses are not physical observables, but formal parameters in the action that depend on the renormalization scheme. In comparison to leptons in the electroweak theory, this is much more pronounced for quarks in QCD due to the strongly coupled character of the theory. Quarks do not exist as physical particles or asymptotic states; and in practice, quarks are never observed directly but as hadronic bound states. However, hadronization per se is not directly the reason for the subtleties concerning quark masses: although the top quark does not hadronize due to its short lifetime ($\sim 10^{-25}$ seconds), all conceptual issues apply to it as well. It is essential that, whenever a quark mass value is stated, the renormalization scheme and scale used to define it are specified.

In the section after that, Chap. 2.3.2, event-shape observables are introduced and the SCET factorization formula is discussed in that context, where the case of massless as well as massive flavors is considered.

2.3.1 Quark Mass Renormalization Schemes and Renormalons

The quark mass parameters as they originally appear in the standard model Lagrangian have to be renormalized, see Chap. 2.2.2. In other words, the UV divergences that arise in the quark self-energy must be absorbed into the quark mass parameters by employing an appropriate regularization technique and renormalization scheme. In addition to the divergent contributions, finite parts can be absorbed as well. Here, the choice of the renormalization scheme comes into play.

At first, the obligation to choose which finite parts to absorb seems to be an additional complication. However, in many observable predictions, a renormalization scheme can be chosen that is especially suitable for the considered type of observable, physical setup, or the energy scale. Choosing that scheme leads to better perturbative convergence and smaller uncertainties of the prediction. With a large number of schemes to choose from and very accurate determinations of various observables, it is necessary to have available the tools (conceptually as well as practical) to convert between schemes in a precise way.

In perturbative QCD, most mass renormalization schemes carry an intrinsic physical scale R, which can be interpreted as an effective energy cutoff where scales larger than R are absorbed into the mass parameter. The cutoff scale is usually much larger than the non-perturbative scale, $R \gg \Lambda_{\mathrm{QCD}}$. This is of great importance since the absorption of non-perturbative scales into the mass parameter leads to strong IR sensitivity and consequently to an IR renormalon, which is addressed later in this section.

Some mass renormalization schemes can be equipped with a renormalization group equation (RGE) that relates two mass values in the same renormalization scheme at different renormalization scales without introducing large logarithms, see also Chap. 2.2.2. Mass schemes equipped with an RGE can be referred to as "running mass" schemes. Just like the scheme itself, the related RGE might be more or less suitable for certain applications and energy scales. This aspect will be discussed in more detail in the following paragraphs. Note that the renormalization scale is in general not equivalent to the intrinsic scale.

To illustrate how intrinsic physical scales appear in quark mass renormalization schemes and how the scheme-associated RGEs give rise to different kinds of renormalization scale running, a few examples are given in the following. After briefly discussing the $\overline{\mathrm{MS}}$ mass as an example of a high-energy scheme, the low-energy 1S mass scheme is reviewed. This sets the stage for introducing the MSR scheme, one of the central topics of this thesis.

The $\overline{\mathrm{MS}}$ mass $\overline{m}(\mu)$ is a running mass that is defined in analogy to the strong coupling, i.e. it absorbs only the DimReg $1/\varepsilon^{n>0}$ contributions into the mass parameter. In the approximation that all quark flavors that are lighter than the heavy quark Q are massless, the relation of the $\overline{\mathrm{MS}}$ mass $\overline{m}_Q(\mu)$ of the quark Q to the pole mass m_Q^{pole} is given by

$$m_Q^{\mathrm{pole}} - \overline{m}_Q(\mu) = \overline{m}_Q(\mu) \sum_{n=1}^{\infty} \sum_{k=0}^{n} a_{n,k}^{\overline{\mathrm{MS}}} \left(\frac{\alpha_s^{(n_\ell+1)}(\overline{m}_Q(\mu))}{4\pi} \right)^n \log^k \frac{\overline{m}(\mu)}{\mu} \,, \tag{2.30}$$

where $\{a_{n,k}^{\overline{\mathrm{MS}}}\}$ are the perturbative coefficients of the pole-$\overline{\mathrm{MS}}$ relation, and $(n_\ell + 1)$ is the flavor number scheme of the strong coupling with n_ℓ the number of flavors that are lighter than the heavy quark Q. The intrinsic scale of the $\overline{\mathrm{MS}}$ mass is the mass scale itself, i.e. if $\mu \sim \overline{m}_Q \equiv \overline{m}_Q(\overline{m}_Q)$ there are no large logarithms:

$$m_Q^{\mathrm{pole}} - \overline{m}_Q = \overline{m}_Q \sum_{n=1}^{\infty} a_n^{\overline{\mathrm{MS}}} \left(\frac{\alpha_s^{(n_\ell+1)}(\overline{m}_Q)}{4\pi} \right)^n . \tag{2.31}$$

Having a closer look at Eq. (2.31), the intrinsic scale of the mass scheme appears in two places: as an argument in the strong coupling, and as a factor in front of the perturbative expansion. Another feature that can be observed immediately is the natural flavor number scheme $(n_\ell+1)$, i.e. the heavy quark itself is included as an active flavor. The $\overline{\mathrm{MS}}$ scheme is the de facto standard scheme for high-energy applications and is only physically meaningful for scales $\mu \gtrsim \overline{m}_Q$. The latter is intuitive, due to the natural flavor number scheme as well as the fact that the mass itself is the intrinsic scale, which should, however, be integrated out for scales $\mu \ll \overline{m}_Q$.

The renormalization group equation of the $\overline{\text{MS}}$ scheme has the form

$$\mu \frac{\mathrm{d}\overline{m}_Q(\mu)}{\mathrm{d}\mu} = 2\,\overline{m}_Q(\mu) \sum_{n=0}^{\infty} \gamma_n^{\overline{\text{MS}}} \left(\frac{\alpha_s^{(n_\ell+1)}(\mu)}{4\pi} \right)^n , \tag{2.32}$$

and gives rise to logarithmic scale evolution. Eq. (2.32) is an appropriate RGE for high-energy evolution ($\mu \gtrsim \overline{m}_Q$), as indicated by the scaling, as well as the fact that the strong coupling is in the $(n_\ell + 1)$-flavor scheme.

The low-energy case $\mu \ll \overline{m}_Q$ is e.g. relevant in the context of non-relativistic heavy quarkonium where the non-relativistic quark velocity v gives rise to the low intrinsic scales $\overline{m}_Q v$ and $\overline{m}_Q v^2$, with $\overline{m}_Q \gg \overline{m}_Q v \gg \overline{m}_Q v^2 \gg \Lambda_{\text{QCD}}$ [61, 63].

An example of a popular low-scale scheme is the 1S mass m_Q^{1S} [64–66], which is defined as half the mass of the heavy quarkonium spin-triplet ground state. The perturbative relation to the pole mass has the form

$$m_Q^{\text{1S}} - m_Q^{\text{pole}} = M_B \sum_{n=1}^{\infty} c_n^{\text{1S}} \left(\frac{\alpha_s^{(n_\ell)}(M_B)}{4\pi} \right)^n , \tag{2.33}$$

with $M_B = C_F \alpha_s m_Q^{\text{pole}}$ the inverse Bohr radius. The low-scale character of the 1S scheme is apparent in two places: first, the natural flavor scheme is n_ℓ, which signals that the scheme is defined at a scale where the heavy quark Q is integrated out. Second, the intrinsic scale is the inverse Bohr radius, a scale much lower than the mass scale, e.g. for the top quark $M_B \approx 30$ GeV.

The 1S mass scheme is not equipped with an RGE, i.e. it is not a running mass, since

$$\mu \frac{\mathrm{d}m_Q^{\text{1S}}}{\mathrm{d}\mu} = 0\,. \tag{2.34}$$

There exists a large number of other low-scale masses, and most of them show an analogous structure, e.g. the PS [67], RS [68] or kinetic mass [69, 70].

The MSR mass scheme [71–73] is one of the main results of this thesis and is introduced in Chap. 7 (summarized in Chap. 3.3) and extended in Chap. 8 (summarized in Chap. 3.4). The MSR scheme combines several ideas, each useful on its own: as will be explained in the following, the MSR mass is the low-scale generalization of the $\overline{\text{MS}}$ mass and has a variable intrinsic scale R. In addition, lighter massive flavors can be treated systematically and consistently in the MSR mass scheme by consecutively applying matching and running operations as known from the strong coupling evolution. The relation of the MSR mass $m_Q^{\text{MSR}}(R)$ of the quark Q to the pole mass is given by

$$m_Q^{\text{pole}} - m_Q^{\text{MSR}}(R) = R \sum_{n=1}^{\infty} a_n \left(\frac{\alpha_s^{(n_\ell)}(R)}{4\pi} \right)^n , \tag{2.35}$$

with $a_n = a_n^{\overline{\text{MS}}}|_{n_h=0}$[6]. The removal of the heavy quark as an active flavor is achieved by changing the flavor number scheme from $(n_\ell+1)$ to n_ℓ, by setting $n_h = 0$ in the perturbative coefficients, and by introducing the variable R as the new intrinsic scale, which results in a $\overline{\text{MS}}$-MSR matching condition. The MSR mass is defined directly via the pole-$\overline{\text{MS}}$

[6] The general perturbative coefficients $a_n^{\overline{\text{MS}}}$ of the relation between the pole and the $\overline{\text{MS}}$ scheme (ignoring light massive flavors) depend on the number of massless flavors n_ℓ and the number of heavy flavors n_h, i.e. the number of active flavors as heavy as the considered heavy quark. In the usual $\overline{\text{MS}}$ scheme, $n_h = 1$, while in the MSR scheme the heavy flavor is not active and therefore $n_h = 0$.

mass relation and is thus directly related to the quark self-energy diagrams, automatically inheriting all favorable infrared properties of the $\overline{\text{MS}}$ mass. The variable intrinsic scale allows to control down to which scale self-energy contributions are absorbed into the mass parameter.

The RGE that is associated to the MSR mass is called *R-evolution* and is given by

$$R\frac{\mathrm{d}m_Q^{\text{MSR}}(R)}{\mathrm{d}R} = -R\sum_{n=1}^{\infty}\gamma_n^R\left(\frac{\alpha_s^{(n_\ell)}(R)}{4\pi}\right)^n . \tag{2.36}$$

Note that in this special case, the evolution parameter R is the intrinsic scale. The linear scaling of Eq. (2.36) as well as the n_ℓ-flavor scheme of the strong coupling indicate that this is the appropriate RGE for low-scale evolution. The R-evolution equation has far-reaching consequences and a very broad range of applications that are described in more detail in Chaps. 3.3 and 3.4.

Eq. (2.35) shows that, in the formal limit $R \to 0$ of the MSR mass, the pole mass is obtained. This illustrates that the pole mass is defined to absorb all quark self-energy contributions down to zero momentum. At the same time, it can be seen that in practice one has to deal with the QCD Landau pole in the strong coupling, which emphasizes that the value of the pole mass is ambiguous. Due to the absorption of low IR contributions, the pole mass suffers from an $\mathcal{O}(\Lambda_{\text{QCD}})$ renormalon [67,74]. The ambiguity is related to bad perturbative behavior which can, depending on the scale, be already seen at low perturbative orders in the relation between the pole and renormalon-free schemes. The pole-mass ambiguity is therefore not only of theoretical but of phenomenological interest [75]. To illustrate the renormalon-associated bad perturbative behavior, let's consider the conversion of the charm $\overline{\text{MS}}$ mass $\overline{m}_c \equiv \overline{m}_c(\overline{m}_c) = 1.3$ GeV to the pole scheme, which gives [76–83]

$$m_c^{\text{pole}} = (1.3 + 0.2108 + 0.1984 + 0.2725 + (0.4843 \pm 0.0005))\text{GeV}\,, \tag{2.37}$$

up to 4-loop order in perturbation theory[7], with $\alpha_s^{(5)}(M_Z) = 0.118$. The perturbative coefficients that relate the pole mass to mass schemes that do not suffer from an $\mathcal{O}(\Lambda_{\text{QCD}})$ renormalon diverge factorially with the perturbative order. All mass schemes that are presented above, except for the pole mass, are (leading) renormalon free, as they only absorb self-energy contributions down to a scale $R \gg \Lambda_{\text{QCD}}$. Mass schemes with this property are called *short-distance schemes*.

2.3.2 Event Shapes and their Factorization

The term "event shapes" refers to a class of observables with a long history of usage in studies of the strong interaction [84, 85]. Event shapes are defined through the energy-momentum distribution of final state particles in a collision experiment, or equivalently, through their geometry. Originally, event shapes were mainly used in e^+e^- collisions and deep inelastic scattering experiments. Today, however, the concept is quite general with event shapes specifically constructed to be used in pp and other types of collisions [86, 87]. Mostly, computations and measurements of differential or cumulative cross sections with respect to a specific event shape are compared to examine aspects of QCD, e.g. to extract the value of the strong coupling.

In the context of high-energy collisions that involve strongly interacting particles, the probability of observing certain final-state geometries is enhanced: events with one or several jets of highly boosted, collinear particles, and isotropic, low-energy ("soft") radiation.

[7] The uncertainty of the fourth order coefficient stems from the numerical methods employed in Ref. [83]

The probability distribution in the space of final-state geometries therefore contains a lot of information about the nature of the strong interaction. Event-shape observables make this information accessible: they encode the geometry of the final-state 4-momenta in a 1-dimensional projection, i.e. in terms of a single number or a scalar quantity.

Popular event shapes include thrust [88, 89], hemisphere masses (left and right, heavy and light) [90–92], C-parameter [93], and jet broadening [94]. These event shapes are so-called 2-jet event shapes, which means that the event-shape value is minimal for the configuration of only two narrow, pencil-like jets. In this final-state configuration, a large scale hierarchy emerges between the collision energy, the energy scale of the collinear particles in the jet and the energy scale of the soft radiation. Consequently, large logs are present in the perturbative expansion that invalidate the fixed order results in the corresponding phase-space region. These logarithms can be resummed using effective field theory techniques.

In the context of jet physics with massless quarks, the effective theory of interest is mainly Soft-Collinear Effective Theory [95–97] (SCET). SCET is a top-down EFT that is constructed from QCD in the phase-space region in which mainly low-energy (soft) and highly boosted (collinear) particles are present as degrees of freedom. If massive quark flavors are considered, SCET (in the region $p^2 \sim p^2 - m^2 \sim m^2$, where p^2 is the squared invariant mass of the heavy-quark initiated jet and m is the mass of the heavy quark) as well as boosted Heavy Quark Effective Theory [98, 99] (bHQET) (in the region $p^2 - m^2 \ll m^2 \approx p^2$) are utilized. By using SCET, the leading-order differential cross section in the SCET power counting parameter can be factorized into objects where each encodes the physics at only one specific physical scale. The large logarithms can then be resummed by applying renormalization group evolutions for each of the functions in the factorization formula.

As an example, let's have a look at the factorization formula of thrust, which is given by

$$\tau \equiv 1 - \max_{\hat{t}} \frac{\sum_i |\hat{t} \cdot \vec{p}_i|}{\sum_i |\vec{p}_i|} \,, \tag{2.38}$$

where the sum runs over all final state particles in a collider experiment with momenta $\vec{p}_i$. $\hat{t}$ is called the thrust axis and is a unit vector that maximizes the second term. In the approximation of massless quarks, the SCET factorization formula for the differential cross section with respect to thrust is given by

$$\begin{aligned} \frac{1}{\sigma_0}\frac{\mathrm{d}\sigma}{\mathrm{d}\tau} = QH(Q,\mu_H)U_H(Q,\mu_H,\mu) \int \mathrm{d}s \int \mathrm{d}s'\, U_J(s-s',\mu,\mu_J)J(s',\mu_J) \\ \times \int \mathrm{d}\ell\, U_S(\ell,\mu,\mu_S)S(Q\tau - s/Q - \ell,\mu_S) \,, \end{aligned} \tag{2.39}$$

with σ_0 the total cross section at tree level. H, J and S are the hard, jet, and soft function, respectively, which encode the relevant physics at the scale of the hard interaction, the collinear particles in the jet, and soft radiation. In Eq. (2.39), all factorization functions are written with their renormalization scale μ_i set such that no large logarithms arise in the individual functions. The logarithms of ratios of the individual scales μ_i and the global renormalization scale μ are resummed in the evolution kernels U_i that are given by the solution of the renormalization group equations of the individual factorization functions. Eq. (2.39) is valid up to power corrections in the SCET power counting parameter $\lambda \sim \max(\tau^{1/2}, (\Lambda_{\mathrm{QCD}}/Q)^{1/2})$. The unresummed power corrections can be determined by computing $\frac{\mathrm{d}\sigma}{\mathrm{d}\tau}$ in fixed-order perturbation theory and subtracting the SCET expansion.

When the mass value $m \gg \Lambda_{\mathrm{QCD}}$ of a heavy quark flavor becomes relevant, the massless factorization formula that is shown in Eq. (2.39) needs to be generalized. With the mass

m, an additional scale is introduced and its relation to the already present kinematic hard ($\mu_H \sim Q$), jet ($\mu_J \sim Q\lambda$), and soft ($\mu_S \sim Q\lambda^2$) scales has to be inspected. Following the EFT methodology, the massless factorization formula of Eq. (2.39) can be equipped with a *variable flavor number scheme* [100–103]: the heavy quark mass m is integrated out (or in) at a scale $\mu_m \sim m$, which results in associated matching factors and appropriate flavor number schemes for quantities with scales above or below μ_m. In other words, the given scale hierarchy of the kinematic scales μ_i and the mass scale μ_m determines whether the heavy quark is treated as an active flavor in the respective factorization functions or not. If the evolution of a factorization function between the intrinsic and the global factorization scale crosses the mass scale μ_m, the quark is integrated out (or in) at that scale, leaving a matching factor $\mathcal{M}_i$. The evolution is performed with n_ℓ and $(n_\ell + 1)$ active flavors below and above the mass scale, respectively, where n_ℓ is the number of massless quarks.

Where the mass scale is located in relation to the kinematic scales is described by kinematic *scenarios* [102]: scenario I, II, III and IV refer to the setups where the mass is heavier than the hard scale, between hard and jet scale, between jet and soft scale, and smaller than the soft scale, respectively. To illustrate the variable flavor number scheme described above, let's take a look at scenario III: in that setup, the factorization formula is given by

$$\begin{aligned}\frac{1}{\sigma_0}\frac{\mathrm{d}\sigma}{\mathrm{d}\tau} = {} & QH^{(n_\ell+1)}(Q,\mu_H)U_H^{(n_\ell+1)}(Q,\mu_H,\mu_J)\int \mathrm{d}s \int \mathrm{d}\ell \int \mathrm{d}\ell' \int \mathrm{d}\ell''\, J^{(n_\ell+1)}(s,m,\mu_J) \\ & \times U_S^{(n_\ell+1)}(\ell'',\mu_J,\mu_m)\mathcal{M}_S^{(n_\ell+1)}(\ell'-\ell'',m,\mu_m,\mu_S)U_S^{(n_\ell)}(\ell-\ell',\mu_m,\mu_S) \\ & \times S^{(n_\ell)}\left(Q(\tau-\tau_{\min})-\frac{s}{Q}-\ell,\mu_S\right), \end{aligned} \tag{2.40}$$

where the global renormalization scale is set to the jet scale μ_J for simplicity. In scenario III, the mass scale μ_m is located between the jet scale μ_J and the soft scale μ_S. Consequently, the hard and jet function as well as their evolution kernels U_i are defined in the $(n_\ell + 1)$-flavor scheme, i.e. they include the heavy quark as an active flavor. In contrast, the soft function at the soft scale μ_S is defined in the n_ℓ-flavor scheme, i.e. the heavy quark is not an active flavor. The evolution of the soft function between the soft scale μ_S and the global jet scale μ_J crosses the mass scale μ_m. Therefore, the soft-function evolution, encoded in the evolution kernels U_S, takes place with $(n_\ell + 1)$ active flavors between the jet and mass scale, and with n_ℓ active flavors from the mass to the soft scale. At the mass scale, the heavy quark is integrated out, resulting in a soft matching factor $\mathcal{M}_S$.

The factorization formulas in the other scenarios follow a similar pattern. An exception is the bHQET scenario, in which the mass scale is very close to the jet invariant mass, with fluctuations $(p^2 - m^2)^2 \ll m^2$. Under these circumstances, a new kind of logarithms arises that can not be resummed by SCET. How to resum these logarithms by matching bHQET to SCET, and a much more extensive discussion of scenarios, the associated scale hierarchies and factorization formulas can be found in Refs. [104, 105].

The approach to massive factorization formulas that is described in this section is called the *universal factorization* approach. Another approach is *mass mode factorization*. The differences, advantages, and disadvantages of the two approaches are discussed in Chap. 3.2 and in the publication that is presented in Chap. 6 in the context of the massive SCET jet function.

Part II

Discussion

Chapter 3

Summaries

In the following, I summarize the work presented in the publications in this thesis, put them into context, and give short outlooks on possible future works.

3.1 NLO Massive Event-Shape Differential and Cumulative Distributions

The first issue that is dealt with in this thesis, see Chap. 5, is the computation of differential and cumulative e^+e^- event-shape cross sections for stable massive quarks with full quark mass dependence in an efficient and general way at NLO. Prior to this work, some fixed-order results have been known [106–108], but all were computed on an individual basis and mostly numerically. The issue at hand unfolds into several sub-issues: How are the observable definitions themselves influenced by finite quark masses? How can differential and cumulative event-shape distributions, including stable massive flavor effects, be computed generally and efficiently? How does one get the coefficients of the delta- and plus-distribution terms that are present in differential event-shape observables?

The necessity to reconsider event-shape definitions and to introduce different event-shape *mass schemes* (not to be confused with *mass renormalization schemes*) for measurements that involve massive particles was already pointed out in the past, e.g. in Refs. [109, 110]. In these publications, however, event-shape definitions were examined in the context of non-zero hadron masses and the related non-perturbative power corrections. Naturally, an analog consideration is necessary in the context of non-zero quark masses, where many of the issues discussed in earlier publications are present as well, see also Ref. [111]. Essentially, massive schemes deal with the fact that event shapes were originally formulated for massless particles. These original definitions, however, become ambiguous when generalized to massive particles due to the fact that $E_p \neq |\vec{p}|$ for massive particles, where $\vec{p}$ is the 3-momentum and E_p is the energy of a particle. As an example, we can consider the popular event shape *Thrust*, defined as

$$\tau \equiv \frac{1}{\sum_i |\vec{p}_i|} \min_{\hat{t}} \sum_i (|\vec{p}_i| - |\hat{t} \cdot \vec{p}_i|) \,, \tag{3.1}$$

where the index i refers to all measured particles and $\hat{t}$ is called the *thrust axis*. Thrust is originally defined in the so-called *P-scheme* (where P stands for "momentum"), i.e. $\tau \equiv \tau^P$. The substitution $\vec{p}_i \to (E_{p_i}/\vec{p}_i)\vec{p}_i$ does not have any effect for massless particles, but changes the event-shape values for massive ones. This substitution defines the conversion from the *P-scheme* to the so-called *E-scheme* (where E stands for "energy"). E-scheme thrust is therefore given by

$$\tau^E \equiv \frac{1}{\sum_i E_{p_i}} \min_{\hat{t}} \sum_i \left(E_{p_i} - \frac{E_{p_i}}{|\vec{p}_i|} |\hat{t} \cdot \vec{p}_i| \right) . \tag{3.2}$$

Fig. 3.1 in this chapter shows the fixed-order NLO thrust distribution in the P- and E-scheme for four different values of the reduced mass $\hat{m} = m/Q$, illustrating well how the difference of their values grows with $\hat{m}$.

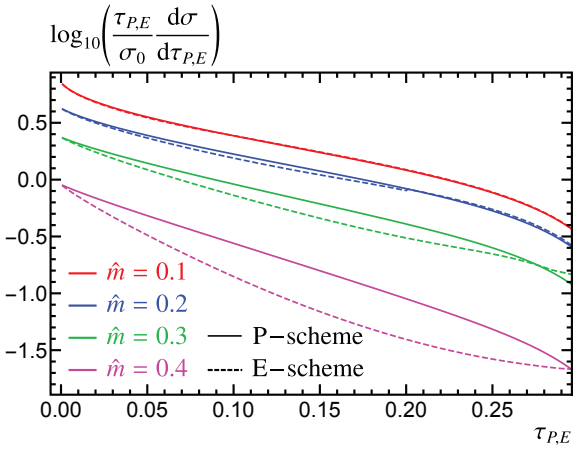

Figure 3.1: The thrust distribution in the P- and E-scheme for different values of the reduced mass $\hat{m}$. For small values of $\hat{m}$, both schemes converge to the same distribution, while their difference grows with large values of $\hat{m}$. The shown values were computed using the algorithm described at the end of this section.

Some event shapes, such as heavy jet mass in its original definition, are mixed and do not belong exclusively to either of the two schemes described above. These definitions are referred to as *massive schemes* or *M-schemes* and it can be useful to add massive-scheme definitions to event shapes that are originally defined in the P- or E-scheme. For thrust, the most popular massive scheme is called *2-jettiness* and is given by

$$\tau_J \equiv \frac{1}{\sum_i E_{p_i}} \min_{\hat{t}} \sum_i \left(E_{p_i} - |\hat{t} \cdot \vec{p}_i| \right) . \tag{3.3}$$

In the present work, event-shape mass schemes are reviewed and the differences in behavior of different schemes are analyzed. One of the key findings is that E- and P-scheme event shapes are insensitive to the quark mass effects at leading order, in contrast to M-scheme ones. This observation can be made use of in setups where it is desirable to increase or decrease quark mass sensitivity. For example, one might want to increase sensitivity in mass measurements or other mass-related measurements, while it is desirable to decrease the mass sensitivity for measurements that focus on the properties of the strong coupling.

The main aim of Chap. 5 is to develop a generally applicable method (analytical and/or numerical) to compute precise predictions for event-shape distributions that involve massive quarks. In this context, we achieve to show that, under a mild assumption, the NLO differential cross section with respect to an observable e (with minimal value $e_{\min}$) generally consists of a non-singular term and two types of Schwartz distributions at threshold $\bar{e} \equiv (e - e_{\min}) = 0$: a delta function $\delta(\bar{e})$ and a plus distribution

$$\left[\frac{1}{\bar{e}}\right]_+ \equiv \lim_{\beta \to 0} \frac{\mathrm{d}}{\mathrm{d}\bar{e}} \left[\Theta(\bar{e} - \beta) \int \frac{\mathrm{d}\bar{e}}{\bar{e}} \right] . \tag{3.4}$$

The overall assumption is that e is linearly sensitive to soft dynamics, which is the case for *all* event shapes of interest at the moment, including thrust, jet masses, C-parameter, jet broadening, and angularities.

As a consequence, the differential cross section $\mathrm{d}\sigma/\mathrm{d}e$ for stable massive quarks with respect

to an event shape e can always be written in the form[1]

$$\frac{1}{\sigma_0}\frac{\mathrm{d}\sigma}{\mathrm{d}e} = R^0(\hat{m})\delta(e-e_{\min}) + C_F\frac{\alpha_s}{\pi}\Bigg\{A_e(\hat{m})\delta(e-e_{\min}) + B_{\text{plus}}(\hat{m})\left[\frac{1}{e-e_{\min}}\right]_+ + F_e^{\text{NS}}(e,\hat{m})\Bigg\} + \mathcal{O}(\alpha_s^2)\,, \tag{3.5}$$

with the coefficient functions R^0, A_e, B_{plus} and the NLO non-singular contribution F_e^{NS} as well as the reduced mass $\hat{m} = m/Q$. The non-singular term F_e^{NS} does not contain any Schwartz-Distributions (except for potential Heaviside functions) and is integrable.[2]

Furthermore, it is shown in the publication that the plus-distribution coefficient B_{plus} is universal for infrared- and collinear-safe event shapes,

$$B_{\text{plus}}(\hat{m}) = \begin{pmatrix} 3-v^2 \\ 2\,v^2 \end{pmatrix}\Big[(1+v^2)L_v - v\Big]\,, \tag{3.6}$$

with $v = \sqrt{1-4\hat{m}}$ and $L_v = \log((1+v)/2\hat{m})$. In contrast to the corresponding massless expressions, the contributions from vector and axial-vector currents differ and are therefore given separately in the first and second line in big parentheses in Eq. (3.6), respectively. On the other hand, the delta-function coefficient A_e can be computed with a general formula that involves only universal terms and a 1-dimensional integral $I_e(\hat{m})$ which is given below in Eq. (3.7) (see also Eq. (3.31) in the publication of Chap. 5 for details and the complete formula).

The strategy to derive the general structure of event-shape distributions as shown in Eq. (3.5), as well as the formulas for A_e and B_{plus}, it to choose a suitable momentum parametrization that makes the soft limit, where the two Schwartz distributions are defined, explicit and easily accessible: at NLO, the 3-particle final state consists of two quarks and one gluon. Defining $x_i = 2E_i/Q$ for the final states ($i = 1, 2$ for the quarks, $i = 3$ for the gluon), the chosen coordinates y and z are defined by $x_1 = 1-(1-z)y$ and $x_2 = 1-zy$, such that $y = x_3$ and the soft limit is realized by $y \to 0$. By conducting as many integrations as possible in full generality and then carefully expanding in the dimensional regularization parameter ε and applying soft subtractions in the remaining integrals, one arrives at the expression in Eq. (3.5) and the explicit formulae for the coefficients therein. The delta-function coefficient is given by a sum of universal terms and a non-universal term. The universal terms contain logarithms, dilogarithms, and polynomials in $\hat{m}$. The non-universal, event-shape dependent term is given by a mass-dependent prefactor and the 1-D integral

$$I_e(\hat{m}) = \frac{1}{2}\int_{z_-}^{z_+}\mathrm{d}z\,\frac{(1-z)z-\hat{m}^2}{(1-z)^2z^2}\log[f_e(z)]\,, \tag{3.7}$$

where

$$z_\pm \equiv \frac{1\pm v}{2}, \qquad f_e(z) \equiv \left.\frac{\mathrm{d}e(y,z)}{\mathrm{d}y}\right|_{y\to 0}. \tag{3.8}$$

I_e can be solved analytically in most cases, with results in the E-, P- and M-scheme given in App. D of Chap. 5 for Heavy Jet Mass, Thrust, C-Parameter, Broadening, and Angularities. In case I_e can not be determined analytically, the integral can be solved numerically with standard methods, as long one can determine the values of $f_e(z)$, at least numerically.

[1] This is a fixed-order statement. In a resummed computation more general Schwartz distributions can appear. In a fixed-order expansion, they cancel with the limits of non-distributional contributions or reduce to delta functions, plus distributions, and non-distributional terms.

[2] Here, the mass m is renormalized in the pole mass scheme.

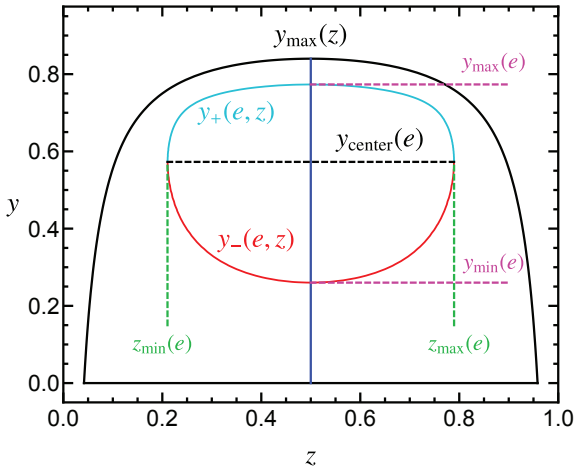

Figure 3.2: Schematic plot of a line of constant event-shape value (colored lines) in phase space (black lines), parametrized by y and z. Some special points and lines necessary to compute the non-singular contribution to the distribution of an event shape e are annotated, such as the minimal and maximal value of z that can be reached by an individual constant event-shape-value line, $z_{\min}$ and $z_{\min}$, respectively.

The same strategy of expanding in the soft limit yields a useful expression for the non-singular term $F_e^{\text{NS}}(e,\hat{m})$, see Eq. (3.29) in the publication of Chap. 5. The expression consists of y-z-parametrized phase-space integrals over the squared matrix element, constrained by delta and Heaviside functions that depend on the event-shape measurement function. Although F_e^{NS} can sometimes be computed analytically (see Sec. 5 of Chap. 5), this is not feasible in most cases. However, the general expression for F_e^{NS} derived in Chap. 5 serves as a valuable starting point to develop numerical algorithms to compute the non-singular contributions very accurately and quickly, see Sec. 4.3 of Chap. 5.

The algorithm developed in Chap. 5 computes the unbinned differential or cumulative distribution of an event shape with in principle arbitrary precision[3], given the event-shape variable and its first derivative in terms of the phase-space parameters y and z. Given these expressions, the task of computing the event-shape distribution (differential or cumulative) numerically reduces to the geometric problem of finding the boundary points on the curves of constant event-shape values in phase space, with a subsequent 1-dimensional integration, see the blue and red colored curves in Fig. 3.2 in this chapter. In our implementation, which is described in detail in Sec. 4.3. of Chap. 5, we first determine as many auxiliary points as possible analytically (such as the phase-space point where the thrust axis can be chosen to point in the direction of either of the 3-momenta of the particles involved in the collision) and use the Brent algorithm to find boundary points numerically. The instructions given in Chap. 5 are very general and can be readily applied to all common event shapes, or, if necessary, easily extended to be applied to new or exotic event shapes.

The geometry of the y-z-parametrized phase space and constant event-shape lines is illustrated in Fig. 3.2 in this chapter, where the phase space boundary is drawn as a black line and an exemplary curve of constant event-shape value as the colored line sections. Additionally, some special points of the event-shape curve required for the numerical computation, such as the extrema in y and z, are marked with dashed lines.

Possible extensions of this work include a generalization to higher orders in perturbation

[3]These are the main advantages of the described technique compared to the common Monte Carlo method, which relies on bins that in general have to be specified ahead, and for which the precision can not be controlled independently.

theory. The inclusion of N^{2}LL contributions from SCET and bHQET has already been achieved in Ref. [112].

The results and instructions presented in the publication in Chap. 5 are useful for anyone interested in event-shape distributions that involve massive quark effects at NLO. The results also represent an important input for future studies related to event-shape based quark mass determinations, e.g. at a future linear collider.

3.2 Two-Loop Massive Quark Jet Functions in SCET

Fixed-order results for event-shape cross sections are most useful in the tail and far tail of the distribution. In the peak and intermediate regions, however, large logarithms invalidate the perturbative series due to large scale hierarchies and the resulting large logarithms. These logarithms can be resummed using effective field theory techniques and factorization, see Chap. 2.3.2.

Similar to fixed-order computations, most calculations of factorization-formula ingredients focus on limiting cases: where all particles are massless (e.g. the massless SCET jet function [113–115]) or where the heavy quark mass is of the order of the associated jet invariant mass (e.g. the bHQET jet function [116]). These approximations are only applicable near their expansion points and general massive results are necessary to achieve high precision in the intermediate regions. General massive SCET results are available: taking the event shape *thrust* as an example (see Chap. 2.3.2 of this thesis), all ingredients to achieve N^{3}LL resummation exist. The last missing piece has been the two-loop massive quark SCET jet function, which describes collinear QCD radiation off a massive quark that is produced at high energy. This missing piece is computed in the second publication included in this thesis, see Chap. 6. The massive quark jet function is, just like most factorization-formula ingredients, not only applicable to thrust but a rather universal function that contributes to many processes like semileptonic meson decays[4] and various event shapes other than thrust.

The quark SCET jet-function matrix element for a jet initiated by the primary quark f in light-like direction n_μ is given by [96, 98]

$$\begin{aligned}\mathscr{J}_f^{(n_\ell+1)}(p^2,m^2) &= \frac{(2\pi)^3}{N_c\,p^-}\,\mathrm{Tr}\left\langle 0\middle|\frac{\bar{n}\!\!\!/}{2}\chi_f^n(0)\,\delta(p^+ + \hat{p}^+)\,\delta(p^- + \overline{\mathcal{P}}_n)\,\delta^{(2)}(p_\perp + \mathcal{P}_{n\perp})\,\overline{\chi}_f^n(0)\middle|0\right\rangle \\ &= \mathrm{Im}\left[\frac{i}{2\pi N_c\,(\bar{n}\cdot p)}\int \mathrm{d}^4x\; e^{-ip\cdot x}\,\mathrm{Tr}\left\langle 0\middle|\mathrm{T}\left\{\frac{\bar{n}\!\!\!/}{2}W^\dagger(0)\,\psi_f(0)\,\overline{\psi}_f(x)\,W(x)\right\}\middle|0\right\rangle\right], \quad (3.9)\end{aligned}$$

where the first line shows the original SCET definition and the second line shows the jet-function matrix element in terms of QCD quark fields [114]. In the two-loop calculation of the jet-function matrix element presented here, the latter option is adopted because it leads to expressions that are easier to evaluate. In Eq. (3.9), the momentum four-vectors are decomposed in lightcone components according to $p^\mu = p^- n^\mu/2 + p^+\bar{n}^\mu/2 + p_\perp^\mu$ with $n^2 = \bar{n}^2 = 0$, $\bar{n}\cdot n = 2$, and $n\cdot p_\perp = \bar{n}\cdot p_\perp = 0$. $\overline{\mathcal{P}}_n$ and $\mathcal{P}_{n\perp}$ are the SCET label momentum operators and $\hat{p}^+$ is the operator of the small plus momentum [97]. $\chi_f^n(x)$ is the SCET jet field, N_c is the number of QCD colors, and $W(x)$ is the n-collinear Wilson line expressed in terms of QCD quark fields. For a more detailed explanation of the ingredients of Eq. (3.9), I refer to Sec. 2 of Chap. 6 and the references therein.

[4] One example is semi-leptonic $B \to X_c\,\ell\,\nu$ decay: the phase-space region of the invariant mass of the hadronic jet that originates from the decaying bottom quark is of order $\sqrt{\Lambda_{\mathrm{QCD}} m_b}$ and is well described by SCET. In this context, the charm quark mass is of the order of the jet invariant mass and the associated mass effect in the jet function must be included to obtain results with satisfying precision.

The jet-function matrix element is in general infrared divergent and includes phase-space regions that overlap with lower-virtuality regions that are already accounted for by other functions in the factorization formula [98, 99]. To receive the infrared-finite jet function and to avoid double counting, subtractions associated with the (equally infrared-divergent) collinear-soft matrix element [117, 118]

$$\mathscr{S}^{(n_\ell+1)}(\ell,m) = \frac{1}{N_c}\mathrm{Tr}\left\langle 0\left|\overline{\mathrm{T}}[V_n^{(0)\dagger}(0)X_n^{(0)}(0)]\,\delta(\ell-\hat{p}^+)\,\mathrm{T}[X_n^{(0)\dagger}(0)V_n^{(0)}(0)]\right|0\right\rangle\,, \quad (3.10)$$

are required, where X_n and V_n are collinear-soft Wilson lines, see Sec. 2 of Chap. 6. The superscript $(n_\ell+1)$ of $\mathscr{S}$ refers to a theory with n_ℓ massless and one heavy quark, see also the explanation below Eq. (3.12). IR-subtractions via the collinear-soft matrix element is an alternative approach to the widely used zero-bin subtractions [119].

The jet function presented in this work includes primary as well as secondary mass effects, i.e. effects that come from the jet-initializing (primary) massive quark as well as from (secondary) pair-produced virtual ones. An essential point that is discussed from a new perspective in the present work is how to deal with collinear-soft subtractions for contributions that contain secondary quark loops. These contributions are infrared divergent if the quark anti-quark pair in the loop is massless, but infrared finite if the pair is massive[5].

As a consequence, one is left with two options to define the infrared-finite quark jet function with secondary massive quarks: either the finite collinear-soft contributions that are related to massive quark loops are subtracted nonetheless, or they are left unsubtracted. The first option leads to the so-called *universal* ("uf", see also Refs. [103, 120]) jet function and the second option to the so-called *mass mode* ("mf", see also Ref. [121]) jet function, respectively. In terms of equations,

$$J_f^{\mathrm{uf},(n_\ell+1)}(p^2,m^2) \equiv \int \mathrm{d}\ell\, \mathscr{J}_f^{(n_\ell+1)}(p^2-(\bar{n}\cdot p)\ell,m^2)\Big(\mathscr{S}^{(n_\ell+1)}(\ell,m^2)\Big)^{-1}\,, \quad (3.11)$$

defines the universal jet function J_f^{uf}, and

$$J_f^{\mathrm{mf},(n_\ell+1)}(p^2,m^2) \equiv \int \mathrm{d}\ell\, \mathscr{J}_f^{(n_\ell+1)}(p^2-(\bar{n}\cdot p)\ell,m^2)\Big(\mathscr{S}^{(n_\ell)}(\ell)\Big)^{-1}\,, \quad (3.12)$$

defines the mass-mode jet function J_f^{mf}, where $\mathscr{J}_f^{(n_\ell+1)}$ and $\mathscr{S}^{(n_\ell+1)}$ are respectively the jet-function and collinear-soft matrix elements in a theory with n_ℓ massless and one heavy quark, and $\mathscr{S}^{(n_\ell)}$ is the collinear-soft matrix element in a theory with only n_ℓ massless flavors. The mass-mode jet function depends on the virtuality renormalization scale μ as well as the rapidity renormalization scale ν and has no well-defined massless limit due to arising infrared singularities[6]. On the other hand, the universal jet function depends on the virtuality renormalization scale μ, but not on the rapidity renormalization scale ν. Furthermore, the universal jet function converges to the known massless result for $m \to 0$. Both jet-function definitions lead to equivalent results when correctly implemented in the factorization formulas, but they allow to study secondary massive quark effects from different perspectives.

[5] These finite contributions are related to mass-mode fluctuations with virtualities $p^2 \sim m^2$. Mass modes arise from collinear as well as soft phase-space regions and lead to rapidity divergences usually associated with $\mathrm{SCET_{II}}$-type observables [102]. This issue also affects the computation of secondary massive quark contributions to the jet function, see below.

[6] The non-existence of a massless limit of the mass-mode jet function is expected: since the massive flavor is not included in the definition of the collinear-soft matrix element, the mass scaling is implicitly assumed to be $m^2 \sim p^2 \sim p^2 - m^2$, i.e. the mass is not an infrared scale, see also the description of factorization theorems below.

Traditionally, the subtractions for secondary massive contributions are approached in the context of soft mass-mode bin subtractions [102, 103, 122], entailing subtle issues concerning power counting. In contrast, the strategy to subtract these modes from the jet-function matrix element with the collinear-soft function is systematic and strongly connected to the philosophy of interpreting the jet function as a matching function describing modes with virtuality $p^2 - m^2 \sim p^2$.

Interpreting the jet function as such a matching function, the universal jet function of Eq. (3.11) is the appropriate definition if $m^2 \ll p^2$ (i.e. if m is an IR scale), while the mass mode jet function of Eq. (3.12) is the natural choice if $m^2 \sim p^2$. However, the universal jet function might also be used in the regime $m^2 \sim p^2$ or any other hierarchy of m with respect to the physical scales and the renormalization scale μ.

This interpolating property leads to the possibility to set up factorization theorems that smoothly interpolate between all possible hierarchies with respect to the mass m [102, 103, 120]. In this *universal factorization approach*, the same factorization formula can be used for any scale hierarchy. Different scale hierarchies are accounted for by mass threshold matching factors and by using the appropriate flavor number scheme for the individual factorization functions. Rapidity logarithms do only appear in mass threshold matching factors.

Let's illustrate the universal factorization approach briefly by considering a setup with the scale hierarchy $s^2/Q^2 \ll m^2 \lesssim s \sim p^2 \ll Q^2$. The corresponding leading power double hemisphere mass factorization theorem in that approach for $s^2/Q^2 < \mu^2 < m^2$, i.e. when the SCET current and the jet functions are evolved below m, has the form

$$\begin{aligned}\frac{1}{\sigma_0}\frac{\mathrm{d}\sigma}{\mathrm{d}M_Q^2\,\mathrm{d}M_{\bar{Q}}^2} = H_Q^{(n_\ell+1)}(Q,\mu) H_m\left(m,\frac{Q}{m},\mu\right)\int \mathrm{d}s_Q\,\mathrm{d}s_{\bar{Q}}\int \mathrm{d}\ell^+\,\mathrm{d}\ell^- \\ \times J_Q^{\mathrm{uf},(n_\ell+1)}(M_Q^2 - s_Q - Q\ell^+, m^2, \mu)\, J_Q^{\mathrm{uf},(n_\ell+1)}(M_{\bar{Q}}^2 - s_{\bar{Q}} - Q\ell^-, m^2, \mu) \\ \times \mathcal{M}_{J_Q}(s_Q, m, \mu)\mathcal{M}_{J_Q}(s_{\bar{Q}}, m, \mu) S^{(n_\ell)}(\ell^+,\ell^-,\mu)\,, \qquad (3.13)\end{aligned}$$

where H_m and $\mathcal{M}_{J_Q}$ are the quark mass threshold matching factors for the SCET current and the universal jet function J_Q^{uf} respectively. For $m^2 < \mu^2 < s$, i.e. where the soft function is evolved above m, the same factorization theorem has the form

$$\begin{aligned}\frac{1}{\sigma_0}\frac{\mathrm{d}\sigma}{\mathrm{d}M_Q^2\,\mathrm{d}M_{\bar{Q}}^2} = H_Q^{(n_\ell+1)}(Q,\mu)\int \mathrm{d}\ell^+\,\mathrm{d}\ell^-\mathrm{d}\ell'^+\,\mathrm{d}\ell'^- \\ \times J_Q^{\mathrm{uf},(n_\ell+1)}(M_Q^2 - Q\ell^+, m^2, \mu) J_Q^{\mathrm{uf},(n_\ell+1)}(M_{\bar{Q}}^2 - Q\ell^-, m^2, \mu) \\ \times \mathcal{M}_S(\ell'^+,\ell'^-,m,\mu) S^{(n_\ell)}(\ell^+ - \ell'^+, \ell^- - \ell'^-, \mu)\,, \qquad (3.14)\end{aligned}$$

where $\mathcal{M}_S$ is the mass threshold matching factor for the soft function S.

Alternatively, in the *mass mode factorization* approach individual factorization formulas are set up for each scale hierarchy of m with respect to the other physical scales [121]. Consequently, each of the factorization formulas is formulated in a way such that only the strictly relevant modes appear for each kinematic scenario. The mass-mode factorization approach is not only economical with respect to the modes present in the individual factorization formulas but also especially transparent since collinear and soft mass-mode contributions do appear explicitly in the formulas. Rapidity resummation is treated on the same footing as virtuality resummation, namely by renormalization group evolutions of the individual factorization-formula ingredients.

To illustrate that strategy, let's again consider the hierarchy $s^2/Q^2 \ll m^2 \ll s \sim p^2 \ll Q^2$. The corresponding factorization theorem in the mass mode factorization approach has the

form

$$\frac{1}{\sigma_0}\frac{\mathrm{d}\sigma}{\mathrm{d}M_Q^2\,\mathrm{d}M_{\bar{Q}}^2} = H_Q^{(n_\ell+1)}(Q,\mu)H_{m,s}\left(m,\mu,\frac{m}{\nu}\right)\int \mathrm{d}\ell^+\,\mathrm{d}\ell^-\mathrm{d}\ell'^+\,\mathrm{d}\ell'^- \\ \times J_q^{(n_\ell+1)}(M_Q^2 - Q\ell^+ - Q\ell'^+,\mu)\,J_q^{(n_\ell+1)}(M_{\bar{Q}}^2 - Q\ell^- - Q\ell'^-,\mu) \\ \times S_c(\ell'^+,m,\mu,\nu)S_c(\ell'^-,m,\mu,\nu)S^{(n_\ell)}(\ell^+,\ell^-,\mu)\,, \tag{3.15}$$

where $H_{m,s}$ is the soft mass mode contribution of the mass threshold hard function

$$H_m(m,Q/m,\mu) = H_{m,n}(m,\mu,Q/\nu)H_{m,\bar{n}}(m,\mu,Q/\nu)H_{m,s}(m,\mu,m/\nu)\,, \tag{3.16}$$

S_c is the collinear-soft function

$$S_c(\ell,m,\mu,\nu) = \int \mathrm{d}\ell\,\mathscr{S}^{(n_\ell+1)}(\ell-\ell',m,\mu,\nu)\Big(\mathscr{S}^{(n_\ell)}(\ell',\mu,\nu)\Big)^{-1} \\ = \frac{1}{\bar{n}\cdot p}\int \mathrm{d}p'^2\,J_f^{\mathrm{mf},(n_\ell+1)}((\bar{n}\cdot p)\ell - p'^2,m^2,\mu,\bar{n}\cdot p/\nu)\big(J_f^{\mathrm{uf},(n_\ell+1)}(p'^2,m^2,\mu)\big)^{-1}\,, \tag{3.17}$$

and $J_q^{(n_\ell+1)}$ is the jet function for $(n_\ell+1)$ *massless* quarks which coincides with the universal jet function for vanishing quark mass, i.e. $J_Q^{\mathrm{uf},(n_\ell+1)}(p^2,0,\mu)$. The (infrared- and rapidity-finite) collinear-soft function S_c encodes the pure collinear-soft contributions associated to the massive quark flavor.

The factorization theorems (3.15), (3.13) and(3.14) provide identical descriptions for the hierarchy $s^2/Q^2 \ll m^2 \ll s \sim p^2 \ll Q^2$ (up to suppressed quark mass power corrections).

For the hierarchy $s^2/Q^2 \ll m^2 \sim s \sim p^2 \ll Q^2$, the mass mode factorization approach states the factorization theorem

$$\frac{1}{\sigma_0}\frac{\mathrm{d}\sigma}{\mathrm{d}M_Q^2\,\mathrm{d}M_{\bar{Q}}^2} = H_Q^{(n_\ell+1)}(Q,\mu)H_{m,s}\left(m,\mu,\frac{m}{\nu}\right)\int \mathrm{d}\ell^+\,\mathrm{d}\ell^- \\ \times J_Q^{\mathrm{mf},(n_\ell+1)}\left(M_Q^2 - Q\ell^+,m^2,\mu,\frac{Q}{\nu}\right)J_Q^{\mathrm{mf},(n_\ell+1)}\left(M_{\bar{Q}}^2 - Q\ell^-,m^2,\mu,\frac{Q}{\nu}\right) \\ \times S^{(n_\ell)}(\ell^+,\ell^-,\mu)\,. \tag{3.18}$$

It is easy to see that Eq. (3.18) and the universal factorization theorems (3.13) and (3.14) provide identical descriptions for $s^2/Q^2 \ll m^2 \sim s \sim p^2 \ll Q^2$ owing to the consistency relations

$$\mathcal{M}_{J_Q}(s,m,\mu) = H_{m,n}^{-1}\,(m,\mu,Q/\nu)\,S_c(s/Q,m,\mu,\nu)\,, \tag{3.19}$$

$$\mathcal{M}_S(\ell^+,\ell^-,m,\mu) = H_{m,s}(m,\mu,m/\nu)S_c(\ell'^+,m,\mu,\nu)S_c(\ell'^{-,m,\mu,\nu})\,, \tag{3.20}$$

together with the definition of the collinear-soft function in Eq. (3.17) and the factorized mass threshold hard function of Eq. (3.16).

For more details, see Sec. 4 of Chap. 6. For a more general description of factorization theorems, see Chap. 2.3.2 of this thesis.

Apart from clarifying the conceptual issues described above, the main goal of the work in Chap. 6 is to compute the two-loop contribution of the massive quark SCET jet function and to present the associated calculations. As expected from a two-loop calculation with finite mass values, elaborate tools developed by the multi-loop community in recent years have to be employed to tackle the problem, including IBP reduction [123], differential-equation techniques [25,124,125], and sector decomposition [126]. For our computation, the Feynman diagrams that have to be evaluated can be separated into three classes: planar diagrams,

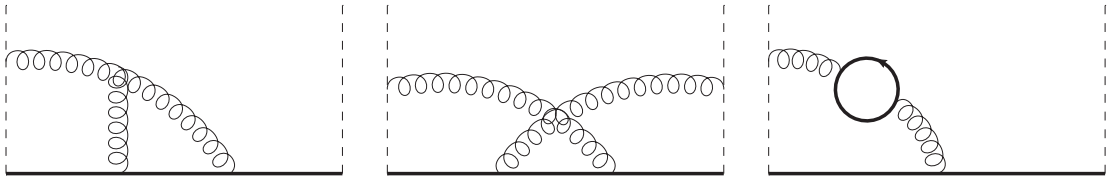

Figure 3.3: Three exemplary Feynman diagrams that contribute to the two-loop massive quark SCET jet function. The solid lines represent massive quarks, the curly lines represent gluons and the dashed lines represent n-collinear (lightlike) Wilson lines. The first diagram belongs to the family of planar topologies, the second one is non-planar, and the third diagram encodes a contribution of secondary massive quarks.

non-planar diagrams, and diagrams with secondary massive quarks. An exemplary diagram is shown for each of these classes in Fig. 3.3 in this chapter. Each class of diagrams requires a distinct strategy to solve them, determined by their complexity and their behavior in the context of eikonal propagators and rapidity divergences. Eikonal propagators $1/(n \cdot k)$ (where n is a light-cone direction and k is a loop momentum) arise from Wilson-line interactions and are the main special feature of this calculation in comparison to most other multi-loop setups. Aside from the fact that many available multi-loop tools are not capable of dealing with this special kind of propagator, the structure in general induces rapidity divergences in Feynman integrals [102, 127], i.e. singularities for $(n \cdot k)/(\bar{n} \cdot k) \to \infty$ or $(n \cdot k)/(\bar{n} \cdot k) \to 0$.

In the following, I shortly describe the strategies that are applied to solve the Feynman diagrams of the individual diagram classes (planar, non-planar, secondary massive) individually. For a more detailed description, I refer to Sec. 5 of Chap. 6.

The class of planar diagrams can be solved in a straightforward way by applying IBP reductions, Feynman parameters, and differential equations. Special care has to be taken only when extracting the imaginary part from the general complex result (see Eq. (3.9)): the imaginary part contains delta and plus distributions at $s = p^2 - m^2$, as well as their derivatives, i.e. there are non-trivial structures at $s = 0$.

For the non-planar diagrams with Wilson-line interactions, the presence of eikonal propagators leads to undefined and wrong results in the IBP reduction (when applied naively) due to rapidity divergences, even for integrals that do not suffer from rapidity divergences initially (i.e. before applying the IBP relations). When additional regulators are added to solve this issue, the procedure becomes well-defined, but the reduction does not lead to a strongly reduced number of easier-to-solve master integrals and is therefore useless. An example of such a case is given in Eq. (5.13) in the publication of Chap. 6. Fortunately, in the case of the two-loop SCET jet function the set of "problematic" non-planar diagrams is small and they can be solved semi-analytically by utilizing analytic information from bHQET and massless limits. Numerically, the semi-analytic contribution G_{fit} in the jet function result is very small compared to all other ingredients, see Fig. 3.4 in this chapter. G_{fit} is given in Eq. (3.16) in the publication of Chap. 6. A more general understanding of arising rapidity divergences in IBP reductions and the development of new techniques that deal with this issue are desirable and should be studied in future works.

The third class of diagrams, which encodes secondary massive quark contributions, requires yet another special treatment: They are evaluated by making use of a dispersion integral that connects the radiation of gluons with finite mass M with the diagrams in which the massive gluon is exchanged with massive quark loops [102, 103]. In other words, instead of solving the massive quark loop diagrams directly, we first evaluate the diagrams where

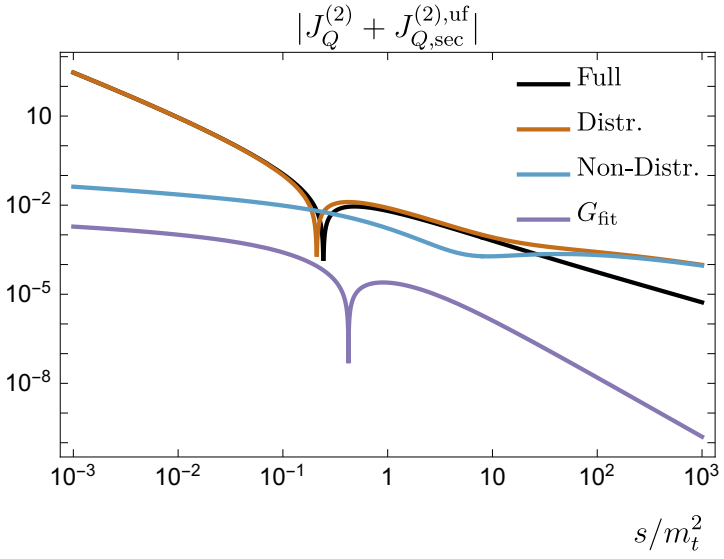

Figure 3.4: A double-logarithmic plot of the absolute values of the two-loop contribution to the massive quark SCET jet function over the mass-scaled virtuality s/m_t^2. The plot illustrates well the impact of different contributions: the distributional part (orange line) is by far the largest contribution for small and intermediate values of s/m_t^2, while the non-distributional part (blue line) takes over at $s/m_t^2 \gtrsim 30$. The non-distributional contribution that is computed numerically (purple line) is always orders of magnitude smaller than the other contributions, except for a small region around the zero-crossing of the jet function.

the quark-bubble-augmented gluon is replaced by a massive gluon with mass M and then compute a dispersion integral over M that involves the absorptive part of the massive quark loop. In the same computation, a gluon mass regulator Λ is incorporated to cleanly separate UV from rapidity divergences[7]. The dispersion relation has the form

$$\frac{-ig^{\mu\rho}}{p^2-\Lambda^2+i0}\,\Pi_{\rho\sigma}(p^2,m^2)\,\frac{-ig^{\sigma\nu}}{p^2-\Lambda^2+i0} = \frac{1}{\pi}\int\limits_{4m^2}^{\infty}\frac{\mathrm{d}M^2}{M^2}\,\frac{-i(g^{\mu\nu}-\frac{p^\mu p^\nu}{p^2})}{p^2-M^2+i0}\,\mathrm{Im}\left[\Pi(M^2,m^2)\right] - \frac{-i\left(g^{\mu\nu}-\frac{p^\mu p^\nu}{p^2}\right)}{p^2-\Lambda^2+i0}\,\Pi(0,m^2)\,, \tag{3.21}$$

where $\Pi(p^2,m^2)$ is the gluon vacuum polarization function and m is the quark mass. To solve the massive-gluon diagrams, it is often convenient to introduce Feynman parameters and to subsequently separate the $M\to\infty$ contribution (which usually has a much simpler structure than the original expression) from the rest (for which the limit $\varepsilon\to 0$ can be taken without any special treatment). For more details concerning the dispersion relation and its application, see Sec. 5.3 of Chap. 6 and the references therein.

For a consistent treatment of cross terms in the renormalization procedure of the two-loop secondary massive quark contributions, the 1-loop contribution to the jet function matrix element has to be computed with the finite Λ gluon-mass regulator as well. This does not lead to any issues. At higher orders, however, this strategy is nearly unfeasible

[7] It is important to take care of rapidity singularities and the associated large logarithms here since secondary massive effects lead to "true" singularities of that type in collinear-soft factorization as known from SCET_{II} observables. The rapidity singularities in the jet-function matrix element either cancel with the collinear-soft matrix element, or need to be renormalized. As described above, this leads to two options to define the massive quark jet function.

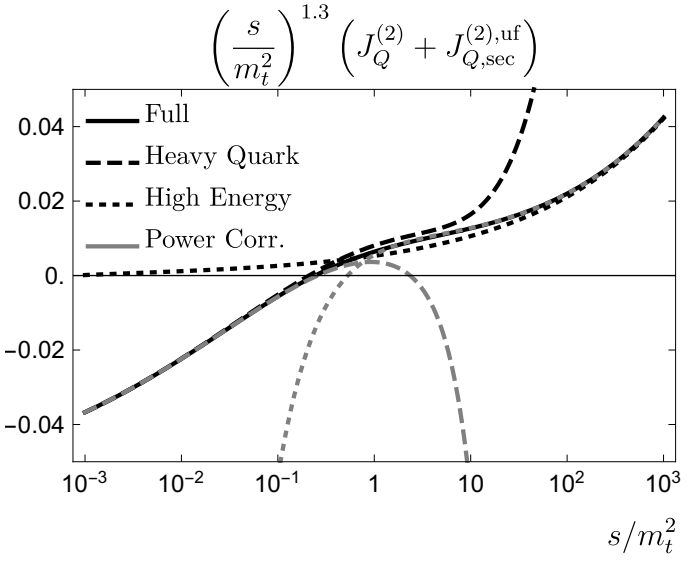

Figure 3.5: The scaled massive quark two-loop SCET jet function (solid black line) over the mass-scaled virtuality s/m_t^2, and its high-energy and heavy-quark limit (dashed and dotted black lines, respectively). The fully massive result nicely interpolates between the two limits. It is unexpected that the two limits are so close to the full result in a very large range and mostly coincidental: adding an additional power-correction term to the limits does not significantly increase their area of validity, or even decrease it in the case of the high-energy limit.

since it involves the computation of all lower-order diagrams with an additional massive-gluon regulator. This includes the various renormalization factors. The development and investigation of new strategies and rapidity regulators to apply to the computation of secondary mass contributions is an interesting project for future work.

The final result of the two-loop massive SCET jet function consists of delta and plus distributions, standard functions, harmonic polylogarithms, elliptic functions, and one-parameter integral functions. However, simple fit functions of the non-distributional results are provided in Chap. 6 to make them easily applicable and implementable. The fit functions only contain polynomials and logarithms of m^2/p^2, coincide with the known massless and heavy-quark limits, and approximate the exact functions with a relative precision of 0.5%. The complete final expressions as well as some of their limiting cases and consistency checks are given in Sec. 3 of Chap. 6. The impact of the fully massive result compared to the high-energy and heavy-quark limit is illustrated in Fig. 3.5 in this chapter.

3.3 The MSR Mass and the $\mathcal{O}(\Lambda_{\rm QCD})$ Renormalon Sum Rule

It is striking that the implementation of mass parameters more often than not leads to additional conceptual and technical issues in high-energy physics. As it turns out, the mass parameter in itself already entails highly involved concepts: first of all, due to confinement in QCD, quark masses are not physical observables and have to be seen as abstract parameters in the QCD action, such that there is no one true physical way of treating them. Additionally, the massive quark self-energy is UV divergent such that the divergences have to be absorbed into the mass parameter by renormalization. The

freedom to absorb additional finite contributions implies that one can define an in principle arbitrarily large number of mass renormalization schemes. A well-chosen renormalization scheme can, however, improve the overall precision of theoretical calculations in QCD and, in many cases, simplify them.

An important problem in the context of mass renormalization schemes for high precision quark mass determinations is the $\mathcal{O}(\Lambda_{\rm QCD})$ renormalon of the pole mass [67, 74]. The pole scheme is often employed when it is assumed that the renormalized mass parameters can be interpreted as being the "physical" masses. For color-charged particles, however, there is no pole in the propagator. An accordingly renormalized mass parameter suffers from an $\mathcal{O}(\Lambda_{\rm QCD})$ renormalon, entailing an inevitable ambiguity of its value. The bad perturbative behavior is caused by the asymptotic nature of the series and renders the fixed-order pole mass to be an order- and observable-dependent quantity. The pole mass renormalization prescription is consequently inappropriate for precision determinations of quark mass parameters. For a more detailed general introduction to mass renormalization schemes, see Chap. 2.3.1 of this thesis.

In the work presented in Chap. 7, the low-scale short-distance MSR mass scheme is discussed[8] in detail and its fundamental aspects are discussed, assuming that all quark flavors lighter than the considered heavy quark flavor are massless, e.g. the formulae describing the top quark MSR mass $m_t^{\rm MSR}$ do not contain any corrections from the non-zero bottom quark mass, etc.[9] In the same article, the MSR scheme is utilized to derive analytic formulae related to $\mathcal{O}(\Lambda_{\rm QCD})$ renormalons and the associated asymptotic high-order behavior of perturbative series. Most importantly, an analytic expression for the normalization of $\mathcal{O}(\Lambda_{\rm QCD})$ renormalons is derived, called the *renormalon sum rule*. In the following, the main concepts and results of Chap. 7 are reviewed.

The MSR mass of a heavy quark is defined via its perturbative series relating it to the pole mass. Assuming all lighter massive flavors to be massless, the relation is given by

$$m_Q^{\rm pole} - m_Q^{\rm MSR}(R) = R \sum_{n=1}^{\infty} a_n \left(\frac{\alpha_s^{(n_\ell)}(R)}{4\pi} \right)^n , \tag{3.22}$$

where the perturbative coefficients a_n are defined analogously to those for the $\overline{\rm MS}$ mass [76–83], but with the contributions from loops of the heavy quark Q in the associated self-energy diagrams removed, see also Sec. 2 of Chap. 7.[10]

There are many ways to express the ideas leading to the defining formula in Eq. (3.22), one of them is the following: we are interested in defining a well-behaved low-scale short-distance mass scheme and are going to derive it in terms of a perturbative series relating it to the pole mass scheme. We choose the $\overline{\rm MS}$ mass as a starting point due to its good infrared behavior and direct relation to quark self-energy diagrams. Since the low-energy and high-order behavior of the pole mass are closely related due to its linear IR-sensitivity, we consider the asymptotic high-order behavior of the pole-$\overline{\rm MS}$ perturbative series to get insights into the correct low-energy behavior. Asymptotically, the series depends only on the number of *massless* quarks n_ℓ, but not on the heavy quark mass m_Q. Furthermore, a linear dependence on the renormalization scale emerges.

[8] Note that the MSR mass scheme was already introduced in Refs. [71, 128], but without a detailed discussion as provided in Chap. 7.

[9] The extension of the MSR mass scheme that includes lighter massive flavor effects is discussed in Chap. 8 and summarized in Chap. 3.4 of this thesis.

[10] Note that in Chap. 7, two versions of the MSR mass are discussed: the natural and the practical definition. Since the natural MSR mass definition is the conceptually cleaner one, I always refer to that definition here.

The reason for the asymptotic linear dependence on the renormalization scale can be easily demonstrated in the large β_0/LL approximation: in that approximation, the pole-$\overline{\rm MS}$ mass relation is given by

$$\begin{aligned}[m_Q^{\rm pole} - \overline{m}]_{\beta_0/\rm LL} &= \overline{m}\frac{a_1}{2\beta_0}\sum_{n=0}^{\infty} n!\left(\frac{\beta_0\alpha_s(\overline{m})}{2\pi}\right)^{n+1} \\ &= \overline{m}\frac{a_1}{2\beta_0}\sum_{n=0}^{\infty} n!\left(\frac{\beta_0\alpha_s(\mu)}{2\pi}\right)^{n+1}\sum_{k=0}^{n}\frac{1}{k!}\log^k\frac{\mu}{\overline{m}}\,, \end{aligned} \tag{3.23}$$

with $\overline{m} \equiv \overline{m}(\overline{m})$. Consequently, the perturbative term of order $n+1$ and its asymptotic form are given by

$$\overline{m}\frac{a_1}{2\beta_0}\left(\frac{\beta_0\alpha_s(\mu)}{2\pi}\right)^{n+1}\sum_{k=0}^{n}\frac{1}{k!}\log^k\frac{\mu}{\overline{m}} \;\sim\; \mu\frac{a_1}{2\beta_0}\left(\frac{\beta_0\alpha_s(\mu)}{2\pi}\right)^{n+1}. \tag{3.24}$$

On the other hand, heavy quark flavors with $m_Q > \Lambda_{\rm QCD}$ do not contribute at asymptotically high orders, since heavy virtual quark loops act as infrared cut-offs that remove the low-scale renormalon contributions [129].

Due to the linear dependence on the renormalization scale at high orders and the convergent nature of diagrams with heavy-quark loops, the intrinsic natural scale of the $\overline{\rm MS}$ mass, m_Q, can be replaced by an arbitrary scale R and the active number of flavors can be reduced from $(n_\ell + 1)$ to n_ℓ without altering the series asymptotics. The resulting relation is then used to define the MSR mass scheme with a matching relation connecting it to the $\overline{\rm MS}$ mass. This procedure leads to linear momentum scaling, the correct high-order/low-energy behavior, which results in improved convergence at low energies.

The freely adjustable universal intrinsic scale R is one of the main features of the MSR mass. The associated renormalization group equation

$$R\frac{{\rm d}m_Q^{\rm MSR}(R)}{{\rm d}R} = -R\sum_{n=0}^{\infty}\gamma_n^R\left(\frac{\alpha_s^{(n_\ell)}(R)}{4\pi}\right)^n, \tag{3.25}$$

is called the R-evolution equation[11]. Here, γ_n^R is the n-th perturbative coefficient of the R-anomalous dimension, see also Sec. 3 of Chap. 7 for more details on the R-evolution equation and its ingredients.

The scale R can be interpreted as an infrared cutoff, such that the MSR mass contains on-shell self-energy corrections only from scales larger than R. This is also nicely illustrated by the fact that in the formal limit $R \to 0$ the MSR mass agrees with the pole mass. In practice, that limit is of course ambiguous (a manifestation of the renormalon ambiguity) due to the Landau pole.

If R is set appropriately, the mass-dependent perturbative higher-order corrections of an observable are resummed, i.e. radiative corrections with kinematic mass dependence are minimized at higher orders and mass-dependent endpoints are not drastically modified by higher-order corrections. Usually, the appropriate choice of R is the observable-dependent intrinsic kinematic scale of the mass sensitivity. One can understand R as a resolution scale below which the virtual self-energy corrections and real radiation corrections that are soft in the heavy-quark rest frame are unresolved. This is analogous to choosing an appropriate scale μ for the strong coupling and in stark contrast to the pole mass, where it

[11] Note that Eq. (3.25) is linear in the evolution scale R, which distinguishes it from most other common renormalization group equations.

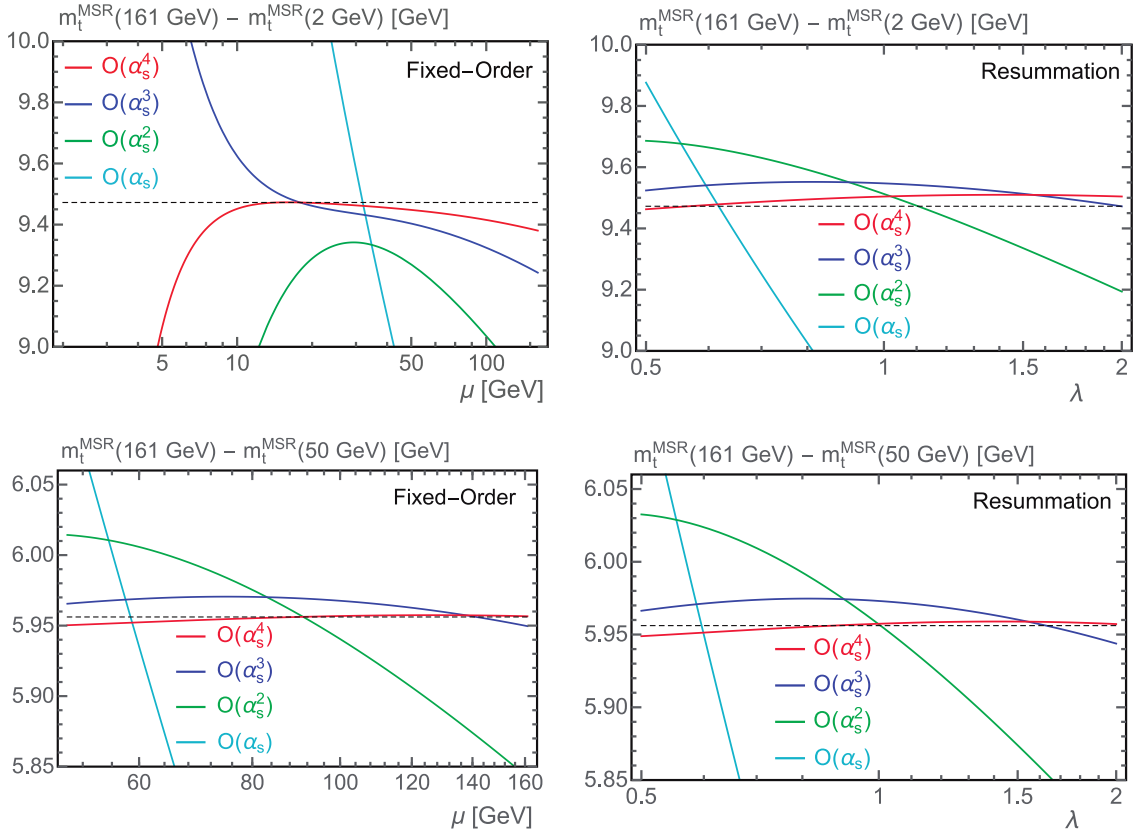

Figure 3.6: The difference of the top quark MSR mass ($n_\ell = 5$) at two different scales R including contributions from one to four loops. Results are shown for the difference between a high scale $R_1 = 161\,\text{GeV}$ and two lower scales $R_2 = 2\,\text{GeV}$ (top two panels) and $R_2 = 50\,\text{GeV}$ (lower two panels). The high and low scales are connected by a fixed-order perturbation theory conversion (left two panels, as a function of the scale μ in $\alpha_s(\mu)$) or via R-evolution (right two panels, as a function of the λ renormalization parameter).

is implicitly assumed that perturbative corrections can be resolved to arbitrarily low scales. This assumption is the reason for the pole-mass renormalon ambiguity.

For further discussion of the physical interpretation of the scale R and R-evolution, see Chap. 3.4 of this theses, where light massive flavor corrections are included and the physical picture is refined further.

One of the main applications of the MSR mass concerns the extraction of mass values from observables where the mass sensitivity is governed by widely separated physical scales. This concerns, for example, the total cross section σ_{tot} and quarkonium masses with their respective intrinsic scales, namely the center-of-mass energy $E_{\text{c.m.}}$ and the inverse Bohr radius $m\alpha_s$. Using the MSR mass, the respective appropriate intrinsic mass scales can be set for each observable, i.e. R can be set at the order of the intrinsic scales, which avoids large logarithms. Subsequently, R-evolution can be applied to evolve the mass values to a single reference scale for comparison, while resumming potentially large logarithms of scale ratios and free of the $\mathcal{O}(\Lambda_{\text{QCD}})$ renormalon. To demonstrate the impact of log-resummation, Fig. 3.6 in this chapter shows the difference of MSR masses at different scales R as computed by the fixed-order formula and the numerical evaluation of the R-evolution equation, respectively. To introduce renormalization-scale variation into the R-evolution equation, a λ-parameter is introduced by expanding $\alpha_s(R)$ in terms of $\alpha_s(\lambda R)$. λ is then varied in the range $[1/2, 2]$ to estimate the remaining uncertainty that originates from the

truncation of the R-anomalous dimension perturbative series.

Similar to the application of R-evolution to mass-extractions at widely separated physical scales, it is possible to relate heavy quark mass values extracted in different mass renormalization schemes with widely separated intrinsic scales. Usually, a perturbative relation between two short-distance mass schemes is derived by eliminating the pole mass systematically from the respective pole-short-distance conversion formulas. When employing those formulas, it is of central importance that the strong coupling α_s is taken in the same flavor-number scheme and at the same scale μ. Otherwise, the renormalon and therefore the bad perturbative behavior present in each of the perturbative relations to the pole mass does not cancel properly. Depending on the intrinsic scales of the to-be-converted mass schemes this can lead to large logarithms. By making use of the freely adjustable intrinsic scale of the MSR mass and R-evolution as described in the previous paragraph, the MSR mass is the optimal tool to circumvent the large-log problem: Let's assume we want to convert from scheme s_1 with intrinsic scale R_1 to scheme s_2 with intrinsic scale R_2, with $R_1 \ll R_2$. The potentially large logarithms of the form $\log(R_1/R_2)$ can be avoided by converting m^{s_1} to the MSR scheme at the scale R_1 in an intermediate step by employing the fixed-order (FO) conversion formulas and using R-evolution in between R_1 and R_2 to resum large logarithms. Finally, $m^{\rm MSR}$ can be converted to m^{s_2} at the scale R_2. Schematically,

$$m^{s_1} \xrightarrow{\rm FO} m^{\rm MSR}(R_1) \xrightarrow{\rm RGE} m^{\rm MSR}(R_2) \xrightarrow{\rm FO} m^{s_2}\,. \tag{3.26}$$

One concrete example where this approach is useful is when converting the top quark mass between the $\overline{\rm MS}$ mass scheme for which the intrinsic scale is the top quark mass $R_1 = m_t \approx 160\,\text{GeV}$ itself, and the 1S mass, with the intrinsic scale $R_2 = M_{\rm 1S} = 4/3\,\alpha_s m_t \approx 30\,\text{GeV}$, i.e. the inverse Bohr radius. In Sec. 5 of Chap. 7, the relation of the MSR mass scheme to various mass renormalization schemes is examined, such as the 1S [64–66], the PS [130], and the $\overline{\rm MS}$ mass.

From the paragraphs above, it is evident that the MSR mass scheme and R-evolution are closely connected to the pole mass renormalon and the high-order asymptotic behavior of the associated perturbative series. It turns out that if one has a closer look at the solution of the R-evolution equation as shown in Eq. (3.25), valuable new insights into the nature of the pole-MSR mass series and the $\mathcal{O}(\Lambda_{\rm QCD})$ renormalon of the pole mass scheme can be gained. The analytic solution to the evolution equation with the lower boundary $R = 0$, which corresponds to the pole mass, is given by

$$\begin{aligned} m_Q^{\rm MSR}(R) - m_Q^{\rm pole} &= -\int_0^{R'} \mathrm{d}R'\,\gamma^R(\alpha_s(R')) \\ &= -\,\Lambda_{\rm QCD}\int_{t_R}^{\infty}\mathrm{d}t\,\gamma^R(t)\,\hat{b}(t)\,\mathrm{e}^{-G(t)} \\ &= \Lambda_{\rm QCD}\sum_{k=0}^{\infty}\mathrm{e}^{i\pi(\hat{b}_1+k)}S_k\int_{t_R}^{\infty}\mathrm{d}t\,t^{-1-k-\hat{b}_1}\mathrm{e}^{-t} \\ &= \Lambda_{\rm QCD}\sum_{k=0}^{\infty}\mathrm{e}^{i\pi(\hat{b}_1+k)}S_k\Gamma(-\hat{b}_1-k,t_R)\,. \end{aligned} \tag{3.27}$$

That expression provides an interesting and useful alternative all-order representation of the original perturbative pole-MSR mass series. Here, $t_R = -2\pi/(\beta_0\alpha_s(R))$, $\hat{b}_1 = \beta_1/(2\beta_0)$ and $\int_{\alpha_0}^{\alpha_1}\mathrm{d}\alpha/\beta(\alpha) = \int_{t_1}^{t_0}\mathrm{d}t\,\hat{b}(t) = G(t_0) - G(t_1)$. $S_k = S_k(\{a_n\},\{\beta_n\})$ is a coefficient function of the perturbative coefficients a_n and β_n. Exact expressions are given in App. A of Chap. 7. See also Sec. 4 of Chap. 7 for more details. Remarkably, the solution to the R-evolution equation in Eq. (3.27) is equivalent to the Borel sum of the original series. The ambiguity of the pole mass that is associated to the factorially divergent renormalon behavior of the

perturbative pole-MSR mass series is encoded in the imaginary part of the incomplete gamma function $\Gamma(c,t)$ with $t<0$ that arises in the integration over the Landau pole at $t=0$.

The sum over k in Eq. (3.27) represents a reordering of the pole-MSR perturbative series in leading and subleading terms with respect to their numerical importance in the asymptotic high-order behavior of the original series, where the first term $k=0$ corresponds to the leading large β_0 contribution.

Taking Eq. (3.27) as a starting point, an analytic expression of the Borel transform of the pole-MSR perturbative series is derived in Sec. 4.1 of Chap. 7 (I refer to that section for details on the derivation), while keeping the useful ordering of the terms in the sum in k. After applying some asymptotic expansions and functional identities, the Borel transform with respect to $\alpha_s(R)$ can be easily obtained[12], giving

$$\begin{aligned} B_{\alpha_s(R)}\left[m_Q^{\rm MSR}(R)-m_Q^{\rm pole}\right](u) = & -N_{1/2}\left[R\,\frac{4\pi}{\beta_0}\sum_{\ell=0}^{\infty} g_\ell \frac{\Gamma(1+\hat{b}_1-\ell)}{\Gamma(1+\hat{b}_1)}(1-2u)^{-1-\hat{b}_1+\ell}\right] \\ & + 2R\sum_{\ell=0}^{\infty} g_\ell\, Q_\ell(u)\,, \end{aligned} \tag{3.28}$$

with the Borel variable u, and with $N_{1/2}$ the normalization of the singular contributions in the Borel transform, see also [68, 131–133]. In this context, "singular contributions" mean the terms in Eq. (3.28) that are non-analytic at $u\geq 1/2$, which corresponds to the $\mathcal{O}(\Lambda_{\rm QCD})$ renormalon in the original series. The normalization $N_{1/2}$ in Eq. (3.28) is given by

$$N_{1/2} = \frac{\beta_0\Gamma(1+\hat{b}_1)}{2\pi}\sum_{k=0}^{\infty}\frac{S_k(\{a_n\},\{\beta_n\})}{\Gamma(1+\hat{b}_1+k)}\,, \tag{3.29}$$

where S_k was already introduced in Eq. (3.27). This formula is called the $\mathcal{O}(\Lambda_{\rm QCD})$ *renormalon sum rule* and is, besides the MSR mass scheme, one of the main topics of the work in Chap. 7.

The factor Q_ℓ in the second line of Eq. (3.28) is a regular polynomial and given by

$$Q_\ell(u) = \sum_{k=0}^{\infty} S_k \sum_{i=0}^{k+\ell-1}\frac{2^i\Gamma(1+\hat{b}_1+i-\ell)}{\Gamma(1+\hat{b}_1+k)\Gamma(i+1)}u^i\,, \tag{3.30}$$

and is finite at $u=1/2$, i.e. the first line of Eq. (3.28) contains all terms that contribute to the leading-renormalon singular behavior.

The renormalon sum rule shown in Eq. (3.29) can be used to probe any perturbative series for an $\mathcal{O}(\Lambda_{\rm QCD})$ renormalon. In practice, the infinite sum has to be truncated and a finite value does, in principle, not provide a rigorous proof of the existence or non-existence of a renormalon. However, the convergence of the known first terms to zero or a finite value provides a strong hint whether a $u=1/2$ renormalon is present or not.

In Secs. 4.3-4.5 of Chap. 7, interesting use cases of the renormalon sum rule are presented. Three of them are summarized in the following paragraphs.

The most obvious application of the renormalon sum rule in Eq. (3.29) is to apply it to the pole-MSR mass relation to determine the normalization $N_{1/2}$ of the $\mathcal{O}(\Lambda_{\rm QCD})$ pole mass renormalon. Inserting the perturbative coefficients of the pole-MSR mass relation up to

[12] The inverse Borel transform is formally given by $f(\alpha_s)=\int_0^\infty {\rm d}u\, B_{\alpha_s}[f](u)$, compare with the third line of Eq. (3.27).

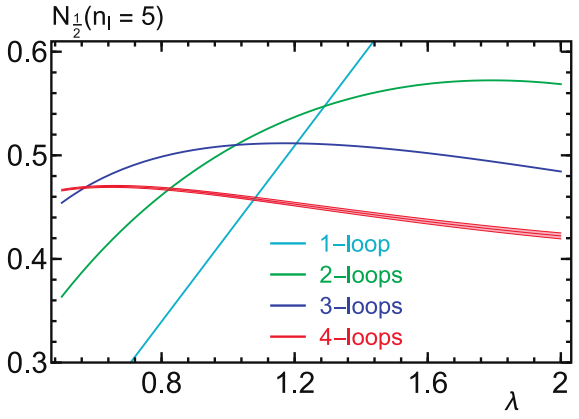

Figure 3.7: The pole mass renormalon normalization $N_{1/2}$ for $n_\ell = 5$ determined by the renormalon sum rule of Eq. (3.29) for different numbers of terms included in the sum over k. The band around the red curve that represents the 4-loop result relates to the numerical uncertainty of the 4-loop coefficient of the pole-$\overline{\rm MS}$ mass relation.

4 loops and the β-function coefficients up to 5 loops (which corresponds to summing the series up to $k = 3$) results in the values

$$\begin{aligned} N_{1/2}(n_\ell = 3) &= 0.526 \pm 0.016\,, \\ N_{1/2}(n_\ell = 4) &= 0.492 \pm 0.020\,, \\ N_{1/2}(n_\ell = 5) &= 0.446 \pm 0.026\,, \end{aligned} \tag{3.31}$$

see also Eqs. (4.12-4.14) in the publication of Chap. 7. The uncertainties quoted in Eq. (3.31) are determined by substituting $R \to \lambda R$ during the derivation of the sum rule and varying λ in the rage $1/2 < \lambda < 2$. Analogously to using a renormalization-scale variation to determine the uncertainty of a truncated perturbative series, the true value of $N_{1/2}$ is independent of R such that its variation with λ is a measure of the uncertainty that is introduced by truncating the sum-rule series. For a visualization of the numerical results of the sum rule for $n_\ell = 5$ and at different loop orders including λ-variation, see Fig. 3.7 in this chapter. The results quoted in Eq. (3.31) are fully compatible with previous estimations of $N_{1/2}$ [68, 133], where other methods were used.

Another interesting application of the findings related to the renormalon sum rule is the derivation of a new formula that describes the asymptotic high-order behavior of the perturbative pole-MSR (or pole-$\overline{\rm MS}$) mass relation. Starting from an intermediate result of the derivation of Eq. (3.28), one can solve for a_n, resulting in

$$a_n = (2\beta_0)^n \sum_{k=0}^{n-1} S_k \sum_{\ell=0}^{n-1-k} g_\ell (1 + \hat{b}_1 + k)_{n-1-\ell-k}\,. \tag{3.32}$$

This result is especially interesting, as the sum over k still involves the ordering of the terms in leading and subleading contributions to the asymptotic high-order behavior. Additionally, the formula involves information about the pure renormalon behavior as well as the subleading contributions to the perturbative coefficients, such that the formula reproduces the known coefficients a_n exactly, while describing their correct high-order behavior beyond the known orders. This is in contrast to the well-known formula [134]

$$a_n^{\rm asy} = 4\pi N_{1/2} (2\beta_0)^{n-1} \sum_{\ell=0}^{\infty} g_\ell (1 + \hat{b}_1)_{n-1-\ell}\,, \tag{3.33}$$

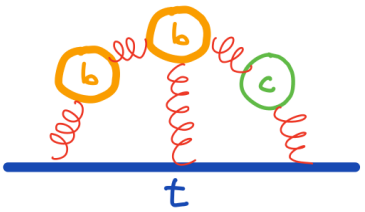

Figure 3.8: Self-energy diagram of a top quark with virtual bottom and charm quark loops, contributing to the relation between the top pole and $\overline{\rm MS}$ masses. If the bottom and charm quarks are treated as being massless, the loop momenta are unrestricted and pick up contributions from non-perturbative regions. If the bottom and charm quarks are treated as being massive ($m > \Lambda_{\rm QCD}$) the virtual massive loops act as an infrared cutoff such that non-perturbative loop momenta are suppressed. [Drawing provided by André Hoang.]

which takes into account only the non-analytic terms in $u = 1/2$ of the Borel transform of the pole-$\overline{\rm MS}$ mass relation. Here, $(x)_n$ is the Pochhammer symbol.

For numerical predictions of the perturbative coefficients of the pole-MSR and pole-$\overline{\rm MS}$ mass relation at the orders $5 \leq n \leq 9$, I refer to Sec. 4.4 of Chap. 7 and specifically to Tab. 2 in that section.

Finally, to demonstrate the applicability of the renormalon sum rule to perturbative series that are not related to the pole mass, I state the results of applying the sum rule to the perturbative series of the QCD β-function, which is known not to be plagued by a $\mathcal{O}(\Lambda_{\rm QCD})$ renormalon. For $n_\ell = 4$, the sum rule yields

$$N^{\beta}_{1/2} = (0.829 \pm 0.497, -0.004 \pm 0.272, 0.065 \pm 0.092, 0.038 \pm 0.032)\,, \tag{3.34}$$

order by order in k, where the stated uncertainties are again derived by varying λ in the range $[1/2, 2]$. As expected, all estimates beyond the $k = 0$ result are compatible with 0,[13] see also Sec. 4.5.4 of Chap. 7.

3.4 On the Light Massive Flavor Dependence of the Large Order Behavior and the Ambiguity of the Pole Mass

In the previous section, the MSR mass and the pole mass renormalon have been discussed under the assumption that all quark flavors lighter than the considered heavy quark are massless. In Chap. 8, a systematic approach is developed that applies a pipeline of running and matching operations to the pole-$\overline{\rm MS}$ mass relation to systematically include the effects of lighter quark flavors and to disentangle the different momentum regions in the relation. This is done by exploiting the concept of the MSR mass and R-evolution. That new and unique approach and the close connection of the MSR mass to the pole-mass renormalon (see the previous section), open up a wide range of applications and topics to study, with interesting implications.

Let's first illustrate the impact of light massive flavors on the perturbative pole-$\overline{\rm MS}$ mass relation. Due to the linear low momentum sensitivity of the pole mass, the pole mass is also linearly sensitive to effects related to lighter massive quarks q with masses $m_q > \Lambda_{\rm QCD}$.

[13] Remember that the renormalon sum rule presented in this section does only probe for renormalon ambiguities of $\mathcal{O}(\Lambda_{\rm QCD})$, not for any higher power $\mathcal{O}(\Lambda^{k>1}_{\rm QCD})$ IR renormalons. However, the sum rule can be easily modified to probe for higher-order renormalons.

These quark masses change the IR sensitivity which entails modifications of the asymptotic behavior of the pole mass. As mentioned in the previous section, virtual massive quark loops act as an effective infrared cutoff in Feynman diagrams, which leads to a modified renormalon structure [129], see Fig. 3.8 in this chapter for a graphical illustration. Due to this infrared cutoff, the correct renormalon structure of the pole mass can only depend on the number of *massless* flavors.

The starting point to study light massive quark corrections in a systematic manner is to write the perturbative series that relates the pole and $\overline{\rm MS}$ mass $\overline{m}(\overline{m})$ of the heavy quark Q in the form

$$m_Q^{\rm pole} - \overline{m}_Q = \underbrace{\overbrace{\overline{m}_Q \sum_{n=0}^{\infty} a_n(n_Q+1,0) \left(\frac{\alpha_s^{(n_Q+1)}(\overline{m}_Q)}{4\pi}\right)^n}^{\text{Renormalon corresponding to } (n_Q+1) \text{ massless flavors}} + \overline{m}_Q\, \overline{\Delta}_Q(\overline{m}_Q, \overline{m}_{Q-1}, \dots)}_{\text{Renormalon corresponding to } n_0 \text{ massless flavors}}, \tag{3.35}$$

with $\overline{m}_Q = \overline{m}_Q(\overline{m}_Q)$. Here, n_Q is the number of flavors lighter than the heavy quark Q, and the arguments of the function $\overline{\Delta}_Q$ represent the masses of all massive quark flavors that are lighter than the heavy quark Q, as well as the mass of the quark Q itself: m_Q is the mass of the heavy quark, m_{Q-1} is the mass of the next lighter quark, and so on.

In this formulation, the first term of Eq. (3.35) represents the pole-$\overline{\rm MS}$ mass relation with *all* masses of virtual quarks (including the heavy quark itself) set to zero: The coefficients $a_n(n_Q+1,0)$ are the perturbative coefficients of the pole-$\overline{\rm MS}$ mass series with (n_Q+1) massless virtual quarks (first argument), and no virtual heavy quarks (second argument). The second term of Eq. (3.35) encodes the finite mass corrections from all virtual quark loops (originating from diagrams like the one shown in Fig. 3.8 in this chapter). More explicitly, the quantity $\overline{\Delta}_Q(\overline{m}_Q, \overline{m}_{Q-1}, \dots)$ can be expanded systematically in the form

$$\begin{aligned}\overline{\Delta}_Q(\overline{m}_Q, \overline{m}_{Q-1}, \dots) = {}& \overline{\delta}_Q^{(Q,q_1,\dots,q_n)}(1, r_{q_1Q}, \dots, r_{q_nQ}) + \overline{\delta}_Q^{(q_1,\dots,q_n)}(r_{q_1Q}, \dots, r_{q_nQ}) \\ & + \dots + \overline{\delta}_Q^{(q_n)}(r_{q_nQ})\,. \end{aligned} \tag{3.36}$$

The terms $\overline{\delta}_Q^{(q,q',\dots)}(r_{qQ}, r_{q'Q}, \dots)$ contain the mass corrections coming from the quark Q on-shell self-energy Feynman diagrams with insertions of virtual massive quark loops. The superscript $(q, q', \dots)$ indicates that each diagram contains at least one insertion of the massive quark q and in addition all possible insertions of the (lighter) massive quarks $q', \dots$ as well as of massless quark and gluonic loops. From each diagram, the corresponding diagram with all the quark loops in the massless limit is subtracted (because these terms are already contained in $a_n(n_Q+1,0)$) in the scheme compatible with the flavor number scheme for the strong coupling α_s. The fractions $r_{qq'} = \overline{m}_q/\overline{m}_{q'}$ stand for the ratios of $\overline{\rm MS}$ masses for massive quarks q and q'.

The unusual (and at first glance unnatural) structure of the arrangement of the terms in Eq. (3.35) is essential to systematically disentangle light massive flavor effects flavor-by-flavor and for properly defining the MSR mass with those effects included, as described in this chapter.

As indicated by the braces in Eq. (3.35), the first term follows an asymptotic renormalon behavior that corresponds to (n_Q+1) massless flavors, while the combined expression suffers from a renormalon corresponding to n_0 massless flavors, where n_0 is the number of quark flavors with masses $m_q < \Lambda_{\rm QCD}$ for which we can adopt the massless approximation. So, there is a renormalon cancellation between the first and the second term. Considering

the top quark ($Q = t$) with heavy bottom and charm quarks as an example, $n_t = 5$ (such that $n_t + 1 = 6$) and $n_0 = 3$.

The quantity $\overline{\Delta}_Q$ is known up to $\mathcal{O}(\alpha_s^3)$ for the insertion of light massive loops of one lighter flavor in addition to the heavy quark Q [77, 135]. Note that the renormalon cancellation between the first and second term in Eq. (3.35) implies that the quantity $\overline{\Delta}_Q$ has itself a divergent asymptotic perturbative series.

For a more detailed discussion of the light massive flavor correction term $\overline{\Delta}_Q$, see Secs. 2.1 and 2.2 of Chap. 8.

It is natural to wonder whether the renormalon cancellation of the two terms in Eq. (3.35) can be made explicit. In other words, to make explicit the n_0 massless-flavor renormalon behavior and the decoupling of massive flavors at asymptotically high orders.

The formalism that is developed in the work presented in Chap. 8 achieves exactly that. This not only allows to work with light massive flavor corrections in a more systematic way, but also to predict yet uncalculated perturbative orders of $\overline{\Delta}_Q$, to describe their asymptotic large-order behavior, and to derive a value for the best possible estimate of the top quark pole mass that takes massive bottom and charm quarks into account.

The approach to disentangle the different momentum modes in the pole-$\overline{\text{MS}}$ mass relation is inspired by the usual pipeline of renormalization group running and matching as known e.g. from the strong coupling. To illustrate this, let's start by integrating out the closed virtual loops of the heavy quark Q, which results in the pole-MSR mass relation

$$m_Q^{\text{pole}} - m_Q^{\text{MSR}}(R) = R \sum_{n=0}^{\infty} a_n(n_Q, 0) \left(\frac{\alpha_s^{(n_Q)}(\overline{m}_Q)}{4\pi} \right)^n + \overline{m}_Q \, \Delta_Q(\overline{m}_Q, \overline{m}_{Q-1}, \dots) \,. \quad (3.37)$$

Note that the quantities Δ_Q in Eq. (3.37) and $\overline{\Delta}_Q$ in the pole-$\overline{\text{MS}}$ mass relation of Eq. (3.35) are different because all diagrams with virtual loops of the heavy quark Q are removed in Δ_Q.

The associated matching contribution is the $\overline{\text{MS}}$-MSR matching

$$m_Q^{\text{MSR}}(\overline{m}_Q) - \overline{m}_Q = \Delta m_Q^{(n_Q+1\to n_Q)}(\overline{m}_Q) + \delta m_{Q,q_1,\dots,q_n}^{(n_Q+1\to n_Q)}(\overline{m}_Q) \,. \quad (3.38)$$

Here, $\Delta m_Q^{(n_Q+1\to n_Q)}$ is the renormalon-free matching contribution under the assumption that all quarks lighter than the heavy quark Q are massless. The second term, $\delta m_{Q,q_1,\dots,q_n}^{(n_Q+1\to n_Q)}$, represents the renormalon-free contributions from virtual loops of massive quarks q_i lighter than the heavy quark Q. That second term starts at $\mathcal{O}(\alpha_s^3)$ and is quadratic in the mass ratios $r_{q_iQ} = m_{q_i}/m_Q$, with m_{q_i} the mass of the quark q_i that is lighter than the quark Q. Therefore, that term is extremely small (it does never exceed 0.01 MeV for all physical cases) and can be neglected for practical purposes. Taking the top quark mass m_t as an example for the heavy quark Q, the contribution $\Delta m_t^{(6\to5)}$ contains the contributions from virtual top loops, and $\delta m_{t,b,c}^{(6\to5)}$ contains the contributions from diagrams that contain *both* virtual top loops and the mass corrections (with respect to the case $m_b = m_c = 0$) arising from the finite masses of virtual massive bottom or charm loops. An exemplary diagram that contributes to $\Delta m_t^{(6\to5)}$ is shown in the top figure of Fig. 3.9 in this summary. For explicit expressions of the two terms in Eq. (3.38), see Sec. 3.1 of Chap. 8, for numerical values of $\Delta m_Q^{(n_Q+1\to n_Q)}$ in physical setups, see Tab. 3 in the same section.

The second type of matching that has to be considered for our goal to fully decouple all the momentum regions in Eq. (3.35) results from integrating out contributions from massive virtual loops of the next lighter massive flavor with respect to the heavy quark Q. In the

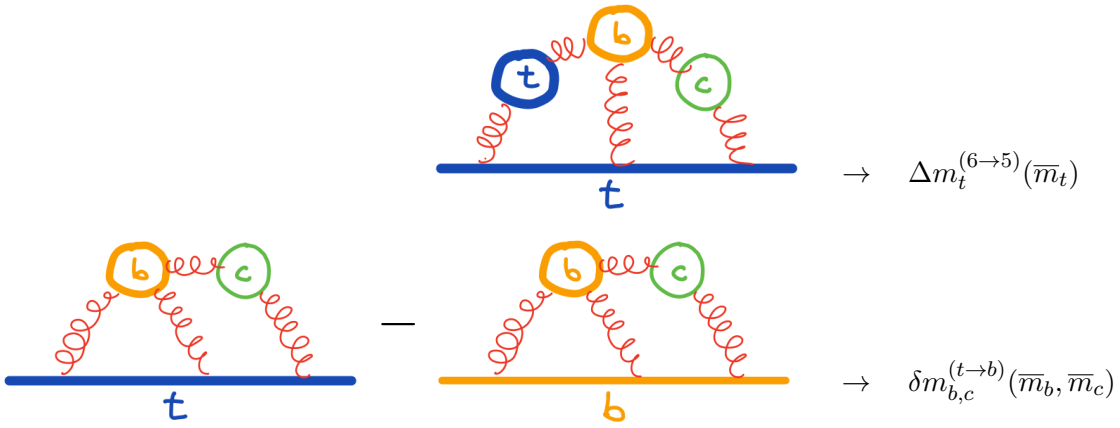

Figure 3.9: *Top figure*: example diagram with a virtual top quark loop that contributes to the top quark $\overline{\text{MS}}$-MSR matching term $\Delta m_t^{(6\to5)}(\overline{m}_t)$. *Bottom figure:* example diagrams that contribute to the top quark heavy quark symmetry breaking term $\delta m_{b,c}^{(t\to b)}(\overline{m}_b, \overline{m}_c)$. [Drawings provided by André Hoang.]

case of the top quark, this concerns diagrams that contain virtual bottom loops. For the purpose of deriving useful expressions for that matching contribution, it is helpful to note that the pole-MSR mass relation of the heavy quark Q as given in Eq. (3.37) would be equivalent to the pole-$\overline{\text{MS}}$ mass relation of the next lighter quark $(Q-1)$ for $R = \overline{m}_{Q-1}$ if the virtual loops of all quark flavors lighter than the quark Q (including the next lighter flavor) are treated as massless. This fact is far from trivial and a consequence of heavy quark symmetry [59]. However, in the presence of lighter massive quarks, this is no longer true. The associated correction can be encoded in a heavy quark symmetry breaking term. The heavy quark symmetry breaking term for the top quark due to the finite bottom mass is defined by

$$\left[m_t^{\text{pole}} - m_t^{\text{MSR}}(\overline{m}_b)\right] - \left[m_b^{\text{pole}} - \overline{m}_b\right] =: \delta m_{b,c}^{(t\to b)}(\overline{m}_b, \overline{m}_c)\,. \tag{3.39}$$

In words, this heavy quark symmetry breaking term encodes the difference between the contributions of virtual massive bottom and charm quark loops in primary (i.e. external) top-quark self-energy diagrams and virtual massive bottom and charm quark loops in primary bottom-quark self-energy diagrams, see the bottom figure of Fig. 3.9 in this chapter for an illustration. It is important to note that the heavy quark symmetry breaking term is, just as the matching contributions from integrating out the heavy quark Q, renormalon free: since the pole-mass renormalon does only depend on the number of massless flavors, m_t^{pole} and m_b^{pole} do actually suffer from the *same* renormalon if lighter quark flavor masses are accounted for, such that the renormalon cancels in the difference on the left-hand side of Eq. (3.39).

Analogously, the heavy quark symmetry breaking term associated to the difference of virtual finite-mass charm quark loops in bottom-quark and charm-quark self-energy diagrams is given by

$$\left[m_b^{\text{pole}} - m_b^{\text{MSR}}(\overline{m}_c)\right] - \left[m_c^{\text{pole}} - \overline{m}_c\right] = \delta m_c^{(b\to c)}(\overline{m}_c)\,. \tag{3.40}$$

For explicit expressions and numerical values of the physical heavy quark symmetry breaking terms, see Sec. 3.2 of Chap. 8 and Tab. 4 therein.

Combining the $\overline{\text{MS}}$-MSR mass matching, the heavy quark symmetry breaking contributions, and R-evolution, it is now possible to decouple the momentum regions in the pole-$\overline{\text{MS}}$ mass relation of Eq. (3.35). For the top quark, with massive bottom and charm quarks,

the decoupled version of Eq. (3.35) is

$$\begin{aligned} m_t^{\text{pole}} - \overline{m}_t = {} & \Delta m_t^{(6\to5)}(\overline{m}_t) + \Delta m^{(5)}(\overline{m}_t, \overline{m}_b) + \delta m_{b,c}^{(t\to b)}(\overline{m}_b, \overline{m}_c) + \Delta m_b^{(5\to4)}(\overline{m}_b) \\ & + \Delta m^{(4)}(\overline{m}_b, \overline{m}_c) + \delta m_c^{(b\to c)}(\overline{m}_c) + \Delta m_c^{(4\to3)}(\overline{m}_c) \\ & + \Delta m^{(3)}(\overline{m}_c, R) + R \sum_{n=1}^{\infty} a_n(n_\ell = 3, 0) \left(\frac{\alpha_s^{(3)}(R)}{4\pi} \right)^n , \end{aligned} \tag{3.41}$$

with $R < \overline{m}_c$ and where $\Delta m^{(n_\ell)}(R, R')$ is the solution of the R-evolution equation with n_ℓ flavors, i.e.

$$\Delta m^{(n_\ell)}(R, R') = m_Q^{\text{MSR}}(R') - m_Q^{\text{MSR}}(R) = \sum_{n=0}^{\infty} \gamma_n^{R,(n_\ell)} \int_{R'}^{R} \mathrm{d}R \left(\frac{\alpha_s^{(n_\ell)}(R)}{4\pi} \right)^{n+1} . \tag{3.42}$$

The exact way how the decoupling formula in Eq. (3.41) is constructed ensures that the R-evolution equation is mass independent and only depends on n_ℓ. This choice is not unique: the article in Ref. [136] includes light massive flavors in the MSR mass definition in a way that results in much more complicated and mass-dependent R-evolution equations.

Eq. (3.41) clearly illustrates the approach of repeated running and matching, evolving down from the top quark mass scale, until all massive flavors are decoupled and all momentum regions are disentangled and logarithms of quark mass ratios are resummed to all orders through R-evolution. The $\mathcal{O}(\Lambda_{\text{QCD}})$ renormalon of the pole mass is contained solely in the very last low-scale term of Eq. (3.41), which encodes the momentum region below $R < \overline{m}_c$ and has contributions only from the massless quark flavors (u, d, s). That last term of Eq. (3.41) is universal for all massive on-shell renormalized quark flavors. This is a profound result that is a consequence of heavy quark symmetry. All other terms shown in Eq. (3.41) are $\mathcal{O}(\Lambda_{\text{QCD}})$ renormalon free.

It should be stressed again that, in order to obtain Eq. (3.41), it is essential to start from the pole-$\overline{\text{MS}}$ mass relation as written in Eq. (3.35). Otherwise, the connection between the $\overline{\text{MS}}$ and MSR mass of different massive flavors and, consequently, the possibility to systematically exploit heavy quark symmetry, is obscured and far from obvious.

To understand the nature of Eq. (3.41), it is illustrative to have a closer look at it by adding the right-hand side term by term, starting from the last one, and to write down the respective fixed-order expressions:

$$\begin{aligned} R \sum_{n=1}^{\infty} a_n(n_\ell = 3, 0) \left(\frac{\alpha_s^{(3)}(R)}{4\pi} \right)^n \quad &\to \quad m_c^{\text{pole}} - m_c^{\text{MSR}}(R) \\ +\Delta m^{(3)}(\overline{m}_c, R) \quad &\to \quad m_c^{\text{pole}} - m_c^{\text{MSR}}(\overline{m}_c) \\ +\Delta m_c^{(4\to3)}(\overline{m}_c) \quad &\to \quad m_c^{\text{pole}} - \overline{m}_c(\overline{m}_c) \\ +\delta m_c^{(b\to c)}(\overline{m}_c) \quad &\to \quad m_b^{\text{pole}} - m_b^{\text{MSR}}(\overline{m}_c) \\ +\Delta m^{(4)}(\overline{m}_b, \overline{m}_c) \quad &\to \quad m_b^{\text{pole}} - m_b^{\text{MSR}}(\overline{m}_b) \\ &\vdots \end{aligned} \tag{3.43}$$

The individual expressions on the right-hand side of the arrow correspond to *the sum of all lines of the left-hand side up to that line*. Obviously, a generalization of Eq. (3.41) to other flavors is straightforward. A graphical illustration of the running and matching contributions is depicted in Fig. 3.10 above.

The disentanglement of the series into a renormalon-plagued low-scale term that depends only on the number of massless flavors ($n_f = 3$ in a physical setup where we account for

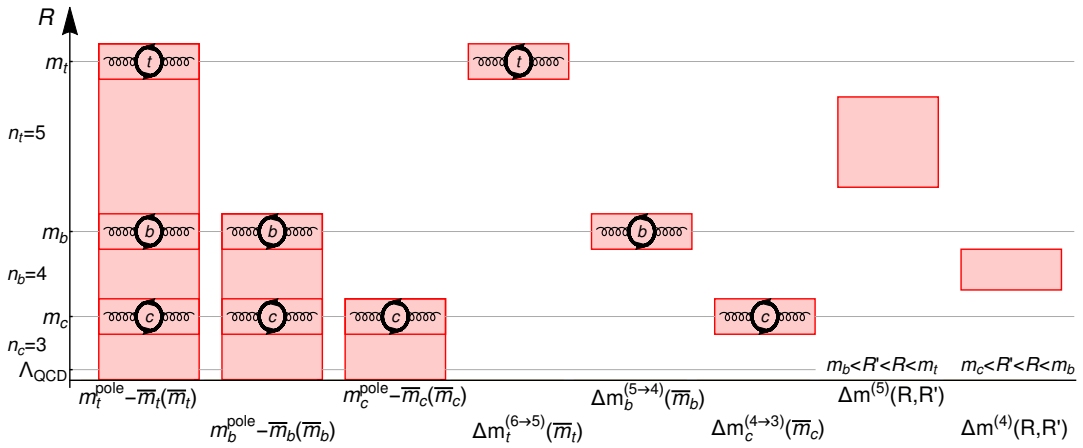

Figure 3.10: Graphical illustration of the running and matching contributions in the pole-$\overline{\text{MS}}$ mass relations and their associated momentum region.

finite charm and bottom masses), and renormalon-free terms that have good convergence properties, has interesting consequences that are immediately exploited in Secs. 3.3, 3.4, 3.5, and 4 of Chap. 8. In the following, some of them are shortly summarized.

First of all, the asymptotic high-order behavior of the pole-$\overline{\text{MS}}$ mass relation that includes the effects from lighter massive flavors can be determined very easily by combining the systematic decoupling that is described above with the methods described in Chap. 7 (and summarized in Chap. 3.3 of this thesis), e.g. Eq. (3.32) of this section, which describes the asymptotic high-order behavior of the perturbative pole-$\overline{\text{MS}}$ relation for the case of massless lighter quarks: All terms in Eq. (3.41) except for the last low-scale one, which carries the renormalon ambiguity, have excellent convergence properties. Therefore, the high-order asymptotic behavior of the full series is only weakly affected by the known perturbative corrections of these convergent contributions. The high-order asymptotic behavior of the low-scale term on the other hand is given by Eq. (3.32) of this section. This systematic approach is in contrast to other heuristic techniques that were used up to now, e.g. by artificially enforcing light flavor decoupling [68]. As it turns out, the heuristic technique works well for charm mass effects in the bottom quark, but gives wrong results for bottom quark mass effects in the top quark. For more details and numerical results, I refer to Sec. 3.5 of Chap. 8.

Secondly, due to the small size and excellent convergence properties of the heavy quark symmetry breaking terms (for all physical setups, their overall size is only a few MeV, and the size of the $\mathcal{O}(\alpha_s^3)$ contributions is only $\sim 1\,\text{MeV}$), the yet unknown $\mathcal{O}(\alpha_s^4)$ perturbative coefficient of Δ_Q in Eq. (3.37) (and equivalently $\overline{\Delta}_Q$ in Eq. (3.35)) can be predicted with a precision better than 1 MeV. This can be achieved by approximating the unknown $\mathcal{O}(\alpha_s^4)$ terms of the heavy quark symmetry breaking contribution with zero, and re-expanding the resulting expression in terms of the original perturbative coefficients of Eq. (3.35). The estimation of the $\mathcal{O}(\alpha_s^4)$ light massive flavor correction term for a single lighter massive

quark flavor q is then given by

$$\begin{aligned}
&\delta^{(q)}_{Q,4}(r_{qQ}) \\
&\approx r_{qQ}\left[\delta^{(q)}_{q,4}(1) + \left(6\beta_0^{(n_Q)}\delta^{(q)}_{q,3}(1) + 4\beta_1^{(n_Q)}\delta_2(1)\right)\ln\left(\frac{\mu}{\overline{m}_q}\right) + 12\delta_2(1)\left(\beta_0^{(n_Q)}\log\left(\frac{\mu}{\overline{m}_q}\right)\right)^2\right] \\
&\quad - \left(6\beta_0^{(n_Q)}\delta^{(q)}_{Q,3}(r_{qQ}) + 4\beta_1^{(n_Q)}\delta_2(r_{qQ})\right)\log\left(\frac{\mu}{\overline{m}_Q}\right) - 12\delta_2(r_{qQ})\left(\beta_0^{(n_Q)}\log\left(\frac{\mu}{\overline{m}_Q}\right)\right)^2,
\end{aligned} \tag{3.44}$$

so that (see Eq. (3.37))

$$\Delta_Q(\overline{m}_Q,\overline{m}_q) = \delta^{(q)}_Q(r_{qQ}) = \delta_2(r_{qQ})\left(\frac{\alpha_s^{(n_Q)}(\overline{m}_Q)}{4\pi}\right)^2 + \sum_{n=3}^{\infty}\delta^{(q)}_{Q,n}(r_{qQ})\left(\frac{\alpha_s^{(n_Q)}(\overline{m}_Q)}{4\pi}\right)^n, \tag{3.45}$$

with $r_{qQ} = \overline{m}_q/\overline{m}_Q$. The expression on the RHS of Eq. (3.44) should provide an approximation to $\delta^{(q)}_{Q,4}$ accurate to $\mathcal{O}(1\,\text{MeV})$. It is interesting to note that the rapid convergence of the heavy quark symmetry breaking term and the resulting precision of the estimation in Eq. (3.44) implies that the perturbative series of Δ_Q is essentially completely governed by its asymptotic high-order behavior already at $\mathcal{O}(\alpha_s^4)$. For a more detailed derivation and numerical analyses, see Sec. 3.3 of Chap. 8.

Last but not least, the framework that is described in this section allows to determine the top quark pole mass renormalon ambiguity and the best estimate of the top quark pole mass with a rigorous implementation of bottom and charm mass effects. The strategy that is used to determine the top pole mass ambiguity and the top pole mass best estimate is the following:

First, we use the known asymptotic behavior of the renormalon series in Eq. (3.41) (the last term) and the convergence properties of the other terms to determine the minimal correction term to the pole-MSR mass series $\Delta(n_{\text{min}})$ with $\Delta(n) = m^{\text{pole}}(n) - m^{\text{pole}}(n-1)$, where $m^{\text{pole}}(n)$ is the partial sum at $\mathcal{O}(\alpha_s^n)$. There is a range of orders for which the partially summed series grows linearly, i.e. where the correction terms have approximately the same size. According to the theory of asymptotic series, this is the relevant range for determining the ambiguity of the series and its best estimate. Consequently, we choose a set of orders $\{n\}_f = \{n : \Delta(n) \leq f\Delta(n_{\text{min}})\}$ with $f \gtrsim 1$ a real number larger but close to 1 at a default renormalization scale. Finally, half the range of values that is covered by $m^{\text{pole}}(n)$, $n \in \{n\}_f$, including renormalization scale variation, is used as an estimate of the top quark pole mass renormalon ambiguity. The best possible estimate is taken to be the midpoint of the resulting range. This method respects heavy quark symmetry in the sense that the resulting pole mass ambiguity is independent of the heavy quark mass value itself, or equivalently, the value of R.

For the numerical evaluation, we choose $f = 5/4$, $\overline{m}_t = 163\,\text{GeV}$, $\overline{m}_b = 4.2\,\text{GeV}$, $\overline{m}_c = 1.3\,\text{GeV}$ and repeat the procedure for $R = 163, 20, 4.2, 1.3\,\text{GeV}$. The renormalization scale variation is performed in the range $1.5 \leq \mu \leq 5\,\text{GeV}$ for $R = 1.3\,\text{GeV}$ and $R/2 \leq \mu \leq 2R$ otherwise.

The results for the best possible estimates of the top quark pole mass and the associated

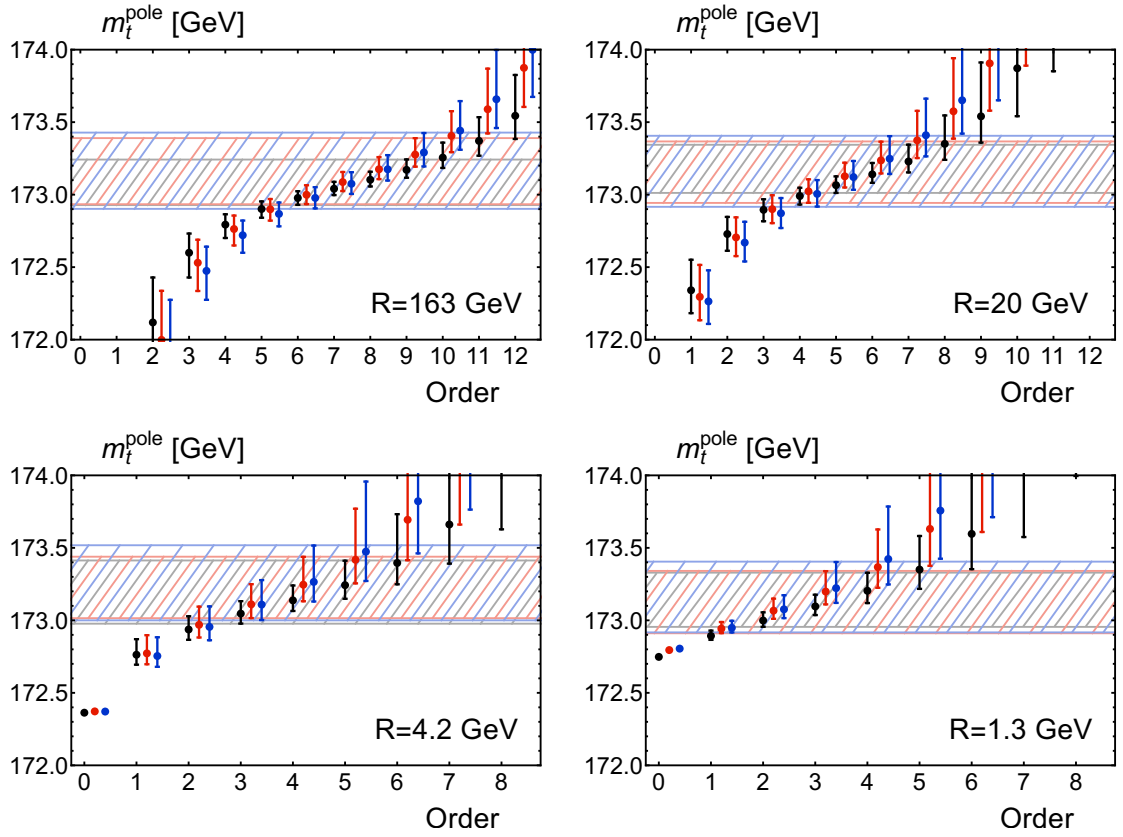

Figure 3.11: The top quark pole mass m_t^{pole} as a function of the perturbative order with $\overline{m}_t = \overline{m}_t(\overline{m}_t) = 163$ GeV. The central dots are obtained for the default renormalization scales for the strong coupling and the error bands represent the scale variation as explained in the text. The light colored hatched horizontal bands bounded by equal colored lines show the best possible estimate for the respective light-flavor-mass configuration. The results obtained for massless bottom and charm quarks are colored black, the results for $(\overline{m}_b, \overline{m}_c) = (4.2, 0)$ GeV are colored in red, and the results for $(\overline{m}_b, \overline{m}_c) = (4.2, 1.3)$ GeV are colored blue. The top left panel shows results for $R = 163$ GeV, the top right panel for $R = 20$ GeV, the bottom left panel for $R = 4.2$ GeV, and the bottom right panel for $R = 1.3$ GeV.

ambiguity with massive bottom and charm quarks and for different values of R are

$$\begin{aligned} m_t^{\text{pole}}\Big|_{R=163\,\text{GeV}} &= (173.165 \pm 0.263)\,\text{GeV}\,, \\ m_t^{\text{pole}}\Big|_{R=20\,\text{GeV}} &= (173.161 \pm 0.245)\,\text{GeV}\,, \\ m_t^{\text{pole}}\Big|_{R=4.2\,\text{GeV}} &= (173.259 \pm 0.259)\,\text{GeV}\,, \\ m_t^{\text{pole}}\Big|_{R=1.3\,\text{GeV}} &= (173.159 \pm 0.244)\,\text{GeV}\,. \end{aligned} \tag{3.46}$$

All values are perfectly compatible with each other, which is a valuable cross-check of our method with respect to heavy quark symmetry. The mean over Eqs. (3.46) of the best possible estimate is 173.186 GeV, while the mean of the ambiguity is 253 MeV. Note that, due to heavy quark symmetry, the value of the pole mass ambiguity is universal for the top, bottom, and charm quark (if m_t, m_b and m_c are non-zero), i.e. this value is also valid for the ambiguity of the bottom and charm quark pole masses.

In comparison, the result for the pole mass for massless bottom and charm quarks is

173.150 GeV for the best possible estimate, and 182 MeV for the ambiguity. So, while the value of the best possible estimate does not change significantly, the value for the ambiguity is much smaller, as expected from $\Lambda_{\rm QCD}^{(n_\ell=5)} < \Lambda_{\rm QCD}^{(n_\ell=3)}$.

In Fig. 3.11 below, the pole mass as a function of the perturbative order, as well as the pole mass ambiguity as determined with the described approach is shown for the individual values of R and for different lighter flavor mass setups, i.e. massive bottom and charm, massive bottom and massless charm, and massless bottom and charm. Note that the order of the minimal correction term is lower for lower values of R.

The best possible estimate and ambiguity of the top quark pole mass was also discussed in Ref. [133] by using a different approach with a resulting value of the ambiguity of 110 MeV. However, as discussed in detail in Sec. 4 of Chap. 8, the approach of Ref. [133] does not respect heavy quark symmetry and does not take light massive quark flavors into account in a rigorous and systematic way.

For a more extensive discussion and numerical values, see Secs. 4.2-4.4 of Chap. 8.

3.5 `REvolver`: Automated Running and Matching of Couplings and Masses in QCD

In Chaps. 7 and 8, summarized in Chaps. 3.3 and 3.4, new concepts and tools related to the MSR mass are developed that are useful for a large group of researchers in the high-energy community. To make the new developments easily available, we developed the `C++` library `REvolver`, which is presented and extensively documented in Chap. 9. The code is available as open-source software and is aimed at both theorists and experimentalists. To make the possible range of applications as broad as possible, the code provides additional interfaces to `Mathematica` [137] as well as `Python` [138]. The examples in this section are given for the `Mathematica` interface.

`REvolver` combines access to the innovations in Chaps. 7 and 8 with a rich set of standard features for coupling and mass evolution as well as the conversion between mass renormalization schemes. This includes

- renormalization group evolution of the strong coupling, the $\overline{\rm MS}$ as well as the MSR mass (complex renormalization scales are supported) with automatic flavor number matching, whereby the MSR mass is treated as the low-energy extension of the $\overline{\rm MS}$ mass. The implemented algorithms allow to solve the renormalization group equations to in principle arbitrary precision, where the equations are treated as exact up to the specified perturbative order;
- mass scheme conversions to and from various short distance masses. At the moment, the following short-distance mass schemes are supported apart from the $\overline{\rm MS}$ and MSR mass:
  - 1S scheme [64–66],
  - kinetic scheme [139],
  - potential subtracted scheme [130, 140],
  - renormalon subtracted scheme [68],
  - RGI scheme [141].

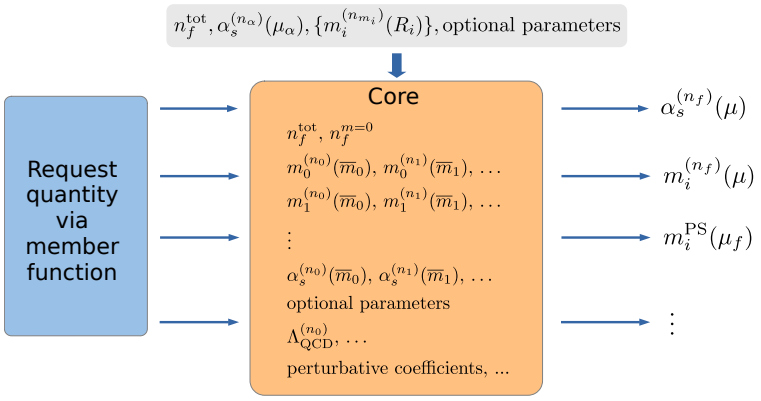

Figure 3.12: Diagrammatical illustration of the `Core` concept in `REvolver`. To create a `Core`, some fundamental parameters have to be specified, such as the number of quark flavors, a value of the strong coupling in a specified flavor number scheme and at a specified scale, as well as quark mass values. A number of optional parameters can be set as well. The `Core` object then provides all functionalities of `REvolver` via member functions, such as the extraction of coupling values, masses, etc. At `Core` creation, some fundamental parameters such as strong coupling values at mass thresholds are precomputed and stored.

Here, the usual fixed-order conversion is supported as well as the conversion with intermediate R-evolution to resum potentially large logarithms of the ratio of the respective intrinsic scales. Whenever known, light massive flavor effects are implemented consistently[14];

- conversion to and from the fixed-order pole mass at arbitrary large perturbative orders by utilizing the asymptotic renormalon behavior of the pole mass;
- conversion to and from the asymptotic pole mass, i.e. the best possible estimate of its value;
- determination of the pole mass renormalon ambiguity, whereby the strategy developed in Chap. 8 as well as the one applied in Ref. [133] can be applied;
- determination of the renormalon normalization $N_{1/2}$ by utilizing the framework developed in Chap. 7;
- determination of the QCD scale Λ_{QCD} in different conventions.

The β-function, the anomalous dimensions, the matching coefficients, as well as the light massive flavor corrections are implemented to the highest perturbative order currently available, i.e. the 5-loop β-function, 5-loop $\overline{\text{MS}}$-anomalous dimension, etc.

The codebase of `REvolver` is written in such a way that its functionalities can be easily extended and modified in the future. This concerns minor additions such as the implementation of new loop corrections to mass scheme relations and anomalous dimensions, as well as major extensions such as including electroweak interactions.

A fundamental concept of `REvolver` is the `Core` object, which can be viewed as the encoding of a certain physical scenario, and from which all desired parameters like coupling and mass values can be extracted, see Fig. 3.12 in this chapter for a diagrammatic illustration. A physical scenario is defined by

[14] "Consistent" here means that in a conversion between short-distance masses, light massive flavor effects are included up to the same perturbative order for both mass schemes. This is crucial for correct renormalon cancellation.

- an initial strong coupling value in a specified flavor number scheme and at a specified scale,
- the total number of quark flavors,
- optional mass values for the quark flavors, specified either in the $\overline{\text{MS}}$ or MSR mass scheme in a specified flavor number scheme and at a specified scale,
- the number of perturbative orders that should be used for the evolution and matching of the running quantities,
- the matching scales.

For example, in `Mathematica` a simple `Core` with six quark flavors, with massive top, bottom and charm quarks can be created by

```
alphaPar = {5, amZdef, mZdef};
mPar = {{4, 1.3, 1.3}, {5, 4.2, 4.2}, {6, 163.0, 163.0}};
CoreCreate["core1", 6, alphaPar, mPar]
```

Here, `CoreCreate` is the `REvolver` function to create a `Core` object, `core1` is the name of the newly defined `Core`, `6` is the total number of quark flavors, `alphaPar` defines the flavor number scheme, value and renormalization scale of the strong coupling, and `mPar` is a list, where each element specifies the flavor number scheme, value, and scale of a massive quark flavor. In this example, the mass values are given in terms of $\overline{m} \equiv \overline{m}(\overline{m})$, however, every consistent flavor number scheme and scale can serve as an input. `mPar` has to be sorted in ascending order with respect to the associated $\overline{\text{MS}}$ mass $\overline{m}$.

The $\overline{\text{MS}}$ and MSR mass schemes are the fundamental schemes in the `Core` framework. The mass parameters in `mPar` have to be given in one of these schemes, where the specified flavor number scheme determines if the parameters are interpreted as $\overline{\text{MS}}$ or MSR ($\overline{\text{MS}}$ if the concerned heavy quark flavor is included in the flavor number scheme, MSR otherwise).

Note that, although the `Core` object must be initialized with mass values in the $\overline{\text{MS}}$ or MSR mass scheme, massive quark flavors with masses specified in other schemes can be added to an already existing `Core` object by using dedicated member functions, see Sec. 6.3 of Chap. 9. Internally, quark masses are always converted to the $\overline{\text{MS}}$ mass $\overline{m}$, which serves as a starting point for all subsequent computations.

By default, renormalization group evolution and matching is performed by using all available perturbative orders, and the matching scales are set to the $\overline{\text{MS}}$ mass $\overline{m}$.

Optional parameters for the creation of a `Core` can be set in `Mathematica` via the options parameter syntax. E.g. to create a `Core` with name `core2` with the matching scale associated to the charm quark mass set to $2\overline{m}_c$ instead of $\overline{m}_c$, the parameter `fMatch` can be set via

```
CoreCreate["core2", 6, alphaPar, mPar, fMatch->{2.0, 1.0, 1.0}]
```

where each element of `fMatch` corresponds to one massive quark flavor.

For more details on the creation of `Core` objects, including available additional parameters and how to create `Core`s in `C++` and `Python`, see Sec. 6.1 of Chap. 9.

In the following, I describe some examples to demonstrate a selection of the functionalities that `REvolver` provides.

To extract couplings and masses from an existing `Core` object, one uses `Core` member functions. In `C++` and `Python`, the usual syntax for `C++` member functions or `Python` methods is used, while in `Mathematica`, the respective functions take the name of a `Core` as an input. For example, the command

```
In[]:= AlphaQCD["core1", -10.0 + 0.1 I]
Out[]= 0.11619771241600231 - 0.08307724827828394 I
```

extracts the strong coupling at the complex renormalization scale $\mu = (-10+0.1i)\,\text{GeV}$ from the `Core` with the name `core1`. Due to the automatic matching procedure implemented in `REvolver`, the flavor number scheme is automatically set to 5, since $|\mu| = 10.0005\,\text{GeV}$ exceeds the bottom mass value $\overline{m}_b = 4.2\,\text{GeV}$ in `core1`, but is smaller than the top mass value $\overline{m}_t = 163\,\text{GeV}$. If desired, the flavor number scheme can be set by hand with an optional parameter, see Sec. 6.2.1 of Chap. 9.

Similarly, in analogy to the strong coupling, the $\overline{\text{MS}}$ or MSR mass is extracted with the function `MassMS` in `Mathematica`, or with the associated `Core` member functions in `C++` and `Python`. Again, automatic flavor matching is applied, with an optional parameter to set the flavor number scheme by hand, see Sec. 6.2.1 of Chap. 9.

Dedicated member functions also exist for all other supported short-distance masses. For example, to extract the potential subtracted mass of the 5-th lightest flavor (the bottom quark in the physical setup of `core1`) at the scale 2 GeV, $m^{\text{PS}}(2\,\text{GeV})$, from the `Core` with name `core1`, one can execute

```
In[]:= MassPS["core1", 5, 2.0]
Out[]= 4.521091787631138
```

Here, R-evolution is used automatically to resum potentially large logarithms of the intrinsic scale ratio between 2 GeV and 4.2 GeV. Fixed-order conversion can be specified with an optional parameter. For more details and optional parameters, see Sec. 6.2.2 of Chap. 9.

Finally, let's demonstrate some functionalities related to the pole mass scheme.

To extract the fixed-order pole mass of the 6-th lightest quark (the top quark in the physical setup of `core1`), at $\mathcal{O}(\alpha_s^{16})$ (for $\mathcal{O}(\alpha_s^{n>4})$ the asymptotic form as described in Chaps. 3.3 and 3.4 is used), converted from the 5-flavor scheme MSR mass with $\mu = R = 20\,\text{GeV}$, the command

```
In[]:= MassPoleFO["core1", 6, 5, 20.0, 20.0, 16]
Out[]= 1190.2576448418606
```

is used. On the other hand, to return the best possible estimate of the top quark pole mass, its ambiguity, and the order of the smallest correction term, one uses

```
In[]:= MassPoleDetailed["core1", 6, 10.0, "min"]
Out[]= {173.09681693689498, 0.1307735468951421, 4}
```

where the third argument specifies the scale $R = 10\,\text{GeV}$ and the fourth argument specifies the method that is used to determine the returned values. In this case, the method `min` is specified, which refers to the strategy of Ref. [133]. For more details on the pole-mass related functions and the respective functions in the `C++` interface, I refer to Sec. 6.2.3 of Chap. 9.

At the beginning of this section, it is stated that renormalization group equations are solved by `REvolver` up to in principle arbitrary precision[15] at the specified perturbative order.

[15] In practice, the accuracy that can be achieved with `REvolver` is limited by the number of digits that a `double` precision variable in `C++` can handle.

To demonstrate this capability, I shortly describe the iterative algorithm that is used to solve the QCD β-function.

The QCD β-function is given by

$$\mu\frac{\mathrm{d}\alpha_s(\mu)}{\mathrm{d}\mu} = \beta_{\mathrm{QCD}}(\alpha_s(\mu)) = -2\alpha_s(\mu)\sum_{n=0}^{\infty}\beta_n\left[\frac{\alpha_s(\mu)}{4\pi}\right]^{n+1}, \tag{3.47}$$

and its solution can be written as

$$\log\frac{\mu}{\mu_0} = \int_{\alpha_0}^{\alpha_\mu}\frac{\mathrm{d}\alpha}{\beta_{\mathrm{QCD}}(\alpha)} = -\frac{2\pi}{\beta_0}\int_{\alpha_0}^{\alpha_\mu}\frac{\mathrm{d}\alpha}{\alpha^2}\left[1+\sum_{i=1}^{\infty}c_i\Big(\frac{\alpha}{4\pi}\Big)^i\right], \tag{3.48}$$

with $\alpha_\mu \equiv \alpha_s(\mu)$, $\alpha_0 \equiv \alpha_s(\mu_0)$. In the second term, the inverse β-function is simply expanded in terms of the strong coupling. The series coefficients c_i can be determined via the recursive relation

$$c_{n+1} = -\sum_{i=1}^{n+1}c_{n+1-i}b_i\,, \tag{3.49}$$

with $b_i \equiv \beta_i/\beta_0$.

The integral in the last term of Eq. (3.48) can be easily solved term by term, which gives

$$\log\frac{\mu}{\mu_0} = -\frac{1}{2\beta_0}\left[\frac{1}{a_0}-\frac{1}{a_\mu}+c_1\log\Big(\frac{a_\mu}{a_0}\Big)+\sum_{i=1}\frac{c_{i+1}}{i}\left(a_\mu^i-a_0^i\right)\right], \tag{3.50}$$

with $a_i \equiv \alpha_i/(4\pi)$.

A trivial transformation leads to

$$a_\mu = \frac{1}{\frac{1}{a_\mu^{\mathrm{LL}}}+c_1\log\Big(\frac{a_\mu}{a_0}\Big)+\sum_{i=1}\frac{c_{i+1}}{i}[a_\mu^i-a_0^i]}\,. \tag{3.51}$$

with the leading-log solution

$$a_\mu^{\mathrm{LL}} = \frac{a_0}{1+2\beta_0 a_0\log(\mu/\mu_0)}. \tag{3.52}$$

Finally, Eq. (3.51) can be implemented as the iterative formula

$$[a_\mu]_{n+1} = \frac{1}{\frac{1}{a_\mu^{\mathrm{LL}}}+c_1\log\Big(\frac{[a_\mu]_n}{a_0}\Big)+\sum_{i=1}\frac{c_{i+1}}{i}[([a_\mu]_n)^i-a_0^i]}\,. \tag{3.53}$$

Note that in practice, there are two iterations to take care of in Eq. (3.53): The iteration in n, and the infinite sum in the denominator.

Eq. (3.53) converges very quickly (usually a relative precision of around 10^{-15} can be achieved after 10 iterations) and automatically deals with coupling evolutions to complex scales, as the starting point is always the leading-log solution.

Chapter 4

Conclusions and Outlook

In this thesis, various aspects related to heavy quarks have been studied, in order to broaden and deepen the understanding of conceptual issues, to provide the results of mass-related corrections, and to develop computational tools and methods that incorporate the gained conceptual insights and make them easily accessible. The results obtained are applicable in many contexts, either combined or individually.

In the following, I recapitulate the results that are presented in the publications in Part. III and summarized in Chap. 3 with a focus on potential use cases and future work.

In Chap. 5 (full article) and Chap. 3.1 (summary) a general method to compute differential and cumulative NLO event-shape cross sections with stable massive quarks is developed. As it turns out, differential cross sections for event shapes that are linearly sensitive to soft momenta (which applies to all common event shapes such as 2-jettiness, C-parameter, jet broadening, jet masses, and angularities) can be written as the sum of a delta-distribution term, a plus-distribution term, and a non-distributional term. General formulas are derived in Chap. 5 to compute the distributional terms analytically, and an algorithm is presented that can compute the non-distributional term numerically (but unbinned) up to in principle arbitrary precision without employing Monte Carlo methods. Interestingly, the coefficient of the delta distribution can be written as a sum of terms that are universal for all event shapes under very mild constraints, and an event-shape dependent 1-parameter integral that depends only on the event-shape measurement function in the soft limit. The coefficient of the plus distribution is universal for the same set of event shapes that contains all popular event shapes such as thrust, C-parameter, hemisphere masses, broadening, and angularities. The methods developed in Chap. 5 can be applied to differential as well as cumulative cross sections and are numerically stable, even in the dijet region.

The results of Chap. 5 are useful for precision-calculations of event-shape cross sections with massive quarks, even for newly defined observables. At future linear colliders that will measure the top quark mass, the methods will help to facilitate the accurate computation of NLO event-shape cross sections, and the analytic formula for the delta-function coefficient can be used to supplement numerical methods that are not capable of properly resolving that contribution.

In future work, the method that is presented in Chap. 5 can be extended with regard to several factors:

- Although the formulas for the coefficients of the distributional terms can be readily applied to event shapes with additional continuous parameters such as angularities, the numerical algorithm is described only for event shapes without additional parameters.
- Observables that imply jet algorithms or are non-global in other ways can not be treated with the methods described here. However, it might be possible to extend the presented methods by applying a similar reasoning.
- The presented methods focus on event-shape distributions at $\mathcal{O}(\alpha_s)$. It might be possible to extend some of the methods to $\mathcal{O}(\alpha_s^2)$, although this is most probably an extensive task. Such a method would be extremely useful to attain even higher

precision in event-shape cross section distributions with massive quarks, even if it can only be applied to specific terms. General $\mathcal{O}(\alpha_s^2)$ results could also provide hints regarding the universality of the coefficients of the distributional terms and provide additional, possibly unforeseen general insights into the structure of event-shape cross sections.

- A systematic inclusion of $\mathrm{N^2LL}$ contributions from SCET and bHQET has already been achieved in Ref. [112].

In addition, some of the results of Chap. 5 can be applied in other contexts. For example, the delta-function coefficient that can be easily obtained with the presented formula can be used as an IR subtraction in parton-level Monte Carlo generators.

In Chap. 6 (full article) and Chap. 3.2 (summary), the computation and results of the NNLO (two-loop) corrections to the massive quark SCET jet function are presented. The result includes the mass-dependencies that come from primary as well as secondary massive quarks in full generality, i.e. without any additional expansions in the mass parameter. The result is especially important in the phase-space region $p^2 \sim p^2 - m^2 \sim m^2$, i.e. the intermediate region where neither the massless approximation $m^2/p^2 \to 0$ nor the super-massive approximation $p^2 - m^2 \to 0$ can be trusted to provide accurate results.

The two-loop contribution to the massive quark SCET jet function depends on two scales: the invariant mass of the jet p^2, and the mass of the massive quark m. This makes the calculation non-trivial. The most interesting technical issue, however, comes from the fact that SCET Feynman diagrams contain Wilson lines that lead to eikonal propagators of the form $1/n \cdot k$ in Feynman integrals, where n is a light-like 4-vector and k is a loop momentum. These eikonal propagators potentially give rise to rapidity divergences in loop integrals. For some integral classes, namely the ones associated to non-planar Feynman diagrams, the potential rapidity divergences prevent the naive application of the common IBP reduction. Even for a rapidity-finite integral in this class, it can not be guaranteed that the IBP relations only contain rapidity-finite integrals. An additional rapidity regulator can be introduced to circumvent this issue, but this leads to a significantly increased number of master integrals, for which several orders in the rapidity regulator have to be evaluated in order to obtain all required terms. Fortunately, in the calculation of the two-loop jet function, there are only two diagrams that are affected by this issue. Those diagrams can be evaluated analytically in the massless and super-massive limit and the remaining contribution can be evaluated numerically. Those numerical contributions are small in comparison to the other terms in the two-loop contribution to the jet function.

The issue described in the previous paragraph gives rise to interesting future studies. The complication of eikonal propagators and the associated potential rapidity divergences is not only relevant for the two-loop jet function, but also for other quantities in SCET for which, sooner or later, higher loop corrections will become relevant. It is therefore useful and interesting to have a closer look at that problem. One possible solution could be a new kind of rapidity regulator that does not blow up the number of master integrals, or a modification to the Laporta algorithm.

Another interesting issue that appears in the computation of the massive two-loop jet function is related to secondary massive quark contributions, i.e. contributions that come from virtual massive quark loops. For those contributions, it is crucial to cleanly separate rapidity, IR, and UV divergences. In Chap. 6 this is achieved by regulating IR divergences with a gluon-mass regulator and, in addition, a symmetric η rapidity regulator [127, 142] if required. The loop integrations are then carried out by using a dispersion relation. Due to the gluon-mass regulator, all quantities that mix into the contributions that come from secondary massive quarks must be computed with that regulator, including the 1-loop

massive jet function and the mass renormalization factor. This is feasible in a two-loop computation, at three loops, however, it is worthwhile to find alternative techniques. Similar to the IBP-reduction problem, a new type of regulator might facilitate the computation, or an entirely different approach could be developed to separate the types of divergences.

It is also described in Chap. 6 that there are in fact two options to define the massive quark two-loop SCET jet function: To avoid double-counting and render the jet function IR-finite, collinear-soft modes that are associated with *massless* virtual quark loops have to be removed from the jet function matrix element. Traditionally, this is often done by applying zero-bin subtractions. Alternatively, the mode subtraction can be performed via the so-called collinear-soft matrix element, which is more intuitive and systematic. Collinear-soft modes associated with *massive* quark loops are IR-finite and can be either subtracted from the jet-function matrix element (the resulting jet function is called the *universal jet function*) or left unsubtracted (resulting in the so-called *mass-mode jet function*). In the mass-mode jet function case, the massive collinear-soft modes are handled separately in the so-called collinear-soft function, while in the case of the universal jet function, the collinear-soft modes are handled as parts of the jet function. The two definitions of the jet function, universal and mass-mode, can both be employed in factorization theorems and provide different perspectives on mode separation and log resummation, while giving equivalent results.

The freedom of choice of how to subtract collinear-soft modes does not only apply to the massive quark SCET jet function but is more general. For example, the reasoning also applies for bHQET jet functions with lighter secondary massive quarks, which can be explored in future work.

Finally, the contributions of virtual massive quark loops with masses that are different from the primary quark mass to the 2-loop massive quark jet function can be computed in a future project. Although lighter massive flavor corrections (e.g. bottom quark mass effects in the top quark jet function) are small and are not relevant at the current level of precision, the analytic form of the corrections and their expansions might provide insights into the behavior and general structure of this kind of contributions.

The results of Chap. 6 were the last missing pieces to perform $\mathrm{N^3LL}$ resummation for some event shapes with massive quarks, including 2-jettiness. Consequently, many precision analyses for those observables that already exist at NNLL can now be updated and made even more precise. The results are most important in the "intermediate region" of the jet invariant mass, in the transition between the peak and the tail.

In Chap. 7 (full article) and Chap. 3.3 (summary), the MSR quark mass renormalization scheme, $m_Q^{\mathrm{MSR}}(R)$, is discussed in detail, a low-scale short-distance scheme that is the low-scale extension of the $\overline{\mathrm{MS}}$ mass $\overline{m}_Q(\mu)$ for scales R below the heavy quark mass. The MSR mass has a variable intrinsic scale R that is used to derive its R-evolution equation, a renormalization group equation that is *linear* in the renormalization scale. Due to the clean definition of the MSR mass through quark self-energy diagrams, and the adjustable scale R, the MSR mass is the perfect tool for determining heavy quark masses from quark-mass dependent observables governed by small dynamical scales and comparing them with mass determinations that were carried out at higher scales. The accurate conversion between mass renormalization schemes with widely separated intrinsic scales can be achieved by employing the R-evolution equation to resum large logarithms. This is especially useful for the top quark mass, for which the scale hierarchy between the mass scale and the optimal kinematic scale where the mass is extracted can be very large.

In the formal limit $R \to 0$, the MSR mass is equivalent to the pole mass. However, this limit is ambiguous since taking the limit requires circumventing the Landau pole in a

non-unique way. This illustrates the $\mathcal{O}(\Lambda_{\rm QCD})$ renormalon ambiguity of the pole mass. The solution of the R-evolution equation with the lower scale set to zero encodes the same contributions as the perturbative pole-MSR mass relation. However, the terms of the solution of the R-evolution equation are re-arranged in comparison to the usual perturbative relation such that they are ordered with respect to their numerical impact in the high-order asymptotic behavior of the perturbative series. Also, the analytic solution makes the pole-mass renormalon ambiguity explicit through a non-zero imaginary part. The expression is equivalent to the Borel sum of the perturbative pole-MSR mass relation and can be used to derive useful formulas for the high-order asymptotic behavior of the pole-MSR and pole-$\overline{\rm MS}$ mass relations as well as the normalization of their asymptotic renormalon behavior, $N_{1/2}$. The derived formula for the normalization is called the "$\mathcal{O}(\Lambda_{\rm QCD})$ renormalon sum rule" and can be applied to any perturbative series, not just the pole-MSR mass relation.

The renormalon sum rule can be used to probe any perturbative series for an $\mathcal{O}(\Lambda_{\rm QCD})$ renormalon by checking if the sum converges to zero or not. Since the renormalon sum rule is a series that is always truncated in practice, the apparent convergence of the formula is not a strict proof of the presence or absence of a renormalon. However, the result can provide precious hints, as in most cases rigorous renormalon analyses are unfeasible.

The concept of the MSR mass is extended in Chap. 8 (full article) and Chap. 3.4 (summary) to include effects of massive flavors that are lighter than the considered heavy quark. Virtual quark loops of massive quarks with mass $m > \Lambda_{\rm QCD}$ act as infrared cutoffs in Feynman diagrams. Consequently, massive lighter flavors decouple in the asymptotic high order behavior of the pole-MSR mass relation that is governed by the $\mathcal{O}(\Lambda_{\rm QCD})$ renormalon of the pole mass. The formalism that is developed in Chap. 8 makes this light-flavor decoupling at high orders explicit by setting up a running and matching pipeline that systematically disentangles the different momentum regions in the perturbative pole-MSR or pole-$\overline{\rm MS}$ mass relation. This is achieved by acknowledging that the pole-MSR mass relation $m_Q^{\rm pole} - m_Q^{\rm MSR}(R)$ contains the contribution from quark self-energy diagrams from the energy range between 0 and R (or μ for the pole-$\overline{\rm MS}$ mass relation). In the spirit of effective field theory, that energy range can be factorized into regions with different active flavor numbers by iteratively applying a running and matching procedure. The procedure is analogous to the running and matching procedure that is known from the strong coupling and resums potentially large logarithms of quark mass ratios.

By using this formalism, it is possible to study the light massive flavor corrections to the pole-MSR and pole-$\overline{\rm MS}$ mass relation in a new systematic way. The concepts of heavy quark symmetry, heavy quark symmetry breaking, and flavor universality are explicit in the formalism and can be studied systematically in that context, which was not possible before.

By examining heavy quark symmetry breaking, analytic formulas for the asymptotic high-order behavior of the light massive flavor corrections to the pole-MSR and pole-$\overline{\rm MS}$ mass relations can be derived and studied. Interestingly, it turns out that light massive flavor corrections are governed by their larger-order behavior already at relatively low orders, such that these corrections can be predicted with a precision of around 1 MeV already at 4-loop order. Explicit expressions are given in Sec. 3.3 of Chap. 8. Additionally, by using the developed formalism, pole-mass differences (that are renormalon free) are computed with a precision of 20 MeV.

An essential part of the work in Chap. 8 is the re-examination of the large order asymptotic behavior of the pole mass and the numeric size of the associated renormalon ambiguity with a special focus on the top quark. The very frequent use of the pole mass scheme for the top quark, also in LHC analyses, makes the study of the size of the ambiguity especially interesting. Once again, the running and matching formalism that is developed in the

same article, and especially heavy quark symmetry, allow studying this problem in a new, systematic way that does not rely on heuristics.

In agreement with the predictions of heavy quark symmetry, the value we determine for the pole-mass renormalon ambiguity does not depend on the mass value of the heavy quark, or on the number of lighter quark flavors with mass values $m_q > \Lambda_{\rm QCD}$. With the method that is developed in Chap. 8, the pole-mass renormalon ambiguity is determined to be 250 MeV. This value is in stark contrast to the value of 110 MeV that is determined in Ref. [133] and that does not follow the constraints of heavy quark symmetry.

It is important to realize that the value of the pole-mass ambiguity of 250 MeV does only incorporate the principle precision with which the pole-mass value can be determined, and does not involve any other sources of uncertainty whatsoever. Also, in a practical application, to achieve the best possible value of the pole mass, one has to incorporate perturbative orders up to the minimal perturbative correction term to its value. The required loop order depends on the typical physical scale of the process and is usually beyond reach if that scale is of the order of the top quark. That being said, even if one only considers the fundamentally irreducible ambiguity of 250 MeV, this is a practically relevant issue for HL-LHC top quark mass measurements, which are projected to reach a precision of 200 MeV [143]. However, even for LHC Run-2, the 250 MeV pole mass ambiguity is practically relevant in precision measurements.

As a consequence, short-distance mass schemes, such as the $\overline{\rm MS}$ or MSR scheme should be used instead of the pole mass scheme to avoid the pole-mass ambiguity problem. The $\overline{\rm MS}$ and MSR mass schemes are perfectly suited for precision analyses of heavy quark masses: They are short-distance masses, have a simple and clean definition, their renormalization factor is known up to $\mathcal{O}(\alpha_s^4)$, and the effects of lighter massive flavors can be implemented systematically. In addition, the relation between the MSR and the $\overline{\rm MS}$ mass is known with a precision of $\mathcal{O}(10\,\text{MeV})$.

In Chap. 9 (full article) and Chap. 3.5 (summary), the `C++` library `REvolver` is presented that features accurate conversions between the most popular mass renormalization schemes and renormalization group evolution of masses and the strong coupling with automatic flavor matching in QCD. `REvolver` introduces the concept of the `Core` object that encodes a physical setup that includes values of the strong coupling and quark masses at specified scales and flavor number schemes. R-evolution is used to resum potentially large logarithms in the conversion between short-distance mass schemes. Furthermore, `REvolver` implements the techniques that are developed in Chaps. 7 and 8. This includes the fixed-order conversions to and from the pole mass at an arbitrary perturbative order by exploiting its know asymptotic high-order behavior, and the conversion to and from the asymptotic pole mass, i.e. its best possible value.

`REvolver` is aimed at theorists and experimentalists alike. In a phenomenological context, `REvolver` was prominently used in Refs. [144, 145] (the author of this thesis is a coauthor of these references) to demonstrate the consistency of bottom-quark $\overline{\rm MS}$-mass values measured at different characteristic dynamical scales with the $\overline{\rm MS}$ renormalization-group evolution as predicted by standard-model QCD. The mass values have been extracted at the bottom quark mass scale $\overline{m}_b$ itself (PDG world average, extracted at a typical scale of the bottomonium mass), the Z-boson mass scale m_Z (extracted from LEP and SLC measurements at the Z-pole), and the Higgs-mass scale m_H (extracted from Higgs-boson branching-ratio measurements at the LHC). In the near future, when experimental data from HL-LHC and other "Higgs factories" are available, studying the running of the bottom quark mass and comparing theoretical predictions with actual mass-value measurements at different energy scales can provide precise tests of standard-model QCD, e.g. by ruling out

(or confirming) exotic heavy color-charged states. Having a tool like `REvolver` at one's disposal for studies of this kind will prove extremely valuable.

`REvolver` can be easily extended, such that newly derived loop corrections of anomalous dimensions, matching factors, etc. can be easily added. The same is true for additional renormalization schemes that might be of interest in the future.

In the long term, however, the most interesting and useful extension of `REvolver` is to implement electroweak interactions and the accordingly interacting particle classes. In that way, a `Core` could encode complete standard-model-like setups from which particle masses or couplings can be extracted at arbitrary scales. By generalizing the algorithms that were developed for the current version of `REvolver`, complex multi-interaction effects can be included in renormalization scheme conversions as well as in running and matching computations very accurately.

In order to illustrate once again the high relevance and usefulness of the works presented in this thesis, let's briefly consider the possible improvements to a currently much discussed and very active research area, namely the top quark Monte Carlo mass interpretation problem and the effort to calibrate it [128,146–150]. The most precise method for extracting the top quark mass today is direct reconstruction [151]. This means that a kinematic fit is made to top-mass sensitive observables that have been reconstructed from experimental data, in order to determine the top quark mass parameter in a Monte Carlo simulation. The problem of how this "Monte Carlo mass" can be related to a field-theoretically well-defined mass scheme or even how the problem should be formulated or which uncertainty to assign is not yet fully known. However, significant progress has been made in recent years [148–150], e.g. it was shown that the Monte Carlo top quark mass is compatible with the MSR mass $m^{\mathrm{MSR}}(\Lambda_c)$ at the shower cutoff Λ_c within uncertainties [149]. The results presented in this thesis can be used to improve existing and future studies in the following way:

- the results of Chap. 5, related to the general and efficient computation of NLO massive event-shape distributions facilitate the extension of existing thrust-based analyses to different event shapes by providing all fixed-order ingredients for $\mathrm{N^2LL}$ resummation. This helps in assessing the generality of existing analyses that use thrust, with the constraint that Chap. 5 only deals with stable quarks;
- the two-loop massive quark jet function of Chap. 6 can be used, together with other already known contributions, to increase the order of the theoretical computations to $\mathrm{N^3LL}$. The two-loop massive quark jet function contains SCET non-singular contributions and is especially important in the intermediate region between the peak and the tail. The inclusion of this result would increase the precision of the current analysis and further refine the estimate of compatibility between the Monte Carlo mass and the MSR mass at the shower cut-off;
- the MSR mass in Chaps. 7 and 8, and the development of the `REvolver` library presented in Chap. 9 facilitates and increases the speed of the numerical calibration process. In addition, the extensive feature set and open-source nature of the code enable the analyses involved to be easily extended, refined, and traceable.

Overall, the presented works do not only offer valuable advances in the field of high-energy physics with regard to heavy quark masses but also open up the possibility of various interesting follow-up works. I hope that the newly provided insights, results, and tools will have long-term impacts due to their generality, extensibility, and the effort to make their key results easily accessible.

Part III

Publications

Chapter 5

NLO Massive Event-Shape Differential and Cumulative Distributions

Christopher Lepenik and Vicent Mateu

NLO massive event-shape differential and cumulative distributions

Published in: JHEP **03** (2020) 024

Preprint version: arXiv:1912.08211 [hep-ph]

Contributions to this article:
Conceptual innovations (together with other authors), derivation and cross-checks of all analytical calculations and formulas (together with other authors), numerical analyses.

Some aspects build on the foundations already established in the author's master thesis [152].

Published for SISSA by Springer

Received: December 21, 2019
Revised: February 7, 2020
Accepted: February 12, 2020
Published: March 4, 2020

NLO massive event-shape differential and cumulative distributions

Christopher Lepenik[a] **and Vicent Mateu**[b,c]

[a] *Faculty of Physics, University of Vienna, Boltzmanngasse 5, A-1090 Wien, Austria*
[b] *Departamento de Física Fundamental e IUFFyM, Universidad de Salamanca, E-37008 Salamanca, Spain*
[c] *Instituto de Física Teórica UAM-CSIC, E-28049 Madrid, Spain*

E-mail: christopher.lepenik@univie.ac.at, vmateu@usal.es

Abstract: We provide a general method to effectively compute differential and cumulative event-shape distributions to $\mathcal{O}(\alpha_s)$ precision for massive quarks produced primarily at an e^+e^- collider. In particular, we show that at this order, due to the screening of collinear singularities by the quark mass, for all event shapes linearly sensitive to soft dynamics, there appear only two distributions at threshold: a Dirac delta function and a plus distribution. Furthermore, we show that the coefficient of the latter is universal for any infra-red and collinear safe event shape, and provide an analytic expression for it. Likewise, we compute a general formula for the coefficient of the Dirac delta function, which depends only on the event-shape measurement function in the soft limit. Finally, we present an efficient algorithm to compute the differential and cumulative distributions, which does not rely on Monte Carlo methods, therefore achieving a priory arbitrary precision even in the extreme dijet region. We implement this algorithm in a numeric code and show that it agrees with analytic results on the distribution for 2-jettiness, heavy jet mass and a massive generalization of C-parameter.

Keywords: Perturbative QCD, Heavy Quark Physics, Quark Masses and SM Parameters

ArXiv ePrint: 1912.08211

https://doi.org/10.1007/JHEP03(2020)024

JHEP03(2020)024

Contents

JHEP03(2020)024

1 Introduction

Recent years have seen tremendous progress in the understanding and computation of event-shape cross sections for e^+e^- machines such as LEP or the future linear and circular colliders. This is mainly achieved with the use of factorized expressions (see e.g. refs. [1, 2]) derived in the frame of the effective field theory (EFT)[1] known as Soft-Collinear Effective Theory (SCET) [8–12]. The state of the art for massless event shapes is next-to-next-to-leading-log ($\mathrm{N^2LL}$) [13–15] and next-to-next-to-next-to-leading-log ($\mathrm{N^3LL}$) [16–20].[2] The computation of the soft function has been fully automatized analytically at $\mathcal{O}(\alpha_s)$ in ref. [18] and numerically at $\mathcal{O}(\alpha_s^2)$ in refs. [24, 25] (in those articles one can also find analytic results for some event shapes such as C-parameter). Analytic fixed-order perturbative predictions exist at $\mathcal{O}(\alpha_s)$ for thrust, heavy jet mass (HJM) and C-parameter, while for other event shapes such as angularities or jet broadening, the cross sections can be expressed as a 1D numerical integral. Numerical results exist at $\mathcal{O}(\alpha_s^2)$ [26, 27] and $\mathcal{O}(\alpha_s^3)$ [28–33]. In ref. [34] the fixed-order cross sections for oriented event shapes have been computed up to $\mathcal{O}(\alpha_s^2)$. These results have been used, in particular, to determine the strong coupling constant with very high precision [14, 17, 35–39].

The theoretical knowledge for event shapes involving massive quarks is comparatively much poorer. Fixed-order predictions have been obtained numerically at $\mathcal{O}(\alpha_s)$ (analytic results at this order exist but are scarce) and $\mathcal{O}(\alpha_s^2)$ [40–42]. Factorization and resummation for 2-jettiness with massive quarks [43, 44] has recently achieved $\mathrm{N^3LL}$ precision through the computation of matrix elements at two loops [45–49]. These results have been used in ref. [50] to calibrate the PYTHIA 8.205 [51] top quark mass parameter in terms of the short-distance MSR scheme [52, 53]. In this direction, further theoretical progress has been made, and a p_T cutoff as implemented in angular ordered parton showers has been included in ref. [54]. Event-shapes for massive particles shall play an important role at the future linear collider, where they will presumably be used to determine the top quark mass from boosted events in a well defined scheme within quantum field theory. This measurement is complementary to threshold scans with partially orthogonal experimental uncertainties. Furthermore, from the conclusions that can be drawn from this article, they might also be a useful tool to determine the strong coupling α_s.

For a complete description of massive event shapes with $\mathrm{N^2LL}$ accuracy in the peak region where the SCET and bHQET effective theories can be applied,[3] but also valid in the tail and far-tail of the distribution, the resummed cross section has to be matched to the fixed-order prediction at $\mathcal{O}(\alpha_s)$. In full generality, the differential cross section for massive

[1] Factorization formulas can also be derived in the Collins, Soper and Sterman (CSS) formalism [3–7].

[2] Resummation can also be worked out in the coherent branching formalism [21], which achieves $\mathrm{N^2LL}$ precision in an automated, numeric way [22, 23].

[3] The logarithmic counting refers to the kinematic limit $p_J^2 \sim m_q^2 \sim Q^2\lambda^2$, with p_J^μ the jet four-momentum and λ de EFT power-counting parameter. In this limit, the set of terms summed up at leading log in the cumulative cross section have the form $\log^{n+1}(\lambda)\alpha_s^n$ for any integer $n > 0$. At threshold there are no double logs and therefore the meaning of logarithmic accuracy is different.

JHEP03(2020)024

particles up to this order can be written as

$$\frac{1}{\sigma_0^C}\frac{\mathrm{d}\sigma_C}{\mathrm{d}e} = R_C^0(\hat{m})\,\delta(e-e_{\min}) + C_F\frac{\alpha_s}{\pi}A_e^C(\hat{m})\delta(e-e_{\min}) \tag{1.1}$$
$$+ C_F\frac{\alpha_s}{\pi}B_{\text{plus}}^C(\hat{m})\left[\frac{1}{e-e_{\min}}\right]_+ + C_F\frac{\alpha_s}{\pi}F_e^{\text{NS}}(e,\hat{m}) + \mathcal{O}(\alpha_s^2)\,,$$

with F_e^{NS} a function regular at $e_{\min}$, the lower endpoint of the distribution, σ_0^C the massless Born-cross section and R_C^0 the tree level R-ratio. The sub- and super-scripts C denote the type of current considered (vector or axial-vector), omitted for F_e^{NS} to keep the notation simple. In this paper we compute the differential and cumulative cross sections for all event shapes, for both vector and axial-vector currents, reaching the same standard as for massless quarks at this order (where essentially all results are known analytically in terms of relatively simple expressions), by obtaining analytical results for A_e and B_{plus}, and computing F_e^{NS} through 1-dimensional numerical integrals in a way which is almost as precise and stable as for a full analytic result. Our calculation shows that A_e and F_e^{NS} depend on the specific event-shape variable, and B_{plus} is a universal function of the reduced mass $\hat{m} \equiv m/Q$. This matching program has already been carried out in previous work [50] in a less efficient way. While at the time of the "NLO revolution" the $\mathcal{O}(\alpha_s)$ results seem completely standard, having a dedicated article on those is still useful because: a) known results are mainly numeric and provided as binned distributions, which makes the matching to resummed results unpractical, b) analytic results are faster and easier to implement; c) non-zero quark masses entail that different event-shape schemes can be used, allowing to control the sensitivity to the mass, to the best of our knowledge a possibility never discussed so far;[4] d) new strategies to efficiently compute the cross section are presented, which we believe will be useful for future work; e) our results are an important input for further studies of massive event shapes, which aim to improve our understanding of heavy quark mass determinations in general. This article provides all ingredients that are needed for a full N^{2}LL computation in a way which is useful and easy to implement, and in that sense it will be a reference for many future analysis in this field. In particular our results will help to clarify the top quark Monte Carlo (MC) mass interpretation problem.

This article is organized as follows: in section 2 we introduce massive schemes, and show how to implement them into massive event shapes. In section 3 we provide a direct computation of our main analytic result, A_e, the coefficient of the delta function, computing the real and virtual contributions directly, canceling the infrared singularities explicitly. Section 4 deals with F_e^{NS}, describing our numerical algorithm, which is applied to differential and cumulative cross sections as well as moments. Analytic results for cross sections of a few event shapes are shown in section 5. Our conclusions are summarized in section 7. We provide a second analytic computation of the delta-function coefficient in appendix A, requiring that the integration of the differential cross section over its entire physical range

[4] Schemes for event shapes were first introduced in ref. [55] to study hadron mass effects in hadronization power corrections. Here we extend the analysis to heavy quarks, and study how to gain/loose sensitivity to their mass.

reproduces the total hadronic cross section. Applications of our master formula for a selection of event shapes, analytic formulae for the massive total hadronic cross section and some master integrals are provided in the remaining appendices.

2 Event shapes for massive particles

In this section we introduce generalizations of classic event shapes for massive heavy quarks, for which we present analytic results of the delta-function coefficient in appendix D. These generalizations go under the name of "mass schemes", and have no effect on the partonic cross section for massless particles, but for massive quarks dramatically modify the sensitivity to their mass already at parton level even at the lowest order. This control on the sensitivity to the mass is of high interest, and in particular sets the effective renormalization scale of the heavy quark mass. No systematic study of these schemes exists yet for massive quarks, and here we intend to fill this gap.

Mass schemes for event shapes were originally introduced to study non-perturbative power corrections in the context of non-zero hadron masses [55, 56]. In the case of massless quarks, partonic cross sections are unaffected by scheme changes, but power corrections substantially depend on the scheme choice. In particular it has been shown that the leading non-perturbative power correction is universal for the so-called E-scheme. They have been also used to study power corrections in the dressed-gluon approximation [57] and to determine the mass of heavy quarks in boosted events [44]. Due to increasing theoretical and experimental precision, it is necessary to include the finite bottom quark mass in high-precision calculations, e.g. for extracting the strong coupling constant [35]. On the other hand, mass effects are dominant and have to be included when extracting the quark mass itself or when carrying out mass-related studies such as analyzing the properties of the top quark Monte Carlo mass parameter.

When using classical event shapes like thrust, C-parameter, jet broadening etc. in presence of massive quarks, the way how one treats energies and three-momenta magnitudes is important, since (unlike for massless particles) $E_p \neq |\vec{p}|$. To categorize different ways of how to treat energies and three-momenta, several "schemes" can be defined for massive event shapes, which are distinguished exactly by the way how E_p and $|\vec{p}|$ are interpreted. Obviously, all these schemes reduce to the original definition in the massless case.

Starting from the original definition of event shapes, the "E-scheme" is defined by the replacement $\vec{p} \to (E_p/|\vec{p}|)\,\vec{p}$, while the "P-scheme" is defined by the substitution $E_p \to |\vec{p}|$. Some event shapes originally defined in P-scheme are thrust [58],

$$\tau \equiv \tau^P = \frac{1}{Q_P}\sum_i p_{i,\perp} \mathrm{e}^{-|\eta_i|} = \frac{1}{Q_P}\min_{\hat{t}}\sum_i (|\vec{p}_i| - |\hat{t}\cdot\vec{p}_i|)\,, \tag{2.1}$$

C-parameter [59, 60] (it is often useful to define the reduced C-parameter as $\widetilde{C} = C/6$)

$$C \equiv C^P = \frac{3}{2Q_P^2}\sum_{i,j}|\vec{p}_i||\vec{p}_j|\sin^2\theta_{ij} = \frac{3}{2}\left[1 - \frac{1}{Q_P^2}\sum_{i,j}\frac{(\vec{p}_i\cdot\vec{p}_j)^2}{|\vec{p}_i||\vec{p}_j|}\right], \tag{2.2}$$

JHEP03(2020)024

and broadening [61]

$$B_T \equiv B_T^P = \frac{1}{2Q_P}\sum_i p_{i,\perp} = \frac{1}{2Q_P}\sum_i (|\vec{p}_i| - |\hat{t}\cdot\vec{p}_i|)^{1/2}(|\vec{p}_i| + |\hat{t}\cdot\vec{p}_i|)^{1/2}\,, \tag{2.3}$$

while angularities [62] were originally defined in the E-scheme:

$$\tau_a \equiv \tau_a^E = \frac{1}{Q}\sum_i \frac{E_i}{|\vec{p}_i|} p_{i,\perp} \mathrm{e}^{-|\eta_i|(1-a)} = \frac{1}{2Q}\sum_i \frac{E_i}{|\vec{p}_i|}(|\vec{p}_i| - |\hat{t}\cdot\vec{p}_i|)^{1-\frac{a}{2}}(|\vec{p}_i| + |\hat{t}\cdot\vec{p}_i|)^{\frac{a}{2}}\,, \tag{2.4}$$

where η denotes the pseudo-rapidity, $p_\perp \equiv |\vec{p}_\perp|$ the transverse momentum measured with respect to the thrust axis, and $m_\perp \equiv \sqrt{p_\perp^2 + m^2}$ is the transverse mass. The P-scheme version of angularities and E-scheme versions of the other event shapes listed here can be found in appendix D. Note that the substitutions have to be done for the event-shape normalization as well, such that E-scheme event shapes are usually normalized using $Q = \sum_i E_{p,i}$, while P-scheme event shapes are normalized by $Q_P = \sum_i |\vec{p}_i|$. The definition of the thrust axis itself does not change with the scheme, i.e. it is always defined with respect to the original P-scheme thrust definition. The minimal value for these event shapes remains $e_{\min} = 0$, meaning that these observables are insensitive to parton masses at leading order, which can be useful in cases where mass effects are preferred to be small.

Some event shapes are, in their original definitions, neither P- nor E-scheme, sometimes referred to as "massive scheme" or "M-scheme", usually containing full momentum information.[5] One of these is heavy jet mass [64–66], defined as the heavier of the two hemisphere invariant masses, normalized by Q^2

$$\rho = \frac{1}{Q^2}\left(\sum_{i\in\text{heavy}} p_i\right)^2, \tag{2.5}$$

where the hemispheres are defined to be separated by the plane orthogonal to the thrust axis. It can be useful to define massive scheme versions of other event shapes as well. Examples include the massive version of thrust (2-jettiness) [67] and C-parameter (C-jettiness) [57]. 2-jettiness is defined by generalizing the original definition to

$$\tau_J = \frac{1}{Q}\sum_i (|E_i| - |\hat{t}\cdot\vec{p}_i|)\,, \tag{2.6}$$

while C-jettiness is based on the Lorentz-invariant form

$$C_J = \frac{3}{2}\left[2 - \sum_{i\neq j}\frac{(p_i\cdot p_j)^2}{(p_i\cdot q)(p_j\cdot q)}\right], \tag{2.7}$$

introduced in ref. [68], with $q = \sum_i p_i$. These event shapes usually have a non-zero minimal value $e_{\min} \neq 0$ and are therefore mass sensitive already at leading order. The increased mass sensitivity can be useful when studying mass related issues, e.g. 2-jettiness was used

[5] For more detailed information on how to define consistent substitution rules, see ref. [63].

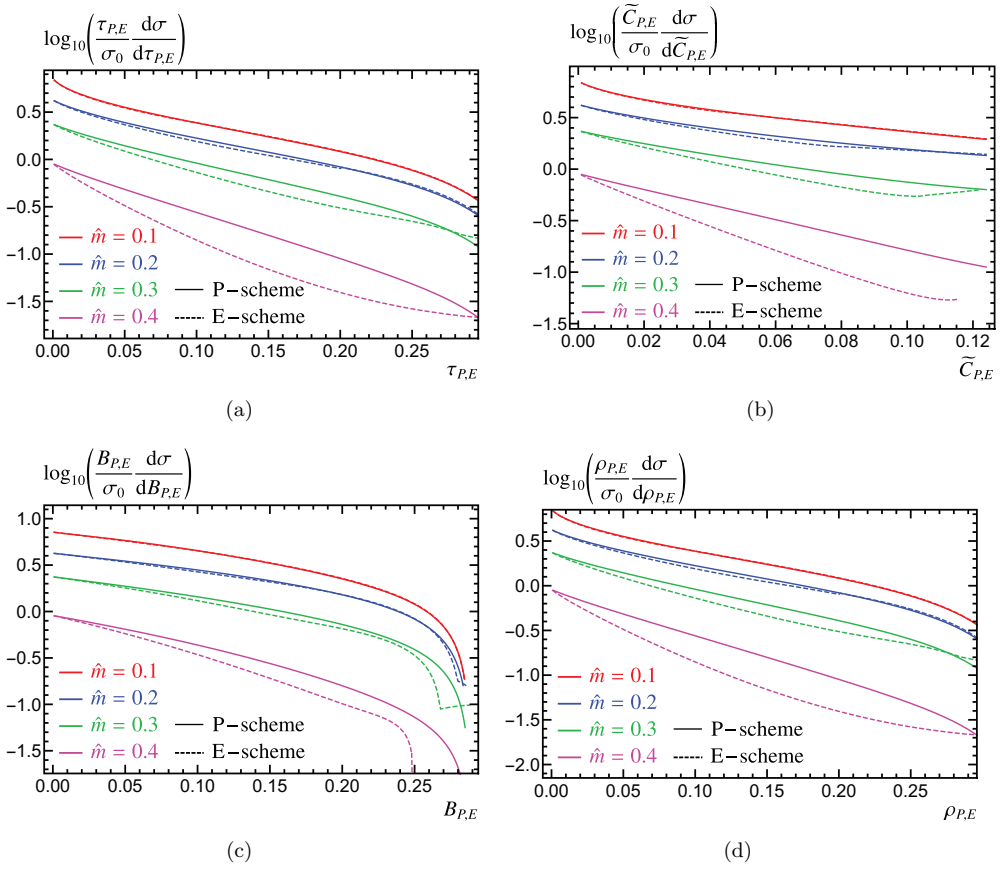

Figure 1. Event-shape differential distributions for the vector current in the P (solid lines) and E schemes (dashed lines). Panels (a), (b), (c), and (d) show the cross section for thrust, C-parameter, jet broadening, and heavy jet mass, respectively. All curves are multiplied by $e - e_{\min}$, with e the event-shape value and $e_{\min}$ its minimal value, such that the cross section is finite for $e = e_{\min}$. Red, blue, green and magenta show the results for $\hat{m} = 0.1$, 0.2, 0.3 and 0.4, respectively.

to calibrate the PYTHIA 8.205 MC top quark mass [50] and has been proposed to measure the top quark mass at a future linear collider [44].

In appendix D we present some analytic results for the delta-function coefficients of differential cross sections for the event shapes listed above in various schemes, together with respective characteristic information on the event shapes.

Differential cross sections in the E- and P-schemes for a selection of event shapes can be seen in figure 1. The plots have been generated using the algorithm described in section 4.3. We do not show massive-scheme cross sections in this plot since their lower endpoint is different from zero. We have chosen the plot-range of the P-scheme allowed values, since they are mass-independent, and our y axis is in a logarithmic scale to make the curves with small values of $\hat{m}$ visible. In general E-scheme maximal values do depend on the

JHEP03(2020)024

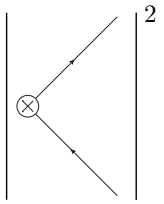

Figure 2. Diagrammatic contribution to the $\mathcal{O}(\alpha_s^0)$ differential event shape distribution. The diagram has to be squared and contributes only as a Dirac delta function.

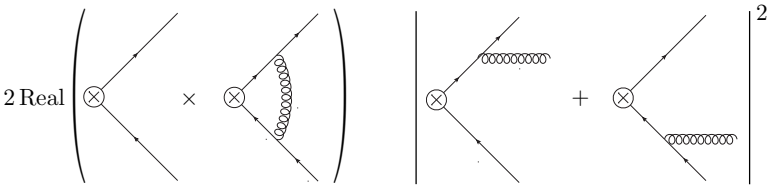

Figure 3. Contributions to the $\mathcal{O}(\alpha_s)$ differential cross section for event shapes. Panel (a) shows the virtual contribution as twice the interference of the three-level and one one-loop diagrams, while in panel (b) the two real-radiation diagrams that have to be added and squared are drawn.

reduced mass (see appendix D for some examples). Since the scheme dependence vanishes for $m = 0$, curves are very similar for small values of the reduced mass, resulting in nearly identical red lines in all four panels of the figure. As the mass increases, the differences grow, and for $\hat{m} = 0.4$ the curves in both schemes are clearly different. We observe that the cross section is smaller in the E-scheme for most of the spectrum.

3 Analytic results for the distributions at threshold

In this section we provide the computation of one of our main results, an integral expression for the delta-function coefficient of event-shape differential cross sections in full QCD. Obviously, the results are different for vector and axial-vector currents, but the computation is analogous to both processes. Along the computation we show that the coefficient of the plus distribution is the same for any observable linearly sensitive to soft momentum. The delta-function coefficient receives contributions from the virtual- and real-radiation diagrams, which are separately IR divergent, although the sum is finite. The Feynman diagrams at LO and NLO are shown in figures 2 and 3, respectively. In the virtual term, the divergence originates from a loop integration, while in the real-radiation it is a consequence of the phase-space integration. The cancellation can be achieved by computing the two terms explicitly, as in the approach followed in section 3.3 for the differential cross section, or, in the case of inclusive quantities such as the total hadronic cross section, by taking the imaginary part of the forward scattering amplitude. In this approach, IR divergences that might appear in individual Feynman diagrams are always a consequence of loop integrals. Furthermore, one never has to deal with squaring matrix elements. We

exploit this fact in appendix A, and analytically compute the delta-function coefficient by simply imposing that the differential cross section integrated across the whole spectrum reproduces the total hadronic cross section.

3.1 Born cross section and $\mathcal{O}(\alpha_s^0)$ distribution

It is customary to present event-shape distributions normalized to the Born cross section, which is defined as the cross section for massless quarks at tree-level in four dimensions. The Born cross section is different for vector and and axial-vector currents: the former gets contributions from both photon and Z-boson exchange, while the letter is mediated by the Z boson only. Taking into account the finite width Γ_Z of the Z boson, one obtains

$$\sigma_0^V = \frac{N_c}{3}\frac{4\pi\alpha_{\text{em}}^2}{Q^2}\left[Q_q^2 + \frac{v_f^2(v_e^2+a_e^2)}{(1-\hat{m}_Z^2)^2+\left(\frac{\Gamma_Z}{m_Z}\right)^2} + \frac{2\,Q_q v_e v_q(1-\hat{m}_Z^2)}{(1-\hat{m}_Z^2)^2+\left(\frac{\Gamma_Z}{m_Z}\right)^2}\right], \tag{3.1}$$
$$\sigma_0^A = \frac{N_c}{3}\frac{4\pi\alpha_{\text{em}}^2}{Q^2}\left[\frac{a_q^2(v_e^2+a_e^2)}{(1-\hat{m}_Z^2)^2+\left(\frac{\Gamma_Z}{m_Z}\right)^2}\right],$$

with α_{em} the electromagnetic coupling, $\hat{m}_Z = m_Z/Q$ the reduced Z-boson mass, Q_q the quark electric charge, N_c the number of colors, and v_e and a_e (v_q and a_q) the electron (quark) vector and axial-vector couplings to the Z boson. Here and in what follows, the leptonic trace is always computed in four dimensions. This poses no problem since we are taking the electroweak interactions at leading order only. For non-zero quark masses, the normalized tree-level cross section is different for vector and axial-vector currents:

$$\frac{\sigma_{0,m}^V}{\sigma_0^V} \equiv R_0^V(\hat{m}) = \frac{(3-v^2)\,v}{2}\,, \qquad \frac{\sigma_{0,m}^A}{\sigma_0^A} \equiv R_0^A(\hat{m}) = v^3\,, \tag{3.2}$$

with $v = \sqrt{1-4\hat{m}^2}$ the velocity of the on-shell massive quarks in the center of mass frame. The functions R_0^V and R_0^A are shown graphically as a function of $\hat{m}$ in figure 4(a). In the massless limit $R_0^C(v=1) = 1$, while both vanish at threshold ($v \to 0$). At $\mathcal{O}(\alpha_s^0)$ the differential cross section is obviously

$$\frac{1}{\sigma_0^C}\frac{\mathrm{d}\sigma_0}{\mathrm{d}e} = R_0^C(\hat{m})\,\delta(e-e_{\text{min}})\,, \tag{3.3}$$

with $C = V, A$ for vector and axial-vector currents, respectively, and e_{min} the minimal value the event shape can take.

3.2 Phase space and kinematic variables

In this section we introduce some notation and write down the 2- and 3-body phase space in $d = 4-2\varepsilon$ dimensions in terms of kinematic variables that facilitate our computation. All masses appearing in this article are understood in the pole scheme. The phase space for n particles in $d = 4-2\varepsilon$ dimensions is defined as

$$\int \mathrm{d}\Phi_n = (2\pi)^d \int\left(\prod_{i=1}^n \frac{\mathrm{d}^{d-1}\vec{p}_i}{2E_i(2\pi)^{d-1}}\right)\delta^{(d)}\left(P^\mu - \sum_{i=1}^n p_i^\mu\right), \tag{3.4}$$

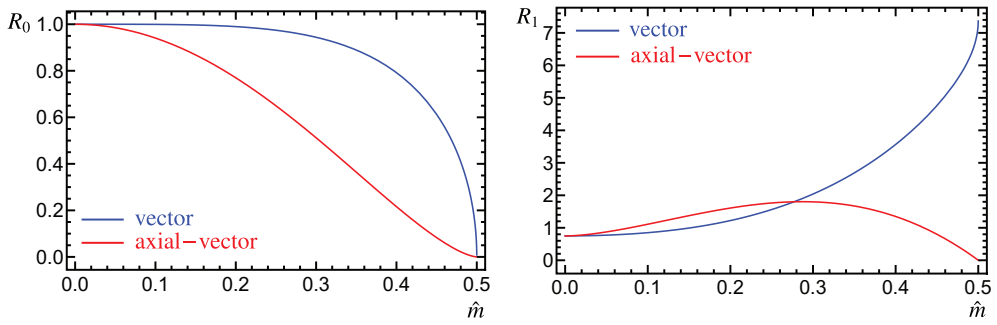

(a) (b)

Figure 4. Massive total hadronic cross section for vector (blue) and axial-vector (red) currents, at tree-level in panel (a) and one loop in panel (b).

with $E_i = \sqrt{|\vec{p}_i|^2 + m_i^2}$, since the particles are on-shell. Let us start with the 2-body phase space for particles with the same mass m:

$$\Phi_2 = (1 - 4\hat{m}^2)^{\frac{1}{2}-\varepsilon}\, \Phi_2^{m=0}\,, \qquad \Phi_2^{m=0} = \frac{\Gamma(1-\varepsilon)}{2\,\Gamma(2-2\varepsilon)} \frac{Q^{-2\varepsilon}}{(4\pi)^{1-\varepsilon}}\,, \tag{3.5}$$

where, for convenience, we have factored out the d-dimensional 2-body phase space for massless particles. For three particles, with particle 1 (quark) and 2 (anti-quark) having the same mass m, while particle 3 (gluon) is massless, and adding the flux factor one obtains

$$\begin{aligned} \frac{\tilde{\mu}^{2\varepsilon}}{2Q^2} P(Q,\varepsilon) \int \mathrm{d}\Phi_3 = \frac{\left(\frac{4\pi\tilde{\mu}^2}{Q^2}\right)^{\varepsilon}}{256\pi^3\Gamma(1-\varepsilon)} \int \mathrm{d}x_1\, \mathrm{d}x_2 \Big\{ (1-x_1)(1-x_2)(x_1+x_2-1) \\ - \hat{m}^2 (2-x_1-x_2)^2 \Big\}^{-\varepsilon}\,, \\ P(Q,\varepsilon) \equiv \frac{\Phi_2^{m=0}|_{\varepsilon\to 0}}{\Phi_2^{m=0}}\,, \end{aligned} \tag{3.6}$$

with $x_i = 2\,E_i/Q$, and E_i the energy of the i-th particle such that energy conservation implies $x_1 + x_2 + x_3 = 2$. For convenience we have multiplied by the ratio of the $d = 4$ and $d = 4 - 2\varepsilon$ massless 2-body phase-space factors. This helps taking the $\varepsilon \to 0$ limit after canceling the IR divergences. Next we implement the following variable transformation: $x_1 = 1 - (1-z)\,y$, $x_2 = 1 - z\,y$, such that $y = 2E_g/Q$, which makes the soft limit $y \to 0$ manifest:

$$\frac{\tilde{\mu}^{2\varepsilon}}{2Q^2} P(Q,\varepsilon) \int \mathrm{d}\Phi_3 = \frac{\left(\frac{4\pi\tilde{\mu}^2}{Q^2}\right)^{\varepsilon}}{256\pi^3\Gamma(1-\varepsilon)} \int \mathrm{d}y\, \mathrm{d}z\, y^{1-2\varepsilon} \left[\, z(1-z)(1-y) - \hat{m}^2 \,\right]^{-\varepsilon}. \tag{3.7}$$

This result shows how collinear singularities, that would be located at $z = 0, 1$ for massless particles, are screened by the finite quark mass. In these coordinates the Dalitz region is

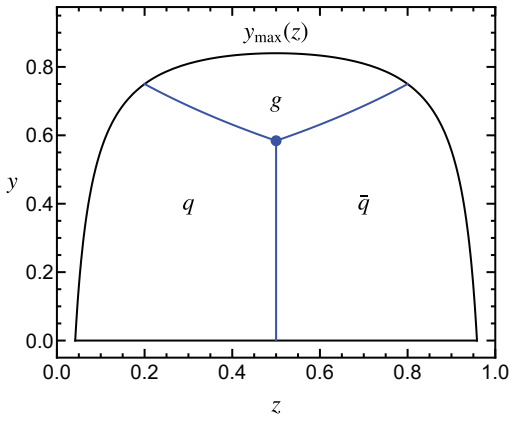

Figure 5. Phase space diagram in (z, y) coordinates for two particles with equal mass (quark and anti-quark) and a massless particle (gluon). The plot is generated with the numerical value $m/Q = 0.2$. The available phase space is contained between the $y = 0$ and $y = y_{\max}(z)$ curves, which intersect at the points $(z = z_{\pm}, y = 0)$. Blue lines split the phase space into regions where the thrust axis points into the direction of the quark, anti-quark or gluon momenta. The three lines meet at the point $(1/2, y_{\text{middle}})$, marked by a blue dot.

parametrized as

$$0 \leq y \leq y_{\max}(z) \equiv 1 - \frac{\hat{m}^2}{z(1-z)}\,, \qquad z_- \leq z \leq z_+\,, \tag{3.8}$$
$$z_\pm \equiv \frac{1 \pm v}{2}\,.$$

In figure 5 we show the phase-space boundaries for the numerical value $\hat{m} = 0.2$. The phase-space limits in the z variable satisfy $z_+ z_- = \hat{m}^2$ and $z_+ + z_- = 1$, while the upper limit in the y variable has its maximum at $y_{\max}(1/2) = v^2$. Another useful relation is given by $(z - z_-)(z_+ - z) = z(1-z) - \hat{m}^2$, a positive quantity inside the Dalitz region. In the massless limit the Dalitz plot is simply a square: $0 \leq y \leq 1$, $|z| \leq 1$. The phase space (as well as all matrix elements and event-shape measurement functions) are invariant under the change $z \to 1 - z$ (mirror symmetry with respect to the $z = 1/2$ vertical line), since all results remain the same when exchanging quark and anti-quark.

For later use, it is convenient to split the 3-body phase space into regions where the thrust axis points into the direction of the quark, anti-quark or gluon momenta. To that end we define

$$y_\tau(\hat{m}, z) = \frac{\sqrt{1 - 4\hat{m}^2(1-z^2)} - z}{1 - z^2}\,, \tag{3.9}$$

such that these three regions are given by

$$\begin{aligned}
&0 \leq z \leq \frac{1}{2}\,, && 0 \leq y \leq y_\tau(\hat{m}, z), && \text{quark}\,,\\
&\frac{1}{2} \leq z \leq 1\,, && 0 \leq y \leq y_\tau(\hat{m}, 1-z), && \text{anti-quark}\,,\\
&0 \leq z \leq 1\,, && \max\left[\, y_\tau(\hat{m}, z), y_\tau(\hat{m}, 1-z)\,\right] \leq y \leq y_{\max}(z), && \text{gluon}\,,
\end{aligned} \tag{3.10}$$

and the lines separating the three regions meet at the point $y_{\text{middle}} = 4\big(\sqrt{1-3\hat{m}^2}-1/2\big)/3$, $z = 1/2$. The quark [anti-quark] boundary meets the phase-space boundary at $z = \hat{m}$ [$z = 1-\hat{m}$], $y = (1-2\hat{m})/(1-\hat{m})$.

The value of any event-shape variable for events with three particles in the final state (two quarks and a gluon) can be expressed as a function of the reduced mass $\hat{m}$ and the z and y phase-space variables. This function, which is not always smooth or continuous, will be referred to as the measurement function $\hat{e}(y,z)$ (for simplicity we will omit its mass dependence). Massive event-shape measurement functions $\hat{e}(z,y)$ take their minimal value if $y = 0$, regardless of the value of z, i.e. $\hat{e}(z,0) = e_{\min}$, and in the soft limit $y \to 0$ the measurement function can be expanded as follows:[6]

$$\hat{e}(z,y) = e_{\min} + y f_e(z) + \mathcal{O}(y^2) \equiv \bar{e}(y,z) + \mathcal{O}(y^2)\,, \tag{3.12}$$

where we have defined the soft event-shape variable $\bar{e}$ associated to e,[7] with measurement function $\bar{e}(y,z) = e_{\min} + y f_e(z)$. The soft event shape has the same minimal value $\bar{e}_{\min} = e_{\min}$ as the original one, but has a different maximal value, generally larger, that is attained at the highest point of the Dalitz plot, $(z,y) = (1/2, v^2)$, as can be seen in figure 6:

$$\bar{e}_{\max} = e_{\min} + v^2 f_e(1/2)\,. \tag{3.13}$$

3.3 Direct computation of $\mathcal{O}(\alpha_s)$ results

In this approach we directly compute the differential distribution adding up real- and virtual-radiation diagrams. Our computation reproduces the few known results (either analytic or numeric), but is more general. In this approach for carrying out the calculation we explicitly show how IR singularities cancel in the sum for IR safe observables already at the differential level. We regulate them using $d = 4-2\varepsilon$ dimensions (dimreg) and use plus-distribution identities to keep the computations as general and simple as possible. We have also written the 3-body phase space in a way in which IR singularities look as close as possible to UV ones.

3.3.1 Virtual radiation

We start with the virtual radiation diagrams, which at this order have only two particles in the final state and are common to all event shapes. The contribution to the differential cross section at $\mathcal{O}(\alpha_s)$ comes from the interference of the tree-level and one-loop diagrams (which have IR divergences treated in dimensional regularization), and since momenta

[6] We consider only the usual case of event shapes linearly sensitive to soft momentum, that is with $f_e(z) \neq 0$. For event shapes with quadratic (or higher) sensitivity to soft momenta, that is with

$$\left.\frac{\mathrm{d}^n \hat{e}(y,z)}{\mathrm{d}y^n}\right|_{y=0} \neq 0\,, \tag{3.11}$$

only for some $n > 1$, one finds that the differential distribution contains up to the $(n-1)$-th derivative of delta and plus distributions. Since those event shapes are scarce and of little interest, we do not show any explicit results for them.

[7] See appendix D for some event-shape specific expressions for $f_e(z)$.

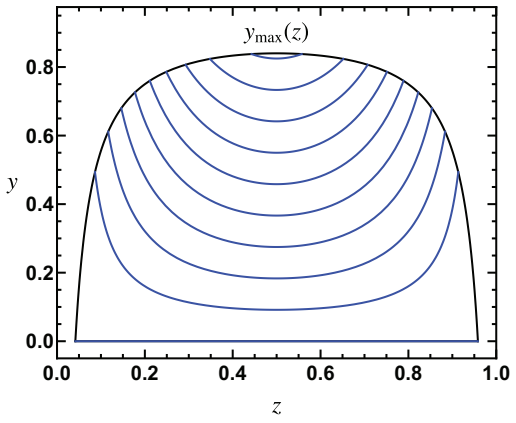

Figure 6. Phase space diagram in (z, y) coordinates (black lines) showing curves with constant value of the C-parameter measurement function in the soft limit $\overline{C}$ (blue lines) with $\hat{m} = 0.2$. The lines correspond to 10 equally spaced values of $\overline{C}$ between 0 and 0.681. For the event shape maximal value $\overline{C}_{\max} = v^2 f_C(1/2)$, the corresponding contour line intersects with the phase space boundary at one point only, the maximum $(1/2, v^2)$.

are fully constrained by energy-momentum conservation, it only contributes to the delta-function coefficient. The general form of the vector and axial-vector massive form factors up to one loop take the form[8]

$$V^\mu = \left[1 + C_F \frac{\alpha_s}{\pi} A(\hat{m})\right] \gamma^\mu + C_F \frac{\alpha_s}{\pi} \frac{B(\hat{m})}{2m} (p_1 - p_2)^\mu \,, \tag{3.14}$$
$$A^\mu = \left[1 + C_F \frac{\alpha_s}{\pi} C(\hat{m})\right] \gamma^\mu \gamma_5 + C_F \frac{\alpha_s}{\pi} \frac{D(\hat{m})}{2m} \gamma_5 \, q^\mu \,,$$

with $q = p_1 + p_2$ the photon or Z-boson momentum, and p_i the quark and anti-quark momenta. The vector form factor satisfies the Ward identity $q_\mu V^\mu = 0$, while the longitudinal part of the axial form factor does not contribute to the cross section. Their real parts take the form [69, 70]

$$\begin{aligned}
\mathrm{Re}[C(\hat{m})] &= \mathrm{Re}[A(\hat{m})] + \frac{4\hat{m}^2}{v} L_v \,, \\
\mathrm{Re}[D(\hat{m})] &= 2\,\hat{m}^2 \left[1 - \frac{2 + v^2}{v} L_v\right], \\
\mathrm{Re}[B(\hat{m})] &= \frac{2\,\hat{m}^2}{v} L_v \,, \\
\mathrm{Re}[A(\hat{m})] &= \left(\frac{1 + v^2}{2v} L_v - \frac{1}{2}\right) \left[\frac{1}{\varepsilon} - 2 \log\left(\frac{m}{\mu}\right)\right] + A_{\mathrm{reg}}(\hat{m}) \,, \\
A_{\mathrm{reg}}(\hat{m}) &= \frac{3}{2}\, v\, L_v - 1 + \frac{1 + v^2}{4v} \left[\pi^2 - 2L_v^2 - 2\,\mathrm{Li}_2\left(\frac{2v}{1 + v}\right)\right],
\end{aligned} \tag{3.15}$$

[8] Here we already include the wave-function renormalization in the OS scheme Z_q^{OS} and the term coming from pole mass renormalization.

with

$$L_v \equiv \log\left(\frac{1+v}{2\hat{m}}\right). \tag{3.16}$$

IR singularities look the same for both currents, and are fully contained in the transverse form factors A and C (note that due to current conservation the form factors are UV finite, and therefore all singularities left after carrying out the QCD renormalization program are IR). The results are singular in the $\hat{m} \to 0$ limit since collinear singularities are regulated by the finite quark mass. Furthermore in this limit the longitudinal form factors B and D vanish, and the transverse form factors become identical for the two currents.

The form factor contribution at $\mathcal{O}(\alpha_s)$ is

$$\begin{aligned}
\frac{1}{\sigma_0^C}\frac{\mathrm{d}\sigma^V_{2,\mathrm{virt}}}{\mathrm{d}e} &= \frac{\alpha_s}{\pi} C_F R_C^{\mathrm{virt}}(\hat{m})\,\delta(e-e_{\min})\,, \qquad (3.17)\\
R_V^{\mathrm{virt}}(\hat{m}) &= P(Q,\varepsilon)\,v^{1-2\varepsilon}\Big\{2\,\mathrm{Re}[A(\hat{m})](1+2\hat{m}^2-\varepsilon) - v^2\mathrm{Re}[B(\hat{m})]\Big\}\\
&= P(Q,\varepsilon)v\Big\{(3-v^2)\mathrm{Re}[A] - [1+2\log(v)]\left(\frac{1+v^2}{v}L_v - 1\right) - v^2\,\mathrm{Re}[B] + \mathcal{O}(\varepsilon)\Big\},\\
R_A^{\mathrm{virt}}(\hat{m}) &= 2\,P(Q,\varepsilon)v^{3-2\varepsilon}(1-\varepsilon)\,\mathrm{Re}[C(\hat{m})]\\
&= 2\,P(Q,\varepsilon)v^3\left\{\mathrm{Re}[C] - [1+2\log(v)]\left(\frac{1+v^2}{v}L_v - \frac{1}{2}\right) + \mathcal{O}(\varepsilon)\right\}.
\end{aligned}$$

When adding these results to the real radiation contributions the $1/\varepsilon$ term present in the A and C form factors cancel, along with the associated μ dependence.

3.3.2 Real radiation

Real radiation diagrams exhibit IR singularities in phase-space integrals, originating from the zero gluon-momentum limit. The matrix element squared, summed over the polarization of final-state particles and averaged over the lepton spins can be written as

$$\begin{aligned}
\frac{|\sum_{\mathrm{spin}}\mathcal{M}_C|^2}{4\sigma_0^C} &= \frac{256\pi^2\alpha_s\tilde{\mu}^{2\varepsilon}C_F}{y^2}M_C(y,z,\hat{m},\varepsilon)\,, \qquad (3.18)\\
M_C(y,z,\hat{m},\varepsilon) &= M_C^0(z,\hat{m}) + \varepsilon M_C^1(z,\hat{m}) + yM_C^{\mathrm{hard}}(y,z) + \mathcal{O}(\varepsilon^2)\,,\\
M_V^0(z,\hat{m}) &= -(1+2\hat{m}^2)M_V^1(z,\hat{m})\,, \quad M_V^1(z,\hat{m}) = -\frac{(1-z)z-\hat{m}^2}{(1-z)^2z^2}\,,\\
M_A^0(z,\hat{m}) &= -M_A^1(z,\hat{m}) = -v^2M_V^1(z,\hat{m})\,,
\end{aligned}$$

with $C = V, A$ labeling the current type and $\mu^2 \equiv 4\pi\tilde{\mu}^2\mathrm{e}^{-\gamma_E}$. We denote the pieces which vanish for $y \to 0$ as the "hard matrix elements" M_C^{hard}. Our results agree with those in refs. [71–73] (note that there is a known sign error in ref. [71]). The hard matrix elements can be further split as $M_C^{\mathrm{hard}}(y,z,\hat{m}) = M_C^2(z,\hat{m}) + yM_C^3(z,\hat{m})$, with

$$\begin{aligned}
M_C^2(z,\hat{m}) &= -\begin{pmatrix}1+2\hat{m}^2\\ v^2\end{pmatrix}\frac{1}{z(1-z)}\,, \qquad (3.19)\\
M_C^3(z,\hat{m}) &= \frac{1}{2z(1-z)}\begin{pmatrix}1\\ 1+2\hat{m}^2\end{pmatrix} - 1\,,
\end{aligned}$$

with the upper (lower) part of the expression in parentheses belonging to the vector (axial-vector) current. The radiative one-loop contribution to the differential distribution, partially expanded around $\varepsilon = 0$, reads

$$\begin{aligned}
&\frac{1}{\sigma_0^C}\frac{\mathrm{d}\sigma_C^{\mathrm{real}}}{\mathrm{d}e} = \qquad (3.20)\\
&\quad P(Q,\varepsilon)C_F\frac{\alpha_s}{\pi}\frac{\left(\frac{4\pi\tilde{\mu}^2}{Q^2}\right)^{\varepsilon}}{\Gamma(1-\varepsilon)}\int\frac{\mathrm{d}y\,\mathrm{d}z}{y^{1+2\varepsilon}}\left[\,z(1-z)(1-y)-\hat{m}^2\,\right]^{-\varepsilon}\delta[e-\hat{e}(y,z)]\,M_C(y,z,\hat{m},\varepsilon)\\
&= P(Q,\varepsilon)C_F\frac{\alpha_s}{\pi}\Bigg\{-\frac{\delta(e-e_{\min})}{2}\int\mathrm{d}z\left[M_C^1(z,\hat{m})+M_C^0(z,\hat{m})\left(\frac{1}{\varepsilon}+2\log\left(\frac{\mu}{Q}\right)\right.\right.\\
&\quad\left.\left.-\log\left[z(1-z)-\hat{m}^2\right]\right)\right]+\int\mathrm{d}z\,\mathrm{d}y\left[M_C^0(z,\hat{m})\left[\frac{1}{y}\right]_+ + M_C^{\mathrm{hard}}(y,z)\right]\delta[e-\hat{e}(y,z)]\Bigg\}.
\end{aligned}$$

To get to the second line we have collected powers in y and used the identity

$$y^{-1-2\varepsilon} = -\frac{1}{2\varepsilon}\delta(y)+\left[\frac{1}{y}\right]_+ + \mathcal{O}(\varepsilon)\,, \qquad (3.21)$$

in the terms containing $M_C^{0,1}$. The coefficient of the Dirac delta function is not yet fully explicit, as the integral over the plus function still hides singular terms. The distributional structure is completely determined in the $y \to 0$ limit, therefore we add and subtract the following term to the last integrand

$$M_C^0(z,\hat{m})\left[\frac{1}{y}\right]_+\delta[e-\bar{e}(y,z)]\,, \qquad (3.22)$$

such that in the sum of the original and subtracted terms the plus prescription can be dropped (this can be done because the integrand goes to zero linearly with y). This strategy is similar to subtraction algorithms used in NLO and NNLO parton-level Monte Carlos to achieve cancellation of IR singularities between real- and virtual-radiation contributions. In our case, the subtraction helps isolating the distributional structure of the cross section. For the added term we proceed as follows

$$\begin{aligned}
&\int\mathrm{d}z\,\mathrm{d}y\,M_C^0(z,\hat{m})\left[\frac{1}{y}\right]_+\delta[e-\bar{e}(y,z)]\,\Theta[y_{\max}(z)-y] =\\
&\int\mathrm{d}z\,\frac{M_C^0(z,\hat{m})}{f_e(z)}\left[\frac{f_e(z)}{e-e_{\min}}\right]_+\Theta\big[y_{\max}(z)-h(e,z)\big] = \qquad (3.23)\\
&-\delta(e-e_{\min})\int\mathrm{d}z\,M_C^0(z,\hat{m})\log[f_e(z)]+\left[\frac{1}{e-e_{\min}}\right]_+\int\mathrm{d}z\,M_C^0(z,\hat{m})\,\Theta\big[y_{\max}(z)-h(e,z)\big]\,,
\end{aligned}$$

with

$$h(e,z)\equiv\frac{e-e_{\min}}{f_e(z)}\,, \qquad (3.24)$$

representing a curve in phase space defined by the condition $\bar{e}(y,z)=e$ (that is, a contour line with constant value of the soft event-shape measurement function). This line has the important property of always intersecting with the phase-space boundary $y_{\max}$ at two

symmetric points, which will be denoted by $z_\pm(e)$, as shown in figure 7 for the C-parameter event shape. To get to the last line of eq. (3.23) we have used the rescaling identity

$$\left[\frac{\log^n(bx)}{bx}\right]_+ = \frac{1}{b}\left\{\frac{\log^{n+1}(b)}{n+1}\,\delta(x) + \sum_{i=0}^{n}\binom{n}{i}\log^{n-i}(b)\left[\frac{\log^n(x)}{x}\right]_+\right\}, \tag{3.25}$$

and the fact that if $e = e_{\min}$ then $h(e_{\min}, z) = 0$ and the constraint imposed by the Heaviside function $\Theta[y_{\max}(z)]$ is automatically satisfied [since $y_{\max}(z) > 0$ for $z_- \le z \le z_+$]. The second term in the last line of eq. (3.23) is not a pure distribution yet, but can be converted to such using the relation

$$f(x)\left[\frac{1}{x}\right]_+ = f(0)\left[\frac{1}{x}\right]_+ + \frac{f(x)-f(0)}{x}\,. \tag{3.26}$$

Finally we arrive at

$$\begin{aligned}\int \mathrm{d}z\,\mathrm{d}y\, M_C^0(z,\hat{m})\left[\frac{1}{y}\right]_+\delta[e-\bar{e}(y,z)] &= -\delta(e-e_{\min})\int \mathrm{d}z\, M_C^0(z,\hat{m})\log[f_e(z)] \\ &+ \left[\frac{1}{e-e_{\min}}\right]_+\int \mathrm{d}z\, M_C^0(z,\hat{m}) - \int \mathrm{d}z\, M_C^0(z,\hat{m})\,\frac{\Theta[e-e_{\min}-y_{\max}(z)f_e(z)]}{e-e_{\min}}\,,\end{aligned} \tag{3.27}$$

where we have used the identity $\Theta(x) + \Theta(-x) = 1$ in the last term. The Heaviside theta function in the last integral requires $h(e,z) > y_{\max}(z)$, and therefore restricts the z integration to the two disconnected segments shown in figure 7 as purple double-pointed arrows: $z_- \le z \le z_-(e)$ and $z_+(e) \le z \le z_+$, where $z_\pm(e)$ are the two solutions of the equation $e = \bar{e}[z, y_{\max}(z)]$ that lay on the original integration path $z_- \le z \le z_+$. The points $z_\pm(e)$ depend on e and fulfill $z_- < z_-(e) < z_+(e) < z_+$, since $f_e(z)$ is positive (given that by definition $e \ge e_{\min}$). It is useful to write the Heaviside theta in the last term as an integral over a Dirac delta function:

$$\frac{\Theta[e-e_{\min}-y_{\max}(z)f_e(z)]}{e-e_{\min}} = \int \mathrm{d}y\,\frac{\Theta[y-y_{\max}(z)]}{y}\,\delta[e-e_{\min}-yf_e(z)]\,. \tag{3.28}$$

These results provide the contribution of the real-radiation diagrams to the differential cross section shown in eq. (1.1):

$$A_e(\hat{m}) = A_e^{\mathrm{real}}(\hat{m}) + R_C^{\mathrm{virt}}(\hat{m})\,, \tag{3.29}$$

$$A_e^{\mathrm{real}}(\hat{m}) = -\frac{P(Q,\varepsilon)}{2}\int \mathrm{d}z\left\{M_C^1(z,\hat{m}) + M_C^0(z,\hat{m})\left[\frac{1}{\varepsilon} + 2\log\left(\frac{\mu}{Q}\right) - \log\left(\frac{z(1-z)-\hat{m}^2}{[f_e(z)]^2}\right)\right]\right\},$$

$$B_{\mathrm{plus}}(\hat{m}) = \int \mathrm{d}z\, M_C^0(z,\hat{m})\,,$$

$$\begin{aligned}F^{\mathrm{NS}} = \int \mathrm{d}z\,\mathrm{d}y\,\Bigg\{&M_C^{\mathrm{hard}}(y,z)\delta[e-\hat{e}(y,z)] + \frac{M_C^0(z,\hat{m})}{y}\Big[\delta[e-\hat{e}(y,z)] \\ &- \Theta[y-y_{\max}(z)]\,\delta[e-\bar{e}(y,z)] - \delta[e-\bar{e}(y,z)]\Big]\Bigg\} \equiv F^{\mathrm{NS}}_{\mathrm{hard}} + F^{\mathrm{NS}}_{\mathrm{soft}}\,.\end{aligned}$$

In F^{NS} (which can only be computed analytically for some simple event shapes), in those terms where no explicit Heaviside function is shown, a $\Theta[y_{\max}(z) - y]$ is understood. $F^{\mathrm{NS}}_{\mathrm{hard}}$

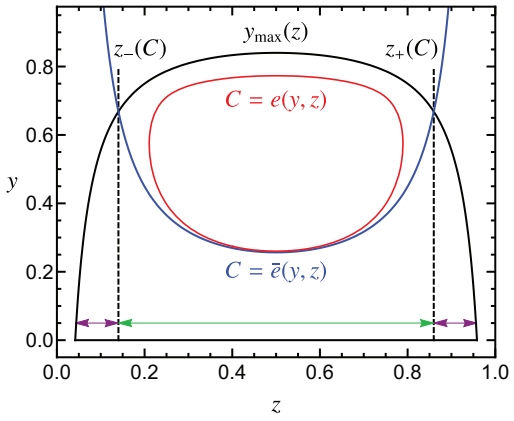

Figure 7. Phase space diagram in (z, y) coordinates (black solid lines) showing a curve with constant value of the C-parameter event shape measurement function (red line) and its soft limit (blue line), using $\hat{m} = 0.2$, $C = 0.42$. The latter corresponds to eq. (3.24), which cuts the phase-space boundary at the points $z_\pm(C)$. The dashed lines divide the $y = 0$ axis into three segments, marked with double-pointed arrows.

and $F^{\rm NS}_{\rm soft}$ correspond to the terms containing $M^{\rm hard}_C$ and M^0_C, respectively. This intermediate result already shows that the coefficient of the plus distribution is identical for all event shapes linearly sensitive to soft momentum. The non-singular term contains no distributions, and there is no singularity in the integration domain: the hard function tends linearly to zero for $y \to 0$, while the soft term contains one piece which is the difference of two delta functions with the same $y \to 0$ limit (therefore again going linearly to zero in the soft limit), and a theta function such that small values of y are left out.

3.3.3 Final result for the direct computation

We first give an analytic expression for the $B_{\rm plus}$ coefficient in eq. (3.29). The z integration is carried out using the first line in eq. (B.3), yielding

$$B_{\rm plus}(\hat{m}) = \begin{pmatrix} 3 - v^2 \\ 2\,v^2 \end{pmatrix} \left[(1 + v^2) L_v - v \right] , \tag{3.30}$$

where again the first and second line of the expression in big parentheses correspond to vector and axial-vector currents, respectively. The result exhibits a log-type singularity for $m \to 0$, since in that limit the log-plus distribution associated to collinear singularities is no longer screened by the heavy quark mass.

To obtain the coefficient of the delta term we need to perform two integrals analytically, which are given in eq. (B.3). Adding the results in eqs. (3.17) and (3.29) we cancel the $1/\varepsilon$ singularity along with the μ dependence. Therefore taking the limit $\varepsilon \to 0$ amounts to

setting $P(Q,\varepsilon)\to 1$, and we get

$$\begin{aligned}
A_e^V(\hat{m}) &= (1+2\hat{m}^2)\Big\{(1-2\hat{m}^2)\Big[\mathrm{Li}_2\Big(-\frac{v(1+v)}{2\hat{m}^2}\Big)-3\,\mathrm{Li}_2\Big(\frac{v(1-v)}{2\hat{m}^2}\Big)+2\log^2(\hat{m})+\pi^2\\
&\quad -2\log^2\Big(\frac{1+v}{2}\Big)\Big]+2v\big[\log(\hat{m})-1\big]-2I_e(\hat{m})\Big\}+(4+v^2-16\hat{m}^4)L_v\,,\\
A_e^A(\hat{m}) &= v^2\Big\{(4+v^2)L_v+2v\big[\log(\hat{m})-1\big]-2I_e(\hat{m})+(1-2\hat{m}^2)\\
&\quad \times\Big[\mathrm{Li}_2\Big(-\frac{v(1+v)}{2\hat{m}^2}\Big)-3\,\mathrm{Li}_2\Big(\frac{v(1-v)}{2\hat{m}^2}\Big)+\pi^2+2\log^2(\hat{m})-2\log^2\Big(\frac{1+v}{2}\Big)\Big]\Big\},
\end{aligned}\tag{3.31}$$

where the only event shape dependent piece is the integral

$$I_e(\hat{m})=\frac{1}{2}\int_{z_-}^{z_+}\mathrm{d}z\,\frac{(1-z)z-\hat{m}^2}{(1-z)^2z^2}\log[f_e(z)]=\int_{z_-}^{1/2}\mathrm{d}z\,\frac{(1-z)z-\hat{m}^2}{(1-z)^2z^2}\log[f_e(z)]\,,\tag{3.32}$$

where we have used the $z\leftrightarrow(1-z)$ symmetry to simplify the integration range.

4 Numerical algorithms

Before we describe the algorithms to compute the differential and cumulative event-shape cross sections, we show how to write down the four-momenta of the three-particle phase space in terms of the (z,y) coordinates. This is very useful to figure out an analytic expression for the event-shape measurement function. These expressions can in turn be used to compute the values of $e_{\min}$ and $e_{\max}$, and can be expanded around $y=0$ to obtain $f_e(z)$. Since we are not dealing with oriented event shapes, without any loss of generality we can choose the three particles contained in the $x-y$ plane, with the gluon 3-momenta pointing into the positive z direction. With the notation $p=[E,\vec{p}]=[E,p_x,p_y,p_z]$ one has:[9]

$$\begin{aligned}
p_g &= \frac{y}{2}\,[1,0,0,1]\,,\\
p_q &= \left[\frac{1-y(1-z)}{2},0,\sqrt{(1-y)(1-z)z-\hat{m}^2},\frac{1-y(1-z)-2z}{2}\right],\\
p_{\bar{q}} &= \left[\frac{1-yz}{2},0,-\sqrt{(1-y)(1-z)z-\hat{m}^2},\frac{2z-1-y\,z}{2}\right].
\end{aligned}\tag{4.1}$$

The magnitude of the (anti-)quark three-momentum reads

$$|\vec{p}_{\bar{q}}|=\frac{1}{2}\sqrt{(1-y\,z)^2-4\hat{m}^2}\,,\qquad |\vec{p}_q|=|\vec{p}_{\bar{q}}|_{z\to 1-z}\,,\tag{4.2}$$

such that E-scheme 4-momenta are obtained by multiplying the spatial components in eq. (4.1) by $E/|\vec{p}|$, while P-scheme 4-momenta require replacing the temporal component by $|\vec{p}|$, see section 2. The thrust axis is simply $\hat{z}$ when pointing in the gluon direction [see eq. (3.10)], while it equals $\vec{p}_q/|\vec{p}_q|$ and $\vec{p}_{\bar{q}}/|\vec{p}_{\bar{q}}|$ when pointing to the quark and anti-quark direction, respectively.

[9] One can generate vectors with non-zero x component by taking vector products, e.g. when computing jet broadening.

Since to compute the radiative tails of the distributions (either differential or cumulative) and the moments of the differential distributions one only needs the real radiation contribution, in this section we adopt the shorthand notation

$$M_C(y,z) \equiv M_C(y,z,\hat{m},\varepsilon=0)\,. \tag{4.3}$$

4.1 Computation of moments

An especially convenient way to compute the n-th moment of the distribution is expressing it in terms of the total hadronic cross section and displaced moments:

$$\langle (e-e_{\rm min})^n\rangle \equiv \frac{1}{\sigma_0^C}\int_{e_{\rm min}}^{e_{\rm max}} {\rm d}e\,(e-e_{\rm min})^n \frac{{\rm d}\sigma}{{\rm d}e}\,, \qquad \langle (e-e_{\rm min})^0\rangle = R(\hat{m})\,. \tag{4.4}$$

The reduced moments at $\mathcal{O}(\alpha_s)$ and for $n>0$ can be computed directly using a numerical 2D integration, which is convergent due to the insertion of the displaced measurement function

$$\langle (e-e_{\rm min})^n\rangle = C_F\frac{\alpha_s}{\pi}\int {\rm d}y\,{\rm d}z\,[\,\hat{e}(y,z)-e_{\rm min}\,]^n\,\frac{M_C(y,z)}{y} + \mathcal{O}(\alpha_s^2)\,. \tag{4.5}$$

The integration can be carried out with a MC procedure, but it is faster and more efficient to use a deterministic integrator in 2D. For our numerical checks we have used the `dblquad` routine included in the `scipy.integrate` [74] python module. Finally, an efficient way of numerically computing regular moments is

$$\langle e\rangle^n = e_{\rm min}^n\,R(\hat{m}) + C_F\frac{\alpha_s}{\pi}\int {\rm d}y\,{\rm d}z\,[\hat{e}(y,z)^n - e_{\rm min}^n]\,\frac{M_C(y,z)}{y} + \mathcal{O}(\alpha_s^2)\,, \tag{4.6}$$

such that the numerical integral is convergent and can be directly computed in a standard way.

4.2 Computation of cross sections using a MC

Before we describe our novel numerical algorithm to directly compute the differential and cumulative cross sections, we briefly review how this is done using MC methods. The MC can only access the radiative tail of the distribution, and therefore one needs to consider only real radiation diagrams. To obtain the differential distribution one needs to integrate over a Dirac delta function of the event-shape measurement function. Since there is no known way of doing this in the MC approach, one instead bins the distribution, such that the delta gets replaced by the difference of Heaviside functions. More specifically, by integrating first over the event-shape bin we obtain

$$\begin{aligned}\Sigma(e_2)-\Sigma(e_1) = &\int\frac{{\rm d}y\,{\rm d}z}{y}\,{\rm d}e\,\delta[e-\hat{e}(y,z)]M_C(y,z)\,\Theta(e-e_1)\,\Theta(e_2-e) = \\ &\int\frac{{\rm d}y\,{\rm d}z}{y}\,\Theta[\hat{e}(y,z)-e_1]\,\Theta[e_2-\hat{e}(y,z)]M_C(y,z)\,.\end{aligned} \tag{4.7}$$

The advantage of the MC method is that one can compute the binned distribution for all event shapes in a single run. In practice one chooses a set of bins for each event-shape

JHEP03(2020)024

variable ahead of time. In our implementation of the MC algorithm, we match the (y, z) phase space into the unit square with the following change of variables:

$$y = v^2\, t_1\,, \qquad z = \frac{1}{2} + \left(t_2 - \frac{1}{2}\right)\sqrt{1 - \frac{4\hat{m}^2}{1-y}}\,, \tag{4.8}$$
$$\mathrm{d}y\,\mathrm{d}z = v^2\sqrt{1 - \frac{4\hat{m}^2}{1-y}}\,\mathrm{d}t_1\,\mathrm{d}t_2\,.$$

Now eq. (4.7) has a nice interpretation in terms of MC's: a) generate a sample of points in the (t_1, t_2) unit square, compute for each one of them (y, z) and from that get numerical values for all event-shape variables, matrix elements and the Jacobian; b) for each random point and for every event shape, figure out which bin it corresponds to; c) add the numerical values of the matrix element (times Jacobian) for each bin; d) normalize each bin to the total number of points in the random sample. Statistical uncertainties can be obtained in the usual way, and several independent runs can be combined. The method can of course be refined using importance sampling, and in our numerical code we use the python implementation of VEGAS [75]. The advantage of the MC is that a single run can be used to compute the full distribution for all event shapes at once, and even to compute other quantities such as moments of the distribution or the cumulative cross-section.

4.3 Direct computation of the differential cross section

In this section we describe an alternative method which does not have the limitations inherent to a MC (can only compute binned cross sections, and in general one needs to specify the bins ahead of time). The direct method computes directly the (unbinned) differential cross section, and since it only uses "deterministic" integration methods, it can in principle achieve arbitrary precision in very small run-time. The only requirement for the method to be applicable is that one can compute the value of the event shape and its first derivative in terms of the phase-space variables y and z. On the other hand, as compared to the MC method, one needs to compute a numerical integral for each current, each event shape and each point in the spectrum. We denote the radiative tail of the distribution by $F_e(e, \hat{m})$, defined as

$$F_e(e, \hat{m}) \equiv \frac{B_{\text{plus}}(\hat{m})}{e - e_{\min}} + F_e^{\text{NS}}(e, \hat{m})\,. \tag{4.9}$$

Since we can compute F_e numerically with high precision and the values of B_{plus} and $e_{\min}$ are known analytically, F_e^{NS} can be readily obtained. This is the last ingredient for the full description of the $\mathcal{O}(\alpha_s)$ differential cross section. It should be noted that even in the massless limit $F_e(e, 0)$ is not always analytically known (e.g. for angularities or broadening). On the other hand, in the $m \to 1/2$ limit $F_e(e, 1/2) = 0$ and only singular terms survive, which are analytically computed in section 3.

Let us first discuss how to obtain the cross section for a toy model: an event shape whose measurement function coincides with the soft limit of some regular event shape. We proceed by integrating the y variable analytically, followed by a numerical integration of

the z variable. The z integration boundaries are set by $z_\pm(e)$, the intersection of $h(e,z)$ with $y_{\max}(z)$, see figure 7. Therefore we get

$$\frac{1}{\sigma_0^C}\frac{\mathrm{d}\sigma_C}{\mathrm{d}\bar{e}} = C_F\frac{\alpha_s}{\pi}\int \mathrm{d}y\,\mathrm{d}z\,\frac{M_C(y,z)}{y}\,\delta[\bar{e}-e_{\min}-yf_e(z)] \tag{4.10}$$
$$= \frac{C_F}{\bar{e}-e_{\min}}\frac{\alpha_s}{\pi}\int_{z_-(e)}^{z_+(e)}\mathrm{d}z\,M_C\left(\frac{\bar{e}-e_{\min}}{f_e(z)},z\right).$$

To illustrate how the method works for "real" event shapes, let us assume for now that we are dealing with an observable such that contour lines with constant event-shape value (that is, that the curve defined by the condition $\hat{e}(y,z)=e$ for some value of e satisfying $e_{\min}<e<e_{\max}$) is continuous, convex and does not intersect with the phase-space boundary (the method can be adapted for observables not satisfying this criteria, as will be explained later). Every event shape we considered, except for 2-jettiness, C-jettiness and HJM (that intersect with the phase-space boundaries for some values of e), and E-scheme variables other than C-parameter (that are not continuous) satisfy this condition. Curves for all event shapes which use the thrust axis have kinks, but this does not pose a problem for the method. We proceed by integrating y with the Dirac delta function first, while the z integral is performed numerically afterwards. The first step is finding the maximal and minimal value of y in the contour line of constant event-shape value, which we call $y_{\max}(e)$ and $y_{\min}(e)$, respectively. Since the curve is convex and symmetric under $z\to 1-z$, these two values are attained for $z=1/2$. To find them, one has to solve the equation

$$\hat{e}\Big(y,\frac{1}{2}\Big)=e\,, \tag{4.11}$$

which can be done e.g. with the Brent algorithm [76]. In our numerical code we use the function `brentq` from the `scipy.optimize` python module. The two roots are easily found since $y_{\min}$ is between 0 and y_{middle}, while $y_{\max}$ is between y_{middle} and $v=\sqrt{1-4\hat{m}^2}$, with $(0.5, y_{\text{middle}})$ being the point at which the lines that divide the phase space into regions with the thrust axis pointing to the quark, anti-quark, or gluon 3-momentum coincide:[10]

$$y_{\text{middle}}=\frac{4}{3}\left(\sqrt{1-3\hat{m}^2}-\frac{1}{2}\right). \tag{4.12}$$

In the second step we obtain the contour lines of constant e parametrized as two functions of y. This is obtained by solving the equation $\hat{e}(y,z)=e$ for z at a given value of y. There are two solutions to this equation, which we call $z_\pm(e,y)$, but we will numerically obtain only $z_-(e,y)<1/2$, since the other solution can be obtained by symmetry. Again, we employ the Brent algorithm, since we know the solution is always contained between $z=1/2$ and the phase-space boundary $z_-^{\text{border}}(y)$, which as a function of y is written as

$$z_\pm^{\text{border}}(y)=\frac{1}{2}\left(1\pm\sqrt{\frac{1-y-4\hat{m}^2}{1-y}}\right). \tag{4.13}$$

[10] This is the point in phase space at which most event shapes obtain their maximal value $e_{\max}$, or a value very close to it. The algorithm can be slightly refined figuring out ahead of time at which exact value of y $e_{\max}$ is attained.

JHEP03(2020)024

In our numerical code we again use the `brentq` function. Since we compute the distribution solving the Dirac delta function in terms of the variable y, the next step is figuring out the lower integration limit in the z variable, dubbed $z_{\min}(e)$. Since the integrand is symmetric around $z = 1/2$, we will integrate in the range $z = [\, z_{\min}(e), 1/2]$ and double the result. The value of the point with the smallest z value for a given event-shape value e, $[\, z_{\min}(e), y_{\text{center}}(e)\,]$, is obtained numerically as the minimum of the function $z_-(e, y)$. The minimum lies between the values $y_{\max}(e)$ and $y_{\min}(e)$ previously determined, and we use the Brent algorithm implemented in the `minimize_scalar` function from the `scipy.optimize` python module, which finds the minimum in a given interval. The maximum event shape value $e_{\max}$ satisfies $z_{\min}(e_{\max}) = z_{\max}(e_{\max}) = 1/2$. The last ingredient we need to determine before performing the numerical integral in z is the contour line of constant e as a function of z. It is obtained by solving the equation $\hat{e}(y, z) = e$ for y at a given value of z, which has two solutions which we denote by $y_\pm(e, z)$, corresponding to the two zeroes of the Dirac delta function argument when integrating the y variable. The lower and upper solutions are contained in the intervals $[\, y_{\min}(e), y_{\text{center}}(e)\,]$ and $[\, y_{\text{center}}(e), y_{\max}(e)\,]$, respectively, and are easily found numerically, once again employing the Brent algorithm already described. In figure 8 we show graphically the position of $z_{\min,\max}(e)$, $y_{\text{center}}(e)$ and $y_{\min,\max}(e)$, as well as the curves $y_\pm(e, z)$, while figure 9 shows the $z_\pm^{\text{border}}(z)$ and $z_\pm(e, z)$ lines. Putting everything together, the differential distribution can be written as[11]

$$F_e(e, \hat{m}) = \int \mathrm{d}z\, \mathrm{d}y\, \frac{M_C(y, z)}{y}\, \delta[e - \hat{e}(y, z)] = 2 \int_{z_{\min}(e)}^{1/2} \mathrm{d}z \sum_{y = y_\pm(e,z)} \frac{M_C(y, z)}{y \left| \frac{\mathrm{d}\hat{e}(y,z)}{\mathrm{d}y} \right|}\,, \tag{4.15}$$

where the sum in y means that we evaluate the y-dependent expression for both $y = y_\pm(e, z)$ and add the results. The derivative of the event-shape measurement function with respect to y is performed analytically, while the value of $y_\pm(e, z)$ is obtained numerically with the procedure outlined above. Our code computes the numerical integral using the python `quad` function, which is the quadpack [77] package implementation of the `scipy.integrate` module.

We close the section explaining how to modify the algorithm to compute E-scheme thrust, broadening and HJM. The contour lines for these event shapes never intersect with the phase-space boundaries (at most they are tangent to it at a single point), but are not always continuous. It turns out that if $\tau^E < \hat{m}$, $B^E < \hat{m}/2$ or $\rho^E < \hat{m}(1 - 2\hat{m})/(1 - \hat{m})$, the event-shape contour lines are continuous and convex, such that the algorithm described above can be used. For larger values, the lines of constant event-shape value show discontinuities exactly along the lines that delimit the regions with the thrust axis

[11] Note that it is also possible to integrate the delta function in terms of z, leaving a numerical y integral

$$F_e(e, \hat{m}) = 2 \int_{y_{\min}(e)}^{y_{\max}(e)} \mathrm{d}y\, \frac{M_C(y, z)}{y \left| \frac{\mathrm{d}\hat{e}(y,z)}{\mathrm{d}z} \right|} \Bigg|_{z = z_-(e,y)}\,. \tag{4.14}$$

We use this alternative expression to cross check our results. Both implementations agree within 15 digits. We choose to integrate in y first because then a) event shapes with kinks in their curves with constant e value can be treated with the algorithm just described, b) the algorithms for differential and cumulative distributions are very similar.

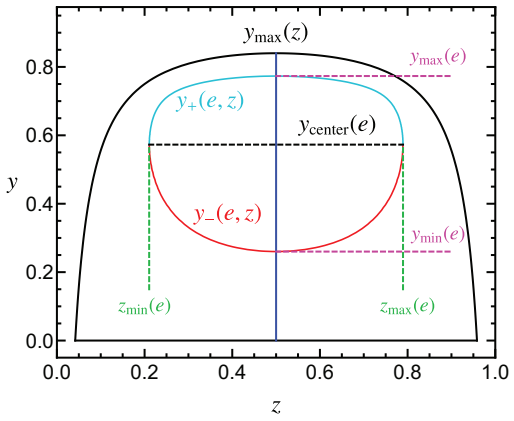

Figure 8. Phase space diagram in (z, y) coordinates (black lines) showing in red and cyan the contour line with constant value of C-parameter, corresponding to the functions $y_+(e, z)$ and $y_-(e, z)$, respectively. The two curves meet at the points $[z_{\min,\max}(e), y_{\text{center}}(e)]$, joined by the black, dashed line. These curves meet the $z = 1/2$ vertical blue line for $y = y_{\min,\max}(e)$, respectively. Dashed magenta [green] lines mark the points of maximal and minimal values that y $[z]$ can take within the red curve. To generate this plot the values $\hat{m} = 0.2$ and $C = 0.42$ were used.

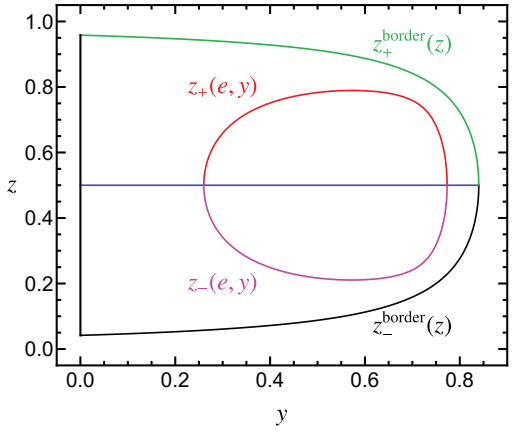

Figure 9. Phase space diagram in (y, z) coordinates depicted as green and black lines, corresponding to the functions $z_+^{\text{border}}(z)$ and $z_-^{\text{border}}(z)$, respectively. The red and magenta lines show a contour line with constant value of C-parameter, corresponding to the functions $z_+(e, y)$ and $z_-(e, y)$, respectively. To generate this plot the numerical values $\hat{m} = 0.2$ and $C = 0.42$ were used.

pointing in the gluon or (anti-)quark direction. Therefore we find it convenient to define event-shape measurement functions in each of the three regions: $\hat{e}_q(y, z)$, $\hat{e}_{\bar{q}}(y, z)$ and $\hat{e}_g(y, z)$. It is clear that one should first determine the intersection points of the contour lines in the quark and gluon regions with $y_\tau(\hat{m}, z)$, defined in eq. (3.10), which we call $z_\pm^q(e)$ and $z_\pm^g(e)$, with $z_+^{q,g}(e) = 1 - z_-^{q,g}$. We find that in all cases $z_-^g(e) > z_-^q(e)$. These points are computed solving the equations $\hat{e}_q[\, y_\tau(\hat{m}, z), z\,] = e$ and $\hat{e}_g[\, y_\tau(\hat{m}, z), z\,] = e$ for

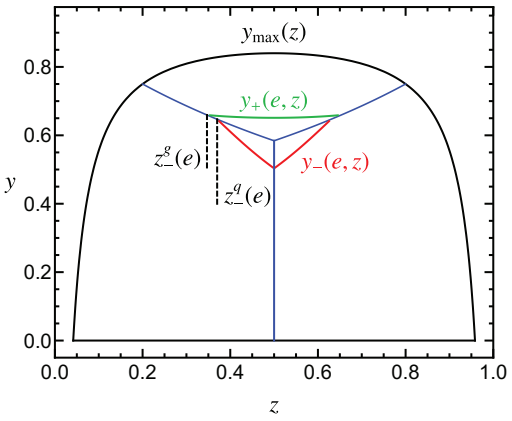

Figure 10. Phase-space diagram in (z, y) coordinates (black curves) split by blue lines into regions in which the thrust axis points in the direction of the quark, anti-quark or gluon momenta. In green and red we show the contour lines for constant value of τ^E corresponding to the functions $y_+(e,z)$ and $y_-(e,z)$, respectively. The two curves do not meet at any point, but intersect with the boundary separating the gluon and quark regions at the points $z_-^q(e)$ and $z_-^g(e)$, marked with dashed black lines. To generate this plot the parameters $\hat{m} = 0.2$ and $\tau^E = 0.27$ were used.

z. In our code we employ the Brent algorithm again, and use that the solutions are to be found in the interval $z \in [\hat{m}, 1/2]$.

For E-scheme thrust and HJM one only needs to compute $y_-(e,z)$ and $y_+(e,z)$, which now coincide with the contours in the quark and gluon regions, respectively. Therefore the equations to solve are $\hat{e}_q(y,z) = e$ and $\hat{e}_g(y,z) = e$, for which we use the Brent algorithm, and use the fact that the solutions have to be contained in the ranges $y \in [\,0, y_\tau(\hat{m},z)\,]$ and $y \in [\,y_\tau(\hat{m},z), y_{\max}(z)\,]$, respectively. In figure 10, for $\tau^E = 0.27$ we show the functions $y_\pm(e,z)$ in red and blue, as well as the points $z_\pm^q(e)$ and $z_\pm^g(e)$ with dashed black lines. The cross section then is computed as

$$F_e(e,\hat{m}) = 2\int_{z_-^q(e)}^{1/2} \mathrm{d}z \left| \frac{M_C(y,z)}{y\,\frac{\mathrm{d}\hat{e}(y,z)}{\mathrm{d}y}} \right|_{y=y_-(e,z)} + 2\int_{z_-^g(e)}^{1/2} \mathrm{d}z \left| \frac{M_C(y,z)}{y\,\frac{\mathrm{d}\hat{e}(y,z)}{\mathrm{d}y}} \right|_{y=y_+(e,z)} . \tag{4.16}$$

The most involved event shape is E-scheme broadening, which requires a specific algorithm. For $B_T^E > \hat{m}/2$ but smaller than a certain critical value $B_T^{E,\mathrm{crit}}$, and for the small range $z \in [\,z_{\min}(e), z_-^q(e)\,]$, there are two solutions to the equation $\hat{e}_q(y,z) = e$, which we call $y_-(e,z)$ and $y_{\mathrm{up}}(e,z)$. The value of $z_{\min}(e)$ is computed using the algorithm already explained for continuous event shapes, and the values of $z_-^{q,g}(e)$ are computed as described in the previous paragraph. In figure 11 we show the functions $y_\pm(e,z)$ and $y_{\mathrm{up}}(e,z)$ in green, red and cyan, respectively. The points $z_{\min}(e)$ and $z_-^{q,g}(e)$ are marked with black, dashed lines. Therefore, while for $B_T > B_T^{E,\mathrm{crit}}$,[12] one simply uses eq. (4.16), if $\hat{m}/2 < B_T^E < B_T^{E,\mathrm{crit}}$

[12]The value of $B_T^{E,\mathrm{crit}}$ is obtained solving $z_{\min}(B_T^{E,\mathrm{crit}}) = z_-^q(B_T^{E,\mathrm{crit}})$. In practice we do not compute it explicitly, but simply use eq. (4.16) if $z_{\min}(e) > z_-^q(e)$.

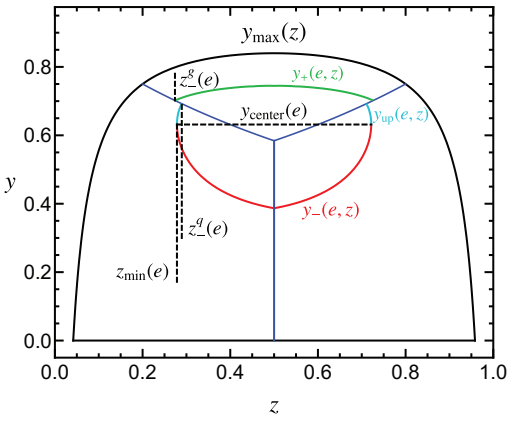

Figure 11. Phase space diagram in (z, y) coordinates (black curves) split by blue lines into regions in which the thrust axis points in the direction of the quark, anti-quark or gluon momenta. In green, cyan and red we show the contour lines for constant value of τ^E corresponding to the functions $y_+(e,z)$, $y_{\text{up}}(e,z)$ and $y_-(e,z)$, respectively. The cyan and green curves do not meet at any point, but intersect with the boundary separating the gluon and quark regions at the points $z_-^q(e)$ and $z_-^g(e)$, marked with dashed black lines. The cyan and red curves meet at the points $[z^q_{\text{min,max}}(e), y_{\text{center}}(e)]$. To generate this plot the values $\hat{m} = 0.2$ and $B_T^E = 0.2$ were used.

the following expression has to be employed:

$$F_e(e,\hat{m}) = 2\int_{z_{\min}(e)}^{z_-^q(e)} \mathrm{d}z \sum_{y=y_-(e,z)}^{y_{\text{up}}(e,z)} \frac{M_C(y,z)}{y\left|\frac{\mathrm{d}\hat{e}(y,z)}{\mathrm{d}y}\right|} + 2\int_{z_-^q(e)}^{1/2} \mathrm{d}z \left|\frac{M_C(y,z)}{y\,\frac{\mathrm{d}\hat{e}(y,z)}{\mathrm{d}y}}\right|_{y=y_-(e,z)} + 2\int_{z_-^g(e)}^{1/2} \mathrm{d}z \left|\frac{M_C(y,z)}{y\,\frac{\mathrm{d}\hat{e}(y,z)}{\mathrm{d}y}}\right|_{y=y_+(e,z)} . \tag{4.17}$$

For e larger than a certain value e_{th}, the contour lines for thrust, HJM and broadening in the E-scheme exist only in the gluon region, or in other words, $z_\pm^q(e_{\text{th}}) = 1/2$, such that only the second term in eq. (4.16) contributes. $e_{\max}$ obviously satisfies $z_\pm^g(e_{\max}) = 1/2$. Some results for differential and cumulative distributions of 2-jettiness, C-jettiness and HJM will be discussed in section 5.

4.4 Computation of the cumulative distribution

We define the cumulative distribution as

$$\Sigma(e_c) = \frac{1}{\sigma_0}\int_0^{e_c} \mathrm{d}e\, \frac{\mathrm{d}\sigma}{\mathrm{d}e} = R_0(\hat{m})\,\Theta(e_c - e_{\min}) + C_F\frac{\alpha_s}{\pi}\,\Sigma^1(e_c) + \mathcal{O}(\alpha_s^2)\,. \tag{4.18}$$

Once again, since we can compute $\Sigma^1(e_c)$ with very high precision, the non-singular $\Sigma^{\text{NS}}(e_c)$ function can be obtained by removing the contributions from the delta and plus functions, which are known analytically. This is the last ingredient for the complete description of the cumulative cross section at $\mathcal{O}(\alpha_s)$.

The cumulative distribution provides an alternative, numeric way of computing the delta coefficient, that will be used as an additional cross check of our computation in section 4 (see appendix A)

$$A_e(\hat{m}) = \lim_{e_c \to e_{\min}} \Sigma^1(e_c) - B_{\text{plus}}(\hat{m}) \log(e_c - e_{\min}) \,. \tag{4.19}$$

In practice one can compute the one-loop contribution to the cumulative distribution by adding and subtracting the total hadronic cross section $R_1^C(\hat{m}) = \Sigma_C^1(e_{\max})$, and then using $1 - \Theta(x) = \Theta(-x)$, to obtain the relation

$$\Sigma_C^1(e_c) = R_1^C(\hat{m}) + \Sigma_C^1(e_c) - \Sigma_C^1(e_{\max}) = R_1^C(\hat{m}) - \int \mathrm{d}y\, \mathrm{d}z\, \Theta[\hat{e}(y,z) - e_c]\, \frac{M_C(y,z)}{y} \,. \tag{4.20}$$

The functions R_1^C are shown graphically in figure 4(b). The cancellation of IR singularities is already realized in R_1^C and the integral left over involves only real radiation. Since the Heaviside function limits the y integration on the lower side, the integral is convergent, and consequently can be carried out using standard methods. For instance, the MC method described in section 4.2 can be easily adapted by simply summing up the events of all bins with lower endpoint larger larger than e_c.

In the rest of this section we describe a direct method along the lines of section 4.3. We again start with our toy model, namely the event shape defined as the soft limit of another variable:

$$\begin{aligned} \Sigma_C^1(\bar{e}_c) &= R_1^C(\hat{m}) - \int_{z_-(\bar{e}_c)}^{z_+(\bar{e}_c)} \mathrm{d}z \int_{h(\bar{e}_c,z)}^{y_{\max}(z)} \mathrm{d}y\, \frac{M_C(y,z)}{y} \\ &= R_1^C(\hat{m}) - \int_{z_-(\bar{e}_c)}^{z_+(\bar{e}_c)} \mathrm{d}z\, \mathcal{M}_C[\, y_{\max}(z), h(\bar{e}_c,z), z, \hat{m}] \,, \end{aligned} \tag{4.21}$$

where, given that the matrix element is a rank-two polynomial in y, the innermost integration can be performed analytically

$$\begin{aligned} \int_{y_1}^{y_2} \mathrm{d}y\, \frac{M_C(y,z)}{y} \equiv \mathcal{M}_C(y_1,y_2,z,\hat{m}) &= M_C^0(z,\hat{m}) \log\left(\frac{y_1}{y_2}\right) \\ &+ M_C^2(z,\hat{m})\,(y_1 - y_2) + \frac{1}{2} M_C^3(z,\hat{m})\,(y_1^2 - y_2^2) \,. \end{aligned} \tag{4.22}$$

The logarithm multiplying M_C^0 reflects the soft singularity and diverges if $\bar{e}_c = e_{\min}$. The z integration in eq. (4.21) can be easily performed numerically, and it corresponds to the area marked with II in figure 21.[13]

For regular event shapes whose contour lines for constant e are continuous, convex and do not intersect with the phase-space boundaries, the cumulative distribution can be computed easily using the ingredients described in section 3.3:

$$\Sigma_C^1(\bar{e}_c) = R_1^C(\hat{m}) - 2 \int_{z_{\min}(e)}^{1/2} \mathrm{d}z\, \mathcal{M}_C[\, y_+(e,z), y_-(e,z), z, \hat{m}] \,. \tag{4.23}$$

[13] Note that a "direct" computation of the cumulative distribution (not based on the difference with respect to the total hadronic cross section), corresponds to the sum or areas marked as III and IV in figure 21, which suffers from an IR singularity.

The z integration is performed numerically as described in section 3.3. We have checked that taking a numerical derivative of our cumulative distribution reproduces the differential cross section as computed in the previous section.

For E-scheme thrust and HJM the above formula has to be modified. From the analysis in the previous section and looking at figure 10, one can readily conclude that between $z_-^g(e)$ and $z_-^q(e)$ the area to be integrated is limited by $y_\tau(\hat{m}, z)$ and $y_+(e, z)$, while between between $z_-^q(e)$ and $1/2$ it is limited by $y_-(e, z)$ and $y_+(e, z)$:

$$\begin{aligned}\Sigma_C^1(\bar{e}_c) = R_1^C(\hat{m}) &- 2\int_{z_-^g(e)}^{z_-^q(e)} \mathrm{d}z\, \mathcal{M}_C[\, y_+(e,z), y_\tau(\hat{m},z), z, \hat{m}] \\ &- 2\int_{z_-^q(e)}^{1/2} \mathrm{d}z\, \mathcal{M}_C[\, y_+(e,z), y_-(e,z), z, \hat{m}]\,.\end{aligned} \tag{4.24}$$

Finally, for E-scheme broadening, if $\hat{m}/2 < B_T^E < B_T^{E,\mathrm{crit}}$ one has to use the following expression:

$$\begin{aligned}\Sigma_C^1(\bar{e}_c) = R_1^C(\hat{m}) &- 2\int_{z_{\min}(e)}^{z_-^q(e)} \mathrm{d}z\, \mathcal{M}_C[\, y_{\mathrm{up}}(e,z), y_-(e,z), z, \hat{m}] \\ &- 2\int_{z_-^g(e)}^{z_-^q(e)} \mathrm{d}z\, \mathcal{M}_C[\, y_+(e,z), y_\tau(\hat{m},z), z, \hat{m}] \\ &- 2\int_{z_-^q(e)}^{1/2} \mathrm{d}z\, \mathcal{M}_C[\, y_+(e,z), y_-(e,z), z, \hat{m}]\,.\end{aligned} \tag{4.25}$$

All the z numerical integrals in this section are performed using the python quadpack implementation in the `scipy` module.

The cumulative distribution for event shapes whose contour lines intersect with the phase space will be discussed in the next section taking 2-jettiness as an example.

5 Cross sections for mass-sensitive event shapes

As an application of the approach presented in this work, we now work out differential and cumulative cross sections for those event shapes whose contour lines intersect with the phase-space boundaries: HJM, 2-jettiness and C-jettiness. These happen to be the most sensitive to the heavy quark mass, since their threshold gets displaced from zero to a mass-dependent position. Analytic results for the differential 2-jettiness [78] and C-jettiness distributions [79][14] are already known, but in this section we will carry out the manipulations necessary to bring their computation into 1D integrals over z. We shall show how to obtain analytical results for the differential heavy jet mass and cumulative 2-jettiness distributions. Since the coefficients of the delta functions are already collected in appendix D and the plus-distribution coefficient is universal, the only missing piece is the non-singular contribution, which can be computed in $d = 4$ dimensions.

[14] In this reference the coefficient of the delta function was determined numerically.

JHEP03(2020)024

5.1 Differential HJM

In order to derive the HJM differential distribution it is useful to split the phase space into the usual three regions, as described by eq. (3.10) and shown in figure 5. For three particles, one of them massless and the other two with same mass m, $\rho(y,z)$ takes the following form in these regions:[15]

$$\rho_q = \hat{m}^2 + yz\,, \qquad \rho_{\bar{q}} = \hat{m}^2 + y(1-z)\,, \qquad \rho_g = 1-y\,. \tag{5.1}$$

Consequently, the measurement delta functions in the respective regions are very simple and given by

$$\delta(\rho - yz - \hat{m}^2) = \frac{1}{z}\delta\left(y - \frac{\rho-\hat{m}^2}{z}\right), \quad \delta[\rho - y(1-z) - \hat{m}^2] = \frac{1}{1-z}\delta\left(y - \frac{\rho-\hat{m}^2}{1-z}\right),$$
$$\delta(\rho - 1 + y)\,. \tag{5.2}$$

To figure out the correct integration boundaries for y and z we consider the quark and anti-quark region first. In this region, the lines of constant ρ meet either the phase-space boundary [for $\rho < \hat{m}(1-\hat{m}-\hat{m}^2)/(1-\hat{m})$], or the boundary to the gluon region (for larger values). Defining $\xi_\rho \equiv \sqrt{t_\rho^2 - 4\rho}$ and $t_\rho = 1+\rho-\hat{m}^2$, the intersections with the phase-space boundary are located at $z = z_1 \equiv (t-\xi_\rho)/2$ and $z = 1-z_1$, while the intersections with the gluon-region boundary are located at $z = z_2 \equiv (t_\rho - 1)/\sqrt{(1-\rho)^2 - 2\hat{m}^2(1+\rho) + \hat{m}^4}$ and $z = 1-z_2$. The gluon region, on the other hand, contributes only for $\rho > 4\hat{m}^2$, intersecting the phase-space boundary [for $\rho < \hat{m}/(1-\hat{m})$] or the region boundary (for larger values). The phase-space boundary intersections are located at $z = z_-^2 \equiv \left[\,1 - \sqrt{1-4\hat{m}^2/\rho}\,\right]/2$ and $z = z_+^2 \equiv 1 - z_-^2$ for $\rho < \hat{m}/(1-\hat{m})$, while the region boundary intersections are located at $z = z_-^3 \equiv \left[\,1 - \sqrt{(1-\rho^2) + 4\hat{m}^2}\,\right]/(1-\rho)$ and $z = z_+^3 \equiv 1 - z_-^3$. All those cases are shown in figure 12. Note that that the constant event-shape lines of the (anti-)quark and the gluon region do not meet at the region boundaries.

Taking all this into account, the differential cross section in $d = 4$ is given by

$$F_\rho(\rho,\hat{m}) = 2\int_{\max(z_1,z_2)}^{\frac{1}{2}} \frac{\mathrm{d}z}{\rho-\hat{m}^2} M_C\left(\frac{\rho-\hat{m}^2}{z}, z\right) + \frac{2\,\Theta(\rho-4\hat{m}^2)}{1-\rho}\int_{\max(z_-^2,z_-^3)}^{\frac{1}{2}} \mathrm{d}z\, M_C(1-\rho,z)$$
$$= f_1[\max(z_1,z_2)] + f_2[\max(z_-^2,z_-^3)]\,, \tag{5.3}$$

[15] The sum of hemisphere masses takes the same form in the last region, while in the first two regions the squared mass gets a factor of 2. Therefore, the calculation presented in this section can be easily modified to give results for this event shape.

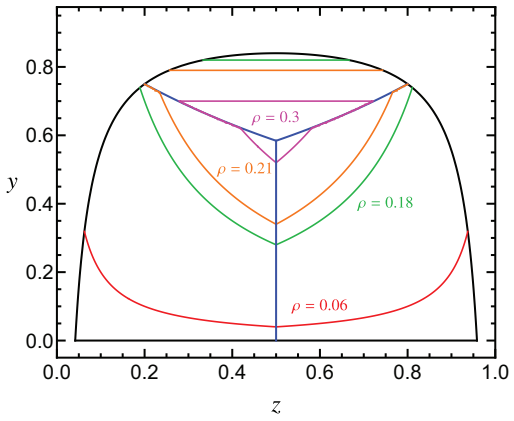

Figure 12. Three-particle phase space (black lines), thrust boundaries (blue lines) and constant ρ value contour lines, with $\hat{m} = 0.2$.

with the integral solutions

$$f_1^V(z) = \frac{(1-2z)\big[\,\rho(1-z)(\rho-4z) - 2\hat{m}^2(\rho+2(1-2\rho)z^2+3\rho z) + \hat{m}^4(1-z-8z^2)\,\big]}{2(1-z)z^2(\rho-\hat{m}^2)}$$
$$+\left(\rho-2-5\hat{m}^2+2\frac{1-4\hat{m}^4}{\rho-\hat{m}^2}\right)\log\left(\frac{1-z}{z}\right),$$
$$f_1^A(z) = 4-8\hat{m}^2(2+\rho)+8\hat{m}^4+\frac{1}{2(\rho-\hat{m}^2)}\left\{\frac{(1+2\hat{m}^2)(\rho-\hat{m}^2)^2}{z^2}+\frac{4(1-4\hat{m}^2)\hat{m}^2}{1-z}\right.$$
$$-2\,\frac{\rho(2+\rho)-2\hat{m}^2\rho(5+\rho)+\hat{m}^4(1+4\rho)-2\hat{m}^6}{z}$$
$$\left.+2\big[\,2-(2-\rho)\rho+2\hat{m}^2(\rho(\rho+3)-5)+\hat{m}^4(9-4\rho)+2\hat{m}^6\big]\log\left(\frac{1-z}{z}\right)\right\},$$
$$f_2^V(z) = \frac{1}{t}\left\{[2-(2-t)t-4\hat{m}^2t-8\hat{m}^4]\log\left(\frac{1}{z}-1\right)-\frac{(1-2z)\big[(1-z)z\,t^2+2\hat{m}^2+4\hat{m}^4\big]}{(1-z)z}\right\},$$
$$f_2^A(z) = \frac{\big[2-2t+t^2+2\hat{m}^2(t^2+4t-6)+16\hat{m}^4\big]\log\left(\frac{1}{z}-1\right)-\frac{(1-2z)[t^2(1-z)z+2\hat{m}^2-8\hat{m}^4]}{(1-z)z}}{t}.$$

The integral boundaries arise as follows: while making use of the symmetry axis $z = 1/2$ by integrating z only up to $1/2$ and multiplying by 2, the boundaries automatically choose the appropriate intersection of the constant event-shape line with the phase-space or region boundary.

5.2 Cumulative 2-jettiness

2-jettiness is defined as

$$\tau_J = \frac{1}{Q}\min_{\hat{n}}\sum_i (E_i - |\hat{n}\cdot\vec{p}_i|)\,, \tag{5.4}$$

which, for the same setup of three partons, two of them massive, takes the simple form

$$\tau_J = \min\big[\,1-y, 1-\ \mathrm{mod}(y,z), 1-\ \mathrm{mod}(y,1-z)\,\big]\,, \tag{5.5}$$

with $\mathrm{mod}(y,z) \equiv \sqrt{(1-yz)^2 - 4\hat{m}^2}$. The three values in the list correspond to the thrust axis pointing into the direction of the gluon, quark and anti-quark momenta, respectively, see eq. (3.10).

Therefore, in these three regions the measurement δ functions read

$$\begin{aligned}
&\delta(\tau_J + y - 1)\,, \\
&\delta[\tau_J + \mathrm{mod}(y,z) - 1] = \frac{t_\tau}{z\xi_\tau}\,\delta\!\left(y - \frac{1-\xi_\tau}{z}\right), \\
&\delta[\tau_J + \mathrm{mod}(y,z) - 1] = \frac{t_\tau}{(1-z)\xi_\tau}\,\delta\!\left(y - \frac{1-\xi_\tau}{1-z}\right),
\end{aligned} \tag{5.6}$$

with $t_\tau = 1 - \tau_J$, $\xi_\tau = \sqrt{t_\tau^2 + 4\hat{m}^2}$. In analogy to the previous section, we analyze the various intersections of the constant event-shape line with the phase-space and region boundaries to figure out the correct integration limits: the constant event-shape line in the gluon region is equivalent to the one for heavy jet mass in the previous section and can be adopted. In the (anti-)quark region, the constant event-shape line intersects the phase-space boundary for $\tau_J < \hat{m}/(1-\hat{m})$, or the boundary to the gluon region for larger values. These intersections take place at $z = z_-^1 \equiv (1 + \tau_J - \xi_\tau)/2$, $z = z_+^1 \equiv 1 - z_-^1$, and $z = z_-^3 \equiv (1-\xi_\tau)/t$, $z = z_+^3 \equiv 1 - z_-^3$, respectively. In contrast to heavy jet mass, the constant τ_J-lines meet at the region boundaries, making the structure of the integration boundaries simpler.

Using the expression in eq. (4.20) the cumulative distribution is given by

$$\begin{aligned}
\Sigma_C^1(\tau_J^c < 4\hat{m}^2) &= R_1^C(\hat{m}) - 2\int_{z_-^1}^{\frac{1}{2}} \mathrm{d}z \int_{\frac{1-\xi}{z}}^{y_{\max}(z)} \mathrm{d}y\, \frac{M_C(y,z)}{y}, \\
\Sigma_C^1(\tau_J^c > 4\hat{m}^2) &= R_1^C(\hat{m}) - 2\int_{\max(z_-^1, z_-^3)}^{\frac{1}{2}} \mathrm{d}z \int_{\frac{1-\xi}{z}}^{\min[y_{\max}(z),t]} \mathrm{d}y\, \frac{M_C(y,z)}{y},
\end{aligned} \tag{5.7}$$

where the integral corresponds to the region in between the limiting value τ_J^c and (potentially) the phase-space boundary, see figure 13. All integrals can be computed analytically, resulting in a long expression containing logs and dilogs. The expressions are available from the authors on request.

5.3 C-jettiness

We finish the discussion on the computation of event-shape differential and cumulative distributions with the special case of C_J, whose contour lines are continuous and smooth, but can intersect with the phase-space boundaries in various ways, some of which are shown in figure 14. For the cumulative distribution one can find a simple expression that covers all possible scenarios

$$\Sigma_C^1(\bar{e}_c) = R_1(\hat{m}) - 2\int_{z_m(e)}^{1/2} \mathrm{d}z\, \mathcal{M}_C[\,\min\{y_{\max}(z), y_+(e,z)\}, y_-(e,z), z, \hat{m}\,], \tag{5.8}$$

with z_m the minimal value that z can attain in the contour line within the phase-space boundaries. Therefore z_m can be either $z_{\min}(e)$, the point at which the contour line has

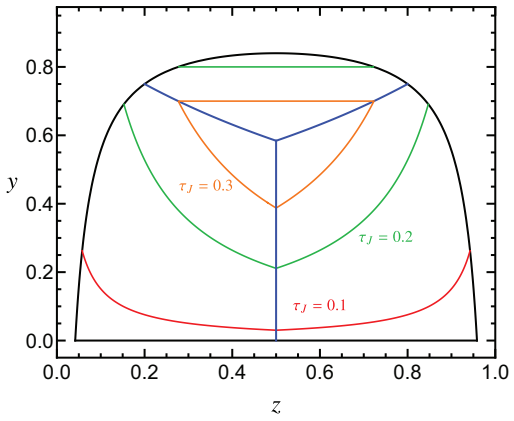

Figure 13. Three-particle phase space (black lines), thrust boundaries (blue lines) and constant τ_J value contour lines, with $\hat{m} = 0.2$.

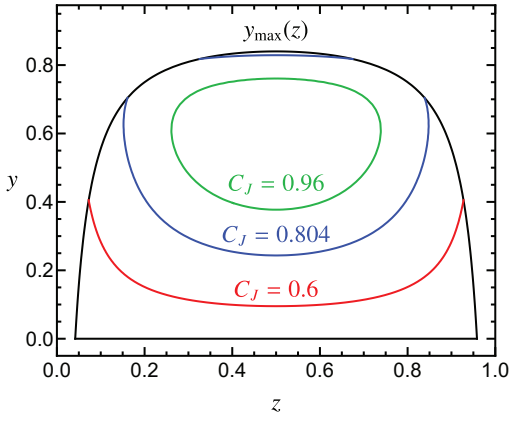

Figure 14. Three-particle phase space (black lines) showing contour lines for the C-jettiness event shape in red ($C_J = 0.6$), blue ($C_J = 0.804$) and green ($C_J = 0.96$). The plot uses the numerical value $\hat{m} = 0.3$.

infinite slope, or z_-^{cut}, the point at which it intersects with the phase-space boundary on the left side (if it intersects more than once, then the lower intersection has always smaller z value). Analytic expressions for $y_\pm(z)$ can also be found. A careful examination of those and their interplay with $y_{\max}$ allows to find a general analytic expression for z_m. These results are given in ref. [79]. The z integration has to be performed numerically, and we use the quadpack package for that.

For the differential cross section one can also write down a unique expression by carefully defining the "upper" and lower contour lines

$$F_e(e,\hat{m}) \;=\; 2\int_{z_m(e)}^{1/2} \mathrm{d}z \sum_{y=y_\pm(e,z)} \Theta[y_{\max}(z) - y]\, \frac{M_C(y,z)}{y\left|\frac{\mathrm{d}\hat{e}(y,z)}{\mathrm{d}y}\right|}\,. \tag{5.9}$$

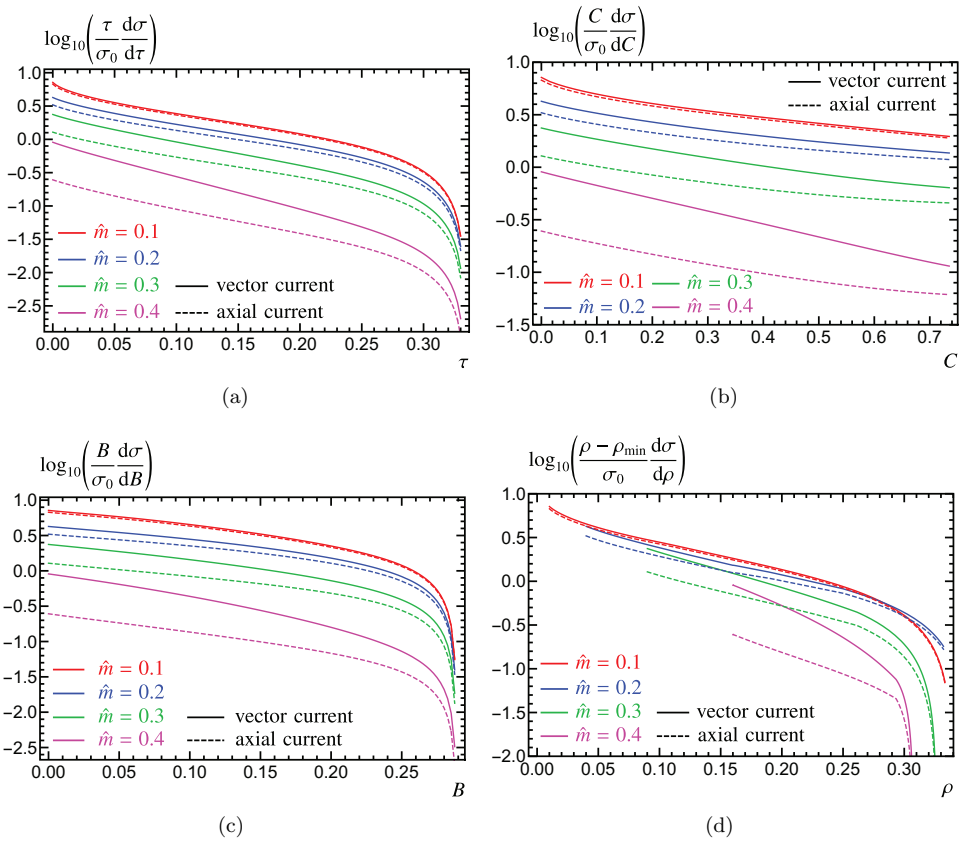

Figure 15. Event-shape distributions for vector (solid curves) and axial-vector (dashed curves) currents. Panels (a), (b), (c), and (d) show results for thrust, C-parameter, jet broadening, and heavy jet mass, respectively. All curves are multiplied by $e - e_{\min}$, with e the event-shape value and $e_{\min}$ its minimal value, such that the cross section is finite for $e = e_{\min}$. Red, blue, green and magenta lines show the results for $\hat{m} = 0.1$, 0.2, 0.3 and 0.4, respectively.

Here the Heaviside function splits the two z integrals in various sub-integrals corresponding to different segments, which are sometimes disconnected. After a careful analysis one can disentangle all possible scenarios that eq. (5.9) encompasses. These depend of course on the value of C_J, but also on $\hat{m}$. After working those out, the resulting z integrals can be performed analytically in terms of incomplete Elliptic functions. A detailed computation, together with the final analytic expressions, is given in ref. [79].

6 Numerical analysis

We start this section by showing differential cross section results for different values of m/Q in figure 15. Since the only singular term at threshold diverges like $\sim 1/(e - e_{\min})$, we plot $(e - e_{\min})$ times the distribution, such that the curves are finite in the whole range. We also use a logarithmic scale on the y axis to make the curves with small reduced mass

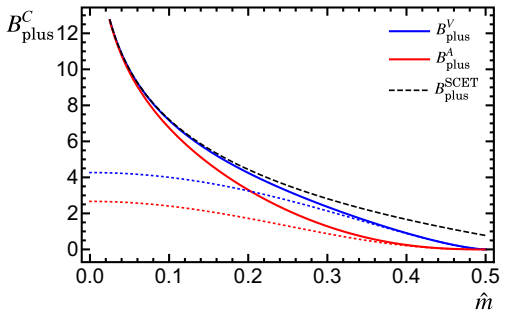

Figure 16. The universal coefficient of the plus distribution $B^C_{\rm plus}$ as a function of the reduced mass $\hat{m}$. We show the coefficient in the case of an axial-vector current (red solid line), a vector current (blue solid line) and the SCET limit (black dashed line). The SCET limit agrees with both the full QCD vector and axial cases in the limit $\hat{m} \to 0$. We also show the respective threshold limits as dotted lines, expanded up to $\mathcal{O}(v^5)$. Both full QCD expressions approach zero in this limit, as expected.

value more visible. We show results for the most common event shapes, namely thrust, C-parameter, jet broadening and heavy jet mass in their original definition, although our code can yield results for those in any other scheme.[16] With the exception of HJM, $e_{\rm min}$ and $e_{\rm max}$ are mass-independent, and therefore the main sensitivity of the cross section is through the magnitude of the curves: smaller masses result in larger cross sections in the tail. Vector and axial-vector cross sections are similar for small values of the reduced mass, but clearly different for e.g. $\hat{m} = 0.4$. We observe that the axial-vector distributions are always lower than their vector counterparts. That hierarchy is also true for the plus and delta-function coefficients, as well as for the cumulative distribution. The HJM endpoints are mass-dependent, such that $\rho_{\rm min}$ [$\rho_{\rm max}$] increases [decreases] with $\hat{m}$. Therefore for this event shape (and all other mass-dependent ones) the mass sensitivity comes partly from the cross-section magnitude, but mainly from the peak position [the peak is not visible in the plots because of the $(\rho - \rho_{\rm min})$ factor, and the missing resummation and convolution with a non-perturbative shape function].

In figure 16 we show the dependence of the plus-function coefficient on $\hat{m}$. For very small reduced masses one recovers the result predicted by SCET or bHQET,

$$B^{\rm SCET}_{\rm plus} = -2\,[\,1 + 2\log(\hat{m})\,]\,, \tag{6.1}$$

in which powers of $\hat{m}$ are suppressed and the mass-dependence is purely logarithmic. Since the squared matrix elements in QCD do not depend on $\log(\hat{m})$, the mass dependence of $B^{\rm SCET}_{\rm plus}$ must come from phase-space restrictions and the event shape definition. Hence, the massless limit has to be the same for both vector and axial-vector currents, as can be seen in figure 16 or by Taylor expanding the corresponding analytic formulas [as in eq. (6.1)]. For $v \to 0$ both vector and axial-vector versions of $B_{\rm plus}$ tend to zero (faster for the axial current), which can be explained by physical arguments. In the threshold limit,

[16] While the aim of figure 1 was to highlight the difference between schemes, here we want to show the difference between vector and axial-vector currents, together with the mass dependence.

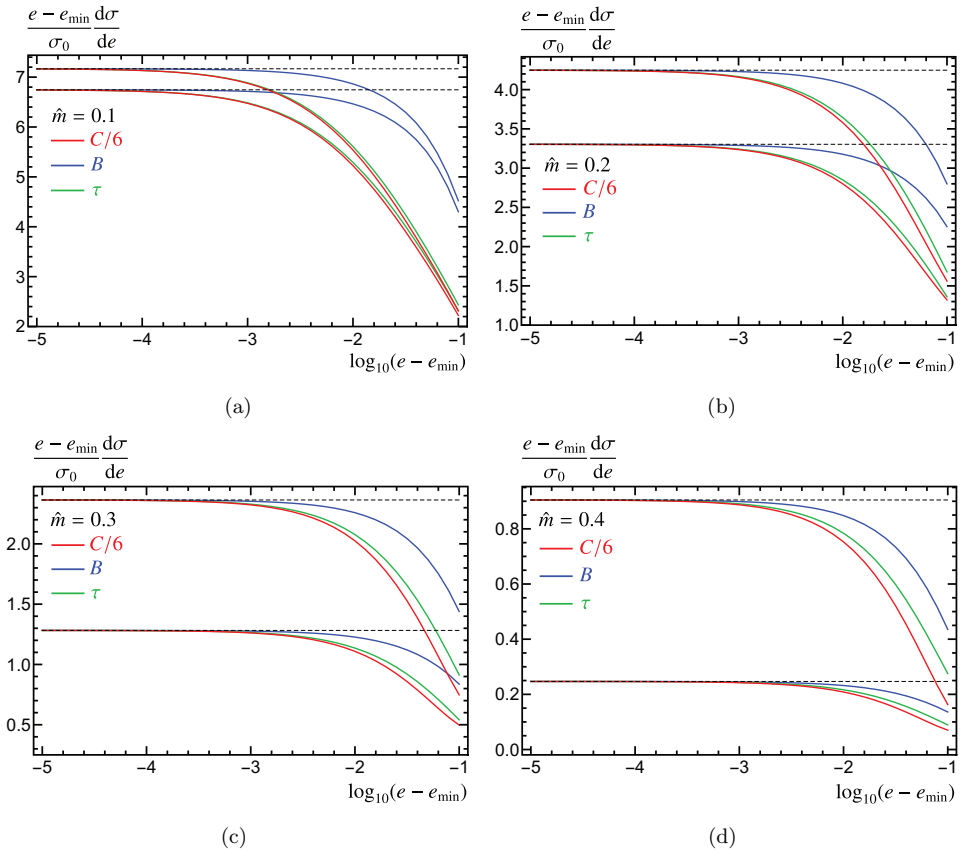

Figure 17. Numerical determination of the plus-function coefficient. Panels (a), (b), (c) and (d) correspond to $\hat{m} = 0.1$, 0.2, 0.3 and 0.4, respectively. In each panel curves converging to the upper (lower) horizontal dashed line show vector (axial-vector) current results. The dashed lines show the analytical result of B_{plus} for both currents. Thrust is shown in green, jet broadening in blue, and reduced C-parameter ($\widetilde{C} = C/6$) in red.

all the energy coming from the e^+e^- collision is invested in creating a heavy $q\bar{q}$ pair at rest. Therefore either no gluon (or massless quark) is radiated, or they have zero energy and momentum. No extra massive particles can be created. In this situation it is clear that $e = e_{\min} = e_{\max}$, and therefore there is no radiative tail. Hence both the plus distribution and non-singular cross section identically vanish, and only the delta function can remain. As a numerical check of the universality of B^C_{plus}, shown in figure 16, we use the fact that

$$B_{\text{plus}} = \lim_{e \to e_{\min}} (e - e_{\min}) F_e(e, \hat{m}) \,, \tag{6.2}$$

to determine graphically the plus-function coefficient for three distinct event shapes. For the vector and axial-vector currents separately, the cross sections approach the same horizontal line, matching our theoretical prediction. We have shown this behavior for $\hat{m} = 0.1$, 0.2, 0.3 and 0.4 in the four panels of figure 17. We have checked that univer-

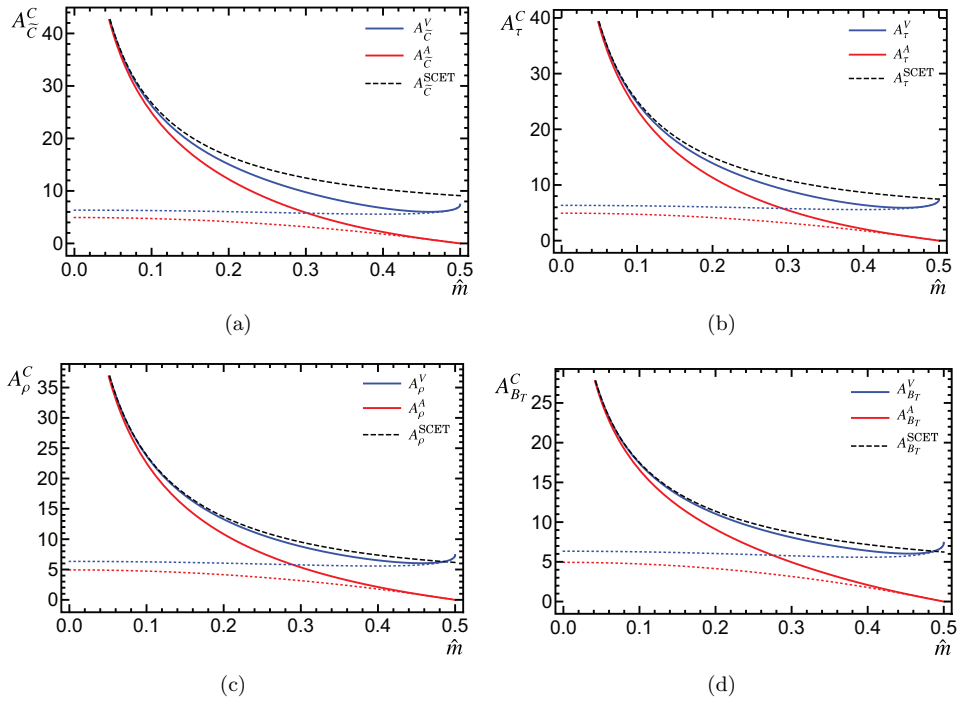

Figure 18. The delta-function coefficients for reduced C-parameter, thrust, heavy jet mass and jet broadening (all in their original definitions) as a function of the reduced mass $\hat{m}$. The red solid lines show the coefficients for an axial-vector current, the blue solid lines for a vector current. We also show the respective threshold limits as dotted lines, including terms up to $\mathcal{O}(v^2)$. The SCET limit, shown as black dashed lines, coincides with the vector as well as axial currents for $\hat{m} \to 0$. The values in the threshold limit are universal, approaching $3\pi^2/4$ and zero in the vector and axial-vector cases, respectively.

sality holds for all 16 event shapes considered in this article, and for 50 values of the reduced mass.[17]

In figure 18 we show the A_e^C coefficients as a function of the reduced mass for thrust, C-parameter, jet broadening and heavy jet mass. We again see that in the SCET/bHQET limit ($\hat{m} \to 0$), the result for both currents is the same. This follows from the same reasoning as in the previous paragraph. Moreover, since the axial total hadronic cross section vanishes for $v \to 0$, A_e^A also vanishes in this limit. Furthermore, $A_e^V(\hat{m} = 1/2) = R_1^V(v = 0) = 3\pi^2/4$ takes the same value for all event shapes in the limit $v \to 0$. This can be easily understood since the event-shape dependent integral in eq. (3.32) appears multiplied in eq. (3.31) precisely by the plus-function coefficient, and we already argued that in the threshold limit $B_{\rm plus} \to 0$. Another interesting property of the Dirac delta-

[17] We have also checked analytically that $B_{\rm plus}$ coincides with the plus-distribution coefficient implied by the high-energy limit of the bare one-loop massive hemisphere soft function, given in eq. (59) of ref. [80].

JHEP03(2020)024

function coefficient is that

$$\lim_{\hat{m}\to 0}[A_{e^M}(\hat{m}) - A_{e^P}(\hat{m})] = \lim_{\hat{m}\to 0}[A_{e^M}(\hat{m}) - A_{e^E}(\hat{m})] = \text{constant}\,, \tag{6.3}$$

where the constant is the difference of the Fourier-space jet functions in the massive and E/P schemes that appear in the bHQET factorization theorem for massive event shapes. This shall be shown in more detail in ref. [81], but it is based on the fact that the hard and H_m functions are the same for any event shape, and the soft function is the same in any scheme since it is mass independent at one loop order. Therefore the consistency condition requires that the jet anomalous dimensions and hence also the logs of $\hat{m}$ are the same in any scheme. Specifically, the logarithmic terms of the delta-function coefficients in the SCET limit $\hat{m} \to 0$ take the form

$$A_{e_{\rm I}}^{\rm SCET}\Big|_{\log(\hat{m})} = 4\log^2(\hat{m}) + \log(\hat{m})\,, \tag{6.4}$$

for pure $\text{SCET}_{\rm I}$ type event shapes like thrust, heavy jet mass and C-parameter, and

$$A_{e_{\rm II}}^{\rm SCET}\Big|_{\log(\hat{m})} = 2\log^2(\hat{m}) - \log(\hat{m})\,, \tag{6.5}$$

for $\text{SCET}_{\rm II}$ type ones like jet broadening. For similar reasons, the SCET/bHQET limit is equal for the same event shape in the E or P scheme, as well as with normalization Q or Q_P. In figure 19 we use eq. (4.19) to graphically determine the delta-function coefficient, checking that it agrees with our analytic computation. To make it visually clearer, we use logarithmic scaling in the horizontal axis, such that the log-subtracted cumulative distribution becomes a horizontal line as the event-shape value approaches the threshold. This plot also shows how reliable our numerical code is, even for very small values of the event shape. We choose the same event-shape measurement functions and reduced-mass values as for the rest of analyses in this section.

7 Conclusions

In this article we have shown how to accurately compute differential and cumulative massive event-shape distributions at $\mathcal{O}(\alpha_s)$. We have analytically calculated all singular terms: the plus-distribution coefficient, which we found to be the same for all event shapes linearly sensitive to soft momenta, and the delta-function coefficient. In our computation of the latter we add the contributions of virtual- and real-radiation diagrams, which are individually IR-divergent, although the sum is finite. We find that the delta-function coefficient only depends on the soft limit of the event-shape measurement function, and can be expressed as the sum of a universal term plus an observable-dependent integral times the plus-function coefficient.

We have developed a numerical algorithm to compute the non-singular distribution efficiently and with high accuracy which does not require binning the distributions. The method directly solves the measurement delta function and figures out the integration limits using standard numerical methods to find the roots of an equation or to minimize

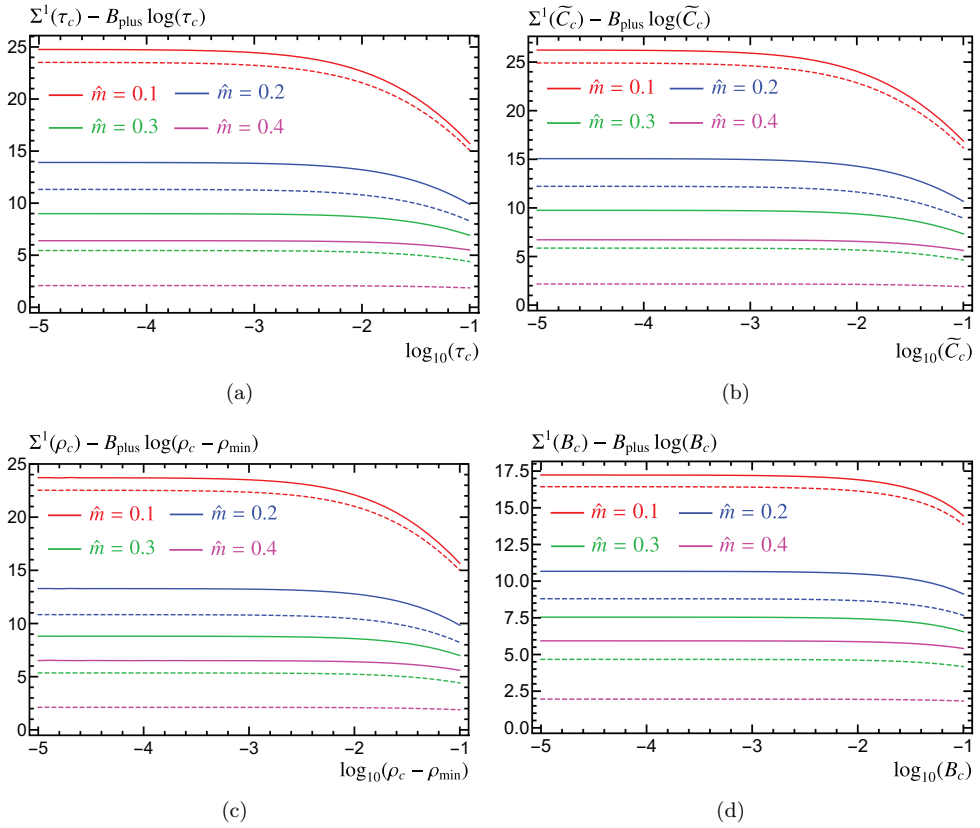

Figure 19. Numerical determination of the delta-function coefficient. Panel (a) is for thrust, (b) for reduced C-parameter, (c) for heavy jet mass and (d) for jet broadening, respectively. Solid (dashed) lines show the vector (axial-vector) current. Red, blue, green and magenta have reduced masses of $\hat{m} = 0.1$, 0.2 0.3 and 0.4, respectively. Each curve becomes a horizontal line as the event shape approaches its minimal value, reproducing exactly our analytic computations for A_e.

functions. The remaining integration is performed numerically. Our method serves for both differential and cumulative cross sections, can be used for massless quarks, and provides very accurate results even for extreme dijet configurations. Possible additional applications of the algorithm are a) event-shape distributions depending on a continuous parameter, such as angularities; b) non-global observables implying a jet algorithm and grooming, such as Soft Drop [82]. Our approach is very different from conventional MC methods, which are based on binned distributions. Although at $\mathcal{O}(\alpha_s)$ one does not yet need to implement subtractions, our strategy to compute the delta-function coefficient could be implemented in NLO parton-level MCs to achieve a much more effective cancellation of IR divergences, that could happen at an early stage.

Extending our calculation of the singular terms to $\mathcal{O}(\alpha_s^2)$ could be possible, provided one can find an analytic form for the event-shape measurement function in the soft limit.

JHEP03(2020)024

Computing the next order could provide hints to figure out if the universality of the plus distribution holds to all orders. Another approach to compute the delta and plus distributions at two loops is using EFT language. Since these parameters are defined in the limit of very soft gluon momenta, one can imagine building an EFT of heavy quarks (not necessarily boosted) interacting with soft particles (massless quarks or gluons), such that $E_{\text{soft}} \ll m_q$. In this way one could derive a factorized form for the cross section in terms of a universal matching coefficient and an event-shape dependent soft function. This could simplify the computation, since the cross section provided by the EFT would be already purely singular, and the problem would be naturally split into simpler pieces, treating one scale at a time. Moreover, such a theory would allow to sum large logarithms of ratios of scales to all orders in perturbation theory. A step in this direction has been taken already in ref. [80].

Our results will be a reference for ongoing and future research carried out in the context of event shapes with massive particles. In particular they will play an important role in the calibration of the MC top quark mass parameter, and will be even more relevant for the top quark mass measurement program at future linear colliders. In this direction, the results presented in this article will help computing efficiently e^+e^- event-shape distributions at $\mathcal{O}(\alpha_s)$ for unstable top quarks, since in that case, the delta function that sits at threshold for stable quarks radiates into the tail through the top decay products. Therefore, already at $\mathcal{O}(\alpha_s)$ one has to deal with the cancellation of IR divergences away from threshold, and our strategy for computing the delta-function coefficient could be adapted for this situation.

Acknowledgments

This work was supported in part by FWF Austrian Science Fund under the Project No. P28535- N27, the Spanish MINECO Ramón y Cajal program (RYC-2014-16022), the MECD grant FPA2016-78645-P, the IFT Centro de Excelencia Severo Ochoa Program under Grant SEV-2012-0249, the EU STRONG-2020 project under the program H2020-INFRAIA-2018-1, grant agreement no. 824093 and the COST Action CA16201 PARTICLEFACE. CL is supported by the FWF Doctoral Program "Particles and Interactions" No. W1252-N2. CL thanks the University of Salamanca for hospitality while parts of this work were completed. We thank A. H. Hoang for many valuable comments.

A Indirect computation

In this appendix we recover the main result of eq. (3.31) imposing that the integrated event-shape distribution over its entire domain reproduces the known total hadronic cross section. This method was discussed in the introduction as a way of obtaining, in a numeric form, the delta-function coefficient if an analytic form for the differential cross section is available in $d = 4$ dimensions. Here we show that if the event shape integration is performed before the phase-space integrals, analytic results can be obtained for any event

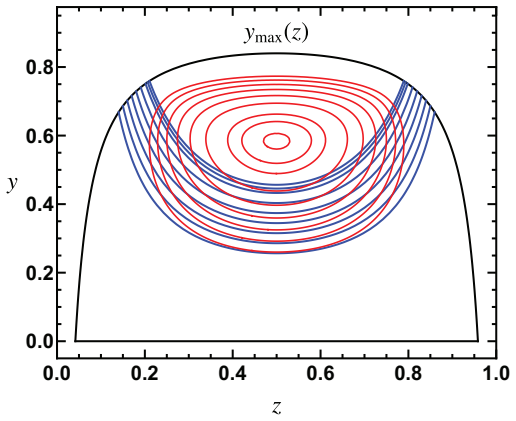

Figure 20. Phase space diagram in (z, y) coordinates (black lines) showing curves with constant value of the C-parameter event-shape measurement function (in red) and for its soft limit (in blue), for the same set of C values $\{0.42, 0.468, 0.516, 0.564, 0.612, 0.66, 0.708, 0.729, 0.747\}$, while $\hat{m} = 0.2$. Red curves are always contained withing the phase-space boundaries, and the enclosed area becomes smaller as the value of C approaches its maximum value, when it collapses to a single point. Blue curves always intersect with the phase-space boundary, and have a finite extension even for $C = C_{\max}$. Blue and red curves are similar for small values of y.

shape considered in this article. Moreover, the result is equivalent to what we have already found by the direct computation.

Writing the massive total hadronic cross section as

$$R(\hat{m}) = R_0(\hat{m}) + C_F \frac{\alpha_s}{\pi} R_1(\hat{m}) + \mathcal{O}(\alpha_s^2)\,, \tag{A.1}$$

one observes the non-trivial constraint

$$R_1(\hat{m}) = A_e(\hat{m}) + B_{\text{plus}}(\hat{m}) \log(e_{\max} - e_{\min}) + \int_{e_{\min}}^{e_{\max}} \mathrm{d}e\, F^{\text{NS}}(e, \hat{m})\,, \tag{A.2}$$

where F_e^{NS}, defined in eq. (3.29), has to be integrated in the whole e domain $[e_{\min}, e_{\max}]$. This is done before integrating in y and z. The e integration in $F_{\text{hard}}^{\text{NS}}$ effectively only replaces the Dirac delta function by 1, since the entire phase space is exactly covered by the full event shape range,

$$\int_{e_{\min}}^{e_{\max}} \mathrm{d}e\, F_{\text{hard}}^{\text{NS}}(e, \hat{m}) = \int \mathrm{d}z\, \mathrm{d}y\, M_C^{\text{hard}}(y, z, \hat{m})\,. \tag{A.3}$$

It is convenient to write the soft non-singular distribution with explicit Heaviside functions in y, such that the two terms with the soft measurement function in eq. (3.29) can be added together

$$F_{\text{soft}}^{\text{NS}} = \int \mathrm{d}z\, \mathrm{d}y\, \frac{M_C^0(z, \hat{m})}{y}\, \Theta(y) \Big\{ \Theta[y_{\max}(z) - y]\, \delta[e - \hat{e}(y, z)] - \delta[e - \bar{e}(y, z)] \Big\}\,, \tag{A.4}$$

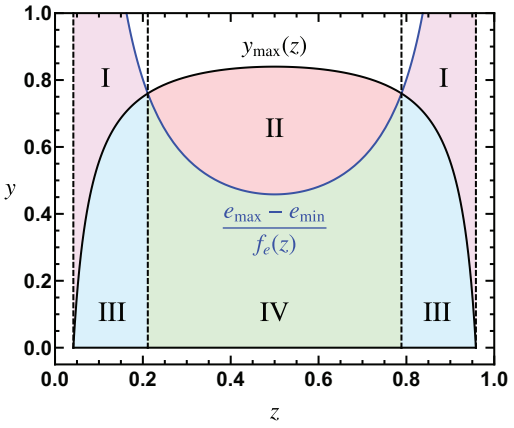

Figure 21. Phase space diagram in (z, y) coordinates (black lines) showing the curve for which the C-parameter soft measurement function equals the maximum allowed value $C_{\max} = 0.75$. Different colors correspond to the different integration regions of the soft non-singular distribution. To make this plot we use the numerical value $\hat{m} = 0.2$.

understanding that the z integration is still between z_- and z_+. To evaluate the $F^{\rm NS}_{\rm soft}$ contribution it is convenient to insert $\Theta(e_{\max} - e)$ before performing the e integral over the Dirac delta functions. In this way we obtain

$$\int_{e_{\min}}^{e_{\max}} \mathrm{d}e\, F^{\rm NS}_{\rm soft}(e,\hat{m}) = \int \mathrm{d}z\,\mathrm{d}y\, \frac{M^0_C(z,\hat{m})}{y}\,\Theta(y)\Big\{\Theta[y_{\max}(z)-y]-\Theta[h(e_{\max},z)-y]\Big\}\,. \quad \text{(A.5)}$$

Graphically, the integral of the first term corresponds to the areas marked as II, III and IV in figure 21, while the second integral is the sum of regions I, III and IV. The sum of III and IV corresponds to integrating the last term in eq. (3.29), while the pieces marked with I are the integration of the one-to-last term in eq. (3.29). Adding the two terms, the resulting y integration has the boundaries $[h(e_{\max}, z), y_{\max}(z)]$ in the whole z range, which can be expressed as

$$\int_{e_{\min}}^{e_{\max}} \mathrm{d}e\, F^{\rm NS}_{\rm soft}(e,\hat{m}) = \int_{z_-}^{z_+} \mathrm{d}z\, M^0_C(z,\hat{m}) \log\left[\frac{1-\frac{\hat{m}^2}{z(1-z)}}{\frac{e_{\max}-e_{\min}}{f_e(z,\hat{m})}}\right], \quad \text{(A.6)}$$

and graphically corresponds to subtracting the portions marked with I from the area labeled II in figure 21. Combining this result with the plus function term and using eq. (3.29) the dependence on $e_{\max}$ cancels. The y integration can be performed analytically, giving

$$\begin{aligned} &B_{\rm plus}(\hat{m})\log(e_{\max}-e_{\min}) + \int_{e_{\min}}^{e_{\max}} \mathrm{d}e\, F^{\rm NS}_{\rm soft}(e,\hat{m}) \\ &= \int \mathrm{d}z\, M^0_C(z,\hat{m})\left\{\log\left[1-\frac{\hat{m}^2}{z(1-z)}\right] + \log[f_e(z)]\right\}, \quad \text{(A.7)} \\ &\int \mathrm{d}y\,\mathrm{d}z\, M^{\rm hard}_C(y,z) = \int \mathrm{d}z\left(1-\frac{\hat{m}^2}{z(1-z)}\right)\left[M^2_C(z,\hat{m}) + \frac{1}{2}M^3_C(z,\hat{m})\left(1-\frac{\hat{m}^2}{z(1-z)}\right)\right]. \end{aligned}$$

With this we conclude with the alternative, but analytically equivalent, expression for the δ coefficient

$$A_e(\hat{m}) = R_1(\hat{m}) - \int_{z_-}^{z_+} \mathrm{d}z \left\{ M_C^0(z,\hat{m}) \big[\log\big[z(1-z) - m^2\big] - \log[z(1-z)] + \log[f_e(z)] \big] \right.$$
$$\left. + \left(1 - \frac{\hat{m}^2}{z(1-z)}\right) \left[M_C^2(z,\hat{m}) + \frac{1}{2} M_C^3(z,\hat{m}) \left(1 - \frac{\hat{m}^2}{z(1-z)}\right) \right] \right\}. \tag{A.8}$$

The integral over hard matrix elements can be performed using eqs. (B.2), while the other integrals are explicitly given in eqs. (B.3). Using these analytic results we arrive at

$$A_e^V(\hat{m}) = R_1^V(\hat{m}) - (3-v^2) I_e(\hat{m}) - (1+2\hat{m}^4) L_v - \frac{v}{4} \left[11 + 34\hat{m}^2 - 8(3-v^2) \log\left(\frac{v}{\hat{m}}\right) \right]$$
$$+2\,v^2 \left[\mathrm{Li}_2\left(\frac{2v}{1+v}\right) - 2\log\left(\frac{v^2}{\hat{m}}\right) L_v + \mathrm{Li}_2\left(\frac{1-v}{2}\right) - \mathrm{Li}_2\left(\frac{2v}{v-1}\right) - \mathrm{Li}_2\left(\frac{1+v}{2}\right) \right],$$
$$A_e^A(\hat{m}) = R_1^A(\hat{m}) - 2v^2 I_e(\hat{m}) - (1 + 2\hat{m}^2 - 6\hat{m}^4 + 12\hat{m}^6) L_v - \frac{v}{4} \left[11 - 68\hat{m}^2 + 12\hat{m}^4 \right.$$
$$\left. -16v^2 \log\left(\frac{v}{\hat{m}}\right) \right] + 2(1 - 6\hat{m}^2 + 8\hat{m}^4) \left[\mathrm{Li}_2\left(\frac{2v}{1+v}\right) + \mathrm{Li}_2\left(\frac{1-v}{2}\right) \right.$$
$$\left. - 2\log\left(\frac{v^2}{\hat{m}}\right) L_v - \mathrm{Li}_2\left(\frac{2v}{v-1}\right) - \mathrm{Li}_2\left(\frac{1+v}{2}\right) \right]. \tag{A.9}$$

Using the known results for the total hadronic cross section, collected for convenience in eq. (C.1) of appendix C, it can be checked that the above result is analytically equivalent to eqs. (3.31).

B Phase-space integrals

Almost every integral in the phase-space variable z we have computed for various event-shape measurement functions can, due to the symmetry under $z \to 1-z$, be cast in the one these forms:

$$\int_{\frac{1}{2}}^{z_+} \mathrm{d}z \frac{\log(z-a)}{z} = \mathrm{Li}_2\left(1 - \frac{1+v}{2a}\right) + \log\left(\frac{1+v}{2a}\right) \log\left(\frac{1-2a+v}{2}\right) \tag{B.1}$$
$$- \mathrm{Li}_2\left(1 - \frac{1}{2a}\right) + \log\left(\frac{1}{2} - a\right) \log(2a)\,, \quad a \le \frac{1}{2}\,,$$
$$\int_{\frac{1}{2}}^{z_+} \mathrm{d}z \frac{\log(a-z)}{z} = \mathrm{Li}_2\left(1 - \frac{1+v}{2a}\right) + \log\left(\frac{1+v}{2a}\right) \log\left(\frac{2a-1-v}{2}\right)$$
$$- \mathrm{Li}_2\left(1 - \frac{1}{2a}\right) + \log\left(a - \frac{1}{2}\right) \log(2a)\,, \quad a \ge z_+\,,$$
$$\int_{\frac{1}{2}}^{z_+} \mathrm{d}z \frac{\log(z-a)}{z^2} = \frac{1}{a} \left\{ \log\left(\frac{1-2a+v}{1+v}\right) - 2a\log(2) - (1-2a)\log(1-2a) \right.$$
$$\left. - \frac{2a \log\left(\frac{1-2a+v}{2}\right)}{1+v} \right\}, \quad a \le \frac{1}{2}\,,$$

$$\int_{\frac{1}{2}}^{z_+} \mathrm{d}z \frac{\log(a-z)}{z^2} = \frac{1}{a}\Bigg\{\log\left(-\frac{1-2a+v}{1+v}\right) - 2\,a\log(2) - (1-2a)\log(2a-1) - \frac{2a\log\left(-\frac{1-2a+v}{2}\right)}{1+v}\Bigg\}, \quad a \geq z_+\,.$$

For integrals in which no event-shape measurement function is involved, the results are even simpler

$$\int_{z_-}^{z_+} \mathrm{d}z = v\,, \qquad \int_{z_-}^{z_+} \frac{\mathrm{d}z}{z} = \int_{z_-}^{z_+} \frac{\mathrm{d}z}{1-z} = 2\,L_v\,, \tag{B.2}$$

$$\int_{z_-}^{z_+} \frac{\mathrm{d}z}{z^2} = \int_{z_-}^{z_+} \frac{\mathrm{d}z}{(1-z)^2} = \frac{v}{\hat{m}^2}, \quad \int_{z_-}^{z_+} \frac{\mathrm{d}z}{z^3} = \int_{z_-}^{z_+} \frac{\mathrm{d}z}{(1-z)^3} = \frac{v}{2\hat{m}^4}\,,$$

$$\int_{z_-}^{z_+} \mathrm{d}z \frac{\log[z(1-z)-\hat{m}^2]}{z^2} = \int_{z_-}^{z_+} \mathrm{d}z \frac{\log[z(1-z)-\hat{m}^2]}{(1-z)^2} = \frac{2v\log(v) - 2L_v}{\hat{m}^2}\,,$$

$$\int_{z_-}^{z_+} \mathrm{d}z \frac{\log[z(1-z)-\hat{m}^2]}{z} = \int_{z_-}^{z_+} \mathrm{d}z \frac{\log[z(1-z)-\hat{m}^2]}{1-z} = \mathrm{Li}_2\left(\frac{2v}{v-1}\right) - \mathrm{Li}_2\left(\frac{2v}{1+v}\right) + 4\log(v)L_v\,.$$

With these one can easily compute the integrals for the real radiation contribution

$$\begin{aligned}
\int_{z_-}^{z_+} \mathrm{d}z\, \frac{(1-z)z-\hat{m}^2}{(1-z)^2z^2} &= 2\big[(1+v^2)L_v - v\big] \\
\int_{z_-}^{z_+} \mathrm{d}z\, \frac{(1-z)z-\hat{m}^2}{(1-z)^2z^2} \log[z(1-z)-\hat{m}^2] &= 4\,L_v - 4\,v\log(v) + (1+v^2)\left[\mathrm{Li}_2\left(\frac{2v}{v-1}\right)\right. \\
&\quad \left. - \mathrm{Li}_2\left(\frac{2v}{1+v}\right) + 4\log(v)\,L_v\right], \\
\int_{z_-}^{z_+} \mathrm{d}z\, \frac{(1-z)z-\hat{m}^2}{(1-z)^2z^2} \log[z(1-z)] &= (1+v^2)\left[\mathrm{Li}_2\left(\frac{1-v}{2}\right) - \mathrm{Li}_2\left(\frac{1+v}{2}\right)\right] \\
&\quad + 2\big[(1+v^2)\log(\hat{m}) + 4\hat{m}^2\big]L_v - 2v\big[1+2\log(\hat{m})\big]\,.
\end{aligned} \tag{B.3}$$

Note that the integrands given in eq. (B.3) are invariant under the substitution $z \to (1-z)$ and therefore $\int_{z_-}^{z_+} \mathrm{d}z = 2\int_{z_-}^{1/2} \mathrm{d}z = 2\int_{1/2}^{z_+} \mathrm{d}z$.

C Total hadronic cross section

It is convenient to write the total hadronic cross section in the following way, such that it can be implemented in eq. (A.9)

$$\begin{aligned}
R_1^V(\hat{m}) &= 4(1-4\hat{m}^4)\left[3L_v^2 + 2\,\mathrm{Li}_2\left(\frac{1-v}{v+1}\right) + \mathrm{Li}_2\left(\frac{v-1}{v+1}\right) - \log\left(\frac{v^2}{\hat{m}^3}\right)L_v\right] \\
&\quad + 2(3-2\hat{m}^2-7\hat{m}^4)L_v + v\left[\frac{3}{4}(1+6\hat{m}^2) - (3-v^2)\log\left(\frac{v^2}{\hat{m}^3}\right)\right], \\
R_1^A(\hat{m}) &= 2\,v^2(1+v^2)\left[3\,L_v^2 + 2\,\mathrm{Li}_2\left(\frac{1-v}{v+1}\right) + \mathrm{Li}_2\left(\frac{v-1}{v+1}\right) - \log\left(\frac{v^2}{\hat{m}^3}\right)L_v\right] \\
&\quad + 2(3-11\hat{m}^2+5\hat{m}^4+6\hat{m}^6)L_v - \frac{21}{16}v - v^3\left[2\log\left(\frac{v^2}{\hat{m}^3}\right) - \frac{15}{8} - \frac{3}{16}v^2\right],
\end{aligned} \tag{C.1}$$

coinciding with ref. [83].

D Analytic delta-function coefficients for some event shapes

In this appendix we present some analytic results for the delta-function coefficient of massive event-shape differential cross sections. Specifically, we list the following information:

- The general definition of the event shape e.
- The expression $e_q(y,z)$ describing the event shape in the phase-space region in which the thrust axis $\hat{t}$ is aligned with the quark momentum in terms of y, z. When evaluating the integral I_e, we use the $z \leftrightarrow (1-z)$ symmetry and integrate only in this region.
- The minimal value of the event shape $e_{\min}$, valid to all orders in perturbation theory.
- The maximal value of the event shape $e_{\max}$, valid at one-loop level.
- The soft term $f_e(z)$ of the event shape required for the integral I_e, derived from $e_q(y,z)$ and therefore valid in the same phase-space region only. It is straight forward to obtain the expression for the region where $\hat{t}$ is proportional to the anti-quark momentum by applying the substitution $z \to (1-z)$.
- The solution of the integrals $I_e(\hat{m})$, which can be inserted into eq. (3.31) or (A.9) to obtain the delta-function coefficient A_e^C.

For simplicity, we define

$$r = \sqrt{1-3\hat{m}^2}\,, \qquad \mathrm{mod}(y,z) = \sqrt{(1-yz)^2-4\hat{m}^2}\,,$$
$$\mathcal{I}(\hat{m}) \equiv \int_{z_-}^{\frac{1}{2}} \mathrm{d}z\, \frac{z(1-z)-\hat{m}^2}{z^2(1-z)^2} = \big(1+v^2\big)L_v - v\,, \tag{D.1}$$

frequently appearing in expressions for $e_{\max}$, $e_q(y,z)$ and relations between event shapes, respectively. Moreover, we use the pseudo-rapidity η, transverse momentum $p_\perp \equiv |\vec{p}_\perp|$ and transverse mass $m_\perp \equiv \sqrt{p_\perp^2+m^2}$ in some event-shape definitions, where the transverse momentum is measured with respect to the thrust axis. The solutions of the integrals needed to compute the various expressions for $I_e(\hat{m})$, are provided in appendix B.

Sometimes it can be useful to define a P-scheme event shape $e^{P,Q}$ with $1/Q^n$ normalization instead of $1/Q_P^n$. The relation between the related event shape dependent integrals $I_e(\hat{m})$ is trivial, as long as $e_{\min}=0$:

$$I_{e^{P,Q}}(\hat{m}) = I_{e^P}(\hat{m}) + n\log(v)\,\mathcal{I}(\hat{m})\,. \tag{D.2}$$

Heavy jet mass.

Original definition

- $\rho = \frac{1}{Q^2}\Big(\sum_{i\in\text{heavy}} p_i\Big)^2$
- $\rho_q(y,z) = \hat{m}^2 + yz$

- $\rho_{\min} = \hat{m}^2$
- $\rho_{\max} = (5-4r)/3$
- $f_\rho(z) = z$
- $I_\rho(\hat{m}) = \frac{1}{4}\Big[(1+v^2)\mathrm{Li}_2\Big(\frac{v+1}{v-1}\Big) + \frac{\pi^2}{6}(1+v^2) - 2v(v+1) - [1+(4-v)v]\log\Big(\frac{1-v}{1+v}\Big) - 4v\log\Big(\frac{v+1}{2}\Big)\Big]$

P-scheme

- $\rho^P = \frac{1}{Q_P^2}\sum_{i,j\in\text{heavy}}(|\vec{p}_i||\vec{p}_j| - \vec{p}_i\cdot\vec{p}_j)$
- $\rho_q^P(y,z) = \frac{Q^2}{2Q_P^2}y\big[\mathrm{mod}(y,1-z) + y(1-z) + 2z - 1\big]$
- $\rho_{\min}^P = 0$
- $\rho_{\max}^P = 1/3$
- $f_{\rho^P}(z) = \frac{2z+v-1}{2v^2}$
- $I_{\rho^P}(\hat{m}) = (1-2\hat{m}^2)\Big[\mathrm{Li}_2(1-v) + \mathrm{Li}_2\Big(\frac{1}{v+1}\Big)\Big] + \frac{1}{2}\log\Big(\frac{1+v}{1-v}\Big)[1-2(1-2\hat{m}^2)\log(2v^2)] - \frac{1}{2}(1-2\hat{m}^2)\log^2(1-v) - \frac{1}{3}(1-2\hat{m}^2)[\pi^2 - 3\log^2(v+1)] - v\log(\hat{m}) + v\log(v)$

E-scheme

- $\rho^E = \frac{1}{Q^2}\sum_{i,j\in\text{heavy}}\frac{E_iE_j}{|\vec{p}_i||\vec{p}_j|}(|\vec{p}_i||\vec{p}_j| - \vec{p}_i\cdot\vec{p}_j)$
- $\rho_q^E(y,z) = \frac{y(1-y(1-z))[\mathrm{mod}(y,1-z)+y(1-z)-1+2z]}{2\,\mathrm{mod}(y,1-z)}$
- $\rho_{\min}^E = 0$
- $\rho_{\max}^E = \frac{(2-r)^2}{3}$
- $f_{\rho^E}(z) = v f_{\rho^P}(z)$
- $I_{\rho^E}(\hat{m}) = I_{\rho^P}(\hat{m}) + \log(v)\,\mathcal{I}(\hat{m})$

Thrust / 2-jettiness.

P-scheme, original definition

- $\tau = \frac{1}{Q_P}\sum_i p_{i,\perp} \mathrm{e}^{-|\eta_i|} = \frac{1}{Q_P}\min_{\hat{t}}\sum_i(|\vec{p}_i| - |\hat{t}\cdot\vec{p}_i|)$
- $\tau_q(y,z) = \mathrm{mod}(y, 1-z) - \mathrm{mod}(y,z) + y$
- $\tau_{\min} = 0$
- $\tau_{\max} = \rho^P_{\max}$
- $f_\tau(z) = f_{\rho^P}(z)$
- $I_\tau(\hat{m}) = I_{\rho^P}(\hat{m})$

E-scheme

- $\tau^E = \frac{1}{Q_P}\min_{\hat{t}}\sum_i \frac{E_i}{|\vec{p}_i|}(|\vec{p}_i| - |\hat{t}\cdot\vec{p}_i|)$
- $\tau^E_q(y,z) = \frac{1}{2}\left(\frac{[1-y(1-z)][4\hat{m}^2+y^2(1-z)z-1+y]}{\mathrm{mod}(y,z)\,\mathrm{mod}(y,1-z)} - \frac{y[1+(y-2)z]}{\mathrm{mod}(y,z)} - y(1-z) + 1 + y\right)$
- $\tau^E_{\min} = 0$
- $\tau^E_{\max} = \rho^E_{\max}$
- $f_{\tau^E}(z) = f_{\rho^E}(z)$
- $I_{\tau^E}(\hat{m}) = I_{\rho^E}(\hat{m})$

2-jettiness

- $\tau_J = \frac{1}{Q}\sum_i m_{i,\perp} \mathrm{e}^{-|\eta_i|} = \frac{1}{Q}\min_{\hat{t}}\sum_i(E_i - |\hat{t}\cdot\vec{p}_i|)$
- $\tau_{J,q}(y,z) = 1 - \mathrm{mod}(y,z)$
- $\tau_{J,\min} = 1 - v$
- $\tau_{J,\max} = \rho_{\max}$
- $f_{\tau_J}(z) = z/v$
- $I_{\tau_J}(\hat{m}) = I_\rho(\hat{m}) - \log(v)\,\mathcal{I}(\hat{m})$

JHEP03(2020)024

C-parameter / C-jettiness. Here we provide results for reduced C-parameter $\widetilde{C} = C/6$. The relation to the original version for the event shape dependent integral is simply

$$I_C(\hat{m}) = I_{\widetilde{C}}(\hat{m}) - \log(6)\,\mathcal{I}(\hat{m})\,. \tag{D.3}$$

P-scheme, original definition

- $\widetilde{C} = \frac{1}{4}\Big[1 - \frac{1}{Q_P^2}\sum_{i,j}\frac{(\vec{p}_i\cdot\vec{p}_j)^2}{|\vec{p}_i||\vec{p}_j|}\Big]$
- $\widetilde{C}_q(y,z) = \frac{2y\,[(1-y)(1-z)z-\hat{m}^2]}{\mathrm{mod}(y,1-z)\,\mathrm{mod}(y,z)[\mathrm{mod}(y,1-z)+\mathrm{mod}(y,z)+y]}$
- $\widetilde{C}_{\min} = 0$
- $\widetilde{C}_{\max} = 1/8$
- $f_{\widetilde{C}}(z) = \frac{(1-z)z-\hat{m}^2}{v^3}$
- $I_{\widetilde{C}}(\hat{m}) = (1-2\hat{m}^2)\Big[-2\log^2(2\hat{m}) + 2\,\mathrm{Li}_2\Big(\frac{1-v}{1+v}\Big) + 2\log^2(1+v) - \frac{\pi^2}{3} + 3\log(v)\log\Big(\frac{1-v}{1+v}\Big) + 2\log(2)\log\Big(\frac{1-v}{1+v}\Big)\Big] + v\log(v) - \log\Big(\frac{1-v}{1+v}\Big)$

E-scheme

- $\widetilde{C}^E = \frac{1}{4}\Big[1 - \frac{1}{Q^2}\sum_{i,j}\frac{E_iE_j(\vec{p}_i\cdot\vec{p}_j)^2}{|\vec{p}_i|^2|\vec{p}_j|^2}\Big]$
- $\widetilde{C}^E_q(y,z) = \frac{y\{\hat{m}^2[y(6(1-z)z+1)-3y^2(1-z)z-4(1-z)z-1]-2\hat{m}^4(y-2)+(1-y)(1-z)z[1-y(1-z)](1-yz)\}}{\mathrm{mod}^2(y,z)\;\mathrm{mod}^2(y,1-z)}$
- $\widetilde{C}^E_{\min} = 0$
- $\widetilde{C}^E_{\max} = 1/8$
- $f_{\widetilde{C}^E}(z) = v f_{\widetilde{C}}(z)$
- $I_{\widetilde{C}^E}(\hat{m}) = I_{\widetilde{C}}(\hat{m}) + \log(v)\,\mathcal{I}(\hat{m})$

C-jettiness

- $\widetilde{C}_J = \frac{1}{4}\Big[2 - \frac{1}{Q^2}\sum_{i\neq j}\frac{(p_i\cdot p_j)^2}{E_iE_j}\Big]$
- $\widetilde{C}_{J,q}(y,z) = \frac{z(1-z)y(1-y)+2\hat{m}^2(1-y)-2\hat{m}^4}{(1-zy)[1-(1-z)y]}$
- $\widetilde{C}_{J,\,\min} = 2\hat{m}^2(1-\hat{m}^2)$
- $\widetilde{C}_{J,\,\max} = \begin{cases}(1+16\hat{m}^2+32\hat{m}^4)/(1+2\hat{m}^2)^2/8 & (\hat{m} < 0.39307568887871164)\\ 4\hat{m}^2(1+2\hat{m}^2)/(1+4\hat{m}^2)^2 & (\hat{m} > 0.39307568887871164)\end{cases}$
- $f_{\widetilde{C}_J}(z) = z(1-z) - 2\hat{m}^4$

- $I_{\widetilde{C}_J}(\hat{m}) = \frac{1}{2}(2\hat{m}^2-1)\Big\{-2\mathrm{Li}_2\Big(\frac{1-v}{1+u}\Big)+2\,\mathrm{Li}_2\Big(\frac{1-u}{1-v}\Big)-2\,\mathrm{Li}_2\Big(\frac{1-u}{1+v}\Big)$
$+2\,\mathrm{Li}_2\Big(\frac{1+v}{1+u}\Big)+\log^2\Big(\frac{1-v}{1+v}\Big)+2\log\Big(\frac{1-v}{1+v}\Big)\log\Big[\frac{(1+u)(1+v)}{4}\Big]\Big\}$
$-\frac{1}{2\hat{m}^2}\Big[\log\Big(\frac{1-v}{1+v}\Big)-u\log\Big(\frac{u-v}{u+v}\Big)\Big]-v\log\big[\hat{m}^2(1-2\hat{m}^2)\big]$

with $u \equiv \sqrt{1-8\hat{m}^4}$.

Broadening.

P-scheme, original definition

- $B_T = \frac{1}{2Q_P}\sum_i p_{i,\perp} = \frac{1}{2Q_P}\sum_i(|\vec{p}_i| - |\hat{t}\cdot\vec{p}_i|)^{1/2}(|\vec{p}_i| + |\hat{t}\cdot\vec{p}_i|)^{1/2}$
- $B_{T,q}(y,z) = \frac{Q}{Q_P}\Bigg\{\frac{\sqrt{\mathrm{mod}(y,z)\,\mathrm{mod}(y,1-z)-v^2+y^2(1-z)z+y}\sqrt{\mathrm{mod}(y,z)\,\mathrm{mod}(y,1-z)+v^2-y^2(1-z)z-y)}}{4\mathrm{mod}(y,z)}$
$+\frac{y\sqrt{[\mathrm{mod}(y,z)+(2-y)z-1][\mathrm{mod}(y,z)+1-(2-y)z]}}{4\,\mathrm{mod}(y,z)}\Bigg\}$
- $B_{T,\min} = 0$
- $B_{T,\max} = \frac{1}{2\sqrt{3}}$
- $f_{B_T}(z) = \sqrt{\frac{f_{\widetilde{C}}(z)}{v}}$
- $I_{B_T}(\hat{m}) = \frac{1}{2}\big[I_{\widetilde{C}}(\hat{m}) - \log(v)\,\mathcal{I}(\hat{m})\big]$

E-scheme

- $B_T^E = \frac{1}{2Q}\sum_i \frac{E_i}{|\vec{p}_i|}(|\vec{p}_i| - |\hat{t}\cdot\vec{p}_i|)^{1/2}(|\vec{p}_i| + |\hat{t}\cdot\vec{p}_i|)^{1/2}$
- $B_{T,q}^E(y,z) = \frac{y\mathrm{mod}(y,1-z)\sqrt{(1-y)(1-z)z-\hat{m}^2}}{2\,\mathrm{mod}(y,z)\,\mathrm{mod}(y,1-z)}$
$+\frac{(1-y(1-z))\sqrt{\mathrm{mod}(y,z)\,\mathrm{mod}(y,1-z)-v^2+y^2(1-z)z+y}\sqrt{\mathrm{mod}(y,z)\,\mathrm{mod}(y,1-z)+v^2-y^2(1-z)z-y}}{4\,\mathrm{mod}(y,z)\,\mathrm{mod}(y,1-z)}$
- $B_{T,\min}^E = 0$
- $B_{T,\max}^E = \frac{2-r}{2\sqrt{3}}$
- $f_{B_T^E}(z) = \frac{1+v}{2} f_{B_T}(z)$
- $I_{B_T^E}(\hat{m}) = I_{B_T}(\hat{m}) + \log\big(\frac{v+1}{2}\big)\,\mathcal{I}(\hat{m})$

JHEP03(2020)024

Angularities. Here, we consider angularities in the parameter region $a < 1$ only. The soft expansion of the event shape contains a term proportional to y^{2-a}, which therefore only contributes to f_{τ_a} if $a = 1$. This case has already been considered separately since $\tau_a \to 2B_T$ $(a \to 1)$.

E-scheme, original definition

- $\tau_a = \frac{1}{Q}\sum_i \frac{E_i}{|\vec{p}_i|} p_{i,\perp} \mathrm{e}^{-|\eta|(1-a)} = \frac{1}{2Q}\sum_i \frac{E_i}{|\vec{p}_i|}(|\vec{p}_i| - |\hat{t}\cdot\vec{p}_i|)^{1-\frac{a}{2}}(|\vec{p}_i| + |\hat{t}\cdot\vec{p}_i|)^{\frac{a}{2}}$
- $\tau_{a,q}(y,z) = \frac{1}{2}\left\{\left[\frac{y[\mathrm{mod}(y,z)-(2-y)z+1]}{\mathrm{mod}(y,z)}\right]^{\frac{a}{2}}\left[y - \frac{y[1-(2-y)z]}{\mathrm{mod}(y,z)}\right]^{1-\frac{a}{2}}\right.$
  $\left. + \frac{[1-y(1-z)][\mathrm{mod}(y,z)\,\mathrm{mod}(y,1-z) - v^2 + y^2(1-z)z + y]^{1-\frac{a}{2}}[\mathrm{mod}(y,z)\,\mathrm{mod}(y,1-z) + v^2 - y^2(1-z)z - y]^{\frac{a}{2}}}{\mathrm{mod}(y,z)\mathrm{mod}(y,1-z)}\right\}$
- $\tau_{a,\min} = 0$
- $\tau_{a,\max} = 3^{\frac{a}{2}-1}(2-r)$
- $f_{\tau_{a<1}}(z) = \frac{(1+v-2z)^{\frac{a}{2}}(v+2z-1)^{1-\frac{a}{2}}}{2v}$
- $I_{\tau_{a<1}}(\hat{m}) = \frac{1-a}{4}\left\{(1+v^2)\left[2\,\mathrm{Li}_2(1-v) + 2\,\mathrm{Li}_2\left(\frac{1}{1+v}\right) - 2\,\mathrm{Li}_2\left(\frac{1-v}{1+v}\right) - \frac{\pi^2}{3}\right.\right.$
  $\left.\left. - \frac{1}{2}\log^2\left(\frac{1-v}{1+v}\right) + \log^2(1+v)\right] - 4v\log(\hat{m})\right\} - 2\log\left(\frac{1-v}{1+v}\right)$
  $+ \frac{1+v^2}{4}\left[2\mathrm{Li}_2\left(\frac{1-v}{1+v}\right) - \frac{1}{2}\log^2\left(\frac{1-v}{1+v}\right) - 2\log\left(\frac{1+v}{2v}\right)\log\left(\frac{1-v}{1+v}\right) - \frac{\pi^2}{3}\right]$

P-scheme

- $\tau_a^P = \frac{1}{Q_P}\sum_i (|\vec{p}_i| - |\hat{t}\cdot\vec{p}_i|)^{1-\frac{a}{2}}(|\vec{p}_i| + |\hat{t}\cdot\vec{p}_i|)^{\frac{a}{2}}$
- $\tau_{a,q}^P(y,z) = \frac{1}{2}\left\{\left[\frac{y[\mathrm{mod}(y,z)-(2-y)z+1]}{\mathrm{mod}(y,z)}\right]^{\frac{a}{2}}\left[y - \frac{y[1-(2-y)z]}{\mathrm{mod}(y,z)}\right]^{1-\frac{a}{2}}\right.$
  $\left. + \frac{[\mathrm{mod}(y,z)\,\mathrm{mod}(y,1-z) - v^2 + y^2(1-z)z + y]^{1-\frac{a}{2}}[\mathrm{mod}(y,z)\,\mathrm{mod}(y,1-z) + v^2 - y^2(1-z)z - y]^{\frac{a}{2}}}{\mathrm{mod}(y,z)}\right\}$
- $\tau_{a,\min}^P = 0$
- $\tau_{a,\max}^P = 3^{\frac{a}{2}-1}$
- $f_{\tau_{a<1}^P}(z) = \frac{f_{\tau_{a<1}}(z)}{v}$
- $I_{\tau_a^P} = I_{\tau_a} - \log(v)\,\mathcal{I}(\hat{m})$

JHEP03(2020)024

References

[1] M.D. Schwartz, *Resummation and NLO matching of event shapes with effective field theory*, *Phys. Rev.* **D 77** (2008) 014026 [arXiv:0709.2709] [INSPIRE].

[2] C.W. Bauer, S.P. Fleming, C. Lee and G.F. Sterman, *Factorization of e^+e^- Event Shape Distributions with Hadronic Final States in Soft Collinear Effective Theory*, *Phys. Rev.* **D 78** (2008) 034027 [arXiv:0801.4569] [INSPIRE].

[3] J.C. Collins and D.E. Soper, *Back-To-Back Jets in QCD*, *Nucl. Phys.* **B 193** (1981) 381 [*Erratum ibid.* **B 213** (1983) 545] [INSPIRE].

[4] G.P. Korchemsky, *Shape functions and power corrections to the event shapes*, in *QCD and high energy hadronic interactions. Proceedings of 33rd Rencontres de Moriond*, Les Arcs France (1998), pg. 489 [hep-ph/9806537] [INSPIRE].

[5] G.P. Korchemsky and G.F. Sterman, *Power corrections to event shapes and factorization*, *Nucl. Phys.* **B 555** (1999) 335 [hep-ph/9902341] [INSPIRE].

[6] G.P. Korchemsky and S. Tafat, *On power corrections to the event shape distributions in QCD*, *JHEP* **10** (2000) 010 [hep-ph/0007005] [INSPIRE].

[7] C.F. Berger, T. Kucs and G.F. Sterman, *Event shape/energy flow correlations*, *Phys. Rev.* **D 68** (2003) 014012 [hep-ph/0303051] [INSPIRE].

[8] C.W. Bauer, S. Fleming and M.E. Luke, *Summing Sudakov logarithms in $B \to X_s\gamma$ in effective field theory*, *Phys. Rev.* **D 63** (2000) 014006 [hep-ph/0005275] [INSPIRE].

[9] C.W. Bauer, S. Fleming, D. Pirjol and I.W. Stewart, *An Effective field theory for collinear and soft gluons: Heavy to light decays*, *Phys. Rev.* **D 63** (2001) 114020 [hep-ph/0011336] [INSPIRE].

[10] C.W. Bauer and I.W. Stewart, *Invariant operators in collinear effective theory*, *Phys. Lett.* **B 516** (2001) 134 [hep-ph/0107001] [INSPIRE].

[11] C.W. Bauer, D. Pirjol and I.W. Stewart, *Soft collinear factorization in effective field theory*, *Phys. Rev.* **D 65** (2002) 054022 [hep-ph/0109045] [INSPIRE].

[12] C.W. Bauer, S. Fleming, D. Pirjol, I.Z. Rothstein and I.W. Stewart, *Hard scattering factorization from effective field theory*, *Phys. Rev.* **D 66** (2002) 014017 [hep-ph/0202088] [INSPIRE].

[13] A. Hornig, C. Lee and G. Ovanesyan, *Effective Predictions of Event Shapes: Factorized, Resummed and Gapped Angularity Distributions*, *JHEP* **05** (2009) 122 [arXiv:0901.3780] [INSPIRE].

[14] T. Becher and G. Bell, *NNLL Resummation for Jet Broadening*, *JHEP* **11** (2012) 126 [arXiv:1210.0580] [INSPIRE].

[15] G. Bell, A. Hornig, C. Lee and J. Talbert, *e^+e^- angularity distributions at NNLL′ accuracy*, *JHEP* **01** (2019) 147 [arXiv:1808.07867] [INSPIRE].

[16] T. Becher and M.D. Schwartz, *A precise determination of α_s from LEP thrust data using effective field theory*, *JHEP* **07** (2008) 034 [arXiv:0803.0342] [INSPIRE].

[17] Y.-T. Chien and M.D. Schwartz, *Resummation of heavy jet mass and comparison to LEP data*, *JHEP* **08** (2010) 058 [arXiv:1005.1644] [INSPIRE].

JHEP03(2020)024

[18] A.H. Hoang, D.W. Kolodrubetz, V. Mateu and I.W. Stewart, *C-parameter distribution at N^3LL' including power corrections*, *Phys. Rev.* **D 91** (2015) 094017 [arXiv:1411.6633] [INSPIRE].

[19] I. Moult and H.X. Zhu, *Simplicity from Recoil: The Three-Loop Soft Function and Factorization for the Energy-Energy Correlation*, *JHEP* **08** (2018) 160 [arXiv:1801.02627] [INSPIRE].

[20] A.H. Hoang, V. Mateu, M. Schwartz and I.W. Stewart, *Precision e^+e^- Hemisphere Masses with Power Corrections*, work in progress (2019).

[21] S. Catani, L. Trentadue, G. Turnock and B.R. Webber, *Resummation of large logarithms in e^+e^- event shape distributions*, *Nucl. Phys.* **B 407** (1993) 3 [INSPIRE].

[22] A. Banfi, G.P. Salam and G. Zanderighi, *Principles of general final-state resummation and automated implementation*, *JHEP* **03** (2005) 073 [hep-ph/0407286] [INSPIRE].

[23] A. Banfi, H. McAslan, P.F. Monni and G. Zanderighi, *A general method for the resummation of event-shape distributions in e^+e^- annihilation*, *JHEP* **05** (2015) 102 [arXiv:1412.2126] [INSPIRE].

[24] G. Bell, R. Rahn and J. Talbert, *Two-loop anomalous dimensions of generic dijet soft functions*, *Nucl. Phys.* **B 936** (2018) 520 [arXiv:1805.12414] [INSPIRE].

[25] G. Bell, R. Rahn and J. Talbert, *Generic dijet soft functions at two-loop order: correlated emissions*, *JHEP* **07** (2019) 101 [arXiv:1812.08690] [INSPIRE].

[26] S. Catani and M.H. Seymour, *A General algorithm for calculating jet cross-sections in NLO QCD*, *Nucl. Phys.* **B 485** (1997) 291 [*Erratum ibid.* **B 510** (1998) 503] [hep-ph/9605323] [INSPIRE].

[27] L.J. Dixon, M.-X. Luo, V. Shtabovenko, T.-Z. Yang and H.X. Zhu, *Analytical Computation of Energy-Energy Correlation at Next-to-Leading Order in QCD*, *Phys. Rev. Lett.* **120** (2018) 102001 [arXiv:1801.03219] [INSPIRE].

[28] A. Gehrmann-De Ridder, T. Gehrmann, E.W.N. Glover and G. Heinrich, *Second-order QCD corrections to the thrust distribution*, *Phys. Rev. Lett.* **99** (2007) 132002 [arXiv:0707.1285] [INSPIRE].

[29] A. Gehrmann-De Ridder, T. Gehrmann, E.W.N. Glover and G. Heinrich, *NNLO corrections to event shapes in e^+e^- annihilation*, *JHEP* **12** (2007) 094 [arXiv:0711.4711] [INSPIRE].

[30] S. Weinzierl, *NNLO corrections to 3-jet observables in electron-positron annihilation*, *Phys. Rev. Lett.* **101** (2008) 162001 [arXiv:0807.3241] [INSPIRE].

[31] A. Gehrmann-De Ridder, T. Gehrmann, E.W.N. Glover and G. Heinrich, *EERAD3: Event shapes and jet rates in electron-positron annihilation at order α_s^3*, *Comput. Phys. Commun.* **185** (2014) 3331 [arXiv:1402.4140] [INSPIRE].

[32] S. Weinzierl, *Event shapes and jet rates in electron-positron annihilation at NNLO*, *JHEP* **06** (2009) 041 [arXiv:0904.1077] [INSPIRE].

[33] V. Del Duca et al., *Jet production in the CoLoRFulNNLO method: event shapes in electron-positron collisions*, *Phys. Rev.* **D 94** (2016) 074019 [arXiv:1606.03453] [INSPIRE].

[34] V. Mateu and G. Rodrigo, *Oriented Event Shapes at $N^3LL + O(\alpha_S^2)$*, *JHEP* **11** (2013) 030 [arXiv:1307.3513] [INSPIRE].

JHEP03(2020)024

[35] R. Abbate, M. Fickinger, A.H. Hoang, V. Mateu and I.W. Stewart, *Thrust at N^3LL with Power Corrections and a Precision Global Fit for $\alpha_s(m_Z)$*, *Phys. Rev.* **D 83** (2011) 074021 [arXiv:1006.3080] [INSPIRE].

[36] R. Abbate, M. Fickinger, A.H. Hoang, V. Mateu and I.W. Stewart, *Precision Thrust Cumulant Moments at N^3LL*, *Phys. Rev.* **D 86** (2012) 094002 [arXiv:1204.5746] [INSPIRE].

[37] T. Gehrmann, G. Luisoni and P.F. Monni, *Power corrections in the dispersive model for a determination of the strong coupling constant from the thrust distribution*, *Eur. Phys. J.* **C 73** (2013) 2265 [arXiv:1210.6945] [INSPIRE].

[38] A.H. Hoang, D.W. Kolodrubetz, V. Mateu and I.W. Stewart, *Precise determination of α_s from the C-parameter distribution*, *Phys. Rev.* **D 91** (2015) 094018 [arXiv:1501.04111] [INSPIRE].

[39] A.H. Hoang, V. Mateu, M. Schwartz and I.W. Stewart, *A Precise Determination of α_s from the Heavy Jet Mass Distribution*, work in progress (2019).

[40] P. Nason and C. Oleari, *Next-to-leading order corrections to the production of heavy flavor jets in e^+e^- collisions*, *Nucl. Phys.* **B 521** (1998) 237 [hep-ph/9709360] [INSPIRE].

[41] W. Bernreuther, A. Brandenburg and P. Uwer, *Next-to-leading order QCD corrections to three jet cross-sections with massive quarks*, *Phys. Rev. Lett.* **79** (1997) 189 [hep-ph/9703305] [INSPIRE].

[42] G. Rodrigo, M.S. Bilenky and A. Santamaria, *Quark mass effects for jet production in e^+e^- collisions at the next-to-leading order: Results and applications*, *Nucl. Phys.* **B 554** (1999) 257 [hep-ph/9905276] [INSPIRE].

[43] S. Fleming, A.H. Hoang, S. Mantry and I.W. Stewart, *Top Jets in the Peak Region: Factorization Analysis with NLL Resummation*, *Phys. Rev.* **D 77** (2008) 114003 [arXiv:0711.2079] [INSPIRE].

[44] S. Fleming, A.H. Hoang, S. Mantry and I.W. Stewart, *Jets from massive unstable particles: Top-mass determination*, *Phys. Rev.* **D 77** (2008) 074010 [hep-ph/0703207] [INSPIRE].

[45] A. Jain, I. Scimemi and I.W. Stewart, *Two-loop Jet-Function and Jet-Mass for Top Quarks*, *Phys. Rev.* **D 77** (2008) 094008 [arXiv:0801.0743] [INSPIRE].

[46] S. Gritschacher, A.H. Hoang, I. Jemos and P. Pietrulewicz, *Secondary Heavy Quark Production in Jets through Mass Modes*, *Phys. Rev.* **D 88** (2013) 034021 [arXiv:1302.4743] [INSPIRE].

[47] P. Pietrulewicz, S. Gritschacher, A.H. Hoang, I. Jemos and V. Mateu, *Variable Flavor Number Scheme for Final State Jets in Thrust*, *Phys. Rev.* **D 90** (2014) 114001 [arXiv:1405.4860] [INSPIRE].

[48] A.H. Hoang, A. Pathak, P. Pietrulewicz and I.W. Stewart, *Hard Matching for Boosted Tops at Two Loops*, *JHEP* **12** (2015) 059 [arXiv:1508.04137] [INSPIRE].

[49] A.H. Hoang, C. Lepenik and M. Stahlhofen, *Two-Loop Massive Quark Jet Functions in SCET*, *JHEP* **08** (2019) 112 [arXiv:1904.12839] [INSPIRE].

[50] M. Butenschoen, B. Dehnadi, A.H. Hoang, V. Mateu, M. Preisser and I.W. Stewart, *Top Quark Mass Calibration for Monte Carlo Event Generators*, *Phys. Rev. Lett.* **117** (2016) 232001 [arXiv:1608.01318] [INSPIRE].

JHEP03(2020)024

[51] T. Sjöstrand, S. Mrenna and P.Z. Skands, *A Brief Introduction to PYTHIA 8.1*, *Comput. Phys. Commun.* **178** (2008) 852 [arXiv:0710.3820] [INSPIRE].

[52] A.H. Hoang, A. Jain, I. Scimemi and I.W. Stewart, *Infrared Renormalization Group Flow for Heavy Quark Masses*, *Phys. Rev. Lett.* **101** (2008) 151602 [arXiv:0803.4214] [INSPIRE].

[53] A.H. Hoang et al., *The MSR mass and the $\mathcal{O}(\Lambda_{\rm QCD})$ renormalon sum rule*, *JHEP* **04** (2018) 003 [arXiv:1704.01580] [INSPIRE].

[54] A.H. Hoang, S. Plätzer and D. Samitz, *On the Cutoff Dependence of the Quark Mass Parameter in Angular Ordered Parton Showers*, *JHEP* **10** (2018) 200 [arXiv:1807.06617] [INSPIRE].

[55] G.P. Salam and D. Wicke, *Hadron masses and power corrections to event shapes*, *JHEP* **05** (2001) 061 [hep-ph/0102343] [INSPIRE].

[56] V. Mateu, I.W. Stewart and J. Thaler, *Power Corrections to Event Shapes with Mass-Dependent Operators*, *Phys. Rev.* **D 87** (2013) 014025 [arXiv:1209.3781] [INSPIRE].

[57] E. Gardi and L. Magnea, *The C parameter distribution in e^+e^- annihilation*, *JHEP* **08** (2003) 030 [hep-ph/0306094] [INSPIRE].

[58] E. Farhi, *A QCD Test for Jets*, *Phys. Rev. Lett.* **39** (1977) 1587 [INSPIRE].

[59] G. Parisi, *Super Inclusive Cross-Sections*, *Phys. Lett.* **B 74** (1978) 65 [INSPIRE].

[60] J.F. Donoghue, F.E. Low and S.-Y. Pi, *Tensor Analysis of Hadronic Jets in Quantum Chromodynamics*, *Phys. Rev.* **D 20** (1979) 2759 [INSPIRE].

[61] P.E.L. Rakow and B.R. Webber, *Transverse Momentum Moments of Hadron Distributions in QCD Jets*, *Nucl. Phys.* **B 191** (1981) 63 [INSPIRE].

[62] C.F. Berger and G.F. Sterman, *Scaling rule for nonperturbative radiation in a class of event shapes*, *JHEP* **09** (2003) 058 [hep-ph/0307394] [INSPIRE].

[63] M. Preisser, *Jet Shapes with Massive Quarks for e^+e^--Annihilation*, Ph.D. thesis, Vienna University, Vienna Austria (2019).

[64] L. Clavelli, *Jet Invariant Mass in Quantum Chromodynamics*, *Phys. Lett.* **B 85** (1979) 111 [INSPIRE].

[65] T. Chandramohan and L. Clavelli, *Consequences of Second Order QCD for Jet Structure in e^+e^- Annihilation*, *Nucl. Phys.* **B 184** (1981) 365 [INSPIRE].

[66] L. Clavelli and D. Wyler, *Kinematical Bounds on Jet Variables and the Heavy Jet Mass Distribution*, *Phys. Lett.* **B 103** (1981) 383 [INSPIRE].

[67] I.W. Stewart, F.J. Tackmann and W.J. Waalewijn, *Factorization at the LHC: From PDFs to Initial State Jets*, *Phys. Rev.* **D 81** (2010) 094035 [arXiv:0910.0467] [INSPIRE].

[68] R.K. Ellis, D.A. Ross and A.E. Terrano, *Calculation of Event Shape Parameters in e^+e^- Annihilation*, *Phys. Rev. Lett.* **45** (1980) 1226 [INSPIRE].

[69] J. Jersak, E. Laermann and P.M. Zerwas, *Electroweak Production of Heavy Quarks in e^+e^- Annihilation*, *Phys. Rev.* **D 25** (1982) 1218 [*Erratum ibid.* **D 36** (1987) 310] [INSPIRE].

[70] B.W. Harris and J.F. Owens, *The Two cutoff phase space slicing method*, *Phys. Rev.* **D 65** (2002) 094032 [hep-ph/0102128] [INSPIRE].

[71] G. Kramer, G. Schierholz and J. Willrodt, *Cross-sections and Angular Distributions of Three Jet Final States in e^+e^- Annihilation for Heavy Quarks*, *Z. Phys.* **C 4** (1980) 149 [INSPIRE].

[72] B.L. Ioffe, *Associated production of gluonic jets and heavy mesons in e^+e^- annihilation*, *Phys. Lett.* **B 78** (1978) 277 [INSPIRE].

[73] H.P. Nilles, *Isolating gluon jets*, *Phys. Rev. Lett.* **45** (1980) 319 [INSPIRE].

[74] P. Virtanen et al., *SciPy 1.0 — Fundamental Algorithms for Scientific Computing in Python*, *Nature Meth.* (2020) [arXiv:1907.10121] [INSPIRE].

[75] G.P. Lepage, *VEGAS: An Adaptive Multidimensional integration program*, CLNS-80/447 (1980).

[76] R. Brent, *Algorithms for minimization without derivatives*, Prentice-Hall, Upper Saddle River U.S.S. (1973).

[77] R. Piessens, E. de Doncker-Kapenga, C. W. Überhuber and D. K. Kahaner, *Quadpack: a subroutine package for automatic integration*, Springer, Heidelberg Germany (1983).

[78] B. Dehnadi, *Heavy quark mass determinations with sum rules and jets*, Ph.D. thesis, Vienna University, Vienna Austria (2016).

[79] M. Preisser, *C-Parameter with massive quarks*, Msc. thesis, Vienna University, Vienna Austria (2014).

[80] A. von Manteuffel, R.M. Schabinger and H.X. Zhu, *The two-loop soft function for heavy quark pair production at future linear colliders*, *Phys. Rev.* **D 92** (2015) 045034 [arXiv:1408.5134] [INSPIRE].

[81] A. Bris, V. Mateu and M. Preisser, *Jet function for P- and E-scheme massive event shapes*, work in progress.

[82] A.J. Larkoski, S. Marzani, G. Soyez and J. Thaler, *Soft Drop*, *JHEP* **05** (2014) 146 [arXiv:1402.2657] [INSPIRE].

[83] K.G. Chetyrkin, J.H. Kuhn and A. Kwiatkowski, *QCD corrections to the e^+e^- cross-section and the Z boson decay rate*, hep-ph/9503396 [INSPIRE].

JHEP03(2020)024

Chapter 6

Two-Loop Massive Quark Jet Functions in SCET

André H. Hoang, Christopher Lepenik and Maximilian Stahlhofen

Two-loop massive quark jet functions in SCET

Published in: JHEP **08** (2019) 112

Preprint version: arXiv:1904.12839 [hep-ph]

Contributions to this article:
All analytical and numerical calculations, all numerical analyses, conceptual innovations (together with other authors).

PUBLISHED FOR SISSA BY SPRINGER

RECEIVED: *May 8, 2019*
ACCEPTED: *July 29, 2019*
PUBLISHED: *August 21, 2019*

Two-loop massive quark jet functions in SCET

André H. Hoang,[a,b] **Christopher Lepenik**[a] **and Maximilian Stahlhofen**[c]

[a] *University of Vienna, Faculty of Physics, Boltzmanngasse 5, A-1090 Wien, Austria*
[b] *Erwin Schrödinger International Institute for Mathematical Physics, University of Vienna, Boltzmanngasse 9, A-1090 Wien, Austria*
[c] *PRISMA Cluster of Excellence, Johannes Gutenberg University, D-55128 Mainz, Germany*

E-mail: andre.hoang@univie.ac.at, christopher.lepenik@univie.ac.at, mastahlh@uni-mainz.de

ABSTRACT: We calculate the $\mathcal{O}(\alpha_s^2)$ corrections to the primary massive quark jet functions in Soft-Collinear Effective Theory (SCET). They are an important ingredient in factorized predictions for inclusive jet mass cross sections initiated by massive quarks emerging from a hard interaction with smooth quark mass dependence. Due to the effects coming from the secondary production of massive quark-antiquark pairs there are two options to define the SCET jet function, which we call universal and mass mode jet functions. They are related to whether or not a soft mass mode (zero) bin subtraction is applied for the secondary massive quark contributions and differ in particular concerning the infrared behavior for vanishing quark mass. We advocate that a useful alternative to the common zero-bin subtraction concept is to define the SCET jet functions through subtractions related to collinear-soft matrix elements. This avoids the need to impose additional power counting arguments as required for zero-bin subtractions. We demonstrate how the two SCET jet function definitions may be used in the context of two recently developed factorization approaches to treat secondary massive quark effects. We clarify the relation between these approaches and in which way they are equivalent. Our two-loop calculation involves interesting technical subtleties related to spurious rapidity divergences and infrared regularization in the presence of massive quarks.

KEYWORDS: Jets, NLO Computations

ARXIV EPRINT: 1904.12839

https://doi.org/10.1007/JHEP08(2019)112

JHEP08(2019)112

Contents

JHEP08(2019)112

1 Introduction

Gaining higher precision in theoretical predictions for the production of massive quarks in hard particle collisions represents an important field of research in the context of the LHC as well as future colliders (see e.g. refs. [1–3]). Factorized predictions are of special relevance since they provide a separation of physical effects from different momentum scales for cases where the scale hierarchies are large, such as for kinematic edges or endpoint regions or when there are hierarchies between particle masses and dynamical scales. Once factorization is established for a given observable, it can be written as a product or a convolution of functions encoding the dynamics of particular phase space regions. The resulting factorization formulae (or theorems) provide an approximation in the limit where one can expand in the ratios of the hierarchical scales. This allows to sum large logarithms related to these scales and in addition may provide the basis for a field theoretic treatment

of low-energy hadronization effects for processes dominated by the strong interaction. As such, factorization theorems provide important pieces of information that are not accessible directly in corresponding calculations obtained in fixed-order perturbation theory within full QCD. Factorization also entails that the various functions occurring in the factorization theorems frequently have a universal character and can be applied for different processes.

For the description of the dynamics related to energetic radiation that is emitted collinearly to a quark produced at high energy, the so-called quark jet function is an essential ingredient in factorization theorems for a variety of processes where the inclusive invariant mass of all the collinear radiation (including the energetic quark) enters. The quark jet function was first introduced in the context of the factorization framework of the Soft-Collinear Effective Theory (SCET) [4–6] for the theoretical description of inclusive semileptonic or radiative B meson decays in the kinematic regions where the produced hadrons form a jet. For the case of massless quarks the jet function is defined as a non-local correlation function of two SCET massless quark jet fields. It was calculated at $\mathcal{O}(\alpha_s)$ and $\mathcal{O}(\alpha_s^2)$ in refs. [7] and [8], respectively, and recently also the $\mathcal{O}(\alpha_s^3)$ corrections became available in ref. [9]. These results are applicable for the treatment of light quarks but can also be applied for massive quarks as long as the jet invariant mass $\sqrt{p^2}$ is much larger than the quark mass m, i.e. $p^2 \gg m^2$, and the associated mass corrections are negligible.

When quark mass effects are considered, it is useful to distinguish two types of mass effects. One is related to the quark produced by the hard interaction and which initiates the jet, called *primary*, and the other is related to quark-antiquark vacuum polarization effects, called *secondary*. Interestingly, primary as well as secondary quark mass effects introduce new kinds of subtleties.

For an inclusive jet initiated by a primary heavy quark and with invariant mass p^2, two kinematic regions where quark mass effects are important emerge: $p^2 \sim p^2 - m^2 \sim m^2$ and $p^2 - m^2 \ll m^2 \approx p^2$. The region $p^2 \sim p^2 - m^2 \sim m^2$, called SCET region, is relevant for processes where the jet invariant mass is close to the primary quark mass m but is also allowed to fluctuate at the same level. The corresponding jet function(s) can be formulated with SCET massive collinear quark jet fields and require that the massless quark SCET formalism is extended to account for mass effects modifying the propagation and interactions of collinear quarks [10–12]. Jet functions of this kind are therefore called SCET jet functions. In the context of bottom and charm quark production in hard collisions the SCET regime $p^2 \sim p^2 - m^2 \sim m^2$ is essentially the only one that can ever arise in practical applications where quark mass effects are important due to the sizable momentum smearing coming from non-perturbative effects [13]. The region $p^2 - m^2 \ll m^2 \approx p^2$, also called bHQET limit or heavy quark limit, is relevant for processes where the jet invariant mass is very close to the primary quark mass m and only allowed to fluctuate at a scale much smaller than m. Here, the SCET description does not provide a full separation of all dynamical effects because $\hat{s} \equiv (p^2 - m^2)/m \ll m \approx \sqrt{p^2}$ emerges as a new relevant scale. This separation is achieved in the context of boosted Heavy Quark Effective Theory (bHQET) where the corresponding collinear SCET sector is matched on a theory containing a super-heavy quark with its small offshell field component being integrated out [12, 14]. Jet functions of this kind are therefore called bHQET jet functions.

JHEP08(2019)112

In practice, the bHQET limit $p^2 - m^2 \ll m^2 \approx p^2$ can only arise in the context of top quark production due to the large size of the top quark mass. Here, scales below the top quark mass may be resolved and not smeared out by hadronization effects [13, 15].[1] The bHQET regime is particularly important for the theoretical understanding of top quark mass determinations from observables tied to kinematic regions with top invariant masses close to the reconstructed top quark resonance [18–20]. The $\mathcal{O}(\alpha_s)$ primary massive quark SCET and the bHQET jet functions were calculated in ref. [14]. The $\mathcal{O}(\alpha_s^2)$ corrections to the bHQET jet function were computed in ref. [21].

Secondary massive quark effects in a jet function occur at $\mathcal{O}(\alpha_s^2)$ (NNLO) in the fixed-order expansion and thus only become relevant in high precision predictions. Their treatment in a factorization approach that separates collinear and soft quantum fluctuations, however, inevitably leads to SCET_{II}-type rapidity singularities and associated large logarithms in factorization theorems for physical cross sections [22]. These large logarithms contribute at the next-to leading logarithmic (NLL) order. They arise from modes of equal virtuality (i.e. invariant mass $k^2 \sim k_+k_- \sim m^2$) but widely separated rapidity (i.e. the size of the ratio k_+/k_-), see e.g. ref. [23]. The treatment of these rapidity singularities in the context of jet functions is tied to the definition of jet functions being infrared finite (matching) functions describing collinear fluctuations with virtuality of order p^2. Traditionally the required infrared (IR) subtractions are associated to so-called zero-bin subtractions [24] (that can be understood from the point of view of the SCET label formalism [6], where the collinear label momentum zero is removed as it may not be power-counted as containing collinear modes) or are simply ignored [8] (since frequently they are related to scaleless integrals that vanish identically in dimensional regularization). However, when secondary massive quark effects (or, conceptually equivalent, the exchange of massive gauge bosons [22]) are considered, these subtractions are associated to non-vanishing contributions that need to be computed and specified in a well-defined and systematic fashion. Here, the concept of a zero-bin subtraction gets tied up with the concept of a soft mass mode bin subtraction [22, 25, 26]. The $\mathcal{O}(\alpha_s^2)$ secondary massive quark corrections for the SCET jet function for primary massless quarks with imposing zero-bin as well as soft mass mode bin subtractions were calculated in ref. [26]. However, the difference between both types of subtractions makes the treatment of secondary quark mass effects subtle since the mass mode subtractions may or may not be associated to lower virtuality modes that are, depending on the application, located in separated phase space regions (i.e. having different power counting).

We propose that an alternative and in fact more transparent view is to associate the subtractions needed to define the jet functions to so-called collinear-soft matrix elements [27, 28], an idea that was already explored in different contexts in refs. [29, 30]. This leads to jet function results that agree with the results based on the zero-bin and mass mode bin subtraction concepts, but avoids the need to impose power counting arguments to determine whether a bin subtraction for a given diagram is relevant. Interestingly, there are two alternative ways to define the subtractions which entail two options to define jet

[1] For similar discussions in the context of groomed jets see e.g. refs. [16, 17, 19].

functions, both of which differ analytically once secondary quark mass effects at $\mathcal{O}(\alpha_s^2)$ are accounted for. Both options differ in whether or not the collinear-soft matrix element used for subtractions accounts for secondary massive quark corrections. The former option leads to what we call "universal" jet functions which merge into the well known massless quark jet functions in the limit $m \to 0$ and which were already introduced in refs. [26, 31]. The latter option leads to what we call "mass mode" jet functions, which are divergent in the limit $m \to 0$ and contain (universal) rapidity singularities. The mass mode jet functions are analogous to a corresponding definition for invariant mass dependent beam functions introduced in ref. [32]. Both types of jet functions are useful to gain a transparent view on the treatment of secondary massive quark effects and can be employed in practical applications. They are also useful to better understand the relation between the secondary massive quark factorization approaches provided in refs. [22, 26, 31] and in ref. [32] which lead to equivalent results. We stress that the concepts of the "universal" and the "mass mode" jet functions also applies to the analogous situation when the effects of massive (e.g. electroweak) gauge bosons are accounted for. This is because the structure of the relevant dynamical modes is equivalent [22]. For the exchange of massive gauge bosons, however, the mass effects arise already at $\mathcal{O}(\alpha_{em})$, α_{em} being the electromagnetic coupling, which will be explored elsewhere. Furthermore, the same concepts can also be applied for invariant mass dependent beam functions [33].

The main aim of this paper is to present the $\mathcal{O}(\alpha_s^2)$ results (and some details of their computation) for the primary massive quark SCET jet functions. They represent important ingredients in factorization theorems for massive quark production within an inclusive jet where the massive quark is produced by the hard interaction and where the jet masses are similar in size to the mass of the quark. To illustrate the application of the universal and the mass mode jet functions we also discuss their role in the equivalent factorization approaches of refs. [22, 26] and [32] using as an example the double differential hemisphere mass distribution in e^+e^- annihilation (for the hard production of a boosted massive quark-antiquark pair). This discussion also clarifies the relation between both approaches and furthermore emphasizes that a smooth dependence on the value of the quark mass m (in the sense that assumptions on the hierarchy of m with respect to the other physical scales are not mandatory) can be achieved with them. The latter issue was already fully accounted for in refs. [22, 26, 31] but not explored in ref. [32]. On the other hand, in ref. [32] a more systematic representation of the building blocks to sum virtuality and rapidity logarithms on an equal footing was provided.

The content of the paper is organized as follows. In section 2 we set up our notation and provide the definition of the universal and the mass mode SCET jet functions in the context of subtractions based on collinear-soft matrix elements. In section 3 we present our results for both SCET jet functions for massive primary quarks at $\mathcal{O}(\alpha_s^2)$ and show that (and in which way) the results are consistent with respect to available $\mathcal{O}(\alpha_s^2)$ results in the limit of massless quarks [8] and the bHQET limit [21]. The practical use of the jet functions in the context of the factorization approaches of refs. [22, 26, 31] and of ref. [32] is discussed in section 4 for the example of the double differential hemisphere mass distribution in e^+e^- annihilation. The discussion should be sufficient to illustrate how the jet functions can be

JHEP08(2019)112

used for other processes in the context of QCD as well as the electroweak theory. Here, we also show how both approaches, considered together, are useful to gain a clearer view on the summation of virtuality and rapidity logarithms, the structure of collinear and soft mass mode corrections and on how a smooth dependence on the quark mass m can be achieved in practical applications. Section 5 contains details of the calculations for the $\mathcal{O}(\alpha_s^2)$ corrections to the massive primary quark SCET jet functions. This section is self-contained and focuses on computational details because the calculations are involved and require specific methods for different types of diagrams that may be useful for similar future work. The readers not interested in these technical details may skip this section except for section 5.1 which summarizes the results for the jet-function and collinear-soft matrix elements with different infrared regulators. In section 6 we provide a brief numerical analysis of the universal primary massive quark SCET jet function at $\mathcal{O}(\alpha_s^2)$ in comparison to the corresponding known result in the massless quark and the bHQET limits. Finally, in section 7 we conclude. The paper also contains a number of appendices. In appendix A we provide the expressions for the universal and the mass mode jet functions at $\mathcal{O}(\alpha_s^2)$ for massless primary quarks for the sake of future use. The latter can be extracted from ref. [26] but was not given there. The massless limit of the non-distributional corrections of the primary massive SCET jet function is provided in appendix B, and a number of virtuality and rapidity anomalous dimensions used in the discussion of section 4 are collected in appendix C. Finally, in appendix D we provide the results for the two-loop master integrals needed for our calculations.

2 Jet function definitions and notation

Quark jet functions in SCET are based on the vacuum correlator of two SCET jet fields, encoding the inclusive collinear dynamics of quark fields coherently accounting for the collinear gluon radiation from all other color sources of a process. *We work in QCD with n_ℓ massless quark flavors and one quark flavor Q with mass m.* The SCET jet-function matrix element (ME) for a jet initiated by the primary quark f in light-like direction n^μ ($\vec{n}^2 = 1$) is given by [5, 12][2]

$$\begin{aligned}\mathscr{J}_f^{(n_\ell+1)}(p^2, m^2) &= \frac{(2\pi)^3}{N_c\, p^-}\,\mathrm{Tr}\left\langle 0\middle|\frac{\bar{n}\!\!\!/}{2}\chi_f^n(0)\,\delta(p^+ + \hat{p}^+)\,\delta(p^- + \overline{\mathcal{P}}_n)\,\delta^{(2)}(p_\perp + \mathcal{P}_{n\perp})\,\overline{\chi}_f^n(0)\middle|0\right\rangle \\ &= \delta(p^2 - m^2) + \mathcal{O}(\alpha_s)\,. \end{aligned} \tag{2.1}$$

We decompose four-vectors in lightcone components according to $p^\mu = p^- n^\mu/2 + p^+ \bar{n}^\mu/2 + p_\perp^\mu$ with $n^2 = \bar{n}^2 = 0$, $\bar{n}\cdot n = 2$, and $n\cdot p_\perp = \bar{n}\cdot p_\perp = 0$. The SCET label momentum operators $\overline{\mathcal{P}}_n$ and $\mathcal{P}_{n\perp}$ yield the sum of the large minus and perpendicular light-cone momentum labels of the fields on their right, respectively [6], while $\hat{p}^+$ is the momentum operator of the small plus momentum. The trace is over color ($N_c = 3$) and spinor indices. The SCET jet fields $\chi_f^n(x)$ are defined by

$$\chi_f^n(x) = W_n^\dagger(x)\xi_f^n(x)\,, \tag{2.2}$$

[2] We note that in this paper we write jet functions and jet-function MEs as functions of the invariant mass $p^2 \geq m^2$ in order to make all dependence on the quark mass m explicit.

where $\xi_f^n(x)$ is the SCET primary quark field and the n-collinear Wilson line can be written as

$$W_n(x) = \sum_{\text{perms}} \exp\left(\frac{-g}{\bar{n}\cdot\mathcal{P}}\,\bar{n}\cdot A_n(x)\right). \tag{2.3}$$

The Wilson lines in eq. (2.1) encode the universal coherent dynamics of collinear gluons coming from other color sources, which are boosted in direction $\vec{n} = -\vec{n}$ with respect to the direction of motion of the primary quark. They entail that the jet-function ME is gauge-invariant with respect to collinear gauge transformations [4].

After BPS field redefinition the collinear sectors of the (leading-order) SCET Lagrangian are equivalent to boosted versions of the QCD Lagrangian [4, 5]. We can thus express the n-collinear jet-function ME also in terms of QCD quark fields as [8]

$$\begin{aligned}\mathscr{J}_f^{(n_\ell+1)}(p^2,m^2) &= \frac{1}{4\pi N_c\,(\bar{n}\cdot p)}\int \mathrm{d}^4x\; e^{-ip\cdot x}\,\mathrm{Tr}\left\langle 0\middle|\frac{\bar{\not{n}}}{2}W^\dagger(0)\,\psi_f(0)\,\overline{\psi}_f(x)\,W(x)\middle|0\right\rangle \\ &= \mathrm{Im}\left[\frac{i}{2\pi N_c\,(\bar{n}\cdot p)}\int \mathrm{d}^4x\; e^{-ip\cdot x}\,\mathrm{Tr}\left\langle 0\middle|\mathrm{T}\left\{\frac{\bar{\not{n}}}{2}W^\dagger(0)\,\psi_f(0)\,\overline{\psi}_f(x)\,W(x)\right\}\middle|0\right\rangle\right], \end{aligned}\tag{2.4}$$

with the corresponding QCD definition for the n-collinear Wilson line

$$W(x) = \mathrm{P}\,\exp\left[i\,g\int_{-\infty}^{0}\mathrm{d}s\,\bar{n}\cdot A(x+s\bar{n})\right]. \tag{2.5}$$

In eq. (2.4) we have reexpressed the jet-function ME as the imaginary part of a jet field correlator. Taking the imaginary part is equivalent to half the discontinuity w.r.t. $s = p^2 - m^2 > 0$. In practice, for the computation of the two-loop corrections it is more convenient to work with eq. (2.4) rather than with the corresponding SCET expression of eq. (2.1), because the QCD Feynman rules are simpler than the SCET Feynman rules and lead to less diagrams.

In eqs. (2.1) and (2.4) the quark flavor index f stands for the flavor of the incoming primary quark and can either be one of the n_ℓ massless quarks, generically referred to as q, or the massive quark Q. The argument m represents the dependence on the mass of quark Q and arises either from secondary Q effects (due to gluon splitting) if the primary quark is a massless flavor q or from primary and secondary Q effects. The superscript $(n_\ell+1)$ in eqs. (2.1) and (2.4) (and for ME definitions and factorization functions used throughout this paper) indicates that we consider the MEs in the context of QCD with n_ℓ massless quarks and the massive quark Q. We stress, however, that here and throughout this work the superscript $(n_\ell+1)$ (or n_ℓ) on MEs or factorization functions does not automatically imply that also the corresponding flavor scheme for the $\overline{\text{MS}}$ strong coupling is used. The latter can in principle be chosen independently, particularly for renormalization scales μ close to the quark mass m. We therefore specify explicitly the flavor scheme of α_s when we quote results parametrized by either $\alpha_s^{(n_\ell)}$ or $\alpha_s^{(n_\ell+1)}$.

It is well known [12, 14] that the jet-function ME $\mathscr{J}_f^{(n_\ell+1)}(p^2,m^2)$ defined in eqs. (2.1) and (2.4) is per se not infrared-finite and commonly said to implicitly require as part of its definition zero-bin subtractions [24] to avoid double counting concerning the collinear

overlap with softer or lower virtuality regions described by other functions in factorization theorems where the jet function appears. *Alternatively*, one can consider the jet function as an IR-finite matching function that describes fluctuations with virtualities $p^2 - m^2 \sim p^2 \gtrsim m^2$ and that is defined by the jet-function ME $\mathscr{J}_f^{(n_\ell+1)}(p^2, m^2)$ with *additional* (i.e. independent) ME subtractions related to (soft and possibly collinear) modes at smaller virtualities. So far in the literature the required subtractions, when they contributed non-vanishing terms, were implemented mostly via the zero-bin [12, 14] or soft mass mode bin [22, 26, 34] prescriptions that are imposed by hand. However, from the point of view of being matching functions, the jet functions can also be defined in a conceptually more systematic way by explicitly dividing out fluctuations with momenta $n \cdot k = k^+ \sim p^2/Q$ and virtualities $k^2 \ll p^2 - m^2$ in terms of a so-called collinear-soft ME. This also has the advantage that no additional power counting arguments are mandatory to identify which contributions have to be accounted for (and which not), as it is necessary when implementing a bin subtraction.

In case that all $(n_\ell + 1)$ quarks are massless this results in the jet function definition

$$J_f^{(n_\ell+1)}(p^2, 0) \equiv \int \mathrm{d}\ell\, \mathscr{J}_f^{(n_\ell+1)}(p^2 - (\bar{n}\cdot p)\ell, 0) \Big(\mathscr{S}^{(n_\ell+1)}(\ell, 0)\Big)^{-1} . \tag{2.6}$$

Here $\mathscr{S}^{(n_\ell+1)}(\ell, m)$ is the collinear-soft ME of our $(n_\ell + 1)$ flavor theory (with n_ℓ massless quarks q and one quark Q with mass m) and defined as[3]

$$\mathscr{S}^{(n_\ell+1)}(\ell, m) = \frac{1}{N_c} \mathrm{Tr} \left\langle 0 \left| \overline{\mathrm{T}}\big[V_n^{(0)\dagger}(0) X_n^{(0)}(0)\big]\, \delta(\ell - \hat{p}^+)\, \mathrm{T}\big[X_n^{(0)\dagger}(0) V_n^{(0)}(0)\big] \right| 0 \right\rangle , \tag{2.7}$$

with the collinear-soft Wilson lines [27, 28]

$$\begin{aligned} X_n(x) &= \sum_{\text{perms}} \exp\left(\frac{-g}{n\cdot\mathcal{P}} \frac{\nu^{\eta/2}}{|\bar{n}\cdot\mathcal{P}|^{\eta/2}}\, n \cdot A_{cs}(x) \right) , \\ V_n(x) &= \sum_{\text{perms}} \exp\left(\frac{-g}{\bar{n}\cdot\mathcal{P}} \frac{\nu^{\eta/2}}{|\bar{n}\cdot\mathcal{P}|^{\eta/2}}\, \bar{n} \cdot A_{cs}(x) \right) , \end{aligned} \tag{2.8}$$

including the symmetric analytic rapidity regularization of ref. [23]. The inverse of the collinear-soft ME is defined by the convolution

$$\int \mathrm{d}\ell'\, \mathscr{S}^{(n_\ell+1)}(\ell - \ell', m) \Big(\mathscr{S}^{(n_\ell+1)}(\ell', m)\Big)^{-1} = \delta(\ell) , \tag{2.9}$$

and we use the analogue relations for defining the inverse of all (factorization) functions depending on dynamical variables. The combination of MEs in eq. (2.6) yields the well known IR finite massless quark jet function at one [7], two [8] and three loops [9]. The analogous definition (with the appropriate color representation for the Wilson lines) can be applied also for the gluon jet function [35–37]. For $(n_\ell + 1)$ massless quarks the subtraction

[3] Note that the collinear-soft matrix element is universal in the sense that it only depends on the color representations of the partons involved as noted in ref. [27]. Therefore the result is equivalent to the one given in eq. (B.51) of ref. [32] where massive quark effects in exclusive Drell-Yan were considered.

of the low virtuality modes is from the purely computational point of view, however, not strictly mandatory for computations of the jet function when dimensional regularization for UV and IR divergences is used because then $\mathscr{S}^{(n_\ell+1)}(\ell,0)$ yields vanishing scaleless integrals beyond tree-level.

On the other hand, when considering the quark Q having a finite mass m, $\mathscr{S}^{(n_\ell+1)}(\ell,m)$ is not anymore scaleless and yields non-vanishing $\mathcal{O}(\alpha_s^2 C_F T_F)$ contributions in dimensional regularization due to mass mode fluctuations with virtualities $k^2 \sim m^2$. We note that the mass mode contributions in the collinear-soft ME $\mathscr{S}^{(n_\ell+1)}(\ell,m)$ are only related to secondary effects of the massive quark Q due to closed Q loops, so that it is the same for the jet functions for a massless and a massive primary quark.

Interestingly, secondary massive quark effects do not lead to IR divergences (as long as one does not take the massless limit) that must always be subtracted. It is therefore not mandatory to use the massive quark analogue of eq. (2.6) to define the jet function. This is also related to the emergence of rapidity singularities, which one may not associate to be of either UV or IR type and leads to two options to define the SCET jet function in the context of QCD with n_ℓ massless flavors and one quark Q with mass m.

The first option is just the analogue of eq. (2.6) but with the $(n_\ell+1)$st quark Q having mass m,

$$J_f^{\text{uf},(n_\ell+1)}(p^2,m^2) \equiv \int \mathrm{d}\ell\, \mathscr{J}_f^{(n_\ell+1)}(p^2-(\bar{n}\cdot p)\ell,m^2)\Big(\mathscr{S}^{(n_\ell+1)}(\ell,m^2)\Big)^{-1}. \tag{2.10}$$

The primary jet-initiating quark flavor f can either be one of the n_ℓ massless quarks q or the massive quark Q. Here the collinear-soft ME is calculated in the full $(n_\ell+1)$ flavor theory and thus encodes in particular the secondary effects coming from the massive quark Q. This jet function yields by construction the massless quark jet function $J_f^{(n_\ell+1)}(p^2,0)$ of eq. (2.6) in the limit $m \to 0$. $J_f^{\text{uf},(n_\ell+1)}(p^2,m^2)$ and $J_f^{(n_\ell+1)}(p^2,0)$ have the same anomalous dimension and are furthermore free of rapidity divergences as well as of any large rapidity logarithms. For $J_f^{\text{uf},(n_\ell+1)}(p^2,m^2)$ both cancel between $\mathscr{J}_f^{(n_\ell+1)}$ and $\mathscr{S}^{(n_\ell+1)}$. Upon renormalizing $J_f^{\text{uf},(n_\ell+1)}$ the only dependence on a renormalization scale is that on the virtuality scale μ. Following the philosophy of the SCET jet function being a matching function describing fluctuations with virtuality $p^2-m^2 \sim p^2$, the jet function of eq. (2.10) is the mandatory definition for the case where $m^2 \ll p^2$ where the quark mass m is an IR scale and mass effects represent power corrections. In that regime, however, one may as well use the massless quark jet function $J_f^{(n_\ell+1)}(p^2,0)$. The jet function $J_f^{\text{uf},(n_\ell+1)}(p^2,m^2)$ can, however, also be employed for $p^2 \sim p^2-m^2 \sim m^2$ following the approach of refs. [22, 26] (originally developed for massless primary quark jet functions) where universal hard, jet and soft (and in principle also invariant mass dependent beam) functions can be defined valid for *any* value of m^2, with respect to the other dynamic scales and the renormalization scale μ. This approach makes the μ-evolution in n_ℓ or $(n_\ell+1)$ flavor schemes to sum virtuality logarithms particularly transparent and allows to formulate factorization theorems that smoothly interpolate all possible hierarchies as far as the value of m with respect to the other kinematic scales is concerned. The approach of refs. [22, 26] also entails that rapidity singularities (and the respective resummation of logarithms) only

JHEP08(2019)112

arise within the mass threshold matching conditions for the individual hard, jet (as well as beam) and soft factorization functions. Since these threshold matching conditions consist of a few universal collinear and soft mass mode factors, there can be cancellations among them in the context of a factorization theorem related to consistency relations. So mass mode factors can arise in the matching conditions that are physically not relevant for a particular observable and eventually cancel in the corresponding factorization theorem. We call this the "universal factorization function" approach and therefore give the jet function definition in eq. (2.10) the superscript "uf". In the following we call it the "universal jet function".

The second option is to define the jet function in the presence of a massive quark by

$$J_f^{\mathrm{mf},(n_\ell+1)}(p^2,m^2) = \int \mathrm{d}\ell\, \mathscr{J}_f^{(n_\ell+1)}(p^2-(\bar{n}\cdot p)\ell, m^2)\Big(\mathscr{S}^{(n_\ell)}(\ell)\Big)^{-1}, \tag{2.11}$$

where the collinear-soft ME is calculated in the n_ℓ flavor theory, i.e. containing the n_ℓ massless quarks but not accounting for the massive quark Q. Like for the jet function $J_f^{\mathrm{uf},(n_\ell+1)}$, the primary jet-initiating quark f can either be one of the n_ℓ massless quarks q or the massive quark Q. The jet function $J_f^{\mathrm{mf},(n_\ell+1)}$ is IR divergent for $m \to 0$ and furthermore has rapidity singularities that are treated by rapidity renormalization. So upon renormalization, $J_f^{\mathrm{mf},(n_\ell+1)}$ depends on the (virtuality) renormalization scale μ and in addition on the (rapidity) renormalization scale ν. Following the philosophy of the SCET jet function being a matching function describing the fluctuations with virtuality $p^2 - m^2 \sim p^2$, the jet function of eq. (2.11) is the natural option for the case where $m^2 \sim p^2 \sim p^2 - m^2$, when the mass is not an IR scale. It has also been advocated for this scale hierarchy in ref. [32] (originally developed for the massless primary quark and invariant mass dependent beam function [38]). In the factorization approach of ref. [32] separate factorization theorems are formulated for each possible hierarchy of the mass scale m with respect to the other kinematic scales. The approach is not designed to provide smooth dependence on m, but is more economical (in the sense of being minimalistic) concerning the appearance of collinear and soft mass mode contributions so that no cancellations arise between them in the context of a factorization theorem. Furthermore, the collinear and soft mass mode contributions adopt the status of genuine factorization functions. The resulting structure of factorization theorems makes the structure of ν-evolution to sum rapidity logarithms particularly transparent as it appears at the same level as the virtuality μ-evolution. We call this the "mass mode factorization" approach and therefore give the jet function definition in eq. (2.11) the superscript "mf". In the following we call it the "mass mode jet function".

The difference between both $\overline{\mathrm{MS}}$-renormalized massive quark jet function definitions yields[4]

$$\begin{aligned} S_c(\ell,m,\mu,\nu) &= \frac{1}{\bar{n}\cdot p}\int \mathrm{d}p'^2\, J_f^{\mathrm{mf},(n_\ell+1)}((\bar{n}\cdot p)\ell - p'^2, m^2, \mu, \bar{n}\cdot p/\nu)\big(J_f^{\mathrm{uf},(n_\ell+1)}(p'^2,m^2,\mu)\big)^{-1} \\ &= \int \mathrm{d}\ell\, \mathscr{S}^{(n_\ell+1)}(\ell-\ell',m,\mu,\nu)\Big(\mathscr{S}^{(n_\ell)}(\ell',\mu,\nu)\Big)^{-1}, \end{aligned} \tag{2.12}$$

[4]The inverse jet function is defined in analogy to eq. (2.9).

and is called the "collinear-soft function" in ref. [32]. It is IR-finite for finite m and has a dependence on the virtuality and the rapidity renormalization scales μ and ν, respectively.

In section 4 we illustrate the practical use of both types of jet functions and the two factorization approaches of refs. [22, 26] and [32] exemplarily for the double differential hemisphere mass distribution in e^+e^- collisions for the hierarchies $m^2 \sim p^2 \sim p^2 - m^2$ and $m^2 \ll p^2$. We also stress that the form of the collinear-soft ME of eq. (2.7) and the two options of using either eq. (2.10) or eq. (2.11) for IR finite jet functions in the presence of massive quarks can also be applied in a fully equivalent way for invariant mass dependent beam functions [38] and the bHQET jet function [12, 14].[5] The approach also applies in an analogous way for the treatment of massive gauge bosons which is conceptually related to the issues of secondary quark mass effects as was discussed in [22].

3 Analytic results: primary massive quark SCET jet functions

In this section we present the analytic results for the $\mathcal{O}(\alpha_s^2)$ primary quark SCET jet functions. Details on the computation of the $\mathcal{O}(\alpha_s^2)$ corrections, which are all new, are given in section 5. We use the abbreviations

$$a_s^{(n_f)} \equiv \frac{\alpha_s^{(n_f)}(\mu)}{4\pi} \qquad \text{and} \qquad s \equiv p^2 - m^2\,, \tag{3.1}$$

for the strong coupling in the n_f-flavor scheme and the squared jet function invariant mass p^2, respectively,

$$L_m \equiv \log\frac{m^2}{\mu^2}\,, \tag{3.2}$$

as well as

$$\mathcal{L}_n(x) \equiv \frac{1}{\mu^\lambda}\left[\frac{\Theta(x)\log^n(x/\mu^\lambda)}{x/\mu^\lambda}\right]_+, \tag{3.3}$$

for plus-distributions for a variable x having mass dimension λ, where μ is the common $\overline{\text{MS}}$ renormalization scale. They are defined such that $\int_0^1 \mathrm{d}x\, \mathcal{L}_n(x) = 0$. Furthermore we define

$$y \equiv \frac{m^2}{p^2}\,, \qquad \bar{y} \equiv \frac{s}{p^2} = 1 - y\,, \qquad L_y \equiv \log(y)\,, \qquad L_{\bar{y}} \equiv \log(\bar{y})\,. \tag{3.4}$$

In the physical kinematic region we have $0 \le y, \bar{y} \le 1$. Note that we also use the notation

$$Q \equiv (\bar{n}\cdot p) = p^-\,, \tag{3.5}$$

and that we carry out all computations in $d = 4 - 2\varepsilon$ dimensions.

[5] In the context of bHQET [12, 14] we refer to the situation that some of the n_ℓ light flavors have finite masses smaller than the mass m of the primary HQET quark, but larger than the hadronization scale Λ_{QCD}. The equivalence of the collinear-soft MEs (or the zero-bin subtractions) for SCET and bHQET is a consequence of a rescaling property of the bHQET and SCET soft gluon eikonal couplings that can e.g. be trivially seen from the structure of the zero-bin diagrams in both effective theories.

JHEP08(2019)112

3.1 Mass mode jet function

The result for the renormalized primary massive mass mode jet function $J_Q^{\mathrm{mf},(n_\ell+1)}$, defined in eq. (2.11), in the pole mass scheme at $\mathcal{O}(\alpha_s^2)$ can be written in the form

$$J_Q^{\mathrm{mf},(n_\ell+1)}(p^2,m^2,\mu,Q/\nu) = \delta(p^2-m^2) + a_s^{(n_\ell)} J_Q^{(1)}(p^2,m^2,\mu) + \left(a_s^{(n_\ell)}\right)^2 \left(J_Q^{(2)}(p^2,m^2,\mu) + J_{Q,\mathrm{sec}}^{(2),\mathrm{mf}}(p^2,m^2,\mu,Q/\nu)\right) + \mathcal{O}\left(\alpha_s^3\right), \tag{3.6}$$

where we adopt the n_ℓ flavor scheme for the strong coupling. This can be considered the natural scheme choice for the mass mode jet function since it matches directly to the bHQET jet function, see section 3.3. It is of course straightforward to switch to the $(n_\ell+1)$ flavor scheme using eq. (3.30). At $\mathcal{O}(\alpha_s^2)$ we distinguish between the corrections from diagrams containing only one single quark Q line ($J_Q^{(2)}$) and those from diagrams containing the $Q\bar{Q}$ vacuum polarization correction ($J_{Q,\mathrm{sec}}^{(2)}$). The mass mode jet function contains rapidity singularities from the $Q\bar{Q}$ vacuum polarization diagrams which are renormalized following the approach of [23, 39] and which lead to the dependence on the rapidity renormalization scale ν. For the prototypical application of the mass mode jet function within factorization theorems where all logarithms are resummed by explicit renormalization group evolution factors the natural choice for the rapidity renormalization scale is $\nu \sim Q$. This is indicated by the argument Q/ν. Throughout this paper we adopt this convention for the rapidity scale ν in an analogous way. In case the natural choice for ν is process (or factorization theorem) dependent, only ν appears as the argument.

The $\mathcal{O}(\alpha_s)$ contribution accounting for terms up to $\mathcal{O}(\varepsilon^2)$ in order to maintain all information mandatory for $\mathcal{O}(\alpha_s^2)$ calculations reads

$$\begin{aligned}
J_Q^{(1)}(p^2,m^2,\mu) = C_F \Bigg\{ & \left(2L_m^2 + L_m - \frac{\pi^2}{3} + 8\right)\delta(s) + (-4L_m - 4)\mathcal{L}_0(s) + 8\mathcal{L}_1(s) \\
& + G_1 \Theta(p^2-m^2) \\
& + \varepsilon \Bigg[\left(\frac{3}{2}L_m^2 - \frac{2\pi^2}{3}L_m + 16 - \frac{5\pi^2}{12} - \frac{16\zeta_3}{3}\right)\delta(s) + \left(-2L_m^2 - 4L_m - 8 + \pi^2\right)\mathcal{L}_0(s) \\
& \quad + (8 + 8L_m)\mathcal{L}_1(s) - 8\mathcal{L}_2(s) + G_1^{(\varepsilon)}\Theta(p^2-m^2) \Bigg] \\
& + \varepsilon^2 \Bigg[\left(\frac{1}{6}L_m^4 + \frac{1}{6}L_m^3 + \left(4 - \frac{\pi^2}{6}\right)L_m^2 + \left(-\frac{7\pi^2}{12} - 4\zeta_3\right)L_m + 32 - \frac{2\pi^2}{3} - \frac{\pi^4}{120} - 5\zeta_3\right)\delta(s) \\
& \quad + \left(-\frac{2}{3}L_m^3 - 2L_m^2 + (-8+\pi^2)L_m - 16 + \pi^2 + \frac{28\zeta_3}{3}\right)\mathcal{L}_0(s) \\
& \quad + \left(4L_m^2 + 8L_m + 16 - 2\pi^2\right)\mathcal{L}_1(s) + (-8 - 8L_m)\mathcal{L}_2(s) + \frac{16}{3}\mathcal{L}_3(s) + G_1^{(\varepsilon^2)}\Theta(p^2-m^2) \Bigg] \Bigg\}.
\end{aligned} \tag{3.7}$$

Here, all distributional contributions are displayed explicitly and the non-distributional contributions are contained in the functions

$$G_1 = \frac{1}{s}\left[\bar{y}^2 + 4L_y\right] = -\frac{4}{m^2} + \mathcal{O}\left(\frac{s}{m^4}\right), \tag{3.8}$$

$$\begin{aligned}
G_1^{(\varepsilon)} &= \frac{1}{s}\left[\left(-\bar{y}^2 - 4L_y\right)L_m + L_y\left(-8L_{\bar{y}} + y^2 - 2y + 5\right) - 2\bar{y}^2 L_{\bar{y}} + \bar{y}^2 + 6L_y^2\right] \\
&= -\frac{4}{m^2}\left(-2\log(\bar{y}/y) - L_m + 1\right) + \mathcal{O}\left(\frac{s}{m^4}\right),
\end{aligned} \tag{3.9}$$

$$
\begin{aligned}
G_1^{(\varepsilon^2)} &= \frac{1}{s}\Bigg[\Big(L_y\left(8L_{\bar y}-y^2+2y-5\right)+2\bar y^2 L_{\bar y}-\bar y^2-6L_y^2\Big)L_m+\left(\frac{\bar y^2}{2}+2L_y\right)L_m^2 \\
&\quad + L_y^2\left(\frac{1}{2}\left(y^2-2y+13\right)-12L_{\bar y}\right)+2\bar y^2 L_{\bar y}^2-2\bar y^2 L_{\bar y}-\frac{1}{4}\left(\pi^2-8\right)\bar y^2+\frac{14}{3}L_y^3 \\
&\quad + L_y\Big(-2\left(y^2-2y+5\right)L_{\bar y}+8L_{\bar y}^2+y^2-2y-\pi^2+9\Big)\Bigg] \\
&= \frac{1}{m^2}\left[\left(4-8\log(\bar y/y)\right)L_m-8\log^2(\bar y/y)+8\log(\bar y/y)-2L_m^2+\pi^2-8\right]+\mathcal{O}\left(\frac{s}{m^4}\right).
\end{aligned}
\tag{3.10}
$$

These functions do not contribute to the singular behavior in the bHQET limit $s = p^2 - m^2 \ll m^2$ and thus represent power corrections in this kinematic region. They constitute the so-called $\mathcal{O}(\alpha_s)$ bHQET non-singular corrections that are important for physical factorization predictions in the region $s \lesssim m^2$ to achieve a smooth transition between bHQET and SCET factorization theorems [12, 13]. For completeness we also quoted the $s \to 0$ limit of the G_1-functions. The $\varepsilon \to 0$ limit of eq. (3.7) was already given in ref. [14], and we refer to this reference for pictures of the Feynman diagrams and details of the calculation. The determination of the $\mathcal{O}(\varepsilon)$ and $\mathcal{O}(\varepsilon^2)$ contributions is straightforward.

The $\mathcal{O}(\alpha_s^2)$ contributions arising from Feynman diagrams containing only one single quark Q line (see all diagrams in figure 1 with the diagrams (o)-(r) containing only massless quark bubbles) read

$$
\begin{aligned}
J_Q^{(2)}(p^2,m^2,\mu) &= C_F^2\Bigg\{\Bigg[2L_m^4+2L_m^3+\left(\frac{33}{2}-2\pi^2\right)L_m^2+\left(-56\zeta_3+\frac{13}{2}-\pi^2\right)L_m \\
&\quad -38\zeta_3-\frac{\pi^4}{2}+\frac{433}{8}+\pi^2\left(-\frac{1}{3}-8\log 2\right)\Bigg]\delta(s) \\
&\quad +\left[-8L_m^3-12L_m^2+\left(\frac{20\pi^2}{3}-36\right)L_m+64\zeta_3+\frac{20\pi^2}{3}-32\right]\mathcal{L}_0(s) \\
&\quad +\left[32L_m^2+40L_m-\frac{40}{3}\left(\pi^2-6\right)\right]\mathcal{L}_1(s)+[-48L_m-48]\mathcal{L}_2(s)+32\mathcal{L}_3(s) \\
&\quad +G_{C_F}^{(1Q)}\Theta(p^2-m^2)+G^{(3Q)}\Theta(p^2-(3m)^2)\Bigg\} \\
&\quad +C_F C_A\Bigg\{\Bigg[\left(\frac{367}{18}-\frac{2\pi^2}{3}\right)L_m^2+\left(20\zeta_3+\frac{341}{18}-\frac{56\pi^2}{9}\right)L_m-\frac{188\zeta_3}{9}-\frac{2\pi^4}{15}+\frac{60221}{648} \\
&\quad +\pi^2\left(4\log 2-\frac{169}{54}\right)\Bigg]\delta(s) \\
&\quad +\left[-\frac{22}{3}L_m^2+\frac{4}{9}\left(3\pi^2-100\right)L_m+\frac{4}{27}\left(135\zeta_3-547+42\pi^2\right)\right]\mathcal{L}_0(s) \\
&\quad +\left[\frac{88}{3}L_m-\frac{8\pi^2}{3}+\frac{800}{9}\right]\mathcal{L}_1(s)-\frac{88}{3}\mathcal{L}_2(s)+G_{C_A}^{(1Q)}\Theta(p^2-m^2)-\frac{1}{2}G^{(3Q)}\Theta(p^2-(3m)^2)\Bigg\} \\
&\quad +C_F T_F n_\ell\Bigg\{\left[-\frac{58}{9}L_m^2+\frac{2}{9}\left(8\pi^2-37\right)L_m+\frac{1}{162}\left(288\zeta_3-6037+132\pi^2\right)\right]\delta(s) \\
&\quad +\left[\frac{8}{3}L_m^2+\frac{128}{9}L_m-\frac{16}{27}\left(3\pi^2-47\right)\right]\mathcal{L}_0(s)+\left[-\frac{32}{3}L_m-\frac{256}{9}\right]\mathcal{L}_1(s)+\frac{32}{3}\mathcal{L}_2(s) \\
&\quad +G_{T_F}\Theta(p^2-m^2)\Bigg\}.
\end{aligned}
\tag{3.11}
$$

The distributional contributions are again displayed explicitly. There are two sets of non-distributional contributions. One set ($\propto \Theta(p^2-m^2)$) is related to terms that are non-vanishing above the one-particle cut and the other ($\propto \Theta(p^2-(3m)^2)$) is related to terms that are non-vanishing above the three particle $QQ\bar{Q}$ cut. Even though the term $J_Q^{(2)}$ exclusively arises from diagrams with one single quark Q line, see figure 1, three particle $QQ\bar{Q}$ cuts can arise due to the antiparticle component of the quark Q propagator. The non-distributional contributions $\propto \Theta(p^2-m^2)$ read

$$
\begin{aligned}
G_{C_F}^{(1Q)} = \frac{1}{s}\Big\{ & L_m^2\left(2\bar{y}^2+8L_y\right)+L_m\Big[4\bar{y}^2L_{\bar{y}}+L_y\left(16L_{\bar{y}}-4(2(y-2)y+5)\right)-7\bar{y}^2-24L_y^2\Big] \\
& +L_y\Big[\frac{4}{\bar{y}}\Big(3y\left(y^2+y+5\right)-13\Big)L_{\bar{y}}+24L_{\bar{y}}^2-8\,\mathrm{Li}_2(-\bar{y}/y)-\frac{2}{\bar{y}} \\
& \quad -2y\Big(y(3y-17)+35\Big)-\frac{16\pi^2}{3}+47\Big]+L_y^2\Big[-36L_{\bar{y}}-\frac{32}{\bar{y}}+8y(y+5)+76\Big] \\
& +2L_{\bar{y}}\Big[8\,\mathrm{Li}_2(-\bar{y}/y)+y(y(3y-17)+37)-7\Big]-8(y-2)\bar{y}L_{\bar{y}}^2 \\
& +\frac{4}{\bar{y}}\Big((2-21y)y+7\Big)\,\mathrm{Li}_2(-\bar{y}/y)+32\,\mathrm{Li}_3(\bar{y})-16\,\mathrm{Li}_3(-\bar{y}/y)+\frac{97}{90}\pi^4y\bar{y} \\
& +8(3y-13)\zeta_3\bar{y}+\frac{1}{3}\pi^2\bar{y}\Big(y(72\log 2-49)+15\Big)+\frac{68}{3}L_y^3-\frac{3}{2}y^2-65y+\frac{33}{2}+G_{\mathrm{fit}}(y)\Big\} \\
= & \frac{1}{m^2}\Big[L_m\Big(12-16\log(\bar{y}/y)\Big)-15.0\log^2(\bar{y}/y)+22.0992\log(\bar{y}/y)-8L_m^2-13.8568\Big] \\
& +\mathcal{O}\Big(\frac{s}{m^4}\Big),
\end{aligned}
\tag{3.12}
$$

$$
\begin{aligned}
G_{C_A}^{(1Q)} = \frac{1}{s}\Big\{ & L_m\frac{11}{3}\left(-\bar{y}^2-4L_y\right)+2L_y\Big[-2L_{\bar{y}}^2+\Big(-\frac{8}{\bar{y}}+12y-\frac{5}{3}\Big)L_{\bar{y}} \\
& \quad -\frac{1}{9\bar{y}}\Big(54\bar{y}\,\mathrm{Li}_2(-\bar{y}/y)-3\pi^2\bar{y}+y\Big(3y(5y+18)+107\Big)-212\Big)\Big] \\
& +L_y^2\Big(-2L_{\bar{y}}+\frac{16}{\bar{y}}-28y+\frac{25}{3}\Big)+2(y-3)\bar{y}L_{\bar{y}}^2-\frac{2}{3}\Big(y(5y+17)+2\Big)L_{\bar{y}} \\
& -\frac{2}{3\bar{y}}\Big[y\Big(3y(y-24)+40\Big)-7\Big]\,\mathrm{Li}_2(-\bar{y}/y)-32\,\mathrm{Li}_3(\bar{y})-24\,\mathrm{Li}_3(-\bar{y}/y) \\
& +\frac{4}{9}\Big(9(13-3y)\zeta_3\bar{y}+46y^2-17y+43\Big)-\frac{97}{180}\pi^4y\bar{y} \\
& -\frac{1}{3}\pi^2\bar{y}\Big(y(36\log 2-26)+9\Big)-2L_y^3-\frac{G_{\mathrm{fit}}(y)}{2}\Big\} \\
= & \frac{1}{m^2}\left[-0.5\log^2(\bar{y}/y)+26.2837\log(\bar{y}/y)+\frac{44}{3}L_m-37.1102\right]+\mathcal{O}\Big(\frac{s}{m^4}\Big),
\end{aligned}
\tag{3.13}
$$

$$
\begin{aligned}
G_{T_F} = \frac{1}{s}\Big\{ & L_m\Big[\frac{4}{3}\bar{y}^2+\frac{16}{3}L_y\Big]+\frac{8}{3}\bar{y}^2L_{\bar{y}}+L_y\Big[\frac{32}{3}L_{\bar{y}}+\frac{4}{9\bar{y}}\Big(y(6(y-3)y+29)-35\Big)\Big] \\
& -\frac{2}{9}\Big[24\,\mathrm{Li}_2(-\bar{y}/y)+y(19y-26)+43\Big]-\frac{32}{3}L_y^2\Big\}
\end{aligned}
\tag{3.14}
$$

$$
= -\frac{8}{9m^2}\Big(6L_m+12\log(\bar{y}/y)-19\Big)+\mathcal{O}\Big(\frac{s}{m^4}\Big)\,.
$$

The non-distributional contributions $\propto \Theta(p^2-(3m)^2)$ read

$$
\begin{aligned}
G^{(3Q)} = \frac{1}{s}\Bigg[& \frac{\sqrt{\left(1-\sqrt{y}\right)\left(1+3\sqrt{y}\right)}\left(3y^2+44y-7\right)}{\left(\sqrt{y}+1\right)} \mathrm{E}\left(\frac{\left(1-3\sqrt{y}\right)\left(1+\sqrt{y}\right)^3}{\left(1+3\sqrt{y}\right)\left(1-\sqrt{y}\right)^3}\right) \\
& - \frac{8\sqrt{1+3\sqrt{y}}\left(3y^{5/2}-18y^{3/2}+3y^3+43y^2-y+3\sqrt{y}-1\right)}{3\left(1-\sqrt{y}\right)^{5/2}\left(1+\sqrt{y}\right)} \mathrm{K}\left(\frac{\left(1-3\sqrt{y}\right)\left(1+\sqrt{y}\right)^3}{\left(1+3\sqrt{y}\right)\left(1-\sqrt{y}\right)^3}\right) \\
& + I_3(y)\frac{8y(1+y)^2}{3\bar{y}}\Bigg] \\
= & \frac{\pi(p^2-(3m)^2)^2}{3456\sqrt{3}m^6} + \mathcal{O}\left(\frac{(p^2-(3m)^2)^3}{m^8}\right).
\end{aligned}
\tag{3.15}
$$

The non-distributional contributions $\propto \Theta(p^2-m^2)$ coming from diagrams (b) and (c) in figure 1 could only be computed numerically for general values of p^2 and m^2, and are parametrized by the fit function G_{fit} which has the convenient form[6]

$$
\begin{aligned}
G_{\text{fit}}(y) = \bar{y}\Bigg[& c_{11}\left(\frac{1}{6}\pi^2 y + L_{\bar{y}}\right) + c_{12}\left(L_{\bar{y}}^2 - 2y\zeta_3\right) + c_{21}\left(\frac{1}{6}\left(\pi^2-6\right)y + \bar{y}L_{\bar{y}}\right) \\
& + c_{22}\left(\bar{y}L_{\bar{y}}^2 - 2y(\zeta_3-1)\right) + c_{23}\left(\frac{1}{15}\left(\pi^4-90\right)y + \bar{y}L_{\bar{y}}^3\right)\Bigg],
\end{aligned}
\tag{3.16}
$$

with

$$
c_{11} = -41.9008,\ c_{12} = 1.0,\ c_{21} = -20.2744,\ c_{22} = -10.5870,\ c_{23} = -7.1277\,. \tag{3.17}
$$

With the values of the fitting parameters c_{ij} quoted in eq. (3.17) the fit function G_{fit} approximates the corresponding numerical results obtained in section 5.2.2 with a relative precision of better than 0.5%. Also accounting for the intrinsic uncertainty of the numerical results we reach an accuracy of at least 1% for G_{fit}. Besides that we note that the contributions parametrized in the fit function account for less then 0.5% of the $\mathcal{O}(\alpha_s^2)$ corrections for all physical values of $y = m^2/p^2$. So for all practical purposes the uncertainties associated to G_{fit} are negligible, and we did not quote uncertainties in eq. (3.17).

The $\mathcal{O}(\alpha_s^2)$ contributions arising from Feynman diagrams containing the $Q\bar{Q}$ vacuum polarization subdiagrams (see diagrams (o)-(r) in figure 1 with only massive quark bubbles) read

$$
\begin{aligned}
J_{Q,\text{sec}}^{(2),\text{mf}}(p^2,m^2,\mu,Q/\nu) = C_F T_F \Bigg\{ & \Bigg[2L_m^2 + \left(\frac{2}{3}+\frac{8\pi^2}{9}\right)L_m + \frac{3139}{162} - \frac{4\pi^2}{3} + \frac{8\zeta_3}{3} \\
& - \left(\frac{8}{3}L_m^2 + \frac{80}{9}L_m + \frac{224}{27}\right)\log\left(\frac{Q}{\nu}\right)\Bigg]\delta(s) + G_{\text{sec}}^{(3Q)}\Theta\big(p^2-(3m)^2\big)\Bigg\},
\end{aligned}
\tag{3.18}
$$

where again the distributional contributions are displayed explicitly. The dependence on the rapidity renormalization scale ν is displayed explicitly in terms of the logarithm

[6] We note that the function G_{fit} contains contributions arising both from Q and $QQ\bar{Q}$ final states.

JHEP08(2019)112

$\log(Q/\nu)$. In the $(n_\ell+1)$ flavor scheme for the strong coupling the coefficient $J^{(2),\mathrm{mf}}_{Q,\mathrm{sec}}$ is the only one that is modified: $J^{(2),\mathrm{mf}}_{Q,\mathrm{sec}} \to J^{(2),\mathrm{mf}}_{Q,\mathrm{sec}} + 4/3 L_m J^{(1)}_Q$.

The non-distributional contributions arise entirely from the three particle $QQ\bar{Q}$ cut and its result reads

$$
\begin{aligned}
G^{(3Q)}_{\mathrm{sec}} = \frac{1}{s}\Bigg[& -\frac{8\left(252y^{9/2}+570y^{7/2}+822y^{5/2}+118y^{3/2}+45y^5+357y^4+720y^3+524y^2\right)}{27\sqrt{1+3\sqrt{y}}\left(1-\sqrt{y}\right)^{5/2}\left(\sqrt{y}+1\right)^3} \\
& \times \frac{8\left(y+10\sqrt{y}+5\right)}{9\sqrt{1+3\sqrt{y}}\left(1-\sqrt{y}\right)^{5/2}\left(\sqrt{y}+1\right)^3}\,\mathrm{K}\left(\frac{\left(1-3\sqrt{y}\right)\left(1+\sqrt{y}\right)^3}{\left(1+3\sqrt{y}\right)\left(1-\sqrt{y}\right)^3}\right) \\
& + \frac{2\sqrt{\left(1-\sqrt{y}\right)^3\left(1+3\sqrt{y}\right)}\left(81y^4+54y^3-24y^2-54y+71\right)}{27\bar{y}^3}\,\mathrm{E}\left(\frac{\left(1-3\sqrt{y}\right)\left(1+\sqrt{y}\right)^3}{\left(1+3\sqrt{y}\right)\left(1-\sqrt{y}\right)^3}\right) \\
& + \frac{32y^{1/4}\left(15y^3+27y^2+25y+5\right)}{9\sqrt{\left(1-\sqrt{y}\right)^3\left(3\sqrt{y}+1\right)\bar{y}}}\,\Pi\left(\frac{\left(1-3\sqrt{y}\right)\left(1+\sqrt{y}\right)}{\left(1-\sqrt{y}\right)^2};\frac{\left(1-3\sqrt{y}\right)\left(1+\sqrt{y}\right)^3}{\left(1+3\sqrt{y}\right)\left(1-\sqrt{y}\right)^3}\right) \\
& + \frac{16}{3}\hat{I}(y)\Bigg] = \frac{11\pi(p^2-(3m)^2)^2}{5184\sqrt{3}m^6} + \mathcal{O}\left(\frac{(p^2-(3m)^2)^3}{m^8}\right).
\end{aligned}
\tag{3.19}
$$

The non-distributional three particle $QQ\bar{Q}$ cut contributions in $J^{(2)}_Q$ and $J^{(2)}_{Q,\mathrm{sec}}$ involve the elliptic functions

$$
\mathrm{K}(m) \equiv \int_0^{\frac{\pi}{2}} \mathrm{d}t\, \frac{1}{\sqrt{1-m\sin^2 t}}\,, \tag{3.20}
$$

$$
\mathrm{E}(m) \equiv \int_0^{\frac{\pi}{2}} \mathrm{d}t\, \sqrt{1-m\sin^2 t}\,, \tag{3.21}
$$

$$
\Pi(n;m) \equiv \int_0^{\frac{\pi}{2}} \mathrm{d}t\, \frac{1}{(1-n\sin^2 t)\sqrt{1-m\sin^2 t}}\,, \tag{3.22}
$$

and the integral functions

$$
I_3(y) = \int_9^{1/y} \mathrm{d}t\, \frac{2\,(t-9)}{(t-1)\sqrt{(\sqrt{t}+3)(\sqrt{t}-1)^3}}\,\mathrm{K}\left(\frac{\left(\sqrt{t}-3\right)\left(\sqrt{t}+1\right)^3}{(\sqrt{t}+3)(\sqrt{t}-1)^3}\right), \tag{3.23}
$$

$$
\tilde{I}(y) = \int_y^{\frac{1}{4}(1-\sqrt{y})^2} \mathrm{d}z\, \frac{\sqrt{z-y}\,\log\left(\frac{y-4z-1-\sqrt{(y+4z-1)^2-16yz}}{y-4z-1+\sqrt{(y+4z-1)^2-16yz}}\right)}{z^{3/2}}\,, \tag{3.24}
$$

which can be readily evaluated numerically. For related discussions see e.g. ref. [40]. In practical applications it is, however, useful to have an approximate representation of $G^{(3Q)}$ and $G^{(3Q)}_{\mathrm{sec}}$ involving only elementary functions. Such approximate representations are

provided by

$$
\begin{aligned}
G^{(3Q)} \approx \frac{1}{m^2}\Bigg\{ & c_1^{C_F(3Q)}\left[81y^2\left(9y+\frac{1}{4}\right)\log(9y)-\frac{81}{8}y^2(9y-1)(27y+7)\right] \\
& + c_2^{C_F(3Q)}\left[81y^2\left(81y^2-\frac{1}{3}\right)\log(9y)-27y^2(9y-1)(45y-3)\right] \\
& - \frac{1}{256}y(9y-1)\Bigg[-243y^2\Big(-64\left(176\zeta_3-209+8\log^2 3-8\log 3\right)+9\sqrt{3}\pi \\
& \quad + 128\pi^2(16\log 2-11)\Big)+9y\Big(-64\left(1584\zeta_3-1869+72\log^2 3-88\log 3\right) \\
& \quad + 45\sqrt{3}\pi+1152\pi^2(16\log 2-11)\Big)+256(4\log 3-7)\Bigg] \\
& + 9y\log(9y)\Bigg[9y\Big(\frac{1}{18}\left(-528\zeta_3+611-24\log^2 3+40\log 3\right)+\frac{\sqrt{3}\pi}{128} \\
& \quad + \frac{1}{3}\pi^2(16\log 2-11)\Big)-\frac{2}{9}\Bigg]\Bigg\} \qquad (3.25) \\
= \frac{9y}{m^2}\big[& -1.4175(1-9y)+1.6758(1-9y)^2-0.5478(1-9y)^3-1.4175\log(9y) \\
& + 2.3420(1-9y)\log(9y)-1.3552(1-9y)^2\log(9y)+0.2085(1-9y)^3\log(9y)\big], \\
G^{(3Q)}_{\rm sec} \approx \frac{1}{m^2}\Bigg\{ & c^{T_F(3Q)}\left[81y^2\left(9y+\frac{1}{4}\right)\log(9y)-\frac{81}{8}y^2(9y-1)(27y+7)\right] \\
& + \frac{y(9y-1)}{3456}\Bigg[-64\Big(81y^2\left(432\zeta_3-2053+576\log^3 3+72\log^2 3+816\log 3\right) \\
& \quad + 9y\left(-1296\zeta_3+6491-1728\log^3 3+360\log^2 3-2688\log 3\right) \\
& \quad + 4\left(359+144\log^2 3-348\log 3\right)\Big)+8019\sqrt{3}\pi y(27y-5) \\
& \quad + 384\pi^2\Big(243y^2(8\log 3-9)+9y(89-72\log 3)+8\Big)\Bigg] \\
& + 9y\log(9y)\Bigg[9y\Big(\frac{1}{81}\left(-144\zeta_3+863-192\log^3 3+168\log^2 3-448\log 3\right) \\
& \quad + \frac{11\pi}{64\sqrt{3}}+\frac{2}{81}\pi^2(24\log 3-35)\Big)-\frac{4}{81}(24\log 3-29)\Bigg]+\frac{8}{3}y\log^2(9y)\Bigg\} \qquad (3.26) \\
= \frac{9y}{m^2}\big[& -0.2586(1-9y)+0.5931(1-9y)^2-0.0707(1-9y)^3-0.2586\log(9y) \\
& + 0.7070(1-9y)\log(9y)-0.3183(1-9y)^2\log(9y)+0.2963\log^2(9y)\big],
\end{aligned}
$$

with $c_1^{C_F(3Q)} = -0.7298$, $c_2^{C_F(3Q)} = -0.2085$, $c^{T_F(3Q)} = -0.3183$. They both approximate the exact expressions to better than 0.5% over the physical kinematic range and provide exact analytic results in the limit $p^2 \to 9m^2$ and $m \to 0$. We also quoted a fully numerical version of the expressions useful for practical applications.

JHEP08(2019)112

In analogy to the non-distributional terms at $\mathcal{O}(\alpha_s)$ the non-distributional G-functions at $\mathcal{O}(\alpha_s^2)$ do not contribute to the singular contributions in the bHQET limit $s = p^2 - m^2 \ll m^2$. They represent power corrections in this kinematic region and constitute the $\mathcal{O}(\alpha_s^2)$ bHQET non-singular corrections. For completeness we also quoted the respective results in the limit $p^2 \to m^2$ (eqs. (3.12)–(3.14)) and in the limit $p^2 \to 9m^2$ (eqs. (3.15) and (3.19)).

For completeness we also provide the result for the renormalized mass mode jet function $J_q^{\mathrm{mf},(n_\ell+1)}(p^2, m^2, \mu, Q/\nu)$ for massless primary quarks in eq. (A.1), which can be extracted from the calculations in ref. [26], but was not given in the literature before. The μ (virtuality) and ν (rapidity) anomalous dimensions of the mass mode jet functions for massive and massless primary quarks agree identically.

3.2 Universal jet function

The result for the renormalized primary massive universal jet function $J_Q^{\mathrm{uf},(n_\ell+1)}$, defined in eq. (2.10), in the pole mass scheme at $\mathcal{O}(\alpha_s^2)$ can be written in the form

$$\begin{aligned} J_Q^{\mathrm{uf},(n_\ell+1)}(p^2, m^2, \mu) &= \delta(p^2 - m^2) + a_s^{(n_\ell+1)} J_Q^{(1)}(p^2, m^2, \mu) \\ &\quad + \left(a_s^{(n_\ell+1)}\right)^2 \left(J_Q^{(2)}(p^2, m^2, \mu) + J_{Q,\mathrm{sec}}^{(2),\mathrm{uf}}(p^2, m^2, \mu)\right) + \mathcal{O}(\alpha_s^3)\,, \end{aligned} \tag{3.27}$$

where we adopt the $(n_\ell + 1)$ flavor scheme for the strong coupling, which is the natural scheme choice for the universal jet function. The universal jet function does not contain rapidity divergences and thus only depends on the UV renormalization scale μ coming from dimensional regularization. The $\mathcal{O}(\alpha_s)$ coefficient $J_Q^{(1)}$ and the $\mathcal{O}(\alpha_s^2)$ contribution from diagrams containing only one single quark Q line $J_Q^{(2)}$ (see all diagrams in figure 1 with the diagrams (o)-(r) containing only massless quark bubbles) are identical to the mass mode jet function and given in eqs. (3.7) and (3.11), respectively.

The $\mathcal{O}(\alpha_s^2)$ contributions arising from Feynman diagrams containing the $Q\bar{Q}$ vacuum polarization subdiagrams (see diagrams (o)-(r) in figure 1 containing only massive quark bubbles) read

$$\begin{aligned} J_{Q,\mathrm{sec}}^{(2),\mathrm{uf}}(p^2, m^2, \mu) = C_F T_F \Bigg[&\left(\frac{32}{9} L_m^3 + \frac{70}{9} L_m^2 + \frac{754}{27} L_m - \frac{32\zeta_3}{9} - \frac{46\pi^2}{27} + \frac{7075}{162}\right) \delta(s) \\ &+ \left(-8L_m^2 - \frac{128}{9} L_m - \frac{224}{27}\right) \mathcal{L}_0(s) + \frac{32}{3} L_m \mathcal{L}_1(s) \\ &+ \frac{4}{3} L_m G_1 \Theta(p^2 - m^2) + G_{\mathrm{sec}}^{(3Q)} \Theta(p^2 - (3m)^2) \Bigg]\,, \end{aligned} \tag{3.28}$$

where again the distributional contributions are displayed explicitly. The non-distributional contributions come from the single heavy quark Q cut and from the three particle $QQ\bar{Q}$ cut. The Q cut term is given in eq. (3.8) and arises from using the $(n_\ell + 1)$ flavor scheme for the strong coupling. The $QQ\bar{Q}$ cut term $G_{\mathrm{sec}}^{(3Q)}$ is given in eq. (3.19).

The non-distributional G-functions represent power corrections in the bHQET limit $s = p^2 - m^2 \ll m^2$ and represent $\mathcal{O}(\alpha_s^2)$ bHQET non-singular corrections. For completeness

we also quoted the respective results in the limit $p^2 \to m^2$ (eqs. (3.12)–(3.14)) and in the limit $p^2 \to 9m^2$ (eqs. (3.15) and (3.19)).

For completeness we also quote the result for the renormalized universal jet function $J_q^{\text{uf},(n_\ell+1)}(p^2, m^2, \mu)$ for primary massless quarks in eq. (A.6), which was computed in ref. [26]. The renormalization Z-factor as well as the μ (virtuality) anomalous dimension of the universal jet functions (to all orders as well as for primary massive and massless quarks) agree with those of the well known massless quark jet functions [8].

3.3 Consistency checks and kinematic limits

There are a number of essential consistency properties the $\mathcal{O}(\alpha_s^2)$ primary massive quark jet functions have to satisfy and which provide important consistency checks. These concern the relation between the mass mode and universal jet functions, the limit of massless quarks and the bHQET limit of a supermassive quark. We discuss them in the following.

As explained in section 2, the difference between the mass mode and the universal jet functions is related to the collinear-soft function S_c [32] via eq. (2.12). Using the results of eqs. (3.6) and (3.27) and accounting for the result for the renormalized collinear-soft function determined in ref. [32], which in our notation has the form

$$\begin{aligned} S_c(\ell, m, \mu, \nu) = \delta(\ell) + \left(a_s^{(n_\ell)}\right)^2 C_F T_F \Bigg\{ \Bigg[\left(\frac{8}{3}L_m^2 + \frac{80}{9}L_m + \frac{224}{27}\right) \log\left(\frac{\nu}{\mu}\right) - \frac{8}{9}L_m^3 - \frac{40}{9}L_m^2 \\ + \frac{4}{27}\left(3\pi^2 - 112\right) L_m + \frac{2}{27}\left(84\zeta_3 - 328 + 5\pi^2\right) \Bigg] \delta(\ell) \\ + \left[\frac{8}{3}L_m^2 + \frac{80}{9}L_m + \frac{224}{27}\right] \mathcal{L}_0(\ell) \Bigg\} + \mathcal{O}(\alpha_s^3)\,, \end{aligned} \tag{3.29}$$

it is straightforward to check the validity of eq. (2.12). Here one has to account for the decoupling relation

$$\begin{aligned} \alpha_s^{(n_\ell+1)}(\mu) = \alpha_s^{(n_\ell)}(\mu) \Bigg\{ 1 - \frac{\alpha_s^{(n_\ell)}(\mu)}{4\pi} T_F \Bigg[\frac{4}{3}L_m + \varepsilon\left(-\frac{2}{3}L_m^2 - \frac{\pi^2}{9}\right) \\ + \varepsilon^2\left(\frac{2}{9}L_m^3 + \frac{\pi^2}{9}L_m + \frac{4\zeta_3}{9}\right) + \mathcal{O}(\varepsilon^3) \Bigg] \Bigg\} + \mathcal{O}(\alpha_s^3)\,, \end{aligned} \tag{3.30}$$

for α_s in the n_ℓ and $(n_\ell + 1)$ flavor schemes (where we also displayed the $\mathcal{O}(\varepsilon)$ and $\mathcal{O}(\varepsilon^2)$ terms useful for divergent expressions). The sole dependence of the collinear-soft function on the rapidity scale ν indicates that the natural choice for ν in general depends on the process and the structure of the factorization theorem.

The definition of the universal jet function $J_f^{\text{uf},(n_\ell+1)}$ given in eq. (2.10) entails that for $m \to 0$ it converges to the jet function $J_f^{(n_\ell+1)}$ for $(n_\ell + 1)$ massless quarks, see eq. (2.6), which at $\mathcal{O}(\alpha_s^2)$ was computed in ref. [8]. In the limit $m \to 0$, the non-distributional G-functions also yield distributions and the corresponding limiting expressions are given in appendix B. Accounting for these results our expression for universal jet function correctly approaches the massless quark two-loop jet function for $m \to 0$.

JHEP08(2019)112

Finally, we discuss the bHQET limit $s = p^2 - m^2 \ll m^2$, the jet mass threshold region. Taking the double differential hemisphere jet mass distribution in e^+e^- annihilation (w.r.t. the thrust axis) as an example, one can consider the kinematic region where both jet masses are close to threshold. The corresponding factorization theorem for boosted top quarks ($Q \gg m$) has the form [12, 41][7]

$$\begin{aligned}\frac{1}{\sigma_0}\frac{\mathrm{d}\sigma}{\mathrm{d}M_Q^2\,\mathrm{d}M_{\bar{Q}}^2} &= H_Q^{(n_\ell+1)}(Q,\mu) H_m\left(m,\frac{Q}{m},\mu\right)\int \mathrm{d}\ell^+\,\mathrm{d}\ell^-\, S^{(n_\ell)}(\ell^+,\ell^-,\mu)\\ &\quad\times J_B^{(n_\ell)}\left(\frac{M_Q^2 - Q\ell^+}{m} - m,\mu\right) J_B^{(n_\ell)}\left(\frac{M_{\bar{Q}}^2 - Q\ell^-}{m} - m,\mu\right)\\ &\quad\times\left[1 + \mathcal{O}\left(\frac{m\alpha_s}{Q}\right) + \mathcal{O}\left(\frac{m^2}{Q^2}\right) + \mathcal{O}\left(\frac{s_{Q,\bar{Q}}^2}{m^4}\right)\right],\end{aligned} \tag{3.31}$$

where $M_{Q,\bar{Q}}$ stand for the hemisphere masses, σ_0 denotes the tree level cross section for $e^+e^- \to Q\bar{Q}$. The term $H_Q^{(n_\ell+1)}$ is the hard function related to the matching of the QCD $Q\bar{Q}$ current to the SCET massive quark dijet current at the scale Q and the term H_m is the mass threshold hard function related to the matching of the SCET dijet current to the bHQET current at the scale m. The terms $J_B^{(n_\ell)}$ and $S^{(n_\ell)}$ denote the bHQET jet function [12, 21] and dijet soft function, respectively. The soft function $S^{(n_\ell)}$ describes ultrasoft cross talk between the two jets at the scale s_Q/Q. The bHQET jet function $J_B^{(n_\ell)}$ [12, 21] describes the effects of the ultra-collinear radiation inside the jets (i.e. soft radiation in the rest frame of the massive quarks) at the scales $s_{Q,\bar{Q}}/m$ and contain all the dynamical (ultra) collinear effects for $s_{Q,\bar{Q}} \ll m^2$. The mass threshold hard function $H_m(m, Q/m, \mu)$ consists of n-collinear, $\bar{n}$-collinear and soft mass mode contributions which can be written in factorized form as [41]

$$H_m\left(m,\frac{Q}{m},\mu\right) = H_{m,n}\left(m,\mu,\frac{Q}{\nu}\right) H_{m,\bar{n}}\left(m,\mu,\frac{Q}{\nu}\right) H_{m,s}\left(m,\mu,\frac{m}{\nu}\right). \tag{3.32}$$

Each of the collinear $(n,\bar{n})$ and soft (s) mass mode factors depends on the rapidity renormalization scale ν. The natural scaling for the collinear factors is $\nu \sim Q$ and for the soft factor it is $\nu \sim m$. They were calculated at $\mathcal{O}(\alpha_s^2)$ in ref. [41] (see eqs. (5.7) and (5.8) in ref. [41] and note that $H_{m,n} = H_{m,\bar{n}}$ for the symmetric regulator of ref. [23], see eq. (2.8)).

Up to power-suppressed (for $s_{Q,\bar{Q}} \ll m^2$) and non-distributional contributions the factorization theorem in eq. (3.31) is also valid in the kinematic region $s_{Q,\bar{Q}} = p_{Q,\bar{Q}}^2 - m^2 \sim m^2 \lesssim p_{Q,\bar{Q}}^2$. Interestingly, in ref. [32] it was pointed out in the context of invariant mass dependent beam functions for exclusive Drell-Yan gauge boson production, that for this kinematic region the collinear-soft function S_c describes dynamical fluctuations located in the same phase space region as those contained in the jet function. The most economical formulation (w.r.t. the number of factorization functions containing the dynamical effects of the collinear and soft mass mode contributions) for $s_{Q,\bar{Q}} = p_{Q,\bar{Q}}^2 - m^2 \sim m^2 \sim p^2$

[7] Note that throughout this paper we do not account for renormalization group functions to sum (virtuality or rapidity) logarithms in our discussions of factorization theorems in order to keep the notations brief.

is therefore the one where the contributions of the collinear-soft function are *included* in the definition of the (invariant mass dependent) beam function, which corresponds to the mass mode definition of eq. (2.11). For the double differential hemisphere jet function this implies that for $s_{Q,\bar{Q}} = p^2_{Q,\bar{Q}} - m^2 \sim m^2 \sim p^2_{Q,\bar{Q}}$ one can formulate a factorization theorem of the form

$$\begin{aligned}\frac{1}{\sigma_0}\frac{\mathrm{d}^2\sigma}{\mathrm{d}M_Q^2\,\mathrm{d}M_{\bar{Q}}^2} &= H_Q^{(n_\ell+1)}(Q,\mu) H_{m,s}\left(m,\mu,\frac{m}{\nu}\right)\int \mathrm{d}\ell^+\,\mathrm{d}\ell^-\, S^{(n_\ell)}(\ell^+,\ell^-,\mu) \\ &\quad\times J_Q^{\mathrm{mf},(n_\ell+1)}\left(M_Q^2 - Q\ell^+, m^2, \mu, \frac{Q}{\nu}\right) J_Q^{\mathrm{mf},(n_\ell+1)}\left(M_{\bar{Q}}^2 - Q\ell^-, m^2, \mu, \frac{Q}{\nu}\right) \\ &\quad\times \left[1 + \mathcal{O}\left(\frac{m\alpha_s}{Q}\right) + \mathcal{O}\left(\frac{m^2}{Q^2}\right)\right]. \end{aligned} \tag{3.33}$$

This in turn implies the relation

$$J_Q^{\mathrm{mf},(n_\ell+1)}\left(p^2 \to m^2, m^2, \mu, \frac{Q}{\nu}\right) = H_{m,n}\left(m,\mu,\frac{Q}{\nu}\right) J_B^{(n_\ell)}\left(\frac{p^2}{m} - m, \mu\right) + \text{non-sing. terms}, \tag{3.34}$$

between the primary massive quark mass mode jet function and the bHQET jet function up to non-singular terms integrable in p^2 at the threshold m^2. Using the $\mathcal{O}(\alpha_s^2)$ results for the bHQET jet function (naturally given in the n_ℓ-flavor scheme for α_s) in ref. [21] (see eq. (39)), the collinear mass mode hard functions $H_{m,n}$ in ref. [41] (see eq. (5.7)) and our result for the mass mode jet function in eq. (2.11), accounting for the fact that *all* G-functions are power-suppressed in the bHQET limit, it is straightforward to see that the relation in eq. (3.34) is indeed satisfied. As discussed in more detail in section 5.2.2, our calculations of the $\mathcal{O}(\alpha_s^2)$ corrections for the mass mode jet function provide a high precision semi-analytic check of eq. (3.34) as some loop integrals could only be determined by numerical methods. The relation (3.34) was then used as an input to analytically parametrize the jet functions result of eqs. (2.11) and (2.10).

4 Alternative factorization approaches and practical use

The non-trivial conceptual aspect of the $\mathcal{O}(\alpha_s^2)$ primary massive quark SCET jet function concerns the mass mode contribution due to secondary radiation. Since these are tied to corrections arising from collinear as well as soft phase space sectors with invariant masses of order the quark mass m, their treatment entails rapidity singularities (and the resummation of associated logarithms) within a $\mathrm{SCET_{II}}$ type approach regardless of whether the observable is $\mathrm{SCET_I}$ or $\mathrm{SCET_{II}}$. As already pointed out in section 2, in the literature two alternative factorization formulations to account for mass mode corrections have been advocated which are (or can be rendered) conceptually and phenomenologically equivalent due to consistency relations. We emphasize that none of these approaches may be considered superior to the respective other and, by emphasizing different and complementary aspects of the mass mode effects, together provide a thorough and comprehensive treatment and understanding from the conceptual as well as practical point of view.

JHEP08(2019)112

In this section we discuss the relation between the approaches employing the mass mode and the universal jet functions for primary massive quarks and using the double differential hemisphere mass distribution already introduced in section 3.3 as an example. To keep the discussion brief we also restrict the discussion to the kinematic regions $s^2/Q^2 \ll m^2 \ll s \sim p^2 \ll Q^2$ and $s = p^2 - m^2 \sim p^2 \sim m^2$ where the quark mass effects calculated in this paper are most relevant. We emphasize, however, that the discussion can be extended in a straightforward way to all kinematic situations and also to other types of factorization theorems where mass mode effects shall be treated (and where factorization functions other than jet functions arise).

The universal factorization approach of refs. [22, 26, 31, 34] was devised with the motivation to obtain universal hard, jet and soft functions defined such that they can smoothly cover all possible choices for the quark mass m in the context of the strict hierarchy $s^2/Q^2 \ll s \ll Q^2$. The resulting factorization theorems therefore contain power corrections w.r.t. mass mode contributions in at least some of the factors in any kinematic region, which, in case they are known, may be expanded away accordingly if a smooth description of mass effects is not wanted. The approach was also constructed to allow for the formulation of universal and simple rules to implement the summation of logarithms through flavor number dependent renormalization evolution factors of the hard, jet and soft function for arbitrary choices of the global renormalization scale μ. The approach also entails that only the hard, jet and soft functions and, depending on the choice of μ, their respective threshold matching factors appear in the factorization theorems (in case they are evolved through the massive quark flavor threshold). By construction in the universal factorization approach, all rapidity logarithms (and their summations) *are fully contained within* these individual quark mass threshold matching factors at the scale $\mu_m \sim m$.

Let us consider the situation $s^2/Q^2 \ll m^2 \lesssim s \sim p^2 \ll Q^2$. The corresponding leading power factorization theorem in the universal factorization function approach for $s^2/Q^2 < \mu^2 < m^2$ (when the SCET current and the jet functions are evolved below m) has the form

$$\begin{aligned}\frac{1}{\sigma_0}\frac{\mathrm{d}\sigma}{\mathrm{d}M_Q^2\,\mathrm{d}M_{\bar{Q}}^2} &= H_Q^{(n_\ell+1)}(Q,\mu) H_m\left(m,\frac{Q}{m},\mu\right) \int \mathrm{d}s_Q\,\mathrm{d}s_{\bar{Q}} \int \mathrm{d}\ell^+\,\mathrm{d}\ell^- \\ &\quad \times J_Q^{\mathrm{uf},(n_\ell+1)}(M_Q^2 - s_Q - Q\ell^+, m^2, \mu)\, J_Q^{\mathrm{uf},(n_\ell+1)}(M_{\bar{Q}}^2 - s_{\bar{Q}} - Q\ell^-, m^2, \mu) \\ &\quad \times \mathcal{M}_{J_Q}(s_Q, m, \mu)\mathcal{M}_{J_Q}(s_{\bar{Q}}, m, \mu) S^{(n_\ell)}(\ell^+, \ell^-, \mu)\,, \end{aligned} \tag{4.1}$$

where H_m and $\mathcal{M}_{J_Q}$ are the quark mass threshold matching factors for the SCET current and the universal jet function J_Q^{uf} respectively. For $m^2 < \mu^2 < s$ (where the soft function is evolved above m) the *same* factorization theorem has the form

$$\begin{aligned}\frac{1}{\sigma_0}\frac{\mathrm{d}\sigma}{\mathrm{d}M_Q^2\,\mathrm{d}M_{\bar{Q}}^2} &= H_Q^{(n_\ell+1)}(Q,\mu) \int \mathrm{d}\ell^+\,\mathrm{d}\ell^-\mathrm{d}\ell'^+\,\mathrm{d}\ell'^- \\ &\quad \times J_Q^{\mathrm{uf},(n_\ell+1)}(M_Q^2 - Q\ell^+, m^2, \mu) J_Q^{\mathrm{uf},(n_\ell+1)}(M_{\bar{Q}}^2 - Q\ell^-, m^2, \mu) \\ &\quad \times \mathcal{M}_S(\ell'^+, \ell'^-, m, \mu) S^{(n_\ell)}(\ell^+ - \ell'^+, \ell^- - \ell'^-, \mu)\,, \end{aligned} \tag{4.2}$$

where $\mathcal{M}_S$ is the mass threshold matching factor for the soft function S. It is straightforward to consider other choices of μ as well.

For a strong hierarchy $m^2 \ll s$ one may replace the universal primary massive quark jet function $J_Q^{\mathrm{uf},(n_\ell+1)}$ by the jet function $J_q^{(n_\ell+1)}$ for $(n_\ell+1)$ massless quark flavors (calculated at $\mathcal{O}(\alpha_s^2)$ in [8]). But using $J_Q^{\mathrm{uf},(n_\ell+1)}$ provides validity of eqs. (4.1) and (4.2) smoothly covering *all* cases between $m^2 \ll s$ and $m^2 \sim s$. The resummation of virtuality logarithms (with respect to μ) is achieved by the flavor number dependent μ-anomalous dimensions of the hard currents and jet functions known from SCET (with $(n_\ell+1)$ flavors) and bHQET (with n_ℓ flavors) and of the soft function (with $(n_\ell+1)$ flavors for scales above m and n_ℓ flavors for scales below m). Furthermore one has to account for the natural scales of the hard, jet and soft function being $\mu_Q \sim Q$, $\mu_J \sim s^{1/2}$ and $\mu_S \sim s/Q$, respectively. In eq. (4.1) the mass threshold matching functions H_m and $\mathcal{M}_J$ account for the change between $(n_\ell+1)$-flavor SCET evolution (above the mass threshold) and n_ℓ-flavor bHQET evolution (below the mass threshold) for the hard current (see ref. [41]) and universal jet function, respectively, at the mass threshold scale $\mu_m \sim m$. For the universal jet function for a massive primary quark this matching relation reads

$$J_B^{(n_\ell)}\left(\frac{p^2}{m} - m, \mu\right) = \int \mathrm{d}s\, \mathcal{M}_{J_Q}(p^2 - s, m, \mu)\, J_Q^{\mathrm{uf},(n_\ell+1)}\left(s, m^2, \mu\right) + \text{non-singular terms for } p^2 \to m^2\,. \tag{4.3}$$

(The analogous relation for the massless primary quark case has been given in eq. (119) of ref. [26].) In eq. (4.2) the mass threshold matching function $\mathcal{M}_S$ accounts for the corresponding change between the corresponding n_ℓ- and $(n_\ell+1)$-flavor evolution of the soft function (see eqs. (136) and (139) of ref. [26]). Rapidity logarithms and their summation take place only inside each of the mass threshold matching functions H_m, $\mathcal{M}_{J_Q}$ and $\mathcal{M}_S$ (see for example eq. (3.32)), and the jet and soft functions are free of any rapidity logarithms. The ν-anomalous dimensions are the same for primary massive and primary massless quarks and were provided in refs. [31, 41]. Finally, consistency between eqs. (4.1) and (4.2) implies the consistency identity

$$H_m\left(m, \frac{Q}{m}, \mu\right) \mathcal{M}_J(Q\ell^+, m, \mu)\mathcal{M}_J(Q\ell^-, m, \mu) = \mathcal{M}_S(\ell^+, \ell^-, m, \mu)\,. \tag{4.4}$$

The mass mode factorization approach of ref. [32] was devised with the motivation to formulate distinct and unique factorization theorems for the different possible scale hierarchies of the mass m with respect to Q, $s^{1/2}$ and s/Q, where the physically relevant n- and $\bar{n}$-collinear and soft mass mode effects appear explicitly within three distinct factors to achieve a transparent and economic representation of their contributions. In contrast to the universal factorization approach, the mass mode factorization approach does not result in two options to formulate the same factorization theorem, such as eqs. (4.1) and (4.2), which are equivalent due to consistency relations such as eq. (4.4). The factorization theorems in the mass mode approach contain functions that have explicit μ and ν dependence, and the summation of virtuality and rapidity logarithms is carried out on equal footing. The summation of the associated logarithms, on the other hand (and in contrast to the universal factorization approach), does explicitly involve consistency relations among the

JHEP08(2019)112

anomalous dimensions to allow for a transparent treatment of renormalization group evolution with either n_ℓ or $(n_\ell+1)$ dynamical flavors with respect to the mass threshold scale m. In addition, in the formulation of the mass mode factorization approach of ref. [32] the resulting factorization theorems have been free of any power corrections in the quark mass m and did not provide a smooth dependence on the quark mass m. The latter is mandatory for smooth predictions of differential cross sections when the quark mass threshold is crossed.

Let us consider the situation $s^2/Q^2 \ll m^2 \ll s \sim p^2 \ll Q^2$. The corresponding factorization theorem in the mass mode factorization approach has the form

$$\begin{aligned}\frac{1}{\sigma_0}\frac{\mathrm{d}\sigma}{\mathrm{d}M_Q^2\,\mathrm{d}M_{\bar{Q}}^2} &= H_Q^{(n_\ell+1)}(Q,\mu) H_{m,s}\left(m,\mu,\frac{m}{\nu}\right)\int \mathrm{d}\ell^+\,\mathrm{d}\ell^-\mathrm{d}\ell'^+\,\mathrm{d}\ell'^- \\ &\quad\times J_q^{(n_\ell+1)}(M_Q^2 - Q\ell^+ - Q\ell'^+,\mu)\, J_q^{(n_\ell+1)}(M_{\bar{Q}}^2 - Q\ell^- - Q\ell'^-,\mu) \\ &\quad\times S_c(\ell'^+,m,\mu,\nu) S_c(\ell'^-,m,\mu,\nu) S^{(n_\ell)}(\ell^+,\ell^-,\mu)\,, \end{aligned} \tag{4.5}$$

where $H_{m,s}$ is the soft mass mode contribution of the mass threshold hard function H_m quoted in eq. (3.32), S_c is the collinear-soft function of eqs. (2.12) and (3.29), and $J_q^{(n_\ell+1)}$ is the jet function for $(n_\ell+1)$ *massless* quarks which coincides with the universal jet function for vanishing quark mass, i.e. $J_Q^{\mathrm{uf},(n_\ell+1)}(p^2,0,\mu)$. Since the factorization theorems (4.5) and (4.1) as well as (4.2) provide identical descriptions for the situations $s^2/Q^2 \ll m^2 \ll s \sim p^2 \ll Q^2$ (up to suppressed quark mass power corrections), they imply the following consistency relations for the mass threshold matching factors $\mathcal{M}_{J_Q}$ for the universal function $J_Q^{\mathrm{uf},(n_\ell+1)}$ and $\mathcal{M}_S$ for the soft function $S^{(n_\ell)}$:

$$\mathcal{M}_{J_Q}(s,m,\mu) = H_{m,n}^{-1}\left(m,\mu,\frac{Q}{\nu}\right) S_c\left(\frac{s}{Q},m,\mu,\nu\right), \tag{4.6}$$

$$\mathcal{M}_S(\ell^+,\ell^-,m,\mu) = H_{m,s}\left(m,\mu,\frac{m}{\nu}\right) S_c(\ell'^+,m,\mu,\nu) S_c(\ell'^-,m,\mu,\nu)\,, \tag{4.7}$$

where $H_{m,n}$ and $H_{m,s}$ are the collinear and soft mass mode contributions of the mass threshold hard function H_m, see eq. (3.32), which appears in the universal factorization theorem eq. (4.1).

In the situation $s^2/Q^2 \ll m^2 \sim s \sim p^2 \ll Q^2$ the mass mode factorization approach states the factorization theorem

$$\begin{aligned}\frac{1}{\sigma_0}\frac{\mathrm{d}\sigma}{\mathrm{d}M_Q^2\,\mathrm{d}M_{\bar{Q}}^2} &= H_Q^{(n_\ell+1)}(Q,\mu) H_{m,s}\left(m,\mu,\frac{m}{\nu}\right)\int \mathrm{d}\ell^+\,\mathrm{d}\ell^- \\ &\quad\times J_Q^{\mathrm{mf},(n_\ell+1)}\left(M_Q^2 - Q\ell^+, m^2,\mu,\frac{Q}{\nu}\right) J_Q^{\mathrm{mf},(n_\ell+1)}\left(M_{\bar{Q}}^2 - Q\ell^-, m^2,\mu,\frac{Q}{\nu}\right) \\ &\quad\times S^{(n_\ell)}(\ell^+,\ell^-,\mu)\,. \end{aligned} \tag{4.8}$$

Using the consistency relations (4.6) and (4.7) as well as the relation between the mass mode jet function J_Q^{mf}, the universal jet function J_Q^{uf} and the collinear-soft function of eq. (2.12), it is easy to see that eq. (4.8) and the universal factorization theorems (4.1) and (4.2) provide identical descriptions for $s^2/Q^2 \ll m^2 \sim s \sim p^2 \ll Q^2$. The relations and the analogous

equivalence for eq. (4.5) show that the factorization theorem (4.5) — upon replacing the massless quark jet function $J_q^{(n_\ell+1)}$ by the universal jet function $J_Q^{\mathrm{uf},(n_\ell+1)}$ — fully accounts for the content of the factorization theorem (4.8) for $s^2/Q^2 \ll m^2 \ll s \sim p^2 \ll Q^2$. Thus in this modified form, (4.5) is applicable for the entire region $s^2/Q^2 \ll m^2 \lesssim s \sim p^2 \ll Q^2$ and exactly equivalent to the universal factorization theorems (4.1) and (4.2).

Thus from a practical application point of view the mass mode factorization theorems (4.5) and (4.8) can be considered as special cases of the universal factorization theorems (4.1) and (4.2). On the other hand, the mass mode factorization approach for the case $s^2/Q^2 \ll m^2 \ll s \sim p^2 \ll Q^2$ makes explicit use of the collinear-soft function S_c and provides a representation of the quark mass threshold matching factors for the jet and soft functions that disentangle the relevant process-independent collinear and soft mass mode contributions. So, eqs. (4.6) and (4.7) in connection with eq. (3.32) clarify the interplay of the different elementary (collinear and soft) mass mode functions $(H_{m,n}, H_{m,\bar{n}}, H_{m,s}, S_c)$. Interestingly, by simply replacing the collinear mass mode factors $H_{m,n}$ and $H_{m,\bar{n}}$ valid for primary massive quarks by the corresponding mass mode factors for primary massless quarks (see eqs. (4.10) and (4.12) in ref. [32] for analytic expressions) the analogous versions of eqs. (3.32), (4.6) and (4.7) are also valid for the corresponding factorization theorems for primary massless quarks. In fact, upon making these modifications and replacing the primary massive quark jet functions $J_Q^{\mathrm{mf},(n_\ell+1)}$ and $J_Q^{\mathrm{uf},(n_\ell+1)}$ by the corresponding jet functions for primary massless quarks, eq. (4.1), (4.2) (and (4.5), (4.8)) agree identically with the results given in ref. [26]. This demonstrates the universal structure of the mass mode corrections and illustrates how to obtain them in an economic way in factorization theorems for other applications.

Our final comment concerns the summation of logarithms. Combining the information from the universal factorization and the mass mode factorization approaches provides a modular and transparent method to resum virtuality as well as rapidity logarithms (where we acknowledge, however, that complete treatments of correctly summing both types of logarithms is available in both approaches, see [32] and [31]).

From the point of view of summing virtuality logarithms, the universal factorization theorems (4.1) and (4.2) may be seen as more transparent and practical because all anomalous dimensions coincide with those known from factorization theorems where secondary massive quark effects (which entail rapidity singularities) are absent: one only has to keep track of the dependence on the number of dynamical flavors n_f being either equal to n_ℓ, when the evolution is below the quark mass m or $(n_\ell+1)$ when it is above. If we write the virtuality μ-anomalous dimensions of the SCET and bHQET quark-antiquark production currents ($\mathcal{J}_{\mathrm{SCET}}$ and $\mathcal{J}_{\mathrm{bHQET}}$, respectively [12, 14]), the hard factor, the universal and bHQET jet function, and the soft function in the form ($\hat{s} = s/m$)

$$\begin{aligned}
\frac{\mathrm{d}}{\mathrm{d}\log\mu}\mathcal{J}_{\mathrm{SCET}}^{(n_f)}(\mu) &= \gamma_c^{(n_f)}(Q,\mu)\mathcal{J}_{\mathrm{SCET}}^{(n_f)}(\mu)\,,\\
\frac{\mathrm{d}}{\mathrm{d}\log\mu}\mathcal{J}_{\mathrm{bHQET}}^{(n_f)}(\mu) &= \gamma_{c_B}^{(n_f)}(Q,m,\mu)\mathcal{J}_{\mathrm{bHQET}}^{(n_f)}(\mu)\,,\\
\frac{\mathrm{d}}{\mathrm{d}\log\mu}H_Q^{(n_f)}(Q,\mu) &= \Big(\gamma_Q^{(n_f)}(Q,\mu) + \gamma_Q^{(n_f)*}(Q,\mu)\Big)\,H_Q^{(n_f)}(Q,\mu)\,,
\end{aligned} \tag{4.9}$$

JHEP08(2019)112

$$\frac{\mathrm{d}}{\mathrm{d}\log\mu} J_Q^{\mathrm{uf},(n_f)}(p^2,m^2,\mu) = \int \mathrm{d}p'^2\, \gamma_J^{(n_f)}(p^2-p'^2,\mu) J_Q^{\mathrm{uf},(n_f)}(p'^2,m^2,\mu)\,,$$
$$\frac{\mathrm{d}}{\mathrm{d}\log\mu} J_B^{(n_f)}(\hat{s},\mu) = \int \mathrm{d}\hat{s}'\, \gamma_{J_B}^{(n_f)}(\hat{s}-\hat{s}',\mu) J_B^{(n_f)}(\hat{s}',\mu)\,,$$
$$\frac{\mathrm{d}}{\mathrm{d}\log\mu} S^{(n_f)}(\ell^+,\ell^-,\mu) = \int \mathrm{d}\ell^{+\prime}\,\mathrm{d}\ell^{-\prime}\, \gamma_S^{(n_f)}(\ell^+-\ell^{+\prime},\ell^--\ell^{-\prime},\mu) S^{(n_f)}(\ell^{+\prime},\ell^{-\prime},\mu)\,,$$

the μ-anomalous dimensions of the corresponding mass threshold matching factors appearing in the factorization theorems (4.5) and (4.8) read

$$\begin{aligned}
\frac{\mathrm{d}}{\mathrm{d}\log\mu} H_m\left(m,\frac{Q}{m},\mu\right) &= \Big[\gamma_{c_B}^{(n_\ell)}(Q,m,\mu) + \gamma_{c_B}^{(n_\ell)*}(Q,m,\mu) \\
&\quad - \left(\gamma_Q^{(n_\ell+1)}(Q,\mu) + \gamma_Q^{(n_\ell+1)*}(Q,\mu)\right)\Big] H_m(Q,m,\mu)\,, \\
\frac{\mathrm{d}}{\mathrm{d}\log\mu} \mathcal{M}_{J_Q}(s,m,\mu) &= \int \mathrm{d}s' \left[\gamma_{J_B}^{(n_\ell)}\left(\frac{s}{m}-\frac{s'}{m},\mu\right) - \gamma_J^{(n_\ell+1)}(s-s',\mu)\right] \mathcal{M}_{J_Q}(s',m,\mu)\,, \\
\frac{\mathrm{d}}{\mathrm{d}\log\mu} \mathcal{M}_S\left(\ell^+,\ell^-,\mu\right) &= \int \mathrm{d}\ell^{+\prime}\,\mathrm{d}\ell^{-\prime}\Big[\gamma_S^{(n_\ell+1)}\left(\ell^+-\ell^{+\prime},\ell^--\ell^{-\prime},\mu\right) \\
&\quad - \gamma_S^{(n_\ell)}(\ell^+-\ell^{+\prime},\ell^--\ell^{-\prime},\mu)\Big] \mathcal{M}_S(\ell^{+\prime},\ell^{-\prime},\mu)\,.
\end{aligned} \tag{4.10}$$

Their form expresses the fact that the mass threshold matching functions H_m, $\mathcal{M}_J$ and $\mathcal{M}_S$ simply account for the appropriate change between $(n_\ell+1)$ and n_ℓ flavor μ-evolution. In this context one just has to take into account that for primary massive quarks the n_ℓ-flavor evolution for the jet and the hard functions is carried out in bHQET. For sake of completeness we have displayed all μ-anomalous dimensions up to $\mathcal{O}(\alpha_s^2)$ in appendix C.

From the point of view of summing rapidity logarithms the structure provided by the mass mode factorization theorems (4.5) and (4.8) may be seen as most transparent because the universal structure of the ν-anomalous dimensions of the collinear and soft mass mode factors is fully determined by quoting the results

$$\begin{aligned}
\frac{\mathrm{d}}{\mathrm{d}\log\nu} H_{m,n}\left(m,\mu,\frac{Q}{\nu}\right) &= \gamma_\nu(m,\mu)\, H_{m,n}\left(m,\mu,\frac{Q}{\nu}\right), \\
\frac{\mathrm{d}}{\mathrm{d}\log\nu} H_{m,s}\left(m,\mu,\frac{m}{\nu}\right) &= -2\gamma_\nu(m,\mu)\, H_{m,s}\left(m,\mu,\frac{m}{\nu}\right), \\
\frac{\mathrm{d}}{\mathrm{d}\log\nu} S_c\left(\ell,m,\mu,\nu\right) &= \gamma_\nu\left(m,\mu\right)\, S_c\left(\ell,m,\mu,\nu\right), \\
\frac{\mathrm{d}}{\mathrm{d}\log\nu} J_Q^{\mathrm{mf},(n_\ell+1)}\left(p^2,m^2,\mu,\frac{Q}{\nu}\right) &= \gamma_\nu(m,\mu)\, J_Q^{\mathrm{mf},(n_\ell+1)}\left(p^2,m^2,\mu,\frac{Q}{\nu}\right).
\end{aligned} \tag{4.11}$$

Interestingly, owing to the consistency relations (3.32), (4.6) and (4.7), the ν-anomalous dimensions of all collinear and soft mass mode factors are identical to all orders in α_s up to trivial factors and signs which are determined from the fact that the rapidity divergences within each of the threshold matching functions H_m, $\mathcal{M}_{J_Q}$ and $\mathcal{M}_S$ cancel. The consistency relations also entail that the ν-anomalous dimensions of the collinear-soft function S_c and the mass mode jet function $J_Q^{\mathrm{mf},(n_\ell+1)}$ are proportional to a δ-function. The convolution in their anomalous dimension therefore reduces to a simple multiplication which we have

already accounted for in the formulae above. The universal ν-anomalous dimension up to $\mathcal{O}(\alpha_s^2)$ reads

$$\gamma_\nu(m,\mu) = a_s^2 C_F T_F \left(\frac{8}{3}L_m^2 + \frac{80}{9}L_m + \frac{224}{27}\right) + \mathcal{O}(\alpha_s^3)\,. \tag{4.12}$$

To resum virtuality as well as rapidity logarithms in the universal factorization approach, one evaluates the factorization theorems of eqs. (4.1) or (4.2) and uses the μ-anomalous dimensions in eq. (4.9) to sum all virtuality logarithms by evolving the hard ($H_Q^{(n_\ell+1)}$), jet ($J_Q^{\text{uf},(n_\ell+1)}$) and soft ($S^{(n_\ell)}$) functions from their natural scale to the global renormalization scale. Whenever one of their μ-evolution crosses the mass threshold m, so that the anomalous dimension is modified, the corresponding matching factor H_m, $\mathcal{M}_{J_Q}$ or $\mathcal{M}_S$ has to be included. The rapidity logarithms are fully contained within each of the mass threshold matching factors H_m, $\mathcal{M}_{J_Q}$ and $\mathcal{M}_S$ evaluated at $\mu \sim m$ and can be resummed by using (3.32), (4.6) and (4.7) and the ν-anomalous dimensions of eq. (4.11).

5 Calculation of massive quark jet functions at $\mathcal{O}(\alpha_s^2)$

5.1 Comment on the calculations and summary of matrix element results

In this section we provide details on the calculation of the SCET primary massive quark jet functions at $\mathcal{O}(\alpha_s^2)$. The universal and mass modes SCET jet functions differ concerning the $\mathcal{O}(\alpha_s^2 C_F T_F)$ corrections coming from diagrams with secondary massive quarks (which for the jet functions refers to diagrams with a closed massive quark-antiquark loop subdiagram). These corrections involve a number of conceptual and technical subtleties, and we briefly address these in the following before presenting details of the computations in the subsequent sections. We also summarize the individual results for the jet-function ME (calculated in the subsequent sections) and the two collinear-soft MEs (extracted from [32]) which are needed to determine the universal and mass mode SCET jet functions. We believe that this makes the conceptual subtleties of the calculations explicit.

The conceptual starting point is the calculation of the jet-function ME $\mathscr{J}_f(p^2,m^2)$, defined in eq. (2.1), which is *infrared divergent* and defined in the $(n_\ell+1)$ flavor theory. The *infrared finite* universal jet function $J_f^{\text{uf},(n_\ell+1)}(p^2,m^2)$ and the mass mode jet function $J_f^{\text{mf},(n_\ell+1)}(p^2,m^2)$ are then given via subtractions related to the likewise *infrared divergent* collinear-soft MEs $\mathscr{S}^{(n_\ell+1)}(\ell,m)$ and $\mathscr{S}^{(n_\ell)}(\ell,m)$, respectively, defined in the $(n_\ell+1)$ flavor theory (i.e. containing n_ℓ massless quarks and one quark Q with mass m, see eq. (2.7)) and in the n_ℓ flavor theory (i.e. containing only n_ℓ massless quarks), respectively. The corresponding definitions are given in eq. (2.10) and eq. (2.11), respectively. We stress that the concept of zero-bin subtractions [24] *does not play any role* in our calculation, and we also believe that our approach can be generalized to other calculations in the context of SCET factorization theorems. As already explained in section 1, the universal jet function $J_f^{\text{uf},(n_\ell+1)}(p^2,m^2)$ by construction approaches the well-known massless quark jet function [8] in the limit $m \to 0$. It can therefore be thought of as the mandatory jet function definition for $m^2 \ll q^2$ that involves subtractions related to the mass singularity coming from the

JHEP08(2019)112

secondary quark mass effects in this limit. On the other hand, the mass mode jet function $J_f^{\mathrm{mf},(n_\ell+1)}(p^2,m^2)$ does not involve subtractions related to the secondary quark mass effects and can be thought of as the jet function definition suitable for $m^2 \sim q^2$, where the quark mass m does not represent an infrared scale. It is useful for the computations to keep these conceptual aspects of the two jet functions in mind, even though we emphasize that both jet functions can be applied in a broader kinematic context and are related through the collinear-soft function $S_c(\ell,m)$ via eq. (2.12) (see the discussion in section 4).[8]

On the technical level an additional subtlety arises because it turns out that — at least at this time — the only feasible way to determine the full set of $\mathcal{O}(\alpha_s^2)$ corrections is to use two completely separate calculational schemes: one for the purely gluonic and the massless quark corrections at $\mathcal{O}(\alpha_s^2 C_F^2, \alpha_s^2 C_F C_A, \alpha_s^2 C_F T_F n_\ell)$ and another one for the secondary massive quark corrections at $\mathcal{O}(\alpha_s^2 C_F T_F)$. This separation arises because the $\mathcal{O}(\alpha_s^2 C_F T_F)$ secondary massive quark corrections involve rapidity singularities. To quantify them analytically it is mandatory to introduce an explicit dimensionful infrared regulator (for which we adopt a gluon mass Λ), such that UV and rapidity divergences can be disentangled and identified unambiguously. The treatment of subdivergences at $\mathcal{O}(\alpha_s^2 C_F T_F)$ then also requires a calculation of the $\mathcal{O}(\alpha_s)$ corrections with a finite gluon mass for consistency. These calculations have to be carried out for the jet-function ME $\mathscr{J}_f(p^2,m^2)$ and the collinear-soft MEs $\mathscr{S}^{(n_\ell+1)}(\ell,m)$ and $\mathscr{S}^{(n_\ell)}(\ell,m)$ which also entails infrared gluon mass dependent $\overline{\mathrm{MS}}$ renormalization Z-factors for each of them. For the renormalized universal and mass mode jet functions as well as for their virtuality and rapidity renormalization group equations contributing at $\mathcal{O}(\alpha_s^2 C_F T_F)$ it can then be explicitly checked that the dependence on the infrared gluon mass cancels. In contrast, the purely gluonic as well as the massless quark corrections at $\mathcal{O}(\alpha_s^2 C_F^2, \alpha_s^2 C_F C_A, \alpha_s^2 C_F T_F n_\ell)$ (as well as the $\mathcal{O}(\alpha_s)$ corrections) do not involve rapidity singularities and just using dimensional regularization without an additional infrared regulator is in principle sufficient. In fact using this simpler regularization is the only feasible way to compute the gluonic $\mathcal{O}(\alpha_s^2)$ corrections due to their complexity. For these corrections then all diagrams contributing to the collinear-soft MEs $\mathscr{S}^{(n_\ell+1)}(\ell,m)$ and $\mathscr{S}^{(n_\ell)}(\ell,m)$ lead to vanishing scaleless integrals which just turn all $1/\varepsilon^n$ IR singularities in the infrared divergent jet-function ME $\mathscr{J}_f(p^2,m^2)$ into $1/\varepsilon^n$ UV singularities of the infrared finite jet functions $J_f^{\mathrm{uf},(n_\ell+1)}(p^2,m^2)$ and $J_f^{\mathrm{mf},(n_\ell+1)}(p^2,m^2)$. Both jet functions thus agree concerning their $\mathcal{O}(\alpha_s)$ and $\mathcal{O}(\alpha_s^2 C_F^2, \alpha_s^2 C_F C_A, \alpha_s^2 C_F T_F n_\ell)$ corrections. This justifies that for the $\mathcal{O}(\alpha_s^2)$ corrections involving only diagrams with massless partons (in addition to the primary massive quark line), at least at the computational level, the subtractions associated to collinear-soft MEs or zero-bins can be ignored. The treatment of subdivergences in this calculation also requires the calculations of the $\mathcal{O}(\alpha_s)$ corrections, which differ from the corresponding results with a gluon mass regulator. The lack of having an infrared regularization scheme that allows the computation of all $\mathcal{O}(\alpha_s^2)$ corrections in a uniform and manageable way entails that — at least at the present time — the computation of the $\mathcal{O}(\alpha_s^3)$ corrections to the SCET jet functions in the presence of massive quarks would represent an extremely challenging task.

[8] In previous literature on the factorization concerning secondary massive quark corrections these subtleties were hidden.

We present the calculations of the purely gluonic and massless quark corrections at $\mathcal{O}(\alpha_s^2 C_F^2, \alpha_s^2 C_F C_A, \alpha_s^2 C_F T_F n_\ell)$ for the jet-function ME $\mathscr{J}_f(p^2, m^2)$ in section 5.2, and those of the secondary massive quark corrections at $\mathcal{O}(\alpha_s^2 C_F T_F)$ in section 5.3. The reader not interested in the computational technical details may skip these two subsections. In the following we summarize the analytic results for jet-function ME and the two collinear-soft MEs within the two calculational schemes. Results needed for the calculation of the $\mathcal{O}(\alpha_s^2 C_F^2, \alpha_s^2 C_F C_A, \alpha_s^2 C_F T_F n_\ell)$ corrections to the jet function are computed in the massless gluon computational scheme (where the $\mathcal{O}(\alpha_s^2 C_F T_F)$ corrections cannot be given) and are quoted with the subscript "$\cancel{C_F T_F}$". In contrast all results needed for the calculation of the $\mathcal{O}(\alpha_s^2 C_F T_F)$ terms from secondary mass effects are computed in the massive gluon computational scheme (where the $\mathcal{O}(\alpha_s^2 C_F^2, \alpha_s^2 C_F C_A, \alpha_s^2 C_F T_F n_\ell)$ corrections cannot be given) and are quoted with the subscript "$C_F T_F$". Note that we use this labeling also for the corresponding one-loop results that contribute (through the treatment of subdivergences) to the determination of the respective renormalized two-loop jet functions and their anomalous dimensions.[9]

In the computational scheme with a massless gluon the renormalized jet-function ME can be written in the form

$$\mathscr{J}_Q^{(n_\ell+1)}(p^2, m^2, \Lambda^2 = 0, \mu, Q/\nu)\Big|_{\cancel{C_F T_F}} = \delta(p^2 - m^2) + a_s^{(n_\ell+1)} J_Q^{(1)}(p^2, m^2, \mu) + \left(a_s^{(n_\ell+1)}\right)^2 J_Q^{(2)}(p^2, m^2, \mu) + \mathcal{O}(\alpha_s^3)\,, \tag{5.1}$$

where the $\mathcal{O}(\alpha_s)$ coefficient $J_Q^{(1)}(p^2, m^2, \mu)$ agrees with the well-known one-loop SCET primary massive quark jet function result from ref. [14] and is given up to $\mathcal{O}(\varepsilon^2)$ in eq. (3.7). The two-loop coefficient $J_Q^{(2)}$ containing the $\mathcal{O}(\alpha_s^2 C_F^2, \alpha_s^2 C_F C_A, \alpha_s^2 C_F T_F n_\ell)$ corrections is given in eq. (3.11). Both are free of rapidity divergences and therefore do not carry an argument with respect to the rapidity renormalization scale ν. For convenience, we also provide the corresponding renormalized result for the massless primary quark jet-function ME $\mathscr{J}_q^{(n_\ell+1)}(p^2, m^2, \Lambda^2 = 0, \mu, Q/\nu)\Big|_{\cancel{C_F T_F}}$ in appendix A.

The divergent Z-factor of the jet-function ME reads

$$\begin{aligned}
Z_{\mathscr{J}_Q}^{(n_\ell+1)}(p^2, m^2, \Lambda^2 = 0, \mu, Q/\nu)\Big|_{\cancel{C_F T_F}} &= \delta(p^2) + a_s^{(n_\ell+1)} C_F \left\{ \left[\frac{4}{\varepsilon^2} + \frac{3}{\varepsilon}\right] \delta(p^2) - \frac{4}{\varepsilon} \mathcal{L}_0(p^2) \right\} \\
&+ \left(a_s^{(n_\ell+1)}\right)^2 \left\{ C_F T_F n_\ell \left[\left(\frac{4}{\varepsilon^3} - \frac{2}{9\varepsilon^2} + \left(-\frac{121}{27} - \frac{2\pi^2}{9} \right) \frac{1}{\varepsilon} \right) \delta(p^2) + \left(-\frac{8}{3\varepsilon^2} + \frac{40}{9\varepsilon} \right) \mathcal{L}_0(p^2) \right] \right. \\
&\quad + C_F C_A \left[\left(-\frac{11}{\varepsilon^3} + \left(\frac{35}{18} - \frac{\pi^2}{3} \right) \frac{1}{\varepsilon^2} + \left(-20\zeta_3 + \frac{1769}{108} + \frac{11\pi^2}{18} \right) \frac{1}{\varepsilon} \right) \delta(p^2) \right. \\
&\qquad \left. + \left(\frac{22}{3\varepsilon^2} + \left(\frac{2\pi^2}{3} - \frac{134}{9} \right) \frac{1}{\varepsilon} \right) \mathcal{L}_0(p^2) \right] \\
&\quad + C_F^2 \left[\left(\frac{8}{\varepsilon^4} + \frac{12}{\varepsilon^3} + \left(\frac{9}{2} - \frac{4\pi^2}{3} \right) \frac{1}{\varepsilon^2} + \left(12\zeta_3 + \frac{3}{4} - \pi^2 \right) \frac{1}{\varepsilon} \right) \delta(p^2) \right. \\
&\qquad \left. \left. + \left(-\frac{16}{\varepsilon^3} - \frac{12}{\varepsilon^2} \right) \mathcal{L}_0(p^2) + \frac{16}{\varepsilon^2} \mathcal{L}_1(p^2) \right] \right\} + \mathcal{O}(\alpha_s^3)\,.
\end{aligned} \tag{5.2}$$

[9] We note that all statements made before in section 5.1 apply for massless ($f = q$) and massive primary quarks ($f = Q$).

JHEP08(2019)112

By definition it contains *all* $1/\varepsilon$-divergent terms and quantifies the difference between the renormalized and bare jet-function MEs,

$$\mathscr{J}_Q^{(n_\ell+1),\text{bare}}(p^2,m^2,\mu) = \int \mathrm{d}p'^2\, Z_{\mathscr{J},Q}^{(n_\ell+1)}(p^2-p'^2,\mu)\mathscr{J}_Q^{(n_\ell+1)}(p'^2,Z_m^2m^2)\,. \tag{5.3}$$

In the context of our jet-function ME computation it includes UV and IR divergent $1/\varepsilon$ terms. We stress that, upon (literally) replacing the color factor $C_FT_Fn_\ell$ by $C_FT_F(n_\ell+1)$ in eq. (5.2), one obtains the *full* $\mathcal{O}(\alpha_s^2)$ $\overline{\text{MS}}$ Z-factor for the universal SCET jet functions $J_f^{\text{uf},(n_\ell+1)}$ (for massless or massive primary quarks) as well as for the SCET jet function for $(n_\ell+1)$ massless quark flavors, where *all* $1/\varepsilon$ divergent terms are UV divergences.[10] This relation is required by consistency and can be used as a cross check for calculations.

In the massless gluon computational scheme the loop corrections to the bare collinear-soft ME $\mathscr{S}^{(n_\ell)}$ are given by scaleless integrals and thus vanish to all orders in perturbation theory

$$\mathscr{S}^{(n_\ell),\text{bare}}(\ell,m,\Lambda=0) = \delta(\ell)\,. \tag{5.4}$$

The corresponding bare collinear-soft ME $\mathscr{S}^{(n_\ell+1)}$, on the other hand, corresponds to scaleless integrals only at $\mathcal{O}(\alpha_s)$ and $\mathcal{O}(\alpha_s^2C_F^2,\alpha_s^2C_FC_A,\alpha_s^2C_FT_Fn_\ell)$:

$$\mathscr{S}^{(n_\ell+1),\text{bare}}(\ell,m,\Lambda=0)\Big|_{\cancel{C_FT_F}} = \delta(\ell)+\mathcal{O}(\alpha_s^3)\,. \tag{5.5}$$

In the computational scheme with an infinitesimal gluon mass Λ the terms of the renormalized jet-function ME relevant for the calculation of the $\mathcal{O}(\alpha_s^2C_FT_F)$ secondary quark mass effects read

$$\begin{aligned}
\mathscr{J}_Q^{(n_\ell+1)}(p^2,m^2,\Lambda^2,\mu,Q/\nu)\Big|_{C_FT_F} &= \delta(s) + a_s^{(n_\ell+1)}C_F\bigg\{\bigg[2L_m^2+L_m+2\log^2\left(\frac{\Lambda^2}{\mu^2}\right)\\
&\quad + 4\log\left(\frac{\Lambda^2}{\mu^2}\right)\log\left(\frac{Q}{\nu}\right)+8\bigg]\delta(s)+\left[-4L_m-4\log\left(\frac{\Lambda^2}{\mu^2}\right)-4\right]\mathcal{L}_0(s)+8\mathcal{L}_1(s)\\
&\quad + \Theta(p^2-m^2)\left[\frac{s}{(m^2+s)^2}-\frac{4\log\left(\frac{s}{m^2}+1\right)}{s}\right]\bigg\}\\
&+\left(a_s^{(n_\ell+1)}\right)^2C_FT_F\bigg\{\bigg[\left(\frac{8}{3}\log^2\left(\frac{\Lambda^2}{\mu^2}\right)+\frac{8\pi^2}{9}+\frac{34}{3}\right)L_m+\frac{8}{3}L_m^3+\frac{10}{3}L_m^2\\
&\quad + \log\left(\frac{Q}{\nu}\right)\left(\frac{16}{3}\log\left(\frac{\Lambda^2}{\mu^2}\right)L_m-\frac{80}{9}L_m-\frac{8}{3}L_m^2-\frac{224}{27}\right)+\frac{8\zeta_3}{3}-\frac{4\pi^2}{3}+\frac{3139}{162}\bigg]\delta(p^2)\\
&\quad + \left[\left(-\frac{16}{3}\log\left(\frac{\Lambda^2}{\mu^2}\right)-\frac{16}{3}\right)L_m-\frac{16}{3}L_m^2\right]\mathcal{L}_0(p^2)+\frac{32}{3}L_m\mathcal{L}_1(p^2)\\
&\quad + L_m\left[\frac{4s}{3\,(m^2+s)^2}-\frac{16\log\left(\frac{s}{m^2}+1\right)}{3s}\right]\Theta(p^2-m^2)+G_{\text{sec}}^{(3Q)}\Theta(p^2-(3m)^2)\bigg\}+\mathcal{O}(\alpha_s^3)\,,
\end{aligned} \tag{5.6}$$

[10] Note that the Z-factor for the mass mode jet function $J_f^{\text{mf},(n_\ell+1)}$ can be obtained from the results for the bare and renormalized jet-function ME $\mathscr{J}_Q^{(n_\ell+1)}$ and collinear-soft ME $\mathscr{S}^{(n_\ell)}$. Because both are defined in theories with different number of quark flavors, the Z-factor for the mass mode jet function cannot be quoted in the $\overline{\text{MS}}$ scheme and in general has finite contributions.

where $G_{\text{sec}}^{(3Q)}$ is given in eq. (3.19). For convenience, we also provide the analogous results for the renormalized massless primary quark jet-function ME $\mathscr{J}_q^{(n_\ell+1)}(p^2,m^2,\Lambda^2,\mu,Q/\nu)\big|_{C_FT_F}$ in appendix A. The $\overline{\text{MS}}$ renormalization Z-factor associated with the jet-function ME contributions in eq. (5.6) (which is identical for massive and massless primary quarks) accounts for UV and rapidity divergences and reads

$$\begin{aligned}
&Z_{\mathscr{J}}(p^2,m^2,\Lambda^2,\mu,Q/\nu)\big|_{C_FT_F} = \delta(p^2)\\
&\quad + a_s^{(n_\ell+1)} C_F \left\{ \left[\frac{4}{\varepsilon} - 4\log\left(\frac{\Lambda^2}{\mu^2}\right) + \mathcal{O}(\varepsilon) \right] \frac{1}{\eta} + \left[3 - 4\log\left(\frac{Q}{\nu}\right) \right] \frac{1}{\varepsilon} \right\} \delta(p^2)\\
&\quad + \left(a_s^{(n_\ell+1)}\right)^2 C_F T_F \left\{ \left[\frac{8}{3\varepsilon^2} - \frac{40}{9\varepsilon} + \frac{8}{3}L_m^2 + \left(\frac{80}{9} - \frac{16}{3}\log\left(\frac{\Lambda^2}{\mu^2}\right) \right) L_m + \frac{224}{27} + \mathcal{O}(\varepsilon) \right] \frac{1}{\eta} \right.\\
&\qquad \left. + \left[2 - \frac{8}{3}\log\left(\frac{Q}{\nu}\right) \right] \frac{1}{\varepsilon^2} + \left[\frac{40}{9}\log\left(\frac{Q}{\nu}\right) - \frac{4\pi^2}{9} - \frac{1}{3} \right] \frac{1}{\varepsilon} \right\} \delta(p^2) + \mathcal{O}(\alpha_s^3)\,. \qquad (5.7)
\end{aligned}$$

The corresponding results for the two different renormalized collinear-soft MEs are

$$\begin{aligned}
&\mathscr{S}^{(n_\ell)}(\ell,m,\Lambda,\mu,\nu)\Big|_{C_FT_F} = \delta(\ell)\\
&\quad + a_s^{(n_\ell)} C_F \left\{ \left[-4\log\left(\frac{\nu}{\mu}\right)\log\left(\frac{\Lambda^2}{\mu^2}\right) + 2\log^2\left(\frac{\Lambda^2}{\mu^2}\right) + \frac{\pi^2}{3} \right] \delta(\ell) - 4\mathcal{L}_0(\ell)\log\left(\frac{\Lambda^2}{\mu^2}\right) \right\}\\
&\quad + \mathcal{O}(\alpha_s^3)\,, \qquad (5.8)
\end{aligned}$$

and

$$\begin{aligned}
&\mathscr{S}^{(n_\ell+1)}(\ell,m,\Lambda,\mu,\nu)\Big|_{C_FT_F} = \delta(\ell)\\
&\quad + a_s^{(n_\ell+1)} C_F \left\{ \left[-4\log\left(\frac{\nu}{\mu}\right)\log\left(\frac{\Lambda^2}{\mu^2}\right) + 2\log^2\left(\frac{\Lambda^2}{\mu^2}\right) + \frac{\pi^2}{3} \right] \delta(\ell) - 4\mathcal{L}_0(\ell)\log\left(\frac{\Lambda^2}{\mu^2}\right) \right\}\\
&\quad + \left(a_s^{(n_\ell+1)}\right)^2 C_F T_F \left\{ \left[-\frac{8}{9}L_m^3 + \left(\frac{8}{3}\log\left(\frac{\nu}{\mu}\right) - \frac{40}{9} \right) L_m^2 \right.\right.\\
&\qquad + L_m \left(-\frac{16}{3}\log\left(\frac{\Lambda^2}{\mu^2}\right)\log\left(\frac{\nu}{\mu}\right) + \frac{8}{3}\log^2\left(\frac{\Lambda^2}{\mu^2}\right) + \frac{80}{9}\log\left(\frac{\nu}{\mu}\right) + \frac{8\pi^2}{9} - \frac{448}{27} \right)\\
&\qquad \left. + \frac{56\zeta_3}{9} + \frac{10\pi^2}{27} - \frac{656}{27} + \frac{224}{27}\log\left(\frac{\nu}{\mu}\right) \right] \delta(\ell)\\
&\qquad \left. + \left[\left(\frac{80}{9} - \frac{16}{3}\log\left(\frac{\Lambda^2}{\mu^2}\right) \right) L_m + \frac{8}{3}L_m^2 + \frac{224}{27} \right] \mathcal{L}_0(\ell) \right\} + \mathcal{O}(\alpha_s^3)\,. \qquad (5.9)
\end{aligned}$$

Their respective $\overline{\text{MS}}$ renormalization Z-factors accounting for UV and rapidity divergences read

$$\begin{aligned}
Z_{\mathscr{S}}^{(n_\ell)}(\ell,m,\Lambda,\mu,\nu)\Big|_{C_FT_F} &= \delta(\ell) + 4\, a_s^{(n_\ell)} C_F \left\{ \left[\frac{1}{\varepsilon} - \log\left(\frac{\Lambda^2}{\mu^2}\right) + \mathcal{O}(\varepsilon) \right] \frac{1}{\eta}\delta(\ell) \right.\\
&\quad \left. + \left[-\frac{1}{\varepsilon^2} + \log\left(\frac{\nu}{\mu}\right) \right] \delta(\ell) + \mathcal{L}_0(\ell)\frac{1}{\varepsilon} \right\} + \mathcal{O}(\alpha_s^3)\,, \qquad (5.10)
\end{aligned}$$

JHEP08(2019)112

and

$$
\begin{aligned}
Z_{\mathscr{I}}^{(n_\ell+1)}(\ell,m,\Lambda,\mu,\nu)\Big|_{C_F T_F} &= \delta(\ell) + 4\, a_s^{(n_\ell)} C_F \Bigg\{ \left[\frac{1}{\varepsilon} - \log\left(\frac{\Lambda^2}{\mu^2}\right) + \mathcal{O}(\varepsilon)\right] \frac{1}{\eta}\delta(\ell) \\
&\quad + \left[-\frac{1}{\varepsilon^2} + \log\left(\frac{\nu}{\mu}\right)\right] \delta(\ell) + \mathcal{L}_0(\ell)\frac{1}{\varepsilon} \Bigg\} \\
&\quad + \left(a_s^{(n_\ell+1)}\right)^2 C_F T_F \Bigg\{ \left[\frac{8}{3\varepsilon^2} - \frac{40}{9\varepsilon} - \frac{16}{3}\log\left(\frac{\Lambda^2}{\mu^2}\right) L_m + \frac{8L_m^2}{3} + \frac{80 L_m}{9} + \frac{224}{27}\right] \frac{1}{\eta}\delta(p^2) \\
&\quad + \left[-\frac{4}{\varepsilon^3} + \left(\frac{20}{9} + \frac{8}{3}\log\left(\frac{\nu}{\mu}\right)\right)\frac{1}{\varepsilon^2} + \left(-\frac{40}{9}\log\left(\frac{\nu}{\mu}\right) - \frac{2\pi^2}{9} + \frac{112}{27}\right)\frac{1}{\varepsilon}\right] \delta\left(p^2\right) \\
&\quad + \left[\frac{8}{3\varepsilon^2} - \frac{40}{9\varepsilon}\right] \mathcal{L}_0(p^2) \Bigg\} + \mathcal{O}(\alpha_s^3)\,. \qquad (5.11)
\end{aligned}
$$

These results can be extracted from ref. [32], and we have explicitly cross checked their results.[11]

From the results quoted above it is straightforward to obtain the results for the universal (see eqs. (2.10) and (3.27)) and the mass mode SCET jet functions (see eqs. (2.11) and (3.6)). The virtuality and rapidity anomalous dimensions for the universal and mass mode SCET jet functions (and the collinear-soft function) (see eqs. (4.9) and (4.11) and appendix C) are related to the corresponding anomalous dimensions for the jet-function and the collinear-soft MEs (see appendix C as well).

5.2 Gluonic and massless quark corrections

In figure 1 all two-loop Feynman diagrams relevant for the calculation of the two-loop jet-function ME in eq. (2.4) using QCD Feynman rules and Feynman gauge are displayed. In this section we discuss the computation of the $\mathcal{O}(\alpha_s^2 C_F^2, \alpha_s^2 C_F C_A, \alpha_s^2 C_F T_F n_\ell)$ corrections using the computational scheme with a massless gluon, as explained in the previous subsection.

After evaluating the Dirac trace in eq. (2.4) the contribution of each diagram for the jet function forward scattering ME can be expressed as a linear combination of dimensionally regularized ($d = 4 - 2\varepsilon$) scalar integrals of the generic form

$$
\begin{aligned}
&\int \frac{\mathrm{d}^d k\, \mathrm{d}^d \ell\ \ [-\bar{n}\cdot k]^{-c_1}[-\bar{n}\cdot \ell]^{-c_2}}{[-k^2]^{a_1}[-\ell^2]^{a_2}[-(k-\ell)^2]^{a_3}[-(p+k)^2+m^2]^{b_1}[-(p+\ell)^2+m^2]^{b_2}[-(p+k+\ell)^2+m^2]^{b_3}} \\
&= -\pi^d (-s)^{d-a_1-a_2-a_3-b_1-b_2-b_3} (\bar{n}\cdot p)^{-c_1-c_2} \mathcal{I}(-m^2/p^2; a_1, a_2, a_3, b_1, b_2, b_3, c_1, c_2)\,, \qquad (5.12)
\end{aligned}
$$

where all propagator denominators have the usual $-i0$ term and the prescription $s \to s + i0$ for the jet virtuality $s = p^2 - m^2 \geq 0$ is understood. In the second line we pulled out the conventional factor of $i\pi^{d/2}$ per loop integral. We also pulled out the factor $(\bar{n}\cdot p)^{-c_1-c_2}$ as this dependence is fixed by the behavior of the integral under the rescaling of $\bar{n}$ or Lorentz covariance. The power of $(-s)$ is then determined by choosing $\mathcal{I}$ to be dimensionless. This

[11] Note that eq. (B.55) of ref. [32] has a typo due to a missing global factor of 4.

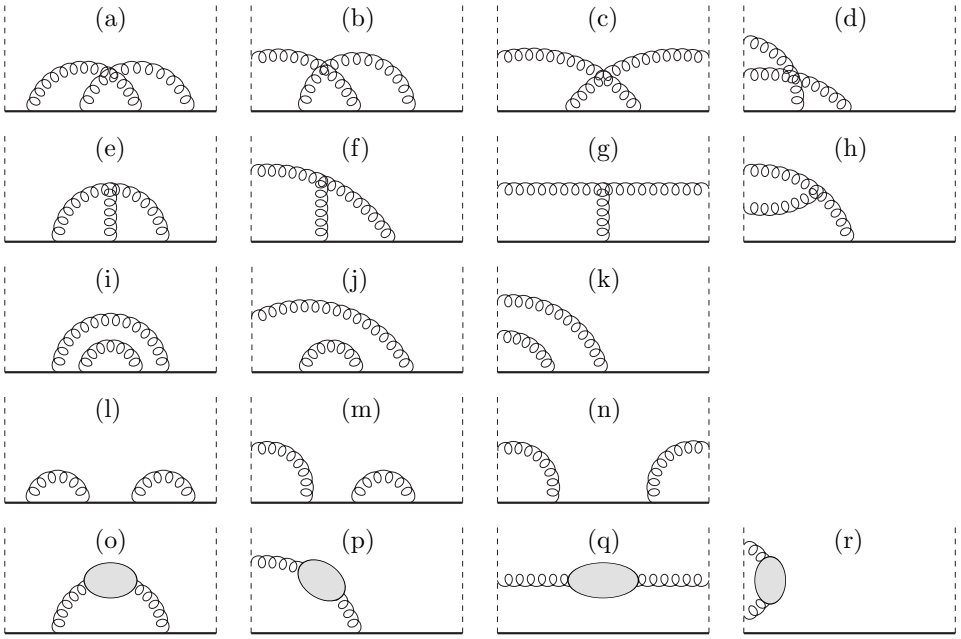

Figure 1. QCD Feynman diagrams contributing to the jet field correlator in eq. (2.4) at two-loop order in Feynman gauge. The dashed lines represent n-collinear (lightlike) Wilson lines. The gray blob symbolizes the set of all 1-loop gluon self-energy subdiagrams. Left-right mirror graphs are understood. Diagrams that are trivially zero (as $\bar{n}^2 = 0$) are not shown.

factor encodes the full s dependence in the massless limit ($s \to p^2$), where $\mathcal{I}$ becomes a function of ε only.

The set of propagator denominators in eq. (5.12) does not represent a linearly independent basis. Either a_3 or b_3 can be rendered zero by partial fraction decomposition. We therefore can arrange all integrals into two integral families: family A, where $b_3 = 0$, and family B, where $a_3 = 0$. Integrals where $a_3 = b_3 = 0$ are for convenience assigned to family A. Some family B integrals with only two massive propagators can be mapped by loop momentum shifts to family A. Diagrams (g) and (c) contain the top sector integrals of family A and B, respectively (i.e. where all propagator powers are positive). We distinguish two types of diagrams: the "planar" diagrams (e)-(q), which contain the leading color contributions, and the "nonplanar" diagrams (a)-(d) which are proportional to $C_F^2 - C_F C_A/2$ and therefore color-suppressed. The planar diagrams only involve family A integrals, while the "nonplanar" diagrams contain integrals of family A and B. Diagrams (r) are scaleless and vanish.

The classification in family A and B integrals is useful for two reasons. The first is that they are closed under integration by parts (IBP) reductions and require different sets of IBP identities. The second is related to the different mathematical properties of family A and B integrals. Family A integrals have at most two massive propagators and involve at most harmonic polylogarithms in the ε expanded results. In contrast, family B integrals can

JHEP08(2019)112

contain elliptic functions in the ε expanded expressions, which makes their evaluation more complicated. This is connected to the fact that they admit a triple massive-particle cut. Moreover, we observed that some family B integrals (including cases with only two massive propagators) are ill-defined in pure dimensional regularization due to rapidity singularities even though the Feynman diagrams are individually rapidity finite. Further, using IBP reductions on rapidity finite family B integrals can lead to rapidity singular integrals. Therefore, the computations of family B integrals in general require a rapidity regulator.

Let us briefly illustrate this issue for the following rapidity-finite family B integral

$$\begin{aligned}&\int \frac{\mathrm{d}^d k\, \mathrm{d}^d \ell}{[-\ell^2][-(p+k)^2+m^2][-(p+\ell)^2+m^2][-(p+k+\ell)^2+m^2][-\bar{n}\cdot k]^{1+\eta}} \\ &\quad = -\pi^d (-s)^{d-5} (\bar{n}\cdot p)^{-1-\eta}\, \mathcal{I}(-y;0,1,0,1,1,1,1+\eta,0)\,, \end{aligned} \tag{5.13}$$

where we introduced an analytic rapidity regulator η for the k-integration, see e.g. refs. [23, 39, 42]. Applying the IBP relation

$$\begin{aligned}0 = \Big(&a_1 - b_1 + a_1 \mathbf{a_1^+} - \frac{1+y}{1-y} b_1 \mathbf{b_1^+} - 2\frac{y}{1-y} b_3 \mathbf{b_3^+} + c_1 \mathbf{c_1^+} + b_1 \mathbf{b_1^+ a_1^-} + b_3 \mathbf{b_3^+ a_1^-} \\ &+ b_3 \mathbf{b_3^+ a_2^-} - a_1 \mathbf{a_1^+ b_1^-} - b_3 \mathbf{b_3^+ b_1^-} - b_3 \mathbf{b_3^+ b_2^-}\Big)\, \mathcal{I}\,, \end{aligned} \tag{5.14}$$

where the bold letters represent operators that increase (+) or decrease (−) the corresponding propagator powers in $\mathcal{I}$, we obtain

$$\begin{aligned}\mathcal{I}(-y;0,1,0,1,1,1,1+\eta,0) &= (1+\eta)\,\mathcal{I}(-y;0,1,0,1,1,1,2+\eta,0) \\ &- \mathcal{I}(-y;0,1,0,0,1,2,1+\eta,0) + \mathcal{I}(-y;0,0,0,1,1,2,1+\eta,0) \\ &- \frac{1+y}{1-y}\,\mathcal{I}(-y;0,1,0,2,1,1,1+\eta,0) - 2\frac{y}{1-y}\,\mathcal{I}(-y;0,1,0,1,1,2,1+\eta,0) \\ &+ \mathcal{I}(-y;-1,1,0,2,1,1,1+\eta,0) + \mathcal{I}(-y;-1,1,0,1,1,2,1+\eta,0) \\ &- \mathcal{I}(-y;0,1,0,1,0,2,1+\eta,0)\,. \end{aligned} \tag{5.15}$$

The first three integrals on the right hand side turn out to be individually rapidity divergent, i.e. they have $1/\eta$ poles as can e.g. be checked numerically with the sector decomposition program `pySecDec` [43]. These $1/\eta$ poles cancel in the sum. Without a rapidity regulator, i.e. naively setting $\eta = 0$ in eq. (5.15) literally, however, gives an incorrect relation because the term $\eta\,\mathcal{I}(-y;0,1,0,1,1,1,2+\eta,0)$ leads to finite contributions which are missed when the rapidity regularization is introduced after using the IBP relation. An analogous issue also arises when using a dimensionful rapidity regulator such as the Δ regulator proposed in ref. [25]. We stress that the IBP reduction with a rapidity regulator (no matter of what kind) in general leads to a substantially increased number of master integrals. Moreover, these are typically more complicated to compute than comparable integrals where this kind of problem does not arise and an additional rapidity regularization is not necessary.

Interestingly, the IBP reduction of family A integrals does not give rise to spurious rapidity divergences and works consistently without any rapidity regulator in the standard way. This is (currently) an empirical observation as we are lacking a simple systematic

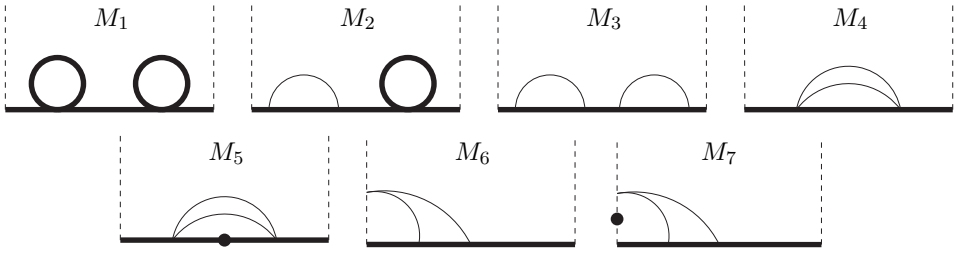

Figure 2. The seven master integrals of family A. Bold solid lines represent massive propagators, thin solid lines represent massless propagators and dashed lines represent (lightlike) Wilson line propagators. A dot on a line means that the associated propagator is squared. Note that the offshell quark propagators $\propto 1/s$ are not included in the definition of the master integrals M_i and are only drawn here for illustration. The corresponding solutions for the $\mathcal{I}_i$ according to eq. (5.12) are given in appendix D.

criterion that would allow us to identify when the problem of spurious rapidity divergences arises and to possibly avoid or treat them in an automatized way. We therefore explicitly verified all family A integral reductions used in our computations numerically in order to dispel any doubt about their validity. In this context the known (or easily computed) massless primary quark limit of each individual diagram provides a valuable cross check of our calculations.

The calculation of the planar diagrams (e)-(q) can thus be performed with standard modern multi-loop technology as explained in section 5.2.1. For the nonplanar diagrams (a)-(d), the issue of the spurious rapidity divergences and the elliptic nature of certain family B integrals forced us to use different and less uniform methods as explained in section 5.2.2. As a general strategy, we analytically compute the two-loop master integrals for the jet field correlator to the required order in ε first, insert them into the different diagrams, and finally take the imaginary part of the total contribution to the jet field correlator according to eq. (2.4) for each color factor. The only exceptions are diagrams (b) and (c), for which we take a different semi-numerical approach, as explained in section 5.2.2. We renormalize the resulting jet-function MEs $\mathscr{J}_Q^{(n_\ell+1)}\big|_{\cancel{C_F}\cancel{T_F}}$ according to eq. (5.3), i.e. we absorb *all* divergent terms into the Z-factor, and we use the pole mass scheme for the quark mass. The necessary counterterms for the pole mass m (and the $\overline{\text{MS}}$ coupling $\alpha_s^{(n_\ell+1)}$) can e.g. be found in ref. [44]. We note that in the pole mass scheme derivatives of the distributions $\delta(s)$ and $\mathcal{L}_n(s)$ do not arise in the final result.

5.2.1 Planar diagrams

The calculation of the planar diagrams (e)-(q) (including only massless partonic loops in the gluon self-energy) is rather straightforward. They involve $\mathcal{O}(100)$ family A integrals. We reduced this set of integrals to the seven master integrals depicted in figure 2 using the IBP program `FIRE5` [45].

The master integrals M_1-M_5 can be computed using Feynman parameters for arbitrary ε in terms of hypergeometric functions. They can be expanded in terms of harmonic

polylogarithms (HPLs) [46, 47] with the help of the `Mathematica` package `HypExp` [48]. We also used the `Mathematica` package `HPL` [49] to exploit relations among the HPLs for the simplification of expressions or to make their singular behavior for $s \to 0$ explicit, see below.

For M_6, M_7 we used the method of differential equations [50–52]. To this end we take their derivatives with respect to $y = m^2/p^2$. The result can be expressed via IBP reduction in terms of M_1-M_7. The coupled system of seven homogeneous first-order differential equations can also be rewritten in terms of a coupled system of two first-order differential equations for M_6, M_7 with linear combinations of M_1-M_5 as (known) inhomogeneous terms:

$$\begin{aligned}\frac{\partial M_6}{\partial y} = & -\frac{(1-\varepsilon)^2(1-y)}{2\varepsilon y^2}M_1 + \frac{(1-2\varepsilon)(1-\varepsilon)}{2\varepsilon y^2}M_2 - \frac{\left(2-7\varepsilon+6\varepsilon^2\right)\left(1-\varepsilon(5-y)\right)}{4\varepsilon^2(1-y)y}M_4 \\ & - \frac{(1-2\varepsilon)\left((2-y^2)\varepsilon-(2-7\varepsilon)y\right)}{4\varepsilon^2(1-y)^2y}M_5 - \frac{\varepsilon(3-y)}{y(1-y)}M_6 + \frac{3}{2y}M_7\,, \qquad (5.16)\\ \frac{\partial M_7}{\partial y} = & \frac{1-3\varepsilon+2\varepsilon^2}{y^2}M_2 + \frac{2-7\varepsilon+6\varepsilon^2}{y(1-y)}M_4 - \frac{(1-2\varepsilon)(1+y)}{y(1-y)^2}M_5 \\ & - \frac{4\varepsilon^2}{y(1-y)}M_6 + \frac{2\varepsilon}{y(1-y)}M_7\,. \qquad (5.17)\end{aligned}$$

These can be decoupled into two separate second-order inhomogeneous differential equations for M_6 and M_7. Upon expansion in ε these can be iteratively rewritten in second-order inhomogeneous differential equations where only derivatives of expansion coefficients of M_6 or M_7 arise. These differential equations happen to have a particularly simple form because these derivatives appear in a combination, such that upon integration the resulting differential equations only involve first derivatives of the expansion coefficients. Another integration w.r.t. y then yields the result depending on two integration constants (boundary values) that can be fixed by taking the (massless) limit $y \to 0$, where the integrals are known [8]. We give the explicit solutions for M_1-M_7 in appendix D. We checked all of them numerically to the required order in ε using the Sector Decomposition codes `FIESTA4` [53] and `pySecDec` [43].

In order to take the imaginary part of the planar contributions we proceed as follows. Defining $f(s)$ as the contribution of the planar diagrams at the correlator level we want to determine

$$\mathrm{Im}[f(s+i0)] = \frac{1}{2i}\mathrm{Disc}[f(s)] = \frac{1}{2i}\lim_{\beta\to 0}\left[f(s+i\beta) - f(s-i\beta)\right]. \qquad (5.18)$$

The result involves the distributions $\delta(s)$ and $\mathcal{L}_n(s)$ and their derivatives prior to pole mass renormalization. (These derivatives only arise from diagrams that contain quark self-energy subdiagrams.) In practice we compute eq. (5.18) for $s > 0$ first. We write the HPLs from the solutions of the master integrals with the help of the `HPL` package in a form, where the branch cuts are made explicit as $\log^n(-s/\mu^2)$ terms. We can now easily take the imaginary part of these terms according to eq. (5.18). The remaining terms are regular in s and thus do not contribute. In the next step we promote the terms $\log^n(s/\mu^2)/s$ and $[n\log^{n-1}(s/\mu^2) - \log^n(s/\mu^2)]/s^2$ for $s > 0$ to the corresponding plus distributions $\mathcal{L}_n(s)$

and their derivatives, respectively. We fix the coefficient of the $\delta(s)$ term by evaluating the imaginary part of the integral of $f(s+i0)$ over a small region around $s=0$:

$$\mathrm{Im}\left[\int_{-\Lambda_1}^{\Lambda_2} \mathrm{d}s\; f(s+i0)\right] \quad \text{with} \quad \Lambda_1, \Lambda_2 > 0\,. \tag{5.19}$$

The result is independent of Λ_1, as the imaginary part of $f(s+i0)$ does not have support for $s<0$. For $\Lambda_2 \to 0$ the result involves a constant and terms $\log^k(\Lambda_2)/\Lambda_2^n$ which match the structure of the distributions $\mathcal{L}_n(s)$ and their derivatives. The constant term determines the coefficient of $\delta(s)$ in $\mathrm{Im}[f(s+i0)]$. The coefficients of first and second derivatives of $\delta(s)$ are determined in an analogous way considering eq. (5.19) with additional weight functions s and s^2, respectively. Upon imposing pole mass renormalization all derivatives of $\delta(s)$ and $\mathcal{L}_n(s)$ consistently cancel, which provides an important cross check.

5.2.2 Nonplanar diagrams

For the calculation of the nonplanar diagrams (a) and (d) we proceed in the same way as described for the planar diagrams in the previous subsection. Regarding the IBP reductions, no rapidity regulator is required for diagram (a), because it does not involve any Wilson line propagators. In the reduction of diagram (d) issues related to spurious rapidity divergences may in principle arise. However, we were able to exclude by hand IBP relations such as eq. (5.14), which generate (possibly ill-defined) rapidity divergent integrals at intermediate steps. Interestingly, diagram (d) then happens to reduce to already known family A master integrals. We explicitly checked the IBP reduction numerically using `pySecDec` [43] together with our analytical results for the master integrals.

For diagram (a) family B master integrals cannot be avoided and a suitable basis for them is depicted in figure 3. It contains so-called sunrise and kite integrals for which generic results can be found in the literature. All three master integrals admit a triple massive particle cut, which is reflected by the $\Theta(p^2-(3m)^2) = \Theta(1-9y)$ terms in their imaginary part, and evaluate to (integrals of) elliptic functions. The master integrals contribute to the jet field correlator with prefactors proportional to $(-s-i0)^{-2\varepsilon}$ and upon ε-expansion in practice we only need the imaginary part of the combination $(-s-i0)^{-2\varepsilon} M_i$ when $s>0$. To determine the coefficients of the $\delta(s)$ and its derivatives we additionally need the first few terms in the expansion of the master integrals in $s = p^2\bar{y} = p^2(1-y)$. All these results are given in appendix D. They are straightforwardly determined or directly taken from refs. [54–56].

To compute diagrams (b) and (c) we are forced to take a different approach. The reason is that diagram (b) and (c) already involve rapidity divergent family B integrals before any reduction. These rapidity divergences cancel in the sum for each diagram. An IBP reduction method without additional regulator, as used for diagram (d) therefore seems impractical. Using a rapidity regulator, on the other hand, results in new types of master integrals which involve three massive propagators, several massless propagators, as well as regularized Wilson line propagators. Such integrals appear too difficult to be solved with the tools at hand. We therefore decided to refrain from using IBP reductions and

JHEP08(2019)112

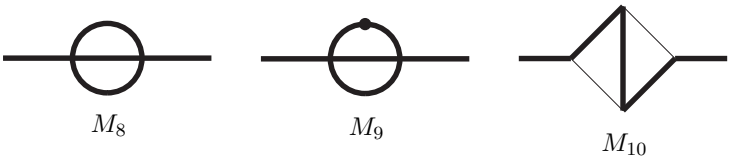

Figure 3. Master integrals of family B contributing to diagram (a). Bold solid lines represent massive propagators, thin solid lines represent massless propagators. A dot on a line means that the associated propagator is squared. The solutions for these offshell sunrise and kite type integrals can be found in the literature. We give the results for their imaginary parts and small s expansion necessary for our calculation in appendix D.

compute them directly using numerical methods and exploiting consistency conditions on their analytical structure as explained in the following.

Numerical calculation of the contributions from diagrams (b) and (c). In a first step we use the sector decomposition code `pySecDec` [43] to obtain numerical results for the real and imaginary parts of the contributions of diagrams (b) and (c) to the jet field correlator expanded in ε up to $\mathcal{O}(\varepsilon^0)$. To this end we set $\mu^2 = s$, separately write the integrands of the two diagrams in Feynman parameter representation and solve as many integrals analytically as possible. For both diagrams four integrations over rational functions of the parameters are remaining and are carried out with `pySecDec`. We furthermore multiply the integrands by $p^2(1-y)^2 = s^2/p^2$ to render them dimensionless and to damp the singular behavior in the (bHQET) limit $y \to 1$. We then obtained numerical results at 100 points in the physical region $0 \leq y < 1$. From these numerical data points we verified that the coefficients of the $1/\varepsilon$ poles together with the divergences of the already computed diagrams correctly reproduce within numerical uncertainties (which are typically at the sub-percent level) the divergence structure related to the renormalization Z-factor in eq. (5.2). This provides an important cross check for our approach, in particular confirms the correctness concerning the μ dependence.

Due to the multiplication of the factor $p^2(1-y)^2 = s^2/p^2$ we do not have direct numerical access to the coefficient of the $\delta(s)$ term. We will come back to this point at the end of this subsection. However, analytic information on the contribution of diagrams (b) and (c) to the jet-function ME is known in various kinematic limits. Using IBP reduction[12] and the master integrals given in [8], it is straightforward to compute the diagrams in the massless limit. Upon taking the imaginary part the result, including mirror diagrams, reads

$$\mathscr{J}_{\text{fin}}^{\text{b+c}}(p^2,0) = a_s^2\left(C_F^2 - \frac{C_F C_A}{2}\right)\left[\left(-\frac{10\zeta_3}{3} - 68 + 2\pi^2 + \frac{\pi^4}{6}\right)\delta(p^2)\right.$$
$$\left. + \left(-40\zeta_3 + 24 + \frac{4\pi^2}{3}\right)\mathcal{L}_0(p^2) + \frac{16}{3}\pi^2\mathcal{L}_1(p^2) - 8\mathcal{L}_2(p^2)\right], \qquad (5.20)$$

where the $1/\varepsilon$ divergences have been subtracted. We can also extract the corresponding expression in the bHQET limit ($y \to 1$) from eq. (3.34). Combining the results for the

[12] Note that in the massless case no rapidity divergences arise.

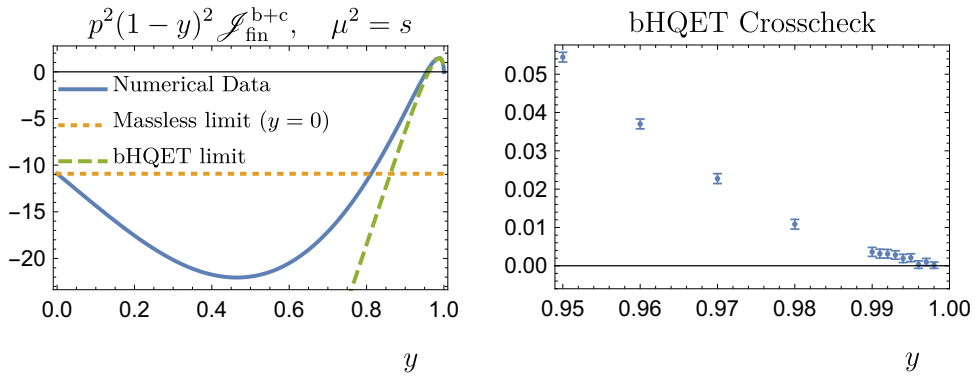

Figure 4. *Left:* Contribution of diagrams (b) and (c) to the jet-function ME finite part multiplied with the singularity-damping factor $p^2(1-y)^2$ as a function of $y \equiv m^2/p^2$ for $\mu^2 = s$. The numerical data from `pySecDec` is shown as the solid blue line. The associated numerical uncertainty is too small to be visible in the plot. The corresponding heavy quark (bHQET) limit, according to eq. (5.21), is shown as dashed green line. The dotted orange line represents the value of the jet-function ME times damping factor in the massless limit ($y = 0$), i.e. to the $\mathcal{L}_0(p^2)$ term in eq. (5.20). *Right:* Difference between numerical data points and analytic bHQET limit, normalized to the massless limit, for $\mu^2 = s$. The error bars indicate the uncertainty of the numerical integration using `pySecDec`.

two-loop bHQET jet function $J_B^{(n_\ell)}$ [21] and the collinear mass mode matching coefficient $H_{m,n}$ [41] with our results for the other diagrams, we find

$$\begin{aligned}\mathscr{J}_{\text{fin}}^{\text{b+c}}(p^2, m^2) = a_s^2 \left(C_F^2 - \frac{C_F C_A}{2}\right) \Bigg\{ \delta(s) \Bigg[&\left(-72\zeta_3 + 24 + 18\pi^2\right) L_m \\ &+ \left(\frac{8\pi^2}{3} - 16\right) L_m^2 - \frac{154\zeta_3}{3} - \frac{\pi^4}{45} + \frac{50\pi^2}{3} - 68 - 24\pi^2 \log 2 \Bigg] \\ &+ \left[16 L_m^2 + \left(32 - \frac{16\pi^2}{3}\right) L_m + 64\zeta_3 - 18\pi^2\right] \mathcal{L}_0(s) \\ &+ \left[-64 L_m + \frac{32\pi^2}{3} - 32\right] \mathcal{L}_1(s) + 40\mathcal{L}_2(s) + \mathcal{O}(m^{-2}) \Bigg\}. \end{aligned} \tag{5.21}$$

Note that this expression contains all distributional terms in $\mathscr{J}^{\text{b+c}}(p^2, m^2)$.

In the left panel of figure 4 we plot our (interpolated) numerical result for $p^2(1-y)^2\mathscr{J}_{\text{fin}}^{\text{b+c}}$ (solid blue line) and the corresponding analytical expression for $s \ll m^2$ according to eq. (5.21) (dashed green line) for $\mu^2 = s$ in the range $0 < y < 1$. Note that for $s > 0$ and $\mu^2 = s$ only the $\mathcal{L}_0(s)$ term in eq. (5.21) survives. With the factor $p^2(1-y)^2$ and for $\mu^2 = s \to p^2 > 0$ the massless result in eq. (5.20) collapses to a single value, namely the coefficient of the $\mathcal{L}_0(p^2)$ distribution. This is indicated by the dotted orange line which agrees with the numerical data point at $y = 0$ within numerical uncertainty. We also observe that in the limit $y \to 1$ the numerical data and the bHQET curve correctly approach each other nicely. To better illustrate this we show in the right panel of figure 4

JHEP08(2019)112

the difference between numerical data points and bHQET result normalized to the $y = 0$ value (dotted orange line in the left panel) in the range $0.95 < y < 1$ including the numerical uncertainties as quoted by `pySecDec`. We clearly see that for $y \gtrsim 0.996$ the difference is zero within the numerical uncertainties. This represents a strong cross check of our combined numerical and analytical evaluation.

In order to obtain a practical fit function that parametrizes our numerical results respecting at the same time the analytic constraints from the bHQET and massless limits we proceed as follows. We start with an ansatz for $\mathscr{J}^{\text{b+c}}_{\text{fin}}(p^2, m^2, \mu^2 = s)$ valid for $s > 0$ of the form

$$s\,\mathscr{J}^{\text{b+c}}_{\text{fin,ansatz}}(p^2, m^2, \mu^2 = s) = a_s^2 \left(C_F^2 - \frac{C_F C_A}{2}\right) \sum_{m=0}^{2} \sum_{n=0}^{3} c_{mn} (1-y)^m \log^n(1-y)\,. \quad (5.22)$$

Note that we multiplied $\mathscr{J}^{\text{b+c}}_{\text{fin}}(p^2, m^2)$ on the l.h.s. with the factor s. We can now fix[13]

$$c_{00} = -18\pi^2 + 64\zeta_3, \qquad c_{01} = \frac{16}{3}(\pi^2 - 6), \qquad c_{02} = 16, \qquad c_{03} = 0, \quad (5.23)$$

by comparing eq. (5.22) in the (bHQET) limit $y \to 1$ to the coefficient of $\mathcal{L}_0(s)$ in eq. (5.21). Similarly, we can take the massless limit ($y \to 0$) of eq. (5.22) and compare it to the coefficient of $\mathcal{L}_0(p^2)$ in eq. (5.20), which fixes

$$c_{10} = -c_{00} - c_{20} + 24 + \frac{4}{3}\pi^2 - 40\zeta_3\,. \quad (5.24)$$

It is straightforward to generalize the ansatz function to arbitrary values of $\mu^2 \neq s$ using the renormalization Z-factor in eq. (5.2) and our results from the other diagrams. The full distributional ansatz $\mathscr{J}^{\text{b+c}}_{\text{fin,ansatz}}(p^2, m^2, \mu^2)$ for arbitrary μ and $s \geq 0$ is then obtained by promoting the $\log^n(s/\mu^2)/s$ terms to $\mathcal{L}_n(s)$ distributions and adding the $\delta(s)$ term of eq. (5.21). To also include the nontrivial analytic information from the $\delta(p^2)$ term in the massless quark result of eq. (5.20), we integrate the full distributional ansatz over a finite interval around $s = 0$, take the limit $m \to 0$ and compare to the corresponding integral of eq. (5.20). In this way we find the additional constraint

$$\begin{aligned} c_{20} = &-\frac{\pi^2}{6}c_{01} + 2\zeta_3 c_{02} - \frac{\pi^4}{15}c_{03} - \frac{\pi^2}{6}c_{11} + 2\zeta_3 c_{12} - \frac{\pi^4}{15}c_{13} + \left(1 - \frac{\pi^2}{6}\right)c_{21} + 2(\zeta_3 - 1)c_{22} \\ &+ \left(6 - \frac{\pi^4}{15}\right)c_{23} - 56\zeta_3 - \frac{17\pi^4}{90} - 8\pi^2(3\log 2 - 2)\,. \end{aligned} \quad (5.25)$$

From the same computation (using arbitrary integration limits) one obtains analogous constraints for c_{01}, c_{02}, and c_{03} which fully agree with eq. (5.23). This represents a nontrivial check of our values for c_{01}, c_{02}, and c_{03} and implies consistency with the L_m dependent terms in the $\delta(s)$ coefficient of eq. (5.21).

Furthermore, one can argue on physical grounds that

$$c_{13} = 0\,, \quad (5.26)$$

[13] We note that a numerical fit of the coefficients in eq. (5.23) from the numerical data points provides results that agree with the values shown within numerical uncertainties.

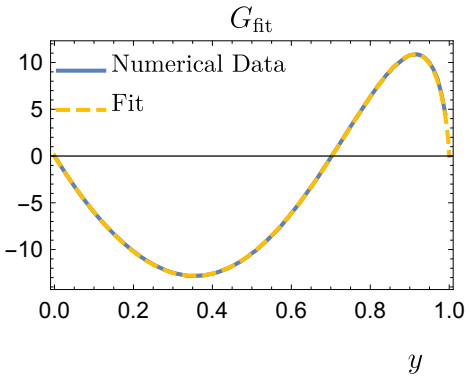

Figure 5. Fit function G_{fit} (dashed orange line) as given in eq. (3.16) compared to the (interpolated) numerical data from `pySecDec` (solid blue line). The numerical uncertainties are too small to be visible in the plot.

because we expect the first subleading bHQET power correction at two loops to have a similar logarithmic structure as eq. (5.21), i.e. is should not contain any cubic logarithmic terms.[14] A dedicated numerical analysis in the bHQET regime confirms eq. (5.26) and moreover yields

$$c_{12} = 1.0\,. \tag{5.27}$$

The values for the remaining coefficients in eq. (5.22) are obtained by a weighted fit to the numerical data from `pySecDec`. We find

$$c_{11} = -41.9008, \qquad c_{21} = -20.2744, \qquad c_{22} = -10.5870, \qquad c_{23} = -7.1277\,. \tag{5.28}$$

With these values the ansatz approximates our numerical data points to a precision better than 0.5%, while the uncertainty of the points themselves is at most 1%.

To check consistency of our numerical computation with the coefficient of $\delta(s)$ term given in eq. (5.21), we performed the same fit as described above, but without including the additional constraint of eq. (5.25). We find that the fitted value for c_{20} satisfies eq. (5.25) within the numerical uncertainties. Since the massless limit for diagrams (b) and (c) was explicitly computed, this consistency check reliably verifies the analytic input for the $\delta(s)$ term in eq. (5.21).

Finally, we separate the analytical part in eq. (5.22) from the purely numerical part given by the terms associated with the coefficients in eqs. (5.27) and (5.28), which we call G_{fit}, see eq. (3.16). We plot the fit function $G_{\text{fit}}(y)$ together with the associated numerical results in figure 5. Since the relative contribution of $G_{\text{fit}}(y)$ to the entire $\mathcal{O}(\alpha_s^2)$ corrections of the jet-function ME is smaller then 0.5% in the whole physical range, we do not bother to quote uncertainties in eqs. (5.27) and (5.28).

[14] Analogously, one could argue that there is no c_{23} term. Unlike the c_{13} term it is however regular for $y \to 1$ and we will use it to model other regular terms in our fit.

JHEP08(2019)112

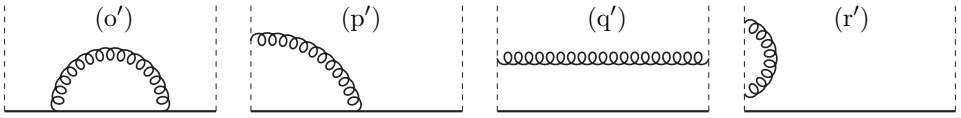

Figure 6. One-loop Feynman diagrams with massive gluons required for the calculation of the secondary mass effects, i.e. the $\mathcal{O}(\alpha_s^2 C_F T_F)$ terms, in the jet-function ME using the dispersion relation in eq. (5.29). They are associated with the diagrams (o), (p), (q) and (r) in figure 1 with a massive quark Q bubble. Left-right mirror graphs are understood.

5.3 Secondary massive quark corrections

In this section we compute the $\mathcal{O}(\alpha_s^2 C_F T_F)$ secondary massive quark corrections to the jet-function ME $\mathscr{J}_f(p^2, m^2)$. The relevant Feynman graphs are diagrams (o), (p), (q) and (r) in figure 1, where the vacuum polarization subdiagram is a massive quark Q bubble. We adopt the approach of refs. [22, 26] where the corrections are calculated starting from the $\mathcal{O}(\alpha_s)$ graphs describing radiation of a gluon with mass M. The corresponding one-loop diagrams are shown in figure 6. In a second step a dispersion relation to account for the gluon splitting into a pair of a quark and antiquark with mass m is applied. Using the dispersion relation the gluon propagator with the insertion of the bare massive quark vacuum polarization function in Feynman gauge and including the (infinitesimal) gluon mass regulator Λ can be written as

$$\frac{-ig^{\mu\rho}}{p^2-\Lambda^2+i0}\,\Pi_{\rho\sigma}(p^2,m^2)\,\frac{-ig^{\sigma\nu}}{p^2-\Lambda^2+i0} = \frac{1}{\pi}\int\limits_{4m^2}^{\infty}\frac{\mathrm{d}M^2}{M^2}\,\frac{-i(g^{\mu\nu}-\frac{p^\mu p^\nu}{p^2})}{p^2-M^2+i0}\,\mathrm{Im}\left[\Pi(M^2,m^2)\right] - \frac{-i\left(g^{\mu\nu}-\frac{p^\mu p^\nu}{p^2}\right)}{p^2-\Lambda^2+i0}\,\Pi(0,m^2)\,. \tag{5.29}$$

Here $\Pi(p^2, m^2)$ is the gluon vacuum polarization function arising from a massive quark bubble defined by

$$\Pi^{AB}_{\mu\nu}(p^2,m^2) = -i(p^2 g_{\mu\nu} - p_\mu p_\nu)\Pi(p^2,m^2)\delta^{AB} \equiv \int \mathrm{d}x^4\, \mathrm{e}^{ipx}\langle 0|\mathrm{T}J^A_\mu(x)J^B_\nu(0)|0\rangle\,, \tag{5.30}$$

with the vector current $J^A_\mu \equiv ig\bar{Q}T^A\gamma_\mu Q$. The imaginary part of the one-loop coefficient $\Pi^{(1)}$ in $d = 4-2\varepsilon$ dimensions evaluates to ($\tilde{\mu} \equiv \mu\, e^{\gamma_E/2}(4\pi)^{-1/2}$)

$$\mathrm{Im}\big[\Pi^{(1)}(p^2,m^2)\big] = \Theta\big(p^2-4m^2\big)T_F\left(\frac{p^2}{\tilde{\mu}^2}\right)^{-\varepsilon}\frac{2^{4\varepsilon}\pi^{\frac{3}{2}+\varepsilon}}{\Gamma(\frac{5}{2}-\varepsilon)}\left(\frac{2m^2}{p^2}+1-\varepsilon\right)\left(1-\frac{4m^2}{p^2}\right)^{\frac{1}{2}-\varepsilon}. \tag{5.31}$$

Note that the Heaviside Θ-function restricts the gluon mass integration in the dispersion relation to $M > 2m$. We could therefore safely set $\Lambda = 0$ in the first term of eq. (5.29).

Using eq. (5.29) for the gluon propagator with a heavy quark loop insertion in figure 1 (o), (p), (q) and (r) we see that we effectively need to compute the $\mathcal{O}(\alpha_s)$ jet-function ME $\mathscr{J}_f^{(1)}$ with finite gluon mass M, i.e. the corresponding diagrams in figure 6. This is needed

for the contribution from the first term on the r.h.s. of eq. (5.29) (before integration over M^2). To include the contribution from the second term we also need the result expanded for $M \to \Lambda \ll M, p^2$.

The $p^\mu p^\nu$ terms on the r.h.s. of eq. (5.29) can be dropped in our computation due to gauge invariance of quantum electrodynamics with a massive photon field [57, 58] and the fact that the secondary $\mathcal{O}(\alpha_s^2 C_F T_F)$ massive quark corrections are up to color factors identical in an Abelian gauge theory. Dropping the $p^\mu p^\nu$ terms in eq. (5.29) we immediately see that diagrams (q′) and (r′) are proportional to $\bar{n}\cdot\bar{n} = 0$ and thus vanish.

The contribution of diagram (o′) to eq. (2.4) before taking the imaginary part reads ($s \equiv p^2 - m^2 + i0$)

$$\begin{aligned}(\mathrm{o}') &= -i\frac{4\,\alpha_s C_F \tilde{\mu}^{2\varepsilon}}{(2\pi)^d(\bar{n}\cdot p)s^2}\int \mathrm{d}^d k\,\frac{(\bar{n}\cdot k)(d-2)s + (\bar{n}\cdot p)(4m^2 - (d-2)(2p\cdot k + s))}{[-(p+k)^2+m^2][-k^2+M^2]} \\ &= \alpha_s C_F\,\frac{\tilde{\mu}^{2\varepsilon}\,\Gamma(\varepsilon)}{2^{1-2\varepsilon}\pi^{2-\varepsilon}}\frac{1}{s^2}\int_0^1 \mathrm{d}u\,\frac{(\varepsilon-1)s(u-1) + 2m^2((\varepsilon-1)u-1)}{(M^2(1-u)+u(s(u-1)+m^2u))^\varepsilon}\,,\end{aligned} \tag{5.32}$$

where the integration variable u represents a Feynman parameter. This expression is well-behaved in the large M limit. It is convenient to separate the leading term for $M \to \infty$ in $d = 4 - 2\varepsilon$ dimensions,

$$(\mathrm{o}')_{M\to\infty} = \alpha_s C_F \Gamma(\varepsilon) 2^{-1+2\varepsilon}\pi^{-2+\varepsilon}\left(\frac{M}{\tilde{\mu}}\right)^{-2\varepsilon}\frac{2(2\varepsilon-3)m^2 + (-1+\varepsilon)^2 s}{(\varepsilon-2)(\varepsilon-1)s^2}\,. \tag{5.33}$$

In the remaining contribution, which vanishes for $M^2 \to \infty$, we can safely set $d = 4$:

$$\begin{aligned}(\mathrm{o}') - (\mathrm{o}')_{M\to\infty} = -\frac{C_F\alpha_s}{2\pi^2}\frac{1}{s^2}\int_0^1 \mathrm{d}u\,\big[s(u-1) + 2m^2(1+u)\big] \\ \times\Big[\log\Big(M^2(1-u)\Big) - \log\Big(M^2(1-u) + u(s(u-1)+m^2u)\Big)\Big] + \mathcal{O}(\varepsilon)\,.\end{aligned} \tag{5.34}$$

We now take the imaginary part according to eq. (5.18). For the non-logarithmic $1/s$ and $1/s^2$ terms we use $\mathrm{Im}[(s+i0)^{-1}] = -\pi\delta(s)$ and $\mathrm{Im}[(s+i0)^{-2}] = \pi\delta'(s)$, respectively. In addition, we get a nonzero contribution from the second logarithm in eq. (5.34) for $p^2 > (M+m)^2$ which also restricts the relevant integration range of the Feynman parameter u. Adding the $\mathcal{O}(\alpha_s)$ counterterm from the renormalization of m in the pole mass scheme at tree level we obtain ($\xi \equiv \sqrt{1-4m^2/M^2}$)

$$\begin{aligned}&\mathrm{Im}\big[(\mathrm{o}')\big] - 2\,a_s m\,\delta m_M^{(1)}\,\delta'(s) = a_s C_F \\ &\times\Bigg[-\Theta\left(p^2-(m+M)^2\right)\frac{\sqrt{(M^2-s)^2-4m^2M^2}\,\big[4m^4+2m^2(M^2+2s)+s(M^2-s)\big]}{s^2(m^2+s)^2} \\ &-2\,\delta(s)\,\mathrm{e}^{\gamma_E\varepsilon}\left(\frac{M}{\tilde{\mu}}\right)^{-2\varepsilon}\Gamma(\varepsilon)\frac{\varepsilon-1}{\varepsilon-2} + \delta(s)\frac{3\,\xi\left(2m^4-M^4\right)\log\left(\frac{m^2}{M^2}\right)}{2m^4\xi} \\ &+\delta(s)\frac{3\left[\left(-4m^4-2m^2M^2+M^4\right)\log\left(\frac{1-\xi}{1+\xi}\right) - m^2\xi(3m^2+2M^2)\right]}{2m^4\xi}\Bigg] + \mathcal{O}(\varepsilon)\,.\end{aligned} \tag{5.35}$$

Note that the $\delta'(s)$ terms from diagram (o′) and the contribution due to the quark pole mass counterterm δm_M (where the subscript indicates the nontrivial dependence on the gauge boson mass M) cancel in the sum.

Diagram (p′) is rapidity divergent. With the symmetric η regulator [23, 39] we have

$$\begin{aligned}(\mathrm{p}') &= -i\frac{8\,\alpha_s C_F \tilde{\mu}^{2\varepsilon}\nu^{\eta}}{(2\pi)^d}\frac{1}{s}\int \mathrm{d}^d k\,\frac{\bar{n}\cdot(p+k)}{[-(p+k)^2+m^2][-k^2+M^2][-\bar{n}\cdot k]^{1+\eta}}\\ &= \alpha_s C_F \frac{\tilde{\mu}^{2\varepsilon}\Gamma(\varepsilon)}{\pi^{2-\varepsilon}2^{1-2\varepsilon}}\left(\frac{\bar{n}\cdot p}{\nu}\right)^{-\eta}\frac{1}{s}\int_0^\infty \mathrm{d}u\,\mathrm{d}v\,\frac{vu^{-\eta-1}(u+v)^{2\varepsilon+\eta-2}\delta(1-u-v)}{(m^2u^2+v\,(M^2(u+v)-su))^{\varepsilon}}\,. \end{aligned} \tag{5.36}$$

To compute the integral we use the same approach as for diagram (o′). The $M\to\infty$ piece is given by

$$(\mathrm{p}')_{M\to\infty} = \alpha_s C_F 2^{-1+2\varepsilon}\pi^{-2+\varepsilon}\left(\frac{\bar{n}\cdot p}{\nu}\right)^{-\eta}\left(\frac{M}{\tilde{\mu}}\right)^{-2\varepsilon}\frac{\Gamma(\varepsilon)\Gamma(2-\varepsilon)\Gamma(-\eta)}{\Gamma(2-\varepsilon-\eta)}\frac{1}{s}\,, \tag{5.37}$$

and the remainder term reads

$$\begin{aligned}(\mathrm{p}') - (\mathrm{p}')_{M\to\infty} = \frac{C_F\alpha_s}{2\pi^2}\frac{1}{s}\int_0^1 \mathrm{d}u\frac{1-u}{u}\\ \times\left[\log\left(M^2(1-u)\right) - \log\left(m^2u^2+(1-u)\left(M^2-su\right)\right)\right] + \mathcal{O}(\varepsilon,\eta)\,.\end{aligned} \tag{5.38}$$

At this point the rapidity regularization has done its job and is in particular not needed anymore for the dispersion integration. One may therefore expand in η keeping only the divergent and finite terms. To take the imaginary part we proceed in the same way as for diagram (o′).

Accounting for the equivalent contribution from the mirror diagram of (p′) the complete result for the bare primary massive quark jet-function ME with gluon mass M to $\mathcal{O}(\alpha_s)$ reads

$$\begin{aligned}&\mathscr{J}_Q^{\mathrm{bare}}(p^2,m^2,M^2) = \delta(s)\\ &+ a_s C_F\left\{\Theta\left(p^2-(m+M)^2\right)\left[\frac{4\log\left(\frac{\sqrt{(M^2-s)^2-4m^2M^2}+M^2+s}{-\sqrt{(M^2-s)^2-4m^2M^2}+M^2+s}\right)}{s}\right.\right.\\ &\qquad\left.-\frac{\left(2m^2+s\right)\sqrt{(M^2-s)^2-4m^2M^2}\left(2m^2+M^2+3s\right)}{s^2\left(m^2+s\right)^2}\right]\\ &+\delta(s)\left[2\mathrm{e}^{\gamma_\varepsilon}\Gamma(\varepsilon)\left(\frac{M^2}{\tilde{\mu}^2}\right)^{-\varepsilon}\left(\frac{2}{\eta}-2\log\left(\frac{Q}{\nu}\right)+2H_{1-\varepsilon}-\frac{\varepsilon-1}{\varepsilon-2}\right)\right.\\ &+\frac{\left(4m^4-10m^2M^2+3M^4\right)\log\left(\frac{1-\xi}{1+\xi}\right)}{2m^4\xi}\\ &\left.\left.-\frac{m^2\left(-8m^2\log\left(\frac{1-\xi}{2}\right)\log\left(\frac{\xi+1}{2}\right)+m^2+6M^2\right)+\left(2m^4-4m^2M^2+3M^4\right)\log\left(\frac{m^2}{M^2}\right)}{2m^4}\right]\right\}\\ &+\mathcal{O}(\varepsilon,a_s^2)\,,\end{aligned} \tag{5.39}$$

where m is the quark pole mass and H_n denotes the n-th harmonic number. For the expression shown here we have kept the exact dependence on $d = 4 - 2\varepsilon$ for the terms that need regularization in the $M^2 \to \infty$ limit of the dispersion integration. Otherwise the expansions in ε and η are carried out.

From eq. (5.39) we can determine the $\mathcal{O}(\alpha_s)$ bare primary massive quark jet-function ME with the infinitesimal gluon mass regulator Λ,

$$\begin{aligned}\mathscr{J}_Q^{\text{bare},(1)}(p^2,m^2,\Lambda^2) = C_F\Bigg\{ &\left[\frac{4}{\varepsilon} - 4\log\left(\frac{\Lambda^2}{\mu^2}\right) + \mathcal{O}(\varepsilon)\right]\delta(s)\frac{1}{\eta} + \left[3 - 4\log\left(\frac{Q}{\nu}\right)\right]\delta(s)\frac{1}{\varepsilon} \\ &+ \delta(s)\left[2L_m^2 + L_m + 2\log^2\left(\frac{\Lambda^2}{\mu^2}\right) + 4\log\left(\frac{\Lambda^2}{\mu^2}\right)\log\left(\frac{Q}{\nu}\right) + 8\right] \\ &+ \mathcal{L}_0(s)\left[-4L_m - 4\log\left(\frac{\Lambda^2}{\mu^2}\right) - 4\right] + 8\mathcal{L}_1(s) + \Theta(s)\left[\frac{s}{(m^2+s)^2} - \frac{4\log\left(\frac{s}{m^2}+1\right)}{s}\right]\Bigg\}. \end{aligned} \tag{5.40}$$

We stress once again that a dimensionful regularization parameter such as the gluon mass is mandatory to fully separate the rapidity and IR singularities such that all remaining $1/\varepsilon$ terms are UV.

Using the dispersion identity eq. (5.29) the unrenormalized secondary massive quark $\mathcal{O}(\alpha_s^2 C_F T_F)$ correction to the jet-function ME $\mathscr{J}_Q(p^2,m^2)$ with an infinitesimal gluon mass regulator reads

$$\begin{aligned}\mathscr{J}_Q^{\text{bare},(2)}(p^2,m^2,\Lambda^2)\Big|_{C_F T_F} &= \frac{1}{\pi}\int\limits_{4m^2}^{\infty}\frac{\mathrm{d}M^2}{M^2}\mathscr{J}_Q^{\text{bare},(1)}(p^2,m^2,M^2)\,\mathrm{Im}\left[\Pi^{(1)}(M^2,m^2)\right] \\ &\quad - \left(\Pi^{(1)}(m^2,0) - \frac{4T_F}{3\varepsilon}\right)\mathscr{J}_Q^{\text{bare},(1)}(p^2,m^2,\Lambda^2) \\ &= Z_{\mathscr{J}}^{(2)}(s,m^2,\Lambda^2,\mu,Q/\nu)\Big|_{C_F T_F} + \mathscr{J}_Q^{(2)}(p^2,m^2,\Lambda^2,\mu,Q/\nu)\Big|_{C_F T_F}. \end{aligned} \tag{5.41}$$

The $4T_F/(3\varepsilon)$ term in the second line of eq. (5.41) is associated with the counterterm coming from the heavy quark loop and is required to implement the $\overline{\text{MS}}$ strong coupling in the $(n_\ell+1)$ flavor scheme. The dispersion integral in the first line of eq. (5.41) can be solved analytically in terms of elementary functions and standard complete elliptic integrals using `Mathematica` with appropriate changes of integration variables, except for the logarithmic real radiation term shown in the second line of eq. (5.39). The latter can be integrated numerically very efficiently. It contributes to the corrections related to the three-particle $QQ\bar{Q}$-cut and corresponds to eq. (3.24). The final result for the finite (renormalized) contribution $\mathscr{J}_Q^{(2)}\big|_{C_F T_F}$ is displayed in eq. (5.6) and the divergent terms $Z_{\mathscr{J}}^{(2)}\big|_{C_F T_F}$ are given in eq. (5.7).

6 Numerical analysis

In this section we provide a brief numerical study concerning the structure and importance of the $\mathcal{O}(\alpha_s^2)$ corrections to the primary massive quark SCET jet function. To be definite

JHEP08(2019)112

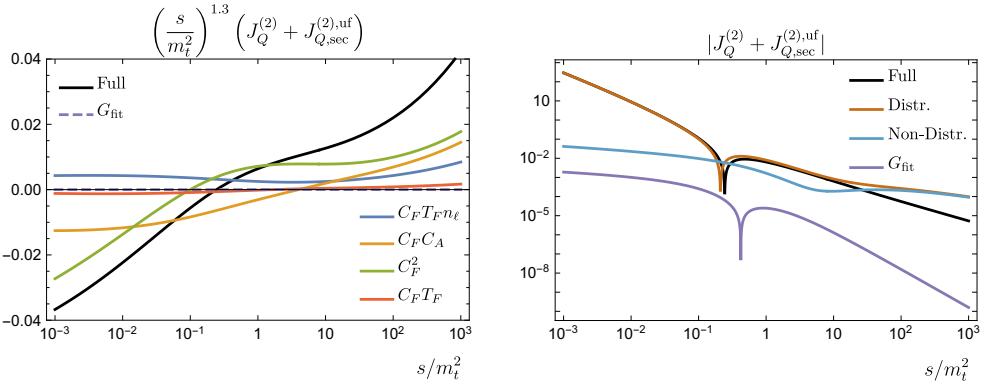

Figure 7. *Left:* Size of contributions to the $\mathcal{O}(\alpha_s^2)$ coefficient of the universal SCET massive primary quark jet function from different color structures as a function of s/m_t^2 for $\mu = \sqrt{s}+5\,\text{GeV}$, $n_\ell = 5$ and $m = m_t = 173\,\text{GeV}$ multiplied by $(s/m_t^2)^{1.3}$. *Right:* Double logarithmic plot of the modulus of the full $\mathcal{O}(\alpha_s^2)$ corrections and the corresponding contribution coming from G_{fit}. We also show the sum of all distributional $\mathcal{O}(\alpha_s^2)$ corrections and the non-distributional ones.

we use the universal jet function $J_Q^{\text{uf}(n_\ell+1)}(p^2, m^2, \mu)$ of eq. (3.27) for the analysis since in practice it is sufficient to formulate factorization theorems for all possible scale hierarchies, see the discussion in section 4. We remind the reader that the universal SCET jet function agrees with the massless quark SCET jet function in the limit $m \to 0$, called "massless limit" in the following. However, its relation to the bHQET jet function in the limit $s = p^2 - m^2 \to 0$ involves the collinear-soft function S_c that is singular by itself in this kinematic regime, see eqs. (2.11), (3.29) and (3.34). Since the bHQET factorization theorem (3.31) and the factorization theorem for $p^2 - m^2 \sim p^2 \lesssim m^2$ (4.1) (which is identical to (4.2)) can be smoothly connected, a comparison of the universal function $J_Q^{\text{uf}(n_\ell+1)}$ with its leading singular limit for $s = p^2 - m^2 \to 0$, called "heavy quark limit" in the following, correctly visualizes the size of the mass corrections that are not captured by the leading power bHQET factorization theorem in the region $0 < s = p^2 - m^2 \lesssim m^2$.

In the left panel of figure 7 the size of the contributions of the two-loop coefficient $J_Q^{(2)}(p^2, m^2, \mu) + J_{Q,\text{sec}}^{(2),\text{uf}}(p^2, m^2, \mu)$ coming from the different color structures is displayed as a function of $s/m^2 = (p^2 - m^2)/m^2$ for $\mu = \sqrt{s} + 5\,\text{GeV}$. The terms proportional to C_F^2 (green), $C_F C_A$ (orange), $C_F T_F n_\ell$ (blue) and $C_F T_F$ (red) are displayed individually where we multiplied the factor $(s/m^2)^{1.3}$ to reduce the variation of the values over the whole kinematic regime.[15] The total coefficient is displayed in black. We see that the C_F^2, $C_F C_A$ and $C_F T_F n_\ell$ terms, not unexpectedly, provide the bulk of the $\mathcal{O}(\alpha_s^2)$ corrections, and that the secondary heavy quark corrections are typically more than one order of magnitude smaller. Interestingly, due to the behavior of the C_F^2 and $C_F C_A$ terms, the $\mathcal{O}(\alpha_s^2)$ correction changes sign at $\sqrt{p^2} \approx 1.1m$ which is well within the bHQET regime.

In the left panel of figure 7 we also show the total contribution of the fit function G_{fit}

[15] This convention is also adopted for figure 8. For all numerical discussions we adopt the renormalization scale $\mu = \sqrt{s} + 5\,\text{GeV}$ and $m = m_t = 173\,\text{GeV}$.

JHEP08(2019)112

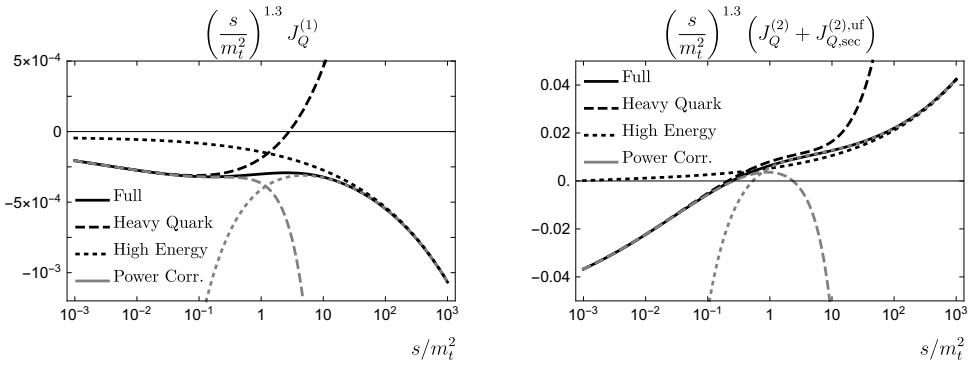

Figure 8. *Left:* $\mathcal{O}(\alpha_s)$ coefficient of the SCET massive primary quark jet function (black solid) in comparison to the leading power results of the massless (black dotted) and bHQET (black dashed) limit. Also shown are the curves including the respective next terms in the small mass and bHQET expansions (gray dotted and dashed, respectively). *Right:* Analogous plot for the $\mathcal{O}(\alpha_s^2)$ coefficient of the universal SCET massive primary quark jet function.

(purple dashed) which is part of the non-distributional terms $G_{C_F}^{(1Q)}$ and $G_{C_A}^{(1Q)}$ contained in the C_F^2 and $C_F C_A$ corrections, see eqs. (3.12) and (3.13) respectively. Typically, it makes up for less than 1% of the total $\mathcal{O}(\alpha_s^2)$ correction, except close to the zero at $\sqrt{p^2} \approx 1.1m$. This is also shown in more detail in the right (double logarithmic) panel of figure 7 where the modulus of the full $\mathcal{O}(\alpha_s^2)$ corrections (black) and the corresponding contribution coming from the function G_{fit} (purple) are displayed. Since the $\mathcal{O}(\alpha_s)$ corrections to the jet function do not have a zero (see below), the overall contribution of G_{fit} to the entire jet function never exceeds the per mille level. In the right panel of figure 7 we have also shown the sum of all distributional $\mathcal{O}(\alpha_s^2)$ corrections (brown) and the non-distributional ones (light blue) which are constituted by the sum of all G-functions quoted in section 3. We see that the non-distributional contributions are strongly suppressed compared to the distributional terms in the bHQET region and still at least an order of magnitude smaller as long as $s \lesssim 10m^2$. In the high energy limit, however, there are strong cancellations between them because the non-distributional corrections develop distributional terms in the limit $m \to 0$, see appendix B. So the contributions of the non-distributional corrections are particularly important for $s/m^2 \gtrsim 10$ where they are not at all negligible.

We also would like to show the numerical impact of the genuine SCET massive primary quark jet function in comparison to the previously known jet functions for massless quarks (i.e. its high energy limit $s/m^2 \to \infty$) and for the bHQET limit $s/m^2 \to 0$. In the left panel of figure 8 the full $\mathcal{O}(\alpha_s)$ coefficient $J_Q^{(1)}(p^2, m^2, \mu)$ is displayed (black solid) in comparison to the singular results of the massless (black dotted) and bHQET (black dashed) limit. We see that both expansions work well in the respective limits, but fail to provide reasonable approximations in the intermediate regime $0.3 \lesssim s/m^2 \lesssim 10$ which corresponds to $1.1 \lesssim \sqrt{p^2}/m \lesssim 3$. In the right panel of figure 8 the analogous results are shown for the $\mathcal{O}(\alpha_s^2)$ coefficient $J_Q^{(2)}(p^2, m^2, \mu) + J_{Q,\text{sec}}^{(2),\text{uf}}(p^2, m^2, \mu)$. Again, the massless as well as the bHQET expansion work well in the respective limits. But, interestingly, both also approximate

JHEP08(2019)112

the exact result within $15-20\%$ in the intermediate regime $0.3 \lesssim s/m^2 \lesssim 10$. That the $\mathcal{O}(\alpha_s)$ and $\mathcal{O}(\alpha_s^2)$ correction of the universal SCET massive primary quark jet function differ in this respect should be considered as an accidental feature. This can be seen by also including the respective next terms in the small mass and bHQET expansions (which represent terms belonging to subleading power expansions in massless quark SCET and bHQET, respectively). These are shown as the gray dotted and dashed lines, respectively, in figure 8. At $\mathcal{O}(\alpha_s)$ as well as $\mathcal{O}(\alpha_s^2)$ these subleading terms improve the approximation of the exact results substantially into the intermediate regime $0.3 \lesssim s/m^2 \lesssim 10$. But we see that, while at $\mathcal{O}(\alpha_s)$ they also improve the approximation to $s/m^2 \approx 1$, the same is not true at $\mathcal{O}(\alpha_s^2)$.

7 Conclusions

In this work we have calculated the $\mathcal{O}(\alpha_s^2)$ corrections to the SCET jet functions for primary massive quarks which are relevant for the inclusive description of jets initiated by massive quarks produced by hard interactions with high energy. The result provides important information for the intermediate region $p^2 \sim p^2 - m^2 = s \sim m^2$, where the previously known $\mathcal{O}(\alpha_s^2)$ jet function results in the massless limit $m^2/p^2 \to 0$ and in the bHQET limit $s \to 0$ do not provide accurate approximations. Thus they represent the essential input to achieve a coherent description that smoothly interpolates these two extreme limits.

The interesting conceptual feature of the primary massive quark SCET jet function is that it can be defined in two different ways depending on whether — in addition to the zero-bin subtractions — one imposes soft mass mode bin subtractions or not for diagrams containing secondary massive quark effects, i.e. a massive quark-antiquark vacuum polarization subdiagram. In the context of the view that jet functions require so-called zero-bin subtractions [24] to constitute infrared finite factorization functions, the relevance of the soft mass mode bin subtraction [22, 25] depends on the assumed power counting of the quark mass w.r.t. the jet invariant mass. An alternative view, that leads to equivalent results, but does not rely on a zero-bin expansion supplemented by power counting arguments, is to define the jet function with a subtraction defined from a collinear-soft matrix element [27, 28] where the effects of secondary massive quarks can be optionally included or not. The collinear-soft matrix elements provide unambiguous prescriptions of the subtractions eliminating the need to impose an additional power counting. The definitions and the results for the collinear-soft matrix elements are identical for massless and massive primary quarks and even apply for bHQET jet functions (to deal with corrections arising from secondary massive quarks that are lighter than the super-heavy primary quark).

If the secondary massive quark is included in the collinear-soft matrix element the resulting jet function is called *universal* jet function. The universal jet function reduces to the massless quark jet function in the limit of zero quark mass and also has the same virtuality (μ) anomalous dimension. It can be used for the kinematic region ranging from $m^2 \sim p^2 \sim p^2 - m^2$ down to the massless limit $p^2 \gg m^2$, where p^2 is the squared jet function invariant mass and m the mass of the primary quark. If the secondary massive quarks are not included in the collinear-soft matrix element the jet function is called *mass mode* jet

function. It is infrared divergent for $m \to 0$ and has a virtuality and a rapidity anomalous dimension. It can be used for the kinematic region $m^2 \sim p^2 \sim p^2 - m^2$. The two types of jet functions are related via the so-called collinear-soft function [32], and we have provided the $\mathcal{O}(\alpha_s^2)$ results for both. We have also demonstrated how both jet functions are used in the factorization approaches of refs. [22, 26, 41] and ref. [32] which were developed to deal with the effects of secondary massive quarks in the context of factorization. While the approach of ref. [32] provides a more transparent view on the modular structure of the collinear, soft and collinear-soft mass modes, the approach of refs. [22, 26, 41] provides a method with a smooth quark mass dependence that allows to treat the cases $p^2 - m^2 \ll m^2 \sim p^2$ and $p^2 - m^2 \sim m^2 \sim p^2$ in a single factorization theorem. Taking a jet mass factorization theorem with the primary massive quark SCET jet function as an example we have shown how both approaches are related and in which way they are or can be rendered equivalent. We emphasize that, considered together, both approaches provide a thorough view on the field theoretic treatment of secondary massive quark effects within factorization approaches that separate soft and collinear quantum effects.

Regarding the calculation, we have treated the two-loop secondary mass corrections due to heavy quark loops separately from the corrections due to massless quark and gluon loops. In fact, the correct treatment of the secondary mass corrections requires to carefully disentangle UV, IR and rapidity divergences present in this case. This is achieved by employing a dimensionful IR regulator (in our case a small gluon mass). The loop integrations are than carried out using the dispersive method of refs. [22, 26, 41].

The remaining $\mathcal{O}(\alpha_s^2)$ corrections (related to diagrams without a closed quark-antiquark loop) have been carried out in pure dimensional regularization. We distinguished two types of relevant diagrams: planar and nonplanar. While the contributions from the planar diagrams can be obtained using standard modern multi-loop techniques, we faced interesting technical issues in the calculation of the nonplanar diagrams. In particular, for two nonplanar diagrams we have not been able to employ (standard automated) IBP reductions without generating spurious rapidity divergences that require an additional rapidity regulator. The latter made the solution of the corresponding master integrals unfeasible. We therefore treated these two diagrams in a semi-numerical approach exploiting analytic information from the massless and bHQET limits. The corresponding numerical results are very accurate and only represent a very small contribution to the full $\mathcal{O}(\alpha_s^2)$ corrections to the jet functions. We have also provided precise numerical approximations of our analytic results (involving elliptic functions) for practical implementations.

Acknowledgments

This work was supported by FWF Austrian Science Fund under the Project No. P28535-N27 and in part by a GFK fellowship and by the clusters of excellence PRISMA (EXC 1098) and PRISMA$^+$ (EXC 2118) at JGU Mainz. We acknowledge partial support by the FWF Austrian Science Fund under the Doctoral Program "Particles and Interactions" No. W1252-N27. We also thank the Erwin-Schrödinger International Institute for Mathematics and Physics for partial support. CL thanks the JGU Mainz and the University of Salamanca

JHEP08(2019)112

for hospitality during parts of this work. We thank A. Carmona, D. Lechner, M. Löschner, P. Pietrulewicz, M. Preisser, and D. Samitz for helpful discussions.

A Other jet functions

The mass mode jet function for massless primary quarks at $\mathcal{O}(\alpha_s^2)$ has the form

$$J_q^{\mathrm{mf},(n_\ell+1)}\left(p^2,m^2,\mu,\frac{Q}{\nu}\right) = \delta(p^2) + a_s^{(n_\ell)} J_q^{(1)}(p^2,\mu) + \left(a_s^{(n_\ell)}\right)^2 \left[J_q^{(2)}(p^2,\mu) + J_{q,\mathrm{sec}}^{(2),\mathrm{mf}}\left(p^2,m^2,\mu,\frac{Q}{\nu}\right)\right] + \mathcal{O}(\alpha_s^3)\,, \tag{A.1}$$

with

$$\begin{aligned} J_q^{(1)}(p^2,\mu) = C_F\Bigg\{ & \left(7-\pi^2\right)\delta(p^2) - 3\mathcal{L}_0(p^2) + 4\mathcal{L}_1(p^2) \\ & + \varepsilon\left[\left(-\frac{28\zeta_3}{3} + 14 - \frac{3\pi^2}{4}\right)\delta(p^2) + \left(\pi^2-7\right)\mathcal{L}_0(p^2) + 3\mathcal{L}_1(p^2) - 2\mathcal{L}_2(p^2)\right] \\ & + \varepsilon^2\left[\left(-7\zeta_3 + 28 - \frac{7\pi^2}{4} - \frac{\pi^4}{24}\right)\delta(p^2) + \left(\frac{28\zeta_3}{3} - 14 + \frac{3\pi^2}{4}\right)\mathcal{L}_0(p^2)\right. \\ & \left. + \left(7-\pi^2\right)\mathcal{L}_1(p^2) - \frac{3}{2}\mathcal{L}_2(p^2) + \frac{2}{3}\mathcal{L}_3(p^2)\right]\Bigg\}, \end{aligned} \tag{A.2}$$

$$\begin{aligned} J_q^{(2)}(p^2,\mu) = {} & C_F^2\left[\left(-18\zeta_3 + \frac{205}{8} - \frac{67\pi^2}{6} + \frac{14\pi^4}{15}\right)\delta(p^2) + \left(-8\zeta_3 - \frac{45}{2} + 7\pi^2\right)\mathcal{L}_0(p^2)\right. \\ & \left. + \left(37 - \frac{20\pi^2}{3}\right)\mathcal{L}_1(p^2) - 18\mathcal{L}_2(p^2) + 8\mathcal{L}_3(p^2)\right] \\ & + C_F C_A\left[\left(-\frac{206\zeta_3}{9} + \frac{53129}{648} - \frac{208\pi^2}{27} - \frac{17\pi^4}{180}\right)\delta(p^2) + \left(40\zeta_3 - \frac{3155}{54} + \frac{22\pi^2}{9}\right)\mathcal{L}_0(p^2)\right. \\ & \left. + \left(\frac{367}{9} - \frac{4\pi^2}{3}\right)\mathcal{L}_1(p^2) - \frac{22}{3}\mathcal{L}_2(p^2)\right] \\ & + C_F T_F n_\ell\left[\left(\frac{494}{27} - \frac{8\pi^2}{9}\right)\mathcal{L}_0(p^2) + \left(\frac{16\zeta_3}{9} - \frac{4057}{162} + \frac{68\pi^2}{27}\right)\delta(p^2)\right. \\ & \left. - \frac{116}{9}\mathcal{L}_1(p^2) + \frac{8}{3}\mathcal{L}_2(p^2)\right], \end{aligned} \tag{A.3}$$

$$\begin{aligned} J_{q,\mathrm{sec}}^{(2),\mathrm{mf}}\left(p^2,m^2,\mu,\frac{Q}{\nu}\right) = C_F T_F\Bigg\{ & \left[\left(-\frac{8}{3}L_m^2 - \frac{80}{9}L_m - \frac{224}{27}\right)\log\left(\frac{Q}{\nu}\right) + 2L_m^2\right. \\ & \left. + \frac{2}{9}\left(3+4\pi^2\right)L_m - \frac{8\zeta_3}{3} + \frac{20\pi^2}{27} + \frac{73}{18}\right]\delta(p^2) + G_{\mathrm{sec}}\Theta\left(p^2-(2m)^2\right)\Bigg\}, \end{aligned} \tag{A.4}$$

$$G_{\rm sec} = \frac{1}{p^2}\Bigg[-\frac{32}{3}\mathrm{Li}_2\left(\frac{b-1}{1+b}\right) + \frac{16}{3}\log\left(\frac{1-b^2}{4}\right)\log\left(\frac{1-b}{1+b}\right) - \frac{8}{3}\log^2\left(\frac{1-b}{1+b}\right) + \left(\frac{1}{2}b^4 - b^2 + \frac{241}{18}\right)\log\left(\frac{1-b}{1+b}\right) - \frac{5}{27}b^3 + \frac{241}{9}b - \frac{8\pi^2}{9}\Bigg] = \frac{(p^2-(2m)^2)^{7/2}}{560m^9} + \mathcal{O}\left(\frac{(p^2-(2m)^2)^{9/2}}{m^{11}}\right), \tag{A.5}$$

where $b \equiv \sqrt{1-4m^2/p^2}$.

The universal jet function for massless primary quarks at $\mathcal{O}(\alpha_s^2)$ has the form [26]

$$J_q^{\mathrm{uf},(n_\ell+1)}(p^2,m^2,\mu) = \delta(p^2) + a_s^{(n_\ell+1)} J_q^{(1)}(p,\mu) + \left(a_s^{(n_\ell+1)}\right)^2 \left[J_q^{(2)}(p,\mu) + J_{q,\rm sec}^{(2),\mathrm{uf}}(p^2,m^2,\mu)\right] + \mathcal{O}(\alpha_s^3)\,, \tag{A.6}$$

with

$$J_{q,\rm sec}^{(2),\mathrm{uf}}(p^2,m^2,\mu) = C_F T_F \Bigg\{ \left[\frac{8}{9}L_m^3 + \frac{58}{9}L_m^2 + \left(\frac{718}{27} - \frac{8\pi^2}{9}\right)L_m + \frac{1531}{54} + \frac{10\pi^2}{27} - \frac{80\zeta_3}{9}\right]\delta(p^2) + \left[-\frac{8}{3}L_m^2 - \frac{116}{9}L_m - \frac{224}{27}\right]\mathcal{L}_0(p^2) + \frac{16}{3}L_m\mathcal{L}_1(p^2) + G_{\rm sec}\Theta\left(p^2-(2m)^2\right)\Bigg\}. \tag{A.7}$$

Both jet functions satisfy eq. (2.12) in the same way as the corresponding primary massive jet functions.

The renormalized primary massless jet-function ME including contributions related to 1-loop corrections and secondary massive quark production at 2-loop in the computational scheme with an infinitesimal gluon mass Λ is given by

$$\mathscr{J}\left(p^2,0,\Lambda^2,\mu,\frac{Q}{\nu}\right)\Big|_{C_F T_F} = \delta(p^2) + a_s^{(n_\ell+1)} C_F \Bigg\{ \left[2\log^2\left(\frac{\Lambda^2}{\mu^2}\right) + 4\log\left(\frac{\Lambda^2}{\mu^2}\right)\log\left(\frac{Q}{\nu}\right) - \frac{2\pi^2}{3} + 7\right]\delta(p^2) + \left[-4\log\left(\frac{\Lambda^2}{\mu^2}\right) - 3\right]\mathcal{L}_0(p^2) + 4\mathcal{L}_1(p^2)\Bigg\} + \left(a_s^{(n_\ell+1)}\right)^2 C_F T_F \Bigg\{ \Bigg[\left(\frac{8}{3}\log^2\left(\frac{\Lambda^2}{\mu^2}\right) + 10\right)L_m + 2L_m^2 + \log\left(\frac{Q}{\nu}\right)\left(\frac{16}{3}\log\left(\frac{\Lambda^2}{\mu^2}\right)L_m - \frac{80}{9}L_m - \frac{8}{3}L_m^2 - \frac{224}{27}\right) - \frac{8\zeta_3}{3} + \frac{20\pi^2}{27} + \frac{73}{18}\Bigg]\delta(p^2) + \left(-\frac{16}{3}\log\left(\frac{\Lambda^2}{\mu^2}\right) - 4\right)L_m\mathcal{L}_0(p^2) + \frac{16}{3}L_m\mathcal{L}_1(p^2) + G_{\rm sec}\Theta(p^2-(2m)^2)\Bigg\} + \mathcal{O}(\alpha_s^3)\,. \tag{A.8}$$

JHEP08(2019)112

The $\mathcal{O}(\alpha_s)$ and $\mathcal{O}(\alpha_s^2 C_F^2, \alpha_s^2 C_F C_A, \alpha_s^2 C_F T_F n_\ell)$ corrections in the computational scheme with a massless gluon in dimensional regularization analytically agree with those of the massless quark SCET jet function, see [8, 26].

B G-functions in the limit $m \to 0$

In the limit that the massive primary quark Q becomes massless the singular limits of the non-distributional G-functions have the form

$$G_1 = \left(-2L_m^2 - L_m - 1 - \frac{2\pi^2}{3}\right)\delta(p^2) + (1+4L_m)\mathcal{L}_0(p^2) - 4\mathcal{L}_1(p^2) + \mathcal{O}\left(\frac{m^2}{p^4}\right), \tag{B.1}$$

$$\begin{aligned} G_1^{(\varepsilon)} = {} & \left(-\frac{3}{2}L_m^2 + \frac{2\pi^2}{3}L_m - 2 - \frac{\pi^2}{3} - 4\zeta_3\right)\delta(p^2) \\ & + (1+4L_m+2L_m^2)\mathcal{L}_0(p^2) + (-5-8L_m)\mathcal{L}_1(p^2) + 6\mathcal{L}_2(p^2) + \mathcal{O}\left(\frac{m^2}{p^4}\right), \end{aligned} \tag{B.2}$$

$$\begin{aligned} G_1^{(\varepsilon^2)} = {} & \left[-\frac{1}{6}L_m^4 - \frac{1}{6}L_m^3 + \left(-4 + \frac{\pi^2}{6}\right)L_m^2 + \left(\frac{7\pi^2}{12} + 4\zeta_3\right)L_m \right. \\ & \left. - 4 - \frac{13\pi^2}{12} - \frac{\pi^4}{30} - 2\zeta_3\right]\delta(p^2) \\ & + \left[\frac{2}{3}L_m^3 + 2L_m^2 + (8-\pi^2)L_m + 2 - \frac{\pi^2}{4}\right]\mathcal{L}_0(p^2) \\ & + [-4L_m^2 - 8L_m - 9 + \pi^2]\mathcal{L}_1(p^2) + \left[8L_m + \frac{13}{2}\right]\mathcal{L}_2(p^2) - \frac{14}{3}\mathcal{L}_3(p^2) + \mathcal{O}\left(\frac{m^2}{p^4}\right), \end{aligned} \tag{B.3}$$

$$\begin{aligned} G_{C_F}^{(1Q)} = {} & \left[-2L_m^4 - 2L_m^3 + \left(2\pi^2 - \frac{35}{2}\right)L_m^2 + L_m\left(56\zeta_3 - \frac{27}{2} + \pi^2\right) \right. \\ & \left. - 68\zeta_3 + \frac{43\pi^4}{30} + \frac{125}{2} + \pi^2\left(24\log 2 - \frac{131}{6}\right)\right]\delta(p^2) \\ & + \left[8L_m^3 + 12L_m^2 + \left(38 - \frac{20\pi^2}{3}\right)L_m - 72\zeta_3 + \frac{\pi^2}{3} + \frac{33}{2}\right]\mathcal{L}_0(p^2) \\ & + \left[-32L_m^2 - 40L_m + \frac{20\pi^2}{3} - 45\right]\mathcal{L}_1(p^2) + 6[8L_m+5]\mathcal{L}_2(p^2) - 24\mathcal{L}_3(p^2) + \mathcal{O}\left(\frac{m^2}{p^4}\right), \end{aligned} \tag{B.4}$$

$$\begin{aligned} G_{C_A}^{(1Q)} = {} & \left[\frac{1}{9}\left(6\pi^2 - 179\right)L_m^2 + \frac{1}{9}L_m\left(-180\zeta_3 - 139 + 56\pi^2\right) + 42\zeta_3 \right. \\ & \left. + \frac{7\pi^4}{180} - \frac{508}{9} + \pi^2\left(\frac{25}{27} - 12\log 2\right)\right]\delta(p^2) \\ & + \frac{1}{9}\left[66L_m^2 + \left(391 - 12\pi^2\right)L_m + 180\zeta_3 - 34\pi^2 + 172\right]\mathcal{L}_0(p^2) \\ & - \frac{4}{9}\left[66L_m - 3\pi^2 + 106\right]\mathcal{L}_1(p^2) + 22\mathcal{L}_2(p^2) + \mathcal{O}\left(\frac{m^2}{p^4}\right), \end{aligned} \tag{B.5}$$

$$G_{T_F} = \left[\frac{58}{9}L_m^2+\left(\frac{74}{9}-\frac{16\pi^2}{9}\right)L_m+\frac{110}{9}+\frac{46\pi^2}{27}\right]\delta(p^2)$$
$$+\left[-\frac{8}{3}L_m^2-\frac{128}{9}L_m-\frac{86}{9}+\frac{8\pi^2}{9}\right]\mathcal{L}_0(p^2)+\left[\frac{32}{3}L_m+\frac{140}{9}\right]\mathcal{L}_1(p^2)$$
$$-8\mathcal{L}_2(p^2)+\mathcal{O}\left(\frac{m^2}{p^4}\right), \tag{B.6}$$

$$G^{(3Q)} = \left[L_m^2+7L_m+88\zeta_3-91+\pi^2(11-16\log 2)\right]\delta(p^2)+[-2L_m-7]\mathcal{L}_0(p^2)$$
$$+2\mathcal{L}_1(p^2)+\mathcal{O}\left(\frac{m^2}{p^4}\right), \tag{B.7}$$

$$G^{(3Q)}_{\rm sec} = \frac{2}{81}\left[-36L_m^3-261L_m^2+3\left(12\pi^2-359\right)L_m+216\zeta_3+171\pi^2-2783\right]\delta(p^2)$$
$$+\frac{2}{27}\left[36L_m^2+174L_m-12\pi^2+359\right]\mathcal{L}_0(p^2)-\frac{4}{9}[12L_m+29]\mathcal{L}_1(p^2)$$
$$+\frac{8}{3}\mathcal{L}_2(p^2)+\mathcal{O}\left(\frac{m^2}{p^4}\right). \tag{B.8}$$

C Anomalous dimensions

The μ-anomalous dimensions as defined in eq. (4.9) are given by

$$\gamma_c^{(n_f)}(Q,\mu) = -\gamma_Q^{(n_f)}(Q,\mu), \tag{C.1}$$

$$\gamma_Q^{(n_f)}(Q,\mu) = \Gamma^{(n_f)}_{\rm cusp}[\alpha_s]\log\left(\frac{-Q^2-i0}{\mu^2}\right)+\gamma_Q^{(n_f)}[\alpha_s], \tag{C.2}$$

$$\gamma_Q^{(n_f)}[\alpha_s] = -6\,C_F a_s^{(n_f)}+\left(a_s^{(n_f)}\right)^2\left[C_F^2\left(-3+4\pi^2-48\zeta_3\right)\right. \tag{C.3}$$
$$\left.+C_F C_A\left(-\frac{961}{27}-\frac{11\pi^2}{3}+52\zeta_3\right)+C_F T_F n_f\left(\frac{260}{27}+\frac{4\pi^2}{3}\right)\right]+\mathcal{O}(\alpha_s^3),$$

$$\gamma_{c_B}^{(n_f)}(Q,m,\mu) = -\Gamma^{(n_f)}_{\rm cusp}[\alpha_s]\log\left(\frac{-Q^2-i0}{m^2}\right)+\gamma_{c_B}^{(n_f)}[\alpha_s], \tag{C.4}$$

$$\gamma_{c_B}^{(n_f)}[\alpha_s] = 4\,C_F a_s^{(n_f)}+\left(a_s^{(n_f)}\right)^2\left[C_F C_A\left(\frac{196}{9}-\frac{4\pi^2}{3}+8\zeta_3\right)+C_F T_F n_f\left(-\frac{80}{9}\right)\right]$$
$$+\mathcal{O}(\alpha_s^3), \tag{C.5}$$

$$\gamma_J^{(n_f)}(p^2,\mu) = -2\Gamma^{(n_f)}_{\rm cusp}[\alpha_s]\mathcal{L}_0(p^2)+\gamma_J^{(n_f)}[\alpha_s]\delta(p^2), \tag{C.6}$$

$$\gamma_J^{(n_f)}[\alpha_s] = 6\,C_F a_s^{(n_f)}+\left(a_s^{(n_f)}\right)^2\left[C_F^2\left(3-4\pi^2+48\zeta_3\right)\right. \tag{C.7}$$
$$\left.+C_F C_A\left(\frac{1769}{27}+\frac{22\pi^2}{9}-80\zeta_3\right)+C_F T_F n_f\left(-\frac{484}{27}-\frac{8\pi^2}{9}\right)\right]+\mathcal{O}(\alpha_s^3),$$

$$\gamma_{J_B}^{(n_f)}(\hat{s},\mu) = -2\Gamma^{(n_f)}_{\rm cusp}[\alpha_s]\mathcal{L}_0(\hat{s})+\gamma_{J_B}^{(n_f)}[\alpha_s]\delta(\hat{s}), \tag{C.8}$$

JHEP08(2019)112

$$\gamma_{J_B}^{(n_f)}[\alpha_s] = 4C_F a_s^{(n_f)} + \left(a_s^{(n_f)}\right)^2 \left[C_F C_A \left(\frac{1396}{27} - \frac{23\pi^2}{9} - 20\zeta_3\right) + C_F T_F n_f \left(\frac{4\pi^2}{9} - \frac{464}{27}\right)\right] + \mathcal{O}(\alpha_s^3)\,, \tag{C.9}$$

$$\gamma_S^{(n_f)}(\ell^+, \ell^-, \mu) = \delta(\ell^+)\gamma_s^{(n_f)}(\ell^-, \mu) + \delta(\ell^-)\gamma_s^{(n_f)}(\ell^+, \mu)\,, \tag{C.10}$$

$$\gamma_s^{(n_f)}(\ell, \mu) = 2\Gamma_{\text{cusp}}^{(n_f)}[\alpha_s]\mathcal{L}_0(\ell) + \gamma_s^{(n_f)}[\alpha_s]\delta(\ell)\,, \tag{C.11}$$

$$\gamma_s^{(n_f)}[\alpha_s] = \left(a_s^{(n_f)}\right)^2 \left[C_F C_A \left(-\frac{808}{27} + \frac{11\pi^2}{9} + 28\zeta_3\right) + C_F T_F n_f \left(\frac{224}{27} - \frac{4\pi^2}{9}\right)\right] + \mathcal{O}(\alpha_s^3)\,, \tag{C.12}$$

$$\Gamma_{\text{cusp}}^{(n_f)} = 4C_F a_s^{(n_f)} + \left(a_s^{(n_f)}\right)^2 \left[C_F C_A \left(\frac{268}{9} - \frac{4\pi^2}{3}\right) + C_F T_F n_f \left(-\frac{80}{9}\right)\right] + \mathcal{O}(\alpha_s^3). \tag{C.13}$$

The μ- and ν-anomalous dimensions of the jet-function ME $\mathscr{J}_f^{(n_\ell+1)}(p^2, m^2)$ and the collinear-soft MEs $\mathscr{S}^{(n_\ell+1)}(\ell, m)$ and $\mathscr{S}^{(n_\ell)}(\ell)$, defined in analogy to eqs. (4.9) and (4.11), read

$$\gamma_{\mathscr{J}}(p^2, \mu, Q/\nu)\big|_{C_F T_F} = a_s^{(n_\ell+1)} C_F \left[6 - 8\log\left(\frac{Q}{\nu}\right)\right]\delta(p^2) + \left(a_s^{(n_\ell+1)}\right)^2 C_F T_F \left[\frac{160}{9}\log\left(\frac{Q}{\nu}\right) - \frac{16\pi^2}{9} - \frac{4}{3}\right]\delta(p^2) + \mathcal{O}(\alpha_s^3)\,, \tag{C.14}$$

$$\gamma_{\mathscr{S}}^{(n_\ell)}(\ell, \mu, \nu) = a_s^{(n_\ell)} C_F \left[8\log\left(\frac{\nu}{\mu}\right)\delta(\ell) + 8\mathcal{L}_0(\ell)\right] + \mathcal{O}(\alpha_s^2)\,, \tag{C.15}$$

$$\gamma_{\mathscr{S}}^{(n_\ell+1)}(\ell, \mu, \nu)\Big|_{C_F T_F} = a_s^{(n_\ell+1)} C_F \left[8\log\left(\frac{\nu}{\mu}\right)\delta(\ell) + 8\mathcal{L}_0(\ell)\right] + \left(a_s^{(n_\ell+1)}\right)^2 C_F T_F \left[\left(-\frac{160}{9}\log\left(\frac{\nu}{\mu}\right) - \frac{8\pi^2}{9} + \frac{448}{27}\right)\delta(\ell) - \frac{160}{9}\mathcal{L}_0(\ell)\right] + \mathcal{O}(\alpha_s^3)\,, \tag{C.16}$$

$$\gamma_{\nu,\mathscr{J}}(m, \Lambda, \mu)\big|_{C_F T_F} = a_s^{(n_\ell+1)} C_F \left[-4\log\left(\frac{\Lambda^2}{\mu^2}\right)\right] + \left(a_s^{(n_\ell+1)}\right)^2 C_F T_F \left[-\frac{16}{3}\log\left(\frac{\Lambda^2}{\mu^2}\right)L_m + \frac{8}{3}L_m^2 + \frac{80}{9}L_m + \frac{224}{27}\right] + \mathcal{O}(\alpha_s^3)\,, \tag{C.17}$$

$$\gamma_{\nu,\mathscr{S}}^{(n_\ell)}(\Lambda, \mu) = a_s^{(n_\ell)} C_F \left[-4\log\left(\frac{\Lambda^2}{\mu^2}\right)\right] + \mathcal{O}(\alpha_s^2)\,, \tag{C.18}$$

$$\gamma_{\nu,\mathscr{S}}^{(n_\ell+1)}(m, \Lambda, \mu)\Big|_{C_F T_F} = a_s^{(n_\ell+1)} C_F \left[-4\log\left(\frac{\Lambda^2}{\mu^2}\right)\right] + \left(a_s^{(n_\ell+1)}\right)^2 C_F T_F \left[-\frac{16}{3}\log\left(\frac{\Lambda^2}{\mu^2}\right)L_m + \frac{8}{3}L_m^2 + \frac{80}{9}L_m + \frac{224}{27}\right] + \mathcal{O}(\alpha_s^3)\,. \tag{C.19}$$

The $\mathcal{O}(\alpha_s^2 C_F^2, \alpha_s^2 C_A C_F, \alpha_s^2 C_F T_F n_\ell)$ contributions to the μ- and ν-anomalous dimensions of the jet-function and collinear-soft MEs are unknown. We therefore only displayed the

$\mathcal{O}(\alpha_s^2 C_F T_F)$ corrections coming from the massive quark Q, which is indicated by subscript "$C_F T_F$".

The virtuality μ-anomalous dimensions for the collinear-soft function S_c and the mass mode jet function $J_f^{\mathrm{mf},(n_\ell+1)}$ are

$$\begin{aligned}\gamma_{S_c}(\ell,m,\mu,\nu) &= a_s^2 C_F T_F \left[\left(-\frac{32}{3}L_m - \frac{160}{9}\right)\mathcal{L}_0(\ell)\right.\\ &\quad\left.+\left(-\frac{32}{3}\log\left(\frac{\nu}{\mu}\right)L_m - \frac{160}{9}\log\left(\frac{\nu}{\mu}\right) - \frac{8\pi^2}{9} + \frac{448}{27}\right)\delta(\ell)\right] + \mathcal{O}(\alpha_s^3), \qquad \text{(C.20)}\\ \gamma_{J^{\mathrm{mf}}}(p^2,m^2,\mu,Q/\nu)\big|_{C_F T_F} &= a_s^{(n_\ell+1)} C_F\left[-8\mathcal{L}_0(p^2)+6\delta(p^2)\right]\\ &\quad+\left(a_s^{(n_\ell+1)}\right)^2 C_F T_F\left[\left(\frac{32}{3}L_m\log\left(\frac{Q}{\nu}\right)+\frac{160}{9}\log\left(\frac{Q}{\nu}\right)-\frac{16\pi^2}{9}-\frac{4}{3}\right)\delta(p^2)\right.\\ &\quad\left.-\frac{32}{3}L_m\mathcal{L}_0(p^2)\right]+\mathcal{O}(\alpha_s^3)\,, \qquad \text{(C.21)}\end{aligned}$$

where the remaining color factor contributions to $\gamma_{J^{\mathrm{mf}}}$ at $\mathcal{O}(\alpha_s^2)$ (which do not arise from diagrams containing the massive quark Q loop) coincide with the $\mathcal{O}(\alpha_s^2)$ contributions of $\gamma_J^{(n_\ell)}$ given in eq. (C.6).

D Master integrals

The family A master integrals depicted in figure 2 evaluate to ($y \equiv m^2/p^2$, $\bar{y} \equiv 1-y$)

$$\begin{aligned}M_1 &= \mathcal{I}(-y;0,0,0,1,1,1,0,0,0) = (-y/\bar{y})^{2-2\varepsilon}\,\Gamma(\varepsilon-1)^2\,, &\text{(D.1)}\\ M_2 &= \mathcal{I}(-y;1,0,0,1,1,1,0,0,0) = -(-y/\bar{y})^{2-2\varepsilon}\,\Gamma(\varepsilon-1)^2\,{}_2F_1(1,2-2\varepsilon;2-\varepsilon;1/\bar{y})\,, &\text{(D.2)}\\ M_3 &= \mathcal{I}(-y;1,1,0,1,1,1,0,0,0) = (-y/\bar{y})^{2-2\varepsilon}\,\Gamma(\varepsilon-1)^2\,{}_2F_1(1,2-2\varepsilon;2-\varepsilon;1/\bar{y})^2\,, &\text{(D.3)}\\ M_4 &= \mathcal{I}(-y;1,0,1,0,1,0,0,0) = -2\Gamma(1-\varepsilon)\Gamma(\varepsilon)\Gamma(2\varepsilon-2)\,{}_2F_1\left(2-2\varepsilon,2\varepsilon-1;2-\varepsilon;1/\bar{y}\right), &\text{(D.4)}\\ M_5 &= \mathcal{I}(-y;1,0,1,0,2,0,0,0) = -\Gamma(1-\varepsilon)\Gamma(\varepsilon-1)\Gamma(2\varepsilon)\,{}_2F_1\left(2-2\varepsilon,2\varepsilon;2-\varepsilon;1/\bar{y}\right), &\text{(D.5)}\\ M_6 &= \mathcal{I}(-y;1,0,1,1,1,0,0,1) = \mathrm{e}^{-2\varepsilon\gamma_E}\left[\frac{\pi^2}{12\varepsilon^2}\right.\\ &\quad+\frac{1}{\varepsilon}\left(\frac{1}{6}\pi^2 H(-1;-y)-H(-2,-1;-y)+H(-2,0;-y)+\frac{7\zeta_3}{2}\right)\\ &\quad+7\zeta_3 H(-1;-y)-\frac{2}{3}\pi^2 H(-2;-y)+H(-3,-1;-y)-H(-3,0;-y)+3H(-2,-2;-y)\\ &\quad+\frac{1}{3}\pi^2 H(-1,-1;-y)-3H(-2,0,0;-y)-2H(-1,-2,-1;-y)+2H(-1,-2,0;-y)\\ &\quad\left.+\frac{11\pi^4}{72}+\mathcal{O}(\varepsilon)\right], &\text{(D.6)}\end{aligned}$$

JHEP08(2019)112

$$
\begin{aligned}
M_7 = \mathcal{I}(-y;1,0,1,1,1,0,0,2) = \mathrm{e}^{-2\varepsilon\gamma_E}\Bigg[&-\frac{1}{4\varepsilon^3}\\
&+\frac{1}{\varepsilon}\left(-H(-1,-1;-y)+H(-1,0;-y)+\frac{5\pi^2}{24}\right)-\frac{1}{6}\pi^2 H(-1;-y)-2H(-2,-1;-y)\\
&+2H(-2,0;-y)+3H(-1,-2;-y)-3H(-1,0,0;-y)+\frac{29\zeta_3}{3}\\
&+\varepsilon\Bigg(-2\zeta_3 H(-1;-y)-\pi^2 H(-2;-y)+2H(-3,-1;-y)-2H(-3,0;-y)\\
&\quad+4H(-2,-2;-y)-7H(-1,-3;-y)+\frac{5\pi^2}{6}H(-1,-1;-y)+\frac{\pi^2}{3}H(-1,0;-y)\\
&\quad-4H(-2,0,0;-y)+4H(-1,-2,-1;-y)-4H(-1,-2,0;-y)\\
&\quad-4H(-1,-1,-1,-1;-y)+4H(-1,-1,-1,0;-y)+7H(-1,0,0,0;-y)+\frac{497\pi^4}{1440}\Bigg)\\
&+\mathcal{O}(\varepsilon^2)\Bigg],
\end{aligned}
\tag{D.7}
$$

where the $H(\vec{n};-y)$ denote HPLs according to the conventions of ref. [49].

The relevant imaginary parts and $\bar{y}$-expansions related to the family B master integrals depicted in figure 3 were determined or directly taken from refs. [54–56] and read

$$
\begin{aligned}
M_8 = \mathcal{I}(-y;0,0,0,1,1,1,0,0) = \mathrm{e}^{-2\varepsilon\gamma_E}\left(\frac{-y}{\bar{y}}\right)^{1-2\varepsilon}\Bigg[&-\frac{3}{2\varepsilon^2}-\frac{\frac{1}{-y}+18}{4\varepsilon}\\
&-\frac{1}{8}\left(59+2\pi^2\right)-\frac{3\bar{y}}{8}-\frac{1}{8}\left(\pi^2-7\right)\bar{y}^2-\frac{1}{96}\left(9\pi^2-56\right)\bar{y}^3+\mathcal{O}\left(\varepsilon,\bar{y}^4\right)\Bigg],
\end{aligned}
\tag{D.8}
$$

$$
\begin{aligned}
\mathrm{Im}\left[(-s-i0)^{-2\varepsilon}M_8\right] \overset{s\geq 0}{=}\ &\Theta(1/9-y)\frac{\pi}{2\bar{y}}\sqrt{1-\sqrt{y}}\sqrt{3\sqrt{y}+1}\\
&\times\left[8y\,\mathrm{K}\left(\frac{\left(\sqrt{y}+1\right)^3\left(3\sqrt{y}-1\right)}{\left(\sqrt{y}-1\right)^3\left(3\sqrt{y}+1\right)}\right)+\left(\sqrt{y}-1\right)\left(1+3y\right)\mathrm{E}\left(\frac{\left(\sqrt{y}+1\right)^3\left(3\sqrt{y}-1\right)}{\left(\sqrt{y}-1\right)^3\left(3\sqrt{y}+1\right)}\right)\right]\\
&+\mathcal{O}(\varepsilon),
\end{aligned}
\tag{D.9}
$$

$$
\begin{aligned}
M_9 = \mathcal{I}(-y;0,0,0,2,1,1,0,0) = \mathrm{e}^{-2\varepsilon\gamma_E}\left(\frac{-y}{\bar{y}}\right)^{-2\varepsilon}\Bigg[&\frac{1}{2\varepsilon^2}+\frac{1}{2\varepsilon}-\frac{1}{12}\left(6-\pi^2\right)\\
&-\left(\frac{\pi^2}{12}-1\right)\bar{y}-\frac{1}{32}\left(4-\pi^2\right)\bar{y}^2+\mathcal{O}\left(\varepsilon,\bar{y}^3\right)\Bigg],
\end{aligned}
\tag{D.10}
$$

$$
\begin{aligned}
\mathrm{Im}\left[(-s-i0)^{-2\varepsilon}M_9\right] \overset{s\geq 0}{=}\ &-\Theta(1/9-y)\frac{\pi\sqrt{3\sqrt{y}+1}}{3\sqrt{1-\sqrt{y}}}\\
&\times\left[4\left(2\sqrt{y}-1\right)\mathrm{K}\left(\frac{\left(\sqrt{y}+1\right)^3\left(3\sqrt{y}-1\right)}{\left(\sqrt{y}-1\right)^3\left(3\sqrt{y}+1\right)}\right)+3\left(\sqrt{y}-1\right)^2\mathrm{E}\left(\frac{\left(\sqrt{y}+1\right)^3\left(3\sqrt{y}-1\right)}{\left(\sqrt{y}-1\right)^3\left(3\sqrt{y}+1\right)}\right)\right]\\
&+\mathcal{O}(\varepsilon),
\end{aligned}
\tag{D.11}
$$

$$M_{10} = \mathcal{I}(-y;1,1,0,1,1,1,0,0) = \bar{y}\left[-\frac{1}{6}\pi^2 H(1;1/y) - 2H(0,1,1;1/y)\right.$$

$$\left. + H(1,0,1;1/y) + \frac{2}{3}\int_9^\infty \mathrm{d}t\, \frac{t-9}{t-1}\log\left(1-\frac{1}{yt}\right)\frac{2\,\mathrm{K}\left(\frac{(\sqrt{t}-3)(\sqrt{t}+1)^3}{(\sqrt{t}-1)^3(\sqrt{t}+3)}\right)}{\sqrt{(\sqrt{t}-1)^3(\sqrt{t}+3)}}\right] + \mathcal{O}(\varepsilon) \quad \text{(D.12)}$$

$$= \bar{y}\left[\left(\frac{17\zeta_3}{4} - \frac{3}{2}\pi^2\log 2\right) + \bar{y}\left(3\log(-\bar{y}) - \log^2(-\bar{y}) - \frac{3\pi^2}{16} - \frac{5}{2}\right)\right] + \mathcal{O}(\varepsilon, \bar{y}^3), \quad \text{(D.13)}$$

$$\mathrm{Im}\left[(-s-i0)^{-2\varepsilon} M_{10}\right] \overset{s\geq 0}{=} \bar{y}\,\pi\left[\Theta(1-y)\left[2\log(y)\log(\bar{y}/y) - 3\mathrm{Li}_2(-\bar{y}/y)\right]\right.$$

$$\left. - \Theta(1/9-y)\frac{4}{3}\int_9^{1/y} \mathrm{d}t\, \frac{t-9}{t-1}\frac{\mathrm{K}\left(\frac{(\sqrt{t}-3)(\sqrt{t}+1)^3}{(\sqrt{t}-1)^3(\sqrt{t}+3)}\right)}{\sqrt{(\sqrt{t}-1)^3(\sqrt{t}+3)}}\right] + \mathcal{O}(\varepsilon). \quad \text{(D.14)}$$

The remaining integral in eq. (D.14) can be evaluated numerically very efficiently. It originates from the branch cut of the logarithm in the explicit integral in the full ε expanded result for M_{10} given in eq. (D.12) when taking the imaginary part. The expansion of M_{10} around $s \sim 0$, i.e. $y \sim 1$, in eq. (D.13) was computed by expanding the integrand and solving the resulting integrals using a PSLQ-type algorithm implemented in `Mathematica`.

All results stated in this appendix were checked numerically using sector decomposition.

References

[1] J.R. Andersen et al., *Les Houches 2017: Physics at TeV Colliders Standard Model Working Group Report*, arXiv:1803.07977 [INSPIRE].

[2] CLICDP collaboration, *Top-Quark Physics at the CLIC Electron-Positron Linear Collider*, arXiv:1807.02441 [INSPIRE].

[3] HL-LHC and HE-LHC WORKING GROUP collaborations, *Standard Model Physics at the HL-LHC and HE-LHC*, arXiv:1902.04070 [INSPIRE].

[4] C.W. Bauer, S. Fleming, D. Pirjol and I.W. Stewart, *An effective field theory for collinear and soft gluons: Heavy to light decays*, *Phys. Rev.* **D 63** (2001) 114020 [hep-ph/0011336] [INSPIRE].

[5] C.W. Bauer, D. Pirjol and I.W. Stewart, *Soft collinear factorization in effective field theory*, *Phys. Rev.* **D 65** (2002) 054022 [hep-ph/0109045] [INSPIRE].

JHEP08(2019)112

[6] C.W. Bauer and I.W. Stewart, *Invariant operators in collinear effective theory*, *Phys. Lett.* **B 516** (2001) 134 [hep-ph/0107001] [INSPIRE].

[7] E. Lunghi, D. Pirjol and D. Wyler, *Factorization in leptonic radiative $B \to \gamma e \nu$ decays*, *Nucl. Phys.* **B 649** (2003) 349 [hep-ph/0210091] [INSPIRE].

[8] T. Becher and M. Neubert, *Toward a NNLO calculation of the $\bar{B} \to X_s \gamma$ decay rate with a cut on photon energy. II. Two-loop result for the jet function*, *Phys. Lett.* **B 637** (2006) 251 [hep-ph/0603140] [INSPIRE].

[9] R. Brüser, Z.L. Liu and M. Stahlhofen, *Three-Loop Quark Jet Function*, *Phys. Rev. Lett.* **121** (2018) 072003 [arXiv:1804.09722] [INSPIRE].

[10] A.K. Leibovich, Z. Ligeti and M.B. Wise, *Comment on quark masses in SCET*, *Phys. Lett.* **B 564** (2003) 231 [hep-ph/0303099] [INSPIRE].

[11] I.Z. Rothstein, *Factorization, power corrections, and the pion form-factor*, *Phys. Rev.* **D 70** (2004) 054024 [hep-ph/0301240] [INSPIRE].

[12] S. Fleming, A.H. Hoang, S. Mantry and I.W. Stewart, *Jets from massive unstable particles: Top-mass determination*, *Phys. Rev.* **D 77** (2008) 074010 [hep-ph/0703207] [INSPIRE].

[13] B. Dehnadi, *Heavy quark mass determinations with sum rules and jets*, Ph.D. Thesis, Vienna University, Austria, (2016).

[14] S. Fleming, A.H. Hoang, S. Mantry and I.W. Stewart, *Top Jets in the Peak Region: Factorization Analysis with NLL Resummation*, *Phys. Rev.* **D 77** (2008) 114003 [arXiv:0711.2079] [INSPIRE].

[15] B. Dehnadi, A.H. Hoang, V. Mateu, M. Preisser and I.W. Stewart, in preparation.

[16] Y. Makris and V. Vaidya, *Transverse Momentum Spectra at Threshold for Groomed Heavy Quark Jets*, *JHEP* **10** (2018) 019 [arXiv:1807.09805] [INSPIRE].

[17] C. Lee, P. Shrivastava and V. Vaidya, *Predictions for energy correlators probing substructure of groomed heavy quark jets*, arXiv:1901.09095 [INSPIRE].

[18] M. Butenschoen, B. Dehnadi, A.H. Hoang, V. Mateu, M. Preisser and I.W. Stewart, *Top Quark Mass Calibration for Monte Carlo Event Generators*, *Phys. Rev. Lett.* **117** (2016) 232001 [arXiv:1608.01318] [INSPIRE].

[19] A.H. Hoang, S. Mantry, A. Pathak and I.W. Stewart, *Extracting a Short Distance Top Mass with Light Grooming*, arXiv:1708.02586 [INSPIRE].

[20] A.H. Hoang, S. Plätzer and D. Samitz, *On the Cutoff Dependence of the Quark Mass Parameter in Angular Ordered Parton Showers*, *JHEP* **10** (2018) 200 [arXiv:1807.06617] [INSPIRE].

[21] A. Jain, I. Scimemi and I.W. Stewart, *Two-loop Jet-Function and Jet-Mass for Top Quarks*, *Phys. Rev.* **D 77** (2008) 094008 [arXiv:0801.0743] [INSPIRE].

[22] S. Gritschacher, A.H. Hoang, I. Jemos and P. Pietrulewicz, *Secondary Heavy Quark Production in Jets through Mass Modes*, *Phys. Rev.* **D 88** (2013) 034021 [arXiv:1302.4743] [INSPIRE].

[23] J.-Y. Chiu, A. Jain, D. Neill and I.Z. Rothstein, *A Formalism for the Systematic Treatment of Rapidity Logarithms in Quantum Field Theory*, *JHEP* **05** (2012) 084 [arXiv:1202.0814] [INSPIRE].

JHEP08(2019)112

[24] A.V. Manohar and I.W. Stewart, *The Zero-Bin and Mode Factorization in Quantum Field Theory*, *Phys. Rev.* **D 76** (2007) 074002 [hep-ph/0605001] [INSPIRE].

[25] J.-y. Chiu, A. Fuhrer, A.H. Hoang, R. Kelley and A.V. Manohar, *Soft-Collinear Factorization and Zero-Bin Subtractions*, *Phys. Rev.* **D 79** (2009) 053007 [arXiv:0901.1332] [INSPIRE].

[26] P. Pietrulewicz, S. Gritschacher, A.H. Hoang, I. Jemos and V. Mateu, *Variable Flavor Number Scheme for Final State Jets in Thrust*, *Phys. Rev.* **D 90** (2014) 114001 [arXiv:1405.4860] [INSPIRE].

[27] C.W. Bauer, F.J. Tackmann, J.R. Walsh and S. Zuberi, *Factorization and Resummation for Dijet Invariant Mass Spectra*, *Phys. Rev.* **D 85** (2012) 074006 [arXiv:1106.6047] [INSPIRE].

[28] M. Procura, W.J. Waalewijn and L. Zeune, *Resummation of Double-Differential Cross Sections and Fully-Unintegrated Parton Distribution Functions*, *JHEP* **02** (2015) 117 [arXiv:1410.6483] [INSPIRE].

[29] C. Lee and G.F. Sterman, *Momentum Flow Correlations from Event Shapes: Factorized Soft Gluons and Soft-Collinear Effective Theory*, *Phys. Rev.* **D 75** (2007) 014022 [hep-ph/0611061] [INSPIRE].

[30] A. Idilbi and T. Mehen, *On the equivalence of soft and zero-bin subtractions*, *Phys. Rev.* **D 75** (2007) 114017 [hep-ph/0702022] [INSPIRE].

[31] A.H. Hoang, P. Pietrulewicz and D. Samitz, *Variable Flavor Number Scheme for Final State Jets in DIS*, *Phys. Rev.* **D 93** (2016) 034034 [arXiv:1508.04323] [INSPIRE].

[32] P. Pietrulewicz, D. Samitz, A. Spiering and F.J. Tackmann, *Factorization and Resummation for Massive Quark Effects in Exclusive Drell-Yan*, *JHEP* **08** (2017) 114 [arXiv:1703.09702] [INSPIRE].

[33] D. Samitz, Ph.D. Thesis, in preparation.

[34] S. Gritschacher, A. Hoang, I. Jemos and P. Pietrulewicz, *Two loop soft function for secondary massive quarks*, *Phys. Rev.* **D 89** (2014) 014035 [arXiv:1309.6251] [INSPIRE].

[35] T. Becher and M.D. Schwartz, *Direct photon production with effective field theory*, *JHEP* **02** (2010) 040 [arXiv:0911.0681] [INSPIRE].

[36] T. Becher and G. Bell, *The gluon jet function at two-loop order*, *Phys. Lett.* **B 695** (2011) 252 [arXiv:1008.1936] [INSPIRE].

[37] P. Banerjee, P.K. Dhani and V. Ravindran, *Gluon jet function at three loops in QCD*, *Phys. Rev.* **D 98** (2018) 094016 [arXiv:1805.02637] [INSPIRE].

[38] I.W. Stewart, F.J. Tackmann and W.J. Waalewijn, *Factorization at the LHC: From PDFs to Initial State Jets*, *Phys. Rev.* **D 81** (2010) 094035 [arXiv:0910.0467] [INSPIRE].

[39] J.-y. Chiu, A. Jain, D. Neill and I.Z. Rothstein, *The Rapidity Renormalization Group*, *Phys. Rev. Lett.* **108** (2012) 151601 [arXiv:1104.0881] [INSPIRE].

[40] J. Ablinger et al., *Iterated Elliptic and Hypergeometric Integrals for Feynman Diagrams*, *J. Math. Phys.* **59** (2018) 062305 [arXiv:1706.01299] [INSPIRE].

[41] A.H. Hoang, A. Pathak, P. Pietrulewicz and I.W. Stewart, *Hard Matching for Boosted Tops at Two Loops*, *JHEP* **12** (2015) 059 [arXiv:1508.04137] [INSPIRE].

[42] T. Becher and G. Bell, *Analytic Regularization in Soft-Collinear Effective Theory*, *Phys. Lett.* **B 713** (2012) 41 [arXiv:1112.3907] [INSPIRE].

JHEP08(2019)112

[43] S. Borowka, G. Heinrich, S. Jahn, S.P. Jones, M. Kerner and J. Schlenk, *Numerical evaluation of two-loop integrals with pySecDec*, *Acta Phys. Polon. Supp.* **11** (2018) 375 [arXiv:1712.05755] [INSPIRE].

[44] K. Melnikov and T. van Ritbergen, *The three loop on-shell renormalization of QCD and QED*, *Nucl. Phys.* **B 591** (2000) 515 [hep-ph/0005131] [INSPIRE].

[45] A.V. Smirnov, *FIRE5: a C++ implementation of Feynman Integral REduction*, *Comput. Phys. Commun.* **189** (2015) 182 [arXiv:1408.2372] [INSPIRE].

[46] T. Gehrmann and E. Remiddi, *Two loop master integrals for $\gamma^* \to 3jets$: The planar topologies*, *Nucl. Phys.* **B 601** (2001) 248 [hep-ph/0008287] [INSPIRE].

[47] E. Remiddi and J.A.M. Vermaseren, *Harmonic polylogarithms*, *Int. J. Mod. Phys.* **A 15** (2000) 725 [hep-ph/9905237] [INSPIRE].

[48] T. Huber and D. Maître, *HypExp: A Mathematica package for expanding hypergeometric functions around integer-valued parameters*, *Comput. Phys. Commun.* **175** (2006) 122 [hep-ph/0507094] [INSPIRE].

[49] D. Maître, *HPL, a mathematica implementation of the harmonic polylogarithms*, *Comput. Phys. Commun.* **174** (2006) 222 [hep-ph/0507152] [INSPIRE].

[50] A.V. Kotikov, *Differential equations method: New technique for massive Feynman diagrams calculation*, *Phys. Lett.* **B 254** (1991) 158 [INSPIRE].

[51] E. Remiddi, *Differential equations for Feynman graph amplitudes*, *Nuovo Cim.* **A 110** (1997) 1435 [hep-th/9711188] [INSPIRE].

[52] T. Gehrmann and E. Remiddi, *Differential equations for two loop four point functions*, *Nucl. Phys.* **B 580** (2000) 485 [hep-ph/9912329] [INSPIRE].

[53] A.V. Smirnov, *FIESTA4: Optimized Feynman integral calculations with GPU support*, *Comput. Phys. Commun.* **204** (2016) 189 [arXiv:1511.03614] [INSPIRE].

[54] S. Laporta and E. Remiddi, *Analytic treatment of the two loop equal mass sunrise graph*, *Nucl. Phys.* **B 704** (2005) 349 [hep-ph/0406160] [INSPIRE].

[55] S. Bauberger, F.A. Berends, M. Böhm and M. Buza, *Analytical and numerical methods for massive two loop selfenergy diagrams*, *Nucl. Phys.* **B 434** (1995) 383 [hep-ph/9409388] [INSPIRE].

[56] E. Remiddi and L. Tancredi, *Differential equations and dispersion relations for Feynman amplitudes. The two-loop massive sunrise and the kite integral*, *Nucl. Phys.* **B 907** (2016) 400 [arXiv:1602.01481] [INSPIRE].

[57] E.C.G. Stueckelberg, *Theory of the radiation of photons of small arbitrary mass*, *Helv. Phys. Acta* **30** (1957) 209 [INSPIRE].

[58] G. Feldman and P.T. Matthews, *Massive Electrodynamics*, *Phys. Rev.* **130** (1963) 1633 [INSPIRE].

JHEP08(2019)112

Chapter 7

The MSR Mass and the $\mathcal{O}(\Lambda_{\rm QCD})$ Renormalon Sum Rule

André H. Hoang, Ambar Jain, Christopher Lepenik, Vicent Mateu, Moritz Preisser, Ignazio Scimemi and Iain W. Stewart

The MSR mass and the $\mathcal{O}(\Lambda_{QCD})$ renormalon sum rule

Published in: JHEP **04** (2018) 003

Preprint version: arXiv:1704.01580 [hep-ph]

Contributions to this article:
Conceptual innovations (together with other authors), most numerical analyses, cross-checks of the analytic calculations and formulas.

The MSR mass scheme is based on Ref. [71], meaning that some of the conceptual foundations of the MSR mass scheme were already introduced before this paper was written.

PUBLISHED FOR SISSA BY SPRINGER
RECEIVED: *May 3, 2017*
REVISED: *December 19, 2017*
ACCEPTED: *March 22, 2018*
PUBLISHED: *April 3, 2018*

The MSR mass and the $\mathcal{O}(\Lambda_{\rm QCD})$ renormalon sum rule

André H. Hoang,[a,b] **Ambar Jain,**[c] **Christopher Lepenik,**[a] **Vicent Mateu,**[d,e] **Moritz Preisser,**[a,f] **Ignazio Scimemi**[g] **and Iain W. Stewart**[f]

[a] *University of Vienna, Faculty of Physics, Boltzmanngasse 5, A-1090 Wien, Austria*
[b] *Erwin Schrödinger International Institute for Mathematical Physics, University of Vienna, Boltzmanngasse 9, A-1090 Wien, Austria*
[c] *Indian Institute of Science Education and Research Bhopal, Bhopal Bypass Road, Bhopal 462066, India*
[d] *Departamento de Física Fundamental e IUFFyM, Universidad de Salamanca, E-37008 Salamanca, Spain*
[e] *Instituto de Física Teórica UAM-CSIC, E-28049 Madrid, Spain*
[f] *Center for Theoretical Physics, Massachusetts Institute of Technology, Cambridge, MA 02139, U.S.A.*
[g] *Departamento de Física Teórica II, Universidad Complutense de Madrid (UCM), E-28040 Madrid, Spain*

E-mail: andre.hoang@univie.ac.at, ambarj@iiserb.ac.in, christopher.lepenik@univie.ac.at, vmateu@usal.es, moritz.preisser@univie.ac.at, ignazios@fis.ucm.es, iains@mit.edu

ABSTRACT: We provide a detailed description and analysis of a low-scale short-distance mass scheme, called the MSR mass, that is useful for high-precision top quark mass determinations, but can be applied for any heavy quark Q. In contrast to earlier low-scale short-distance mass schemes, the MSR scheme has a direct connection to the well known $\overline{\rm MS}$ mass commonly used for high-energy applications, and is determined by heavy quark on-shell self-energy Feynman diagrams. Indeed, the MSR mass scheme can be viewed as the simplest extension of the $\overline{\rm MS}$ mass concept to renormalization scales $\ll m_Q$. The MSR mass depends on a scale R that can be chosen freely, and its renormalization group evolution has a linear dependence on R, which is known as R-evolution. Using R-evolution for the MSR mass we provide details of the derivation of an analytic expression for the normalization of the $\mathcal{O}(\Lambda_{\rm QCD})$ renormalon asymptotic behavior of the pole mass in perturbation theory. This is referred to as the $\mathcal{O}(\Lambda_{\rm QCD})$ renormalon sum rule, and can be applied to any perturbative series. The relations of the MSR mass scheme to other low-scale short-distance masses are analyzed as well.

KEYWORDS: Heavy Quark Physics, Perturbative QCD, Quark Masses and SM Parameters, Renormalization Regularization and Renormalons

ARXIV EPRINT: 1704.01580

https://doi.org/10.1007/JHEP04(2018)003

JHEP04(2018)003

Contents

1 Introduction

Achieving higher precision in theoretical predictions in the framework of quantum chromo dynamics (QCD) is one of the main goals in high-energy physics and an essential ingredient in the indirect search for physics beyond the Standard Model. In this endeavor accurate determinations of the masses of the heavy charm, bottom and top quarks play an important role since they enter the description of many observables that are employed in consistency

tests of the Standard Model and in the exploration of models of new physics. Because quark masses are formally-defined renormalized quantities and not physical observables, the quantities from which the heavy quark masses are extracted need to be computed in perturbative QCD to high order. Among the most precise recent high-order analyses to determine the heavy quark masses are QCD sum rules and the analysis of quarkonium energies for the charm and bottom quark masses [1–10] and the top pair production threshold cross section at a future lepton collider for the top quark mass [11–13]. Over time all of these analyses have been continuously updated and improved by computations of new QCD corrections, and more are being designed and studied currently to also allow for more precise determinations of the top quark mass from available LHC data [14–21].

In all the analyses of refs. [1–13] the use of short-distance mass schemes was essential to achieve a well-converging perturbative expansion and a precision in the mass determination well below the hadronization scale $\Lambda_{\rm QCD} \sim 200$–$300\,\text{MeV}$. The heavy quark pole mass $m_Q^{\rm pole}$, which is the perturbation theory equivalent of the rest mass of an on-shell quark, on the other hand, leads to a substantially worse perturbative behavior due to its linear infrared-sensitivity, also known as the $\mathcal{O}(\Lambda_{\rm QCD})$ renormalon problem [22, 23], and was therefore not adopted as a relevant mass scheme for analyses where a precision better than $\Lambda_{\rm QCD}$ could be achieved. Nevertheless, the pole mass still served as an important intermediate mass scheme during computations because it determines the partonic (but unphysical) poles of heavy quark Green functions. Typical short-distance quark mass schemes which have been employed were the renormalization-scale dependent $\overline{\rm MS}$ mass $\overline{m}_Q(\mu)$ and so-called low-scale short-distance masses such as the kinetic mass [24], the potential-subtracted (PS) mass [25], the 1S mass [26–28], the renormalon-subtracted (RS) mass [29] or the jet mass [30, 31]. The basic difference between the $\overline{\rm MS}$ mass to the low-scale short-distance mass schemes is that the perturbative coefficients of its relation to the pole mass scale linearly with the heavy quark mass, $\overline{m}_Q(\mu) - m_Q^{\rm pole} \sim m_Q(\alpha_s + \ldots)$, while for the low-scale short-distance mass schemes the corresponding series scales linearly with a scale $R \ll m_Q$. This feature enables the low-scale short-distance quark mass schemes to be used for predictions of quantities where the heavy quark dynamics is non-relativistic in nature and fluctuations at the scale of m_Q are integrated out. This is because radiative corrections to the mass in such quantities involve physical scales much smaller than m_Q. One very prominent example in the context of top quark physics is the non-relativistic heavy quarkonium dynamics inherent to the top-antitop pair production cross section at threshold at a future lepton collider [11–13], where the most important dynamical scale is the inverse Bohr radius $m_t\,\alpha_s \sim 25\,\text{GeV} \ll m_t$. On the other hand, the $\overline{\rm MS}$ mass is a good scheme choice for quantities that involve energies much larger than m_Q, such as for high-energy total cross sections, or when the massive quark causes virtual and off-shell effects. This is because in such cases the heavy quark mass yields corrections that either scale with positive or negative powers of m_Q such that QCD corrections associated with the mass have a scaling that is linear in m_Q as well. The difference between the $\overline{\rm MS}$ mass and the low-scale short-distance masses is most important for the case of the top quark because in this case the difference between m_t and the dynamical low-energy scales can be very large numerically.

JHEP04(2018)003

For the top quark mass there are excellent prospects for very precise measurements in low-scale short-distance schemes such as the PS mass or the 1S mass from the top-antitop threshold inclusive cross section at a future lepton collider [11–13]. Current studies indicate that a precision well below 50 MeV can be achieved accounting for theoretical as well as experimental uncertainties [32–34]. Currently, the most precise measurements of the top quark mass come from reconstruction analyses at the LHC [35, 36] and the Tevatron [37] and have uncertainties at the level of 500 MeV or larger. Moreover, the mass is obtained from multivariate fits involving multipurpose Monte Carlo (MC) event generators and thus represents a determination of the top quark mass parameter $m_t^{\rm MC}$ contained in the particular MC event generator. Recently, a first high-precision analysis on how the MC top quark mass parameter can be related to a field theoretically well-defined short-distance top quark mass was provided in refs. [38, 39] and general considerations on the relation were discussed in refs. [40, 41]. For the analysis, hadron level predictions for the 2-jettiness distribution [42] for electron-positron collisions and $\mathcal{O}(\alpha_s)$ QCD corrections together with the resummation of large logarithms at next-to-next-to leading order [31, 43, 44] were employed. Since the 2-jettiness distribution is closely related to the invariant mass distribution of a single reconstructed top quark, the relevant dynamical scales inherent to the problem are governed by the width of the mass distribution which amounts to only about 5 GeV in the peak region of the distribution where the sensitivity to the top mass is the highest. Interestingly, as was shown in ref. [38], the dynamical scales increase continuously considering the 2-jettiness distribution further away from the peak. In the analysis of [38] the MSR mass scheme $m_Q^{\rm MSR}(R)$ was employed which depends on a scale R and for which the dependence on R is described by a renormalization group flow such that R can be continuously adapted according to which part of the distribution is predicted. Other applications of the MSR mass using a flavor number dependent evolution in R to account for the mass effects of lighter quarks were given in refs. [45, 46]. In contrast to the μ-dependent $\overline{\rm MS}$ mass $\overline{m}_Q(\mu)$, which evolves only logarithmically in μ, the MSR mass has logarithmic as well as linear dependence on R.

The MSR mass scheme was succinctly introduced in ref. [47] and discussed conceptually in ref. [41], but a detailed discussion has so far not been provided. A key purpose of this paper is to provide sufficient details such that phenomenological MSR mass analyses, such as the results of ref. [38], can be easily related to other common short-distance mass schemes that are being used in the literature.

The definition of the MSR mass given by the perturbative series for the MSR-pole mass difference $m_Q^{\rm MSR}(R) - m_Q^{\rm pole}$ is obtained directly from the $\overline{\rm MS}$-pole mass relation $\overline{m}_Q(\overline{m}_Q) - m_Q^{\rm pole}$ and is therefore the only low-scale short-distance mass suggested in the literature that is derived directly from on-shell heavy quark self-energy diagrams just like the $\overline{\rm MS}$ mass.[1] The MSR mass thus automatically inherits the clean and good infrared properties of the $\overline{\rm MS}$ mass. Furthermore, by construction, the MSR mass matches to the $\overline{\rm MS}$ mass for $R = \overline{m}_Q(\overline{m}_Q)$ and is known to the same order as the series of $\overline{m}_Q(\overline{m}_Q) - m_Q^{\rm pole}$

[1] The name 'MSR mass' arises from a combination of the letters 'MS' standing for the close relation to the $\overline{\rm MS}$ mass and the letter 'R' standing for R-evolution.

without any further effort, which is currently $\mathcal{O}(\alpha_s^4)$ from the results of refs. [48–55]. As already argued in refs. [40, 47], the MSR mass can therefore be considered as the natural modification of the "running" $\overline{\rm MS}$ mass scheme concept for renormalization scales below m_Q, where the logarithmic evolution of the regular $\overline{\rm MS}$ mass is known to be unphysical.

Since the MSR mass is designed to be employed for scales $R < m_Q$, it can be useful — for applications where a clean treatment of virtual massive-flavor effects is important — to integrate out the virtual effects of the massive quark Q from the MSR mass definition. We therefore introduce two types of MSR masses, one where the virtual effects of the massive quark Q are integrated out, called the *natural MSR mass*, and one where these effects are not integrated out, called the *practical MSR mass*. The difference between these two versions of the MSR mass is quite small and very well behaved for all R values in the perturbative region, and the practical definition should be perfectly fine for most phenomenological applications. But the natural definition has conceptual advantages as its evolution for scales $R < m_Q$ does not include the virtual effects of the massive quark Q, which is conceptually cleaner since these belong physically to the scale m_Q.

We note that the R-evolution concept of a running heavy quark mass scheme for scales $R < m_Q$ elaborated in ref. [47] has already been suggested a long time ago in refs. [56, 57]. The R-evolution equation we discuss for the MSR mass was already quoted explicitly for the renormalization group evolution of the kinetic mass [24] at $\mathcal{O}(\alpha_s)$ in these references, but the conceptual implications of R-evolution and its connection to the $\mathcal{O}(\Lambda_{\rm QCD})$ renormalon problem in the perturbative relations between short-distance masses and the pole mass were first studied systematically in ref. [47]. The second main purpose of this paper is to give further details on R-evolution and also to discuss its relation to the Borel transformation focusing mainly on the case of the MSR mass. We note that the concept of R-evolution is quite general and can in principle be applied to any short-distance mass which depends on a variable infrared cutoff scale (such as the PS and the RS masses) or to cutoff-dependent QCD matrix elements with arbitrary dimensions. In fact, R-evolution has already been examined and applied in a number of other applications which include the factorization-scale dependence in the context of the operator product expansion [58], the scale dependence of the non-perturbative soft radiation matrix element in high-precision determinations of the strong coupling from e^+e^- event-shape distributions [59–62], even accounting for the finite mass effects of light quarks [63, 64] and hadrons [61, 65].

The basic feature of the R-evolution concept is that for the difference of MSR masses at two scales, $m_Q^{\rm MSR}(R) - m_Q^{\rm MSR}(R')$, its linear dependence on the renormalization scale provides, completely within perturbation theory, a resummation of the terms in the asymptotic series associated to the pole-mass renormalon ambiguity to all orders. The R-evolution then resums the factorially growing terms in a systematic way that is $\mathcal{O}(\Lambda_{\rm QCD})$-renormalon free and, at the same time also sums all large logarithms that arise if R and R' are widely separated. This cannot be achieved by more common purely logarithmic renormalization group equations, but is fully compatible with a Wilsonian renormalization group setup. We note that the summations carried out by the R-evolution was achieved prior to ref. [47] for the RS mass in [66] (see also ref. [67]). Their method (and the RS mass) is based on using an approximate expression for the Borel transform function. The summation for a difference

JHEP04(2018)003

of RS masses (for scales R and R') is obtained by computing the inverse Borel integral over the difference of the two respective Borel functions. This method and R-evolution lead to consistent results, but the R-evolution does not rely on the knowledge of the Borel functions.

The essential and probably most interesting conceptual feature of the perturbative series of the R-evolution equations is that it provides a systematic reordering of the terms in the asymptotic series associated to the $\mathcal{O}(\Lambda_{\rm QCD})$ renormalon ambiguity in leading, subleading, subsubleading, etc. contributions. So using the analytic solution of the R-evolution equations allows one to derive analytically (i.e. without any numerical procedure or modeling) the Borel-transform of a given perturbative series from the perspective that it carries an $\mathcal{O}(\Lambda_{\rm QCD})$ renormalon ambiguity. As a result one can rigorously derive an analytic expression for the normalization of the non-analytic terms in the Borel transform that are characteristic for the $\mathcal{O}(\Lambda_{\rm QCD})$ renormalon. The analytic result for this normalization factor was already given and discussed in ref. [47], but no details on the derivation were provided. We take the opportunity to show the details of the derivation here. We call the analytic result for the normalization of the $\mathcal{O}(\Lambda_{\rm QCD})$ renormalon ambiguity the $\mathcal{O}(\Lambda_{\rm QCD})$ *sum rule*, because it can be quickly applied to any given perturbative series. To demonstrate the use and the high sensitivity of the $\mathcal{O}(\Lambda_{\rm QCD})$ renormalon sum rule we apply it also to a number of other cases, pointing out subtleties in its application to avoid inconsistencies and misinterpretations of the results.

We note that also other methods to determine the normalization factor have been used. In ref. [29] it was determined from a computation of the residue of the Borel transform of the series following a proposal in ref. [68]. This approach, which we call *Borel method* can also be carried out analytically and provides the correct result, but has been observed to converge very slowly. We can identify the reason for this analytically from the solutions for the R-evolution equations, and we also discuss the connection of this method to our $\mathcal{O}(\Lambda_{\rm QCD})$ sum rule based on explicit analytic expressions. In ref. [69] the normalization factor was computed taking the ratio of the n-th term of the series to the asymptotic behavior. This *ratio method* converges very fast and provides results very similar to the $\mathcal{O}(\Lambda_{\rm QCD})$ sum rule. Recently, the ratio method was applied in ref. [70], accounting for the $\mathcal{O}(\alpha_s^4)$ corrections to the pole-$\overline{\rm MS}$ mass relation [54, 55]. We show that our $\mathcal{O}(\Lambda_{\rm QCD})$ sum rule provides results that are in full agreement with the ones obtained in ref. [70] and also leads to very similar uncertainties.

The paper is organized as follows: in section 2 we provide the definition of the natural and practical MSR masses, $m_Q^{\rm MSRn}$ and $m_Q^{\rm MSRp}$, based on the perturbative series of the $\overline{\rm MS}$-pole mass relation $\overline{m}_Q(\overline{m}_Q) - m_Q^{\rm pole}$, and we also analyze the difference between these two MSR masses. This section provides the conventions we use for the coefficients of perturbative series, but it can otherwise be skipped by the reader not interested in the MSR masses. In section 3 we present the R-evolution equations which describe the scale dependence of the MSR masses and we also show explicitly how the solutions of the R-evolution equations sum large logarithms together with the high-order asymptotic series terms related to the $\mathcal{O}(\Lambda_{\rm QCD})$ renormalon. We in particular show for the top quark mass under which conditions the use of the R-evolution equations and its resummation is essential and superior to

renormalon-free fixed-order perturbation theory, which does not sum any large logarithms. To our knowledge, such an analysis has not been provided in the literature before. We also point out that the solution of the R-evolution equations is intrinsically related to carrying out an inverse Borel transform over differences of functions in the Borel plane such that the singularities related to the $\mathcal{O}(\Lambda_{\rm QCD})$ renormalon cancel. In section 4 we present the analytic derivation of the $\mathcal{O}(\Lambda_{\rm QCD})$ renormalon sum rule and demonstrate its utility by a detailed analysis concerning the normalization of the $\mathcal{O}(\Lambda_{\rm QCD})$ renormalon ambiguity in the series for the difference of the pole mass and the MSR masses. The derivation of the sum rule allows to derive a new alternative expression for the high-order asymptotic behavior of a series that contains an $\mathcal{O}(\Lambda_{\rm QCD})$ renormalon which we discuss as well. To demonstrate the high sensitivity of the sum rule and to explain its consistent (and inconsistent) application we discuss its strong flavor number dependence and apply it to the massive quark vacuum polarization function, the series for the PS mass-pole mass difference, the QCD β-function, and the hadronic R-ratio. This section can be bypassed by the reader not interested in applications of the $\mathcal{O}(\Lambda_{\rm QCD})$ sum rule, but we note that section 4.5.3 discusses implications for the PS mass that are relevant for section 5 and may be important for high-precision top quark mass determinations. Some subtle issues in the relation of the MSR masses to the PS, 1S and $\overline{\rm MS}$ masses are discussed in section 5. Finally, we conclude in section 6. The paper also contains two appendices. In appendix A we specify our convention for the QCD β-function coefficients and present a number of expressions and formulae for coefficients, quantities and matching relations that arise in the discussion of R-evolution, the $\mathcal{O}(\Lambda_{\rm QCD})$ renormalon and on various mass definitions throughout this paper. In appendix B we provide details on the relation of the Borel method and our sum rule method to determine the normalization of the $\mathcal{O}(\Lambda_{\rm QCD})$ renormalon ambiguity of the pole mass. Finally, in appendix C we quote the coefficients that define the PS and the 1S masses for the convenience of the reader and also show how the MSR masses can be obtained from a given value of the 1S mass in the non-relativistic and Υ-expansion counting scheme [26, 27].

JHEP04(2018)003

2 MSR mass setup

2.1 Basic idea of the MSR mass

The $\overline{\rm MS}$ mass $\overline{m}_Q(\mu)$ serves as the standard short-distance mass scheme for many high-energy applications with physical scales of the order or larger than the mass of the quark Q. It relies on the subtraction of the $1/\epsilon$ divergences in the common $\overline{\rm MS}$ scheme in the on-shell self-energy corrections calculated in dimensional regularization. Despite the fact that it is an unphysical (i.e. theoretically designed) mass definition, it is infrared-safe and gauge invariant to all orders [48, 71] and its series relation to the pole mass $m_Q^{\rm pole}$ thus serves as the cleanest way to precisely quantify the renormalon ambiguity of the pole mass. The relation of $\overline{m}_Q \equiv \overline{m}_Q^{(n_\ell+1)}(\overline{m}_Q^{(n_\ell+1)})$ to the pole mass in the approximation that the masses of all quarks lighter than Q are zero reads

$$m_Q^{\rm pole} - \overline{m}_Q = \overline{m}_Q \sum_{n=1}^{\infty} a_n^{\overline{\rm MS}}(n_\ell, n_h) \left(\frac{\alpha_s^{(n_\ell+1)}(\overline{m}_Q)}{4\pi}\right)^n , \tag{2.1}$$

with

$$
\begin{aligned}
a_1^{\overline{\rm MS}}(n_\ell,n_h) &= \frac{16}{3}\,, \qquad (2.2)\\
a_2^{\overline{\rm MS}}(n_\ell,n_h) &= 213.437 + 1.65707\,n_h - 16.6619\,n_\ell\,,\\
a_3^{\overline{\rm MS}}(n_\ell,n_h) &= 12075. + 118.986\,n_h + 4.10115\,n_h^2 - 1707.35\,n_\ell + 1.42358\,n_h\,n_\ell + 41.7722\,n_\ell^2\,,\\
a_4^{\overline{\rm MS}}(n_\ell,n_h) &= (911588.\pm 417.) + (1781.61\pm 30.72)\,n_h - (60.1637\pm 0.6912)\,n_h^2\\
&\quad - (231.201\pm 0.102)\,n_h\,n_\ell - (190683.\pm 10.)\,n_\ell + 9.25995\,n_h^2\,n_\ell\\
&\quad + 6.35819\,n_h^3 + 4.40363\,n_h\,n_\ell^2 + 11105.\,n_\ell^2 - 173.604\,n_\ell^3\,,
\end{aligned}
$$

where $\alpha_s^{(n_f)}$ stands for the strong coupling that renormalization-group (RG) evolves with n_f active flavors, see eq. (A.1). The coefficients $a_n^{\overline{\rm MS}}$ at $\mathcal{O}(\alpha_s, \alpha_s^2, \alpha_s^3)$ are known analytically from refs. [48–53]. The $\mathcal{O}(\alpha_s^4)$ coefficient $a_4^{\overline{\rm MS}}$ was determined numerically in refs. [54, 55], and the quoted numerical uncertainties have been taken from ref. [55]. Using the method of ref. [72] the uncertainties of the n_ℓ-dependent terms may be further reduced. Using renormalon calculus [22, 23, 73] one can show that the high-order asymptotic behavior series of eq. (2.1) has an ambiguity of order $\Lambda_{\rm QCD}^{(n_\ell)}$, which depends on the number of massless quarks (indicated by the superscript) but is *independent* of the actual value of $\overline{m}_Q$.

A coherent treatment of the mass effects of lighter quarks is beyond the scope of this paper, and we therefore use the approximation that all flavors lighter than Q are massless. These mass corrections come from the insertion of massive virtual quark loops in the self-energy Feynman diagrams and start at $\mathcal{O}(\alpha_s^2)$. At this order and at $\mathcal{O}(\alpha_s^3)$ the mass corrections from the virtual massive quark loops have been calculated analytically for all mass values in ref. [49] and [74], respectively. The dominant linear mass corrections at $\mathcal{O}(\alpha_s^3)$ were determined in ref. [75]. At $\mathcal{O}(\alpha_s^4)$ and the mass corrections are not yet known, but the corrections in the limit of large virtual quark masses are encoded in the ultraheavy flavor threshold matching relations of the RG-evolution $\overline{m}_Q(\mu)$ at scales above m_Q [76].

The idea of the MSR mass is based on the fact that the $\mathcal{O}(\Lambda_{\rm QCD})$ ambiguity of the perturbative series on the r.h.s. of eq. (2.1) does not depend on the value $\overline{m}_Q$, as already mentioned above. This is an exact mathematical statement within the context of the calculus for asymptotic series and means that we can replace the term $\overline{m}_Q$ by the arbitrary scale R on the r.h.s. of eq. (2.1) and use the resulting perturbative series as the definition of the R-dependent MSR mass scheme. It was pointed out in ref. [41] that, for a given value of R, one can also interpret the MSR mass field theoretically as having a mass renormalization constant that contains the on-shell self-energy corrections of the pole mass only for scales larger than R. In other words, the pole mass and the MSR mass at the scale R differ by self-energy corrections from scales below R: while the pole mass absorbs all self-energy corrections for quantum fluctuations up to scales m_Q, the MSR mass at the scale R absorbs only self-energy corrections between R and m_Q. Since the pole mass renormalon problem is related to the self-energy corrections from the scale $\Lambda_{\rm QCD} < R$, this explains why the MSR mass is a short-distance mass. In this illustrative context the $\overline{\rm MS}$ mass absorbs no self-energy corrections up to the scale m_Q. Since the scale R is variable, the MSR mass can serve as a short-distance mass definition for applications governed by different physical scales and

thus can also interpolate between them. Since the MSR mass is expected to have applications primarily for $R < m_Q$, it is further suitable to change the scheme from $n_\ell{+}1$ dynamical flavors, which includes the UV effects of the quark Q, to a scheme with n_ℓ dynamical flavors. This can be achieved in two ways, either by simply rewriting $\alpha_s^{(n_\ell+1)}$ in terms of $\alpha_s^{(n_\ell)}$, or by integrating out the virtual loop corrections of the quark Q. This results in two different ways to define the MSR mass, where we call the former the *practical MSR mass* and the latter the *natural MSR mass*, either one having advantages depending on the application.

We note that the notion of a scale-dependent short-distance mass which was first suggested in refs. [56, 57] has also been adopted for the kinetic [24], the PS [25], RS [29] and jet masses [30, 43]. However, none of these short-distance masses is defined directly from the on-shell self-energy diagrams of the massive quark Q such as the MSR mass. This has a number of advantages, for example when discussing heavy flavor symmetry properties in the pole-$\overline{\rm MS}$ mass relation of different heavy quarks.

2.2 Natural MSR mass

The *natural MSR mass* definition is obtained by integrating out the corrections from the heavy quark Q virtual loops in the self-energy diagrams of the massive quark Q, such that its relation to the pole mass reads

$$m_Q^{\rm pole} - m_Q^{\rm MSRn}(R) = R \sum_{n=1}^{\infty} a_n^{\overline{\rm MS}}(n_\ell, 0) \left(\frac{\alpha_s^{(n_\ell)}(R)}{4\pi}\right)^n , \tag{2.3}$$

where the coefficients are given in eq. (2.2). The natural MSR mass only accounts for gluonic and massless quark corrections, and has a non-trivial matching relation to the $\overline{\rm MS}$ mass. The matching between the natural MSR mass and the $\overline{\rm MS}$ mass can be derived from the relation $[\overline{m}_Q \equiv \overline{m}_Q^{(n_\ell+1)}(\overline{m}_Q^{(n_\ell+1)})]$

$$m_Q^{\rm MSRn}(\overline{m}_Q) - \overline{m}_Q = \overline{m}_Q \sum_{k=1}^{\infty} \left[a_k^{\overline{\rm MS}}(n_\ell, 1) \left(\frac{\alpha_s^{(n_\ell+1)}(\overline{m}_Q)}{4\pi}\right)^k - a_k^{\overline{\rm MS}}(n_\ell, 0) \left(\frac{\alpha_s^{(n_\ell)}(\overline{m}_Q)}{4\pi}\right)^k \right] , \tag{2.4}$$

and will be discussed in more detail in section 5.3.

We note that, formally, the natural MSR mass (as well as the practical MSR mass discussed in the next subsection) agrees with the pole mass in the limit $R \to 0$. However, taking this limit is ambiguous as it involves evolving through the Landau pole of the strong coupling and dealing with its non-perturbative definition for $|R| < \Lambda_{\rm QCD}$. This issue is a manifestation of the renormalon problem of the pole mass.

2.3 Practical MSR mass

The *practical MSR mass* definition is directly related to the $\overline{\rm MS}$-pole perturbative series of eq. (2.1). To obtain its defining series one rewrites $\alpha_s^{(n_\ell+1)}(\overline{m}_Q)$ as a series in $\alpha_s^{(n_\ell)}(\overline{m}_Q)$ in eq. (2.1) using the matching relation given in eq. (A.7) and then replaces $\overline{m}_Q$ by R, obtaining

$$m_Q^{\rm pole} - m_Q^{\rm MSRp}(R) = R \sum_{n=1}^{\infty} a_n^{\rm MSRp}(n_\ell) \left(\frac{\alpha_s^{(n_\ell)}(R)}{4\pi}\right)^n , \tag{2.5}$$

JHEP04(2018)003

with

$$
\begin{aligned}
a_1^{\rm MSRp}(n_\ell) &= \frac{16}{3}\,, \\
a_2^{\rm MSRp}(n_\ell) &= 215.094 - 16.6619\,n_\ell\,, \\
a_3^{\rm MSRp}(n_\ell) &= 12185. - 1705.93\,n_\ell + 41.7722\,n_\ell^2\,, \\
a_4^{\rm MSRp}(n_\ell) &= (911932. \pm 418.) - (190794. \pm 10.)\,n_\ell + 11109.4\,n_\ell^2 - 173.604\,n_\ell^3\,.
\end{aligned}
\tag{2.6}
$$

The practical MSR mass still accounts for the virtual corrections from the massive quark Q with an evolving mass R and has the convenient feature that it agrees with the $\overline{\rm MS}$ mass at the scale of the mass to all orders in perturbation theory [$\overline{m}_Q \equiv \overline{m}_Q^{(n_\ell+1)}(\overline{m}_Q^{(n_\ell+1)})$]:

$$
m_Q^{\rm MSRp}(m_Q^{\rm MSRp}) = \overline{m}_Q(\overline{m}_Q)\,. \tag{2.7}
$$

The formula for the difference of the natural and practical MSR masses at the same scale R up to $\mathcal{O}(\alpha_s^4)$ reads

$$
\begin{aligned}
m_Q^{\rm MSRn}(R) - m_Q^{\rm MSRp}(R) = R\,\Bigg[& 1.65707\left(\frac{\alpha_s^{(n_\ell)}(R)}{4\pi}\right)^2 + \big(110.050 + 1.4236\,n_\ell\big)\left(\frac{\alpha_s^{(n_\ell)}(R)}{4\pi}\right)^3 \\
& + \big((344. \pm 31.) - (111.59 \pm 0.10)\,n_\ell + 4.40\,n_\ell^2\big)\left(\frac{\alpha_s^{(n_\ell)}(R)}{4\pi}\right)^4 + \ldots\Bigg]\,.
\end{aligned}
\tag{2.8}
$$

In figure 1 the difference between the natural and the practical MSR top quark masses $m_t^{\rm MSRn}(R) - m_t^{\rm MSRp}(R)$ is shown for R between 1 and 170 GeV (here $n_\ell = 5$).[2] The numerical difference between these two masses is quite small. The natural MSR mass is larger than the practical MSR mass and the difference increases with R reaching about 30 MeV at $R = 170$ GeV. The error bands reflect variations of the renormalization scale μ in α_s between $R/2$ and $2R$, showing very good convergence, exhibiting a perturbative error of ± 5 MeV for $R \sim 1$ GeV and below ± 1 MeV for $R \gtrsim 3$ GeV due to missing terms of $\mathcal{O}(\alpha_s^5)$ and higher. This indicates that the different way how the natural and practical MSR masses treat the virtual massive quark effects does not reintroduce any infrared sensitivity, as is expected since the mass of the virtual quark provides an infrared cutoff. The numerical uncertainties in the $\mathcal{O}(\alpha_s^4)$ correction are below the level of 0.1 MeV and negligible. Note that the difference between the natural and the practical MSR masses at the common scale R starts at $\mathcal{O}(\alpha_s^2)$ and that the uncertainty band from scale variation is an underestimate at this lowest order. However, the series results and error bands at $\mathcal{O}(\alpha_s^{3,4})$ show good behavior and convergence. In ref. [38] the practical MSR mass was employed, but the numerical difference to the natural MSR mass is subdominant to the uncertainties obtained in the analysis there.

In the rest of the paper we will simply use the notation of the MSR mass with the definition $m_Q^{\rm pole} - m_Q^{\rm MSR}(R) = R\sum_n a_n\big[\alpha_s(R)/(4\pi)\big]^n$ when the difference between the natural and practical definitions and the value of n_ℓ are insignificant but we will specify explicitly our use of the practical or the natural MSR masses (or any other mass scheme) and the massless flavor number n_ℓ for any numerical analysis.

[2] Throughout this article we use $\alpha_s^{(n_f=5)}(m_Z) = 0.118$ and $m_Z = 91.187$ GeV.

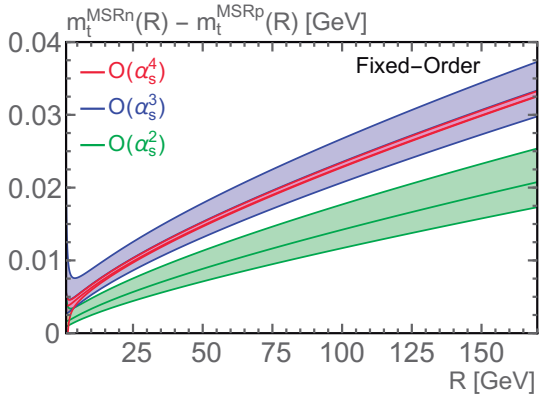

Figure 1. Difference of the natural and practical MSR top quark masses ($n_\ell = 5$) as a function of R in GeV at two, three and four loop order (the one loop result vanishes). The uncertainty bands are obtained from scale variations in $\alpha_s(\mu)$ with $R/2 < \mu < 2R$.

3 R-evolution

The dependence of the MSR mass $m_Q^{\rm MSR}$ on the scale R is described by the R-evolution equation [47], which is derived from the logarithmic derivative of the defining equations (2.3) and (2.5) and using that the pole mass is R independent:

$$R\frac{\rm d}{{\rm d}R}m_Q^{\rm MSR}(R) = -\,R\,\gamma^R(\alpha_s(R)) = -\,R\sum_{n=0}^{\infty}\gamma_n^R\left(\frac{\alpha_s(R)}{4\pi}\right)^{n+1}, \tag{3.1}$$

where

$$\begin{aligned}
\gamma_0^R &= a_1\,,\\
\gamma_1^R &= a_2 - 2\,\beta_0\,a_1\,,\\
\gamma_2^R &= a_3 - 4\,\beta_0\,a_2 - 2\,\beta_1\,a_1\,,\\
\gamma_n^R &= a_{n+1} - 2\sum_{j=0}^{n-1}(n-j)\,\beta_j\,a_{n-j}\,.
\end{aligned} \tag{3.2}$$

The overall minus sign on the r.h.s. of eq. (3.1) indicates that the MSR mass always decreases with R. Note that this equation applies to all MSR schemes and we have therefore suppressed the superscript on the a_n's. The crucial feature of the R-evolution equation is that it is free from the $\mathcal{O}(\Lambda_{\rm QCD})$ ambiguity contained in the series that relates the MSR mass to the pole mass because the ambiguity is R-independent. This is directly related to the fact that for determining the R-evolution equation also the overall linear factor of R on the r.h.s. of eqs. (2.3) and (2.5) has to be accounted for. Therefore the R-evolution equation does not only have a logarithmic dependence on R, as common to usual renormalization group equations (RGEs), but also a linear one. Both of these issues are actually tied together conceptually. The numerical expressions for the coefficients γ_n for the natural and practical MSR masses are given explicitly in eqs. (A.11) and (A.12). We implement

renormalization scale variation in the R-evolution equation by simply expanding $\alpha_s(R)$ in eq. (3.1) as a series in $\alpha_s(\lambda R)$ and by varying λ, typically in the range $0.5 < \lambda < 2$. In principle one may also consider varying the boundaries of integration, as it is common for usual RGEs, but only the former way of implementing scale variations in the R-evolution leads to variations of the scale solely in logarithms, which is the standard used for the usual logarithmic RGEs.

By solving the R-evolution equation one sums, at the same time and systematically, the asymptotic renormalon series as well as the large logarithmic terms in $m_Q^{\rm MSR}(R_0) - m_Q^{\rm MSR}(R_1)$ to all orders in a manner free from the $\mathcal{O}(\Lambda_{\rm QCD})$ renormalon:

$$m_Q^{\rm MSR}(R_0) - m_Q^{\rm MSR}(R_1) = -\sum_{n=0}^{\infty} \gamma_n^R \int_{R_1}^{R_0} {\rm d}R \left(\frac{\alpha_s(R)}{4\pi}\right)^{n+1} . \tag{3.3}$$

It is straightforward to solve the R-evolution equation numerically and it shows very good perturbative stability even for low values of R very close to the Landau pole [58] in the perturbative strong coupling. Details of how to solve the R-evolution equations analytically have already been given in [47] and shall not be repeated here.

It is instructive to briefly discuss what the solution of the R-evolution achieves by considering the difference of the MSR mass, $m_Q^{\rm MSR}(R_0) - m_Q^{\rm MSR}(R_1)$, in the context of fixed-order perturbation theory (FOPT), where it is well-known that the renormalon ambiguity contained in the series for $m_Q^{\rm pole} - m_Q^{\rm MSR}(R_0)$ and the series for $m_Q^{\rm pole} - m_Q^{\rm MSR}(R_1)$ only cancel if one expands in α_s with a common renormalization scale μ. This is nicely illustrated in the β_0/LL (leading log) approximation where the pole-MSR mass relation has the all order form

$$\begin{aligned}\left[m_Q^{\rm pole} - m_Q^{\rm MSR}(R)\right]_{\beta_0/{\rm LL}} &= \frac{a_1}{2\beta_0} R \sum_{n=0}^{\infty} \left(\frac{\beta_0\alpha_s(R)}{2\pi}\right)^{n+1} n! \\ &= \frac{a_1}{2\beta_0} R \sum_{n=0}^{\infty} \left(\frac{\beta_0\alpha_s(\mu)}{2\pi}\right)^{n+1} n! \sum_{k=0}^{n} \frac{1}{k!} \log^k \frac{\mu}{R} .\end{aligned} \tag{3.4}$$

The series by itself is divergent and not summable, but

$$\begin{aligned}&\left[m_Q^{\rm MSR}(R_0) - m_Q^{\rm MSR}(R_1)\right]_{\beta_0/{\rm LL}} = \\ &\quad = \frac{a_1}{2\beta_0} \sum_{n=0}^{\infty} \left(\frac{\beta_0\alpha_s(\mu)}{2\pi}\right)^{n+1} n! \left(R_1 \sum_{k=0}^{n} \frac{1}{k!} \log^k \frac{\mu}{R_1} - R_0 \sum_{k=0}^{n} \frac{1}{k!} \log^k \frac{\mu}{R_0}\right) \\ &\quad = \frac{a_1}{2\beta_0} \sum_{n=0}^{\infty} \left(\frac{\beta_0\alpha_s(R_1)}{2\pi}\right)^{n+1} n! \left(R_1 - R_0 \sum_{k=0}^{n} \frac{1}{k!} \log^k \frac{R_1}{R_0}\right),\end{aligned} \tag{3.5}$$

is easily seen to be convergent. In the context of FOPT, when the sum over n is truncated, the unavoidable appearance of large logarithms $\log(R_0/R_1)$ for let's say $R_0 \ll R_1$ may degrade the convergence and cause sizable perturbative uncertainties. Due to the additional linear dependence on R_0 and R_1, as shown in eq. (3.5), these logarithms cannot be summed by common logarithmic renormalization group (RG) equations. The same type of logarithms also appear for example in the relation of any other low-scale short-distance

mass to the $\overline{\rm MS}$ mass and their effects can be significant particularly for the top quark. By solving the R-evolution equation one sums, at the same time and systematically, the asymptotic terms in the renormalon series as well as the large logarithmic terms in $m_Q^{\rm MSR}(R_0) - m_Q^{\rm MSR}(R_1)$ to all orders in a manner free from the $\mathcal{O}(\Lambda_{\rm QCD})$ renormalon. It is again instructive to see how this is achieved in the β_0/LL approximation of eq. (3.4), which explicitly shows the factorial growth of the perturbative series. When calculating the derivative to get the R-evolution equation, the whole series collapses exactly (i.e. without any truncation!) to

$$\left[R\frac{\mathrm{d}}{\mathrm{d}R}m_Q^{\rm MSR}(R)\right]_{\beta_0/\rm LL} = -a_1\,R\left(\frac{\alpha_s(R)}{4\pi}\right), \tag{3.6}$$

which is the one-loop version of eq. (3.1). Moreover, the exact solution of the R-evolution equation at this order

$$\left[m_Q^{\rm MSR}(R_0) - m_Q^{\rm MSR}(R_1)\right]_{\beta_0/\rm LL} = -\,a_1\int_{R_1}^{R_0}\mathrm{d}R\left(\frac{\alpha_s(R)}{4\pi}\right), \tag{3.7}$$

can be easily seen to be exactly equal to the r.h.s. of eq. (3.5) which sums the renormalon series and the large logarithms at the same time into a convergent series.

Conceptually, the solution of the R-evolution equation is directly related to the Borel space integral over the Borel transform for the series for $m_Q^{\rm MSR}(R_0) - m_Q^{\rm MSR}(R_1)$. Since this has not been shown in [47] we briefly outline this calculation here at the β_0/LL level. Starting from eq. (3.7) one can shuffle the integration over R into an integral over $\alpha_s(R)$ by using the QCD β-function and the relation $\Lambda_{\rm QCD}^{\rm LL} = R\exp\left(-2\pi/\beta_0\alpha_s(R)\right)$. Using the variable $t = -2\pi/(\beta_0\alpha_s(R))$ one can then rewrite the integral as $[t_i = -2\pi/(\beta_0\alpha_s(R_i))]$

$$\begin{aligned}\left[m_Q^{\rm MSR}(R_0) - m_Q^{\rm MSR}(R_1)\right]_{\beta_0/\rm LL} &= -\frac{a_1}{2\beta_0}\Lambda_{\rm QCD}^{\rm LL}\int_{t_1}^{t_0}\frac{\mathrm{d}t}{t}\,\mathrm{e}^{-t} \\ &= -\frac{a_1}{2\beta_0}\Lambda_{\rm QCD}^{\rm LL}\left[\int_{t_1}^{\infty}\frac{\mathrm{d}t}{t}\,\mathrm{e}^{-t} - \int_{t_0}^{\infty}\frac{\mathrm{d}t}{t}\,\mathrm{e}^{-t}\right],\end{aligned} \tag{3.8}$$

where the two integrals in the last line are just the difference of the MSR masses at $R_{0,1}$ to the pole mass, and the pole mass ambiguity is encoded in the singularity at $t = 0$, which arises because $t_{0,1} < 0$,

$$\left[m_Q^{\rm MSR}(R_i) - m_Q^{\rm pole}\right]_{\beta_0/\rm LL} = \frac{a_1}{2\beta_0}\Lambda_{\rm QCD}^{\rm LL}\int_{t_i}^{\infty}\frac{\mathrm{d}t}{t}\,\mathrm{e}^{-t}\,. \tag{3.9}$$

Upon changing variables to the Borel plane parameter $u = -(t/t_i - 1)/2$ and writing $\Lambda_{\rm QCD}$ in terms of R_i and $\alpha_s(R_i)$ in both integrals, this gives

$$\left[m_Q^{\rm MSR}(R_0) - m_Q^{\rm MSR}(R_1)\right]_{\beta_0/\rm LL} = \int_0^{\infty}\mathrm{d}u\,\left[B(R_0,\mu,u) - B(R_1,\mu,u)\right]\mathrm{e}^{-\frac{4\pi u}{\beta_0\alpha_s(\mu)}}\,. \tag{3.10}$$

Here

$$B(R,\mu,u) = \frac{a_1}{2\beta_0}\,R\left(\frac{\mu}{R}\right)^{2u}\frac{1}{u-\frac{1}{2}}\,, \tag{3.11}$$

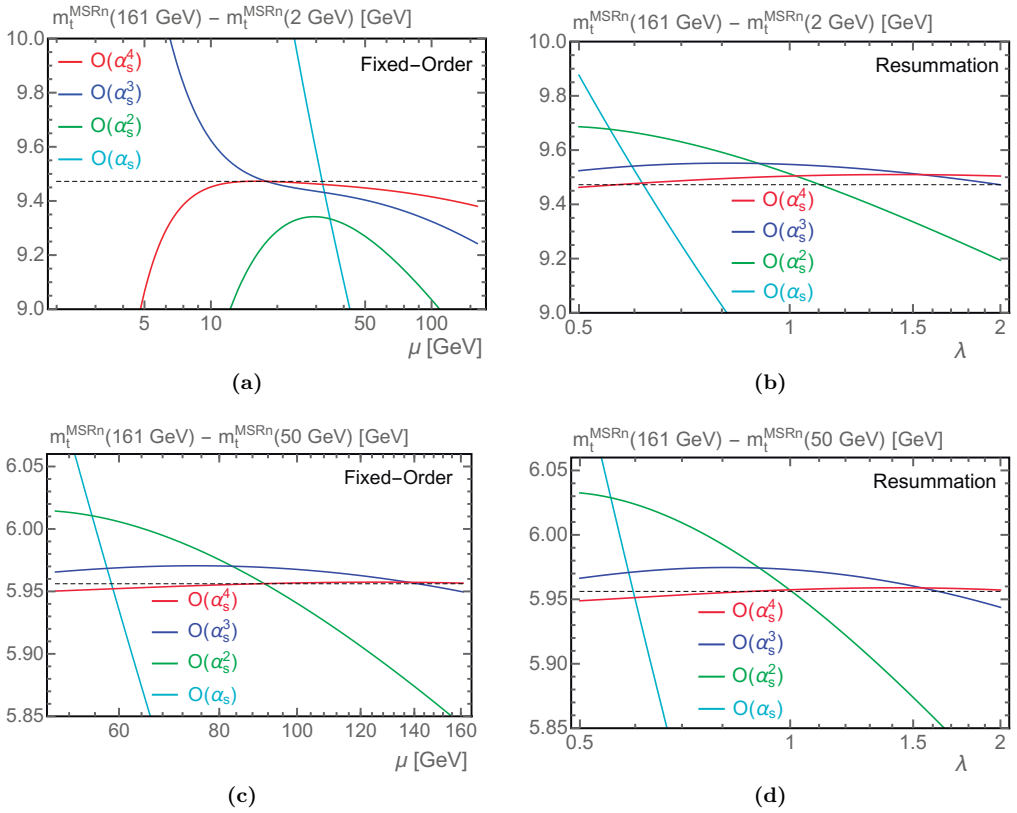

Figure 2. Difference of the natural top quark MSR mass ($n_\ell = 5$) at two different scales R including contributions from one to four loops. Results are shown for the difference between a high scale $R_1 = 161\,\text{GeV}$ and two lower scales $R_2 = 2\,\text{GeV}$ (top two panels) and $R_2 = 50\,\text{GeV}$ (lower two panels). The high and low scales are connected by a fixed-order perturbation theory conversion [left two panels, as a function of the scale μ in $\alpha_s(\mu)$] or via R-evolution [right two panels, as a function of the λ renormalization parameter].

is the well-known Borel transform with respect to $\alpha_s(\mu)$ of the β_0/LL series in eq. (3.4). In eq. (3.10) the singular and non-analytic contributions contained in the individual Borel functions cancel and the integral becomes ambiguity-free.

To illustrate the impact of using R-evolution compared to using FOPT we show in figure 2 the difference of natural MSR masses $\Delta m_t^{\text{MSRn}}(R_0, R_1) \equiv m_t^{\text{MSRn}}(R_0) - m_t^{\text{MSRn}}(R_1)$ for $n_\ell = 5$ in fixed-order perturbation theory (FOPT) and with R-evolution. The curves in figure 2a show Δm_t^{MSRn} for $(R_0, R_1) = (2, 161)\,\text{GeV}$ in FOPT for the common renormalization scale μ between R_0 and R_1 at 1 loop (cyan), 2 loop (green), 3 loop (blue) and 4 loops (red). We see a good convergence for μ around $\sqrt{R_0 R_1}$, but a deterioration of the series when μ gets closer to either R_0 or R_1. For $\mu \lesssim 1/2\sqrt{R_0 R_1}$ the series even gets out of bounds and breaks down completely. If one uses scale variation as an estimate of the remaining perturbative error, one therefore obtains a significant dependence on the

JHEP04(2018)003

choice of the lower bound of the variation, and one has no other choice than to abandon in an ad hoc manner scales closer to R_0 to estimate the scale variation error. The curves in figure 2b show $\Delta m_t^{\rm MSRn}$ for $(R_0, R_1) = (2, 161)\,\text{GeV}$ from numerically solving the R-evolution equation as a function of the renormalization scale parameter λ between 0.5 and 2. The color coding for the order of the R-evolution equation used for the evaluation is the same as for figure 2a. As explained below eq. (3.1), the parameter λ is the renormalization scaling parameter in the R-evolution equation which determines by how much the scale in α_s differs from the scale R. Thus a variation between 0.5 and 2 means that in the solution of the R-evolution equations scales between $R/2$ and $2R$ are covered at each value of R along the evolution, which in this case includes scales between 1 and 322 GeV. Comparing the curves in figure 2a and 2b we see that the renormalization scale variation in the R-evolved results is much smaller than the one of FOPT. For the FOPT result with scale variation between $\sqrt{R_0 R_1}/2$ — which we pick by hand — and R_1 we obtain $\Delta m_t = (9.838 \pm 2.504,\, 8.981 \pm 0.361,\, 9.465 \pm 0.222,\, 9.427 \pm 0.047)\,\text{GeV}$ at $(1, 2, 3, 4)$ loops. Using R-evolution with λ variation between 0.5 and 2 we obtain $\Delta m_t = (8.817 \pm 1.059,\, 9.440 \pm 0.246,\, 9.512 \pm 0.040,\, 9.486 \pm 0.025)\,\text{GeV}$ which is fully compatible with the FOPT result, but shows more stability and smaller errors. It is also quite instructive to see that using R-evolution the 3-loop result is significantly closer to the 4-loop result than the corresponding 3-loop FOPT result. The results show that for $R_0 \ll R_1$ employing R-evolution to calculate MSR mass differences is clearly superior to FO perturbation theory.

To compare to a situation where the scales R_0 and R_1 are of similar size we have also shown in figures 2c and 2d the results for Δm_t in FOPT and from R-evolution for $(R_0, R_1) = (50, 161)\,\text{GeV}$. Here the results from both approaches are completely equivalent showing that the logarithm $\log(R_0/R_1)$ is not large and the summation of the renormalon contributions from higher orders only constitutes very small effects. Furthermore using renormalization scales close to R_0 or R_1 in FOPT is not problematic. Numerically, using FOPT with scale variations between R_0 and R_1 we obtain $\Delta m_t = (5.618 \pm 0.498,\, 5.928 \pm 0.086,\, 5.961 \pm 0.010,\, 5.954 \pm 0.004)\,\text{GeV}$ at $(1, 2, 3, 4)$ loops, while using R-evolution with λ variations between 0.5 and 2 we obtain $\Delta m_t = (5.555 \pm 0.577,\, 5.919 \pm 0.114,\, 5.959 \pm 0.015,\, 5.954 \pm 0.005)\,\text{GeV}$. We find that FOPT and R-evolution give equivalent results even for $(R_0, R_1) = (20, 161)\,\text{GeV}$, and that the use of R-evolution is essential for $R_0/R_1 < 0.1$. Overall we see that, if R_0 and R_1 are of similar size, FO perturbation theory and R-evolution lead to equivalent results, but that it is in general safer to use R-evolution. So the situation is very similar to the one we encounter when considering the relation of the strong coupling for two different renormalization scales.

We note that the possibility to sum the renormalon-type logarithms displayed in eq. (3.5) by considering the Borel integral over the difference of Borel transforms as shown in eq. (3.10) was pointed out already in ref. [66] prior to ref. [47]. However, this exact equivalence [via a transformation of variables as given below eq. (3.9)] of R-evolution and the method using the integration over Borel transform differences can only be analytically shown at the β_0/LL approximation. Beyond that, both approaches sum up the same type of logarithms but differ in subleading terms. Numerically, both approaches converge to the same result and have comparable order-by-order convergence. From a practical point of

JHEP04(2018)003

view, however, the concept of R-evolution may be considered more general. This is because R-evolution can be applied directly to any series having the form of (2.3) or (2.5) while using the Borel integration method requires that the corresponding Borel transforms are known or constructed beforehand. For general series, such as for the difference of MSR masses as discussed above, this is not possible without making additional approximations. In practice, the approach of ref. [66] to sum the renormalon-type logarithms has therefore only been applied for series (referred to as RS-schemes) which were explicitly derived from a given expression for the Borel transform.

4 Analytic Borel transform and renormalon sum rule

Using the solution of the R-evolution equation it is possible to derive, analytically and rigorously, an expression for the Borel transform of the MSR-pole mass relation. This Borel transform is designed to focus on the singular contributions that quantify the $\mathcal{O}(\Lambda_{\rm QCD})$ renormalon of the pole mass. This result was already quoted in the letter [47] where, however, no details on the derivation could be given due to lack of space. In the following we provide these details on how to obtain the analytic result for the normalization of the singular terms. The analytic results for the normalization can be applied to other perturbative series as a probe of $\mathcal{O}(\Lambda_{\rm QCD})$ renormalon ambiguities, and we therefore call it *the* $\mathcal{O}(\Lambda_{\rm QCD})$ *renormalon sum rule*. This sum rule was first given in ref. [47], and is very sensitive to even subtle effects if $\mathcal{O}(\alpha_s^4)$ corrections are known. We apply the sum rule to obtain an updated determination of the size of the pole mass $\mathcal{O}(\Lambda_{\rm QCD})$ ambiguity, accounting for the $\mathcal{O}(\alpha_s^4)$ results of refs. [54, 55] which became available recently but were unknown when ref. [47] appeared. To demonstrate the sum rule's capabilities to probe $\mathcal{O}(\Lambda_{\rm QCD})$ renormalon ambiguities in perturbative series and to clarify subtleties in how to use it properly, we also apply it to a few other cases. Interestingly, the analytic manipulations arising in the derivation of the sum rule lead to an alternative expression for the high-order asymptotic behavior of a series that contains an $\mathcal{O}(\Lambda_{\rm QCD})$ renormalon. This expression differs from the well known asymptotic formula which is known since a long time from [77], and we therefore discuss it as well.

4.1 Derivation

The analytic derivation for the Borel transform of the MSR-pole mass relation starts from its expression related to the solution of the R-evolution equation given in eq. (3.1) which was already derived in ref. [47].

$$\begin{aligned} m_Q^{\rm MSR}(R) - m_Q^{\rm pole} &= -\int_0^R {\rm d}\bar{R}\,\gamma^R(\alpha_s(\bar{R})) \\ &= -\,\Lambda_{\rm QCD}\int_{t_R}^\infty {\rm d}t\,\gamma^R(t)\,\hat{b}(t)\,{\rm e}^{-G(t)} \\ &= \Lambda_{\rm QCD}\sum_{k=0}^\infty {\rm e}^{i\pi(\hat{b}_1+k)} S_k \int_{t_R}^\infty {\rm d}t\, t^{-1-k-\hat{b}_1}{\rm e}^{-t} \\ &= \Lambda_{\rm QCD}\sum_{k=0}^\infty {\rm e}^{i\pi(\hat{b}_1+k)}\, S_k\,\Gamma(-\hat{b}_1-k, t_R)\,, \end{aligned} \tag{4.1}$$

where in the second line we changed variable to $t = -2\pi/(\beta_0\alpha_s(\bar{R}))$ and used the identity (A.6) to scale out $\Lambda_{\rm QCD}$, and in the third line we employed the coefficients given in eq. (A.15). The expression in eq. (4.1) gives an all-order representation of the original series that is more useful for analyzing $\mathcal{O}(\Lambda_{\rm QCD})$ renormalon issues than eqs. (2.3) and (2.5). This is because using the R-evolution equation of eq. (3.1) (which is linear in R) and its solution, provides, through the sum in k, a reordering of the original series in leading and subleading series of terms from the perspective of their numerical importance in the asymptotic high order behavior related to the $\mathcal{O}(\Lambda_{\rm QCD})$ renormalon. This allows to derive rigorously a representation of the Borel transform [given in eq. (4.7)] reflecting efficiently the hierarchy of leading and subleading terms with respect to the $\mathcal{O}(\Lambda_{\rm QCD})$ renormalon, which is the information that is not contained in the original series. That such a separation is possible in a systematic way may not be obvious, but it is achieved by the R-evolution equation. We stress that the result of eq. (4.7) should not be considered as the exact expression for the Borel transform because it does not encode information on possible poles (or non-analytic cuts) other than at $u = 1/2$. We note that these poles and the associated renormalons can be studied by considering solutions of R-evolution equations involving powers of R different from the linear dependence shown in eq. (3.1), see [78].

We note that the expression in the last line of eq. (4.1), which involves the incomplete gamma function $\Gamma(c,t) = \int_t^\infty \mathrm{d}x\, x^{c-1}e^{-x}$, also arises in the analytic solution of the mass difference (3.3),

$$m_Q^{\rm MSR}(R_0) - m_Q^{\rm MSR}(R_1) = \Lambda_{\rm QCD} \sum_{k=0}^{\infty} \mathrm{e}^{i\pi(\hat{b}_1+k)}\, S_k \left[\Gamma(-\hat{b}_1-k,t_0) - \Gamma(-\hat{b}_1-k,t_1)\right]. \quad (4.2)$$

Here the cut in the gamma functions $\Gamma(c,t)$ for $t<0$ cancels in the difference for each k in the sum, and the result on the r.h.s. is real. We mention that the first term ($k=0$) in the sum over k provides the summation of the leading terms in the β_0/LL approximation shown in eqs. (3.5) and (3.7). In eq. (4.1) the cut still remains and arises from the integration of the Landau pole in the strong coupling located at $t=0$ in the integral in the next-to-last line. The resulting imaginary part in the numerical expression corresponds to the imaginary part that arises in the inverse Borel integral for $m_Q^{\rm MSR}(R) - m_Q^{\rm pole}$, see eq. (3.10), and simply reflects the ambiguity of the pole mass. From the point of view of the analytic solution of eq. (4.1) based on a perturbative expansion, the imaginary part is well-defined and analytically unique.

To proceed we asymptotically expand the incomplete gamma function in inverse powers of t (i.e. powers of α_s)

$$\begin{aligned}\Lambda_{\rm QCD}\mathrm{e}^{i\pi(\hat{b}_1+k)}\Gamma(-\hat{b}_1-k,t) &= -R\left[\mathrm{e}^{G(t)}\mathrm{e}^{-t}(-t)^{-\hat{b}_1}\right]\sum_{m=0}^{\infty}\frac{\Gamma(1+\hat{b}_1+k+m)}{\Gamma(1+\hat{b}_1+k)}\,(-t)^{-1-k-m}\\ &= -R\sum_{\ell=0}^{\infty} g_\ell \sum_{m=0}^{\infty}\frac{\Gamma(1+\hat{b}_1+k+m)}{\Gamma(1+\hat{b}_1+k)}\,(-t)^{-1-\ell-k-m}\,, \end{aligned} \quad (4.3)$$

where the coefficients g_ℓ are given in eq. (A.13), and coincide with the s_k coefficients defined in ref. [77]. We stress that the equality in eq. (4.3) is the asymptotic expansion and is not

JHEP04(2018)003

an identity, so that the imaginary part due to the cut in the incomplete gamma function does not arise on the r.h.s.. Inserting eq. (4.3) in eq. (4.1) gives

$$m_Q^{\rm MSR}(R) - m_Q^{\rm pole} = -R \sum_{k=0}^{\infty} S_k \sum_{\ell=0}^{\infty} g_\ell \sum_{m=0}^{\infty} \frac{\Gamma(1+\hat{b}_1+k+m)}{\Gamma(1+\hat{b}_1+k)} (-t)^{-1-\ell-k-m} . \tag{4.4}$$

We then perform the Borel transform with respect to powers of $\alpha_s(R)$ according to the rule $(-t)^{-1-n} \to 2\,(2u)^n/\Gamma(n+1)$ giving

$$\begin{aligned} B_{\alpha_s(R)}\Big[m_Q^{\rm MSR}(R) - m_Q^{\rm pole}\Big](u) = & \\ = & -2R \sum_{\ell=0}^{\infty} g_\ell \sum_{k=0}^{\infty} S_k \sum_{m=0}^{\infty} \frac{\Gamma(1+\hat{b}_1+k+m)}{\Gamma(1+\hat{b}_1+k)\Gamma(1+k+\ell+m)} (2u)^{\ell+k+m} \\ = & -2R \sum_{\ell=0}^{\infty} g_\ell \sum_{k=0}^{\infty} S_k \frac{(2u)^{\ell+k}}{\Gamma(1+k+\ell)}\, {}_2F_1(1, 1+\hat{b}_1+k, 1+k+\ell, 2u) . \end{aligned} \tag{4.5}$$

Using identities for the hypergeometric function we can rewrite

$$\begin{aligned} \frac{(2u)^{\ell+k}}{\Gamma(1+k+\ell)}\, {}_2F_1(1,1+\hat{b}_1+k,1+k+\ell,2u) = & \frac{\Gamma(1+\hat{b}_1-\ell)}{\Gamma(1+\hat{b}_1+k)} (1-2u)^{-1-\hat{b}_1+\ell} \\ & - \frac{1}{(1+\hat{b}_1-\ell)\Gamma(k+\ell)}\, {}_2F_1(1+\hat{b}_1-\ell, 1-k-\ell, 2+\hat{b}_1-\ell, 1-2u) , \end{aligned} \tag{4.6}$$

and the Borel transform can then be cast into the form [47]

$$\begin{aligned} B_{\alpha_s(R)}\left[m_Q^{\rm MSR}(R) - m_Q^{\rm pole}\right](u) = & -N_{1/2}\left[R\,\frac{4\pi}{\beta_0} \sum_{\ell=0}^{\infty} g_\ell \frac{\Gamma(1+\hat{b}_1-\ell)}{\Gamma(1+\hat{b}_1)} (1-2u)^{-1-\hat{b}_1+\ell}\right] \\ & + 2R \sum_{\ell=0}^{\infty} g_\ell\, Q_\ell(u) , \end{aligned} \tag{4.7}$$

where

$$\begin{aligned} N_{1/2} &= \frac{\beta_0\,\Gamma(1+\hat{b}_1)}{2\pi}\, P_{1/2} , \\ P_{1/2} &= \sum_{k=0}^{\infty} \frac{S_k}{\Gamma(1+\hat{b}_1+k)} , \end{aligned} \tag{4.8}$$

and $N_{1/2}$ and $P_{1/2}$ are two conventions for the normalization. Here

$$\begin{aligned} Q_\ell(u) &= \sum_{k=0}^{\infty} \frac{S_k\,(2u)^{k+\ell}}{(1+\hat{b}_1-\ell)\,\Gamma(k+\ell)}\, {}_2F_1(1, 1+\hat{b}_1+k, 2+\hat{b}_1-\ell, 1-2u) \\ &= \sum_{k=0}^{\infty} S_k \sum_{i=0}^{k+\ell-1} \frac{2^i\,\Gamma(1+\hat{b}_1+i-\ell)}{\Gamma(1+\hat{b}_1+k)\,\Gamma(i+1)}\, u^i . \end{aligned} \tag{4.9}$$

Setting $u = 1/2$ in eq. (4.9) one gets $Q_\ell(1/2) = 1/(1+\hat{b}_1-\ell)\sum_{k=0}^{\infty} S_k/\Gamma(k+\ell)$. Since the S_k coefficients are renormalon-free and further damped by the factorial in the denominator, this sum is finite. Furthermore, the sum on the second line of eq. (4.7) is also

finite for $u = 1/2$. Therefore one concludes that the sum of Q_ℓ coefficients is regular at $u = 1/2$, implying that the first line of eq. (4.7) fully contains the leading-renormalon singular behavior. In ref. [47] the expression for the Borel transform in eq. (4.7) was given using $P_{1/2}$, but here we have shown an alternate convention with $N_{1/2}$ which agrees with the terms N_m and N discussed in refs. [8, 70], and hence eases comparison of our numerical results with theirs. For the phenomenological relevant values $n_\ell = (3, 4, 5)$ we have $N_{1/2}/P_{1/2} = (1.27, 1.18, 1.09)$. The analytic difference between these normalizations is that $P_{1/2}$ vanishes in the limit $n_\ell \to -\infty$ while $N_{1/2}$ is finite in this limit. We will predominantly use $N_{1/2}$ for the numerical examinations in the following subsections.

The manipulations that lead to the expressions for $P_{1/2}$ and $N_{1/2}$ involve the rearrangement of the infinite sums over ℓ and k in eq. (4.5). These can be seen to be identities if one assumes that the QCD β-function and its inverse have some region of convergence. In practice, because only the first few terms in perturbation theory are known and one truncates the sums over ℓ and k, no formal convergence issue arises. We note that the analytic manipulations involving the R-evolution equation and the derivation of eq. (4.7) are also valid in schemes for the strong coupling other than $\overline{\rm MS}$, and to apply them to such schemes one simply needs to account for the perturbative rearrangement for the coefficients a_n and the QCD β-function due to the scheme change. As an example, all manipulations and the results simplify considerably in a strong coupling scheme $\bar{\alpha}$ where the coefficients $\hat{b}_n$ vanish for $n > 1$ and which also implies $g_\ell = 0$ for $\ell > 0$ and that the coefficients of the QCD β-function have the exact form $\beta_n = \beta_0(\beta_1/\beta_0)^n$. Since such a scheme change can be achieved via a relation of the form $\alpha_s(\mu) = \bar{\alpha}(\mu) + [\beta_2/\beta_0 - (\beta_1/\beta_0)^2]\,\bar{\alpha}^3(\mu) + \ldots$, which does not contain any $\mathcal{O}(\bar{\alpha}_s^2)$ term, the overall normalization of $N_{1/2}$ (or $P_{1/2}$) remains unchanged [73]. In this scheme we have $S_{k>0} = \tilde{\gamma}_k^R - \hat{b}_1\tilde{\gamma}_{k-1}^R$, and eq. (4.8) can be rewritten in the equivalent form $N_{1/2} = (\beta_0/2\pi)\Gamma(1+\hat{b}_1)\sum_{k=0}^\infty \tilde{\gamma}_k^R(1+k)/\Gamma(2+\hat{b}_1+k)$ and was derived recently in ref. [79]. There is, however, no advantage in using this form, because the coefficients $\tilde{\gamma}_k^R$ in the $\bar{\alpha}$ scheme still have to account for the reordering of the series due to the scheme change from α_s to $\bar{\alpha}$. Other schemes, such as the 't Hooft scheme, where all coefficients of the QCD β-function beyond β_0 and β_1 vanish, have been studied in ref. [78].

We discuss the structure of the non-analytic terms multiplied by $N_{1/2}$ in eq. (4.7) in section 4.4 below. The second term in eq. (4.7) is purely polynomial and represents contributions in the Borel transform $B(u)$ that account for the portions in the original series of eqs. (2.3) and (2.5) that go beyond the pure $\mathcal{O}(\Lambda_{\rm QCD})$ renormalon corrections that numerically dominate the series. These terms may include renormalon contributions of a different kind [such as $\mathcal{O}(\Lambda_{\rm QCD})^{k>1}$], which are however not probed by an R-evolution equation that is linear in R [58]. Moreover, they account for the difference of the pure $\mathcal{O}(\Lambda_{\rm QCD})$ renormalon asymptotic form of the series (encoded in the value of $N_{1/2}$) and the actual coefficients of the original series given in eqs. (2.3) and (2.5). The latter are recovered in the asymptotic limit were the sums over k and ℓ are carried out up to infinity. Note that in practice, for a finite order determination of the Borel transform for a given value of $N_{1/2}$ or $P_{1/2}$, one truncates the sum over k and ℓ in eq. (4.9), and in this case the terms coming from the Q_ℓ represent finite polynomials. For the construction of a Borel transform that reproduces the known coefficients exactly, it may then be more suitable to simply fit

JHEP04(2018)003

the coefficients of the remaining polynomial terms such that the known coefficients in the original series are reproduced exactly.

4.2 Renormalon sum rule

The analytic expression for $N_{1/2}$ is quite useful as it can be applied to any perturbative series as a probe for $\mathcal{O}(\Lambda_{\rm QCD})$ renormalons, given the information on the available coefficients of a perturbative series. We therefore call the formula for $N_{1/2}$ (or equivalently $P_{1/2}$) in eq. (4.8) *the* $\mathcal{O}(\Lambda_{\rm QCD})$ *renormalon sum rule* [47]. Formally to any given order in k, $N_{1/2}$ is a linear functional acting on perturbative series in powers of α_s since the coefficients S_k in eq. (4.8) are linear in the coefficients a_n of the perturbative series, see eq. (A.15). So given two series defined by the sequence $\{c_n\} = (c_1, c_2, \dots)$ and $\{d_n\} = (d_1, d_2, \dots)$, where c_n/d_n are the coefficients of order $[\alpha_s/(4\pi)]^n$ in the series, one has

$$N_{1/2}[\{\alpha\, c_n + \beta\, d_n\}] = \alpha\, N_{1/2}[\{c_n\}] + \beta\, N_{1/2}[\{d_n\}]\,. \tag{4.10}$$

As a word of caution, we emphasize that applying the $N_{1/2}$ sum rule to a truncated series does (like any other type of renormalon calculus in the context of perturbative QCD) not rigorously and mathematically prove or disprove the existence of an $\mathcal{O}(\Lambda_{\rm QCD})$ renormalon, since the existence of renormalons is by definition related to the asymptotic high-order behavior and mathematically strict proofs, if they exist, are related to elaborate all-order studies of Feynman diagrams. So using the sum rule should be better thought of as an analytic projection of the known terms of a perturbative series onto the known pattern of a pure $\mathcal{O}(\Lambda_{\rm QCD})$ renormalon series, which is generated from the singular terms in the Borel transform in eq. (4.7) that are multiplied by $N_{1/2}$ or $P_{1/2}$ and known to all orders. This projection becomes more accurate the more terms of a series are known and mathematically converges (only) if the yet unknown high order terms keep following the renormalon pattern expected from the low order terms.[3]

Although the series in k for $N_{1/2}$ in eq. (4.8) is not ordered in powers of the strong coupling, it is possible to implement renormalization scale variation by rescaling $R \to \lambda R$ in the original series of eqs. (2.3) and (2.5) and subsequently expanding again in $\alpha_s(R)$. This leads to

$$\begin{aligned}
S_0' &= \lambda\, S_0\,,\\
S_1' &= \lambda\big[S_1 - S_0 \log\lambda\big],\\
S_2' &= \lambda\big[S_2 - 2\,S_1 \log\lambda + S_0\big(\log^2\lambda - (\hat{b}_2 + 2\,\hat{b}_1)\log\lambda\big)\big],\\
S_3' &= \lambda\Big[S_3 - 3\,S_2\log\lambda + S_1\big(3\log^2\lambda - (\hat{b}_2 + 3\,\hat{b}_1)\log\lambda\big)\\
&\qquad + S_0\left(-\log^3\lambda + \left(2\,\hat{b}_2 + \frac{9}{2}\,\hat{b}_1\right)\log^2\lambda + \big(3\,\hat{b}_2 + \hat{b}_3 - \hat{b}_1(\hat{b}_2 + 3\,\hat{b}_1)\big)\log\lambda\right)\Big],
\end{aligned} \tag{4.11}$$

[3] For example, applying the sum rule to a series that follows an $\mathcal{O}(\Lambda_{\rm QCD})$ renormalon pattern up to order m, but then changes to a convergent series beyond, the value of $N_{1/2}$ approaches a finite value up to order m, but then decreases and approaches zero when more terms beyond order m are included. Note however that there is no reason to expect a perturbative series in QCD to behave in such a manner.

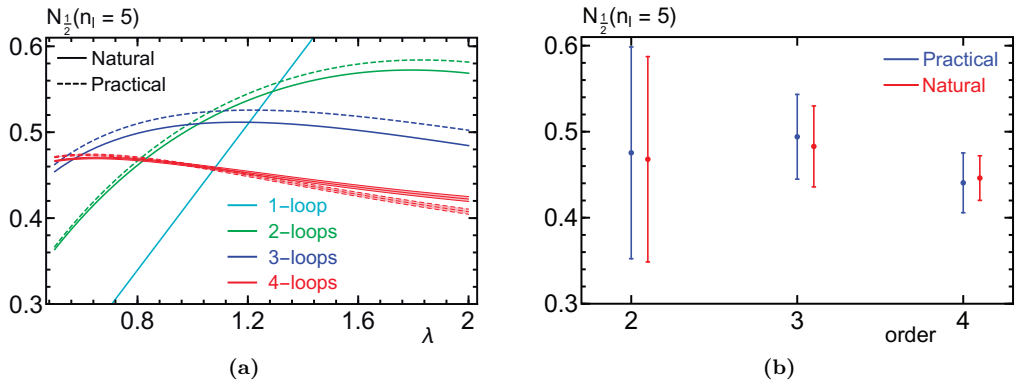

Figure 3. $N_{1/2}(n_\ell = 5)$ for the natural and practical top quark MSR masses. On panel (a) results are shown as a function of λ including contributions from one to four loops. The size of the bands at four loops reflects the error introduced by the numerical uncertainty in the $\mathcal{O}(\alpha_s^4)$ coefficient for the $\overline{\rm MS}$-pole conversion series. On panel (b) results are shown as error bars in blue (red) for the practical (natural) MSR masses at k-loops accounting also for the η parameter variation as described after eq. (4.14).

and one can show that in the asymptotic limit, i.e. to all orders in k, the sum rule expression for $N_{1/2}$ or $P_{1/2}$ is invariant under variations of λ. Thus for a finite order determination of $N_{1/2}$ the λ-dependence decreases with order, and the remaining variation with λ can be taken as an estimate for the uncertainty due to the missing higher order terms in the same way as renormalization scale variation in RG-invariant power series in α_s is commonly used to estimate perturbative uncertainties. The invariance under changes of λ is directly related to the facts that the $\mathcal{O}(\Lambda_{\rm QCD})$ renormalon ambiguity of the series in eqs. (2.3) and (2.5) is R-independent and that carrying out the Borel transform of eq. (4.5) in the previous section with respect to $\alpha_s(\mu)$ instead of $\alpha_s(R)$ leads to the simple rescaling factor μ/R of all the non-analytic terms proportional to $N_{1/2}$.

4.3 Sum rule for the pole mass renormalon

We now apply the sum rule to the series of the MSR-pole mass relations to quantify the $\mathcal{O}(\Lambda_{\rm QCD})$ renormalon of the pole mass. Note, that to fully determine the order k result, the $\mathcal{O}(\alpha_s^{k+1})$ $(k+1)$-loop corrections from eq. (2.3) and eq. (2.5) and the $\mathcal{O}(\alpha_s^{k+3})$ $(k+2)$-loop correction to the QCD β-function, β_{k+1} need to be known. So at $k = 3$, both the recently determined $\mathcal{O}(\alpha_s^4)$ 4-loop correction from eqs. (2.3) and (2.5) [54, 55] and the $\mathcal{O}(\alpha_s^6)$ 5-loop correction to the QCD β-function [80] are required. To simplify terminology we call the result that truncates the series for $N_{1/2}$ after the k-th term the "$(k+1)$-loop" or "$\mathcal{O}(\alpha_s^{k+1})$ result", referring to the order to which the series is being probed with the sum rule.

In figure 3a the numerical results for $N_{1/2}(n_\ell = 5)$ are shown for the natural (solid lines) and practical (dashed lines) MSR masses for $0.5 < \lambda < 2$ using terms in the series for $N_{1/2}$ up to $k = 0$ (cyan), $k = 1$ (blue), $k = 2$ (green) and $k = 3$ (red). The thickness of the $\mathcal{O}(\alpha_s^4)$ curves correspond to the numerical error of the coefficients

JHEP04(2018)003

quoted in [55] and shown in eqs. (2.6) and (2.2) and indicates that this error is more than an order of magnitude smaller than the uncertainty due to missing higher order terms and therefore negligible. We therefore do not account for this uncertainty any further and adopt the central values given in eqs. (2.6) and (2.2). Using the λ dependence in the range $0.5 < \lambda < 2$ as an error estimate due to the missing higher orders we obtain for $N_{1/2}(n_\ell = 5)$ at $\mathcal{O}(\alpha_s^k)$, $k = (1, 2, 3, 4)$ the numerical results $N_{1/2}^{\rm nat}(n_\ell = 5) = (0.531 \pm 0.318, 0.468 \pm 0.104, 0.483 \pm 0.029, 0.446 \pm 0.024)$ for the natural MSR mass and $N_{1/2}^{\rm prac}(n_\ell = 5) = (0.531 \pm 0.318, 0.475 \pm 0.109, 0.494 \pm 0.032, 0.441 \pm 0.033)$ for the practical MSR mass. The central values are the mean of the respective maximal and minimal value obtained in the range $0.5 < \lambda < 2$. Both results are fully compatible, as is expected since the difference of the natural and practical MSR masses is free from an $\mathcal{O}(\Lambda_{\rm QCD})$ renormalon as already discussed in section 2.3. We see that the λ-dependence of $N_{1/2}$ nicely decreases when including more higher-order terms and that there is excellent convergence. The convergence and the reducing λ-dependence both indicate that the numerical size of the recently calculated 4-loop correction in the $\overline{\rm MS}$-pole mass relation [54, 55] is fully compatible with the expectations based on the knowledge of the corrections up to 3 loops and the proposition that the $\overline{\rm MS}$-pole mass is dominated by an $\mathcal{O}(\Lambda_{\rm QCD})$ renormalon behavior already at the known low orders.

It is quite instructive that one can invert this line of arguments and use the sum rule as a tool to determine a prediction for higher order terms in the perturbative series under the assumption that the $\mathcal{O}(\Lambda_{\rm QCD})$ renormalon-type behavior observed at lower orders persists also at higher orders. Indeed, using for example the $\mathcal{O}(\alpha_s^3)$ result for the practical MSR mass $N_{1/2}^{\rm prac}(n_\ell = 5) = 0.494 \pm 0.032$ and the coefficients $a_{1,2,3}^{\rm MSRp}$ of the relation between practical MSR and pole masses [see eqs. (2.6)] and the β-function coefficients up to β_4 as an input, one can fit for the $\mathcal{O}(\alpha_s^4)$ coefficient giving $a_4^{\rm MSRp}(n_\ell = 5) = 224620 \pm 18656$. Converting to the $(n_\ell + 1)$ flavor scheme we obtain for the $\mathcal{O}(\alpha_s^4)$ coefficient in the $\overline{\rm MS}$-pole mass relation $a_4^{\overline{\rm MS}}(n_\ell = 5, 1) = 230192 \pm 14747$ compared to the result $a_4^{\overline{\rm MS}}(n_\ell = 5, 1) = 211807 \pm 5504$ from [54] and $a_4^{\overline{\rm MS}}(n_\ell = 5, 1) = 214828 \pm 422$ from ref. [55]. The prediction for the $\mathcal{O}(\alpha_s^4)$ coefficient based on the sum rules has a larger error but is fully compatible with the results from the explicit loop calculations. This is remarkable given that the sum rule result is obtained with essentially no additional computational effort. We note that estimates for the coefficient $a_4^{\overline{\rm MS}}$ were given before for example in refs. [8, 81–84]. These were not based on the renormalon sum rule but used available information on the high-order asymptotics of the perturbative series (see section 4.4). The analyses of refs. [8] and [84] were quoting an uncertainty for the estimate using the known corrections up to $\mathcal{O}(\alpha_s^3)$ and obtained the results $a_4^{\overline{\rm MS}}(n_\ell = 5, 1) = 241920 \pm 23552$ and $a_4^{\overline{\rm MS}}(n_\ell = 5, 1) = 229632^{+\,7936}_{-\,44800}$, respectively, which are fully compatible with the sum rule estimate we showed above at the same order.

The results for $N_{1/2}(n_\ell = 5)$ represent the $\mathcal{O}(\Lambda_{\rm QCD})$ renormalon ambiguity for the top quark pole mass assuming that the other quark flavors including *the charm and bottom quarks are massless*. The other cases of phenomenological interest are $n_\ell = 3$ and $n_\ell = 4$ and the corresponding results for the natural and practical MSR masses are given in table 1. As our final results for the $N_{1/2}$ values for the *number of massless flavors* $n_\ell = 3, 4, 5$ we

quote the 4-loop results for the natural MSR mass

$$N_{1/2}(n_\ell = 3) = 0.526 \pm 0.016\,, \tag{4.12}$$

$$N_{1/2}(n_\ell = 4) = 0.492 \pm 0.020\,, \tag{4.13}$$

$$N_{1/2}(n_\ell = 5) = 0.446 \pm 0.026\,. \tag{4.14}$$

Note that the uncertainties are slightly larger than the ones quoted in table 1. Following ref. [70] we have also included an additional uncertainty coming from varying the defining coefficients $a_n^{\overline{\rm MS}} = a_n^{\overline{\rm MS}}(n_\ell, 0)$ of the natural MSR mass based on the idea that using the association of R with the $\overline{\rm MS}$ mass at the scale of the $\overline{\rm MS}$ mass is in principle not mandatory. Since one may as well consider different renormalization scales for the $\overline{\rm MS}$ mass and the $\mathcal{O}(\Lambda_{\rm QCD})$ renormalon ambiguity is not affected by this choice, we have determined modified coefficients a_n from eq. (2.3) by setting $R = \overline{m}_Q^{(n_\ell)}(\overline{m}_Q^{(n_\ell)})$ and completely reexpanding the series in terms of $R' = \overline{m}_Q^{(n_\ell)}(\eta\,\overline{m}_Q^{(n_\ell)})$ using the RG equation for the $\overline{\rm MS}$ mass for n_ℓ dynamic flavors. Using the resulting series coefficients we have reevaluated the sum rule using variations in η between 0.5 and 2 and added the resulting uncertainty (while keeping $\lambda = 1$) quadratically to the ones shown in table 1 (which relate to the choice $\eta = 1$). The results including the η variation are shown in figure 3b exemplarily for $n_\ell = 5$.

The results of eqs. (4.12)–(4.14) are compatible with those given in refs. [8, 70]. For example for $n_\ell = 5$ [70] obtained $0.4616^{+0.027}_{-0.070} \pm 0.002$, where the first uncertainty is from a double scale variation similar to ours and the second uncertainty is from the numerical determination of the four loop coefficient. In refs. [8, 70] the determination of the normalization $N_{1/2}$ was based on the ratio method, which arises from a comparison of the perturbative coefficients a_n from explicit QCD loop calculations to the coefficients $a_n^{\rm asy}$ of the series generated by a pure $\mathcal{O}(\Lambda_{\rm QCD})$ renormalon in eq. (4.16) based on the relation that $\lim_{n\to\infty} a_n/a_n^{\rm asy} = 1$. In ref. [8] the static QCD potential and the $\overline{\rm MS}$-pole mass relation were studied, and in ref. [70] the $\overline{\rm MS}$-pole mass was examined. (In ref. [8] the static potential based numbers are roughly 1.4σ higher than those in eqs. (4.12)–(4.14), which may be related to the points discussed below in section 5.1 for the PS mass.) The agreement of our sum rule results and those obtained from the ratio method in ref. [70] underlines the capabilities of R-evolution and the renormalon sum rule concept.

In table 1 we have also shown the results for a number of other n_ℓ values as these results are also of theoretical interest. Our results are in full agreement with and have compatible uncertainties to the results given in table 1 of ref. [70] and in particular confirm that $N_{1/2} \to 1$ for $n_\ell \to -\infty$, which is the classic large-n_ℓ limit where the perturbative series are fully dominated by the massless quark bubble chain and the non-Abelian QCD effects are diluted away. Our result for $n_\ell = 0$ is also in agreement with ref. [8] and the lattice determinations of refs. [69, 85], which found $N_{1/2}(n_\ell = 0) = 0.600 \pm 0.029$, $N_{1/2}(n_\ell = 0) = 0.660 \pm 0.056$ and $N_{1/2}(n_\ell = 0) = 0.620 \pm 0.035$, respectively. We note that our analytic expression for $N_{1/2}$ gets unstable and non-conclusive for $10 \lesssim n_\ell \lesssim 30$ which is the so-called conformal region where the coefficient β_0 of the QCD β-function becomes small and in particular $\hat{b}_1 = \beta_1/(2\beta_0^2)$ becomes large. In this region the analytic formula for $N_{1/2}$ has singularities and does not approach any stable value. This is connected to the

JHEP04(2018)003

n_ℓ	$\mathcal{O}(\alpha_s)$	$\mathcal{O}(\alpha_s^2)$	$\mathcal{O}(\alpha_s^3)$	$\mathcal{O}(\alpha_s^4)$
$N_{1/2}(n_\ell)$ from $m_t^{\rm MSRn}$				
−1000000	0.531 ± 0.318	1.022 ± 0.378	0.817 ± 0.121	1.009 ± 0.068
−10	0.531 ± 0.318	0.654 ± 0.220	0.640 ± 0.062	0.684 ± 0.030
0	0.531 ± 0.318	0.558 ± 0.169	0.567 ± 0.058	0.582 ± 0.017
3	0.531 ± 0.318	0.514 ± 0.140	0.527 ± 0.046	0.526 ± 0.012
4	0.531 ± 0.318	0.494 ± 0.124	0.508 ± 0.039	0.492 ± 0.016
5	0.531 ± 0.318	0.468 ± 0.104	0.483 ± 0.029	0.446 ± 0.024
6	0.531 ± 0.318	0.434 ± 0.079	0.437 ± 0.027	0.381 ± 0.038
7	0.531 ± 0.318	0.387 ± 0.047	0.340 ± 0.059	0.271 ± 0.063
8	0.531 ± 0.318	0.184 ± 0.141	0.165 ± 0.142	0.053 ± 0.097
10	0.531 ± 0.318	-3.381 ± 2.714	-1.811 ± 0.492	-2.434 ± 1.041
$N_{1/2}(n_\ell)$ from $m_t^{\rm MSRp}$				
−1000000	0.531 ± 0.318	1.022 ± 0.378	0.817 ± 0.121	1.009 ± 0.068
−10	0.531 ± 0.318	0.658 ± 0.222	0.641 ± 0.062	0.684 ± 0.028
0	0.531 ± 0.318	0.563 ± 0.172	0.572 ± 0.059	0.583 ± 0.016
3	0.531 ± 0.318	0.520 ± 0.144	0.535 ± 0.048	0.522 ± 0.017
4	0.531 ± 0.318	0.501 ± 0.129	0.517 ± 0.041	0.487 ± 0.023
5	0.531 ± 0.318	0.475 ± 0.109	0.494 ± 0.032	0.441 ± 0.033
6	0.531 ± 0.318	0.442 ± 0.083	0.457 ± 0.023	0.373 ± 0.052
7	0.531 ± 0.318	0.394 ± 0.050	0.366 ± 0.051	0.259 ± 0.083
8	0.531 ± 0.318	0.200 ± 0.134	0.201 ± 0.127	0.027 ± 0.132
10	0.531 ± 0.318	-3.325 ± 2.681	-1.638 ± 0.439	-3.057 ± 0.649

Table 1. $N_{1/2}(n_\ell)$ for the natural and practical heavy quark MSR masses. The results are given for different theoretically interesting values of n_ℓ including contributions from one to four loops. The errors shown are obtained from λ variations in the interval $[0.5, 2]$ and the central values are the mean value of the respective maximal and minimal values obtained in that interval.

fact that in this region no definite statement on the asymptotic large order behavior of the perturbative series and in particular on the $\mathcal{O}(\Lambda_{\rm QCD})$ renormalon can be made because the infrared and ultraviolet structure of the QCD β-function strongly depend on a complicated numerical interplay of the coefficients $\beta_{i>0}$, which can become quite large and have different signs. The unstable behavior of our analytical formula for $10 \lesssim n_\ell \lesssim 30$ differs from the results obtained in refs. [8, 70], where the normalization $N_{1/2}$ was observed being tiny. However, as emphasized in ref. [70], this feature was an artifact of the ratio method used in refs. [8, 70], and again indicates that in this n_ℓ region the canonical renormalon calculus cannot be applied.

In ref. [29] the Borel method to compute $N_{1/2}$ was suggested based on the idea that the Borel function $(1-2u)^{1+\hat{b}_1}B_{\alpha_s}(u)$ eliminates all non-analytic contributions in the first term on the r.h.s. of eq. (4.7) and thus isolates the term $N_{1/2}$ in the limit $u \to 1/2$ [68]. This approach entails that after the low-order terms in the expansion of the Borel transform $B_{\alpha_s}(u)$ around $u = 0$ are determined from the original series, one expands $(1-2u)^{1+\hat{b}_1}B_{\alpha_s}(u)$ in powers of u and subsequently evaluates the resulting series for $u = 1/2$. The results of refs. [29, 68] were based on the assumption that the analytic contributions [involving the functions $Q_\ell(u)$] on the r.h.s. of eq. (4.7) quickly tend to zero when multiplied by $(1-2u)^{1+\hat{b}_1}$ and are unimportant. This is not the case, as the Taylor expansion $(1-2u)^{1+\hat{b}_1}$ around $u = 0$ converges very slowly to zero if one sets $u = 1/2$. This can be traced to the fact that $\hat{b}_1$ is non-integer and in general the convergence radius of the binomial series is 1. Here $u = 1/2$ corresponds exactly to the border of this radius. These terms are therefore numerically sizable at any truncation order. As we show in appendix B, neglecting them leads to a much larger dependence on the renormalization parameter λ at a given truncation order. This is because the λ dependence of these terms is multiplied by a factor converging to zero, but the convergence is rather slow. When many orders are included, as shown in ref. [69] which accounted for terms up to $\mathcal{O}(\alpha_s^{20})$, the dependence vanishes and the method converges to $N_{1/2}$, which we have confirmed through a reanalysis. This observation is consistent with the large scale uncertainties found in the detailed numerical analysis of ref. [8]. The Borel method to determine $N_{1/2}$ is therefore not very precise if only the first few terms of the series are known. Interestingly, accounting for the analytic terms on the r.h.s. of eq. (4.7), which are contained in the polynomials Q_ℓ and are computed systematically from R-evolution as shown in section 4.1, one can derive an improved version of the Borel approach which agrees exactly with our sum rule formula of eq. (4.8). The corresponding analytic calculation and a brief numerical analysis are given in appendix B.

4.4 Asymptotic higher order behavior

In this section we use the analytic manipulations that arise in the derivation of the sum rule to derive an alternative expression for the high-order asymptotic form of a series containing an $\mathcal{O}(\Lambda_{\rm QCD})$ renormalon that differs from the well known formula derived in [77]. The latter formula is related to the sum of the non-analytic terms, which are multiplied by $N_{1/2}$ or $P_{1/2}$ in the Borel function of eq. (4.7), and reads

$$\begin{aligned}\left[m_Q^{\rm pole} - m_Q^{\rm MSR}(R)\right]_{\rm asy} &= N_{1/2}\, R \sum_{n=0}^{\infty} a_{n+1}^{\rm asy} \left(\frac{\alpha_s(R)}{4\pi}\right)^{n+1} \\ &= N_{1/2}\, R \sum_{n=0}^{\infty} 4\pi\,(2\beta_0)^n \left(\frac{\alpha_s(R)}{4\pi}\right)^{n+1} \sum_{\ell=0}^{\infty} g_\ell\, \frac{\Gamma(1+\hat{b}_1+n-\ell)}{\Gamma(1+\hat{b}_1)} \\ &= P_{1/2}\, R \sum_{n=0}^{\infty} (2\beta_0)^{n+1} \left(\frac{\alpha_s(R)}{4\pi}\right)^{n+1} \sum_{\ell=0}^{\infty} g_\ell\, \Gamma(1+\hat{b}_1+n-\ell)\,,\end{aligned} \tag{4.15}$$

giving the asymptotic form of the coefficients

$$a_n^{\rm asy} = 4\pi\, N_{1/2} (2\beta_0)^{n-1} \sum_{\ell=0}^{\infty} g_\ell\, (1+\hat{b}_1)_{n-1-\ell}\,, \tag{4.16}$$

where $(b)_n = b\,(b+1)\cdots(b+n-1) = \Gamma(b+n)/\Gamma(b)$ is the Pochhammer symbol. Given the value for $P_{1/2}$ or $N_{1/2}$ the structure of the perturbative coefficients of eq. (4.15) is completely fixed by the properties of the QCD β-function and does not depend any more on the coefficients of the original series of eqs. (2.3) and (2.5). Thus eq. (4.15) has been frequently used as the standard form for the asymptotic high-order behavior of perturbative series dominated by an $\mathcal{O}(\Lambda_{\rm QCD})$ renormalon. This is also reflected by the fact that the imaginary part of the inverse Borel integration over the non-analytic terms in eq. (4.7) is exactly proportional to $\Lambda_{\rm QCD}$

$$\begin{aligned}\mathrm{Im}\int_0^\infty \mathrm{d}u \left[-N_{1/2}\,R\,\frac{4\pi}{\beta_0}\sum_{\ell=0}^{\infty} g_\ell\,\frac{\Gamma(1+\hat{b}_1-\ell)}{\Gamma(1+\hat{b}_1)}\,(1-2u)^{-1-\hat{b}_1+\ell}\right] \mathrm{e}^{-\frac{4\pi u}{\beta_0\alpha_s(R)}} \\ = P_{1/2}\,\pi\,\Lambda_{\rm QCD} = N_{1/2}\,\frac{2\pi^2}{\beta_0\,\Gamma(1+\hat{b}_1)}\,\Lambda_{\rm QCD}\,,\end{aligned} \tag{4.17}$$

with $\Lambda_{\rm QCD}$ given in eq. (A.6). As a side remark, we note that inserting the series in eq. (4.15), with a given value for $N_{1/2}$, into the sum rule expression of eq. (4.8) one recovers $N_{1/2}$ in the limit of carrying out the sums over k, n and ℓ to infinity.

Interestingly, eq. (4.4) provides a remarkable alternative expression for the high-order asymptotic of the MSR-pole mass series as it can be rewritten in the form

$$m_Q^{\rm pole} - m_Q^{\rm MSR}(R) = R\sum_{n=0}^{\infty}\left(\frac{\alpha_s(R)}{4\pi}\right)^{n+1}\sum_{k=0}^{n}\sum_{\ell=0}^{n-k}(2\beta_0)^{n+1}S_k\,g_\ell\,\frac{\Gamma(1+\hat{b}_1+n-\ell)}{\Gamma(1+\hat{b}_1+k)}\,. \tag{4.18}$$

In contrast to eq. (4.15) this expression still depends on the S_k coefficients non-trivially and thus carries all the information contained in the original series due to the identity

$$a_n = (2\beta_0)^n\sum_{k=0}^{n-1}S_k\sum_{\ell=0}^{n-1-k} g_\ell\,(1+\hat{b}_1+k)_{n-1-\ell-k}\,. \tag{4.19}$$

This relation is interesting because it provides a separation of the coefficients of the original series into leading and subleading terms with respect to the asymptotic high-order behavior. So truncating the sums over k and ℓ in eq. (4.19) (e.g. accounting for the coefficients S_k and g_ℓ up to the order they are known) provides the correct high-order asymptotic behavior for n beyond the truncation order and, at the same time, reproduces exactly the coefficients of the original series up to the truncation order.

Currently the coefficients a_n for the MSR-pole and the $\overline{\rm MS}$-pole mass relations are known to order $\mathcal{O}(\alpha_s^4)$ and the QCD β-function is known to order $\mathcal{O}(\alpha_s^6)$ so that the coefficients S_k and g_ℓ are known up to $k_{\rm max} = \ell_{\rm max} = 3$. We may therefore write down estimates for the still uncalculated coefficients $a_{n>4}$ using the expression

$$a_{n>4}^{\rm asy} = 4\pi\,N_{1/2}\,(2\beta_0)^{n-1}\sum_{\ell=0}^{3} g_\ell\,(1+\hat{b}_1)_{n-1-\ell}\,, \tag{4.20}$$

which is the established formula from [77] shown in eq. (4.15), and

$$a_{n>4}^{\rm asy\,\prime} = (2\beta_0)^n\sum_{k=0}^{3}S_k\sum_{\ell=0}^{\min(n-k-1,3)} g_\ell\,(1+\hat{b}_1+k)_{n-1-\ell-k}\,, \tag{4.21}$$

based on eq. (4.19), which encodes information on both the regular and asymptotic behavior of the series.[4] In table 2 we show estimates for the yet uncalculated coefficients $a_{5\le n\le 9}$ for the relations of the natural MSR mass and the $\overline{\rm MS}$ mass $\overline{m}_Q \equiv \overline{m}_Q^{(n_\ell+1)}(\overline{m}_Q^{(n_\ell+1)})$ to the pole mass using eqs. (4.20) and (4.21) for $n_\ell = 3, 4, 5$ and the results of eqs. (4.12)–(4.14) for $N_{1/2}$. The uncertainties for the coefficients $a_n^{\rm asy}$ are based on the uncertainties shown in eqs. (4.12) – (4.14) and those for the coefficients $a_n^{\rm asy\,\prime}$ are determined from λ variations $1/2 < \lambda < 2$, as explained in section 4.2 and η variations $1/2 < \eta < 2$, as explained below eq. (4.14). The coefficient estimates for the $\overline{\rm MS}$ mass have been obtained by using the second equality of (5.8) and eq. (A.7) to the order shown. We see that both estimates are completely equivalent and have the same uncertainties. Our estimates for the $\overline{\rm MS}$ mass coefficients for $n_\ell = 5$ also agree perfectly with those given in ref. [70] which used the approach of eq. (4.20). We note that the relation (4.19) can also be inverted to provide closed iterative expressions for the S_k coefficients to all orders, which are given in appendix A and in particular in eq. (A.18).

We note that the asymptotic series coefficients $a_n^{\rm asy}$ in eq. (4.16) and the expression for the coefficients a_n in eq. (4.19) allow for an alternative derivation of the renormalon sum rule formula since the ratio $a_n/a_n^{\rm asy}$ approaches unity for $n \to \infty$. Taking that ratio one arrives at

$$N_{1/2}\frac{a_n}{a_n^{\rm asy}} = \frac{(2\beta_0)^n \sum\limits_{k=0}^{n-1} S_k \sum\limits_{\ell=0}^{n-1-k} g_\ell\,(1+\hat{b}_1+k)_{n-1-\ell-k}}{4\pi\,(2\beta_0)^{n-1} \sum\limits_{\ell=0}^{\infty} g_\ell\,(1+\hat{b}_1)_{n-1-\ell}} \tag{4.22}$$

$$= \frac{\beta_0\,\Gamma(1+\hat{b}_1)}{2\pi} \sum_{k=0}^{n-1} \frac{S_k}{\Gamma(1+\hat{b}_1+k)} \frac{\sum\limits_{\ell=0}^{n-1-k} g_\ell\,\Gamma(\hat{b}_1+n-\ell)}{\sum\limits_{\ell=0}^{\infty} g_\ell\,\Gamma(\hat{b}_1+n-\ell)}\,.$$

To the extent that the sums over k in the sum rule formula of eq. (4.8) and in eq. (4.22) for $n \to \infty$ are convergent, one can use the Cauchy convergence criterion to show that the expression of eq. (4.22) is equivalent to eq. (4.8) for $n \to \infty$. This shows analytically the equivalence of the ratio method and the sum rule.

4.5 Other applications of the sum rule

To conclude our considerations concerning the $\mathcal{O}(\Lambda_{\rm QCD})$ renormalon sum rule we discuss in this section a number of subtleties in its proper use and a few interesting applications. As it is sufficient for the purpose of the examinations, we use for simplicity only λ variations, as explained in section 4.2, when quoting uncertainties of the sum rule evaluated here.

4.5.1 Number of massless flavors

An important feature of the $\mathcal{O}(\Lambda_{\rm QCD})$ renormalon sum rule is that it probes the infrared sensitivity of the perturbative series, which physically depends on the number of massless

[4] One can easily write eq. (4.21) as the sum of eq. (4.20) and a term build from the inverse Borel transform of the Q_ℓ polynomials defined in eq. (4.9).

n_ℓ	$a_5^{\rm MSRn}\times 10^{-7}$	$a_6^{\rm MSRn}\times 10^{-9}$	$a_7^{\rm MSRn}\times 10^{-11}$	$a_8^{\rm MSRn}\times 10^{-13}$	$a_9^{\rm MSRn}\times 10^{-15}$
3	3.394 ± 0.105	3.309 ± 0.102	3.819 ± 0.118	5.093 ± 0.157	7.706 ± 0.238
4	2.249 ± 0.090	2.019 ± 0.081	2.147 ± 0.086	2.641 ± 0.106	3.687 ± 0.148
5	1.379 ± 0.080	1.128 ± 0.066	1.095 ± 0.064	1.231 ± 0.072	1.572 ± 0.091
	$a_5^{\rm MSRn\prime}\times 10^{-7}$	$a_6^{\rm MSRn\prime}\times 10^{-9}$	$a_7^{\rm MSRn\prime}\times 10^{-11}$	$a_8^{\rm MSRn\prime}\times 10^{-13}$	$a_9^{\rm MSRn\prime}\times 10^{-15}$
3	3.393 ± 0.105	3.309 ± 0.102	3.819 ± 0.118	5.093 ± 0.157	7.706 ± 0.238
4	2.248 ± 0.090	2.019 ± 0.081	2.147 ± 0.086	2.641 ± 0.106	3.687 ± 0.148
5	1.378 ± 0.080	1.128 ± 0.066	1.095 ± 0.063	1.231 ± 0.072	1.572 ± 0.091
	$a_5^{\overline{\rm MS}}\times 10^{-7}$	$a_6^{\overline{\rm MS}}\times 10^{-9}$	$a_7^{\overline{\rm MS}}\times 10^{-11}$	$a_8^{\overline{\rm MS}}\times 10^{-13}$	$a_9^{\overline{\rm MS}}\times 10^{-15}$
3	3.401 ± 0.105	3.315 ± 0.102	3.824 ± 0.118	5.099 ± 0.158	7.714 ± 0.239
4	2.255 ± 0.090	2.023 ± 0.081	2.151 ± 0.086	2.644 ± 0.106	3.692 ± 0.148
5	1.383 ± 0.080	1.130 ± 0.066	1.097 ± 0.064	1.233 ± 0.072	1.575 ± 0.091
	$a_5^{\overline{\rm MS}\prime}\times 10^{-7}$	$a_6^{\overline{\rm MS}\prime}\times 10^{-9}$	$a_7^{\overline{\rm MS}\prime}\times 10^{-11}$	$a_8^{\overline{\rm MS}\prime}\times 10^{-13}$	$a_9^{\overline{\rm MS}\prime}\times 10^{-15}$
3	3.400 ± 0.106	3.315 ± 0.103	3.824 ± 0.118	5.099 ± 0.158	7.714 ± 0.239
4	2.254 ± 0.091	2.023 ± 0.081	2.151 ± 0.086	2.644 ± 0.106	3.692 ± 0.148
5	1.382 ± 0.081	1.130 ± 0.066	1.097 ± 0.064	1.233 ± 0.072	1.575 ± 0.091

Table 2. Numerical estimates for the perturbative coefficients $a_n^{\rm MSRn}$ (MSRn-pole mass relation in eq. (2.3)) and $a_n^{\overline{\rm MS}}$ [$\overline{\rm MS}$-pole mass relation in eq. (2.1)] for $5 \leq n \leq 9$ and $n_\ell = 3, 4, 5$ using formulae (4.20) and (4.21) for their asymptotic high-order behavior. The quoted errors arise from λ and η variations in the interval $[0.5, 2]$ and the central values are the mean of the maximum and minimum values in that interval.

quarks, n_ℓ, one employs in the computation of the series. In a computation in QCD, however, n_ℓ might not be equal to the number of active flavors, n_f, which governs the ultraviolet behavior and the renormalization group evolution of the strong coupling $\alpha_s^{(n_f)}$ and other renormalized quantities, and a naive application of the sum rule may lead to inconsistent results. In such a case, the series in $\alpha_s^{(n_f)}$ should be better converted to the n_ℓ-flavor scheme for the strong coupling, $\alpha_s^{(n_\ell)}$, before its coefficients are inserted in the sum rule expression. This can be either realized by simply rewriting $\alpha_s^{(n_f)}$ as a series in $\alpha_s^{(n_\ell)}$, as it is done in the definition of the practical MSR mass, or by integrating out the effects of the $n_f - n_\ell$ massive quarks, as it is done in the definition of the natural MSR mass. The latter approach is the physically cleaner way (which was the reason for using the name 'natural'), but both approaches are consistent as far as the application of the sum rule is concerned.

In the following we discuss the pitfalls of using the sum in an inconsistent way. To discuss the issue we recall that, since the $\mathcal{O}(\Lambda_{\rm QCD})$ renormalon sum rule is a functional on the perturbative series, it can also be seen as a function $N_{1/2}[n_\ell, \{a_n\}]$ acting on the coefficients a_n of the $[\alpha_s/(4\pi)]^n$ terms in the series. As indicated, $N_{1/2}$ is a function of the number of massless flavors n_ℓ through its dependence on β_0 and the coefficients $\hat{b}_k$, which

appear in eq. (4.8) and a function of the coefficients a_n contained in the expressions for the S_k as shown in eq. (A.15). The function $N_{1/2}[n_\ell, \{a_n\}]$ is therefore probing the series defined by the set of coefficients $\{a_n\}$ with respect to an $\mathcal{O}(\Lambda_{\rm QCD})$ renormalon for n_ℓ massless flavors, and it is essential for the sum rule to work properly that the value of n_ℓ agrees with the number of massless flavors used for the computation of the coefficients a_n. Let us now apply the sum rule to the coefficients $\{a_n^{\overline{\rm MS},n_\ell}\}$ of the series for $m_Q^{\rm pole} - \overline{m}_Q(\overline{m}_Q)^{(n_\ell+1)}$ in eq. (2.1), which is a series in $\alpha_s^{(n_\ell+1)}$, but contains the effects of n_ℓ massless flavors. Here we use the shorthand notation

$$a_n^{\overline{\rm MS},n_\ell} \equiv a_n^{\overline{\rm MS}}(n_\ell, n_h = 1)\,. \tag{4.23}$$

To be specific we take $n_\ell = 5$. Probing the series with respect to an $\mathcal{O}(\Lambda_{\rm QCD})$ renormalon for $n_\ell + 1 = 6$ massless flavors, in accordance with the scheme for α_s, one obtains $N_{1/2}[6, \{a_n^{\overline{\rm MS},{\rm n}_\ell=5}\}] = (0.531 \pm 0.318, 0.526 \pm 0.1298, 0.623 \pm 0.070, 0.6360 \pm 0.016)$ at order $n = (0, 1, 2, 3)$, where the errors are obtained from varying λ in the range $0.5 < \lambda < 2$ and the central values are the mean value of the respective maximal and minimal values obtained in the λ variation. We see that the sum rule appears to approach a value that is much larger than the correct result of eq. (4.14), but this is a consequence of an inconsistent application of the sum rule. Indeed, one can show by simple algebra in the β_0/LL approximation [where $\hat{b}_{i\geq 1} = \beta_{i\geq 1} = 0$, $a_{n+1}^{{\rm asy},n_\ell} = a_1(2\beta_{0,n_\ell})^n n!$ and $\beta_{0,n_\ell} = 11 - 2/3\, n_\ell$] that the order n expression for $N_{1/2}$ that is obtained — when probing with respect to an $\mathcal{O}(\Lambda_{\rm QCD})$ renormalon for n_f massless flavors — has the form

$$\Big[N_{1/2}^{(n)}[n_f, \{a_n^{{\rm asy},n_\ell}\}]\Big]_{\beta_0/{\rm LL}} = \frac{\beta_0}{2\pi}\sum_{k=0}^{n}\frac{S_k}{k!} = \frac{a_1}{4\pi}\left(\frac{\beta_{0,n_\ell}}{\beta_{0,n_f}}\right)^n . \tag{4.24}$$

As long as $\beta_{0,n}$ is a positive number this expression diverges for $n_f > n_\ell$ in the limit $n \to \infty$, which explains the behavior of the sum rule results shown above. On the other hand, the expression of eq. (4.24) converges to zero for $n_f < n_\ell$. So when probing the coefficients $\{a_n^{\overline{\rm MS},n_\ell}\}$ of the series for $m_Q^{\rm pole} - \overline{m}_Q(\overline{m}_Q)^{(n_\ell+1)}$ with respect to an $\mathcal{O}(\Lambda_{\rm QCD})$ renormalon for $n_\ell - 1 = 4$ massless flavors we obtain $N_{1/2}[4, \{a_n^{\overline{\rm MS},{\rm n}_\ell=5}\}] = (0.531 \pm 0.318, 0.433 \pm 0.089, 0.405 \pm 0.027, 0.327 \pm 0.051)$ at order $n = (0, 1, 2, 3)$ which is a sequence of decreasing terms, as expected from eq. (4.24), which in addition does not behave in a stable way. But, again, the behavior is a consequence of an inconsistent application of the sum rule. On the other hand, if we probe the coefficients $\{a_n^{\overline{\rm MS},n_\ell}\}$ of the series for $m_Q^{\rm pole} - \overline{m}_Q(\overline{m}_Q)^{(n_\ell+1)}$ with respect to an $\mathcal{O}(\Lambda_{\rm QCD})$ renormalon for $n_\ell = 5$ massless flavors we obtain $N_{1/2}[5, \{a_n^{\overline{\rm MS},{\rm n}_\ell=5}\}] = (0.531 \pm 0.318, 0.475 \pm 0.109, 0.494 \pm 0.032, 0.442 \pm 0.033)$ at order $n = (0, 1, 2, 3)$, which converges to the correct result of eq. (4.14). We also learn that adopting for the strong coupling $\alpha_s^{(n_f)}$ a flavor number scheme where n_f agrees with the number of massless flavors is clean conceptually, but not crucial numerically such that the sum rule works reliably. This is related to the fact that the matching relation of the strong coupling in different flavor number schemes does not suffer from an $\mathcal{O}(\Lambda_{\rm QCD})$ renormalon behavior.

JHEP04(2018)003

This brief examination above underlines the importance that the $\mathcal{O}(\Lambda_{\rm QCD})$ sum rule, which probes the infrared sensitivity of the perturbative series, is applied consistently with respect to the number of massless quarks, which may not agree with the number of active flavors in the normalization group equation that is governed by ultraviolet effects. Of course this feature may as well be used as a tool, as studying the convergence of the sum rule may be employed to determine the number of massless flavors used, let's say, in a numerical computation of a perturbative series.

4.5.2 Moments of the vacuum polarization function

The zero-momentum moments M_i, $i = 1, 2, 3, \ldots$, of the massive quark Q vector current correlator $\Pi(q^2)$, defined by $[j^\mu(x) \equiv \overline{\psi}_Q(x)\gamma^\mu\psi_Q(x)]$

$$M_i = \frac{12\pi^2 Q_Q^2}{m!}\frac{\mathrm{d}^i}{\mathrm{d}q^{2i}}\Pi(q^2)\bigg|_{q^2=0}\,, \tag{4.25}$$

$$\left(g_{\mu\nu}q^2 - q_\mu q_\nu\right)\Pi(q^2) = -\,i\int \mathrm{d}x\,\mathrm{e}^{iqx}\,\langle 0|\mathrm{T}j_\mu(x)j_\nu(0)|0\rangle\,,$$

provide one of the most precise methods to determine the charm and bottom quark $\overline{\rm MS}$ masses [1–10] and are known to utterly fail in precision when expressed in terms of the charm and bottom pole masses. This mass sensitivity comes from the fact that the perturbative series for the moments M_i is due to dimensional reasons proportional to m_Q^{-2i} in the form $M_i = m_Q^{-2i}\sum_{n=0}^{\infty} c_{i,n}(m_Q)[\alpha_s^{(n_\ell)}(m_Q)/(4\pi)]^n$, where n_ℓ is the number of massless flavors and we use the n_ℓ-flavor scheme for the strong coupling.[5] The moments M_i are related to weighted integrals over the hadronic R-ratio of $Q\overline{Q}$ production and thus free from the $\mathcal{O}(\Lambda_{\rm QCD})$ renormalon. They can be rewritten in the form

$$m_Q - \left(\frac{M_i}{c_{i,0}}\right)^{-\frac{1}{2i}} = m'_Q\sum_{n=1}^{\infty} a_{i,n}[m_Q, m'_Q]\left(\frac{\alpha_s^{(n_\ell)}(m'_Q)}{4\pi}\right)^n, \tag{4.26}$$

where m_Q and m'_Q may be in general different quark mass schemes.

The moments M_i are suitable quantities to discuss the parametric aspect of renormalon ambiguities and how they affect the proper application of the $\mathcal{O}(\Lambda_{\rm QCD})$ sum rule. The first three moments $M_{1,2,3}$ are known to $\mathcal{O}(\alpha_s^3)$ [86–96] and the corresponding series coefficients $a_{i,n}$ for $n_\ell = 4$ in the $\overline{\rm MS}$ mass scheme $m_Q = m'_Q = \overline{m}_Q^{(n_\ell+1)}(\overline{m}_Q^{(n_\ell+1)})$ and the pole mass scheme $m_Q = m'_Q = m_Q^{\rm pole}$ using the n_ℓ-flavor scheme $\alpha_s^{(n_\ell)}$ for the coupling are quoted in table 3. Applying the sum rule to the series for the $M_{1,2,3}$ on the r.h.s. of eq. (4.26) in the $\overline{\rm MS}$ scheme we obtain for $n_\ell = 4$, relevant for the bottom quark, the results

$$\begin{aligned} N_{1/2}^{i=1} &= (0.477 \pm 0.286, -0.178 \pm 0.261, \quad 0.013 \pm 0.036)\,, \\ N_{1/2}^{i=2} &= (0.241 \pm 0.145, -0.007 \pm 0.083, -0.029 \pm 0.058)\,, \\ N_{1/2}^{i=3} &= (0.127 \pm 0.076, \quad 0.031 \pm 0.026, -0.029 \pm 0.048)\,, \end{aligned} \tag{4.27}$$

[5] In the recent sum-rule analyses [1–10] for the bottom quark mass $n_\ell = 4$ was used, while for charm mass determinations $n_\ell = 3$ was employed, and the $(n_\ell + 1)$ flavor scheme was employed for the renormalization group evolution.

i	$\mathcal{O}(\alpha_s)$	$\mathcal{O}(\alpha_s^2)$	$\mathcal{O}(\alpha_s^3)$	$\mathcal{O}(\alpha_s)$	$\mathcal{O}(\alpha_s^2)$	$\mathcal{O}(\alpha_s^3)$
	$a_{i,n}[m_{\rm pole}, m_{\rm pole}]$			$a_{i,n}[\overline{m}(\overline{m}), \overline{m}(\overline{m})]$		
1	10.1235	83.7296	4669.92	4.79012	− 10.7255	− 310.275
2	7.76049	120.609	4589.81	2.42716	13.5516	− 334.42
3	6.61153	127.821	4754.39	1.2782	14.6354	− 199.81
	$a_{i,n}[m_{\rm pole}, \overline{m}(\overline{m})]$			$a_{i,n}[m_{\rm pole}, \widetilde{M}]$		
1	10.1235	137.721	5719.41	10.1235	186.214	5831.25
2	7.76049	161.998	5695.26	7.76049	180.834	6005.71
3	6.61153	163.082	5829.87	6.61153	171.533	6063.32

Table 3. $a_{i,n}(m_Q, m'_Q)$ coefficients of the perturbative expansion for the mass-subtracted linearized moments, as displayed in eq. (4.26), at one (left column of each block), two (middle column of each block), and three (right column of each block) loops. The numerical values correspond to the case $n_\ell = 4$, studied in this section. The table is split into four blocks: the upper left one corresponds to the pole mass expansion in terms of the pole mass, the upper right one shows the $\overline{\rm MS}$ mass expansion in terms of the $\overline{\rm MS}$ mass, the lower left block displays the pole mass expansion in terms of the $\overline{\rm MS}$ mass, and the lower right displays the linearized iterative expansion for the pole mass.

at order $n = (0, 1, 2)$, where the errors are obtained by λ variations in the range $0.5 < \lambda < 2$ and the central values are obtained from the mean of the respective maximal and minimal values in the λ variation. We see that the results for $N_{1/2}$ are compatible with zero beyond $\mathcal{O}(\alpha_s)$ and have uncertainties that decrease with order, illustrating the known fact that the series are free from an $\mathcal{O}(\Lambda_{\rm QCD})$ renormalon in the $\overline{\rm MS}$ mass scheme.

Applying the sum rule to the series for the $M_{1,2,3}$ in the pole mass scheme $m_Q = m'_Q = m_Q^{\rm pole}$ the corresponding results for $n_\ell = 4$ read

$$\begin{aligned} N_{1/2}^{i=1} &= (1.007 \pm 0.604,\, 0.092 \pm 0.278,\, 0.510 \pm 0.113)\,, \\ N_{1/2}^{i=2} &= (0.772 \pm 0.463,\, 0.345 \pm 0.094,\, 0.420 \pm 0.012)\,, \\ N_{1/2}^{i=3} &= (0.658 \pm 0.395,\, 0.416 \pm 0.053,\, 0.424 \pm 0.013)\,. \end{aligned} \tag{4.28}$$

Apart from the outcome for M_1, which still happens to have a rather large error at order $n = 2$ the results converge to the result 0.42 ± 0.01 which is incompatible with the correct result 0.49 ± 0.02 from eq. (4.13). So the $\mathcal{O}(\Lambda_{\rm QCD})$ renormalon ambiguity inherent to the coefficients in the series of eq. (4.26) in the pole mass scheme appears to be about 15% smaller than for the coefficients of the MSR-pole mass series analyzed before. The discrepancy is resolved by the fact that in the pole scheme with both $m_Q = m'_Q = m_Q^{\rm pole}$ the r.h.s. of eq. (4.26) is expressed using the ambiguous pole mass as a parameter. As a consequence, the perturbative coefficients of the series and factors of $m_Q^{\rm pole}$ on the r.h.s. share the full $\mathcal{O}(\Lambda_{\rm QCD})$ pole mass renormalon ambiguity contained in the l.h.s. of eq. (4.26).

To recover the full $\mathcal{O}(\Lambda_{\rm QCD})$ pole mass renormalon ambiguity in the coefficients on the r.h.s. one has to rewrite the series on the r.h.s. in terms of parameters that are free from the $\mathcal{O}(\Lambda_{\rm QCD})$ renormalon ambiguity. This can be achieved by re-expanding the series for

JHEP04(2018)003

$m_Q^{\rm pole} - (M_m/c_{i,0})^{-1/(2i)}$ completely in terms of the $\overline{\rm MS}$ mass using $m'_Q = \overline{m}_Q^{(n_\ell+1)}(\overline{m}_Q^{(n_\ell+1)})$. The resulting coefficients in powers of $\alpha_s^{(n_\ell)}(m'_Q)$ are given in the lower left column of table 3. Using these coefficients, the renormalon sum rule applied to the series for the $M_{1,2,3}$ and $n_\ell = 4$ gives

$$\begin{aligned} N_{1/2}^{i=1} &= (1.007 \pm 0.604,\, 0.350 \pm 0.159,\, 0.547 \pm 0.047)\,, \\ N_{1/2}^{i=2} &= (0.772 \pm 0.463,\, 0.525 \pm 0.078,\, 0.495 \pm 0.032)\,, \\ N_{1/2}^{i=3} &= (0.658 \pm 0.395,\, 0.535 \pm 0.110,\, 0.501 \pm 0.034)\,, \end{aligned} \tag{4.29}$$

at order $n = (0, 1, 2)$. This is in full agreement with the result 0.49 ± 0.02 given in eq. (4.13), and also shows a substantially better behavior for the moment M_1.

As an alternative to using the series for $m_Q = m_Q^{\rm pole}$ and $m'_Q = \overline{m}_Q^{(n_\ell+1)}(\overline{m}_Q^{(n_\ell+1)})$, one can also define $\widetilde{M}_i \equiv (M_i/c_{i,0})^{-1/2i}$ and re-express the r.h.s. of eq. (4.26) perturbatively in terms of $m'_Q = \widetilde{M}_i$ for the different moments. (We refer to ref. [1] for details on this iterative procedure.) The resulting coefficients in powers of $\alpha_s^{(n_\ell)}(\widetilde{M}_i)$ are given in the lower right column of table 3. Using these coefficients, the renormalon sum rule applied to the series for the $M_{1,2,3}$ and $n_\ell = 4$ gives

$$\begin{aligned} N_{1/2}^{i=1} &= (1.007 \pm 0.604,\, 0.604 \pm 0.075,\, 0.493 \pm 0.071)\,, \\ N_{1/2}^{i=2} &= (0.772 \pm 0.463,\, 0.589 \pm 0.109,\, 0.501 \pm 0.056)\,, \\ N_{1/2}^{i=3} &= (0.658 \pm 0.395,\, 0.568 \pm 0.129,\, 0.516 \pm 0.040)\,. \end{aligned} \tag{4.30}$$

These results behave similarly to those of eq. (4.29) and are again in full agreement with the result 0.49 ± 0.02 given in eq. (4.13).

This analysis underlines the importance of using renormalon-free parameters for series coefficients that are being probed with the $\mathcal{O}(\Lambda_{\rm QCD})$ renormalon sum rule, but also illustrates the high sensitivity of the sum rule to even subtle high order effects.

4.5.3 Infrared sensitivity of the PS mass definition

The PS (potential subtracted) mass [25] is based on the concept that the total static potential energy of a color singlet massive quark-antiquark pair with separation r, $2m_Q^{\rm pole} + V(r)$, is $\mathcal{O}(\Lambda_{\rm QCD})$ renormalon free. It is defined from the integral

$$m_Q^{\rm pole} - m_Q^{\rm PS}(\mu_f) = -\frac{1}{2}\int_{|\vec{q}|<\mu_f} \frac{{\rm d}^3\vec{q}}{(2\pi)^3}\,\tilde{V}(\vec{q}^{\,2})\,, \tag{4.31}$$

where $\tilde{V}(\vec{q}^{\,2})$ is the momentum-space static potential calculated in perturbation theory. To the extent that the total static potential is a well-defined and unambiguous quantity, the PS mass is free from an $\mathcal{O}(\Lambda_{\rm QCD})$ renormalon. The coefficients of the series for $m_Q^{\rm pole} - m_Q^{\rm PS}(\mu_f)$, expressed as a series in powers of $\alpha_s^{(n_\ell)}(\mu_f)/(4\pi)$, are given in eq. (C.1).

We now apply the $\mathcal{O}(\Lambda_{\rm QCD})$ renormalon sum rule to the relation of the pole mass to the potential PS mass. The examination is of interest because the static potential has infrared divergences starting at $\mathcal{O}(\alpha_s^4)$ arising from higher Fock $Q\overline{Q}$-gluon states which

lead to retardation effects that invalidate the frame-independent static limit [97, 98]. The definition of the PS mass at $\mathcal{O}(\alpha_s^4)$ and beyond is therefore known to depend on the scheme used for the subtraction prescription for these infrared divergences. In refs. [99] the authors defined the following convention: the infrared divergence in the $\mathcal{O}(\alpha_s^4)$ corrections to the momentum-space static potential [100, 101] is regularized dimensionally (with the $\overline{\rm MS}$ convention for the definition of μ), and the $1/\epsilon$ divergence together with the corresponding logarithm $\log(\mu/\mu_f)$ that arises from the integral over the momentum-space static potential in eq. (4.31) are subtracted. We call this the standard convention, and it leads to the coefficient $a_4^{\rm PS}$ shown in eq. (C.2), where the term with the logarithm $\log(\mu/\mu_f)$ is dropped. In a minimal subtraction convention, only the $1/\epsilon$ divergence is subtracted and the logarithmic term displayed in $a_4^{\rm PS}$ remains. So the convention of ref. [99] is equivalent to the choice $\mu/\mu_f = 1$ for the dimensional scale in the minimal subtraction convention.

Using the $\mathcal{O}(\Lambda_{\rm QCD})$ renormalon sum rule we can now track quantitatively if and how much the convention for the infrared subtraction may affect the higher-order behavior in the PS-pole mass relation. Applying the sum rule to the PS mass in the standard convention of ref. [99] we obtain for $n_\ell = 5$, relevant for the top quark,

$$N_{1/2}^{\mu/\mu_f=1} = (0.531 \pm 0.318, 0.376 \pm 0.057, 0.503 \pm 0.078, 0.545 \pm 0.045)\,, \tag{4.32}$$

at order $n = (0, 1, 2, 3)$, where the errors come from λ variations in the interval $[0.5,\, 2]$. The order $n = 3$ result that involves the $\mathcal{O}(\alpha_s^4)$ coefficient $a_4^{\rm PS}$ is 22% higher and within errors only marginally compatible with the result $N_{1/2}(n_\ell = 5) = 0.446 \pm 0.026$ of eq. (4.14). This indicates that $a_4^{\rm PS}$ in the standard convention is somewhat larger than expected assuming that the pole-PS mass series is dominated by the pole mass renormalon. The same observation has also been made in refs. [54, 102] in the context of relating the PS mass to the $\overline{\rm MS}$ mass.

It is interesting to consider other minimal subtraction scheme choices that differ from the standard scheme by reasonable variations of the subtraction scale μ. For example, for the choice $\mu/\mu_f = 1/5$ we obtain $N_{1/2}^{\mu/\mu_f=1/5} = 0.455 \pm 0.021$ at order $n = 3$ for $n_\ell = 5$, which is fully compatible with eq. (4.14). That the sum rule result for the PS mass agrees with the correct result of eq. (4.14) much better for a smaller infrared subtraction scale is quite suggestive because the infrared divergence in the static potential is known to be physically regulated by the massive quark kinetic energy, which is of order $\vec{q}^{\,2}/m_Q \sim \mu_f v$ where v is the relative velocity, and hence is parametrically smaller than $|\vec{q}| \sim \mu_f$. We stress that our analysis does neither validate nor invalidate the concept of the standard PS mass as a suitable mass scheme to carry out ongoing high-precision threshold studies [11, 13], as the sum rule only probes the calculated orders and the effect of the retardation singularity on the perturbative coefficients in the static potential beyond $\mathcal{O}(\alpha_s^4)$ on the PS mass scheme is unknown. However, the analysis demonstrates that the scheme dependence in the PS mass coming from the infrared divergences in the static potential at $\mathcal{O}(\alpha_s^4)$ is not a numerically irrelevant issue and may become even more serious beyond $\mathcal{O}(\alpha_s^4)$. As far as the known $\mathcal{O}(\alpha_s^4)$ results are concerned the issue already seems to affect the relation of the standard PS mass to the MSR and $\overline{\rm MS}$ masses as discussed in section 5.1.

JHEP04(2018)003

4.5.4 QCD β-function and massless quark R-ratio

As the concluding part of the discussion in this section we now apply the $\mathcal{O}(\Lambda_{\rm QCD})$ renormalon sum rule to series that are known not to be plagued by any $\mathcal{O}(\Lambda_{\rm QCD})$ renormalon. As examples we take the series for the QCD β-function with

$$a_n^\beta = \beta_{n-1}\,, \tag{4.33}$$

as defined in eq. (A.1) and the hadronic R-ratio for n_ℓ massless quarks

$$R(s) = 3\sum_{f=1}^{n_\ell} Q_f^2 \left[1 + \sum_{n=1}^{\infty} a_n^R \left(\frac{\alpha_s^{(n_\ell)}(\sqrt{s})}{4\pi}\right)^n\right], \tag{4.34}$$

where $\sqrt{s}$ stands for the center-of-mass energy, with [103–107]

$$\begin{aligned} a_1^R &= 4\,, \\ a_2^R &= 31.7712 - 1.8432\,n_\ell\,, \\ a_3^R &= -424.764 - 76.8083\,n_\ell - 0.33152\,n_\ell^2\,, \\ a_4^R &= -40092.2 + 4805.12\,n_\ell - 204.134\,n_\ell^2 + 5.504\,n_\ell^3\,, \end{aligned} \tag{4.35}$$

and Q_f stands for the quark electric charges. Applying the sum rule for $n_\ell = 4$ to the series for the QCD β-function we obtain

$$N_{1/2}^\beta = (0.829 \pm 0.497, -0.004 \pm 0.272, 0.065 \pm 0.092, 0.038 \pm 0.032)\,, \tag{4.36}$$

and applying it to the hadronic R-ratio we obtain

$$N_{1/2}^R = (0.398 \pm 0.239, -0.003 \pm 0.1311, -0.071 \pm 0.105, -0.009 \pm 0.029)\,, \tag{4.37}$$

at order $n = (0, 1, 2, 3)$. The errors are obtained from the variation $0.5 < \lambda < 2$. In both cases all results for $N_{1/2}$ beyond $\mathcal{O}(\alpha_s)$ are compatible with zero as expected. We note that at least for the hadronic R-ratio it is known that its perturbative series given in eq. (4.34) has a renormalon ambiguity that is suppressed and scales with the fourth power of the hadronic scale $\Lambda_{\rm QCD}$. This leads to an ambiguity in the R-ratio of $\mathcal{O}(\Lambda_{\rm QCD}^4/s^2)$, which is associated to the gluon condensate, and adding the effects of the gluon condensate in the context of an operator product expansion in terms of low-energy QCD matrix elements [108, 109] this ambiguity is compensated in a physical prediction. For the QCD β-function no conclusive statements on a higher-order renormalon ambiguity exist. The results in eqs. (4.36) and (4.37) show that the $\mathcal{O}(\Lambda_{\rm QCD})$ renormalon sum rule is only probing for an $\mathcal{O}(\Lambda_{\rm QCD})$ renormalon and not sensitive to any higher order renormalon ambiguity.

It is straightforward to generalize the sum rule discussed here to higher order renormalons, which has already been studied in ref. [78].

5 Relation to other short-distance masses

From the perturbative series that relate other short-distance masses to the pole mass it is straightforward to determine the perturbative series for the difference of these short-distance masses to the MSR masses by eliminating the pole mass systematically such that

the $\mathcal{O}(\Lambda_{\rm QCD})$ renormalon is canceled exactly. If regular fixed-order perturbation theory can be applied this is achieved by simply using a common renormalization scale μ and a consistent scheme for the strong coupling throughout the calculation when the pole mass is eliminated order by order. The corresponding formulae and codes for the relation of frequently used short-distance mass schemes (such as the kinetic mass [24], the PS mass [25], the 1S mass [26–28], the RS mass [29] and the jet mass [30, 43]) to the MSR masses can be obtained on request, and we therefore do not intend to cover all possible cases in this paper. However, we will cover several of them explicitly since there are a number of non-trivial practical and conceptual aspects that arise in the relation of the MSR masses to a number of other short-distance mass schemes we would like to point out in the following.

5.1 Potential subtracted mass

The relations of the PS mass [25] and the natural and practical MSR masses at the common scale R up to $\mathcal{O}(\alpha_s^4)$ have the form [$a_s \equiv \alpha_s^{(n_\ell)}(R)/(4\pi)$]

$$\begin{aligned} m_Q^{\rm PS}(\mu_f = R) - m_Q^{\rm MSRn}(R) = R\Big\{&[40.9928 - 3.6248\,n_\ell]\,a_s^2 + [963.44 - 184.87\,n_\ell \\ &+ 0.422\,n_\ell^2]\,a_s^3 + \Big[-(1749.\pm 417.) - (11168.\pm 10.)\,n_\ell \\ &+ 569.34\,n_\ell^2 - 0.89\,n_\ell^3 - 22739.57\log\Big(\frac{\mu}{R}\Big)\Big]\,a_s^4 + \ldots\Big\}, \end{aligned} \tag{5.1}$$

$$\begin{aligned} m_Q^{\rm PS}(\mu_f = R) - m_Q^{\rm MSRp}(R) = R\Big\{&[42.6499 - 3.6248\,n_\ell]\,a_s^2 + [1073.49 - 183.45\,n_\ell \\ &+ 0.422\,n_\ell^2]\,a_s^3 + \Big[-(1405.\pm 418.) - (11279.\pm 10.)\,n_\ell \\ &+ 573.74\,n_\ell^2 - 0.89\,n_\ell^3 - 22739.57\log\Big(\frac{\mu}{R}\Big)\Big]\,a_s^4 + \ldots\Big\}. \end{aligned} \tag{5.2}$$

For a conversion at the common scale $\mu_f = R$ the $\mathcal{O}(\alpha_s)$ corrections vanish identically indicating that this is the natural way to carry out the conversion. As pointed out already in section 4.5.3, the standard convention for the PS mass [99] corresponds to $\mu/\mu_f = 1$, such that the logarithmic term in the $\mathcal{O}(\alpha_s^4)$ correction is eliminated. In table 4 we show numerical results for the PS-MSR mass difference $m_Q^{\rm PS}(\mu_f = R) - m_Q^{\rm MSR}(R)$ for representative R values for $n_\ell = 5$ (relevant to the top quark) and $n_\ell = 4$ (relevant for the bottom quark) at different orders in α_s. The errors come from the variation of the renormalization scale μ of the strong coupling in the interval $[R/2, 2R]$, and the central values are the mean of the respective maximal and minimal values obtained in that interval. In figure 4a $m_Q^{\rm PS}(\mu_f = R) - m_Q^{\rm MSRn}(R)$ is shown at $\mathcal{O}(\alpha_s^2)$ (green), $\mathcal{O}(\alpha_s^3)$ (blue) and $\mathcal{O}(\alpha_s^4)$ (red) for $n_\ell = 5$ as a function of R between 20 and 160 GeV. The error bands are again obtained from variations of μ in the interval $[R/2, 2R]$. For the top quark case ($n_\ell = 5$) the PS and the MSR masses differ by about 20 to 300 MeV for R values between 2 and 160 GeV and for the bottom quark case ($n_\ell = 4$) they differ by about 30 to 40 MeV for R values below 5 GeV. So the PS and the MSR masses are quite close numerically.

The conspicuous property of the relation of the standard PS mass to the MSR masses at the common scale R is that the $\mathcal{O}(\alpha_s^4)$ correction is very large and far away from the

JHEP04(2018)003

R	$\mathcal{O}(\alpha_s^2)$	$\mathcal{O}(\alpha_s^3)$	$\mathcal{O}(\alpha_s^4)^{\mu/\mu_f=1}$	$\mathcal{O}(\alpha_s^4)^{\mu/\mu_f=1/5}$
	$m_t^{\rm PS}(\mu_f = R) - m_t^{\rm MSRn}(R) \quad (n_\ell = 5)$ [GeV]			
2	0.031 ± 0.016	0.022 ± 0.004	-0.027 ± 0.042	0.017 ± 0.006
5	0.037 ± 0.014	0.032 ± 0.002	0.007 ± 0.017	0.030 ± 0.002
10	0.050 ± 0.016	0.046 ± 0.002	0.024 ± 0.013	0.044 ± 0.002
40	0.110 ± 0.026	0.105 ± 0.003	0.081 ± 0.011	0.103 ± 0.001
80	0.174 ± 0.037	0.168 ± 0.003	0.138 ± 0.013	0.166 ± 0.002
160	0.282 ± 0.054	0.275 ± 0.005	0.236 ± 0.015	0.272 ± 0.002
	$m_t^{\rm PS}(\mu_f = R) - m_t^{\rm MSRp}(R) \quad (n_\ell = 5)$ [GeV]			
2	0.034 ± 0.018	0.028 ± 0.004	-0.024 ± 0.043	0.020 ± 0.007
5	0.040 ± 0.015	0.037 ± 0.003	0.012 ± 0.017	0.034 ± 0.003
10	0.054 ± 0.017	0.052 ± 0.003	0.030 ± 0.013	0.050 ± 0.002
40	0.118 ± 0.028	0.118 ± 0.004	0.094 ± 0.011	0.116 ± 0.002
80	0.186 ± 0.039	0.188 ± 0.005	0.158 ± 0.013	0.186 ± 0.002
160	0.302 ± 0.058	0.306 ± 0.007	0.267 ± 0.015	0.303 ± 0.002
	$m_b^{\rm PS}(\mu_f = R) - m_b^{\rm MSRn}(R) \quad (n_\ell = 4)$ [GeV]			
2	0.044 ± 0.027	0.034 ± 0.007	-0.041 ± 0.065	0.032 ± 0.005
3	0.041 ± 0.021	0.036 ± 0.005	-0.003 ± 0.030	0.036 ± 0.002
4	0.042 ± 0.019	0.038 ± 0.004	0.010 ± 0.021	0.039 ± 0.001
	$m_b^{\rm PS}(\mu_f = R) - m_b^{\rm MSRp}(R) \quad (n_\ell = 4)$ [GeV]			
2	0.047 ± 0.029	0.040 ± 0.009	-0.039 ± 0.068	0.034 ± 0.008
3	0.044 ± 0.022	0.041 ± 0.007	0.001 ± 0.031	0.039 ± 0.003
4	0.045 ± 0.020	0.043 ± 0.006	0.014 ± 0.022	0.043 ± 0.002

Table 4. Differences between the top mass in the PS and MSR schemes, showing both the natural and practical MSR mass definitions. Results are given for various scales $\mu_f = R$ and orders in α_s. At $\mathcal{O}(\alpha_s^4)$ results are shown for two choices of the infrared subtraction scale, $\mu/\mu_f = 1$ and $\mu/\mu_f = 1/5$.

$\mathcal{O}(\alpha_s^3)$ uncertainty band such that the $\mathcal{O}(\alpha_s^4)$ error band from scale variation is three to four times larger than the $\mathcal{O}(\alpha_s^3)$ one. For the top quark ($n_\ell = 5$) for R around 40 to 80 GeV, the typical range employed in studies of top pair production at threshold [11], the $\mathcal{O}(\alpha_s^3)$ and $\mathcal{O}(\alpha_s^4)$ central values differ by 23 MeV compared to scale variations of ± 4 MeV at $\mathcal{O}(\alpha_s^3)$ and ± 12 MeV at $\mathcal{O}(\alpha_s^4)$. For $R = 160$ GeV, the $\mathcal{O}(\alpha_s^3)$ and $\mathcal{O}(\alpha_s^4)$ central values even differ by 40 MeV compared to scale variations of about ± 4 MeV at $\mathcal{O}(\alpha_s^3)$ and ± 15 MeV at $\mathcal{O}(\alpha_s^4)$. A similar observation was made earlier in ref. [54]. Given this situation it is reasonable to use the difference of the $\mathcal{O}(\alpha_s^3)$ and $\mathcal{O}(\alpha_s^4)$ central values as the $\mathcal{O}(\alpha_s^4)$ uncertainty due to the missing higher order terms rather than the scale variation, leading

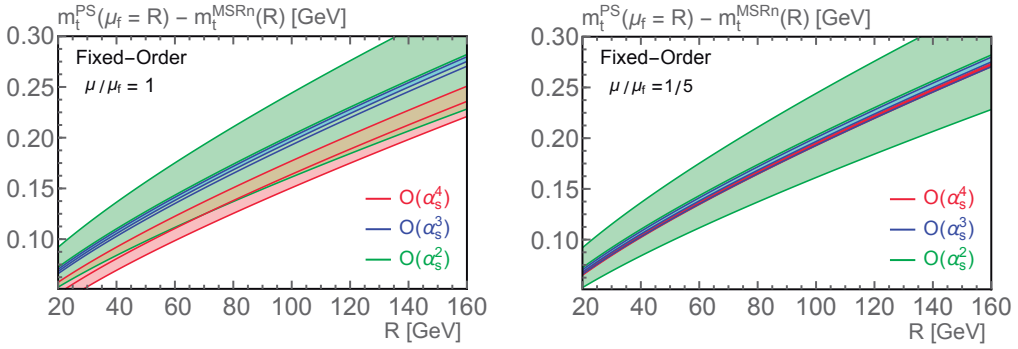

Figure 4. Difference between the natural MSR and PS ($\mu_f = R$) top quark mass ($n_\ell = 5$) as a function of R in GeV at two, three and four loops (the one loop result vanishes). Results are shown for two different choices of the IR subtraction scale, $\mu/\mu_f = 1$ and $\mu/\mu_f = 1/5$.

to uncertainties of about $(20, 25, 30, 40)$ MeV at $R = (10, 40, 80, 160)$ GeV. In ref. [54] the $\mathcal{O}(\alpha_s^4)$ uncertainty in the relation between the $\overline{\rm MS}$ mass $\overline{m}_Q \equiv \overline{m}_Q^{(n_\ell+1)}(\overline{m}_Q^{(n_\ell+1)})$ and the PS mass for $\mu_f = 20\,$GeV was quoted as 23 MeV, defined as half the size of the $\mathcal{O}(\alpha_s^4)$ correction. This issue is directly related to our observation made in section 4.5.3 that the $\mathcal{O}(\alpha_s^4)$ correction in the relation of the pole mass and the PS mass in the standard scheme [99] (with infrared subtraction scale $\mu/\mu_f = 1$) is much larger than expected from the $\mathcal{O}(\Lambda_{\rm QCD})$ renormalon of the pole mass.

In section 4.5.3 we also found that for the PS top mass in the infrared subtraction scheme with $\mu/\mu_f = 1/5$ there is much better consistency concerning the $\mathcal{O}(\Lambda_{\rm QCD})$ sum rule. Using the PS mass in this modified scheme the $\mathcal{O}(\alpha_s^4)$ corrections in this relation to the MSR masses reduce substantially, as can be easily spotted from the corresponding results in table 4 and in figure 4b: for the modified PS mass the $\mathcal{O}(\alpha_s^4)$ result for the PS-MSR mass difference is fully compatible with the $\mathcal{O}(\alpha_s^3)$ result and leads to scale variations that are about half the ones at $\mathcal{O}(\alpha_s^3)$. In this scheme it is therefore reasonable to quote the scale variations as the remaining perturbative error at $\mathcal{O}(\alpha_s^4)$. For all R values above 2 GeV and $n_\ell = 4$ and 5, the error in the $\mathcal{O}(\alpha_s^4)$ relation of the natural and the practical MSR masses and the PS mass in the modified scheme with $\mu/\mu_f = 1/5$ for the infrared scale is only about $\pm 2 - 3\,$MeV.

One may alternatively make the conversion between the PS mass $m_Q^{\rm PS}(\mu_f)$ and the MSR masses $m_Q^{\rm MSR}(R)$ for $\mu_f \neq R$, where we expand consistently in $\alpha_s(\mu)$ with a common scale μ. For the case $\mu_f < R$ we observe in general that the scale dependence of the $\mathcal{O}(\alpha_s^4)$ conversion formula for the standard convention for the PS scheme, $m_Q^{{\rm PS},\mu/\mu_f=1}(\mu_f) - m_Q^{\rm MSR}(R)$, decreases compared to the choice $\mu_f = R$, but the size of the $\mathcal{O}(\alpha_s^4)$ correction is still many times larger than the $\mathcal{O}(\alpha_s^3)$ scale variation. This can be seen for example for the case $(\mu_f, R) = (50, 100)\,$GeV were we obtain for $n_\ell = 5$ the numerical results $m_Q^{{\rm PS},\mu/\mu_f=1}(\mu_f) - m_Q^{\rm MSRn}(R) = (2.612 \pm 0.143, 2.925 \pm 0.042, 2.946 \pm 0.005, 2.922 \pm 0.005)\,$GeV at $\mathcal{O}(\alpha_s^{1,2,3,4})$

JHEP04(2018)003

for the standard PS mass scheme with renormalization scale variation $\mu_f < \mu < R$. This may be compared to the corresponding results for the modified PS mass scheme, which read $m_Q^{\mathrm{PS},\mu/\mu_f=1/5}(\mu_f) - m_Q^{\mathrm{MSRn}}(R) = (2.612 \pm 0.143, 2.925 \pm 0.042, 2.946 \pm 0.005, 2.939 \pm 0.002)$ GeV and show again a fully consistent behavior between the $\mathcal{O}(\alpha_s^3)$ and $\mathcal{O}(\alpha_s^4)$ results and their scale variations. On the other hand, for the case $\mu_f > R$ we observe in general that, at each given order, the size of the scale dependence of $m_Q^{\mathrm{PS},\mu/\mu_f=1}(\mu_f) - m_Q^{\mathrm{MSRn}}(R)$ is much smaller than the next correction. This can be seen for example for the case $(\mu_f, R) = (50, 25)$ GeV were we obtain for $n_\ell = 5$ the numerical results $m_Q^{\mathrm{PS},\mu/\mu_f=1}(\mu_f) - m_Q^{\mathrm{MSRn}}(R) = (-1.468 \pm 0.091, -1.456 \pm 0.005, -1.478 \pm 0.004, -1.504 \pm 0.007)$ GeV at $\mathcal{O}(\alpha_s^{1,2,3,4})$ for the standard PS mass scheme with the renormalization scale variation $R < \mu < \mu_f$. This may be compared to the corresponding results for the modified PS mass scheme which read $m_Q^{\mathrm{PS},\mu/\mu_f=1/5}(\mu_f) - m_Q^{\mathrm{MSRn}}(R) = (-1.468 \pm 0.091, -1.456 \pm 0.005, -1.478 \pm 0.004, -1.4767 \pm 0.0003)$ GeV, and yet again show a better behavior. So, also when the conversion between the standard PS mass and the MSR masses is carried out for $\mu_f \neq R$, the size of the $\mathcal{O}(\alpha_s^4)$ correction and not the usual renormalization scale variation must be taken as an estimate for the remaining perturbative error. Since the $\mathcal{O}(\alpha_s^4)$ corrections are typically in the range 20 – 40 MeV, making the conversion $\mu_f \neq R$ does not lead to any improvement in the perturbative relation between the standard PS mass and the MSR masses.

We conclude that the conversion of the MSR masses to the PS mass in the standard scheme of ref. [99] has, even at $\mathcal{O}(\alpha_s^4)$, perturbative uncertainties due to unknown higher-order terms of about 20 – 40 MeV and that this behavior is related to the fact that the $\mathcal{O}(\alpha_s^4)$ coefficient in the relation of the PS mass to the pole mass in the standard scheme appears to be unnaturally large in the context of its expected size with respect to the pole mass $\mathcal{O}(\Lambda_{\mathrm{QCD}})$ renormalon ambiguity. On the other hand, using an infrared subtraction scheme for the PS mass, where the subtraction scale is much lower, leads to a much better perturbative behavior and to much smaller uncertainties in its relation to the MSR masses. This observation is fully consistent with the conclusions from the renormalon sum rule analysis we carried out for the PS mass in section 4.5.3. Since the MSR masses for $R = \overline{m}_Q$ are very close or identical to the $\overline{\mathrm{MS}}$ mass $\overline{m}_Q(\overline{m}_Q)$ the conclusions we draw on the perturbative relation of the standard PS mass to the MSR masses also applies to the perturbative relation of the standard PS mass to the $\overline{\mathrm{MS}}$ mass. For $R = \overline{m}_Q$ the $\mathcal{O}(\alpha_s^4)$ correction is typically at the level of 40 MeV. We note that this issue of the standard PS mass scheme becomes problematic once a precision in top quarks mass determinations below 30 – 40 MeV can be reached. Given the projections of top mass determinations of a future lepton collider, see e.g. [110, 111], this may become a pressing issue, but for current studies of high-precision top quark mass determinations the standard PS mass scheme is adequate for most applications.

5.2 1S mass

The 1S mass [26–28] is defined as half of the mass of the heavy quarkonium spin triplet ground state. In terms of the pole mass the 1S mass is defined as

$$m_Q^{\mathrm{1S}} = m_Q^{\mathrm{pole}} + \left[C_F \alpha_s^{(n_\ell)}(\mu) m_Q^{\mathrm{pole}}\right] \sum_{n=1}^{\infty} \sum_{k=0}^{n-1} c_{n,k} \left(\frac{\alpha_s^{(n_\ell)}(\mu)}{4\pi}\right)^n \log^k \left(\frac{\mu}{C_F \alpha_s^{(n_\ell)}(\mu) m_Q^{\mathrm{pole}}}\right), \quad (5.3)$$

where the coefficients $c_{n,k}$ are known up to $n = 4$ and given for convenience in eq. (C.3). Because the 1S mass originates from a calculation in the non-relativistic context, there are a few subtleties when calculating its relation to the MSR masses so that the $\mathcal{O}(\Lambda_{\rm QCD})$ renormalon cancels properly.

For the case $R \sim m_Q$ it is essential that terms of order $[C_F\alpha_s m_Q]\alpha_s^n$ are formally counted as $\mathcal{O}(\alpha_s^n)$ in the conversion. This is because $[C_F\alpha_s m_Q]$ is the inverse Bohr radius, which is the relevant physical mass scale and should not be counted as an $\mathcal{O}(\alpha_s)$ correction. This counting is called the Υ-expansion [26, 27] or the relativistic order counting, and must also be used when relating the 1S mass to the $\overline{\rm MS}$ masses in fixed-order perturbation theory. The resulting formula for the 1S mass as a function of the MSR mass for $\mu = R$ up to $\mathcal{O}(\alpha_s^4)$ reads [defining parameters $M_B = C_F\alpha_s^{(n_\ell)}(R)\, m_Q^{\rm MSR}(R)$, $R_B = C_F\alpha_s^{(n_\ell)}(R)\, R$, $a_s = \alpha_s^{(n_\ell)}(R)/(4\pi)$, $L = \log(R/M_B)$ which are all functions of R]

$$
\begin{aligned}
m_Q^{\rm 1S} - m_Q^{\rm MSR}(R) = {}& [R\,a_1 + M_B\,c_{1,0}]\,a_s \\
&+ [R\,a_2 + R_B\,a_1\,c_{1,0} + M_B(c_{2,0}+c_{2,1}L)]\,a_s^2 \\
&+ \Big[R\,a_3 + R_B\Big(a_2\,c_{1,0} + a_1\,(c_{2,0} - c_{2,1}(1-L))\Big) + M_B\,(c_{3,0}+c_{3,1}L+c_{3,2}L^2)\Big]\,a_s^3 \\
&+ \Bigg[R\left(a_4 - \frac{R_B}{2m_Q^{\rm MSR}(R)}\,a_1^2\,c_{2,1}\right) + R_B\Big(a_3\,c_{1,0} + a_2\,(c_{2,0} - (1-L)\,c_{2,1}) \\
&\quad + a_1\,(c_{3,0} - c_{3,1} + (c_{3,1} - 2\,c_{3,2})L + c_{3,2}L^2)\Big) + M_B\,(c_{4,0}+c_{4,1}L+c_{4,2}L^2+c_{4,3}L^3)\Bigg]\,a_s^4 .
\end{aligned}
\tag{5.4}
$$

Here a_n are the coefficients in the MSR scheme. The inverse of eq. (5.4) is given in eq. (C.4).

For the case $R \sim m_Q\alpha_s$, which is relevant for non-relativistic applications where α_s may scale with the quark velocity $\alpha_s \sim v \ll 1$, the non-relativistic counting $R \sim M_B \sim m_Q\alpha_s$ should be used, such that the leading correction in the 1S-MSR mass difference is of order α_s^2. In this case the formula for the 1S mass as a function of the MSR mass for $\mu = R$ up to $\mathcal{O}(\alpha_s^5)$ reads [$M_B = C_F\alpha_s^{(n_\ell)}(R)\, m_Q^{\rm MSR}(R)$, $a_s = \alpha_s^{(n_\ell)}(R)/(4\pi)$, $L = \log(R/M_B)$]

$$
\begin{aligned}
m_Q^{\rm 1S} - m_Q^{\rm MSR}(R) = {}& \big[R\,a_1 + M_B\,c_{1,0}\big]\,a_s \\
&+ \big[R\,a_2 + M_B\,(c_{2,0} + c_{2,1}L)\big]\,a_s^2 \\
&+ \big[R\,(a_3 + 4\pi\,C_F\,a_1\,c_{1,0}) + M_B(c_{3,0} + c_{3,1}L + c_{3,2}L^2)\big]\,a_s^3 \\
&+ \Big[R\Big(a_4 + 4\pi\,C_F\,a_2\,c_{1,0} + 4\pi\,C_F\,a_1\,\big[c_{2,0} - c_{2,1}(1-L)\big]\Big) \\
&\quad + M_B\,\big(c_{4,0} + c_{4,1}L + c_{4,2}L^2 + c_{4,3}L^3\big)\Big]\,a_s^4 .
\end{aligned}
\tag{5.5}
$$

The inverse of eq. (5.5) is given in eq. (C.5). We note that in order to implement a general renormalization scale μ in eqs. (5.4) as well as (5.5), also the dependence of M_B on α_s needs to be accounted for consistently, which leads to quite involved expressions for the relativistic counting of the Υ-expansion. For the top quark and $R \sim m_t\alpha_s \sim 30\,\text{GeV}$ the numerical difference between using the relativistic or the non-relativistic counting is below 10 MeV at the highest order and may be not significant. However, for all other cases the difference can be more sizable such that a consistent use of the order counting is mandatory in general.

JHEP04(2018)003

R	m_t^{1S} [GeV]			
	$\mathcal{O}(\alpha_s)$	$\mathcal{O}(\alpha_s^2)$	$\mathcal{O}(\alpha_s^3)$	$\mathcal{O}(\alpha_s^4)$
160	167.934 ± 0.968	168.315 ± 0.151	168.397 ± 0.019	168.368 ± 0.021
	$\mathcal{O}(\alpha_s^2)$	$\mathcal{O}(\alpha_s^3)$	$\mathcal{O}(\alpha_s^4)$	$\mathcal{O}(\alpha_s^5)$
40	168.156 ± 0.113 (± 0.113)	168.409 ± 0.054 (± 0.054)	168.373 ± 0.019 (± 0.021)	168.372 ± 0.007 (± 0.011)
35	168.197 ± 0.077 (± 0.078)	168.421 ± 0.048 (± 0.049)	168.365 ± 0.026 (± 0.028)	168.371 ± 0.006 (± 0.011)
30	168.232 ± 0.037 (± 0.038)	168.434 ± 0.046 (± 0.047)	168.353 ± 0.036 (± 0.038)	168.372 ± 0.008 (± 0.012)

Table 5. Results for the top mass in the 1S mass scheme at different orders using as input the practical MSR mass $m_t^{\rm MSRp}(m_t^{\rm MSRp}) = 160\,\text{GeV}$. The results at the top of the table show the 1S mass using FOPT conversion in the relativistic order counting of eq. (5.4) with $R = 160\,\text{GeV}$. The conversion still contains large logarithms $\ln(m_Q/M_B)$. The lower three lines show the 1S mass using R-evolution from 160 GeV to $R = (30, 35, 40)\,\text{GeV}$ and then FOPT in the non-relativistic order counting of eq. (5.5) with the scale R. The logarithms $\ln(m_Q/M_B)$ are then summed to all orders, and the uncertainties are about a factor two smaller at the highest order. The uncertainties shown are explained in detail in the text.

In the top line of table 5 the top quark 1S mass is shown for the practical MSR top mass $m_t^{\rm MSRp}(m_t^{\rm MSRp}) = \overline{m}_t(\overline{m}_t) = R_0 = 160\,\text{GeV}$ using directly the relativistic conversion of eq. (5.4) at $\mathcal{O}(\alpha_s)$ to $\mathcal{O}(\alpha_s^4)$, where the quoted uncertainties have been obtained by renormalization scale variations $\sqrt{R_0\,M_B}/2 < \mu < R_0$ with $M_B = 23.2\,\text{GeV}$ and the central values are the mean of the respective maximal and minimal values obtained in the scale variation. In the lower three lines the conversion to the 1S mass is achieved by first using $\mathcal{O}(\alpha_s^4)$ R-evolution of $m_t^{\rm MSRp}(160\,\text{GeV})$ to $R = (30, 35, 40)\,\text{GeV}$, which gives $m_t^{\rm MSRp}(R) = (167.181{\pm}0.010, 166.854{\pm}0.009, 166.535{\pm}0.008)\,\text{GeV}$, where the uncertainties are obtained by variations of λ in the interval $[0.5, 2]$ and central values are the mean of the respective maximal and minimal values. Then the non-relativistic formula of eq. (5.5) is used to determine the 1S mass at $\mathcal{O}(\alpha_s^2)$ to $\mathcal{O}(\alpha_s^5)$. The quoted uncertainties are from renormalization scale variations $R/2 < \mu < 2R$. To these uncertainties the errors from the R-evolution calculation just shown above still have to be added quadratically to obtain the complete conversion uncertainty, which is shown in the parentheses. We see that the direct relativistic conversion, which does not account for the resummation of logarithms and renormalon corrections, leads to uncertainties of $\pm 20\,\text{MeV}$ at highest order, compared to $\pm\,(10-13)$ MeV for the conversion that uses R-evolution from 160 GeV down to non-relativistic scales $\sim M_B$. Given the projections of high precision top mass determinations at future lepton colliders [110–112], the increased precision obtained by using the resummation of higher order terms provided by R-evolution could be relevant, but for the conversion of the MSR mass (and also the $\overline{\rm MS}$ mass) to the 1S mass the fixed-order expansion is adequate for most current applications in top quark physics.

5.3 $\overline{\rm MS}$ mass

The relation of the MSR masses to the $\overline{\rm MS}$ mass is conceptually special since the MSR masses are directly derived from the perturbative series of the pole-$\overline{\rm MS}$ mass relation. The concept of the MSR mass addresses the conceptual question of how the $\overline{\rm MS}$ mass evolves for scales much smaller than the quark mass. This question simply expresses the situation that the $\overline{\rm MS}$ mass $\overline{m}_Q(\mu)$ for $\mu \ll m_Q$ can be readily computed solving its renormalization group equation, but does not have any physical significance, because it breaks the power counting of heavy quark problems involving (non-relativistic) physical scales much smaller than the mass. This power counting breaking comes from the perturbative series of the pole-$\overline{\rm MS}$ mass relation that scales with m_Q even for $\mu \ll m_Q$ and which spoils the perturbative series for non-relativistic problems where smaller dynamical scales govern the size of the perturbative corrections and the scale m_Q is integrated out and hence not a dynamical scale any more.

Since the perturbative series for the pole-MSR mass relations scale with R, which is adjustable, but also match to the pole-$\overline{\rm MS}$ mass series for $R = m_Q$, one can consider the concept of the MSR mass $m_Q^{\rm MSR}(\mu)$ as the most reasonable answer of how the $\overline{\rm MS}$ mass concept should be extended to scales $\mu \lesssim m_Q$. Thus for $\mu \lesssim m_Q$ R-evolution is the proper concept of the renormalization group running of a heavy quark mass for scales below m_Q. Both the natural and the practical MSR masses differ by the way how the virtual massive quark Q effects are treated in their matching relation to the $\overline{\rm MS}$ mass at the scale $\mu \sim m_Q$, and this matching may be considered in analogy to the flavor-number matching of the strong coupling schemes $\alpha_s^{(n_\ell)}(\mu)$ and $\alpha_s^{(n_\ell+1)}(\mu)$ when the scale μ crosses m_Q. In this context, the natural MSR mass is conceptually cleaner than the practical MSR mass, since in the natural MSR mass the virtual massive quark loops are integrated out at the scale $\mu = m_Q$, but this issue is irrelevant for practical applications, where the practical MSR mass has an advantage due to its simpler matching relation to the $\overline{\rm MS}$ mass.

The most efficient way to relate the MSR masses $m_Q^{\rm MSRn}(R)$ and $m_Q^{\rm MSRp}(R)$ to the $\overline{\rm MS}$ mass $\overline{m}_Q(\mu)$ is to (i) evolve the MSR masses from R to m_Q using the R-evolution equations eq. (3.3) with n_ℓ active flavors, (ii) employing the regular renormalization group equation for $\overline{m}_Q(\mu)$ to evolve it from μ to m_Q with $(n_\ell+1)$ active flavors,

$$\overline{m}_Q^{(n_\ell+1)}(m_Q) = \overline{m}_Q^{(n_\ell+1)}(\mu)\, \exp\left[-\sum_{k=0}^{\infty} \gamma_{m,k}^{(n_\ell+1)} \int_{\log \mu^2}^{\log m_Q^2} {\rm d}\log\bar\mu^2 \left(\frac{\alpha_s^{(n_\ell+1)}(\bar\mu)}{4\pi} \right)^{k+1} \right], \quad (5.6)$$

and then (iii) to apply the simple matching relations based on eq. (2.4) or eq. (2.7).

The solution of the R-evolution equation is [47] [$t_m = -2\pi/(\beta_0 \alpha_s^{(n_\ell)}(m_Q))$, $t_R = -2\pi/(\beta_0 \alpha_s^{(n_\ell)}(R))$]

$$\begin{aligned} m_Q^{\rm MSR}(m_Q) - m_Q^{\rm MSR}(R) &= -\sum_{n=0}^{\infty} \gamma_n^R \int_R^{m_Q} {\rm d}R \left(\frac{\alpha_s^{(n_\ell)}(R)}{4\pi} \right)^{n+1} \qquad (5.7) \\ &= \Lambda_{\rm QCD} \sum_{k=0}^{\infty} {\rm e}^{i\pi(\hat b_1+k)} S_k \left[\Gamma(-\hat b_1 - k, t_m) - \Gamma(-\hat b_1 - k, t_R) \right], \end{aligned}$$

where $\Lambda_{\rm QCD}$ and the coefficients γ_n^R, S_k and $\hat{b}_1$ are given in eqs. (A.6), (3.1), (A.15) and (A.4) and the series may be truncated at the desired order. The R-evolution equation can be solved numerically or by using the analytic expression in the second line of eq. (5.7).

The matching relations for the $\overline{\rm MS}$ and the natural MSR mass can be derived from eq. (2.4) and written in various ways quoted in the following. From $\overline{m}_Q \equiv \overline{m}_Q^{(n_\ell+1)}(\overline{m}_Q^{(n_\ell+1)})$ one can determine $m_Q^{\rm MSRn}(\overline{m}_Q)$ using the matching relations [$A_s \equiv \alpha_s^{(n_\ell+1)}(\overline{m}_Q)/(4\pi)$, $a_s \equiv \alpha_s^{(n_\ell)}(\overline{m}_Q)/(4\pi)$]

$$
\begin{aligned}
& m_Q^{\rm MSRn}(\overline{m}_Q^{(n_\ell+1)}) - \overline{m}_Q^{(n_\ell+1)}(\overline{m}_Q^{(n_\ell+1)}) \\
&\quad = \overline{m}_Q^{(n_\ell+1)}(\overline{m}_Q^{(n_\ell+1)})\Big\{ 1.65707\, A_s^2 + [110.05 + 1.424\, n_\ell]\, A_s^3 + [(352. \pm 31.) \\
&\qquad\qquad - (111.59 \pm 0.10)\, n_\ell + 4.40 n_\ell^2]\, A_s^4 \Big\} \\
&\quad = \overline{m}_Q^{(n_\ell+1)}(\overline{m}_Q^{(n_\ell+1)})\Big\{ 1.65707\, a_s^2 + [110.05 + 1.424\, n_\ell]\, a_s^3 + [(344. \pm 31.) \\
&\qquad\qquad - (111.59 \pm 0.10)\, n_\ell + 4.40\, n_\ell^2]\, a_s^4 \Big\},
\end{aligned}
\tag{5.8}
$$

where the superscript $(n_\ell+1)$ is a reminder of the active flavors used to run the $\overline{\rm MS}$ mass. Given $m_Q^{\rm MSRn} \equiv m_Q^{{\rm MSRn},(n_\ell)}(m_Q^{{\rm MSRn},(n_\ell)})$ one can determine $\overline{m}_Q^{(n_\ell+1)}(\overline{m}_Q^{(n_\ell+1)})$ by the relations $\big[\bar{A}_s \equiv \alpha_s^{(n_\ell+1)}(m_Q^{\rm MSRn})/(4\pi)$, $\bar{a}_s \equiv \alpha_s^{(n_\ell)}(m_Q^{\rm MSRn})/(4\pi)\big]$

$$
\begin{aligned}
& \overline{m}_Q^{(n_\ell+1)}(\overline{m}_Q^{(n_\ell+1)}) - m_Q^{{\rm MSRn},(n_\ell)}(m_Q^{{\rm MSRn},(n_\ell)}) \\
&\quad = m_Q^{{\rm MSRn},(n_\ell)}(m_Q^{{\rm MSRn},(n_\ell)})\Big\{ -1.65707\, \bar{A}_s^2 - [101.21 + 1.424\, n_\ell]\, \bar{A}_s^3 \\
&\qquad\qquad + [(349. \pm 31.) + (103.35 \pm 0.10)\, n_\ell - 4.40\, n_\ell^2]\, \bar{A}_s^4 \Big\} \\
&\quad = m_Q^{{\rm MSRn},(n_\ell)}(m_Q^{{\rm MSRn},(n_\ell)})\Big\{ -1.65707\, \bar{a}_s^2 - [101.21 + 1.424\, n_\ell]\, \bar{a}_s^3 \\
&\qquad\qquad + [(357. \pm 31.) + (103.35 \pm 0.10)\, n_\ell - 4.40\, n_\ell^2]\, \bar{a}_s^4 \Big\},
\end{aligned}
\tag{5.9}
$$

where the superscript (n_ℓ) is a reminder of the active flavors used to run the MSR mass. We have displayed the matching relations both for the n_ℓ and the $(n_\ell+1)$-flavor scheme for the strong coupling. The corresponding matching relations for the strong coupling at the scales $\overline{m}_Q$ and $m_Q^{\rm MSRn}$ are shown for convenience in eqs. (A.7) and (A.9), respectively.

Numerically, $m_t^{\rm MSRn}(m_t) - \overline{m}_t(\overline{m}_t)$ is about 30 MeV for $\overline{m}_t(\overline{m}_t)$ around 160 GeV. The perturbative uncertainties in this matching relations from missing higher orders are 1 MeV or lower for all massive quarks. The numerical uncertainties in the $\mathcal{O}(\alpha_s^4)$ coefficients given in eqs. (5.8) and (5.9) are quoted from ref. [55] and smaller than 0.01 MeV. Thus the matching relations can be taken as exact for all foreseeable applications.

The matching relations for the $\overline{\rm MS}$ and the practical MSR mass simply reads

$$
m_Q^{{\rm MSRp},(n_\ell)}(m_Q^{{\rm MSRp},(n_\ell)}) = \overline{m}_Q^{(n_\ell+1)}(\overline{m}_Q^{(n_\ell+1)})\,,
\tag{5.10}
$$

to all orders of perturbation theory, where in comparison to eq. (2.7) we have also explicitly indicated the flavor number of the evolution of the MSR mass and the $\overline{\rm MS}$ mass.

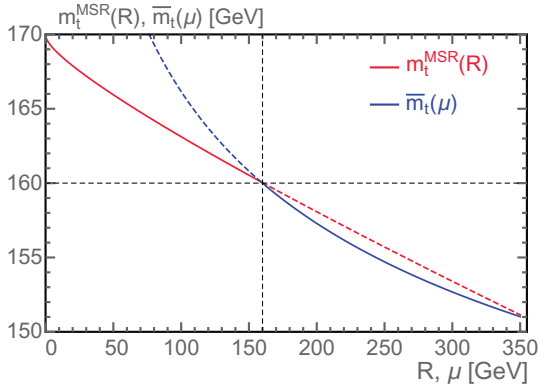

Figure 5. Comparison of the scale dependence for the $\overline{\rm MS}$ and the MSR top quark masses ($n_\ell = 5$) as a function of μ and R in GeV.

In figure 5 we show the scale dependence of the MSR masses $m_t^{\rm MSR}(R)$ (red line) and the $\overline{\rm MS}$ mass $\overline{m}_t(\mu)$ (blue line) for $\overline{m}_t^{(n_\ell+1)}(\overline{m}_t^{(n_\ell+1)}) = 160\,\text{GeV}$. The difference between the natural and practical MSR masses is not visible on the scale of this figure. The solid curves represent the evolution of the masses in regions where they should be used for physical applications in close analogy to the flavor-number-dependent scale dependence of the strong coupling, while the dashed lines show their evolution beyond these regions. At the scale 160 GeV the two mass schemes are matched via eq. (5.8), eq. (5.9) and eq. (5.10). For $R < m_t$ the MSR mass $m_t^{\rm MSR}(R)$ is substantially smaller than the $\overline{\rm MS}$ mass $\overline{m}_t(R)$ and approaches the pole mass for $R \to 0$. The MSR mass remains well defined for all $R \gtrsim \Lambda_{\rm QCD}$, whereas the exact value for the limit $m_t^{\rm MSR}(R \to 0)$ is ambiguous due to the Landau pole in the evolution of the strong coupling in the R-evolution equation (5.7). This illustrates the ambiguity of the pole mass concept.

6 Conclusions

This paper had two main aims. The first aim was to give a detailed presentation of the MSR mass, which is an R-dependent short-distance mass designed for high-precision determinations of heavy quark masses from quantities where the physical scales are smaller than the quark mass, $R < m_Q$. Since such scale hierarchies can only be really large for the top quark, the MSR mass concept is most useful in the context of top quark physics, but it may be useful for bottom and charm quark analyses as well. The MSR mass is obtained from the results of heavy quark on-shell self-energy diagrams which is not the case for any earlier low-scale short-distance mass given in the literature. The MSR mass has therefore a very close relation to the well-known $\overline{\rm MS}$ mass $\overline{m}_Q(\mu)$, and should be viewed as the generalization of the $\overline{\rm MS}$ mass concept for renormalization scales below m_Q, where the $\overline{\rm MS}$ mass is known to be impractical and does not capture the proper physics. The main feature of the MSR mass is that its renormalization group evolution is linear and logarithmic in the scale R, compared to the purely logarithmic evolution of the $\overline{\rm MS}$

mass. This linear scale dependence in the renormalization group flow of the MSR mass is called R-evolution and the MSR mass is well defined for any $R \gtrsim \Lambda_{\rm QCD}$. Formally, in the limit $R \to 0$, the MSR mass can be evolved to the pole mass. However, taking this limit is ambiguous as it involves evolving the strong coupling through the Landau pole, which illustrates the $\mathcal{O}(\Lambda_{\rm QCD})$ ambiguity of the pole mass scheme. Since there are two options to treat the corrections coming from virtual heavy quark loops in the heavy quark self-energy diagrams, we defined two variants of the MSR mass, the *natural MSR mass* $m_Q^{\rm MSRn}(R)$, where these effects are integrated out, and the *practical MSR mass* $m_Q^{\rm MSRp}(R)$, where they are still included in the mass definition. Both MSR masses can be easily related to all other short-distance mass schemes available in the literature. We have provided all necessary formulae such that conversions can be carried out to $\mathcal{O}(\alpha_s^4)$ and we have discussed in detail the cases where there are subtleties in the conversion.

The second aim of the paper was to give a detailed presentation of how R-evolution can be used to derive an analytic expression for the normalization of the high-order asymptotic behavior of the MSR-pole (or $\overline{\rm MS}$-pole) mass perturbative series related to the $\mathcal{O}(\Lambda_{\rm QCD})$ renormalon ambiguity contained in the pole mass. This analytic result can be applied to any perturbative series and be used to probe the known coefficients for the series pattern related to an $\mathcal{O}(\Lambda_{\rm QCD})$ renormalon ambiguity. Since using the result does not involve any numerical comparison of the series coefficients, but is a very simple analytic function of the coefficients, we call it the $\mathcal{O}(\Lambda_{\rm QCD})$ *renormalon sum rule*. Using the sum rule we reanalyzed the $\mathcal{O}(\Lambda_{\rm QCD})$ renormalon in the MSR-pole (and $\overline{\rm MS}$-pole) perturbative series and showed that the sum rule results are fully compatible with previous available methods. We examined the relation between these methods to our sum rule analytically and explained the reason why one of them has very slow convergence. We also applied the sum rule to a number of other quantities known to high order and demonstrated its high sensitivity. These examples included the PS-pole mass relation, the moments of the massive quark vacuum polarization, the hadronic R-ratio and the QCD β-function.

Acknowledgments

We acknowledge partial support by the FWF Austrian Science Fund under the Doctoral Program No. W1252-N27 and the Project No. P28535-N27, the U.S. Department of Energy under the Grant No. DE-SC0011090, the Simons Foundation through the Grant 327942, the Spanish MINECO "Ramón y Cajal" program (RYC-2014-16022), MECD grants FPA2016-78645-P, FPA2014-53375-C2-2-P and FPA2016-75654-C2-2-P, the group UPARCOS, the IFT "Centro de Excelencia Severo Ochoa" Program under Grant SEV-2012-0249 and by the Ramanujan Fellowship of SERB, DST. We also thank the Erwin-Schrödinger International Institute for Mathematics and Physics, the University of Vienna and Cultural Section of the City of Vienna (MA7) for partial support.

Note added. After this paper was originally posted the comments in ref. [113] appeared. We have added appendix B to make a comparison of our sum rule with the method and formulas discussed there.

A QCD β-function and coefficients

For the QCD β-function in the $\overline{\rm MS}$ scheme we use the convention

$$\frac{\mathrm{d}\alpha_s(R)}{\mathrm{d}\log R} = \beta(\alpha_s(R)) = -2\,\alpha_s(R)\sum_{n=0}^{\infty}\beta_n\left(\frac{\alpha_s(R)}{4\pi}\right)^{n+1}, \tag{A.1}$$

where $\beta_0 = 11 - 2/3\,n_\ell$ with n_ℓ being the number of dynamical flavors. The coefficients are known up to β_4 from refs. [80, 114–119]. The equation can be used to write [$\alpha_i \equiv \alpha_s(R_i)$, $t = -2\pi/(\beta_0\alpha_s(R))$]

$$\log\frac{R_1}{R_0} = \int_{\alpha_0}^{\alpha_1}\frac{\mathrm{d}\alpha}{\beta(\alpha)} = \int_{t_1}^{t_0}\mathrm{d}t\,\hat{b}(t) = G(t_0) - G(t_1)\,, \tag{A.2}$$

where

$$\hat{b}(t) = 1 + \sum_{k=1}^{\infty}\frac{\hat{b}_k}{t^k}, \qquad G(t) = t + \hat{b}_1\log(-t) - \sum_{k=2}^{\infty}\frac{\hat{b}_k}{(k-1)\,t^{k-1}}\,, \tag{A.3}$$

and the first four coefficients relevant for renormalon sum rule applications up to $\mathcal{O}(\alpha_s^4)$ are

$$\begin{aligned}
\hat{b}_1 &= \frac{\beta_1}{2\beta_0^2}\,, & \hat{b}_3 &= \frac{1}{8\beta_0^6}(\beta_1^3 - 2\,\beta_0\,\beta_1\beta_2 + \beta_0^2\,\beta_3), \\
\hat{b}_2 &= \frac{1}{4\beta_0^4}(\beta_1^2 - \beta_0\,\beta_2)\,, & \hat{b}_4 &= \frac{1}{16\beta_0^8}(\beta_1^4 - 3\,\beta_0\,\beta_1^2\,\beta_2 + \beta_0^2\,\beta_2^2 + 2\,\beta_0^2\,\beta_1\,\beta_3 - \beta_0^3\,\beta_4)\,.
\end{aligned} \tag{A.4}$$

One can show the following recursion relation for the $\hat{b}_k$ coefficients ($\hat{b}_0 \equiv 1$):

$$\hat{b}_{n+1} = 2\sum_{i=0}^{n}\frac{\hat{b}_{n-i}\,\beta_{i+1}}{(-2\beta_0)^{i+2}}\,, \tag{A.5}$$

which can be used for an automated computation. From eq. (A.2) one can also derive the known relation

$$\Lambda_{\rm QCD} = R_i\,\mathrm{e}^{G(t_i)}\,, \tag{A.6}$$

that gives $\Lambda_{\rm QCD}^{\rm N^kLL}$ if the series in $G(t_i)$ is truncated after the k-th term.

The matching relations for the strong coupling in the n_ℓ and the $(n_\ell{+}1)$-flavor schemes at the scale $\overline{m}_Q \equiv \overline{m}_Q^{(n_\ell+1)}(\overline{m}_Q^{(n_\ell+1)})$ read

$$\begin{aligned}
\alpha_s^{(n_\ell)}(\overline{m}_Q) = \alpha_s^{(n_\ell+1)}(\overline{m}_Q)\Bigg[1 &+ 0.152778\left(\frac{\alpha_s^{(n_\ell+1)}(\overline{m}_Q)}{\pi}\right)^2 \\
&+ (0.972057 - 0.08465\,n_\ell)\left(\frac{\alpha_s^{(n_\ell+1)}(\overline{m}_Q)}{\pi}\right)^3 + \ldots\Bigg]\,,
\end{aligned} \tag{A.7}$$

$$\begin{aligned}
\alpha_s^{(n_\ell+1)}(\overline{m}_Q) = \alpha_s^{(n_\ell)}(\overline{m}_Q)\Bigg[1 &- 0.152778\left(\frac{\alpha_s^{(n_\ell)}(\overline{m}_Q)}{\pi}\right)^2 \\
&- (0.972057 - 0.08465\,n_\ell)\left(\frac{\alpha_s^{(n_\ell)}(\overline{m}_Q)}{\pi}\right)^3 + \ldots\Bigg]\,.
\end{aligned} \tag{A.8}$$

JHEP04(2018)003

The matching relations for the strong coupling in the n_ℓ and the $(n_\ell+1)$ flavor schemes at the scale $m_Q^{\rm MSRn} \equiv m_Q^{{\rm MSRn},(n_\ell)}(m_Q^{{\rm MSRn},(n_\ell)})$ read

$$\alpha_s^{(n_\ell)}(m_Q^{\rm MSRn}) = \alpha_s^{(n_\ell+1)}(m_Q^{\rm MSRn})\biggl[1 + 0.152778\biggl(\frac{\alpha_s^{(n_\ell+1)}(m_Q^{\rm MSRn})}{\pi}\biggr)^2 + (0.93753 - 0.08465\,n_\ell)\biggl(\frac{\alpha_s^{(n_\ell+1)}(m_Q^{\rm MSRn})}{\pi}\biggr)^3 + \ldots\biggr], \tag{A.9}$$

$$\alpha_s^{(n_\ell+1)}(m_Q^{\rm MSRn}) = \alpha_s^{(n_\ell)}(m_Q^{\rm MSRn})\biggl[1 - 0.152778\biggl(\frac{\alpha_s^{(n_\ell)}(m_Q^{\rm MSRn})}{\pi}\biggr)^2 - (0.93753 - 0.08465\,n_\ell)\biggl(\frac{\alpha_s^{(n_\ell)}(m_Q^{\rm MSRn})}{\pi}\biggr)^3 + \ldots\biggr]. \tag{A.10}$$

The R-anomalous dimension coefficients γ_n^R take the following numerical values for the natural MSR mass:

$$\begin{aligned}
\gamma_0^{Rn} &= \frac{16}{3}\,,\\
\gamma_1^{Rn} &= 96.1039 - 9.55076\,n_\ell\,,\\
\gamma_2^{Rn} &= 1595.75 - 269.953\,n_\ell - 2.65945\,n_\ell^2\,,\\
\gamma_3^{Rn} &= (12319.\pm 417.) - (9103.\pm 10.)\,n_\ell + 610.264\,n_\ell^2 - 6.515\,n_\ell^3\,,
\end{aligned} \tag{A.11}$$

whereas for the practical MSR mass the coefficients are:

$$\begin{aligned}
\gamma_0^{Rp} &= \frac{16}{3}\,,\\
\gamma_1^{Rp} &= 97.761 - 9.55076\,n_\ell\,,\\
\gamma_2^{Rp} &= 1632.89 - 264.11\,n_\ell - 2.65945\,n_\ell^2\,,\\
\gamma_3^{Rp} &= (4724.\pm 418.) - (8784.\pm 10.)\,n_\ell + 620.362\,n_\ell^2 - 6.515\,n_\ell^3\,.
\end{aligned} \tag{A.12}$$

The uncertainties appearing in the coefficients $\gamma_3^{Rn,Rp}$ are from numerical errors in the results of ref. [55]. They amount to an uncertainty in the solutions of the R-evolution equation of 1 MeV or less for all relevant cases and are smaller than the uncertainty due to missing higher orders. Therefore they can be neglected for all practical purposes.

The coefficients g_ℓ defined by the series $\sum_{\ell=0}^\infty g_\ell\,(-t)^{-\ell} \equiv {\rm e}^{G(t)}\,{\rm e}^{-t}\,(-t)^{-\hat b_1}$ relevant for the renormalon sum rule up to $\mathcal{O}(\alpha_s^4)$ read

$$g_0 = 1\,,\qquad g_1 = \hat b_2\,,\qquad g_2 = \frac{1}{2}(\hat b_2^2 - \hat b_3)\,,\qquad g_3 = \frac{1}{6}(\hat b_2^3 - 3\,\hat b_2\,\hat b_3 + 2\,\hat b_4)\,. \tag{A.13}$$

One can proof the following recursion relation for g_ℓ:

$$g_{n+1} = \frac{1}{1+n}\sum_{i=0}^{n}(-1)^i\,\hat b_{i+2}\,g_{n-i}\,, \tag{A.14}$$

suitable for automated computation. The coefficients g_ℓ agree with the coefficients s_ℓ given in refs. [73, 77].

The coefficients S_k defined from the series $\sum_{k=0}^{\infty} S_k(-t)^{-k} \equiv -t\gamma^R(t)\,\hat{b}(t)\mathrm{e}^{-G(t)}\mathrm{e}^t(-t)^{\hat{b}_1}$ relevant up to $\mathcal{O}(\alpha_s^4)$ read $[\tilde{\gamma}_k^R = \gamma_k^R/(2\beta_0)^{k+1}]$

$$
\begin{aligned}
S_0 &= \tilde{\gamma}_0^R = \frac{a_1}{2\beta_0}\,, \\
S_1 &= \tilde{\gamma}_1^R - (\hat{b}_1+\hat{b}_2)\,\tilde{\gamma}_0^R = \frac{a_2}{4\beta_0^2} - \frac{a_1}{2\beta_0}(1+\hat{b}_1+\hat{b}_2)\,, \\
S_2 &= \tilde{\gamma}_2^R - (\hat{b}_1+\hat{b}_2)\,\tilde{\gamma}_1^R + \left[(1+\hat{b}_1)\,\hat{b}_2 + \frac{1}{2}(\hat{b}_2^2+\hat{b}_3)\right]\tilde{\gamma}_0^R \\
&= \frac{a_3}{8\beta_0^3} - \frac{a_2}{4\beta_0^2}(2+\hat{b}_1+\hat{b}_2) + \frac{a_1}{2\beta_0}\left[(2+\hat{b}_1)\,\hat{b}_2 + \frac{1}{2}(\hat{b}_2^2+\hat{b}_3)\right], \\
S_3 &= \tilde{\gamma}_3^R - (\hat{b}_1+\hat{b}_2)\,\tilde{\gamma}_2^R + \left[(1+\hat{b}_1)\,\hat{b}_2 + \frac{1}{2}(\hat{b}_2^2+\hat{b}_3)\right]\tilde{\gamma}_1^R \\
&\quad - \left[\left(1+\frac{1}{2}\hat{b}_1+\frac{1}{6}\hat{b}_2\right)\hat{b}_2^2 + \left(1+\frac{1}{2}\hat{b}_1+\frac{1}{2}\hat{b}_2\right)\hat{b}_3 + \frac{1}{3}\,\hat{b}_4\right]\tilde{\gamma}_0^R \\
&= \frac{a_4}{16\beta_0^4} - \frac{a_3}{8\beta_0^3}(3+\hat{b}_1+\hat{b}_2) + \frac{a_2}{4\beta_0^2}\left[(3+\hat{b}_1)\,\hat{b}_2 + \frac{1}{2}(\hat{b}_2^2+\hat{b}_3)\right] \\
&\quad - \frac{1}{2}\frac{a_1}{2\beta_0}\left[\left(3+\hat{b}_1+\frac{1}{3}\hat{b}_2\right)\hat{b}_2^2 + \left(3+\hat{b}_1+\hat{b}_2\right)\hat{b}_3 + \frac{2}{3}\,\hat{b}_4\right].
\end{aligned}
\tag{A.15}
$$

The relation between the S_k coefficients and the R-anomalous dimension can be compactly written as follows:

$$
\begin{aligned}
S_k = \tilde{\gamma}_k^R - (1-\delta_{k,0})\,(\hat{b}_1+\hat{b}_2)\,\tilde{\gamma}_{k-1}^R + \sum_{n=0}^{k-2}\tilde{\gamma}_n^R\Bigg[\tilde{g}_{k-n} + (-1)^{k-n}\hat{b}_{k-n} \\
+ \sum_{\ell=1}^{k-n-1}(-1)^{k-n-\ell}\,\tilde{g}_\ell\,\hat{b}_{k-n-\ell}\Bigg],
\end{aligned}
\tag{A.16}
$$

$$
\tilde{g}_{n+1} = -\frac{1}{1+n}\sum_{i=0}^{n}(-1)^i\,\hat{b}_{i+2}\,\tilde{g}_{n-i}\,, \qquad \tilde{g}_0 = 1\,. \tag{A.17}
$$

In addition one can use eq. (4.19) to write a recursion relation for the S_k coefficients, which are then expressed in terms of a_i :

$$
S_k = \frac{a_{k+1}}{(2\beta_0)^{k+1}} - \sum_{n=0}^{k-1} S_n \sum_{\ell=0}^{k-n} g_\ell\,(1+\hat{b}_1+n)_{k-\ell-n}\,, \tag{A.18}
$$

where $(b)_n = b\,(b+1)\cdots(b+n-1) = \Gamma(b+n)/\Gamma(b)$ is the Pochhammer symbol. This formula can be used for an automated implementation of S_k once the g_ℓ coefficients have been computed. We note that in order to determine the coefficients S_k, one needs all terms up to k loops in the R-evolution equation, and the $(k+1)$-loop QCD β-function.

B Alternative derivation of the $\mathcal{O}(\Lambda_{\rm QCD})$ renormalon sum rule

In section 4.1 we have shown how to directly derive the sum rule formula for $N_{1/2}$ displayed in eq. (4.8) from the computation of the Borel transform of eq. (4.7) starting from the solution of the R-evolution equation given in eq. (4.1). There is an interesting alternative way to determine the sum rule formula which starts from the Borel function $B_{\alpha_s(R)}(u)$

JHEP04(2018)003

given in eq. (4.7) without knowing the expression for $N_{1/2}$. This expression is equivalent to the Borel transform of the original series $-R\sum_{i=1}^{\infty} a_i\,[\alpha_s(R)/(4\pi)]^i$ which has the form:

$$B_{\alpha_s(R)}(u) = -R\sum_{i=1}^{\infty} a_i\,\frac{u^{i-1}}{\Gamma(i)}\,\beta_0^{-i}\,, \tag{B.1}$$

in the fixed-order expansion in powers of the Borel variable u.

Consider now the modified Borel function $(\beta_0/4\pi R)(1-2u)^{1+\hat{b}_1}B_{\alpha_s(R)}(u)$. Inserting eq. (4.7) for $B_{\alpha_s(R)}(u)$ one obtains:

$$\begin{aligned}\frac{\beta_0}{4\pi R}(1-2u)^{1+\hat{b}_1}B_{\alpha_s(R)}(u) = -N_{1/2}\sum_{\ell=0}^{\infty} g_\ell\,\frac{\Gamma(1+\hat{b}_1-\ell)}{\Gamma(1+\hat{b}_1)}\,(1-2u)^{\ell} \\ +\frac{\beta_0}{2\pi}(1-2u)^{1+\hat{b}_1}\sum_{\ell=0}^{\infty} g_\ell\,Q_\ell(u)\,,\end{aligned} \tag{B.2}$$

where the role of analytic and non-analytic terms is just reversed compared to eq. (4.7). Truncating the series in ℓ at order n (which corresponds to including the coefficients a_i, S_k, g_ℓ up to $i=n+1$, $k=n$ and $\ell=n$, respectively), one can see that expanding eq. (B.2) in powers of u up to order n and taking the limit $u\to 1/2$ one singles out $N_{1/2}$ on the r.h.s.:

$$\begin{aligned}-N_{1/2}^{(n)} + \frac{\beta_0}{2\pi}\sum_{k=0}^{n}\sum_{m=0}^{k}\sum_{i=k-m+1}^{n}\sum_{\ell=0}^{i}(-1)^m\,g_\ell\,S_{i-\ell} \\ \times\frac{\Gamma(2+\hat{b}_1)}{\Gamma(m+1)\,\Gamma(2+\hat{b}_1-m)}\,\frac{\Gamma(1+\hat{b}_1+k-m-\ell)}{\Gamma(1+\hat{b}_1+i-\ell)\Gamma(k-m+1)}\,,\end{aligned} \tag{B.3}$$

where $N_{1/2}^{(n)}$ refers to the $(n+1)$-loop approximation for $N_{1/2}$. Applying the same procedure to the Borel transform of eq. (B.1) and solving for $N_{1/2}^{(n)}$ one obtains:

$$\begin{aligned}N_{1/2}^{(n)} = \frac{1}{4\pi}\sum_{k=0}^{n}\sum_{m=0}^{k}\frac{(-1)^m}{(2\beta_0)^{k-m}}\,\frac{\Gamma(2+\hat{b}_1)a_{k-m+1}}{\Gamma(k-m+1)\Gamma(m+1)\Gamma(2+\hat{b}_1-m)} \\ +\frac{\beta_0}{2\pi}\sum_{k=0}^{n}\sum_{m=0}^{k}\sum_{i=k-m+1}^{n}\sum_{\ell=0}^{i}(-1)^m\,g_\ell\,S_{i-\ell} \\ \times\frac{\Gamma(2+\hat{b}_1)}{\Gamma(m+1)\Gamma(2+\hat{b}_1-m)}\,\frac{\Gamma(1+\hat{b}_1+k-m-\ell)}{\Gamma(1+\hat{b}_1+i-\ell)\Gamma(k-m+1)}\,.\end{aligned} \tag{B.4}$$

Although lengthier, it can be checked that this formula agrees exactly with the sum rule of eq. (4.8) at $(n+1)$-loop order (i.e. when truncated with $k\le n$ as shown).

In ref. [29] (see also ref. [68]), a version of the above considerations to determine the normalization of the non-analytic terms in eq. (4.7), which we refer to as the Borel method, was proposed. They made the additional assumption that the analytic terms on the r.h.s. of eq. (4.7) can be neglected because they quickly tend to zero when multiplied by $(1-2u)^{1+\hat{b}_1}$ in the limit $u\to 1/2$. Therefore they did not include the terms related to the polynomials Q_ℓ. This leads to a formula for the normalization that only contains the first term on the

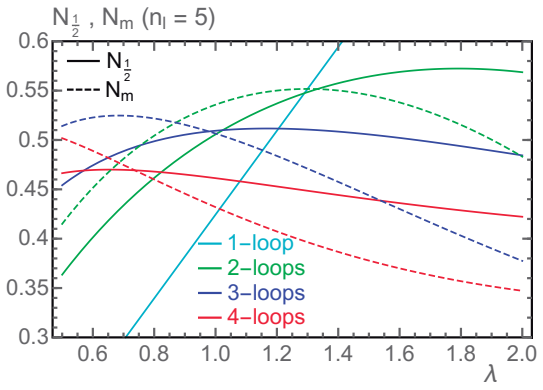

Figure 6. Comparison of $N_{1/2}^{(n)}$ and $N_m^{(n)}$ for $n_\ell = 5$. Results are shown as a function of λ including contributions from one to four loops.

r.h.s. of eq. (B.4), which they called N_m. After a bit of algebra, the double sum of this term can be recast into a single summation, yielding:[6]

$$N_m^{(n)} = \frac{1}{4\pi} \sum_{m=0}^{n} \frac{(-\hat{b}_1)_{n-m}\, a_{m+1}}{(2\beta_0)^m\, m!\, (n-m)!}\,. \tag{B.6}$$

However, the contribution from the second term on the r.h.s. of eq. (B.4) is actually not negligible because it involves the expansion of the $(1-2u)^{1+\hat{b}_1}$ and setting $u = 1/2$ afterwards. In particular, the β-function coefficients $\beta_{n>1}$ contained in the g_ℓ are essential for the cancellation of the λ-dependence with n beyond 2-loop order, i.e. for $n > 1$.

This is shown in figure 6 where we plot $N_{1/2}^{(n)}$ (solid lines) and $N_m^{(n)}$ (dashed lines) obtained from the natural MSR mass for $n = 0$ (cyan), $n = 1$ (green), $n = 2$ (blue) and $n = 3$ (red) for $n_\ell = 5$ as a function of λ in the interval [0.5, 2]. We see that the results for $N_m^{(n)}$ differ substantially from $N_{1/2}^{(n)}$ showing that the terms neglected in the approach of ref. [29] are numerically sizable and, in particular, do not decrease with the order n. Moreover, the results for $N_m^{(n)}$ do not appear to show any reduced λ-dependence beyond 2-loop order, in contrast to the results for $N_{1/2}^{(n)}$. Interestingly, in ref. [69] it has been shown that

[6] We note that no analytic formula for $N_m^{(n)}$ was provided in ref. [29], and that eq. (B.6) correctly encodes the prescription given there. In formula (7) of ref. [113] the following analytic double series formula was given:

$$\begin{aligned} N_m &= \frac{1}{\nu} \sum_{m,n'=0}^{\infty} \frac{\Gamma(2+b)(-1)^m r_{n'}(\nu)}{\Gamma(m+1)\Gamma(n'+1)\Gamma(2+b-m)} \left(\frac{2\pi}{\beta_0}\right)^{n'} \\ &= \frac{1}{4\pi} \sum_{m,n'=0}^{\infty} \frac{\Gamma(2+\hat{b}_1)(-1)^m a_{n'+1}}{\Gamma(m+1)\Gamma(n'+1)\Gamma(2+\hat{b}_1-m)} \frac{1}{(2\beta_0)^{n'}}\,, \end{aligned} \tag{B.5}$$

where in the second line we have converted to our conventions for ease of comparison. Eq. (B.5) is not fully specified because it does not provide a prescription how to systematically truncate the two series in order to compute N_m at $(n+1)$-loop order. The sum for $(1-2u)^{1+\hat{b}_1} = \sum_{m=0}^{\infty}(2u)^m\Gamma(2+\hat{b}_1)/[\Gamma(m+1)\Gamma(2+\hat{b}_1-m)]$ converges to zero at $u = 1/2$, while the other, which is eq. (B.1), is divergent for $u = 1/2$. To obtain eq. (B.6) from eq. (B.5) one switches variable from (m, n') to (k, m) with $k = m + n'$, and then finally truncates with respect to the variable k.

JHEP04(2018)003

when many more terms of the expansion are known [they accounted for terms up to $\mathcal{O}(\alpha_s^{20})$ for the quark and gluino QCD static potential], eq. (B.6) does eventually converge to the right value and shows reduced scale variation. We have numerically confirmed that using series generated from the Borel function of eq. (4.7) setting (by hand) explicit expressions for the functions $Q_\ell(u)$, such as $Q_\ell(u) = \delta_{\ell,0}$. The eventual convergence at very high orders n can be understood from the fact that the contributions in the asymptotic behavior of the perturbative coefficients a_n that arise from the β-function coefficients $\beta_{n>1}$ become $1/n$ suppressed and eventually become also numerically small, see eqs. (4.16) and (4.19). But in any case, its very slow convergence renders the Borel method less practical and less precise for most phenomenological applications, for which only a few terms of the perturbative expansion are known.

C Other short distance masses

The PS mass [25] is defined by the integral of the momentum space color singlet static potential between a quark-antiquark pair, each having infinite mass. The relation of the PS mass to the pole mass has the form

$$m_Q^{\rm pole} - m_Q^{\rm PS}(\mu_f) = \mu_f \sum_{n=1}^{\infty} a_n^{\rm PS} \left(\frac{\alpha_s^{(n_\ell)}(\mu_f)}{4\pi} \right)^n , \tag{C.1}$$

where the coefficients are known up to $\mathcal{O}(\alpha_s^4)$ based on refs. [100, 101, 120–124], and have the form

$$\begin{aligned}
a_1^{\rm PS} &= \frac{16}{3} , \\
a_2^{\rm PS} &= 172.4444 - 13.03704\, n_\ell , \\
a_3^{\rm PS} &= 11111.55 - 1522.482\, n_\ell + 41.350\, n_\ell^2 , \\
a_4^{\rm PS} &= 913336.84 - 179514.95\, n_\ell + 10535.70\, n_\ell^2 - 172.72\, n_\ell^3 + 22739.57 \log\left(\frac{\mu}{\mu_f}\right) .
\end{aligned} \tag{C.2}$$

In the standard convention for the PS mass defined in ref. [99] the term $\log(\mu/\mu_f)$ appearing in $a_4^{\rm PS}$ is set to zero.

The definition of the 1S mass [26–28] in terms of the pole mass is given in eq. (5.3) and the coefficients $c_{n,k}$ up to $\mathcal{O}(\alpha_s^5)$ read [26–28, 124–126]

$$\begin{aligned}
c_{1,0} &= -2.09440 , \\
c_{2,0} &= -135.438 + 10.2393\, n_\ell , \\
c_{2,1} &= -92.1534 + 5.5851\, n_\ell , \\
c_{3,0} &= -11324.72 + 1372.745\, n_\ell - 38.9677\, n_\ell^2 , \\
c_{3,1} &= -7766.02 + 1077.92\, n_\ell - 33.5103\, n_\ell^2 , \\
c_{3,2} &= -3041.06 + 368.61\, n_\ell - 11.1701\, n_\ell^2 , \\
c_{4,0} &= -1005116.33 + 176714.27\, n_\ell - 10088.35\, n_\ell^2 + 168.57\, n_\ell^3 - 63574.35\, \log(\alpha_s^{(n_\ell)}(\mu)) , \\
c_{4,1} &= -901778.56 + 162559.51\, n_\ell - 9263.14\, n_\ell^2 + 163.15\, n_\ell^3 , \\
c_{4,2} &= -303000.33 + 61184.26\, n_\ell - 3823.90\, n_\ell^2 + 74.47\, n_\ell^3 , \\
c_{4,3} &= -89204.48 + 16219.00\, n_\ell - 982.97\, n_\ell^2 + 19.86\, n_\ell^3 .
\end{aligned} \tag{C.3}$$

Employing the Υ-expansion (relativistic order counting) the formula for the MSR masses as a function of the 1S mass up to $\mathcal{O}(\alpha_s^4)$ reads [$M_B^{\rm 1S} = C_F\,\alpha_s^{(n_\ell)}(R)\,m_Q^{\rm 1S}$, $A_R = C_F\,\alpha_s^{(n_\ell)}(R)$, $a_s = \alpha_s^{(n_\ell)}(R)/(4\pi)$, $L = \log(R/M_B^{\rm 1S})$]

$$
\begin{aligned}
m_Q^{\rm MSR}(R) - m_Q^{\rm 1S} =& -\left[R\,a_1 + M_B^{\rm 1S}\,c_{1,0}\right] a_s \\
&- \left[R\,a_2 - M_B^{\rm 1S}\Big(A_R\,c_{1,0}^2 - c_{2,0} - c_{2,1}L\Big)\right] a_s^2 \\
&- \left[R\,a_3 + M_B^{\rm 1S}\Big(A_R^2\,c_{1,0}^3 - A_R\,c_{1,0}\Big(2\,c_{2,0} - c_{2,1} + 2\,c_{2,1}L\Big) + c_{3,0} + c_{3,1}L + c_{3,2}L^2\Big)\right] a_s^3 \\
&- \Bigg[R\,a_4 - M_B^{\rm 1S}\Bigg(A_R^3\,c_{1,0}^4 - A_R^2\,c_{1,0}^2\Big(3\,c_{2,0} - \Big(\frac{5}{2} - 3\,L\Big)\,c_{2,1}\Big) \\
&\quad + A_R\Big(c_{2,0}\,(c_{2,0} - (1-2\,L)\,c_{2,1}) - (1-L)\,c_{2,1}^2 L + c_{1,0}\big(2\,c_{3,0} \\
&\quad - (1-2\,L)\,c_{3,1} - 2\,(1-L)\,c_{3,2}\,L\big)\Big) - c_{4,0} - c_{4,1}L - c_{4,2}L^2 - c_{4,3}L^3\Bigg)\Bigg] a_s^4 .
\end{aligned}
\tag{C.4}
$$

Employing the non-relativistic order counting the formula for the MSR masses as a function of the 1S mass up to $\mathcal{O}(\alpha_s^5)$ reads [$M_B^{1S} = C_F\,\alpha_s^{(n_\ell)}(R)\,m_Q^{\rm 1S}$, $a_s = \alpha_s^{(n_\ell)}(R)/(4\pi)$, $L = \log(R/M_B^{1S})$]

$$
\begin{aligned}
m_Q^{\rm MSR}(R) - m_Q^{\rm 1S} =& -\left[R\,a_1 + M_B^{\rm 1S}\,c_{1,0}\right] a_s \\
&- \left[R\,a_2 + M_B^{\rm 1S}\Big(c_{2,0} + c_{2,1}L\Big)\right] a_s^2 \\
&- \left[R\,a_3 - M_B^{\rm 1S}\Big(4\pi\,C_F\,c_{1,0}^2 - c_{3,0} - c_{3,1}L - c_{3,2}L^2\Big)\right] a_s^3 \\
&- \Big[R\,a_4 - M_B^{\rm 1S}\Big(4\pi\,C_F\,c_{1,0}\big(2\,c_{2,0} - (1-2\,L)\,c_{2,1}\big) \\
&\quad - c_{4,0} - c_{4,1}L - c_{4,2}L^2 - c_{4,3}L^3\Big)\Big] a_s^4 .
\end{aligned}
\tag{C.5}
$$

JHEP04(2018)003

References

[1] B. Dehnadi, A.H. Hoang, V. Mateu and S.M. Zebarjad, *Charm Mass Determination from QCD Charmonium Sum Rules at Order α_s^3*, *JHEP* **09** (2013) 103 [arXiv:1102.2264] [INSPIRE].

[2] S. Bodenstein, J. Bordes, C.A. Dominguez, J. Penarrocha and K. Schilcher, *QCD sum rule determination of the charm-quark mass*, *Phys. Rev.* **D 83** (2011) 074014 [arXiv:1102.3835] [INSPIRE].

[3] S. Bodenstein, J. Bordes, C.A. Dominguez, J. Penarrocha and K. Schilcher, *Bottom-quark mass from finite energy QCD sum rules*, *Phys. Rev.* **D 85** (2012) 034003 [arXiv:1111.5742] [INSPIRE].

[4] A. Hoang, P. Ruiz-Femenia and M. Stahlhofen, *Renormalization Group Improved Bottom Mass from Upsilon Sum Rules at NNLL Order*, *JHEP* **10** (2012) 188 [arXiv:1209.0450] [INSPIRE].

[5] B. Chakraborty et al., *High-precision quark masses and QCD coupling from $n_f = 4$ lattice QCD*, *Phys. Rev.* **D 91** (2015) 054508 [arXiv:1408.4169] [INSPIRE].

[6] B. Colquhoun, R.J. Dowdall, C.T.H. Davies, K. Hornbostel and G.P. Lepage, *Υ and Υ' Leptonic Widths, a_μ^b and m_b from full lattice QCD*, *Phys. Rev.* **D 91** (2015) 074514 [arXiv:1408.5768] [INSPIRE].

[7] M. Beneke, A. Maier, J. Piclum and T. Rauh, *The bottom-quark mass from non-relativistic sum rules at NNNLO*, *Nucl. Phys.* **B 891** (2015) 42 [arXiv:1411.3132] [INSPIRE].

[8] C. Ayala, G. Cvetič and A. Pineda, *The bottom quark mass from the $\Upsilon(1S)$ system at NNNLO*, *JHEP* **09** (2014) 045 [arXiv:1407.2128] [INSPIRE].

[9] B. Dehnadi, A.H. Hoang and V. Mateu, *Bottom and Charm Mass Determinations with a Convergence Test*, *JHEP* **08** (2015) 155 [arXiv:1504.07638] [INSPIRE].

[10] J. Erler, P. Masjuan and H. Spiesberger, *Charm Quark Mass with Calibrated Uncertainty*, *Eur. Phys. J.* **C 77** (2017) 99 [arXiv:1610.08531] [INSPIRE].

[11] A.H. Hoang et al., *Top-anti-top pair production close to threshold: Synopsis of recent NNLO results*, *Eur. Phys. J. direct* **2** (2000) 3 [hep-ph/0001286] [INSPIRE].

[12] A.H. Hoang and M. Stahlhofen, *The Top-Antitop Threshold at the ILC: NNLL QCD Uncertainties*, *JHEP* **05** (2014) 121 [arXiv:1309.6323] [INSPIRE].

[13] M. Beneke, Y. Kiyo, P. Marquard, A. Penin, J. Piclum and M. Steinhauser, *Next-to-Next-to-Next-to-Leading Order QCD Prediction for the Top Antitop S-Wave Pair Production Cross Section Near Threshold in e^+e^- Annihilation*, *Phys. Rev. Lett.* **115** (2015) 192001 [arXiv:1506.06864] [INSPIRE].

[14] M. Czakon, P. Fiedler and A. Mitov, *Total Top-Quark Pair-Production Cross Section at Hadron Colliders Through $O(\alpha_s^4)$*, *Phys. Rev. Lett.* **110** (2013) 252004 [arXiv:1303.6254] [INSPIRE].

[15] CMS collaboration, *Measurement of the t-tbar production cross section in the e-mu channel in proton-proton collisions at $\sqrt{s} = 7$ and 8 TeV*, *JHEP* **08** (2016) 029 [arXiv:1603.02303] [INSPIRE].

[16] ATLAS collaboration, *Measurement of the $t\bar{t}$ production cross-section using $e\mu$ events with b-tagged jets in pp collisions at $\sqrt{s}$=13 TeV with the ATLAS detector*, *Phys. Lett.* **B 761** (2016) 136 [*Erratum ibid.* **B 772** (2017) 879] [arXiv:1606.02699] [INSPIRE].

[17] M. Czakon, P. Fiedler, D. Heymes and A. Mitov, *NNLO QCD predictions for fully-differential top-quark pair production at the Tevatron*, *JHEP* **05** (2016) 034 [arXiv:1601.05375] [INSPIRE].

[18] S. Alioli et al., *A new observable to measure the top-quark mass at hadron colliders*, *Eur. Phys. J.* **C 73** (2013) 2438 [arXiv:1303.6415] [INSPIRE].

[19] S. Frixione and A. Mitov, *Determination of the top quark mass from leptonic observables*, *JHEP* **09** (2014) 012 [arXiv:1407.2763] [INSPIRE].

[20] CMS collaboration, *Measurement of masses in the $t\bar{t}$ system by kinematic endpoints in pp collisions at $\sqrt{s} = 7$ TeV*, *Eur. Phys. J.* **C 73** (2013) 2494 [arXiv:1304.5783] [INSPIRE].

[21] A. Kharchilava, *Top mass determination in leptonic final states with J/ψ*, *Phys. Lett.* **B 476** (2000) 73 [hep-ph/9912320] [INSPIRE].

JHEP04(2018)003

[22] I.I.Y. Bigi, M.A. Shifman, N.G. Uraltsev and A.I. Vainshtein, *The pole mass of the heavy quark. Perturbation theory and beyond*, *Phys. Rev.* **D 50** (1994) 2234 [hep-ph/9402360] [INSPIRE].

[23] M. Beneke and V.M. Braun, *Heavy quark effective theory beyond perturbation theory: Renormalons, the pole mass and the residual mass term*, *Nucl. Phys.* **B 426** (1994) 301 [hep-ph/9402364] [INSPIRE].

[24] A. Czarnecki, K. Melnikov and N. Uraltsev, *NonAbelian dipole radiation and the heavy quark expansion*, *Phys. Rev. Lett.* **80** (1998) 3189 [hep-ph/9708372] [INSPIRE].

[25] M. Beneke, *A Quark mass definition adequate for threshold problems*, *Phys. Lett.* **B 434** (1998) 115 [hep-ph/9804241] [INSPIRE].

[26] A.H. Hoang, Z. Ligeti and A.V. Manohar, *B decay and the Upsilon mass*, *Phys. Rev. Lett.* **82** (1999) 277 [hep-ph/9809423] [INSPIRE].

[27] A.H. Hoang, Z. Ligeti and A.V. Manohar, *B decays in the upsilon expansion*, *Phys. Rev.* **D 59** (1999) 074017 [hep-ph/9811239] [INSPIRE].

[28] A.H. Hoang, *1S and MS-bar bottom quark masses from Upsilon sum rules*, *Phys. Rev.* **D 61** (2000) 034005 [hep-ph/9905550] [INSPIRE].

[29] A. Pineda, *Determination of the bottom quark mass from the $\Upsilon(1S)$ system*, *JHEP* **06** (2001) 022 [hep-ph/0105008] [INSPIRE].

[30] A. Jain, I. Scimemi and I.W. Stewart, *Two-loop Jet-Function and Jet-Mass for Top Quarks*, *Phys. Rev.* **D 77** (2008) 094008 [arXiv:0801.0743] [INSPIRE].

[31] S. Fleming, A.H. Hoang, S. Mantry and I.W. Stewart, *Jets from massive unstable particles: Top-mass determination*, *Phys. Rev.* **D 77** (2008) 074010 [hep-ph/0703207] [INSPIRE].

[32] K. Seidel, F. Simon, M. Tesar and S. Poss, *Top quark mass measurements at and above threshold at CLIC*, *Eur. Phys. J.* **C 73** (2013) 2530 [arXiv:1303.3758] [INSPIRE].

[33] T. Horiguchi et al., *Study of top quark pair production near threshold at the ILC*, arXiv:1310.0563 [INSPIRE].

[34] M. Vos et al., *Top physics at high-energy lepton colliders*, arXiv:1604.08122 [INSPIRE].

[35] CMS collaboration, *Measurement of the top quark mass using proton-proton data at $\sqrt{(s)} = 7$ and 8 TeV*, *Phys. Rev.* **D 93** (2016) 072004 [arXiv:1509.04044] [INSPIRE].

[36] ATLAS collaboration, *Measurement of the top quark mass in the $t\bar{t} \to$ dilepton channel from $\sqrt{s} = 8$ TeV ATLAS data*, *Phys. Lett.* **B 761** (2016) 350 [arXiv:1606.02179] [INSPIRE].

[37] CDF, D0 collaboration, T.E.W. Group, *Combination of CDF and D0 results on the mass of the top quark using up to 9.7 fb^{-1} at the Tevatron*, arXiv:1407.2682 [INSPIRE].

[38] M. Butenschoen, B. Dehnadi, A.H. Hoang, V. Mateu, M. Preisser and I.W. Stewart, *Top Quark Mass Calibration for Monte Carlo Event Generators*, *Phys. Rev. Lett.* **117** (2016) 232001 [arXiv:1608.01318] [INSPIRE].

[39] A.H. Hoang, S. Mantry, A. Pathak and I.W. Stewart, *Extracting a Short Distance Top Mass with Light Grooming*, arXiv:1708.02586 [INSPIRE].

[40] A.H. Hoang and I.W. Stewart, *Top Mass Measurements from Jets and the Tevatron Top-Quark Mass*, *Nucl. Phys. Proc. Suppl.* **185** (2008) 220 [arXiv:0808.0222] [INSPIRE].

JHEP04(2018)003

[41] A.H. Hoang, *The Top Mass: Interpretation and Theoretical Uncertainties*, in *Proceedings, 7th International Workshop on Top Quark Physics (TOP2014)*, Cannes, France, September 28-October 3, 2014 [arXiv:1412.3649] [INSPIRE].

[42] I.W. Stewart, F.J. Tackmann and W.J. Waalewijn, *N-Jettiness: An Inclusive Event Shape to Veto Jets*, *Phys. Rev. Lett.* **105** (2010) 092002 [arXiv:1004.2489] [INSPIRE].

[43] S. Fleming, A.H. Hoang, S. Mantry and I.W. Stewart, *Factorization approach for top mass reconstruction at high energies*, *eConf* **C 0705302** (2007) LOOP06 [arXiv:0710.4205] [INSPIRE].

[44] A.H. Hoang and I.W. Stewart, *Designing gapped soft functions for jet production*, *Phys. Lett.* **B 660** (2008) 483 [arXiv:0709.3519] [INSPIRE].

[45] A.H. Hoang, C. Lepenik and M. Preisser, *On the Light Massive Flavor Dependence of the Large Order Asymptotic Behavior and the Ambiguity of the Pole Mass*, *JHEP* **09** (2017) 099 [arXiv:1706.08526] [INSPIRE].

[46] V. Mateu and P.G. Ortega, *Bottom and Charm Mass determinations from global fits to $Q\bar{Q}$ bound states at N^3LO*, *JHEP* **01** (2018) 122 [arXiv:1711.05755] [INSPIRE].

[47] A.H. Hoang, A. Jain, I. Scimemi and I.W. Stewart, *Infrared Renormalization Group Flow for Heavy Quark Masses*, *Phys. Rev. Lett.* **101** (2008) 151602 [arXiv:0803.4214] [INSPIRE].

[48] R. Tarrach, *The Pole Mass in Perturbative QCD*, *Nucl. Phys.* **B 183** (1981) 384 [INSPIRE].

[49] N. Gray, D.J. Broadhurst, W. Grafe and K. Schilcher, *Three Loop Relation of Quark $\overline{\rm MS}$ and Pole Masses*, *Z. Phys.* **C 48** (1990) 673 [INSPIRE].

[50] K. Melnikov and T.v. Ritbergen, *The Three loop relation between the $\overline{\rm MS}$ and the pole quark masses*, *Phys. Lett.* **B 482** (2000) 99 [hep-ph/9912391] [INSPIRE].

[51] K.G. Chetyrkin and M. Steinhauser, *Short distance mass of a heavy quark at order α_s^3*, *Phys. Rev. Lett.* **83** (1999) 4001 [hep-ph/9907509] [INSPIRE].

[52] K.G. Chetyrkin and M. Steinhauser, *The Relation between the $\overline{\rm MS}$ and the on-shell quark mass at order α_s^3*, *Nucl. Phys.* **B 573** (2000) 617 [hep-ph/9911434] [INSPIRE].

[53] P. Marquard, L. Mihaila, J.H. Piclum and M. Steinhauser, *Relation between the pole and the minimally subtracted mass in dimensional regularization and dimensional reduction to three-loop order*, *Nucl. Phys.* **B 773** (2007) 1 [hep-ph/0702185] [INSPIRE].

[54] P. Marquard, A.V. Smirnov, V.A. Smirnov and M. Steinhauser, *Quark Mass Relations to Four-Loop Order in Perturbative QCD*, *Phys. Rev. Lett.* **114** (2015) 142002 [arXiv:1502.01030] [INSPIRE].

[55] P. Marquard, A.V. Smirnov, V.A. Smirnov, M. Steinhauser and D. Wellmann, *$\overline{\rm MS}$-on-shell quark mass relation up to four loops in QCD and a general* SU(N) *gauge group*, *Phys. Rev.* **D 94** (2016) 074025 [arXiv:1606.06754] [INSPIRE].

[56] M.B. Voloshin, *'Optical' sum rule for form-factors of heavy mesons*, *Phys. Rev.* **D 46** (1992) 3062 [INSPIRE].

[57] I.I.Y. Bigi, M.A. Shifman and N. Uraltsev, *Aspects of heavy quark theory*, *Ann. Rev. Nucl. Part. Sci.* **47** (1997) 591 [hep-ph/9703290] [INSPIRE].

[58] A.H. Hoang, A. Jain, I. Scimemi and I.W. Stewart, *R-evolution: Improving perturbative QCD*, *Phys. Rev.* **D 82** (2010) 011501 [arXiv:0908.3189] [INSPIRE].

JHEP04(2018)003

[59] R. Abbate, M. Fickinger, A.H. Hoang, V. Mateu and I.W. Stewart, *Thrust at N^3LL with Power Corrections and a Precision Global Fit for $\alpha_s(m_Z)$*, *Phys. Rev.* **D 83** (2011) 074021 [arXiv:1006.3080] [INSPIRE].

[60] R. Abbate, M. Fickinger, A.H. Hoang, V. Mateu and I.W. Stewart, *Precision Thrust Cumulant Moments at N^3LL*, *Phys. Rev.* **D 86** (2012) 094002 [arXiv:1204.5746] [INSPIRE].

[61] A.H. Hoang, D.W. Kolodrubetz, V. Mateu and I.W. Stewart, *C-parameter distribution at N^3LL' including power corrections*, *Phys. Rev.* **D 91** (2015) 094017 [arXiv:1411.6633] [INSPIRE].

[62] A.H. Hoang, D.W. Kolodrubetz, V. Mateu and I.W. Stewart, *Precise determination of α_s from the C-parameter distribution*, *Phys. Rev.* **D 91** (2015) 094018 [arXiv:1501.04111] [INSPIRE].

[63] S. Gritschacher, A. Hoang, I. Jemos and P. Pietrulewicz, *Two loop soft function for secondary massive quarks*, *Phys. Rev.* **D 89** (2014) 014035 [arXiv:1309.6251] [INSPIRE].

[64] P. Pietrulewicz, S. Gritschacher, A.H. Hoang, I. Jemos and V. Mateu, *Variable Flavor Number Scheme for Final State Jets in Thrust*, *Phys. Rev.* **D 90** (2014) 114001 [arXiv:1405.4860] [INSPIRE].

[65] V. Mateu, I.W. Stewart and J. Thaler, *Power Corrections to Event Shapes with Mass-Dependent Operators*, *Phys. Rev.* **D 87** (2013) 014025 [arXiv:1209.3781] [INSPIRE].

[66] G.S. Bali and A. Pineda, *QCD phenomenology of static sources and gluonic excitations at short distances*, *Phys. Rev.* **D 69** (2004) 094001 [hep-ph/0310130] [INSPIRE].

[67] F. Campanario and A. Pineda, *Fit to the Bjorken, Ellis-Jaffe and Gross-Llewellyn-Smith sum rules in a renormalon based approach*, *Phys. Rev.* **D 72** (2005) 056008 [hep-ph/0508217] [INSPIRE].

[68] T. Lee, *Renormalons beyond one loop*, *Phys. Rev.* **D 56** (1997) 1091 [hep-th/9611010] [INSPIRE].

[69] G.S. Bali, C. Bauer, A. Pineda and C. Torrero, *Perturbative expansion of the energy of static sources at large orders in four-dimensional* SU(3) *gauge theory*, *Phys. Rev.* **D 87** (2013) 094517 [arXiv:1303.3279] [INSPIRE].

[70] M. Beneke, P. Marquard, P. Nason and M. Steinhauser, *On the ultimate uncertainty of the top quark pole mass*, *Phys. Lett.* **B 775** (2017) 63 [arXiv:1605.03609] [INSPIRE].

[71] A.S. Kronfeld, *The Perturbative pole mass in QCD*, *Phys. Rev.* **D 58** (1998) 051501 [hep-ph/9805215] [INSPIRE].

[72] A.L. Kataev and V.S. Molokoedov, *On the flavour dependence of the $\mathcal{O}(\alpha_s^4)$ correction to the relation between running and pole heavy quark masses*, *Eur. Phys. J. Plus* **131** (2016) 271 [arXiv:1511.06898] [INSPIRE].

[73] M. Beneke, *Renormalons*, *Phys. Rept.* **317** (1999) 1 [hep-ph/9807443] [INSPIRE].

[74] S. Bekavac, A. Grozin, D. Seidel and M. Steinhauser, *Light quark mass effects in the on-shell renormalization constants*, *JHEP* **10** (2007) 006 [arXiv:0708.1729] [INSPIRE].

[75] A.H. Hoang, *Bottom quark mass from Upsilon mesons: Charm mass effects*, hep-ph/0008102 [INSPIRE].

JHEP04(2018)003

[76] K.G. Chetyrkin, B.A. Kniehl and M. Steinhauser, *Decoupling relations to O (alpha-S^3) and their connection to low-energy theorems*, *Nucl. Phys.* **B 510** (1998) 61 [hep-ph/9708255] [INSPIRE].

[77] M. Beneke, *More on ambiguities in the pole mass*, *Phys. Lett.* **B 344** (1995) 341 [hep-ph/9408380] [INSPIRE].

[78] A. Jain, *Heavy quarks in effective field theories*, Ph.D. Thesis, Massachusetts Institute of Technology (2009).

[79] J. Komijani, *A discussion on leading renormalon in the pole mass*, *JHEP* **08** (2017) 062 [arXiv:1701.00347] [INSPIRE].

[80] P.A. Baikov, K.G. Chetyrkin and J.H. Kühn, *Five-Loop Running of the QCD coupling constant*, *Phys. Rev. Lett.* **118** (2017) 082002 [arXiv:1606.08659] [INSPIRE].

[81] M. Beneke and V.M. Braun, *Naive nonAbelianization and resummation of fermion bubble chains*, *Phys. Lett.* **B 348** (1995) 513 [hep-ph/9411229] [INSPIRE].

[82] K.G. Chetyrkin, B.A. Kniehl and A. Sirlin, *Estimations of order α_s^3 and α_s^4 corrections to mass dependent observables*, *Phys. Lett.* **B 402** (1997) 359 [hep-ph/9703226] [INSPIRE].

[83] A.L. Kataev and V.T. Kim, *Peculiar features of the relations between pole and running heavy quark masses and estimates of the $O(\alpha_s^4)$ contributions*, *Phys. Part. Nucl.* **41** (2010) 946 [arXiv:1001.4207] [INSPIRE].

[84] Y. Sumino, *Estimate of 4-loop Pole-MSbar Mass Relation from Static QCD Potential*, *Phys. Lett.* **B 728** (2014) 73 [arXiv:1309.5436] [INSPIRE].

[85] G.S. Bali, C. Bauer and A. Pineda, *The static quark self-energy at $O(\alpha^{20})$ in perturbation theory*, PoS(LATTICE 2013)371 [arXiv:1311.0114] [INSPIRE].

[86] A.O.G. Kallen and A. Sabry, *Fourth order vacuum polarization*, *Kong. Dan. Vid. Sel. Mat. Fys. Med.* **29** (1955) 1 [INSPIRE].

[87] K.G. Chetyrkin, J.H. Kuhn and M. Steinhauser, *Heavy quark vacuum polarization to three loops*, *Phys. Lett.* **B 371** (1996) 93 [hep-ph/9511430] [INSPIRE].

[88] K.G. Chetyrkin, J.H. Kuhn and M. Steinhauser, *Three loop polarization function and $\mathcal{O}(\alpha_s^2)$ corrections to the production of heavy quarks*, *Nucl. Phys.* **B 482** (1996) 213 [hep-ph/9606230] [INSPIRE].

[89] R. Boughezal, M. Czakon and T. Schutzmeier, *Four-Loop Tadpoles: Applications in QCD*, *Nucl. Phys. Proc. Suppl.* **160** (2006) 160 [hep-ph/0607141] [INSPIRE].

[90] M. Czakon and T. Schutzmeier, *Double fermionic contributions to the heavy-quark vacuum polarization*, *JHEP* **07** (2008) 001 [arXiv:0712.2762] [INSPIRE].

[91] A. Maier, P. Maierhofer and P. Marquard, *Higher Moments of Heavy Quark Correlators in the Low Energy Limit at $\mathcal{O}(\alpha_s^2)$*, *Nucl. Phys.* **B 797** (2008) 218 [arXiv:0711.2636] [INSPIRE].

[92] K.G. Chetyrkin, J.H. Kuhn and C. Sturm, *Four-loop moments of the heavy quark vacuum polarization function in perturbative QCD*, *Eur. Phys. J.* **C 48** (2006) 107 [hep-ph/0604234] [INSPIRE].

[93] R. Boughezal, M. Czakon and T. Schutzmeier, *Charm and bottom quark masses from perturbative QCD*, *Phys. Rev.* **D 74** (2006) 074006 [hep-ph/0605023] [INSPIRE].

JHEP04(2018)003

[94] C. Sturm, *Moments of Heavy Quark Current Correlators at Four-Loop Order in Perturbative QCD*, *JHEP* **09** (2008) 075 [arXiv:0805.3358] [INSPIRE].

[95] A. Maier, P. Maierhofer and P. Marqaurd, *The Second physical moment of the heavy quark vector correlator at $\mathcal{O}(\alpha_s^3)$*, *Phys. Lett.* **B 669** (2008) 88 [arXiv:0806.3405] [INSPIRE].

[96] A. Maier, P. Maierhofer, P. Marquard and A.V. Smirnov, *Low energy moments of heavy quark current correlators at four loops*, *Nucl. Phys.* **B 824** (2010) 1 [arXiv:0907.2117] [INSPIRE].

[97] T. Appelquist, M. Dine and I.J. Muzinich, *The Static Potential in Quantum Chromodynamics*, *Phys. Lett.* **B 69** (1977) 231 [INSPIRE].

[98] T. Appelquist, M. Dine and I.J. Muzinich, *The Static Limit of Quantum Chromodynamics*, *Phys. Rev.* **D 17** (1978) 2074 [INSPIRE].

[99] M. Beneke, Y. Kiyo and K. Schuller, *Third-order Coulomb corrections to the S-wave Green function, energy levels and wave functions at the origin*, *Nucl. Phys.* **B 714** (2005) 67 [hep-ph/0501289] [INSPIRE].

[100] C. Anzai, Y. Kiyo and Y. Sumino, *Static QCD potential at three-loop order*, *Phys. Rev. Lett.* **104** (2010) 112003 [arXiv:0911.4335] [INSPIRE].

[101] A.V. Smirnov, V.A. Smirnov and M. Steinhauser, *Three-loop static potential*, *Phys. Rev. Lett.* **104** (2010) 112002 [arXiv:0911.4742] [INSPIRE].

[102] Y. Kiyo, G. Mishima and Y. Sumino, *Strong IR Cancellation in Heavy Quarkonium and Precise Top Mass Determination*, *JHEP* **11** (2015) 084 [arXiv:1506.06542] [INSPIRE].

[103] K.G. Chetyrkin, A.L. Kataev and F.V. Tkachov, *Higher Order Corrections to $\sigma_t(e^+e^- \to \text{Hadrons})$ in Quantum Chromodynamics*, *Phys. Lett.* **B 85** (1979) 277 [INSPIRE].

[104] S.G. Gorishnii, A.L. Kataev and S.A. Larin, *The $O(\alpha_s^3)$-corrections to $\sigma_{tot}(e^+e^- \to hadrons)$ and $\Gamma(\tau^- \to \nu_\tau + hadrons)$ in QCD*, *Phys. Lett.* **B 259** (1991) 144 [INSPIRE].

[105] L.R. Surguladze and M.A. Samuel, *Total hadronic cross-section in e^+e^- annihilation at the four loop level of perturbative QCD*, *Phys. Rev. Lett.* **66** (1991) 560 [INSPIRE].

[106] L.R. Surguladze and M.A. Samuel, *Erratum: Total hadronic cross-section in e^+e^- annihilation at the four loop level of perturbative QCD*, *Phys. Rev. Lett.* **66** (1991) 2461.

[107] P.A. Baikov, K.G. Chetyrkin and J.H. Kuhn, *Order α_s^4 QCD Corrections to Z and tau Decays*, *Phys. Rev. Lett.* **101** (2008) 012002 [arXiv:0801.1821] [INSPIRE].

[108] M.A. Shifman, A.I. Vainshtein and V.I. Zakharov, *QCD and Resonance Physics. Theoretical Foundations*, *Nucl. Phys.* **B 147** (1979) 385 [INSPIRE].

[109] M.A. Shifman, A.I. Vainshtein and V.I. Zakharov, *QCD and Resonance Physics: Applications*, *Nucl. Phys.* **B 147** (1979) 448 [INSPIRE].

[110] F. Simon, *Impact of Theory Uncertainties on the Precision of the Top Quark Mass in a Threshold Scan at Future e^+e^- Colliders*, PoS(ICHEP2016)872 [arXiv:1611.03399] [INSPIRE].

[111] D. d'Enterria, *Physics at the FCC-ee*, in *Proceedings, 17th Lomonosov Conference on Elementary Particle Physics*, Moscow, Russia, August 20–26, 2015, pp. 182–191 (2017) [DOI:10.1142/9789813224568_0028] [arXiv:1602.05043] [INSPIRE].

JHEP04(2018)003

[112] D. d'Enterria et al. eds., *Proceedings, High-Precision α_s Measurements from LHC to FCC-ee*, CERN, Geneva, Switzerland (2015) [arXiv:1512.05194] [INSPIRE].

[113] A. Pineda, *Comment on "The MSR Mass and the $\mathcal{O}(\Lambda_{\rm QCD})$ Renormalon Sum Rule"*, arXiv:1704.05095 [INSPIRE].

[114] O.V. Tarasov, A.A. Vladimirov and A.Yu. Zharkov, *The Gell-Mann-Low Function of QCD in the Three Loop Approximation*, *Phys. Lett.* **B 93** (1980) 429 [INSPIRE].

[115] S.A. Larin and J.A.M. Vermaseren, *The Three loop QCD β-function and anomalous dimensions*, *Phys. Lett.* **B 303** (1993) 334 [hep-ph/9302208] [INSPIRE].

[116] T. van Ritbergen, J.A.M. Vermaseren and S.A. Larin, *The Four loop β-function in quantum chromodynamics*, *Phys. Lett.* **B 400** (1997) 379 [hep-ph/9701390] [INSPIRE].

[117] G.P. Korchemsky and A.V. Radyushkin, *Renormalization of the Wilson Loops Beyond the Leading Order*, *Nucl. Phys.* **B 283** (1987) 342 [INSPIRE].

[118] S. Moch, J.A.M. Vermaseren and A. Vogt, *The three loop splitting functions in QCD: The Nonsinglet case*, *Nucl. Phys.* **B 688** (2004) 101 [hep-ph/0403192] [INSPIRE].

[119] M. Czakon, *The four-loop QCD β-function and anomalous dimensions*, *Nucl. Phys.* **B 710** (2005) 485 [hep-ph/0411261] [INSPIRE].

[120] W. Fischler, *Quark-anti-Quark Potential in QCD*, *Nucl. Phys.* **B 129** (1977) 157 [INSPIRE].

[121] A. Billoire, *How Heavy Must Be Quarks in Order to Build Coulombic $q\bar{q}$ Bound States*, *Phys. Lett.* **B 92** (1980) 343 [INSPIRE].

[122] M. Peter, *The Static quark-anti-quark potential in QCD to three loops*, *Phys. Rev. Lett.* **78** (1997) 602 [hep-ph/9610209] [INSPIRE].

[123] Y. Schröder, *The static potential in QCD to two loops*, *Phys. Lett.* **B 447** (1999) 321 [hep-ph/9812205] [INSPIRE].

[124] R.N. Lee, A.V. Smirnov, V.A. Smirnov and M. Steinhauser, *Analytic three-loop static potential*, *Phys. Rev.* **D 94** (2016) 054029 [arXiv:1608.02603] [INSPIRE].

[125] A.A. Penin and M. Steinhauser, *Heavy quarkonium spectrum at $\mathcal{O}(\alpha_s^5 m_q)$ and bottom/top quark mass determination*, *Phys. Lett.* **B 538** (2002) 335 [hep-ph/0204290] [INSPIRE].

[126] Y. Kiyo and Y. Sumino, *Full Formula for Heavy Quarkonium Energy Levels at Next-to-next-to-next-to-leading Order*, *Nucl. Phys.* **B 889** (2014) 156 [arXiv:1408.5590] [INSPIRE].

JHEP04(2018)003

Chapter 8

On the Light Massive Flavor Dependence of the Large Order Asymptotic Behavior and the Ambiguity of the Pole Mass

André H. Hoang, Christopher Lepenik and Moritz Preisser

On the light massive flavor dependence of the large order behavior and the ambiguity of the pole mass

Published in: JHEP **09** (2017) 099

Preprint version: arXiv:1706.08526 [hep-ph]

Contributions to this article:
All numerical analyses (together with other authors), derivation and checks of most analytical computations and formulas, conceptual innovations (together with other authors).

PUBLISHED FOR SISSA BY SPRINGER
RECEIVED: July 5, 2017
ACCEPTED: August 31, 2017
PUBLISHED: September 20, 2017

On the light massive flavor dependence of the large order asymptotic behavior and the ambiguity of the pole mass

André H. Hoang,[a,b] **Christopher Lepenik**[a] **and Moritz Preisser**[a,c]

[a] *University of Vienna, Faculty of Physics, Boltzmanngasse 5, A-1090 Wien, Austria*
[b] *Erwin Schrödinger International Institute for Mathematical Physics, University of Vienna, Boltzmanngasse 9, A-1090 Wien, Austria*
[c] *Center for Theoretical Physics, Massachusetts Institute of Technology, Cambridge, MA 02139, U.S.A.*

E-mail: andre.hoang@univie.ac.at, christopher.lepenik@univie.ac.at, moritz.preisser@univie.ac.at

ABSTRACT: We provide a systematic renormalization group formalism for the mass effects in the relation of the pole mass $m_Q^{\rm pole}$ and short-distance masses such as the $\overline{\rm MS}$ mass $\overline{m}_Q$ of a heavy quark Q, coming from virtual loop insertions of massive quarks lighter than Q. The formalism reflects the constraints from heavy quark symmetry and entails a combined matching and evolution procedure that allows to disentangle and successively integrate out the corrections coming from the lighter massive quarks and the momentum regions between them and to precisely control the large order asymptotic behavior. With the formalism we systematically sum logarithms of ratios of the lighter quark masses and m_Q, relate the QCD corrections for different external heavy quarks to each other, predict the $\mathcal{O}(\alpha_s^4)$ virtual quark mass corrections in the pole-$\overline{\rm MS}$ mass relation, calculate the pole mass differences for the top, bottom and charm quarks with a precision of around 20 MeV and analyze the decoupling of the lighter massive quark flavors at large orders. The summation of logarithms is most relevant for the top quark pole mass $m_t^{\rm pole}$, where the hierarchy to the bottom and charm quarks is large. We determine the ambiguity of the pole mass for top, bottom and charm quarks in different scenarios with massive or massless bottom and charm quarks in a way consistent with heavy quark symmetry, and we find that it is 250 MeV. The ambiguity is larger than current projections for the precision of top quark mass measurements in the high-luminosity phase of the LHC.

KEYWORDS: Heavy Quark Physics, Perturbative QCD, Quark Masses and SM Parameters, Renormalization Regularization and Renormalons

ARXIV EPRINT: 1706.08526

https://doi.org/10.1007/JHEP09(2017)099

JHEP09(2017)099

Contents

JHEP09(2017)099

1 Introduction

The masses of the heavy charm, bottom and top quarks belong to the most important input parameters in precise theoretical predictions of the Standard Model and models of new physics. Due to the effects of quantum chromodynamics (QCD) and because quarks are states with color charge, however, the mass of a heavy quark Q is not a physical observable and should, in general, be better thought of as a renormalized and scheme-dependent parameter of the theory. This concept is incorporated most cleanly in the so-called $\overline{\text{MS}}$ mass $\overline{m}_Q(\mu)$, which is defined through the same renormalization prescription as the $\overline{\text{MS}}$ QCD coupling $\alpha_s(\mu)$. It can be measured from experimental data very precisely, but does not have any kinematic meaning, and it can be thought of incorporating short-distance information on the mass from scales larger than μ. On the other hand, the

so-called pole mass $m_Q^{\rm pole}$ is defined as the single particle pole in correlation functions involving the massive quark Q as an external on-shell particle, and it determines the kinematic mass of the quark Q in the context of perturbation theory. It is therefore unavoidable that the pole mass scheme appears in one way or another in higher order QCD calculations involving external massive quarks. For perturbative predictions involving the production of top quarks at hadron colliders, the pole mass scheme is therefore the main top quark mass scheme used in the literature, and switching scheme is cumbersome since these computations are predominantly numerical where the pole scheme provides the most efficient approach for the computations. In refs. [1–8] the relation between the $\overline{\rm MS}$ and the pole mass has been computed up to $\mathcal{O}(\alpha_s^4)$ in the approximation that all quarks lighter than Q are massless. Assuming the values $\overline{m}_t \equiv \overline{m}_t(\overline{m}_t) = 163$ GeV, $\overline{m}_b \equiv \overline{m}_b(\overline{m}_b) = 4.2$ GeV and $\overline{m}_c \equiv \overline{m}_c(\overline{m}_c) = 1.3$ GeV we obtain[1]

$$m_t^{\rm pole} = 163 + 7.5040 + 1.6005 + 0.4941 + (0.1944 \pm 0.0004)\,\text{GeV}\,, \tag{1.1}$$

$$m_b^{\rm pole} = 4.2 + 0.3998 + 0.1986 + 0.1443 + (0.1349 \pm 0.0002)\,\text{GeV}\,, \tag{1.2}$$

$$m_c^{\rm pole} = 1.3 + 0.2108 + 0.1984 + 0.2725 + (0.4843 \pm 0.0005)\,\text{GeV}\,, \tag{1.3}$$

where the terms show the series in powers of the strong coupling $\alpha_s(\overline{m}_Q)$ in the scheme that includes Q as a dynamical flavor. The fourth order coefficient displays the numerical uncertainties from [8], which are, however, much smaller than other types of uncertainties considered in this paper.

The pole mass renormalization scheme is infrared-safe and gauge-invariant [1, 11], but suffers from large corrections in the QCD perturbation series. This is because the pole mass scheme involves subtractions of on-shell quark self energy corrections containing virtual gluon and massless quark fluctuations which are linearly sensitive to small momenta. The on-shell approximation of the self energy diagrams entails that this sensitivity increases strongly with the order. The effect this has for the form of the corrections can be seen in eqs. (1.1)–(1.3), which in the asymptotic large order limit have the form

$$m_Q^{\rm pole} - \overline{m}_Q(\overline{m}_Q) \sim \mu \sum_{n=0}^{\infty} \frac{16}{3} (2\beta_0^{(n_\ell)})^n\, n! \left(\frac{\alpha_s^{(n_\ell)}(\mu)}{4\pi}\right)^{n+1}\,, \tag{1.4}$$

in the β_0/LL approximation, which means that the terms in the QCD β-function,

$$\frac{{\rm d}\alpha_s^{(n_\ell)}(\mu)}{{\rm d}\log\mu} = \beta^{(n_\ell)}(\alpha_s(\mu)) = -2\,\alpha_s^{(n_\ell)}(\mu) \sum_{n=0}^{\infty} \beta_n^{(n_\ell)} \left(\frac{\alpha_s^{(n_\ell)}(\mu)}{4\pi}\right)^{n+1}\,, \tag{1.5}$$

beyond the leading logarithmic level (i.e. $\beta_{n>0}$) are neglected. Here n_ℓ is the number of massless quark flavors.

The factorially diverging pattern of the perturbation series and the linear dependence on the renormalization scale μ of the strong coupling displayed in eq. (1.4) are called *the*

[1] We assume $\alpha^{(5)}(M_Z) = 0.1180$ for $M_Z = 91.187$ GeV for the $\overline{\rm MS}$ QCD coupling and account for 5-loop evolution [9] and flavor matching at the scales $\overline{m}_{c,b,t}$ [10], which gives $\alpha_s^{(6)}(\overline{m}_t) = 0.10847$, $\alpha_s^{(5)}(\overline{m}_b) = 0.22430$, $\alpha_s^{(4)}(\overline{m}_c) = 0.38208$.

JHEP09(2017)099

$\mathcal{O}(\Lambda_{\rm QCD})$ *renormalon* of the pole mass [12, 13]. The form of the series on the r.h.s. of eq. (1.4) implies that at asymptotic large orders, and up to terms suppressed by inverse powers of n, the series becomes independent of its intrinsic physical scale m_Q. This and the n-factorial growth is an artifact of the pole mass scheme itself and not related to any physical effect. Technically this issue entails that for computing differences of series containing $\mathcal{O}(\Lambda_{\rm QCD})$ renormalon ambiguities using fixed-order perturbation theory one must consistently expand in powers of the strong coupling at the same renormalization scale such that the renormalon can properly cancel.

The $\mathcal{O}(\Lambda_{\rm QCD})$ renormalon problem of the pole mass has received substantial attention in the literature as it turned out to be not just an issue of pedagogical interest, but one that is relevant phenomenologically [14]. This is because for $\mu = \overline{m}_Q$ the known coefficients of the series in eqs. (1.1)–(1.3) agree remarkably well with the corresponding large order asymptotic behavior already beyond the terms of $\mathcal{O}(\alpha_s)$ (so that the terms of the series are known quite precisely to all orders) and because even for orders where the QCD corrections still decrease with order they can be very large numerically and make phenomenological applications difficult. The pole mass scheme has therefore been abandoned in high precision top, bottom and charm quark mass analyses in favor of quark mass schemes such as $\overline{\rm MS}$ or low-scale short distance masses such as the kinetic mass [15], the potential-subtracted (PS) mass [16], the 1S mass [17–19], the renormalon-subtracted (RS) mass [20], the jet mass [21, 22] or the MSR mass [23, 24]. These mass schemes do not have an $\mathcal{O}(\Lambda_{\rm QCD})$ renormalon and are called short-distance masses. It is commonly agreed from many studies that it is possible to determine short-distance masses with theoretical uncertainties of a few 10 MeV [25, 26], and we therefore neglect any principle ambiguity in their values in this paper.

Using the theory of asymptotic series one can show that the best possible approximation to the l.h.s. of eq. (1.4) is to truncate the series on the r.h.s. at the minimal term at order $n_{\rm min}$ which is approximately $n_{\rm min} \approx 2\pi/(\beta_0^{(n_\ell)}\alpha_s^{(n_\ell)}(\mu))$. The size of the correction of the minimal term is approximately $\Delta(n_{\rm min}) \approx (4\pi\alpha_s^{(n_\ell)}(\mu)/\beta_0^{(n_\ell)})^{1/2}\Lambda_{\rm QCD}^{(n_\ell)}$, and there is a region in the orders n around $n_{\rm min}$ of width $\Delta n \approx (2\pi^2/(\beta_0^{(n_\ell)}\alpha_s^{(n_\ell)}(\mu)))^{1/2}$ in which all series terms have a size close to the minimal term. At orders above $n_{\rm min} + \Delta n/2$ the series diverges quickly and the series terms from these orders are useless even if they are known through an elaborate loop calculation. The uncertainty with which the pole mass can be determined *in principle* given the full information about the perturbative series is called the *pole mass ambiguity*. It is universal, independent on the choice of the renormalization scale μ and exists in equivalent size in any context without the possibility to be circumvented. However, the μ-dependence of $n_{\rm min}$, $\Delta(n_{\rm min})$ and Δn indicates that the way how the renormalon problem appears in practical applications based on perturbative QCD can differ substantially depending on the physical scale of the quantity under consideration and the corresponding choice of the renormalization scale μ. Using the method of Borel resummation the pole mass ambiguity can be estimated to be of order $\Lambda_{\rm QCD}^{(n_\ell)}$, where the superscript (n_ℓ) stands for the dependence of the hadronization scale on the number of massless quark flavors. The norm of the ambiguity, which we call $N_{1/2}^{(n_\ell)}$ in this paper,

and the resulting pattern of the large order asymptotic behavior of the series can be determined very precisely and have been studied in many analyses (see e.g. the recent work of refs. [24, 27–29]). However, when quoting a concrete numerical size of the ambiguity, criteria common for converging series cannot be applied, and it is instrumental to consider more global aspects of the series and the quantity it describes. An essential aspect of the low-energy quantum corrections in heavy quark masses is *heavy quark symmetry (HQS)* [30] on which we put particular focus in this work.

An issue that has received less attention in the literature so far is how the masses of the lighter massive quarks affect the large order asymptotic behavior of the pole-$\overline{\text{MS}}$ mass relation, where we refer to the effects of quarks with masses that are larger than Λ_{QCD}. These corrections come from insertions of virtual quark loops and are known up to $\mathcal{O}(\alpha_s^3)$ [2, 31] from explicit loop calculations. It is known that the masses of lighter massive quarks provide an infrared cutoff and effectively reduce the number n_ℓ of massless flavors governing the large order asymptotic behavior [32]. Due to the n_ℓ-dependence of the QCD β-function the finite bottom and charm quark masses lead to an increased infrared sensitivity of the top quark pole mass and a stronger divergence pattern of the series, as can be seen from eq. (1.4). The ambiguity therefore inflates following the n_ℓ-dependent increase of Λ_{QCD}. In refs. [33, 34] it was pointed out that the $\mathcal{O}(\alpha_s^2)$ and $\mathcal{O}(\alpha_s^3)$ virtual quark mass corrections are already dominated by the infrared behavior related to the $\mathcal{O}(\Lambda_{\text{QCD}})$ renormalon. In ref. [27] it was further observed that the $\mathcal{O}(\alpha_s^3)$ charm mass corrections in the bottom pole-$\overline{\text{MS}}$ mass relation can be rendered small when the series is expressed in terms of $\alpha_s^{(n_\ell=3)}$ rather than $\alpha_s^{(n_\ell=4)}$, i.e. the charm quark effectively decouples. A systematic and precise understanding of the intrinsic structure of the lighter massive quark effects from the point of view of disentangling the different momentum modes and their interplay has, however, not been provided so far in the literature. The task is complicated since apart from being a problem in connection with the behavior of perturbation theory at large orders, it also represents a multi-scale problem with scales given by the quark masses as well as Λ_{QCD} and where, for the top quark, logarithms of mass ratios can be large.

It is the main purpose of this paper to present a formalism that can do exactly that. It is based on the concept of the renormalization group (RG) and allows to successively integrate out momentum modes from the pole-$\overline{\text{MS}}$ mass relation of a heavy quark Q in order to disentangle the contributions coming from the lighter massive quarks and to systematically sum logarithms of the mass ratios. The approach allows to quantify and formulate precisely the effects the masses of the lighter massive quarks have on the pole-$\overline{\text{MS}}$ mass relation and therefore on the pole mass itself and may find interesting applications in other contexts. As the essential new feature the RG formalism entails *linear scaling with the renormalization scale*. The common logarithmic scaling, as known for the strong coupling, cannot capture the linear momentum dependence of QCD corrections to the heavy quark mass for scales below m_Q. The formalism is in particular useful since it fully accounts for all aspects of HQS. It can be used to concretely formulate and study in a transparent way two important properties of the heavy quark pole masses following from HQS: (1) The pole mass ambiguity is independent of the mass of the heavy quark and (2) the ambiguities of all heavy quarks are equal up to power corrections of order $\Lambda_{\text{QCD}}^2/m_Q$.

JHEP09(2017)099

The essential technical tool to set up the formalism is the MSR mass $m_Q^{\rm MSR}(R)$ [23, 24]. Like the perturbative series for the pole-$\overline{\rm MS}$ mass relation, the pole-MSR mass relation is calculated from on-shell heavy quark self energy diagrams, but has also linear dependence on R. It is the basis of the RG formalism we propose, allows to precisely capture the QCD corrections from the different quark mass scales and, in particular, to encode and study issue (1) coming from HQS. The renormalization group evolution in the scale R is described by R-evolution [23, 24], which is free of the $\mathcal{O}(\Lambda_{\rm QCD})$ renormalon, and allows to sum large logarithms of ratios of the quark masses in the evolution between the quark mass scales. Using the concepts of the MSR mass and the R-evolution it is then possible to relate the pole-$\overline{\rm MS}$ masses of the top, bottom and charm quarks to each other. This allows to systematically encode and study issue (2) coming from HQS, and to interpret the small effects of HQS breaking as matching corrections in a renormalization group flow that connects the QCD correction of the top, bottom and charm quarks. The resulting formula can be used to specify the heavy quark pole mass ambiguity in the context of lighter massive quarks and to derive a generalized expression for the large order asymptotic behavior accounting accurately for the light massive flavor dependence. Concerning the accuracy of our description of the virtual quark loop mass effects in the large order asymptotic behavior we reach a precision of a few MeV, which applies equally for top, bottom and charm quarks.

The second main purpose of this paper is to use the RG formalism to specify concretely the ambiguity of the top quark pole mass and also the pole mass of the bottom and charm quarks assuming that their $\overline{\rm MS}$ masses are given. We in particular address the question how the outcome depends on different scenarios for treating the bottom and charm quarks as massive or massless, and we explicitly take into account the consistency requirements of HQS. The aim is to provide a concrete numerical specification of the ambiguity of the top quark pole mass beyond the qualitative statement that the ambiguity is "of order $\Lambda_{\rm QCD}^{(n_\ell)}$" and to make a concrete statement up to which principle precision the top quark pole mass may still be used as a meaningful phenomenological parameter. We stress that in this context we adopt the view that the pole masses have well-defined and unique meaning, so that the pole mass ambiguity acquires the meaning of an intrinsic numerical uncertainty. This differs from the view sometimes used in high-precision analyses, where the pole mass is employed as an intrinsic order-dependent parameter to effectively parameterize the use of a short-distance mass scheme.

Apart from specifying the ambiguity of the pole masses we are also interested in studying the dependence of their value on the different scenarios for treating the bottom and charm quarks as massive or massless. The issue is of particular interest for the top quark pole mass which is still widely used for theoretical predictions and phenomenological studies in top quark physics. The top quark pole mass is, due to its linear sensitivity to small momenta, also linearly sensitive to the masses of the lighter massive quarks. Since many short-distance observables used for top quark pole mass determinations are at most quadratically sensitive to small momenta, the dominant effects of the bottom and charm masses may well come from the top quark pole definition itself. A large dependence of the top quark pole mass value on whether the bottom and charm quarks are treated as massive or massless would therefore affect the ambiguity estimate if one considers the top quark

pole mass as a globally defined mass scheme (valid for any scenario for the bottom and charm quark masses). We can address this question precisely because the RG-formalism we use allows for very accurate numerical calculations of the lighter quark mass effects. Within the size of the ambiguity, we do not find any such dependence. The outcome of our analysis is that the top quark pole mass ambiguity, and the ambiguity of the bottom and charm quark pole masses, is around 250 MeV.

Prior to this work the best estimate and the ambiguity of the top quark pole mass were studied in ref. [28]. They analyzed the top quark pole-$\overline{\rm MS}$ mass series of eq. (1.1) for $\mu = \overline{m}_t$ and massless bottom and charm quarks and in an extended analysis also for massive bottom and charm quarks. They argued that the ambiguity of the top, bottom and charm quark pole masses amounts to 110 MeV. We believe that their ambiguity estimate of 110 MeV is too optimistic, and we explain this in detail from the requirements of HQS. They also quantified the bottom and charm mass effects coming from beyond the known corrections at $\mathcal{O}(\alpha_s^2)$ and $\mathcal{O}(\alpha_s^3)$ by using a heuristic prescription based on an order-dependent reduction of the flavor number. This does not represent a systematic calculation, but we find it to be an adequate approximation for the task of estimating the top quark pole mass renormalon ambiguity.

The paper is organized as follows: in section 2 we review the explicitly calculated corrections up to $\mathcal{O}(\alpha_s^4)$ for the pole-$\overline{\rm MS}$ and the pole-MSR mass relations for the case that all quarks lighter than quark Q are massless and we explain our notation for parameterizing the virtual quark mass corrections due to the light massive quarks. This notation is essential for our setup of the flavor number dependent RG evolution of the MSR mass, which we also review to the extend needed for our studies in the subsequent sections. We also review known basic issues about the large order asymptotic behavior and the renormalon ambiguity of the pole-$\overline{\rm MS}$ and the pole-MSR mass relations, including their dependence on the number of massless quarks. In section 3 we explain details about the matching procedures that allow to integrate out the virtual corrections coming from the heavy quark Q and the lighter massive quarks, and to relate the pole-MSR mass relation of quark Q to the pole-$\overline{\rm MS}$ mass relation of the next lighter massive quark, which is based on heavy quark symmetry. These considerations and the numerical analysis of the latter matching corrections allow us to derive a prediction for the yet uncalculated $\mathcal{O}(\alpha_s^4)$ virtual quark mass corrections and to discuss the large order asymptotic form of the virtual quark mass corrections. As an application of the RG formalism devised in our work we compute the difference of the pole masses of the top, bottom and charm quarks. Since their differences are short-distance quantities we can compute them with a precision of around 20 MeV. We also analyze the validity of the effective flavor decoupling at large orders in the context of the top quark pole mass. In section 4 we finally discuss in detail the best possible estimate of the top quark pole mass and in particular its ambiguity in the context of three different scenarios for the bottom and charm quark masses. We discuss these three scenarios separately because the pole mass concept, strictly speaking, depends on the setup for the lighter quark masses, and we also discuss our results in the context of adopting the view that the top quark pole mass is a general concept. Finally, in section 5 we conclude. In appendix A we provide explicit results for the virtual quark mass corrections at $\mathcal{O}(\alpha_s^3)$ in our

JHEP09(2017)099

notation, using the results from ref. [31], and we complete them concerning the corrections coming from the insertion of two quark loops involving quarks with two arbitrary masses.

2 Preliminaries and notation

2.1 $\overline{\rm MS}$ mass

The perturbative series of the difference between the $\overline{\rm MS}$ mass $\overline{m}_Q(\mu)$ at the scale $\mu = \overline{m}_Q(\overline{m}_Q)$ and the pole mass $m_Q^{\rm pole}$ of a heavy quark Q is the basic relation from which we start our analysis of the renormalon ambiguity of the pole mass. To be more specific we consider

$$\overline{m}_Q \equiv \overline{m}_Q^{(n_Q+1)}(\overline{m}_Q^{(n_Q+1)})\,, \tag{2.1}$$

which is the $\overline{\rm MS}$ mass defined for (n_Q+1) active dynamical flavors, where

$$n_Q \equiv \text{number of flavors lighter than quark } Q\,. \tag{2.2}$$

In this work we use these two definitions for all massive quarks, and depending on the context we also use the lower case letter q for massive quarks. We also define

$$n_\ell \equiv \text{number of flavors lighter than } \Lambda_{\rm QCD}\,, \tag{2.3}$$

which we strictly treat in the massless approximation.

Assuming that $q_1,\ldots,q_n$ are the massive quarks lighter than Q *in the order of decreasing mass* (i.e. $m_Q > m_{q_1} > \ldots > m_{q_n} > \Lambda_{\rm QCD}$ with $n < n_Q$ and $n_\ell = n_Q - n$), the pole-$\overline{\rm MS}$ mass relation for the heavy quark Q can be written in the form

$$\begin{aligned} m_Q^{\rm pole} = \overline{m}_Q + \overline{m}_Q \sum_{n=1}^{\infty} a_n(n_Q+1,0) \left(\frac{\alpha_s^{(n_Q+1)}(\overline{m}_Q)}{4\pi}\right)^n \\ + \overline{m}_Q\Big[\overline{\delta}_Q^{(Q,q_1,\ldots,q_n)}(1,r_{q_1Q},\ldots,r_{q_nQ}) + \overline{\delta}_Q^{(q_1,\ldots,q_n)}(r_{q_1Q},\ldots,r_{q_nQ}) \\ + \cdots + \overline{\delta}_Q^{(q_n)}(r_{q_nQ})\Big]\,, \end{aligned} \tag{2.4}$$

with

$$\begin{aligned} a_1(n_Q,n_h) &= \tfrac{16}{3}\,, \\ a_2(n_Q,n_h) &= 213.437 + 1.65707\,n_h - 16.6619\,n_Q\,, \\ a_3(n_Q,n_h) &= 12075. + 118.986\,n_h + 4.10115\,n_h^2 - 1707.35\,n_Q \\ &\quad + 1.42358\,n_h\,n_Q + 41.7722\,n_Q^2\,, \\ a_4(n_Q,n_h) &= (911588. \pm 417.) + (1781.61 \pm 30.72)\,n_h - (60.1637 \pm 0.6912)\,n_h^2 \\ &\quad - (231.201 \pm 0.102)\,n_h\,n_Q - (190683. \pm 10.)\,n_Q + 9.25995\,n_h^2\,n_Q \\ &\quad + 6.35819\,n_h^3 + 4.40363\,n_h\,n_Q^2 + 11105.\,n_Q^2 - 173.604\,n_Q^3\,, \end{aligned} \tag{2.5}$$

where $\alpha_s^{(n_Q+1)}$ is the strong coupling that evolves with (n_Q+1) active dynamical flavors, see eq. (1.5).

The coefficients $a_n(n_Q, n_h)$ encode the QCD corrections to $m_Q^{\rm pole} - \overline{m}_Q$ for the case that the n_Q quarks lighter than Q are assumed to be massless, and $n_h = 1$ is just an identifier for the corrections coming from virtual loops of the quark Q. The coefficients $a_{1,2,3}$ are known analytically from refs. [1–6], and a_4 was determined numerically in refs. [7, 8], where the quoted numerical uncertainties have been taken from ref. [8]. In ref. [35] an approach was suggested to further reduce the uncertainties of the n_Q-dependent terms. The numerical uncertainties of the coefficient a_4 are, however, tiny and irrelevant for the analysis carried out in this work. We quote them just for completeness throughout this work.

The terms $\overline{\delta}_Q^{(q,q',\dots)}(r_{qQ}, r_{q'Q}, \dots)$ contain the mass corrections coming from the quark Q on-shell self-energy Feynman diagrams with insertions of virtual massive quark loops. We remind the reader that the quarks with mass below the hadronization scale are taken as massless and do not contribute. The superscript $(q, q', \dots)$ indicates that *each diagram contains at least one insertion of the massive quark* q and in addition all possible insertions of the (lighter) massive quarks $q', \dots$ as well as of massless quark and gluonic loops. From each diagram the corresponding diagram with all the quark loops in the massless limit is subtracted in the scheme compatible with the flavor number scheme for the strong coupling α_s. The fraction

$$r_{qq'} \equiv \frac{\overline{m}_q}{\overline{m}_{q'}}\,, \tag{2.6}$$

stands for the ratio of $\overline{\rm MS}$ masses for massive quarks q and q' as defined in eq. (2.1). In the pole-$\overline{\rm MS}$ mass relation for the heavy quark Q only mass ratios with respect to the heavy quark mass $\overline{m}_Q$ arise. By construction, the sum of all virtual quark mass corrections contained in the functions $\overline{\delta}_Q^{(q,q',\dots)}(r_{qQ}, r_{q'Q}, \dots)$ are RG-invariant and do not contain effects from quarks heavier than the external quark Q. The effects on the mass of the quark Q related to quarks heavier than Q are accounted for in the renormalization group evolution of the $\overline{\rm MS}$ mass $\overline{m}_Q(\mu)$ for scales $\mu > m_Q$ and are not considered here. The virtual quark mass corrections satisfy the following two relations to all orders of perturbation theory

$$\overline{\delta}_Q^{(q_1,q_2,\dots,q_n)}(0, 0, \dots, 0) = 0\,, \tag{2.7}$$

$$\overline{\delta}_Q^{(Q,q_1,\dots,q_n)}(1, 0, \dots, 0) = \sum_{n=2}^{\infty} \left[\, a_n(n_Q, 1) - a_n(n_Q + 1, 0) \,\right] \left(\frac{\alpha_s^{(n_Q+1)}(\overline{m}_Q)}{4\pi}\right)^n . \tag{2.8}$$

Due to eq. (2.8) the pole-$\overline{\rm MS}$ mass relation of eq. (2.4) can be rewritten in the alternative form

$$\begin{aligned} m_Q^{\rm pole} = \overline{m}_Q &+ \overline{m}_Q \sum_{n=1}^{\infty} a_n(n_Q, 1) \left(\frac{\alpha_s^{(n_Q+1)}(\overline{m}_Q)}{4\pi}\right)^n \\ &+ \overline{m}_Q \left[\overline{\delta}_Q^{(Q,q_1,\dots,q_n)}(1, r_{q_1Q}, \dots, r_{q_nQ}) - \overline{\delta}_Q^{(Q,q_1,\dots,q_n)}(1, 0, \dots, 0)\right. \\ &\left. + \overline{\delta}_Q^{(q_1,\dots,q_n)}(r_{q_1Q}, \dots, r_{q_nQ}) + \cdots + \overline{\delta}_Q^{(q_n)}(r_{q_nQ})\right] . \end{aligned} \tag{2.9}$$

In the limit that all quarks lighter than Q are massless, all $\overline{\delta}$ terms cancel or vanish in eq. (2.9), and only the first line involving the a_n coefficients remains.

JHEP09(2017)099

The perturbative expansion of the virtual quark mass corrections in the pole-$\overline{\rm MS}$ mass relation of eq. (2.4) and (2.9) can be written in the form

$$\overline{\delta}_Q^{(q,q',\dots)}(r_{qQ}, r_{q'Q}, \dots) = \delta_2(r_{qQ}) \left(\frac{\alpha_s^{(n_Q+1)}(\overline{m}_Q)}{4\pi}\right)^2 + \sum_{n=3}^{\infty} \delta_{Q,n}^{(q,q',\dots)}(r_{qQ}, r_{q'Q}, \dots) \left(\frac{\alpha_s^{(n_Q+1)}(\overline{m}_Q)}{4\pi}\right)^n , \tag{2.10}$$

which together with eq. (2.8) implies that

$$\begin{aligned} \delta_2(1) &= a_2(n_Q, 1) - a_2(n_Q+1, 0) = 18.3189\,, \\ \delta_{Q,n}^{(Q,q,q',\dots)}(1, 0, 0, \dots) &= a_n(n_Q, 1) - a_n(n_Q+1, 0)\,. \end{aligned} \tag{2.11}$$

The $\mathcal{O}(\alpha_s^2)$ correction comes from the on-shell self energy diagram of quark Q with the insertion of a loop of the massive quark q. The result was determined analytically in ref. [2]. At $\mathcal{O}(\alpha_s^3)$, in ref. [31], the virtual quark mass corrections were determined in a semi-analytic form for arbitrary quark masses for insertions of loops of the quark Q and one other massive quark q. The expressions for these virtual quark mass corrections are for convenience collected in appendix A after adapting the results of ref. [31] to our notation. We also provide the $\mathcal{O}(\alpha_s^3)$ result for insertions of loops with two arbitrary massive quarks, which were not given in ref. [31]. The $\mathcal{O}(\alpha_s^4)$ virtual quark mass corrections have not been determined through an explicit loop calculation.

One can interpret the $\overline{\rm MS}$ mass $\overline{m}_Q = \overline{m}_Q^{(n_Q+1)}(\overline{m}_Q^{(n_Q+1)})$ as the pole mass *minus* all self-energy corrections coming from scales *at and below* $\overline{m}_Q$. So $\overline{m}_Q$ only contains mass contributions from momentum fluctuations from above $\overline{m}_Q$, which illustrates that it is a short-distance mass that is strictly insensitive to issues related to low momentum fluctuations at the hadronization scale $\Lambda_{\rm QCD}$. See figure 1 for illustration.

2.2 MSR mass and R-evolution

In order to integrate out high momentum contributions and formulate the renormalization group flow of momentum contributions in the heavy quark masses we use the MSR mass $m_Q^{\rm MSR}(R)$ introduced in ref. [24],[2] extending its definition to account for the mass effects of the lighter massive quarks.

The MSR mass for the heavy quark Q is derived from on-shell self-energy diagrams just like the pole-$\overline{\rm MS}$ mass relation of eq. (2.4), but it does not include any diagrams involving virtual loops of the heavy quark Q, i.e. the contributions from heavy quark Q virtual loops are integrated out. Like the $\overline{\rm MS}$ mass, the MSR mass is a short-distance mass, and since the corrections from the heavy quark Q are short-distance effects, its relation to the pole mass fully contains the pole mass $\mathcal{O}(\Lambda_{\rm QCD})$ renormalon (just as the pole-$\overline{\rm MS}$ mass relation of eqs. (2.4) and (2.9)). Furthermore the MSR mass depends on the arbitrary scale $R \lesssim m_Q$

[2] In refs. [23, 24] the natural and the practical MSR masses were introduced. In this paper we employ the natural MSR mass and call it just the MSR mass for convenience.

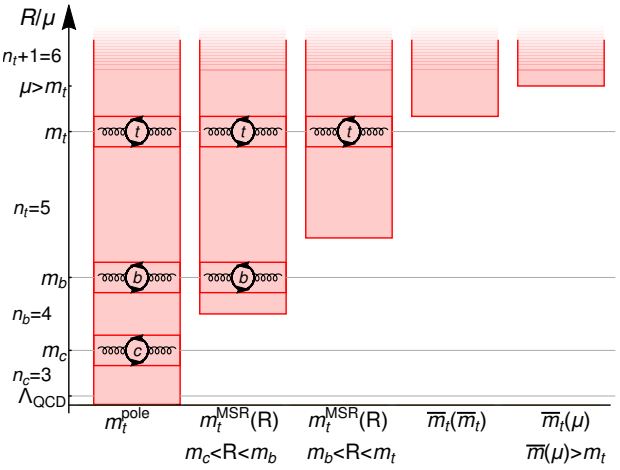

Figure 1. Graphical illustration of the physical contributions contained in the pole, MSR and $\overline{\rm MS}$ mass schemes coming from the different momentum scales for the case of the top quark. The quark loops stand for the contributions of the virtual massive quark loops contained in the masses.

to describe contributions in the mass from the momenta below the scale m_Q, and therefore represents the natural extension of the concept of the $\overline{\rm MS}$ mass for scales below m_Q.

Assuming that $q_1, \ldots, q_n$ are the massive quarks lighter than Q in the order of decreasing mass (i.e. $m_Q > m_{q_1} > \ldots > m_{q_n} > \Lambda_{\rm QCD}$ with $n < n_Q$ and $n_\ell = n_Q - n$), the MSR mass $m_Q^{\rm MSR}(R)$ is *defined* by the relation

$$m_Q^{\rm pole} = m_Q^{\rm MSR}(R) + R \sum_{n=1}^{\infty} a_n(n_Q, 0) \left(\frac{\alpha_s^{(n_Q)}(R)}{4\pi}\right)^n + \overline{m}_Q \left[\delta_Q^{(q_1,\ldots,q_n)}(r_{q_1 Q}, \ldots, r_{q_n Q}) + \cdots + \delta_Q^{(q_n)}(r_{q_n Q})\right], \tag{2.12}$$

where the coefficients a_n are given in eqs. (2.5) and the perturbative expansion is in powers of the strong coupling in the n_Q-flavor scheme since the quark Q is integrated out. The R-dependence of the strong coupling entails that the scale R has to be chosen sufficiently larger than $\Lambda_{\rm QCD}$ to stay away from the Landau pole. The definition generalizes the one already provided in ref. [24], which only considered n_Q massless quarks.

The notation used for the virtual quark mass corrections involving the functions $\delta_Q^{(q,q',\ldots)}(r_{qQ}, r_{q'Q}, \ldots)$ is the same as the one for the $\overline{\rm MS}$ mass described above, and their sum is by construction RG-invariant. Their perturbative expansion has the form

$$\delta_Q^{(q,q',\ldots)}(r_{qQ}, r_{q'Q}, \ldots) = \delta_2(r_{qQ}) \left(\frac{\alpha_s^{(n_Q)}(\overline{m}_Q)}{4\pi}\right)^2 + \sum_{n=3}^{\infty} \delta_{Q,n}^{(q,q',\ldots)}(r_{qQ}, r_{q'Q}, \ldots) \left(\frac{\alpha_s^{(n_Q)}(\overline{m}_Q)}{4\pi}\right)^n, \tag{2.13}$$

where the coefficient functions $\delta_{Q,n}^{(q,q',\dots)}(r_{qQ}, r_{q'Q}, \dots)$ are identical to the ones appearing in eq. (2.10).

In our definition of the MSR mass, the virtual quark mass corrections are independent of R. This entails that the renormalization group evolution of the MSR mass in R does not depend on the masses of the n_Q lighter quarks. So $m_Q^{\rm MSR}(R)$ is defined in close analogy to the μ-dependent $\overline{\rm MS}$ strong coupling and the $\overline{\rm MS}$ masses, whose renormalization group evolution only depends on the number of active dynamical quarks (which is typically the number of quarks lighter than μ) and where mass effects are implemented by threshold corrections when μ crosses a flavor threshold. Moreover, because the $\mathcal{O}(\Lambda_{\rm QCD})$ renormalon ambiguity of the series proportional to R is independent of R and because the corrections from the virtual loops of the heavy quark Q are short-distance effects, the series of the pole-MSR mass relation in eq. (2.12) suffers from the same $\mathcal{O}(\Lambda_{\rm QCD})$ renormalon ambiguity as the pole-$\overline{\rm MS}$ mass relation of eqs. (2.4) and (2.9). It can therefore also be used to study and quantify the $\mathcal{O}(\Lambda_{\rm QCD})$ renormalon of the pole mass $m_Q^{\rm pole}$.

As explained below eq. (1.4), in order to expand the difference of MSR masses at two scales R and R' in the fixed-order expansion in powers of $\alpha_s^{(n_Q)}$ it is necessary to do that at a common renormalization scale μ so that the renormalon in the R-dependent corrections of eq. (2.12) cancels order by order. This unavoidably leads to large logarithms if the scale separation is large, similarly to when considering the fixed-order expansion of the difference of the strong coupling at widely separated scales. To sum the logarithms in the difference of MSR masses we use its RG-evolution equation in R, which reads

$$R\frac{\mathrm{d}}{\mathrm{d}R}m_Q^{\rm MSR}(R) = -R\,\gamma^{R,(n_Q)}(\alpha_s^{(n_Q)}(R)) = -R\sum_{n=0}^{\infty}\gamma_n^{R,(n_Q)}\left(\frac{\alpha_s^{(n_Q)}(R)}{4\pi}\right)^{n+1}, \tag{2.14}$$

where the coefficients are known up to four loops and given by [23, 24]

$$\begin{aligned}
\gamma_0^{R,(n_Q)} &= \frac{16}{3}\,, \\
\gamma_1^{R,(n_Q)} &= 96.1039 - 9.55076\,n_Q\,, \\
\gamma_2^{R,(n_Q)} &= 1595.75 - 269.953\,n_Q - 2.65945\,n_Q^2\,, \\
\gamma_3^{R,(n_Q)} &= (12319.\pm 417.) - (9103.\pm 10.)\,n_Q + 610.264\,n_Q^2 - 6.515\,n_Q^3\,.
\end{aligned} \tag{2.15}$$

The difference of MSR masses at two scales R' and R can then be computed from solving the evolution equation

$$\Delta m^{(n_Q)}(R,R') = m_Q^{\rm MSR}(R') - m_Q^{\rm MSR}(R) = \sum_{n=0}^{\infty}\gamma_n^{R,(n_Q)}\int_{R'}^{R}\mathrm{d}R\left(\frac{\alpha_s^{(n_Q)}(R)}{4\pi}\right)^{n+1}, \tag{2.16}$$

which accounts for the RG-evolution in the presence of n_Q active dynamical quark flavors.

The RG-equation of the MSR mass has a linear as well as logarithmic dependence on R and thus differs from the usual logarithmic RG-equations for α_s and the $\overline{\rm MS}$ mass. Since its linear dependence on R allows to systematically probe linear sensitivity to small momenta it can be used to systematically study the $\mathcal{O}(\Lambda_{\rm QCD})$ renormalon behavior of

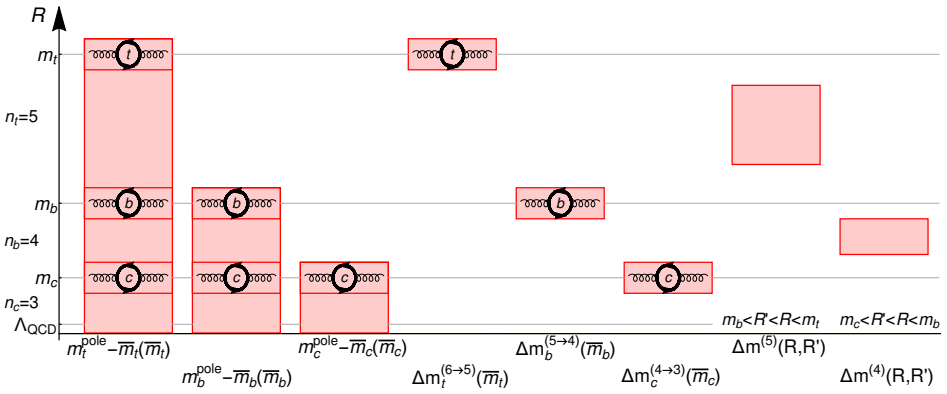

Figure 2. Graphical illustration for pole-$\overline{\rm MS}$ mass differences, the MSR-$\overline{\rm MS}$ mass matching corrections and MSR mass differences for different R scales. They constitute the major contributions in the RG analysis of the heavy quark pole masses.

perturbative series [23, 24]. Since this is impossible for usual logarithmic RG-evolution equations, eq. (2.14) was called the *R-evolution equation* in refs. [23, 24]. Continuing on the thoughts made at the end of section 2.1 we note that one can interpret the MSR mass $m_Q^{\rm MSR}(R)$ as the pole mass *minus* all self-energy contributions coming from scales *below* R and all virtual quark mass corrections from quarks lighter than Q, see figure 1. This also illustrates that the MSR mass $m_Q^{\rm MSR}(R)$ is a short-distance mass. The negative overall sign on the r.h.s. of eq. (2.14) expresses that self-energy contributions are added to the MSR mass when R is evolved to smaller scales, and that $\Delta m^{(n_Q)}(R,R')$ for $R > R'$ is positive and represents the self-energy contributions to the mass in the presence of n_Q active dynamical flavors coming from the scales between R' and R. This is illustrated in figure 2.

In the context of the analyses in this work the essential property is that the $\mathcal{O}(\Lambda_{\rm QCD})$ renormalon ambiguity in the series on the r.h.s. of eq. (2.12) is R-independent. This entails that the R-evolution equation is free of the $\mathcal{O}(\Lambda_{\rm QCD})$ renormalon, and solving the R-evolution equation in eq. (2.16) allows to relate MSR masses at different scales in a way that is renormalon free and, in addition, systematically sums logarithms $\ln(R/R')$ to all orders in a way free of the $\mathcal{O}(\Lambda_{\rm QCD})$ renormalon. So the R-evolution equation resolves the problem of the large logarithms that arise when computing MSR mass differences in the fixed-order expansion. The integral of eq. (2.16) can be readily computed numerically, and an analytic solution has been discussed in detail in [24]. The analytic solution also allows to derive the large-order asymptotic form of the perturbative coefficients a_n. To implement renormalization scale variation in eq. (2.16) one expands $\alpha_s^{(n_Q)}(R)$ as a series in $\alpha_s^{(n_Q)}(\lambda R)$, and by varying λ in some interval around unity. We note that in our analysis we consider the top, bottom and charm mass scales, and using the R-evolution equation is instrumental for our discussion of the top quark pole mass.

In table 1 we show numerical results for various MSR mass differences $\Delta m^{(n_Q)}$ relevant in our examinations below for $n_Q = 3, 4, 5$. We display the results obtained from using the

JHEP09(2017)099

$\mathcal{O}(\alpha_s^n)$	$\Delta m^{(5)}(163, 20)$	$\Delta m^{(5)}(163, 4.2)$	$\Delta m^{(5)}(163, 1.3)$
$n = 1$	7.358 ± 0.811	8.536 ± 1.008	8.864 ± 1.047
$n = 2$	8.007 ± 0.168	9.336 ± 0.225	9.728 ± 0.311
$n = 3$	8.031 ± 0.024	9.368 ± 0.035	9.764 ± 0.066
$n = 4$	8.006 ± 0.009	9.331 ± 0.016	9.716 ± 0.023
$\mathcal{O}(\alpha_s^n)$	$\Delta m^{(4)}(163, 4.2)$	$\Delta m^{(4)}(20, 4.2)$	$\Delta m^{(4)}(4.2, 1.3)$
$n = 1$	8.181 ± 1.026	1.153 ± 0.211	0.337 ± 0.098
$n = 2$	9.064 ± 0.270	1.326 ± 0.073	0.419 ± 0.063
$n = 3$	9.139 ± 0.054	1.346 ± 0.018	0.434 ± 0.026
$n = 4$	9.114 ± 0.014	1.337 ± 0.007	0.423 ± 0.017
$\mathcal{O}(\alpha_s^n)$	$\Delta m^{(3)}(163, 1.3)$	$\Delta m^{(3)}(20, 1.3)$	$\Delta m^{(3)}(4.2, 1.3)$
$n = 1$	8.009 ± 1.044	1.419 ± 0.296	0.328 ± 0.106
$n = 2$	9.008 ± 0.404	1.691 ± 0.166	0.418 ± 0.078
$n = 3$	9.130 ± 0.126	1.741 ± 0.067	0.440 ± 0.037
$n = 4$	9.111 ± 0.032	1.729 ± 0.023	0.434 ± 0.020

Table 1. MSR mass differences $\Delta m^{(n_Q)}(R, R')$ computed from R-evolution, for $n_Q = 3, 4, 5$ active dynamical flavors for scale differences involving top, bottom and charm masses and the scale 20 GeV. The central values are obtained for $\lambda = 1$ and the uncertainties are symmetrized λ variations in the interval $[0.5, 2]$. For entries involving the scale $\overline{m}_c$ the interval $[0.6, 2.5]$ is used for λ variations. The numbers for $\Delta m^{(n_Q)}(R, R')$ are given in units of GeV.

R-evolution equation at $\mathcal{O}(\alpha_s^n)$ for $n = 1, 2, 3, 4$. The uncertainties are from λ variations in the interval $[0.5, 2]$ for the cases where scales above the charm mass scale 1.3 GeV are considered, and in the interval $[0.6, 2.5]$ for cases which involve the charm mass scale. We see an excellent convergence and stability of the results and a significant reduction of scale variation with the order, illustrating that the mass differences $\Delta m^{(n_Q)}(R, R')$ are free of an $\mathcal{O}(\Lambda_{\rm QCD})$ renormalon ambiguity. For our analyses below we use the most precise $\mathcal{O}(\alpha_s^4)$ results shown in the respective lowest lines.

2.3 Asymptotic high order behavior and Borel transform for massless lighter quarks

In this section we review a number of known results relevant for the analyses in the subsequent parts of the paper. The results are already known since refs. [12–14]. We adapt them according to our notation and present updated numerical results accounting for the recent perturbative calculations of the pole-$\overline{\rm MS}$ mass relation and the QCD β-function.

The Borel transform of an α_s power series

$$f(\alpha_s(R)) = R \sum_{n=0}^{\infty} a_{n+1} \left(\frac{\alpha_s(R)}{4\pi}\right)^{n+1}, \tag{2.17}$$

is defined as

$$B[f](u) = R \sum_{n=0}^{\infty} a_{n+1} \frac{u^n}{n!\,\beta_0^{n+1}}\,, \tag{2.18}$$

where β_0 is the one-loop β-function coefficient in the flavor number scheme of α_s. For the approximation that all quarks lighter than the heavy quark Q are massless (i.e. $n_\ell = n_Q$) the Borel transform of the series for the pole-MSR mass reads

$$B\left[m_Q^{\rm pole} - m_Q^{\rm MSR}(R)\right](u) = \\ N_{1/2}^{(n_\ell)}\, R\, \frac{4\pi}{\beta_0^{(n_\ell)}} \sum_{k=0}^{\infty} g_k^{(n_\ell)} \frac{\Gamma(1+\hat{b}_1^{(n_\ell)}-k)}{\Gamma(1+\hat{b}_1^{(n_\ell)})}\,(1-2\,u)^{-1-\hat{b}_1^{(n_\ell)}+k} + \dots\,, \tag{2.19}$$

where the non-analytic (and singular) terms multiplied by the normalization factor $N_{1/2}^{(n_\ell)}$ single out the $\mathcal{O}(\Lambda_{\rm QCD})$ renormalon behavior of the pole-MSR mass series and the ellipses stand for contributions not affected by an $\mathcal{O}(\Lambda_{\rm QCD})$ renormalon. Their form is unambiguously determined by the coefficients $\beta_n^{(n_\ell)}$ of the QCD β-function in eq. (1.5), and the sum over k parametrizes the subleading effects due to the higher order coefficients of the QCD β-function. The coefficients $g_k^{(n_\ell)}$ can be determined from the recursion formulae [24]

$$\hat{b}_{n+1} = 2\sum_{i=0}^{n} \frac{\hat{b}_{n-i}\,\beta_{i+1}}{(-2\beta_0)^{i+2}}\,, \\ g_{n+1} = \frac{1}{1+n}\sum_{i=0}^{n} (-1)^i\,\hat{b}_{i+2}\,g_{n-i} \tag{2.20}$$

with $\hat{b}_0 = g_0 = 1$, where we dropped the superscript (n_ℓ) for simplicity. Currently, coefficients $g_k^{(n_\ell)}$ are known up to $k = 3$. The factor $N_{1/2}^{(n_\ell)}$ precisely quantifies the overall normalization of the $\mathcal{O}(\Lambda_{\rm QCD})$ renormalon behavior and can be determined quite precisely from the coefficients $a_n(n_\ell, 0)$ known from explicit computations. Accounting for the coefficients up to $\mathcal{O}(\alpha_s^4)$ the normalization was determined with very small errors for the relevant flavor numbers $n_\ell = 3, 4, 5$ in refs. [24, 27, 28], all of which are in agreement. We use the results from ref. [24]:

$$N_{1/2}^{(n_\ell=3)} = 0.526 \pm 0.012\,, \\ N_{1/2}^{(n_\ell=4)} = 0.492 \pm 0.016\,, \\ N_{1/2}^{(n_\ell=5)} = 0.446 \pm 0.024\,. \tag{2.21}$$

The uncertainties are not essential for the outcome of our analysis and quoted for completeness. Their small size reflects that the large-order asymptotic behavior of the series is known very precisely.

The inverse Borel transform

$$\int_0^\infty \mathrm{d}u\, B[f](u)\, \mathrm{e}^{-\frac{4\pi u}{\beta_0 \alpha_s(R)}}\,, \tag{2.22}$$

JHEP09(2017)099

has the same α_s power series as the original series $f(\alpha_s(R))$ and provides the exact result if it can be calculated unambiguously from the Borel transform $B[f](u)$. However, for the case of eq. (2.19), due to the singularity at $u = 1/2$ and the cut along the positive real axis for $u > 1/2$, the integral cannot be computed without further prescription and an ambiguity remains. Using an $i\epsilon$ prescription $(1-2u)^\alpha \to (1-2u-i\epsilon)^\alpha$ to shift the cut to the lower complex half plane, the resulting imaginary part of the integral is

$$\begin{aligned}\Delta m_{\rm Borel}^{(n_\ell)} &\equiv \left| {\rm Im} \int_0^\infty {\rm d}u \, \exp\left(-\frac{4\pi u}{\beta_0^{(n_\ell)} \alpha_s^{(n_\ell)}(R)}\right) \right. \\ &\qquad \left. \times \left[N_{1/2}^{(n_\ell)} \, R \, \frac{4\pi}{\beta_0^{(n_\ell)}} \sum_{k=0}^\infty g_k^{(n_\ell)} \frac{\Gamma(1+\hat{b}_1^{(n_\ell)} - k)}{\Gamma(1+\hat{b}_1^{(n_\ell)})} \, (1-2u)^{-1-\hat{b}_1^{(n_\ell)}+k} \right] \right| \\ &= N_{1/2}^{(n_\ell)} \, \frac{2\pi^2}{\beta_0^{(n_\ell)} \Gamma(1+\hat{b}_1^{(n_\ell)})} \Lambda_{\rm QCD}^{(n_\ell)} \,, \end{aligned} \tag{2.23}$$

and represents a quantification of the ambiguity of the pole mass, where $\Lambda_{\rm QCD}^{(n_\ell)}$ is given by the expression ($t_R = -2\pi/\beta_0^{(n_\ell)} \alpha_s^{(n_\ell)}(R)$)

$$\Lambda_{\rm QCD}^{(n_\ell)} = R \, \exp\left(t_R + \hat{b}_1^{(n_\ell)} \log(-t_R) - \sum_{k=2}^\infty \frac{\hat{b}_k^{(n_\ell)}}{(k-1) t_R^{k-1}} \right) . \tag{2.24}$$

In this work we use this expression as the definition of $\Lambda_{\rm QCD}$ for n_ℓ massless flavors. The r.h.s. is R-independent, and truncating at $k = 4$ provides the results

$$\begin{aligned} \Lambda_{\rm QCD}^{(n_\ell=3)} &= 253 \text{ MeV} \,, \\ \Lambda_{\rm QCD}^{(n_\ell=4)} &= 225 \text{ MeV} \,, \\ \Lambda_{\rm QCD}^{(n_\ell=5)} &= 166 \text{ MeV} \,, \end{aligned} \tag{2.25}$$

with uncertainties below 0.5 MeV. $\Lambda_{\rm QCD}^{(n_\ell)}$ increases for smaller flavor numbers n_ℓ since the scale-dependence of α_s, and thus also the infrared sensitivity of QCD quantities, increases with n_ℓ. The expressions for $\Delta m_{\rm Borel}^{(n_\ell)}$ for the size of the imaginary part of the inverse Borel transform in eq. (2.23) provide a parametric estimate for the ambiguity of the pole mass. Using eqs. (2.21) and (2.25) they give $\Delta m_{\rm Borel}^{(3,4,5)} = (329 \pm 8, 295 \pm 10, 213 \pm 11)$ MeV which are around a factor 1.3 larger than the corresponding values for $\Lambda_{\rm QCD}^{(n_\ell)}$.

From the expression for the Borel transform given in eq. (2.19) one can derive the large order asymptotic form of the perturbative coefficients a_n of the pole-MSR mass series (which describe the case that all quarks lighter than Q are massless, i.e. $n_Q = n_\ell$):

$$a_n^{\rm asy}(n_\ell, n_h) = a_n^{\rm asy}(n_\ell, 0) = 4\pi N_{1/2}^{(n_\ell)} (2\beta_0^{(n_\ell)})^{n-1} \sum_{k=0}^\infty g_k^{(n_\ell)} \frac{\Gamma(n+\hat{b}_1^{(n_\ell)} - k)}{\Gamma(1+\hat{b}_1^{(n_\ell)})} \,, \tag{2.26}$$

where the value of n_h is insignificant because the virtual effects of quark Q do not affect the large order asymptotic behavior. The sum in k is convergent, and truncating at $k = 3$ one can use the results for $n > 4$ as an approximation for the yet uncalculated series

n	$a_n^{\rm asy}(n_\ell=3,0)$	$a_n^{\rm asy}(n_\ell=4,0)$	$a_n^{\rm asy}(n_\ell=5,0)$
5	$(3.394 \pm 0.077) \times 10^{7}$	$(2.249 \pm 0.075) \times 10^{7}$	$(1.379 \pm 0.074) \times 10^{7}$
6	$(3.309 \pm 0.075) \times 10^{9}$	$(2.019 \pm 0.067) \times 10^{9}$	$(1.128 \pm 0.060) \times 10^{9}$
7	$(3.819 \pm 0.087) \times 10^{11}$	$(2.147 \pm 0.071) \times 10^{11}$	$(1.095 \pm 0.059) \times 10^{11}$
8	$(5.093 \pm 0.115) \times 10^{13}$	$(2.641 \pm 0.088) \times 10^{13}$	$(1.231 \pm 0.066) \times 10^{13}$
9	$(7.706 \pm 0.175) \times 10^{15}$	$(3.687 \pm 0.123) \times 10^{15}$	$(1.572 \pm 0.084) \times 10^{15}$
10	$(1.305 \pm 0.030) \times 10^{18}$	$(5.762 \pm 0.192) \times 10^{17}$	$(2.250 \pm 0.120) \times 10^{17}$
11	$(2.443 \pm 0.055) \times 10^{20}$	$(9.964 \pm 0.332) \times 10^{19}$	$(3.563 \pm 0.191) \times 10^{19}$
12	$(5.014 \pm 0.114) \times 10^{22}$	$(1.889 \pm 0.063) \times 10^{22}$	$(6.190 \pm 0.331) \times 10^{21}$

Table 2. Coefficients of the pole-MSR mass series for $a_{n>4}(n_\ell,0)$ for $n_\ell = 3,4,5$ estimated from the asymptotic formula of eq. (2.26) and with uncertainties from eq. (2.21).

coefficients. The results up to $n = 12$ for $n_\ell = 3,4,5$ using the values for the $N_{1/2}^{(n_\ell)}$ from eq. (2.21) are displayed in table 2.

With the normalization factors $N_{1/2}^{(n_\ell)}$, which are known to a precision of a few percent and which also entails the same precision for $\Delta m_{\rm Borel}^{(n_\ell)}$ and the asymptotic coefficients $a_n^{\rm asy}$, the series for the pole-MSR and also for the pole-$\overline{\rm MS}$ mass relation are essentially known to all orders for the case of $n_\ell = n_Q$. The task to determine the ambiguity of the pole mass involves to specify how this precisely known pattern limits the principle capability to determine the pole mass numerically, see the discussion in section 4.1. In other words, the ambiguity of the pole mass is known to be proportional to $\Delta m_{\rm Borel}^{(n_\ell)}$ or $\Lambda_{\rm QCD}^{(n_\ell)}$, but the factor of proportionality has to be determined from an additional dedicated analysis.

3 Integrating out hard modes from the heavy quark pole mass

3.1 MSR-$\overline{\rm MS}$ mass matching

Using the MSR mass we can successively separate off, i.e. integrate out, hard momentum contributions from the pole-$\overline{\rm MS}$ mass difference, $m_Q^{\rm pole} - \overline{m}_Q$. We start with the matching relation between the MSR and the $\overline{\rm MS}$ masses at the common scale $\mu = R = \overline{m}_Q$, which can be obtained by eliminating the pole mass from eqs. (2.9) and (2.12). The matching relation accounts for the virtual top quark loop contributions and can be written in the form

$$m_Q^{\rm MSR}(\overline{m}_Q) - \overline{m}_Q = \Delta m_Q^{(n_Q+1\to n_Q)}(\overline{m}_Q) + \delta m_{Q,q_1,\ldots,q_n}^{(n_Q+1\to n_Q)}(\overline{m}_Q)\,. \tag{3.1}$$

The term $\Delta m_Q^{(n_Q+1\to n_Q)}(\overline{m}_Q)$ contains the virtual top quark loop contributions in the approximation that all n_Q quarks lighter than quark Q are massless and has the form [24]

$$\begin{aligned}\Delta m_Q^{(n_Q+1\to n_Q)}(\overline{m}_Q) = \qquad\qquad\qquad\qquad\qquad\qquad\qquad\qquad\qquad\qquad (3.2)\\ \overline{m}_Q \Bigg\{ 1.65707 \left(\frac{\alpha_s^{(n_Q+1)}(\overline{m}_Q)}{4\pi}\right)^2 + [110.05 + 1.424\, n_Q] \left(\frac{\alpha_s^{(n_Q+1)}(\overline{m}_Q)}{4\pi}\right)^3 \\ + \left[352. \pm 31. - (111.59 \pm 0.10)\, n_Q + 4.40\, n_Q^2\right] \left(\frac{\alpha_s^{(n_Q+1)}(\overline{m}_Q)}{4\pi}\right)^4 + \ldots \Bigg\}\,,\end{aligned}$$

$\mathcal{O}(\alpha_s^n)$	$\Delta m_t^{(6\to5)}(\overline{m}_t)$	$\Delta m_b^{(5\to4)}(\overline{m}_b)$	$\Delta m_c^{(4\to3)}(\overline{m}_c)$
2	0.021 ± 0.004	0.003 ± 0.001	0.002 ± 0.002
3	0.033 ± 0.003	0.006 ± 0.002	0.008 ± 0.005
4	0.032 ± 0.001	0.004 ± 0.001	0.005 ± 0.002

Table 3. The MSR-$\overline{\rm MS}$ mass matching corrections for the top, bottom and charm quarks for $(\overline{m}_t, \overline{m}_b, \overline{m}_c) = (163, 4.2, 1.3)$ GeV, given in units of GeV. The uncertainties are obtained from variations of the renormalization scale in the range $0.5\,\overline{m}_Q \le \mu \le 2\,\overline{m}_Q$ for the top and bottom quark and $0.65\,\overline{m}_c \le \mu \le 2.5\,\overline{m}_c$ for the charm quark. The central value is the respective mean of the largest and smallest values obtained in the scale variation.

where we expressed the series in powers of the strong coupling in the (n_Q+1) flavor scheme. The series only contains the hard corrections coming from the virtual heavy quark Q and therefore does not have any $\mathcal{O}(\Lambda_{\rm QCD})$ ambiguity, see figure 2 for illustration.

In table 3 the numerical values for $\Delta m_Q^{(n_Q+1\to n_Q)}(\overline{m}_Q)$ are shown at $\mathcal{O}(\alpha_s^{2,3,4})$ for the top, bottom, and charm quarks for $(\overline{m}_t, \overline{m}_b, \overline{m}_c) = (163, 4.2, 1.3)$ GeV. Also shown is the variation due to changes in the renormalization scale in the range $0.5\,\overline{m}_Q \le \mu \le 2\,\overline{m}_Q$, for the top and bottom quark and $0.65\,\overline{m}_c \le \mu \le 2.5\,\overline{m}_c$ for the charm quark. The $\mathcal{O}(\alpha_s^3)$ corrections are quite sizable compared to the $\mathcal{O}(\alpha_s^2)$ contributions, but the $\mathcal{O}(\alpha_s^4)$ corrections are small indicating that the $\mathcal{O}(\alpha_s^4)$ result and the uncertainty estimate based on the scale variations can be considered reliable. Overall, the matching corrections amount to 32, 4 and 5 MeV for the top, bottom and charm quarks, respectively with an uncertainty at the level of 1 to 2 MeV. The numerical uncertainties of the $\mathcal{O}(\alpha_s^4)$ coefficients displayed in eq. (3.2) are smaller than 0.1 MeV for all cases and therefore irrelevant for practical purposes.

The term $\delta m_{Q,q_1,\ldots,q_n}^{(n_Q+1\to n_Q)}(\overline{m}_Q)$ represents the virtual top quark loop contributions arising from the finite masses of the lighter massive quarks $q_1, \ldots, q_n$. Since at $\mathcal{O}(\alpha_s^2)$ only the loop of quark Q can be inserted, the series for $\delta m_{Q,q_1,\ldots,q_n}^{(n_Q+1\to n_Q)}(\overline{m}_Q)$ starts at $\mathcal{O}(\alpha_s^3)$, where only self energy diagrams with one insertion of a loop of quark Q and one insertion of a loop of one of the lighter massive quarks $q_1, \ldots, q_n$ can contribute. At $\mathcal{O}(\alpha_s^3)$ $\delta m_{Q,q_1,\ldots,q_n}^{(n_Q+1\to n_Q)}(\overline{m}_Q)$ has the form

$$
\begin{aligned}
&\delta m_{Q,q_1,\ldots,q_n}^{(n_Q+1\to n_Q)}(\overline{m}_Q) \\
&\quad = \overline{m}_Q \left\{ \left[\delta_{Q,3}^{(Q,q_1,\ldots,q_n)}(1, r_{q_1Q}, \ldots, r_{q_nQ}) \right.\right. \\
&\qquad\qquad \left.\left. - \delta_{Q,3}^{(Q,q_1,\ldots,q_n)}(1,0,\ldots,0) \right] \left(\frac{\alpha_s^{(n_Q+1)}(\overline{m}_Q)}{4\pi} \right)^3 + \ldots \right\} \\
&\quad = \overline{m}_Q \left\{ \sum_{i=1}^{n} \left[14.2222\, r_{q_iQ}^2 - 18.7157\, r_{q_iQ}^3 + \left(7.3689 - 11.1477 \ln(r_{q_iQ}) \right) r_{q_iQ}^4 \right.\right. \\
&\qquad\qquad \left.\left. + \ldots \right] \left(\frac{\alpha_s^{(n_Q+1)}(\overline{m}_Q)}{4\pi} \right)^3 + \ldots \right\} ,
\end{aligned}
\tag{3.3}
$$

where $r_{qQ} = \overline{m}_q/\overline{m}_Q$, and for simplicity we suppress the masses of the quarks $q_1, \ldots, q_n$ in the argument of $\delta m^{(n_Q+1\to n_Q)}_{Q,q_1,\ldots,q_n}$. Starting at $\mathcal{O}(\alpha_s^4)$ the finite quark mass corrections in $\delta m^{(n_Q+1\to n_Q)}_{Q,q_1,\ldots,q_n}(\overline{m}_Q)$ become also dependent on the flavor threshold corrections relating $\alpha_s^{(n_Q)}(\overline{m}_Q)$ and $\alpha_s^{(n_Q+1)}(\overline{m}_Q)$. In eq. (3.3) we have also displayed the first terms of the expansions in the mass ratios r_{q_iQ}. They start quadratically in the r_{q_iQ} indicating that the corrections are governed by the scale $\overline{m}_Q$ just like the matching term $\Delta m_Q^{(n_Q+1\to n_Q)}(\overline{m}_Q)$ and do not have any linear sensitivity to small momenta and the lighter quark masses, in particular. This feature is realized at any order of perturbation theory.

Because the finite mass corrections $\delta m^{n_Q+1\to n_Q}_{Q,q_1,\ldots,q_n}(\overline{m}_Q)$ start at $\mathcal{O}(\alpha_s^3)$ and are quadratic in the mass ratios r_{q_iQ} they are extremely small and never exceed 0.01 MeV for the top quark (due to the finite bottom or charm masses) and the bottom quark (due to the finite charm mass). We can expect that this is also exhibited at higher orders, so that $\delta m^{(n_Q+1\to n_Q)}_{Q,q_1,\ldots,q_n}(\overline{m}_Q)$ can be neglected for all practical purposes and will not be considered and discussed any further in this work.

3.2 Top-bottom and bottom-charm mass matching

Comparing the pole-MSR mass relation (2.12) for the heavy quark Q to the pole-$\overline{\rm MS}$ mass relation (2.4) for the next lighter massive quark q, one immediately notices that for $R = \overline{m}_q$ the corrections are identical in the approximation that in the *virtual* quark loops all n_Q lighter quarks (i.e. including the quark q) are treated as massless. This identity is a consequence of *heavy quark symmetry* which states that the low-energy QCD corrections to the heavy quark masses coming from massless partons are flavor-independent.

For the top MSR and the bottom $\overline{\rm MS}$ masses (i.e. for $Q = t$ and $q = b$) the resulting matching relation reads

$$\left[m_t^{\rm pole} - m_t^{\rm MSR}(\overline{m}_b)\right] - \left[m_b^{\rm pole} - \overline{m}_b\right] = \delta m_{b,c}^{(t\to b)}(\overline{m}_b, \overline{m}_c)\,, \tag{3.4}$$

where $\delta m_{b,c}^{(t\to b)}(\overline{m}_b, \overline{m}_c)$ encodes the heavy quark symmetry breaking corrections coming from the finite virtual charm and bottom quark masses. Their form can be extracted directly from eqs. (2.4) and (2.12) and written in the form ($r_{qq'} = \overline{m}_q/\overline{m}_{q'}$)

$$\delta m_{b,c}^{(t\to b)}(\overline{m}_b, \overline{m}_c) = \overline{m}_t \left[\delta_t^{(b,c)}(r_{bt}, r_{ct}) + \delta_t^{(c)}(r_{ct})\right] - \overline{m}_b \left[\bar{\delta}_b^{(b,c)}(1, r_{cb}) + \bar{\delta}_b^{(c)}(r_{cb})\right]\,, \tag{3.5}$$

where the first term on the r.h.s. (multiplied by $\overline{m}_t$) represents the virtual bottom and charm mass effects from the top quark self energy and the second term (multiplied by $\overline{m}_b$) represents the virtual bottom and charm mass effects from the bottom quark self energy. Their explicit form up to $\mathcal{O}(\alpha_s^3)$ reads

$$\begin{aligned}\overline{m}_t \left[\delta_t^{(b,c)}(r_{bt}, r_{ct}) + \delta_t^{(c)}(r_{ct})\right] &= \overline{m}_t \left[\,\delta_2(r_{bt}) + \delta_2(r_{ct})\,\right] \left(\frac{\alpha_s^{(5)}(\mu)}{4\pi}\right)^2 \\ &+ \overline{m}_t \left[\delta_{t,3}^{(b,c)}(r_{bt}, r_{ct}) + \delta_{t,3}^{(c)}(r_{ct}) + 4\beta_0^{(5)} \ln\left(\frac{\mu}{\overline{m}_t}\right) \left[\,\delta_2(r_{bt}) + \delta_2(r_{ct})\right]\right] \left(\frac{\alpha_s^{(5)}(\mu)}{4\pi}\right)^3 + \ldots\,,\end{aligned} \tag{3.6}$$

and

$$\overline{m}_b \left[\overline{\delta}_b^{(b,c)}(1, r_{cb}) + \overline{\delta}_b^{(c)}(r_{cb})\right] = \overline{m}_b \left[\, \delta_2(1) + \delta_2(r_{cb}) \,\right] \left(\frac{\alpha_s^{(5)}(\mu)}{4\pi}\right)^2 \tag{3.7}$$
$$+ \overline{m}_b \left[\delta_{b,3}^{(b,c)}(1, r_{cb}) + \delta_{b,3}^{(c)}(r_{cb}) + 4\beta_0^{(5)} \ln\left(\frac{\mu}{\overline{m}_b}\right) \left[\, \delta_2(1) + \delta_2(r_{cb}) \right] \right] \left(\frac{\alpha_s^{(5)}(\mu)}{4\pi}\right)^3 + \dots \,.$$

It is important that the quark mass corrections in (3.5) are expressed coherently in powers of α_s at the common scale μ because the individual δ_n terms carry contributions that modify the infrared sensitivity and therefore each contain $\mathcal{O}(\Lambda_{\rm QCD})$ renormalon ambiguities. In eq. (3.4) these renormalon ambiguities mutually cancel. We also note that $\delta m_{b,c}^{(t\to b)}(\overline{m}_b, \overline{m}_c)$ also depends on the top quark mass $\overline{m}_t$. We have suppressed $\overline{m}_t$ in the argument since $\delta m_{b,c}^{(t\to b)}(\overline{m}_b, \overline{m}_c)$ encodes symmetry breaking corrections due to the finite bottom and charm quark masses.

For the bottom MSR and the charm $\overline{\rm MS}$ masses the corresponding matching relation reads

$$\left[m_b^{\rm pole} - m_b^{\rm MSR}(\overline{m}_c)\right] - \left[m_c^{\rm pole} - \overline{m}_c\right] = \delta m_c^{(b\to c)}(\overline{m}_c) \,, \tag{3.8}$$

with

$$\delta m_c^{(b\to c)}(\overline{m}_c) = \overline{m}_b \delta_b^{(c)}(r_{cb}) - \overline{m}_c \overline{\delta}_c^{(c)}(1) \,, \tag{3.9}$$

where the first term on the r.h.s. (multiplied by $\overline{m}_b$) represents the virtual charm mass effects from the bottom quark self energy and the second term (multiplied by $\overline{m}_c$) represent the virtual charm mass effects from the charm quark self energy. Their explicit form up to $\mathcal{O}(\alpha_s^3)$ reads

$$\overline{m}_b\, \delta_b^{(c)}(r_{cb}) = \overline{m}_b\, \delta_2(r_{cb}) \left(\frac{\alpha_s^{(4)}(\mu)}{4\pi}\right)^2$$
$$+ \overline{m}_b \left[\delta_{b,3}^{(c)}(r_{cb}) + 4\beta_0^{(4)} \delta_2(r_{cb}) \ln\left(\frac{\mu}{\overline{m}_b}\right)\right] \left(\frac{\alpha_s^{(4)}(\mu)}{4\pi}\right)^3 + \dots \,, \tag{3.10}$$

and

$$\overline{m}_c\, \overline{\delta}_c^{(c)}(1) = \overline{m}_c\, \delta_2(1) \left(\frac{\alpha_s^{(4)}(\mu)}{4\pi}\right)^2$$
$$+ \overline{m}_c \left[\delta_{c,3}^{(c)}(1) + 4\beta_0^{(4)} \delta_2(1) \ln\left(\frac{\mu}{\overline{m}_c}\right)\right] \left(\frac{\alpha_s^{(4)}(\mu)}{4\pi}\right)^3 + \dots \,, \tag{3.11}$$

where again we expanded both terms consistently for a common renormalization scale μ in the strong coupling.

In figure 3(a) the top-MSR bottom-$\overline{\rm MS}$ mass matching correction $\delta m_{b,c}^{(t\to b)}(\overline{m}_b, \overline{m}_c)$ of eq. (3.4) is displayed as a function of the renormalization scale μ at $\mathcal{O}(\alpha_s^2)$ (red dashed line) and $\mathcal{O}(\alpha_s^3)$ (red solid line) for $(\overline{m}_t, \overline{m}_b, \overline{m}_c) = (163, 4.2, 1.3)$ GeV. The matching correction at $\mathcal{O}(\alpha_s^3)$ amounts to 6 MeV and has a scale variation of only 1 MeV for $\overline{m}_b \le \mu \le \overline{m}_t$.

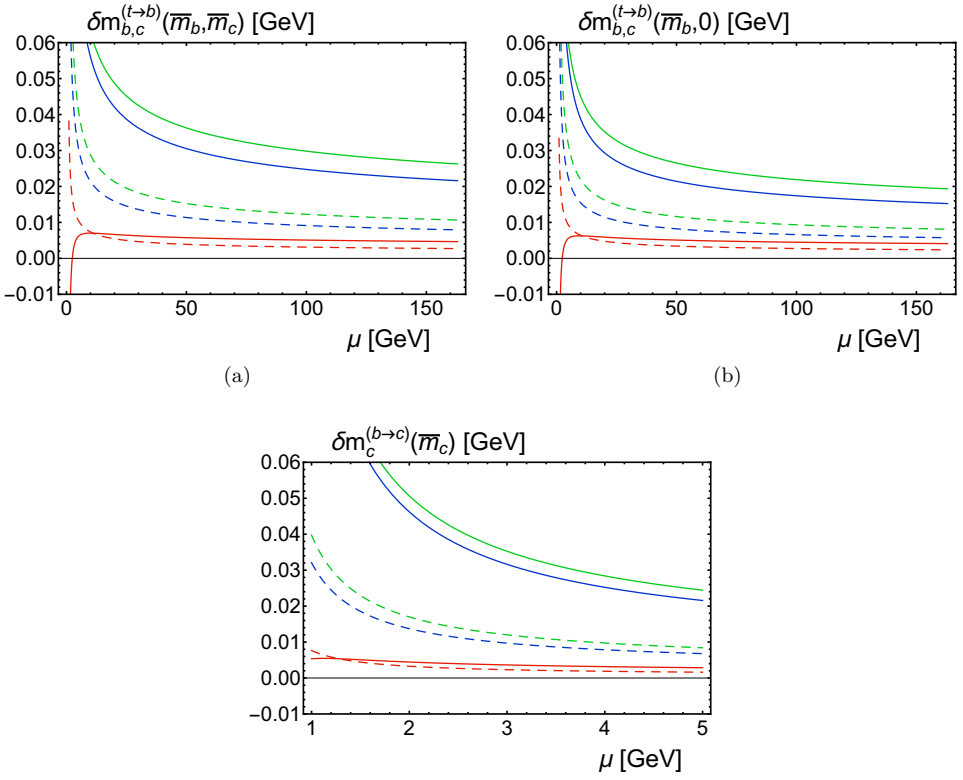

Figure 3. (a) Top-MSR bottom-$\overline{\rm MS}$ mass matching correction $\delta m_{b,c}^{(t\to b)}(\overline{m}_b, \overline{m}_c)$ at $\mathcal{O}(\alpha_s^2)$ (red dashed curve) and $\mathcal{O}(\alpha_s^3)$ (red solid curve) over the renormalization scale μ. The virtual bottom and charm mass effects to the top quark self energy of eq. (3.6) (green curves) and the virtual bottom and charm mass effects to the bottom quark self energy of eq. (3.7) (blue curves) at $\mathcal{O}(\alpha_s^2)$ (dashed) and $\mathcal{O}(\alpha_s^3)$ (solid). For the masses of the top, bottom and charm quarks the values $(\overline{m}_t, \overline{m}_b, \overline{m}_c) = (163, 4.2, 1.3)$ GeV are used. (b) Same quantities as in panel (a) for $\overline{m}_c = 0$. (c) The bottom-MSR charm-$\overline{\rm MS}$ mass matching correction $\delta m_c^{(b\to c)}(\overline{m}_c)$ at $\mathcal{O}(\alpha_s^2)$ (red dashed curve) and $\mathcal{O}(\alpha_s^3)$ (red solid curve) over the renormalization scale μ. The virtual charm mass effects to the bottom quark self energy of eq. (3.10) (green curves) and the virtual charm mass effects to the charm quark self energy of eq. (3.11) (blue curves) are shown at $\mathcal{O}(\alpha_s^2)$ (dashed) and $\mathcal{O}(\alpha_s^3)$(solid).

Compared to the $\mathcal{O}(\alpha_s^2)$ result we see a strong reduction of the scale-dependence at $\mathcal{O}(\alpha_s^3)$. The final numerical results at $\mathcal{O}(\alpha_s^2)$ and $\mathcal{O}(\alpha_s^3)$ are shown in the second column of table 4 where the uncertainties are obtained from variations of the renormalization scale in the range $\overline{m}_b \le \mu \le \overline{m}_t$ and the central values are the respective mean of the largest and smallest values obtained in the scale variation. The corresponding results for a vanishing charm quark mass are shown in figure 3(b) and the third column of table 4. We see that the charm mass effects in the top-MSR bottom-$\overline{\rm MS}$ mass matching correction $\delta m_{b,c}^{(t\to b)}(\overline{m}_b, \overline{m}_c)$ are only around 1 MeV, and the stability for $\overline{m}_c \to 0$ shows that the matching correction

JHEP09(2017)099

$\mathcal{O}(\alpha_s^n)$	$\delta m_{b,c}^{(t\to b)}(\overline{m}_b,\overline{m}_c)$	$\delta m_{b,c}^{(t\to b)}(\overline{m}_b,0)$	$\delta m_c^{(b\to c)}(\overline{m}_c)$
2	0.007 ± 0.004	0.006 ± 0.004	0.004 ± 0.002
3	0.006 ± 0.001	0.005 ± 0.001	0.004 ± 0.001

Table 4. The top-bottom MSR-$\overline{\rm MS}$ mass matching corrections, given in units of GeV, for finite bottom and charm masses (second column), for finite bottom quark mass and massless charm quark (third column), and the bottom-charm MSR-$\overline{\rm MS}$ mass matching correction (fourth column). For the finite masses of the top, bottom and charm quarks the values $(\overline{m}_t, \overline{m}_b, \overline{m}_c) = (163, 4.2, 1.3)$ GeV are used. The uncertainties are obtained from variations of the renormalization scale in the range $\overline{m}_b \le \mu \le \overline{m}_t$ for $\delta m_{b,c}^{(t\to b)}$ and in the range $\overline{m}_c \le \mu \le \overline{m}_b$ for $\delta m_c^{(b\to c)}$. The central values are the respective mean of the largest and smallest values obtained in the scale variation.

is governed by scales of order $\overline{m}_b$ and higher, which reconfirms the range $\overline{m}_b \le \mu \le \overline{m}_t$ for the variation of the renormalization scale.

In figure 3(c) the bottom-MSR charm-$\overline{\rm MS}$ mass matching correction $\delta m_c^{(b\to c)}(\overline{m}_c)$ of eq. (3.8) is displayed as a function of the renormalization scale μ for $\overline{m}_b = 4.2$ GeV and $\overline{m}_c = 1.3$ GeV at $\mathcal{O}(\alpha_s^2)$ and $\mathcal{O}(\alpha_s^3)$ using the same color coding and curve styles as for figures 3(a) and 3(b). In the fourth column of table 4 the final numerical results at $\mathcal{O}(\alpha_s^2)$ and $\mathcal{O}(\alpha_s^3)$ are shown using $\overline{m}_c \le \mu \le \overline{m}_b$ for the renormalization scale variation. The stability and convergence is again excellent, and at $\mathcal{O}(\alpha_s^3)$ the matching correction amounts to 4 MeV with an uncertainty of 1 MeV.

Given that the heavy quark symmetry breaking matching corrections $\delta m_{b,c}^{(t\to b)}(\overline{m}_b,\overline{m}_c)$ and $\delta m_c^{(b\to c)}(\overline{m}_c)$ amount to only 4 to 6 MeV, we note that they may be simply neglected in practical applications where they yield contributions that are much smaller than other sources of uncertainties. In fact, this also applies to our subsequent studies of the top, bottom and charm quark pole masses. However, we include them here for completeness. Due to their small size, we have not explicitly included the heavy quark symmetry breaking matching corrections in the graphical illustration of figure 2.

3.3 Light virtual quark mass corrections at $\mathcal{O}(\alpha_s^4)$ and beyond

The excellent perturbative convergence of the top-MSR bottom-$\overline{\rm MS}$ mass matching correction $\delta m_{b,c}^{(t\to b)}(\overline{m}_b,\overline{m}_c)$ and of the bottom-MSR charm-$\overline{\rm MS}$ mass matching correction $\delta m_c^{(b\to c)}(\overline{m}_c)$ discussed in the previous section illustrates that they both are short-distance quantities and free of an $\mathcal{O}(\Lambda_{\rm QCD})$ renormalon ambiguity. This is also expected theoretically due to heavy quark symmetry. However, the facts that the overall size of the matching corrections only amounts to a few MeV, and that the $\mathcal{O}(\alpha_s^3)$ corrections are only around 1 MeV allows us to draw interesting conceptual implications for the large order asymptotic behavior of the virtual quark mass corrections in the mass relations of eqs. (2.4), (2.9) and (2.12). We discuss these implications in the following. As a consequence we can *predict* the yet uncalculated virtual quark mass corrections at $\mathcal{O}(\alpha_s^4)$ to within a few percent without an additional loop calculation and draw important conclusions on their properties for the orders beyond.

To be concrete, we consider the matching correction $\delta m_q^{(Q\to q)}(\overline{m}_q)$ between the MSR mass of heavy quark Q and the $\overline{\rm MS}$ mass of the next lighter massive quark q assuming the massless approximation for all quarks lighter than quark q i.e. $n_Q = n_q + 1 = n_\ell + 1$ and $n_\ell = n_q$ being the number of massless quarks. This situation applies to the matching relation for the top-MSR and the bottom $\overline{\rm MS}$ masses for a massless charm quark or to the matching relation between the bottom-MSR and the charm-$\overline{\rm MS}$ masses.

In figure 3(a) we have displayed separately the virtual bottom and charm mass effects to the top quark self energy of eq. (3.6) (green curves) and the virtual bottom and charm mass effects to the bottom quark self energy of eq. (3.7) (blue lines) at $\mathcal{O}(\alpha_s^2)$ (dashed) and $\mathcal{O}(\alpha_s^3)$ (solid). In figure 3(b) the charm quark is treated as massless in the same quantities. In figure 3(c) the virtual charm mass effects to the bottom quark self energy of eq. (3.10) and the virtual charm mass effects to the charm quark self energy of eq. (3.11) are shown at $\mathcal{O}(\alpha_s^2)$ and $\mathcal{O}(\alpha_s^3)$ with the analogous line styles and colors. We see that both types of contributions each are quite large and furthermore do not at all converge. The $\mathcal{O}(\alpha_s^3)$ corrections are even bigger than the $\mathcal{O}(\alpha_s^2)$ corrections, which indicates that the corresponding asymptotic large order behavior already dominates the $\mathcal{O}(\alpha_s^2)$ and $\mathcal{O}(\alpha_s^3)$ corrections.

The origin of this behavior has been already mentioned and is understood: the mass of the virtual quark q acts as an infrared cutoff and therefore modifies the infrared sensitivity of the self energy diagrams (of quark Q and of quark q) with respect to the case where the virtual loops of quark q are evaluated in the massless approximation. As a consequence these corrections individually carry an $\mathcal{O}(\Lambda_{\rm QCD})$ renormalon ambiguity. Moreover, at large orders in perturbation theory the sensitivity of the self energy diagrams to infrared momenta increases due to high powers of logarithms from gluonic and massless quark loops. As a consequence, at large orders, the finite mass effects of the virtual loops of quark q in the self energy diagrams of quark Q and the self energy diagrams of quark q become equivalent due to heavy quark symmetry. The strong cancellation in the sum of both types of corrections in $\delta m_q^{(Q\to q)}(\overline{m}_q)$ ($\sim 75\%$ at $\mathcal{O}(\alpha_s^2)$ and $\gtrsim 90\%$ at $\mathcal{O}(\alpha_s^3)$ for the cases displayed in figure 3) thus confirms that the known $\mathcal{O}(\alpha_s^2)$ and $\mathcal{O}(\alpha_s^3)$ self energy corrections coming from virtual quark masses are already dominated by their large order asymptotic behavior.

From the observations that the series for $\delta m_{b,c}^{(t\to b)}(\overline{m}_b, \overline{m}_c)$ and $\delta m_c^{(b\to c)}(\overline{m}_c)$ converge very well and that their $\mathcal{O}(\alpha_s^3)$ corrections amount to only about 1 MeV, we can therefore expect that the two types of corrections that enter $\delta m_{b,c}^{(t\to b)}(\overline{m}_b, \overline{m}_c)$ as well as $\delta m_c^{(b\to c)}(\overline{m}_c)$ agree to even better than 1 MeV at $\mathcal{O}(\alpha_s^4)$ and beyond. This allows us to make an approximate *prediction* for the yet uncalculated $\mathcal{O}(\alpha_s^4)$ finite mass corrections from virtual loops of quark q in the pole-$\overline{\rm MS}$ mass relations of quark Q of eqs. (2.4) and (2.9) by setting the $\mathcal{O}(\alpha_s^4)$ correction in $\delta m_q^{(Q\to q)}(\overline{m}_q)$ to zero:

$$
\begin{aligned}
&\delta_{Q,4}^{(q)}(r_{qQ}) \qquad\qquad (3.12)\\
&\approx r_{qQ}\left[\delta_{q,4}^{(q)}(1)+\left(6\,\beta_0^{(n_Q)}\delta_{q,3}^{(q)}(1)+4\,\beta_1^{(n_Q)}\delta_2(1)\right)\ln\left(\frac{\mu}{\overline{m}_q}\right)+12\,\delta_2(1)\left(\beta_0^{(n_Q)}\ln\left(\frac{\mu}{\overline{m}_q}\right)\right)^2\right]\\
&\quad-\left(6\,\beta_0^{(n_Q)}\delta_{Q,3}^{(q)}(r_{qQ})+4\,\beta_1^{(n_Q)}\delta_2(r_{qQ})\right)\ln\left(\frac{\mu}{\overline{m}_Q}\right)-12\,\delta_2(r_{qQ})\left(\beta_0^{(n_Q)}\ln\left(\frac{\mu}{\overline{m}_Q}\right)\right)^2.
\end{aligned}
$$

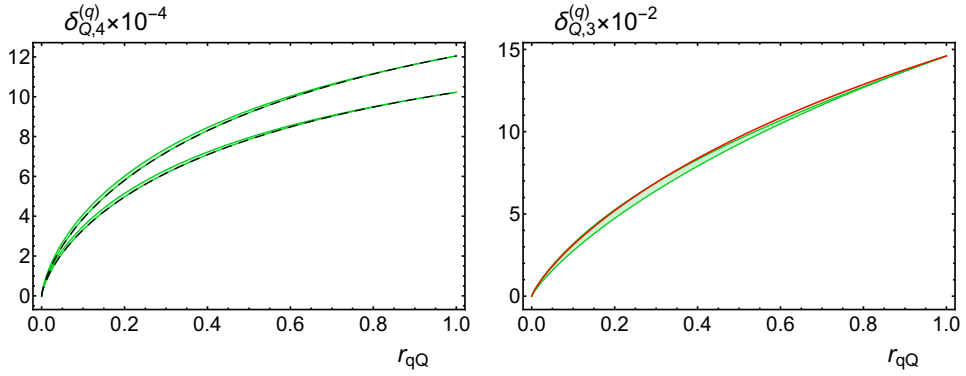

(a) (b)

Figure 4. (a) Prediction for the $\mathcal{O}(\alpha_s^4)$ virtual quark mass correction $\delta^{(q)}_{Q,4}(r_{qQ})$ for $\overline{m}_q \le \mu \le \overline{m}_Q$ (green bands) for $n_Q = n_\ell + 1 = 5$ (lower band) and $n_Q = n_\ell + 1 = 4$ (upper band). The black dashed lines show the prediction for $\mu = \overline{m}_Q$ which gives the simple approximation formula in eq. (3.14). (b) The $\mathcal{O}(\alpha_s^3)$ virtual quark mass correction $\delta^{(q)}_{Q,3}(r_{qQ})$ for $n_Q = n_\ell + 1 = 5$ (red curve). The green band is the prediction for $\delta^{(q)}_{Q,3}(r_{qQ})$ using the method of panel (a) for $\overline{m}_q \le \mu \le \overline{m}_Q$ showing excellent agreement to the exact result within errors.

The prediction has a residual μ-dependence, which would vanish in the formal limit that the virtual quark q mass corrections are entirely dominated by their large order asymptotic behavior. Therefore the dependence on the scale μ can be used as an uncertainty estimate of our approximation.

In figure 4(a) we show the prediction for $\delta^{(q)}_{Q,4}(r_{qQ})$ for $\overline{m}_q \le \mu \le \overline{m}_Q$ (green bands) for $n_Q = n_q + 1 = n_\ell + 1 = 5$ (lower band) and $n_Q = n_q + 1 = n_\ell + 1 = 4$ (upper band). The prediction satisfies exactly the required boundary condition $\delta^{(q)}_{Q,4}(0) = 0$ and eq. (2.11) for $r_{qQ} = 1$ and provides an interpolation for $0 < r_{qQ} < 1$ with an uncertainty of $\pm 3\%$ (for $r_{qQ} \lesssim 0.1$) or smaller (for $r_{qQ} > 0.1$). To judge the quality of the prediction we apply the same method at $\mathcal{O}(\alpha_s^3)$ to "predict" $\delta^{(q)}_{Q,3}(r_{qQ})$ which gives

$$\delta^{(q)}_{Q,3}(r_{qQ}) \approx r_{qQ}\left[\delta^{(q)}_{q,3}(1) + 4\,\beta_0^{(n_Q)}\delta_2(1)\ln\left(\frac{\mu}{\overline{m}_q}\right)\right] - 4\beta_0^{(n_Q)}\delta_2(r_{qQ})\ln\left(\frac{\mu}{\overline{m}_Q}\right). \qquad (3.13)$$

The result for the prediction of $\delta^{(q)}_{Q,3}(r_{qQ})$ is shown in figure 4(b) for $n_Q = n_q+1 = n_\ell+1 = 5$. The green band illustrates again the range of predictions for μ-variations $\overline{m}_q \le \mu \le \overline{m}_Q$, and represents an uncertainty of $\pm 10\%$ (for $r_{qQ} \lesssim 0.1$) or smaller (for $r_{qQ} > 0.1$). Compared to the $\mathcal{O}(\alpha_s^4)$ result, the larger μ variation we observe at $\mathcal{O}(\alpha_s^3)$ is expected because the infrared sensitivity is weaker and the large order asymptotic behavior is less dominating at the lower order. The red curve is the exact result for $\delta^{(q)}_{Q,3}(r_{qQ})$ obtained from the results in ref. [31], see also eq. (A.4). We see that the prediction is fully compatible with the exact result and that the uncertainty estimate based on the μ-variation is reliable. The prediction for $\delta^{(q)}_{Q,3}(r_{qQ})$ for $n_Q = n_q+1 = n_\ell+1 = 4$ has the same good properties but is not displayed since it is numerically very close to the prediction for $n_Q = n_q + 1 = n_\ell + 1 = 5$.

Overall, the examination shows that the prediction and the uncertainty estimate for $\delta^{(q)}_{Q,4}(r_{qQ})$ can be considered reliable. We can also provide a very simple closed analytic expression by evaluating eq. (3.12) for $\mu = \overline{m}_Q$, which gives

$$\begin{aligned}
&\delta^{(q)}_{Q,4}(r_{qQ}) \qquad (3.14)\\
&\approx r_{qQ}\left[\delta^{(q)}_{q,4}(1) - \left(6\,\beta_0^{(n_Q)}\delta^{(q)}_{q,3}(1) + 4\,\beta_1^{(n_Q)}\delta_2(1)\right)\ln(r_{qQ}) + 12\,\delta_2(1)\left(\beta_0^{(n_Q)}\ln(r_{qQ})\right)^2\right]\\
&= r_{qQ}\Big[(203915. \pm 32.) - 22962.\,n_Q + 525.2\,n_Q^2\\
&\qquad + (-130946. + 13831.\,n_Q - 328.5\,n_Q^2)\,\ln(r_{qQ})\\
&\qquad + (26599.1 - 3224.1\,n_Q + 97.70\,n_Q^2)\,\ln(r_{qQ})^2\Big]\,.
\end{aligned}$$

The expression depends via the boundary condition of eq. (2.11) entirely on the coefficients $a_n(n_q, n_h)$ of eq. (2.5), which for this case describe the corrections to the heavy quark q self energy for the case that all lighter quarks are massless, and the coefficients of the β-function. The expression is shown as the black dashed lines in figure 4(a) for $n_Q = n_\ell + 1 = 5$ (lower line) and $n_Q = n_\ell + 1 = 4$ (upper line). This approximation for $\delta^{(q)}_{Q,4}(r_{qQ})$ has a simple overall linear behavior on the mass ratio $r_{qQ} = \overline{m}_q/\overline{m}_Q$. The behavior is just a manifestation of $\delta^{(q)}_{Q,4}(r_{qQ})$ being dominated by the large order asymptotic behavior due to its $\mathcal{O}(\Lambda_{\rm QCD})$ renormalon ambiguity which is related to linear sensitivity to small scales. The overall linear dependence of $\delta^{(q)}_{Q,4}(r_{qQ})$ on $\overline{m}_q$ arises since the mass of quark q represents an infrared cut and thus represents the characteristic physical scale that governs $\delta^{(q)}_{Q,4}(r_{qQ})$. This also explains the origin of the logarithms shown in eq. (3.14): they arise because all virtual quark mass corrections in eqs. (2.4), (2.9) and (2.12) are defined in an expansion in $\alpha_s(\overline{m}_Q)$. We note that for the $\mathcal{O}(\alpha_s^3)$ virtual massive quark correction $\delta^{(q)}_{Q,3}(r_{qQ})$ these aspects were already discussed in ref. [34] and later in ref. [27], where a direct comparison to the explicit calculations from ref. [31] could be carried out. These analyses were, however, using generic considerations and were not carried out within a systematic RG framework.

The expression of eq. (3.14) is a special case of the general statement that the asymptotic large order behavior of the coefficients $\delta^{(q)}_{Q,n}(r_{qQ})$ can be obtained from the relation

$$\begin{aligned}
&\delta_2(r_{qQ})\left(\frac{\alpha_s^{(n_Q)}(\overline{m}_Q)}{4\pi}\right)^2 + \sum_{n=3}^{\infty}\delta^{(q)}_{Q,n}(r_{qQ})\left(\frac{\alpha_s^{(n_Q)}(\overline{m}_Q)}{4\pi}\right)^n \qquad (3.15)\\
&\qquad \approx r_{qQ}\,\bar{\delta}^{(q)}_q(1) = r_{qQ}\left[\delta_2(1)\left(\frac{\alpha_s^{(n_Q)}(\overline{m}_q)}{4\pi}\right)^2 + \sum_{n=3}^{\infty}\delta^{(q)}_{q,n}(1)\left(\frac{\alpha_s^{(n_Q)}(\overline{m}_q)}{4\pi}\right)^n\right],
\end{aligned}$$

where on the r.h.s. of the approximate equality $\alpha_s^{(n_Q)}(\overline{m}_q)$ has to be expanded in powers of $\alpha_s^{(n_Q)}(\overline{m}_Q)$, and we have $\delta_2(1) = 18.3189$, $\delta^{(q)}_{q,3}(1) = 1870.79 - 82.1208\,n_Q$ and $\delta^{(q)}_{q,4}(1) = (203915. \pm 32.) - 22961.6\,n_Q + 525.216\,n_Q^2$. The terms $\delta^{(q)}_{q,n}(1)$ for $n > 4$ can be obtained from using eqs. (2.10) and (2.11) together with the large order asymptotic form of the coefficients a_n shown in eq. (2.26), giving

$$\delta^{(q)}_{q,n>4}(1) \approx a_n^{\rm asy}(n_q) - a_n^{\rm asy}(n_q+1) = a_n^{\rm asy}(n_Q-1) - a_n^{\rm asy}(n_Q)\,, \qquad (3.16)$$

where we would like to remind the reader that for the case we consider here we have $n_Q = n_q + 1 = n_\ell + 1$. Our examination at $\mathcal{O}(\alpha_s^3)$ and $\mathcal{O}(\alpha_s^4)$ above showed that this relation provides an approximation for $\delta^{(q)}_{Q,4}$ within a few percent. For the higher-order terms $\delta^{(q)}_{Q,n}$ with $n > 4$ it should be even more precise, and we therefore believe that it should be sufficient for essentially all future applications in the context of studies of the pole mass scheme.

To conclude we note that it is straightforward to extend eq. (3.12) from the case of having only one massive quark q being lighter than heavy quark Q, i.e. $n_Q = n_q+1 = n_\ell+1$, to the case of having a larger number of lighter massive quarks. For example for the case that there are two massive quarks lighter than quark Q (let's say q and q', in order of decreasing mass) with $n_Q = n_q + 1 = n_{q'} + 2 = n_\ell + 2$, the generalization of the approximation formula (3.12) reads

$$
\begin{aligned}
&\delta^{(q,q')}_{Q,4}(r_{qQ}, r_{q'Q}) + \delta^{(q')}_{Q,4}(r_{q'Q}) \approx r_{qQ} \Bigg\{ \delta^{(q,q')}_{q,4}(1, r_{q'q}) + \delta^{(q')}_{q,4}(r_{q'q}) \\
&\quad + \Big[6\,\beta_0^{(n_Q)} \Big(\delta^{(q,q')}_{q,3}(1, r_{q'q}) + \delta^{(q')}_{q,3}(r_{q'q})\Big) + 4\,\beta_1^{(n_Q)} \big(\delta_2(1) + \delta_2(r_{q'q})\big)\Big] \ln\left(\frac{\mu}{\overline{m}_q}\right) \\
&\quad + 12\,\big(\delta_2(1) + \delta_2(r_{q'q})\big)\,\left(\beta_0^{(n_Q)} \ln\left(\frac{\mu}{\overline{m}_q}\right)\right)^2 \Bigg\} \\
&\quad - \Big[6\,\beta_0^{(n_Q)} \Big(\delta^{(q,q')}_{Q,3}(r_{qQ}, r_{q'Q}) + \delta^{(q')}_{Q,3}(r_{q'Q})\Big) + 4\,\beta_1^{(n_Q)} \big(\delta_2(r_{qQ}) + \delta_2(r_{q'Q})\big)\Big] \ln\left(\frac{\mu}{\overline{m}_Q}\right) \\
&\quad - 12\,\big(\delta_2(r_{qQ}) + \delta_2(r_{q'Q})\big)\,\left(\beta_0^{(n_Q)} \ln\left(\frac{\mu}{\overline{m}_Q}\right)\right)^2 .
\end{aligned}
\tag{3.17}
$$

3.4 Pole mass differences

Using the MSR mass we have set up a conceptual framework to systematically quantify the contributions to the pole mass of a heavy quark coming from the different momentum regions contained in the on-shell self energy diagrams. The pole mass of a heavy quark Q contains the contributions from all momenta, while the $\overline{\rm MS}$ mass $\overline{m}_Q(\mu)$ and the MSR mass $m_Q^{\rm MSR}(R)$ contain the contributions from above the scales μ and R, respectively (see figure 1). The MSR mass is the natural extension of the $\overline{\rm MS}$ mass, which is applied for scales $\mu > m_Q$, to scales $R < m_Q$, and obeys a RG-evolution equation that is linear in R, called R-evolution [23, 24]. The R-evolution equation quantifies in a way free of the $\mathcal{O}(\Lambda_{\rm QCD})$ renormalon the change in the MSR mass when contributions from lower momenta are included into the mass when R is decreased, as long as $R > \Lambda_{\rm QCD}$.

In section 3.1 we discussed the matching corrections $\Delta m_Q^{(n_Q+1\to n_Q)}(\overline{m}_Q)$ that arise when the virtual loop contributions of quark Q are integrated out by switching from $\overline{m}_Q$ to $m_Q^{\rm MSR}(\overline{m}_Q)$. In section 2.2 we discussed the MSR mass difference $\Delta m^{(n_Q)}(R, R') = m_Q^{\rm MSR}(R') - m_Q^{\rm MSR}(R)$, which is determined from solving the R-evolution equation of the MSR mass and which systematically sums logarithms of R/R'. In section 3.2 we examined the matching between the QCD corrections to the MSR mass of the heavy quark Q and the

$\overline{\rm MS}$ mass of the next lighter massive quark q, $\delta m^{(Q\to q)}_{q,q',\dots}(\overline{m}_q, \overline{m}_{q'}, \dots)$ accounting for the mass effects of the quarks $q, q', \dots$. This matching is based on heavy quark symmetry and the small numerical size of $\delta m^{(Q\to q)}_{q,q',\dots}(\overline{m}_q, \overline{m}_{q'}, \dots)$ reflects that the symmetry breaking effects due to the finite quark masses are quite small. These two types of matching corrections and the R-evolution of the MSR mass each are free of $\mathcal{O}(\Lambda_{\rm QCD})$ renormalon ambiguities and show excellent convergence properties in QCD perturbation theory.

An interesting application is the determination of the difference of the pole masses of two massive quarks. Due to heavy quark symmetry, the differences of two heavy quark pole masses are also free of $\mathcal{O}(\Lambda_{\rm QCD})$ renormalon ambiguities and can therefore be determined to high precision. The matching corrections discussed above and the R-evolution of the MSR mass allow us to systematically sum logarithms of the mass ratios that would remain unsummed in a fixed-order calculation, and to achieve more precise perturbative predictions [24]. Taking the example of the top and bottom mass one can then write the difference of the top quark pole-$\overline{\rm MS}$ mass relation and the bottom quark pole-$\overline{\rm MS}$ mass relation in the form

$$\Big[m_t^{\rm pole} - \overline{m}_t\Big] - \Big[m_b^{\rm pole} - \overline{m}_b\Big] = \Delta m_t^{(6\to5)}(\overline{m}_t) + \Delta m^{(5)}(\overline{m}_t, \overline{m}_b) + \delta m_{b,c}^{(t\to b)}(\overline{m}_b, \overline{m}_c)\,. \quad (3.18)$$

The analogous relation for the bottom and charm quarks reads

$$\Big[m_b^{\rm pole} - \overline{m}_b\Big] - \Big[m_c^{\rm pole} - \overline{m}_c\Big] = \Delta m_b^{(5\to4)}(\overline{m}_b) + \Delta m^{(4)}(\overline{m}_b, \overline{m}_c) + \delta m_c^{(b\to c)}(\overline{m}_c)\,. \quad (3.19)$$

Each of the mass differences is the sum of universal matching and evolution building blocks which each can be computed to high precision, as shown in tables 1, 3, 4.

The resulting relations between the top, bottom and charm quark pole masses read

$$m_t^{\rm pole} - m_b^{\rm pole} = [\overline{m}_t - \overline{m}_b] + \Delta m_t^{(6\to5)}(\overline{m}_t) + \Delta m^{(5)}(\overline{m}_t, \overline{m}_b) + \delta m_{b,c}^{(t\to b)}(\overline{m}_b, \overline{m}_c)\,, \quad (3.20)$$

$$m_b^{\rm pole} - m_c^{\rm pole} = [\overline{m}_b - \overline{m}_c] + \Delta m_b^{(5\to4)}(\overline{m}_b) + \Delta m^{(4)}(\overline{m}_b, \overline{m}_c) + \delta m_c^{(b\to c)}(\overline{m}_c)\,, \quad (3.21)$$

$$\begin{aligned} m_t^{\rm pole} - m_c^{\rm pole} = {} & [\overline{m}_t - \overline{m}_c] + \Delta m_t^{(6\to5)}(\overline{m}_t) + \Delta m^{(5)}(\overline{m}_t, \overline{m}_b) + \delta m_{b,c}^{(t\to b)}(\overline{m}_b, \overline{m}_c) \\ & + \Delta m_b^{(5\to4)}(\overline{m}_b) + \Delta m^{(4)}(\overline{m}_b, \overline{m}_c) + \delta m_c^{(b\to c)}(\overline{m}_c)\,, \end{aligned} \quad (3.22)$$

and can be readily evaluated from the highest order results given in tables 1, 3, 4 for the case $(\overline{m}_t, \overline{m}_b, \overline{m}_c) = (163, 4.2, 1.3)$ GeV:

$$\begin{aligned} m_t^{\rm pole} - m_b^{\rm pole} &= 158.800 + (0.032 \pm 0.001) + (9.331 \pm 0.016) + (0.006 \pm 0.001)\ \text{GeV} \\ &= 168.169 \pm 0.016\ \text{GeV}\,, \end{aligned} \quad (3.23)$$

$$\begin{aligned} m_b^{\rm pole} - m_c^{\rm pole} &= 2.9 + (0.004 \pm 0.001) + (0.423 \pm 0.017) + (0.004 \pm 0.001)\ \text{GeV} \\ &= 3.331 \pm 0.017\ \text{GeV}\,, \end{aligned} \quad (3.24)$$

$$m_t^{\rm pole} - m_c^{\rm pole} = 171.500 \pm 0.024\ \text{GeV}\,, \quad (3.25)$$

where we have added all uncertainties quadratically. We can compare our results for the bottom-charm pole mass difference $m_b^{\rm pole} - m_c^{\rm pole}$ to the result obtained in ref. [36] using a fixed-order expansion at $\mathcal{O}(\alpha_s^3)$ for the mass difference. Their result was based on a linear

JHEP09(2017)099

approximation for the virtual charm quark mass effects derived in ref. [34] which is similar to eq. (3.13), but used a numerical calculation of the coefficient linear in r_{qQ} from ref. [37]. In this analysis the pole mass difference was used to eliminate the charm quark mass as a primary parameter in the predictions. They determined $m_b^{\rm pole} - m_c^{\rm pole} = 3.401 \pm 0.013$ GeV and obtained $\overline{m}_c = 1.22 \pm 0.06$ GeV from the fits using $\overline{m}_b = 4.16 \pm 0.05$ GeV as input. Their result for $m_b^{\rm pole} - m_c^{\rm pole}$ is consistent with ours, but one should keep in mind that logarithms of $\overline{m}_c/\overline{m}_b$ were not systematically summed and that their result also included nontrivial QCD corrections to semileptonic B-meson decay spectra for $B \to X_c \ell \nu$ and $B \to X_s \gamma$ which were only known to $\mathcal{O}(\alpha_s^2)$. The mutual agreement is reassuring (also for the theoretical approximations made in the context of the B meson analyses) and in particular shows that the summation of logarithms of $\overline{m}_c/\overline{m}_b$ is not essential for bottom and charm masses, which is expected, and that the $\mathcal{O}(\alpha_s^4)$ corrections are tiny, which can also be seen explicitly in our results. The larger error we obtain in our computation of $m_b^{\rm pole} - m_c^{\rm pole}$ arises from the renormalization scale variation in $\Delta m^{(4)}(\overline{m}_b, \overline{m}_c)$ which includes scales as low as $0.6\,\overline{m}_c$ while in their analysis the lowest renormalization scale was $\overline{m}_c$. Similar determinations of bottom and charm quark masses from B-meson decay spectra were carried out in refs. [38, 39], and they are also consistent with our result for $m_b^{\rm pole} - m_c^{\rm pole}$.

For the case $(\overline{m}_t, \overline{m}_b, \overline{m}_c) = (163, 4.2, 0)$ GeV, the difference between the top and bottom pole masses reads

$$\begin{aligned} m_t^{\rm pole} - m_b^{\rm pole} &= 158.800 + (0.032 \pm 0.001) + (9.331 \pm 0.016) + (0.005 \pm 0.001)\ \text{GeV} \\ &= 168.168 \pm 0.016\ \text{GeV}\,. \end{aligned} \tag{3.26}$$

This result differs from eq. (3.23) by only 1 MeV showing that the effects of the finite charm quark mass are tiny in the difference of the top and bottom pole masses. The uncertainties in the pole mass differences are between 16 and 24 MeV and should be considered as conservative estimates of the theoretical uncertainties due to missing higher order corrections.

3.5 Lighter massive flavor decoupling

Another very instructive application of the RG framework to quantify and separate the contributions to the pole mass of a heavy quark coming from the different physical momentum regions is to examine the effective massive flavor decoupling at large orders. It was observed in ref. [27] that the sum of the known $\mathcal{O}(\alpha_s^2)$ and $\mathcal{O}(\alpha_s^3)$ charm quark mass effects in the bottom quark pole-$\overline{\rm MS}$ mass series expressed in four flavor coupling $\alpha_s^{(4)}(\overline{m}_b)$ (where they amount to about 35 MeV) are essentially fully captured simply by expressing the series in the three flavor coupling $\alpha_s^{(3)}(\overline{m}_b)$ (where they amount to only -2 MeV). This observation entails that one can simply neglect the charm quark mass corrections by computing the bottom quark pole-$\overline{\rm MS}$ mass relation right from start in the three flavor theory without any charm quark (which corresponds to an infinitely heavy charm quark). This effective decoupling of lighter massive quarks is obvious and truly happening at asymptotic large orders. The importance of the observation made in ref. [27] was that the finite

charm quark mass corrections in the decoupled calculation at $\mathcal{O}(\alpha_s^2)$ and $\mathcal{O}(\alpha_s^3)$ were so tiny that there was no need to compute them explicitly in the first place. If this decoupling property would be true in general (i.e. the remaining light quark mass correction become negligible) it would represent a great simplification because it may make an explicit calculation of the lighter massive quark corrections and also the summation of the associated logarithms irrelevant.

Using the RG framework for the lighter massive flavor dependence of the pole mass we can examine systematically in which way this effective lighter massive quark decoupling property is realized. In the following we analyze this issue for $(\overline{m}_t, \overline{m}_b, \overline{m}_c) = (163, 4.2, 1.3)$ GeV. We start with the effects of the charm quark mass in the bottom pole-$\overline{\text{MS}}$ mass relation examined in ref. [27]. Applying the same considerations as for the pole mass differences in section 3.4 for this case we can write down the relation

$$m_b^{\text{pole}} - \left[\overline{m}_b + \overline{m}_b \sum_{n=1}^{\infty} a_n(n_\ell = 3, 0) \left(\frac{\alpha_s^{(3)}(\overline{m}_b)}{4\pi} \right)^n \right] \tag{3.27}$$

$$\begin{aligned} &= \Delta m_b^{(5\to4)}(\overline{m}_b) + \Delta m^{(4)}(\overline{m}_b, \overline{m}_c) + \delta m_c^{(b\to c)}(\overline{m}_c) + \Delta m_c^{(4\to3)}(\overline{m}_c) \\ &\quad - \Delta m^{(3)}(\overline{m}_b, \overline{m}_c) \\ &= (0.004 \pm 0.001) + (0.423 \pm 0.017) + (0.004 \pm 0.001) + (0.005 \pm 0.002) \\ &\quad - (0.434 \pm 0.020)\ \text{GeV} \\ &= 0.002 \pm 0.026\ \text{GeV}\,. \end{aligned} \tag{3.28}$$

The r.h.s. represents a computation of the charm quark mass corrections that remain within a calculation where the charm mass effects are approximated by making the charm infinitely heavy (i.e. $n_\ell = 3$). The individual numerical results have been taken from the highest order results in tables 1, 3 and 4, and for the final numerical result we have conservatively added all uncertainties quadratically. We see that these remaining corrections are essentially zero, fully confirming the observation of ref. [27]. This is not surprising since the bottom and charm quark masses are similar in size and the ratio $\overline{m}_c/\overline{m}_b$ does not lead to large logarithms. So the summation of these logarithms which is contained in our computation does not make an improvement, and the agreement with ref. [27] simply represents a computational cross check of both calculations. The scale uncertainty is larger than the one shown in ref. [27] because we considered variations of the renormalization scale down to $\mu = 0.6\,\overline{m}_c$, which were not considered by them, and because we do not attempt to eliminate the strong correlation in scale-dependence between $\Delta m^{(4)}(\overline{m}_b, \overline{m}_c)$ and $\Delta m^{(3)}(\overline{m}_b, \overline{m}_c)$ from these low scales here.

Let us now investigate the case of the bottom quark mass corrections in the top quark pole-$\overline{\text{MS}}$ mass relation assuming a massless charm quark. We can simply adapt eq. (3.27) through trivial modifications and obtain the relation

$$m_t^{\text{pole}} - \left[\overline{m}_t + \overline{m}_t \sum_{n=1}^{\infty} a_n(n_\ell = 4, 0) \left(\frac{\alpha_s^{(4)}(\overline{m}_t)}{4\pi} \right)^n \right] \tag{3.29}$$

$$\begin{aligned} &= \Delta m_t^{(6\to5)}(\overline{m}_t) + \Delta m^{(5)}(\overline{m}_t, \overline{m}_b) + \delta m_{b,c}^{(t\to b)}(\overline{m}_b, 0) + \Delta m_b^{(5\to4)}(\overline{m}_b) \\ &\quad - \Delta m^{(4)}(\overline{m}_t, \overline{m}_b) \end{aligned}$$

JHEP09(2017)099

$$
\begin{aligned}
&= (0.032 \pm 0.001) + (9.331 \pm 0.016) + (0.005 \pm 0.001) + (0.004 \pm 0.001) \\
&\quad - (9.114 \pm 0.014)\ \text{GeV} \\
&= 0.258 \pm 0.021\ \text{GeV}\,.
\end{aligned}
$$

We see that using the approximation of an infinitely heavy bottom quark for a calculation of the bottom mass effects in the top quark pole-$\overline{\text{MS}}$ mass relation gives a result that is about 260 MeV too small.

We can now go one step further and also consider the case where the masses of both the bottom and charm quark are accounted for. Generalizing the previous two calculations to this case is straightforward and we obtain

$$
\begin{aligned}
m_t^{\text{pole}} &- \left[\, \overline{m}_t + \overline{m}_t \sum_{n=1}^{\infty} a_n(n_\ell = 3, 0) \left(\frac{\alpha_s^{(3)}(\overline{m}_t)}{4\pi} \right)^n \,\right] \qquad (3.30) \\
&= \Delta m_t^{(6\to5)}(\overline{m}_t) + \Delta m^{(5)}(\overline{m}_t, \overline{m}_b) + \delta m_{b,c}^{(t\to b)}(\overline{m}_b, \overline{m}_c) \\
&\quad + \Delta m_b^{(5\to4)}(\overline{m}_b) + \Delta m^{(4)}(\overline{m}_b, \overline{m}_c) + \delta m_c^{(b\to c)}(\overline{m}_c) + \Delta m_c^{(4\to3)}(\overline{m}_c) \\
&\quad - \Delta m^{(3)}(\overline{m}_t, \overline{m}_c)\,. \\
&= (0.032 \pm 0.001) + (9.331 \pm 0.016) + (0.006 \pm 0.001) \\
&\quad + (0.004 \pm 0.001) + (0.423 \pm 0.017) + (0.004 \pm 0.001) + (0.005 \pm 0.002) \\
&\quad - (9.111 \pm 0.032)\ \text{GeV} \\
&= 0.694 \pm 0.040\ \text{GeV}\,.
\end{aligned}
$$

In this case using the approximation of infinitely heavy bottom and charm quarks for a calculation of the bottom and charm mass effects in the top quark pole-$\overline{\text{MS}}$ mass relation gives a result that is almost 700 MeV too small.

Our results show that the approximation of computing the lighter heavy flavor mass corrections in a theory where these heavy flavors are decoupled is an excellent approximation for the charm mass corrections in the bottom quark pole mass, but it is considerably worse for the top quark, where the discrepancy even reaches the 1 GeV level. The reason is that the decoupling limit can in general not capture the true size of the lighter quark mass effects if the hierarchy of scales is large. One should therefore not use this approximation to determine bottom or charm quark mass effects for the top quark.

4 The top quark pole mass ambiguity

4.1 General comments and estimation method

In this section we address the question of the best possible approximation and the ambiguity of the top quark pole mass m_t^{pole} using the RG formalism for the top mass described in the earlier sections. As a reminder and for illustration we show in figure 5 m_t^{pole} as a function of the order obtained from the series for $m_t^{\text{pole}} - m_t^{\text{MSR}}(\overline{m}_t)$ in powers of $\alpha_s^{(5)}$ given in eq. (2.12) for massless bottom and charm quarks, where the central dots are obtained for the default choice of renormalization scale $\mu = \overline{m}_t$ in the strong coupling and the error

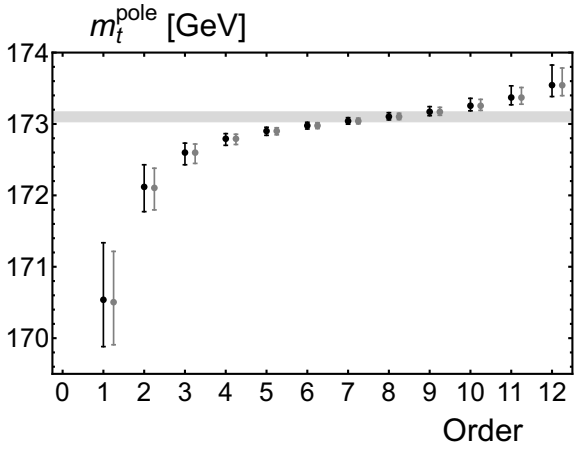

Figure 5. Top quark pole mass as a function of order obtained from the MSR mass $m_t^{\text{MSR}}(\overline{m}_t)$ (black) and $\overline{m}_t = \overline{m}_t(\overline{m}_t) = 163$ GeV (gray) for massless bottom and charm quarks. The central dots refer to the renormalization scale $\mu = \overline{m}_t$ for the strong coupling. The error bars arise from renormalization scale variation $\overline{m}_t/2 \leq \mu \leq 2\,\overline{m}_t$. The gray horizontal band represents the region $m_t^{\text{pole}} = 173.10 \pm 0.07$, which indicates the top quark pole mass and its scale uncertainty obtained from $m_t^{\text{MSR}}(\overline{m}_t)$ at the 8th order.

bars represent the scale variation $\overline{m}_t/2 \leq \mu \leq 2\,\overline{m}_t$. The corresponding results from the series for $m_t^{\text{pole}} - \overline{m}_t$ given in eq. (2.4) in powers of $\alpha_s^{(6)}$, also for massless bottom and charm quarks, are shown in gray. We have used the asymptotic form of the perturbative coefficients shown in table 2 for the series coefficients beyond $\mathcal{O}(\alpha_s^4)$.[3] We note that focusing on the approximation of massless bottom and charm quarks by itself is phenomenologically valuable because it is employed for most current predictions in the context of top quark physics, and since the analytic expressions are most transparent for this case.

The graphics illustrates visually the problematic features associated to the top quark $\mathcal{O}(\Lambda_{\text{QCD}})$ pole mass renormalon, and in particular the specific properties of the series for $\mu \sim m_t$ already mentioned in section 1: the minimal term of the series is obtained at order $n_{\text{min}} = 8$, which according to the theory of asymptotic series is the order that provides the best possible approximation for the top quark pole mass. Furthermore, the corrections are numerically close to the eighth order correction for the orders in the range 6 to 10, i.e. $\Delta n \approx 5$, for which the partially summed series increases linearly with the order. According to the theory of asymptotic series it is this region of orders that is relevant for the size of the principle uncertainty of this best approximation. We also see two very important practical issues appearing already at lower orders which can make dealing with the pole mass in mass determinations difficult: first, the higher order corrections are much larger than indicated by usual renormalization scale variations of the lower order prediction and, second, the common renormalization scale variation at any given truncation order is not an appropriate

[3]The uncertainties of the normalization factors $N_{1/2}^{(n_Q)}$ are about an order of magnitude smaller than the renormalization scale variation of the series beyond $\mathcal{O}(\alpha_s^4)$ and therefore not significant for our analysis.

JHEP09(2017)099

tool to estimate the perturbative uncertainty. In this context it is easy to understand that specifying a concrete numerical value for the principle uncertainty of the top quark pole mass is non-trivial even if the series is known precisely to all orders. So to obtain a top quark pole mass determination with uncertainties close to the principle uncertainty within a phenomenological analysis based on a usual truncated finite order calculation may be quite difficult. As a comparison let us recall the much better perturbative behavior of a series that is free of an $\mathcal{O}(\Lambda_{\rm QCD})$ renormalon ambiguity such as the MSR mass differences $\Delta m^{(n_Q)}(R, R')$ of eq. (2.16) with numerical evaluations given in table 1.

Prior to this work the issue of the best possible estimate and the ambiguity of the top quark pole mass were already studied in ref. [28]. They examined the pole-$\overline{\rm MS}$ mass relation of eq. (2.4) for massless bottom and charm quarks (i.e. $n_Q = n_t = n_\ell = 5$) and their analysis addressed the numerical uncertainty of the top quark pole mass accounting for all series terms displayed in figure 5 for $\mu = \overline{m}_t$. They adopted a prescription given in ref. [14], which *defined* the top quark pole mass uncertainty as the imaginary part of the inverse Borel integral of eq. (2.23), $\Delta m_{\rm Borel}^{(n_\ell=5)}$, divided by π, which gives about 65 MeV. Since this agrees in size with the minimal series term[4] they argued that $\Delta m_{\rm Borel}^{(n_\ell=5)}/\pi$ (or the size of the minimal term) is a reliable quantification of the top quark pole mass ambiguity, which they finally specified as 70 MeV. Interpreting the specification like a numerical uncertainty, this gives $m_t^{\rm pole} = 173.10 \pm 0.07$, which is shown in figure 5 as the thin gray horizontal band. The uncertainty band is about the same size as the renormalization scale variation of the series truncated at the eighth order.

We believe that quoting 70 MeV for the top quark pole mass ambiguity for massless bottom and charm quarks is too optimistic. Given (i) the overall bad behavior of the series, (ii) that there is a sizable range of orders where the corrections have very similar size and (iii) that the partially summed series increases linearly with the order in the range 6 to 10 ($\Delta n \approx 5$), we see no compelling reason to truncate precisely at the order $n_{\rm min} = 8$ and to quote a number at the level of the scale variation of the truncated series or the size of the correction at this order as the principle uncertainty. Our view is also supported by heavy quark symmetry (HQS) [30] which states that the pole mass ambiguity is independent of the mass of the heavy quark up to power corrections of $\mathcal{O}(\Lambda_{\rm QCD}^2/m_Q)$. This is the first aspect following from HQS we discussed in section 1. HQS requires that the criteria and the outcome of the method used to determine the top quark pole mass ambiguity are independent of the top mass value (as long as it is sufficiently bigger than $\Lambda_{\rm QCD}$). So it is straightforward to carry out a test concerning HQS by changing the value of $\overline{m}_t$ while keeping $\mu/\overline{m}_t = 1$ and checking whether the approach to estimate the ambiguity provides stable results.

Concerning ref. [28] this check is best carried out in the five-flavor scheme for the strong coupling, and we therefore evaluate the size of the minimal term in the series for

[4] In ref. [14] the order of the minimal series term $n_{\rm min}$ and the size of the minimal term $\Delta(n_{\rm min})$ were not chosen from the set of the actual series terms but computed from the minimum of a quadratic fit to the series terms in the vicinity of the minimum, so that their $n_{\rm min}$ was a non-integer value and their $\Delta(n_{\rm min})$ value is slightly smaller than the minimal term in the series. There are neither practical nor conceptual advantages of this procedure, and the numerical results are unchanged within their errors if $\Delta(n_{\rm min})$ is taken as the minimal terms in the series.

$m_t^{\rm pole} - m_t^{\rm MSR}(\overline{m}_t)$. Adopting the values 163, 20, 4.2, 2 and 1.3 GeV for $\overline{m}_t$ we obtain 62, 75, 91, 113 and 131 MeV for the minimal term $\Delta(n_{\rm min})$. This behavior is roughly described by the approximate formula $\Delta(n_{\rm min}) \approx (4\pi\alpha_s^{(n_\ell=5)}(\mu)/\beta_0^{(n_\ell=5)})^{1/2}\Lambda_{\rm QCD}^{(n_\ell=5)}$, already mentioned in section 1 and shows that the basic dependence on μ is logarithmic. We can even render the minimal term arbitrarily small if we adopt for $\overline{m}_t$ values much larger than 163 GeV. We see that $\Delta m_{\rm Borel}^{(n_\ell=5)}/\pi$, which is independent of the top mass value and therefore proportional to the ambiguity, agrees with the size of the minimal term only for $\mu \sim 163$ GeV, but disagrees for other choices. So the line of reasoning used for the analysis of the top quark pole mass ambiguity in ref. [28] is not independent of the top quark mass value, and one has to conclude that the ambiguity must be larger than $\Delta m_{\rm Borel}^{(n_\ell=5)}/\pi$ and certainly larger than 130 MeV, which is the size of the minimal term for a very small value of $\overline{m}_t$. Concerning the quoted numbers, we emphasize that we still discuss the case of massless bottom and charm quarks. From the relation $\Delta n \times \Delta(n_{\rm min}) \propto \pi^2 \Lambda_{\rm QCD}^{(n_\ell)}/\beta_0 \propto \Delta m_{\rm Borel}$ we see in particular that a reliable method consistent with HQS has to explicitly account for the range $n_{\rm min} \pm \Delta n/2$ in orders for which the terms in the series have values close to $\Delta(n_{\rm min})$. We stress that the latter issue is not at all new and has been known since the work of refs. [12, 13]. It was also argued in [28] that their approach to estimate the size of the top quark pole mass ambiguity is consistent concerning that issue. However, their approach did not account for the actual size of Δn, which is about 5 for the case discussed in [28] and also shown in figure 5.

In the following subsections we apply a method to determine the best possible estimate and the ambiguity of the top quark pole mass which explicitly accounts for the range $n_{\rm min} \pm \Delta n/2$ in orders where the $\Delta(n)$ are very close to $\Delta(n_{\rm min})$. It also accounts for the practical problems in an order-by-order determination of the pole mass from a series containing the $\mathcal{O}(\Lambda_{\rm QCD})$ renormalon which we discussed above in the context of figure 5. To describe the method we define, for a given series to calculate the top quark pole mass,

$$\Delta(n) \equiv m_t^{\rm pole}(n) - m_t^{\rm pole}(n-1)\,, \tag{4.1}$$

where $m_t^{\rm pole}(n)$ is the partial sum at $\mathcal{O}(\alpha_s^n)$ of the series for the top quark pole mass that contains the $\mathcal{O}(\Lambda_{\rm QCD})$ pole mass renormalon, and thus $\Delta(n)$ is the n-th order correction. The method we use is as follows:

1. We determine the minimal term $\Delta(n_{\rm min})$ and the set of orders $\{n\}_f \equiv \{n : \Delta(n) \leq f\,\Delta(n_{\rm min})\}$ in the series for a default renormalization scale, where f is a number larger but close to unity.

2. We use half of the range of values covered by $m_t^{\rm pole}(n)$ with $n \in \{n\}_f$ evaluated for this setup and include renormalization scale variation in a given range as an estimate for the ambiguity of the top quark mass. We use the midpoint of the covered range as the central value.

While $n_{\rm min}$, $\Delta(n_{\rm min})$ and Δn each can vary substantially depending on which setup one uses to determine $m_t^{\rm pole}$, the method provides results that are setup-independent and is therefore consistent with HQS. Through the RG formalism we developed in the previous

sections we can explicitly implement the other important requirement of HQS, namely that the ambiguities of the pole masses of all heavy quarks agree. To do this we apply our method for three different scenarios which differ on whether the bottom and charm quarks are treated as massive or massless and we furthermore study the pole-MSR mass difference for different values of R.

4.2 Massless bottom and charm quarks

For the case that the bottom and charm quarks are treated as massless we can calculate the top quark pole mass from the top MSR mass $m_t^{\rm MSR}(R)$ at different scales $R \leq \overline{m}_t$. Using the $\overline{\rm MS}$-MSR mass matching contribution $\Delta m_t^{(6\to5)}(\overline{m}_t)$ of eq. (3.2) and R-evolution from the scale $\overline{m}_t$ to R of eq. (2.16) with $n_t = 5$ active dynamical flavors one can write the top quark pole mass as

$$m_t^{\rm pole} = \overline{m}_t + \Delta m_t^{(6\to5)}(\overline{m}_t) + \Delta m^{(5)}(\overline{m}_t, R) + R \sum_{n=1}^{\infty} a_n(n_\ell = 5, 0) \left(\frac{\alpha_s^{(5)}(R)}{4\pi}\right)^n , \quad (4.2)$$

where the sum of the second and third term on the r.h.s. is just $m_t^{\rm MSR}(R) - \overline{m}_t$. The terms $\Delta m_t^{(6\to5)}(\overline{m}_t)$ and $\Delta m^{(5)}(\overline{m}_t, R)$ are free of an $\mathcal{O}(\Lambda_{\rm QCD})$ renormalon ambiguity and can be evaluated to the highest order given in tables 1 and 3. We can then determine the best estimate of the top quark pole mass and its $\mathcal{O}(\Lambda_{\rm QCD})$ renormalon ambiguity from the R-dependent series which is just equal to $m_t^{\rm pole} - m_t^{\rm MSR}(R)$. The outcome of the analysis using the method described in section 4.1 for $\overline{m}_t = 163$ GeV and $R = 163, 20, 4.2$ and 1.3 GeV and $f = 5/4$ is shown in the upper section of table 5.

The entries are as follows: the second column shows $m_t^{\rm MSR}(R) - \overline{m}_t = \Delta m_t^{(6\to5)}(\overline{m}_t) + \Delta m^{(5)}(\overline{m}_t, R)$ at the highest order. The third and fourth column show the order $n_{\rm min}$ and $\Delta(n_{\rm min})$ for the default renormalization scale $\mu = R$ for the cases $R = 163, 20$ and 4.2 GeV and $\mu = 2\overline{m}_c$ for $R = 1.3$ GeV. The values for $\Delta(n_{\rm min})$ for $R = 163$ and 20 GeV have an uncertainty because for these cases $n_{\rm min} > 4$ and the values for $\Delta(n > 4)$ are determined from the asymptotic large order values given in table 2 which have a numerical uncertainty from the normalization factor $N_{1/2}^{(5)}$ in eqs. (2.21). The fifth column shows the sum of the perturbative corrections beyond the explicitly calculated $\mathcal{O}(\alpha_s^4)$ terms up to order $n_{\rm min}$ showing the amount of extrapolation needed to obtain the best possible top quark mass based on the asymptotic approximation. The sixth column shows the set of orders $\{n\}_{f=5/4}$ for which $\Delta(n) \leq f\,\Delta(n_{\rm min})$ and which are used for determining the best estimate and the uncertainty of the top quark pole mass. The seventh column then contains the best estimate and the ambiguity of the series for $m_t^{\rm pole} - m_t^{\rm MSR}(R)$ using the method from section 4.1. To obtain the uncertainties we used renormalization scale variation for $\alpha_s^{(5)}(\mu)$ in the range $R/2 \leq \mu \leq 2\,R$ for the cases $R = 163, 20, 4.2$ GeV and in the range $1.5\,{\rm GeV} \leq \mu \leq 5$ GeV for $R = 1.3$ GeV. For $R = 1.3$ GeV we always use renormalization scales μ of the strong coupling that are larger than 1.5 GeV because the dependence on the renormalization scale grows rapidly for smaller scales. The last column contains the final result for $m_t^{\rm pole}$ combining the results for $m_t^{\rm MSR}(R) - \overline{m}_t$ and $m_t^{\rm pole} - m_t^{\rm MSR}(R)$ where the uncertainties of both are added quadratically to give the final number for the ambiguity of

$\overline{m}_t = 163\,\text{GeV}, \quad \overline{m}_b = \overline{m}_c = 0\,\text{GeV}, \quad n_\ell = n_t = 5$							
R	$m_t^{\text{MSR}}(R) - \overline{m}_t$	n_{min}	$\Delta(n_{\text{min}})$	$\sum_{n=5}^{n_{\text{min}}} \Delta(n)$	$\{n\}_{5/4}$	m_t^{pole} $- m_t^{\text{MSR}}(R)$	m_t^{pole}
163	0.032(1)	8	0.062(3)	0.310(17)	$\{6,7,8,9\}$	10.054(157)	173.086(157)
20	8.038(9)	6	0.075(4)	0.150(8)	$\{5,6,7\}$	2.140(166)	173.178(166)
4.2	9.363(16)	4	0.091	0	$\{3,4,5\}$	0.832(217)	173.195(218)
1.3	9.748(23)	3	0.098	0	$\{2,3,4\}$	0.394(186)	173.142(187)
$\overline{m}_t = 163\,\text{GeV}, \quad \overline{m}_b = 4.2\,\text{GeV}, \quad \overline{m}_c = 0\,\text{GeV}, \quad n_\ell = n_t - 1 = 4$							
R	$m_t^{\text{pole}} - m_b^{\text{pole}}$ $+ m_b^{\text{MSR}}(R) - \overline{m}_t$	n_{min}	$\Delta(n_{\text{min}})$	$\sum_{n=5}^{n_{\text{min}}} \Delta(n)$	$\{n\}_{5/4}$	m_b^{pole} $- m_b^{\text{MSR}}(R)$	m_t^{pole}
163	0.258(21)	7	0.087(3)	0.324(11)	$\{6,7,8,9\}$	9.904(227)	173.162(228)
20	8.035(17)	5	0.104(3)	0.104(3)	$\{4,5,6\}$	2.120(211)	173.155(212)
4.2	9.372(16)	4	0.135	0	$\{3,4\}$	0.855(211)	173.227(212)
1.3	9.795(23)	2	0.124	0	$\{1,2,3\}$	0.331(214)	173.126(215)
$\overline{m}_t = 163\,\text{GeV}, \quad \overline{m}_b = 4.2\,\text{GeV}, \quad \overline{m}_c = 1.3\,\text{GeV}, \quad n_\ell = n_t - 2 = 3$							
R	$m_t^{\text{pole}} - m_c^{\text{pole}}$ $+ m_c^{\text{MSR}}(R) - \overline{m}_t$	n_{min}	$\Delta(n_{\text{min}})$	$\sum_{n=5}^{n_{\text{min}}} \Delta(n)$	$\{n\}_{5/4}$	m_c^{pole} $- m_c^{\text{MSR}}(R)$	m_t^{pole}
163	0.694(40)	7	0.098(2)	0.355(8)	$\{6,7,8,9\}$	9.471(260)	173.165(263)
20	8.076(33)	5	0.116(3)	0.116(3)	$\{4,5,6\}$	2.085(243)	173.161(245)
4.2	9.371(31)	3	0.154	0	$\{3,4\}$	0.888(257)	173.259(259)
1.3	9.805(24)	2	0.128	0	$\{1,2,3\}$	0.354(243)	173.159(244)

Table 5. Details of the numerical results of our method to determine m_t^{pole} for the cases of massless bottom and charm quarks (upper section), massless charm quarks (middle section) and finite bottom and charm quarks (lower section) and exploring different setups to determine m_t^{pole}. The final respective results for m_t^{pole} are shown in the last column. See the text for details. All numbers for masses and mass differences are in units of GeV. Errors are quoted in parentheses.

m_t^{pole}. These results are also displayed graphically in figures 6(a)–6(d) as the gray hatched horizontal bands.

In figures 6 we have also shown in black the results for $m_t^{\text{pole}}(n)$ over the order n for the different setups where the dots are the results for the default renormalization scales that are used to determine n_{min}, $\Delta(n_{\text{min}})$ and $\{n\}_f$. The error bars represent the range of values at each order of the truncated series coming from the variations of the renormalization scale of the strong coupling. The black dot at $n = 0$ visible in figures 6(c), 6(d) shows the highest order result for $m_t^{\text{MSR}}(R)$.

We see that the results for the top quark pole mass m_t^{pole} for the different R values are fully compatible to each other. In particular, the ambiguity estimates based on our method agree within $\pm 15\%$ and average to 182 MeV. Furthermore, the central values for the best estimates vary by at most 110 MeV and average to 173.150 GeV. It is reassuring that the spread of the central values is smaller than the size of the ambiguity. We emphasize that the consistency of our results for the different R values to each other cannot be interpreted in any way statistically since the analyses for different R values are not

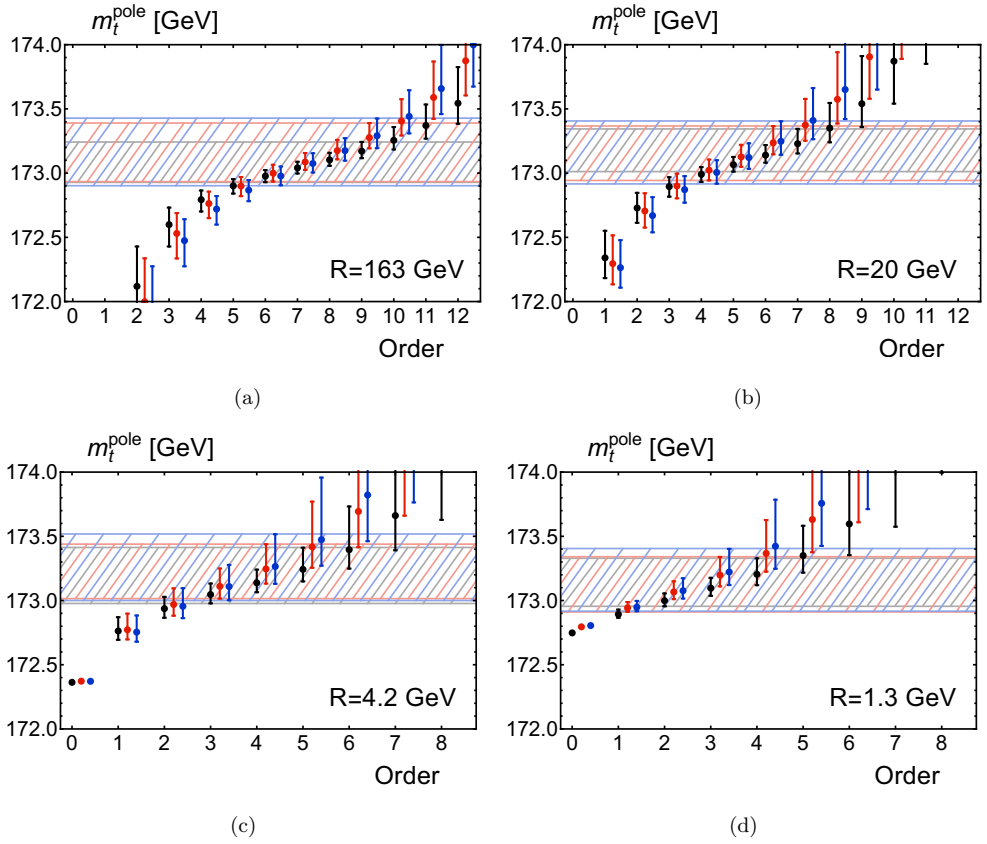

Figure 6. Top quark pole mass $m_t^{\rm pole}$ as a function of order taking $\overline{m}_t = \overline{m}_t(\overline{m}_t) = 163$ GeV as input and using different methods to obtain the best possible estimate and the ambiguity. The central dots are obtained for the default renormalization scales for the strong coupling and the error bands represent the scale variation as explained in the text. The light colored hatched horizontal bands bounded by equal colored lines show the best possible estimate for the respective method also given in the last column in table 5. All results obtained for massless bottom and charm quarks are in black, all results for $(\overline{m}_b, \overline{m}_c) = (4.2, 0)$ GeV are in red, all results for $(\overline{m}_b, \overline{m}_c) = (4.2, 1.3)$ GeV are in blue. Panel (a) shows results for $R = 163$ GeV, panel (b) for $R = 20$ GeV, panel (c) for $R = 4.2$ GeV and panel (d) for $R = 1.3$ GeV.

theoretically independent. The agreement just shows that our method is consistent since the best estimate (and also the ambiguity) of the top quark pole mass is independent of R. Interestingly our estimate for the ambiguity of the top quark pole mass agrees quite well with $\Lambda_{\rm QCD}^{(n_\ell=5)} = 166$ MeV given in eq. (2.24).

As already pointed out in section 4.1, the minimal correction $\Delta(n_{\rm min})$ increases from around 60 MeV for $R = 163$ GeV to about 100 MeV[5] for $R = 1.3$ GeV. At the same time,

[5]This number is obtained for the default renormalization scale $\mu = 2\,\overline{m}_c = 2.6$ GeV. In the short analysis of section 4.1 we quoted 131 MeV for the size of the minimal term for $R = 1.3$ GeV, which was obtained for $\mu = 1.3$ GeV.

the order $n_{\rm min}$ where the minimal correction $\Delta(n_{\rm min})$ arises decreases from $n_{\rm min} = 8$ at $R = \overline{m}_t$ down to $n_{\rm min} = 4$ and 3 for $R = 4.2$ and 1.3 GeV. Moreover, the contribution in the best estimate for $m_t^{\rm pole}$ from orders beyond $n = 4$ until order $n_{\rm min}$ decreases from about 310 MeV at $R = \overline{m}_t$ to about 150 MeV at $R = 20$ GeV. For R scales around the bottom quark mass and below, where $n_{\rm min} \leq 4$, there is no need any more to extrapolate beyond the explicitly calculated four orders to get the best value for $m_t^{\rm pole}$. This information is not just of academic importance but it is also relevant for phenomenology: The MSR mass $m_t^{\rm MSR}(R)$ for some low scale R can serve as a low-scale short-distance mass for a physical application where the characteristic physical scale is R. Typical examples include the top pair inclusive cross section at the production threshold where $R \sim m_t\alpha_s \sim 25$ GeV [25], or the reconstructed invariant top quark mass distribution where R is in the range of 5 to 10 GeV [22, 40, 41]. The behavior of the series for $m_t^{\rm pole} - m_t^{\rm MSR}(R)$ thus reflects the typical behavior of the QCD corrections to the mass for the respective physical applications. The observations we make for the R-dependence of the behavior of the series show that the best possible determination of the top quark mass from an observable characterized by a low characteristic physical scale can in general be achieved at a lower order and also involves smaller perturbative corrections compared to an observable characterized by high characteristic physical scales (such as inclusive top pair cross sections at high energies or virtual top quark effects). This general property is also reflected visually in the graphical illustrations shown in figure 6.

We note that our numerical analysis has a rather weak overall dependence on the choice of f and that the results change by construction in a non-continuous way. Using $f = 4/3$ only the outcome for $R = 20$ GeV is modified to $m_t^{\rm pole} - m_t^{\rm MSR}(R) = 2.100 \pm 0.206$. Using $f = 6/5$ only the outcome for $R = 163$ GeV is modified to $m_t^{\rm pole} - m_t^{\rm MSR}(R) = 10.088 \pm 0.123$. This leaves the overall conclusion about the ambiguity of the top quark pole mass unchanged and we therefore consider $f = 5/4$ as a reasonable default choice.

Comparing our results to those of ref. [28], we find that our estimate of the top quark pole mass ambiguity of 180 MeV exceeds theirs of 70 MeV by a factor of 2.5. The discrepancy arises since their result was only related to the size of the minimal term $\Delta(n_{\rm min})$ for an R value close to 163 GeV and did not account for the number of orders Δn for which the $\Delta(n)$ are close to the minimal term $\Delta(n_{\rm min})$. For $R = 163$ GeV we have $\Delta n = 4$ for $f = 5/4$ and we see the discrepancy is roughly compatible with $\Delta n/2$. Since for other choices of R the values of $\Delta(n_{\rm min})$ and Δn vary individually substantially (while their product is stable) we believe that a specification of the top quark pole mass ambiguity of 70 MeV is not consistent with heavy quark symmetry.

4.3 Massless charm quark

For the case of a massive bottom quark and treating the charm quark as massless we can calculate the top quark pole mass from the bottom MSR mass $m_b^{\rm MSR}(R \leq \overline{m}_b)$ using the top-bottom mass matching contribution $\delta m_{b,c}^{(t\to b)}(\overline{m}_b, 0)$ of eq. (3.5) for $\overline{m}_c = 0$ in combination with the top and bottom $\overline{\rm MS}$-MSR mass matching contributions, $\Delta m_t^{(6\to5)}(\overline{m}_t)$ and $\Delta m_b^{(5\to4)}(\overline{m}_b)$ of eq. (3.2) and R-evolution, see eq. (2.16), with $n_t = 5$ active dynamical

$\overline{m}_t = 163\,\text{GeV}$, $\overline{m}_b = 4.2\,\text{GeV}$, $\overline{m}_c = 0\,\text{GeV}$, $n_\ell = n_t - 1 = 4$			
R	m_t^{pole}	m_b^{pole}	m_c^{pole}
163	173.162 ± 0.228	4.994 ± 0.227	—
20	173.155 ± 0.212	4.987 ± 0.211	—
4.2	173.227 ± 0.212	5.059 ± 0.211	—
1.3	173.126 ± 0.215	4.958 ± 0.215	—
$\overline{m}_t = 163\,\text{GeV}$, $\overline{m}_b = 4.2\,\text{GeV}$, $\overline{m}_c = 1.3\,\text{GeV}$, $n_\ell = n_t - 2 = 3$			
R	m_t^{pole}	m_b^{pole}	m_c^{pole}
163	173.165 ± 0.263	4.996 ± 0.263	1.665 ± 0.262
20	173.161 ± 0.245	4.992 ± 0.245	1.661 ± 0.244
4.2	173.259 ± 0.259	5.090 ± 0.258	1.759 ± 0.258
1.3	173.159 ± 0.244	4.990 ± 0.244	1.659 ± 0.243

Table 6. Upper section: best estimate for the top and bottom quark pole masses for the case $(\overline{m}_t, \overline{m}_b, \overline{m}_c) = (163, 4.2, 0)\,\text{GeV}$ for $R = 163, 20, 4.2, 1.3\,\text{GeV}$. Lower section: best estimate for the top, bottom and charm quark pole masses for the case $(\overline{m}_t, \overline{m}_b, \overline{m}_c) = (163, 4.2, 1.3)\,\text{GeV}$ for $R = 163, 20, 4.2, 1.3\,\text{GeV}$. All numbers are in units of GeV.

flavors from $\overline{m}_t$ to $\overline{m}_b$ and with $n_b = 4$ active dynamical flavors from $\overline{m}_b$ to R. The resulting expression for the top quark pole mass systematically sums all logarithms $\log(\overline{m}_b/\overline{m}_t)$ and uses that the bottom quark pole-MSR mass relation, which specifies the bottom quark pole mass ambiguity, fully encodes the top quark pole mass ambiguity due to heavy quark symmetry. The expression for the top quark pole mass we use reads

$$m_t^{\text{pole}} = \overline{m}_t + \Delta m_t^{(6\to5)}(\overline{m}_t) + \Delta m^{(5)}(\overline{m}_t, \overline{m}_b) + \delta m_{b,c}^{(t\to b)}(\overline{m}_b, 0) + \Delta m_b^{(5\to4)}(\overline{m}_b)$$
$$+ \Delta m^{(4)}(\overline{m}_b, R) + R \sum_{n=1}^{\infty} a_n(n_\ell = 4, 0) \left(\frac{\alpha_s^{(4)}(R)}{4\pi}\right)^n , \qquad (4.3)$$

where the sum of the first four terms on the r.h.s. is just $m_t^{\text{pole}} - m_b^{\text{pole}} + \overline{m}_b$, using eq. (3.20), and the sum of the fifth and sixth term is the difference of the bottom MSR and $\overline{\text{MS}}$ masses $m_b^{\text{MSR}}(R) - \overline{m}_b$. Both quantities are free of an $\mathcal{O}(\Lambda_{\text{QCD}})$ renormalon ambiguity and can be evaluated to the highest order given in tables 1, 3 and 4. We can then study the uncertainty of the top quark pole mass and its $\mathcal{O}(\Lambda_{\text{QCD}})$ renormalon ambiguity from the R-dependent series which is just equal to $m_b^{\text{pole}} - m_b^{\text{MSR}}(R)$.

The outcome of the analysis using the method described in section 4.1 for $(\overline{m}_t, \overline{m}_b) = (163, 4.2)\,\text{GeV}$ as well as $R = 163, 20, 4.2, 1.3\,\text{GeV}$ and $f = 5/4$ is shown in the middle section of table 5. Except for the second and seventh column the entries are analogous to the analysis for $\overline{m}_b = \overline{m}_c = 0$ in section 4.2. Here, the second column shows $m_t^{\text{pole}} - m_b^{\text{pole}} + m_b^{\text{MSR}}(R) - \overline{m}_t$ and the seventh shows $m_b^{\text{pole}} - m_b^{\text{MSR}}(R)$, which contains the $\mathcal{O}(\Lambda_{\text{QCD}})$ renormalon ambiguity. The default choices and the ranges of variation for

the renormalization scale in the strong coupling in the series for $m_b^{\rm pole} - m_b^{\rm MSR}(R)$ are the same as for our analysis for $\overline{m}_b = \overline{m}_c = 0$ in section 4.2 for the corresponding R values. The last column contains again the final result for $m_t^{\rm pole}$ combining the results for $m_t^{\rm pole} - m_b^{\rm pole} + m_b^{\rm MSR}(R) - \overline{m}_t$ and $m_b^{\rm pole} - m_b^{\rm MSR}(R)$ where the uncertainties of both are added quadratically. The results are also displayed graphically in figures 6(a)–6(d) as the light red hatched horizontal bands. In the upper section of table 6 we also show the best estimate for the bottom quark pole mass $m_b^{\rm pole}$ obtained for the respective R values, which can be obtained using eq. (4.3) and the result for the top-bottom pole mass difference of eq. (3.26).

In figures 6 we have shown in red the results for $m_t^{\rm pole}(n)$ over the order n for the different setups where the dots are again the results for the default renormalization scales that are used to determine $n_{\rm min}$, $\Delta(n_{\rm min})$ and $\{n\}_f$. The error bars are the range of values coming from the variations of the renormalization scale of the strong coupling. The red dots at $n = 0$ visible in figures 6(c) and 6(d) show the highest order results for $m_t^{\rm pole} - m_b^{\rm pole} + m_b^{\rm MSR}(R)$.

We again see that the results for the top quark pole mass for the different R values are compatible each other. The ambiguity estimates average to 217 MeV. Interestingly this estimate for the ambiguity of the top quark pole mass roughly agrees with $\Lambda_{\rm QCD}^{(n_\ell=4)} = 225\,\text{MeV}$ given in eq. (2.25). This is larger than $\Lambda_{\rm QCD}^{(5)} = 166\,\text{MeV}$ since the infrared sensitivity of the top quark pole mass increases when the number of massless quarks is decreased (i.e. $\beta_0^{(4)} > \beta_0^{(5)}$). Furthermore, we observe that the central values for the top quark pole mass cover a range that is compatible with case of a massless bottom quark. The central values average to 173.168 GeV which is about 20 MeV larger than for a massless bottom quark, which is, however, insignificant given the range of values covered by the central values or even the size of the ambiguity. So the bottom quark mass does essentially not affect the overall value of the top quark pole mass. We also note that the minimal corrections $\Delta(n_{\rm min})$ are all larger than the corresponding terms for the case of massless bottom and charm quarks. For $R = 4.2$ and 1.3 GeV they amount to about 130 MeV.

4.4 Massive bottom and charm quarks

We now, finally, consider the case that both the bottom and the charm quark masses are accounted for. Since this situation involves three scales, it is the most complicated concerning matching and evolution that systematically sums logarithms $\log(\overline{m}_t/\overline{m}_b)$ and $\log(\overline{m}_b/\overline{m}_c)$. However, the case can be treated in a straightforward way by iterating the top-bottom mass matching procedure of the previous section one more time concerning the bottom-charm mass matching. The resulting formula for the top quark pole mass reads

$$\begin{aligned} m_t^{\rm pole} &= \overline{m}_t + \Delta m_t^{(6\to5)}(\overline{m}_t) + \Delta m^{(5)}(\overline{m}_t, \overline{m}_b) + \delta m_{b,c}^{(t\to b)}(\overline{m}_b, \overline{m}_c) \\ &\quad + \Delta m_b^{(5\to4)}(\overline{m}_b) + \Delta m^{(4)}(\overline{m}_b, \overline{m}_c) + \delta m_c^{(b\to c)}(\overline{m}_c) + \Delta m_c^{(4\to3)}(\overline{m}_c) \\ &\quad + \Delta m^{(3)}(\overline{m}_c, R) + R\sum_{n=1}^{\infty} a_n(n_\ell = 3, 0)\left(\frac{\alpha_s^{(3)}(R)}{4\pi}\right)^n . \end{aligned} \tag{4.4}$$

JHEP09(2017)099

The expression combines the top-bottom and bottom-charm mass matching contributions $\delta m_{b,c}^{(t\to b)}(\overline{m}_b,\overline{m}_c)$ and $\delta m_c^{(b\to c)}(\overline{m}_c)$ from eqs. (3.5) and (3.9), respectively, and the top, bottom and charm $\overline{\rm MS}$-MSR mass matching contributions $\Delta m_t^{(6\to5)}(\overline{m}_t)$, $\Delta m_b^{(5\to4)}(\overline{m}_b)$ and $\Delta m_c^{(4\to3)}(\overline{m}_c)$ of eq. (3.2). Furthermore it contains contributions from R-evolution with $n_t = 5$ active dynamical flavors from $\overline{m}_t$ to $\overline{m}_b$, with $n_b = 4$ active dynamical flavors from $\overline{m}_b$ to $\overline{m}_c$ and with $n_b = 3$ active dynamical flavors from $\overline{m}_c$ to R. We do not employ any evolution to scales below $\overline{m}_c$ due to instabilities of perturbation theory for the charm pole-MSR mass relation at such low scales but we can explore scales above $\overline{m}_c$ using the R-evolution.

On the r.h.s. of eq. (4.4) the sum of the first seven terms is just $m_t^{\rm pole} - m_c^{\rm pole} + \overline{m}_c$, using eq. (3.22), and the eighth term is the charm $\overline{\rm MS}$-MSR matching contribution. Both quantities are free from an $\mathcal{O}(\Lambda_{\rm QCD})$ renormalon ambiguity and can be evaluated to the highest order given in tables 1, 3 and 4. We can then study the ambiguity of the top quark pole mass due to the $\mathcal{O}(\Lambda_{\rm QCD})$ renormalon from the R-dependent series which is just equal to $m_c^{\rm pole} - m_c^{\rm MSR}(R)$. This relation specifies the charm quark pole mass ambiguity, and it fully encodes the top and bottom quark pole mass ambiguities due to heavy quark symmetry.

We note that among all the terms shown in eq. (4.4) the contributions from the MSR mass differences $\Delta m^{(5)}(\overline{m}_t,\overline{m}_b)$, $\Delta m^{(4)}(\overline{m}_b,\overline{m}_c)$ and $\Delta m^{(3)}(\overline{m}_c,R)$, determined with R-evolution, and the series proportional to R, which contains the $\mathcal{O}(\Lambda_{\rm QCD})$ renormalon, constitute the numerically most important terms. They exceed by far the contributions from the matching corrections, which amount to only 50 MeV and, therefore, fully encode the large order asymptotic behavior of the top quark pole-$\overline{\rm MS}$ mass series $m_t^{\rm pole} - \overline{m}_t$ as defined in eq. (2.4) in the presence of finite bottom and charm quark masses. The large order asymptotic form of the coefficients in the expansion in powers of $\alpha_s^{(6)}(\overline{m}_t)$ may then be determined directly from these terms for $R = \overline{m}_c$ using the analytic solution for the MSR mass differences provided in eq. (4.2) of ref. [24] and expanding in $\alpha_s^{(6)}(\overline{m}_t)$. However, the resulting series suffers from the large logarithms involving the ratios of the top, bottom and charm quark masses, and is therefore less reliable for applications than the result shown in eq. (4.4).

The outcome of the analysis using the method described in section 4.1 for $(\overline{m}_t,\overline{m}_b,\overline{m}_c) = (163, 4.2, 1.3)\,\text{GeV}$, as well as $R = 163, 20, 4.2, 1.3\,\text{GeV}$ and $f = 5/4$ is shown in the lower section of table 5. Except for the second and seventh column the entries are analogous to the previous two analyses in sections 4.2 and 4.3. Here, the second column shows $m_t^{\rm pole} - m_c^{\rm pole} + m_c^{\rm MSR}(R) - \overline{m}_t$ and the seventh shows $m_c^{\rm pole} - m_c^{\rm MSR}(R)$, which contains the $\mathcal{O}(\Lambda_{\rm QCD})$ renormalon ambiguity of the top quark pole mass. The default choices and the ranges of variation for the renormalization scale in the strong coupling in the series for $m_c^{\rm pole} - m_c^{\rm MSR}(R)$ are the same as for the two previous analyses in sections 4.2 and 4.3 for the corresponding R values. The last column contains again the final result for $m_t^{\rm pole}$ combining the results for $m_t^{\rm pole} - m_c^{\rm pole} + m_c^{\rm MSR}(R) - \overline{m}_t$ and $m_c^{\rm pole} - m_c^{\rm MSR}(R)$ where all uncertainties are added quadratically. These results are also displayed graphically in figure 6(a)–6(d) as the light blue hatched horizontal bands. In the lower section of table 6

we also show the best estimate for the charm and bottom quark pole masses $m_c^{\rm pole}$ and $m_b^{\rm pole}$, respectively, for the different R values, which can be obtained using eq. (4.4) and the result for the top-bottom and top-charm pole mass difference of eqs. (3.20) and (3.22).

In figure 6 we have also shown in blue the results for $m_t^{\rm pole}(n)$ over the order n for the different setups where the dots are again the results for the default renormalization scales that are used to determine $n_{\rm min}$, $\Delta(n_{\rm min})$ and $\{n\}_f$. The error bars are the range of values coming from the variations of the renormalization scale of the strong coupling. The blue dots visible in figures 6(c) and 6(d) at $n = 0$ shows the highest order result for $m_t^{\rm pole} - m_c^{\rm pole} + m_c^{\rm MSR}(R)$.

We see that the results for the top quark pole mass for the different R values are again fully consistent to each other. The ambiguity estimates average to 253 MeV, which is more than twice the 110 MeV ambiguity obtained in ref. [28]. The reason for the discrepancy is the same as for the analysis for massless bottom and charm quarks already explained in sections 4.1 and 4.2, and we therefore do not discuss it here further. Concerning the size of the minimal corrections $\Delta(n_{\rm min})$, we find that they reach 116, 154 and 128 MeV for $R = 20$, 4.2 and 1.3 GeV, respectively, each of which is larger than 110 MeV. As in the two previous analyses our result for the ambiguity agrees very well with the corresponding value of $\Lambda_{\rm QCD}$, given in eq. (2.24), which in this case is also $\Lambda_{\rm QCD}^{(n_\ell=3)} = 253\,\text{MeV}$. This is larger than the uncertainties we obtained for the cases discussed in the two previous analyses, where either the bottom and charm quarks were massless or just the charm quark, and thus again follows the pattern that the infrared sensitivity of the top quark pole mass increases when the number of massless quarks decreases (i.e. $\beta_0^{(3)} > \beta_0^{(4)} > \beta_0^{(5)}$).

Furthermore, we find that the central values for the top quark pole mass cover a range that is within errors in agreement with the two previous analyses. The range is, however, shifted slightly upwards by about 70 MeV with respect to the case of massless bottom and charm quarks. For the value of the average we have 173.186 GeV which is about 40 MeV higher than the average 173.150 GeV we obtained for massless bottom and charm quarks. This shift may represent a slight trend, but it is overall insignificant compared to the range of values covered by the central values or the size of the ambiguity. This shows that the charm quark mass, like the bottom quark mass, does not affect the value of the top quark pole mass. We can compare to the result of ref. [28], where they found that the finite bottom and charm quark masses increase the top quark pole mass by 80 ± 30 MeV, where the 30 is their estimate for the uncertainty in their computation of the bottom and charm mass effects. This is consistent with the dependence on the bottom and charm masses we find in our analysis. Their prescription was based on a successive order-dependent reduction of the effective flavor number in the series motivated by the decoupling property observed in ref. [27]. It incorporated some basic features of the bottom and charm mass corrections beyond the third order but is otherwise heuristic and does not systematically sum logarithms of $\overline{m}_b/\overline{m}_t$ and $\overline{m}_c/\overline{m}_t$. The consistency shows that concerning the estimate of the top quark pole mass ambiguity and within errors their prescription provides an adequate approximation.

JHEP09(2017)099

4.5 Overall assessment for the pole mass ambiguity

The overall outcome of the analyses above concerning the best possible estimates (and the ambiguities) of the top quark pole mass and the pole masses of the bottom and charm quarks is summarized as follows:

1. Heavy quark symmetry states that the ambiguity of a heavy quark pole mass is independent of the mass of the heavy quark and that the ambiguities of the pole masses of all heavy quarks are equivalent. Our method for estimating the ambiguity is insensible to the masses of the heavy quarks and, within any given setup for the heavy quark mass spectrum, obtains the same ambiguities for all heavy quark pole masses. It is therefore fully consistent with heavy quark symmetry.

2. Our examinations for different setups for the spectrum of the masses of the bottom and charm quarks show that the top quark pole mass ambiguity increases when the number n_ℓ of massless quarks is decreased (which arises when the number of lighter massive quarks is increased). The numerical size we find agrees very well with $\Lambda_{\rm QCD}^{(n_\ell)}$ defined in eqs. (2.24). So our studies show that the well-accepted statement that "heavy quark pole masses have an ambiguity of order $\Lambda_{\rm QCD}$" can be specified to the more precise statement that "the ambiguity of the heavy quark pole masses is $\Lambda_{\rm QCD}^{(n_\ell)}$, where n_ℓ is the number of massless quarks".

3. Considering the value of the top quark pole mass (and not its ambiguity) we find essentially no dependence on whether the bottom and charm quarks are treated massive or massless. This also implies that there is no dependence on actual values of the bottom and charm quark masses (which are know to a precision of a few 10 MeV in the $\overline{\rm MS}$ scheme). Likewise we also find that the value of the bottom quark pole mass has no dependence on whether the charm quark is treated massive or massless. These observations are important because, although the pole mass concept depends, due to the linear sensitivity to small momenta, intrinsically on the spectrum of the lighter massive quarks, they imply that one can give the top and the bottom quark pole masses a unique global meaning irrespective which approximation is used for the bottom and charm masses. In such a global context, however, one has to assign the largest value for $\Lambda_{\rm QCD}$ as the ambiguity of the pole mass. This value is obtained for finite bottom and charm quark masses and amounts to 250 MeV which we adopt as our final specification of the top quark pole mass ambiguity.

5 Conclusions

In this work we have provided a systematic study of the mass effects of virtual massive quark loops in the relation between the pole mass $m_Q^{\rm pole}$ and short-distance masses such as the $\overline{\rm MS}$ mass $\overline{m}_Q(\mu)$ and the MSR mass $m_Q^{\rm MSR}(R)$ [23, 24] of a heavy quark Q, where we mean virtual loop insertions of quarks q with $\Lambda_{\rm QCD} < m_q < m_Q$. In this context it is well-known that the virtual loops of a massive quark act as an infrared cut-off on the virtuality of the gluon exchange that eliminates the effects of that quark from the large

order asymptotic behavior of the series. This effect arises from the $\mathcal{O}(\Lambda_{\rm QCD})$ renormalon contained in the pole mass which means that the QCD corrections have a linear sensitivity of small momenta that increases with the order in the perturbative expansion. The primary aim of this work was to study this effect in detail at the qualitative and quantitative level. We established a renormalization group formalism that allows to discuss the mass effects coming from virtual quark loops in the on-shell self energy diagrams of heavy quarks in a coherent and systematic fashion. We in particular examined (i) how the logarithms of mass ratios that arise in this multi-scale problem can be systematically summed to all orders, (ii) the large order asymptotic behavior and structure of the mass corrections themselves and (iii) the consequences of heavy quark symmetry (HQS).

The basis of our formalism is that the difference of the pole mass and a short-distance mass contains the QCD corrections from all momentum scales between zero and the scale at which the short-distance mass is defined, which is μ for the $\overline{\rm MS}$ mass $\overline{m}_Q(\mu)$ or R for the MSR mass $m_Q^{\rm MSR}(R)$. The MSR mass $m_Q^{\rm MSR}(R)$, which is derived from self energy diagrams like the $\overline{\rm MS}$ mass, is particularly suited to describe the scale-dependence for momentum scales $R < m_Q$ since its renormalization group (RG) evolution is linear in R, called R-evolution [23, 24]. When the finite masses of lighter heavy quarks are accounted for, the MSR mass concept allows to establish a RG evolution and matching procedure where the number of active dynamical flavors governing the evolution changes when the evolution crosses a mass threshold and where threshold corrections arise when a massive flavor is integrated out. This follows entirely the common approach of logarithmic RG equations as known from the n_f flavor dependent μ-evolution of the strong coupling $\alpha_s^{(n_f)}(\mu)$ and reflects the properties of HQS.

Due to heavy quark symmetry, the procedure allows for example to relate the QCD corrections in the top quark pole-$\overline{\rm MS}$ mass difference $m_t^{\rm pole} - \overline{m}_t(\overline{m}_t)$ that are coming from scales smaller than the bottom mass, to the bottom quark pole-$\overline{\rm MS}$ mass difference $m_b^{\rm pole} - \overline{m}_b(\overline{m}_b)$. This relation can be used to generically study and determine the large order asymptotic behavior and the structure of the lighter virtual quark mass corrections in the pole-$\overline{\rm MS}$ mass difference of a heavy quark Q. Within the RG framework we have proposed, we find that the bulk of the lighter virtual quark mass corrections is determined by their large order asymptotic behavior already at $\mathcal{O}(\alpha_s^3)$ (very much like the QCD corrections for massless virtual quarks), which confirms earlier observations made in refs. [33, 34] and [27]. Using our RG framework and heavy quark symmetry we used this property to predict the previously unknown $\mathcal{O}(\alpha_s^4)$ lighter virtual quark mass corrections to within a few percent from the available information on the $\mathcal{O}(\alpha_s^4)$ corrections for massless lighter quarks without an additional loop computation, see eq. (3.14). Furthermore we calculated the differences of the top, bottom and charm quark pole masses with a precision of around 20 MeV, and we analyzed in detail the quality of the coupling approximation of ref. [27], which works in an excellent way for the charm mass effects in the bottom quark pole mass, where in the context of the top quark, it fails.

The second aim of the paper was to use the formalism to determine a concrete numerical specification of the ambiguities of the heavy quark pole masses and in particular of the top quark pole mass. This is of interest because the top quark pole mass is still the most

JHEP09(2017)099

frequently used mass scheme in higher order theoretical predictions for the LHC top physics analyses. The ambiguity of the pole mass is the precision with which the pole mass can be determined *in principle* given that the complete series is known. This ambiguity is universal (i.e. it exists in equivalent size in any context and cannot be circumvented) and its size can therefore be quantified from the relation of the pole mass and any short-distance mass alone for which all terms in the series can be determined to high precision. With the renormalization group formalism we have proposed we carried out an analysis accounting explicitly for the constraints coming from HQS. HQS states (i) that the ambiguity of a heavy quark is independent of its mass, and (ii) that the QCD effects in the heavy quark masses coming from momenta below the lightest massive quark are all equivalent, which implies that the ambiguities of all heavy quarks are equal.

With our formalism both aspects were incorporated and validated in detail at the qualitative and quantitative level. We considered different scenarios for the treatment of the bottom and charm quark masses and employed a method to estimate the ambiguity that does not depend on the mass of the heavy quark in a way that is consistent with heavy quark symmetry. For the case of massless bottom and charm quarks we found that the ambiguity of the top quark pole mass is 180 MeV, when the charm quark is massless we found 215 MeV and when the finite masses of both the bottom and charm quarks are accounted for we obtained 250 MeV. Numerically, the ambiguity turns out be essentially equal to the hadronization scale $\Lambda_{\rm QCD}^{(n_\ell)}$, defined in eq. (2.24), where n_ℓ is the number of massless quarks. Thus, our analysis allows to specify the well-known qualitative statement "the heavy quark pole masses have an ambiguity of order $\Lambda_{\rm QCD}$" to the more specific statement "the ambiguity of heavy quark pole masses is $\Lambda_{\rm QCD}^{(n_\ell)}$, where n_ℓ is the number of massless quarks". This dependence of the top quark pole mass ambiguity on the number of massless flavors is fully consistent with the behavior expected from the pole mass renormalon. Furthermore, we have found that there is no significant dependence of the central value of the top quark pole mass on whether the bottom and charm quarks are treated as massive or massless.

Our results for the ambiguities differ considerably from those of ref. [28]. They estimated the top quark pole mass ambiguity as 70 MeV for the case that bottom and charm masses are neglected and as 110 MeV when the bottom and charm masses are accounted for. We have shown in detail in which ways these values are incompatible with heavy quark symmetry and why our ambiguity estimates should be considered more reliable.

If one considers the top quark pole mass as a globally defined mass scheme valid for all choices of approximations for the bottom and charm quark masses, one should assign it an intrinsic principle ambiguity due to the $\mathcal{O}(\Lambda_{\rm QCD})$ renormalon of 250 MeV. We stress, that this intrinsic uncertainty refers to the best possible precision with which one can in principle theoretically determine the top quark pole mass, and does not account in any way for issues unrelated to the pole mass renormalon in applications for actual phenomenological quantities, which typically involve NLO, NNLO or even NNNLO corrections from perturbative QCD. Furthermore, in order to achieve this theoretical precision it is required to have access to orders where the corrections (in the relation involving the pole mass) become minimal. The order where this happens in an actual phenomenological analysis also

depends on the typical physical scale (i.e. the value of R) governing the examined quantity. If the top quark mass is determined from a quantity which has a low characteristic physical scale (e.g. top pair production close to threshold, kinematic endpoints, reconstructed top invariant mass distributions) then the minimal term is reached at very low orders, which may well be within the orders that can be calculated explicitly. If the top quark mass is determined from a quantity which has a high characteristic scale of the order or the top quark mass (e.g. total inclusive cross sections at high energies, virtual top quark effects) then the minimal term is reached only at high orders, which are not accessible to full perturbative computations. This also explains why top mass sensitive observables involving low characteristic physical scales are more sensitive for top quark mass determinations than observables involving high characteristic physical scales. So reaching the uncertainties in top quark pole mass determinations that come close to the ambiguity limit is in general much harder for observables governed by high physical scales.

Currently, the most precise measurements of the top quark mass from the D0 and CDF experiments at the Tevatron [42, 43] and the ATLAS and CMS collaborations at the LHC [44, 45] use the top reconstruction method and already reach the level of 500 to 700 MeV. Projections for LHC Run-2 further indicate that this uncertainty can be reduced significantly in the future and may reach the level of 200 MeV for the high-luminosity LHC run [46]. The outcome of our analysis disfavors the top quark pole mass as a practically adequate mass parameter in the theoretical interpretation of these measurements.

As a final comment we would like to remind the reader that all tricky issues concerning the convergence of the perturbative series and the way how to properly estimate the ambiguity of top quark pole mass become irrelevant if one employs an adequate short-distance mass definition. This may of course not mean in general that switching to a short-distance mass scheme will automatically lead to smaller uncertainties simply because other unresolved issues may then dominate. The outcome of our analysis, however, implies that even reaching a 250 MeV uncertainty for the top quark pole mass in a reliable way within a practical application is difficult. This is because the $\mathcal{O}(\Lambda_{\rm QCD})$ renormalon prevents using common ways such as scale variation for the truncated series to estimate theoretical uncertainties, and can affect the behavior of the series already at low orders where the corrections still decrease. It is therefore advantageous to abandon the pole mass scheme in favor of an adequately chosen short-distance mass at latest when the available QCD corrections for a mass sensitive quantity yield perturbative uncertainties in the pole mass that become of the order of its ambiguity, which we believe is when they approach 0.5 GeV.

Acknowledgments

We acknowledge partial support by the FWF Austrian Science Fund under the Doctoral Program No. W1252-N27 and the Project No. P28535-N27 and the U.S. Department of Energy under the Grant No. DE-SC0011090. We also thank the Erwin-Schrödinger International Institute for Mathematics and Physics for partial support.

A Virtual quark mass corrections up to $\mathcal{O}(\alpha_s^3)$

The virtual quark mass corrections of $\mathcal{O}(\alpha_s^2)$ were determined in ref. [2] and read

$$\delta_2(1) = 8\left(\frac{\pi^2}{3} - 1\right) = 18.3189 \tag{A.1}$$

$$\begin{aligned}\delta_2(r) = {} & \frac{8}{9}\pi^2 + \frac{16}{3}\ln^2 r - \frac{16}{3}r^2\left(\frac{3}{2} + \ln r\right) \\ & + \frac{16}{3}(1+r)(1+r^3)\left(\frac{\pi^2}{6} - \frac{1}{2}\ln^2 r + \ln r\,\ln(1+r) + \mathrm{Li}_2(-r)\right) \\ & + \frac{16}{3}(1-r)(1-r^3)\left(-\frac{\pi^2}{3} - \frac{1}{2}\ln^2 r + \ln r\,\ln(1-r) + \mathrm{Li}_2(r)\right).\end{aligned} \tag{A.2}$$

The expansion of δ_2 for small r has the form $\delta_2(r) = (8\pi^2/3)r - 16r^2 + (8\pi^2/3)r^3 + \ldots$. At $\mathcal{O}(\alpha_s^3)$ the virtual quark mass corrections were determined semi-analytically in ref. [31] for the case of one more massive quark q in the heavy quark Q self-energy. The corrections from the insertions of virtual loops of two different massive quarks q and q' were not provided and are given in eq. (A.12). In the following we provide the results for the full set of $\mathcal{O}(\alpha_s^3)$ virtual quark mass corrections using the results from ref. [31] in the expansion for $\overline{m}_q/\overline{m}_Q \ll 1$ adapted to our notation. The expressions for general $\overline{m}_q/\overline{m}_Q$, which are extensive, can be downloaded at https://backend.univie.ac.at/fileadmin/user_upload/i_particle_physics/publications/hpw.m.

We consider the $\mathcal{O}(\alpha_s^3)$ virtual quark mass corrections to the pole-$\overline{\mathrm{MS}}$ mass relation of the heavy quark Q coming from n lighter massive quarks q_1, q_2, $\ldots q_n$ in the *order of decreasing mass* and n_ℓ additional quarks lighter than Λ_{QCD}, which we treat as massless. So, the number n_Q of quark flavors lighter than quark Q is $n_Q = n + n_\ell$. The expressions for the functions $\delta_{Q,3}$ defined in eqs. (2.10) and (2.13) can be written in the form

$$\delta_{Q,3}^{(Q,q_1,q_2,\ldots,q_n)}(1, r_{q_1Q}, \ldots, r_{q_nQ}) = h(1) + (n_Q+1)\,p(1) + \sum_{i=1}^{n} w(1, r_{q_iQ})\,, \tag{A.3}$$

$$\delta_{Q,3}^{(q_1,q_2,\ldots,q_n)}(r_{q_1Q}, r_{q_2Q}, \ldots, r_{q_nQ}) = h(r_{q_1Q}) + n_Q\,p(r_{q_1Q}) + \sum_{i=2}^{n} w(r_{q_1Q}, r_{q_iQ})\,, \tag{A.4}$$

$$\begin{aligned}\delta_{Q,3}^{(q_m,q_{m+1},\ldots,q_n)}(r_{q_mQ}, r_{q_{m+1}Q}, \ldots, r_{q_nQ}) = {} & h(r_{q_mQ}) + (n_Q - m + 1)\,p(r_{q_mQ}) \\ & + \sum_{i=m+1}^{n} w(r_{q_mQ}, r_{q_iQ})\,.\end{aligned} \tag{A.5}$$

All three formulae follow the same general scheme, where the number multiplying the function $p(r)$ is just the number of massive quarks in the superscript plus the number of massless quarks, n_ℓ. We have displayed them nevertheless for clarity. The explicit form of the functions h, p and w is

$$\begin{aligned}h(1) &= 1870.7877\,, \\ h(r) &= r\,(1486.55 - 1158.03\ln r)\end{aligned} \tag{A.6}$$

$$
\begin{aligned}
&+ r^2\,(-884.044 - 683.967\ln r) + r^3\,(906.021 - 1126.84\ln r)\\
&+ r^4\,(225.158 + 11.4991\ln r - 80.3086\ln^2 r + 21.3333\ln^3 r)\\
&+ r^5\,(126.996 - 182.478\ln r) + r^6\,(-22.8899 + 38.3536\ln r - 54.5284\ln^2 r)\\
&+ r^7\,(15.3830 - 34.8914\ln r) + r^8\,(2.52528 - 3.82270\ln r - 20.4593\ln^2 r) + \mathcal{O}(r^9)\,,
\end{aligned}
\tag{A.7}
$$

and

$$
p(1) = -82.1208\,, \tag{A.8}
$$

$$
\begin{aligned}
p(r) &= \frac{32}{27}\int_0^\infty \mathrm{d}z \left[\frac{z}{2} + \left(1 - \frac{z}{2}\right)\sqrt{1+\frac{4}{z}}\right] \mathrm{P}\left(\frac{r^2}{z}\right)\left(\ln z - \frac{5}{3}\right) \\
&= r\,(-66.4668 + 70.1839\ln r) + r^2\,14.2222 + r^3\,(15.4143 + 70.1839\ln r)\\
&\quad + r^4\,(-23.1242 + 18.0613\ln r + 15.4074\ln^2 r - 4.74074\ln^3 r) - 31.5827\,r^5\\
&\quad + r^6\,(11.9886 - 1.70667\ln r) - 4.17761\,r^7 + r^8\,(2.40987 - 0.161088\ln r) + \mathcal{O}(r^9)\,,
\end{aligned}
\tag{A.9}
$$

as well as

$$
w(1,1) = 6.77871\,, \tag{A.10}
$$

$$
\begin{aligned}
w(1,r) &= r^2\,14.2222 - 18.7157\,r^3 + r^4\,(7.36885 - 11.1477\ln r)\\
&\quad + r^6\,(3.92059 - 3.60296\ln r + 1.89630\ln^2 r)\\
&\quad + r^8\,(0.0837382 - 0.0772789\ln r + 0.457144\ln^2 r) + \mathcal{O}(r^9)\,,
\end{aligned}
\tag{A.11}
$$

$$
w(r_1,r_2) = p(r_2) + \frac{32}{27}\int_0^\infty \mathrm{d}z \left[\frac{z}{2} + \left(1 - \frac{z}{2}\right)\sqrt{1+\frac{4}{z}}\right] \mathrm{P}\left(\frac{r_1^2}{z}\right)\mathrm{P}\left(\frac{r_2^2}{z}\right)\,, \tag{A.12}
$$

where

$$
\Pi(x) = \frac{1}{3} - (1-2\,x)\left[2 - \sqrt{1+4\,x}\ln\left(\frac{\sqrt{1+4\,x}+1}{\sqrt{1+4\,x}-1}\right)\right]\,, \tag{A.13}
$$

$$
\mathrm{P}(x) = \Pi(x) + \ln x + \frac{5}{3}\,. \tag{A.14}
$$

References

[1] R. Tarrach, *The pole mass in perturbative QCD*, *Nucl. Phys.* **B 183** (1981) 384 [INSPIRE].

[2] N. Gray, D.J. Broadhurst, W. Grafe and K. Schilcher, *Three loop relation of quark (modified) Ms and pole masses*, *Z. Phys.* **C 48** (1990) 673 [INSPIRE].

[3] K.G. Chetyrkin and M. Steinhauser, *Short distance mass of a heavy quark at order α_s^3*, *Phys. Rev. Lett.* **83** (1999) 4001 [hep-ph/9907509] [INSPIRE].

[4] K.G. Chetyrkin and M. Steinhauser, *The Relation between the MS-bar and the on-shell quark mass at order α_s^3*, *Nucl. Phys.* **B 573** (2000) 617 [hep-ph/9911434] [INSPIRE].

JHEP09(2017)099

[5] K. Melnikov and T.v. Ritbergen, *The three loop relation between the MS-bar and the pole quark masses*, *Phys. Lett.* **B 482** (2000) 99 [hep-ph/9912391] [INSPIRE].

[6] P. Marquard, L. Mihaila, J.H. Piclum and M. Steinhauser, *Relation between the pole and the minimally subtracted mass in dimensional regularization and dimensional reduction to three-loop order*, *Nucl. Phys.* **B 773** (2007) 1 [hep-ph/0702185] [INSPIRE].

[7] P. Marquard, A.V. Smirnov, V.A. Smirnov and M. Steinhauser, *Quark mass relations to four-loop order in perturbative QCD*, *Phys. Rev. Lett.* **114** (2015) 142002 [arXiv:1502.01030] [INSPIRE].

[8] P. Marquard, A.V. Smirnov, V.A. Smirnov, M. Steinhauser and D. Wellmann, $\overline{\text{MS}}$*-on-shell quark mass relation up to four loops in QCD and a general* SU(N) *gauge group*, *Phys. Rev.* **D 94** (2016) 074025 [arXiv:1606.06754] [INSPIRE].

[9] P.A. Baikov, K.G. Chetyrkin and J.H. Kühn, *Five-loop running of the QCD coupling constant*, *Phys. Rev. Lett.* **118** (2017) 082002 [arXiv:1606.08659] [INSPIRE].

[10] B.A. Kniehl, A.V. Kotikov, A.I. Onishchenko and O.L. Veretin, *Strong-coupling constant with flavor thresholds at five loops in the anti-MS scheme*, *Phys. Rev. Lett.* **97** (2006) 042001 [hep-ph/0607202] [INSPIRE].

[11] A.S. Kronfeld, *The perturbative pole mass in QCD*, *Phys. Rev.* **D 58** (1998) 051501 [hep-ph/9805215] [INSPIRE].

[12] I.I.Y. Bigi, M.A. Shifman, N.G. Uraltsev and A.I. Vainshtein, *The pole mass of the heavy quark. Perturbation theory and beyond*, *Phys. Rev.* **D 50** (1994) 2234 [hep-ph/9402360] [INSPIRE].

[13] M. Beneke and V.M. Braun, *Heavy quark effective theory beyond perturbation theory: renormalons, the pole mass and the residual mass term*, *Nucl. Phys.* **B 426** (1994) 301 [hep-ph/9402364] [INSPIRE].

[14] M. Beneke, *Renormalons*, *Phys. Rept.* **317** (1999) 1 [hep-ph/9807443] [INSPIRE].

[15] A. Czarnecki, K. Melnikov and N. Uraltsev, *Non-abelian dipole radiation and the heavy quark expansion*, *Phys. Rev. Lett.* **80** (1998) 3189 [hep-ph/9708372] [INSPIRE].

[16] M. Beneke, *A quark mass definition adequate for threshold problems*, *Phys. Lett.* **B 434** (1998) 115 [hep-ph/9804241] [INSPIRE].

[17] A.H. Hoang, Z. Ligeti and A.V. Manohar, *B decay and the Upsilon mass*, *Phys. Rev. Lett.* **82** (1999) 277 [hep-ph/9809423] [INSPIRE].

[18] A.H. Hoang, Z. Ligeti and A.V. Manohar, *B decays in the upsilon expansion*, *Phys. Rev.* **D 59** (1999) 074017 [hep-ph/9811239] [INSPIRE].

[19] A.H. Hoang, *1S and MS-bar bottom quark masses from Upsilon sum rules*, *Phys. Rev.* **D 61** (2000) 034005 [hep-ph/9905550] [INSPIRE].

[20] A. Pineda, *Determination of the bottom quark mass from the* $\Upsilon(1S)$ *system*, *JHEP* **06** (2001) 022 [hep-ph/0105008] [INSPIRE].

[21] A. Jain, I. Scimemi and I.W. Stewart, *Two-loop jet-function and jet-mass for top quarks*, *Phys. Rev.* **D 77** (2008) 094008 [arXiv:0801.0743] [INSPIRE].

[22] S. Fleming, A.H. Hoang, S. Mantry and I.W. Stewart, *Jets from massive unstable particles: top-mass determination*, *Phys. Rev.* **D 77** (2008) 074010 [hep-ph/0703207] [INSPIRE].

[23] A.H. Hoang, A. Jain, I. Scimemi and I.W. Stewart, *Infrared renormalization group flow for heavy quark masses*, *Phys. Rev. Lett.* **101** (2008) 151602 [arXiv:0803.4214] [INSPIRE].

JHEP09(2017)099

[24] A.H. Hoang et al., *The MSR mass and the $\mathcal{O}(\Lambda_{\rm QCD})$ renormalon sum rule*, arXiv:1704.01580 [INSPIRE].

[25] A.H. Hoang et al., *Top-anti-top pair production close to threshold: synopsis of recent NNLO results*, *Eur. Phys. J. direct* **2** (2000) 3 [hep-ph/0001286] [INSPIRE].

[26] PARTICLE DATA GROUP collaboration, C. Patrignani et al., *Review of Particle Physics*, *Chin. Phys.* **C 40** (2016) 100001 [INSPIRE].

[27] C. Ayala, G. Cvetič and A. Pineda, *The bottom quark mass from the $\Upsilon(1S)$ system at NNNLO*, *JHEP* **09** (2014) 045 [arXiv:1407.2128] [INSPIRE].

[28] M. Beneke, P. Marquard, P. Nason and M. Steinhauser, *On the ultimate uncertainty of the top quark pole mass*, arXiv:1605.03609 [INSPIRE].

[29] J. Komijani, *A discussion on leading renormalon in the pole mass*, *JHEP* **08** (2017) 062 [arXiv:1701.00347] [INSPIRE].

[30] N. Isgur and M.B. Wise, *Weak decays of heavy mesons in the static quark approximation*, *Phys. Lett.* **B 232** (1989) 113 [INSPIRE].

[31] S. Bekavac, A. Grozin, D. Seidel and M. Steinhauser, *Light quark mass effects in the on-shell renormalization constants*, *JHEP* **10** (2007) 006 [arXiv:0708.1729] [INSPIRE].

[32] P. Ball, M. Beneke and V.M. Braun, *Resummation of (beta0 α_s)**n corrections in QCD: Techniques and applications to the tau hadronic width and the heavy quark pole mass*, *Nucl. Phys.* **B 452** (1995) 563 [hep-ph/9502300] [INSPIRE].

[33] A.H. Hoang and A.V. Manohar, *Charm effects in the MS-bar bottom quark mass from Υ mesons*, *Phys. Lett.* **B 483** (2000) 94 [hep-ph/9911461] [INSPIRE].

[34] A.H. Hoang, *Bottom quark mass from Υ mesons: charm mass effects*, hep-ph/0008102 [INSPIRE].

[35] A.L. Kataev and V.S. Molokoedov, *On the flavour dependence of the $\mathcal{O}(\alpha_s^4)$ correction to the relation between running and pole heavy quark masses*, *Eur. Phys. J. Plus* **131** (2016) 271 [arXiv:1511.06898] [INSPIRE].

[36] A.H. Hoang and A.V. Manohar, *Charm quark mass from inclusive semileptonic B decays*, *Phys. Lett.* **B 633** (2006) 526 [hep-ph/0509195] [INSPIRE].

[37] M. Melles, *Massive fermionic corrections to the heavy quark potential through two loops*, *Phys. Rev.* **D 58** (1998) 114004 [hep-ph/9805216] [INSPIRE].

[38] O. Buchmuller and H. Flacher, *Fit to moment from $B \to X_c l\bar{\nu}$ and $B \to X_s\gamma$ decays using heavy quark expansions in the kinetic scheme*, *Phys. Rev.* **D 73** (2006) 073008 [hep-ph/0507253] [INSPIRE].

[39] P. Gambino, K.J. Healey and S. Turczyk, *Taming the higher power corrections in semileptonic B decays*, *Phys. Lett.* **B 763** (2016) 60 [arXiv:1606.06174] [INSPIRE].

[40] M. Butenschoen et al., *Top quark mass calibration for Monte Carlo event generators*, *Phys. Rev. Lett.* **117** (2016) 232001 [arXiv:1608.01318] [INSPIRE].

[41] A.H. Hoang, S. Mantry, A. Pathak and I.W. Stewart, *Extracting a short distance top mass with light grooming*, arXiv:1708.02586.

[42] CDF, D0 collaboration, T.E.W. Group, *Combination of CDF and D0 results on the mass of the top quark using up to 9.7 fb^{-1} at the Tevatron*, arXiv:1407.2682 [INSPIRE].

[43] D0 collaboration, V.M. Abazov et al., *Combination of D0 measurements of the top quark mass*, *Phys. Rev.* **D 95** (2017) 112004 [arXiv:1703.06994] [INSPIRE].

JHEP09(2017)099

[44] ATLAS collaboration, *Measurement of the top quark mass in the $t\bar{t} \to$ dilepton channel from $\sqrt{s} = 8$ TeV ATLAS data*, *Phys. Lett.* **B 761** (2016) 350 [arXiv:1606.02179] [INSPIRE].

[45] CMS collaboration, *Measurement of the top quark mass using proton-proton data at $\sqrt{s} = 7$ and 8 TeV*, *Phys. Rev.* **D 93** (2016) 072004 [arXiv:1509.04044] [INSPIRE].

[46] CMS collaboration, *Updates on projections of physics reach with the upgraded CMS detector for high luminosity LHC*, CMS-DP-2016-064 (2016).

JHEP09(2017)099

Chapter 9

REvolver
Automated Running and Matching of Couplings and Masses in QCD

André H. Hoang, Christopher Lepenik and Vicent Mateu

REvolver: Automated running and matching of couplings and masses in QCD

Published in: Comput. Phys. Commun. **270** (2022) 108145

Preprint version: arXiv:2102.01085 [hep-ph]

Contributions to this article:
Bulk of the code, most analytical and numerical calculations (together with other authors), most numerical analyses, conceptual innovations (together with other authors).

Computer Physics Communications 270 (2022) 108145

Contents lists available at ScienceDirect

Computer Physics Communications

www.elsevier.com/locate/cpc

REvolver: Automated running and matching of couplings and masses in QCD ☆,☆☆

André H. Hoang [a,b], Christopher Lepenik [a,*], Vicent Mateu [c,d]

[a] University of Vienna, Faculty of Physics, Boltzmanngasse 5, A-1090 Wien, Austria
[b] Erwin Schrödinger International Institute for Mathematical Physics, University of Vienna, Boltzmanngasse 9, A-1090 Wien, Austria
[c] Departamento de Física Fundamental e IUFFyM, Universidad de Salamanca, E-37008 Salamanca, Spain
[d] Instituto de Física Teórica UAM-CSIC, E-28049 Madrid, Spain

ARTICLE INFO

Article history:
Received 7 March 2021
Received in revised form 5 July 2021
Accepted 1 August 2021
Available online 23 August 2021

Keywords:
QCD
Renormalization group
Heavy quarks

ABSTRACT

In this article we present `REvolver`, a `C++` library for renormalization group evolution and automatic flavor matching of the QCD coupling and quark masses, as well as precise conversion between various quark mass renormalization schemes. The library systematically accounts for the renormalization group evolution of low-scale short-distance masses which depend linearly on the renormalization scale and sums logarithmic terms of high and low scales that are missed by the common logarithmic renormalization scale evolution. The library can also be accessed through `Mathematica` and `Python` interfaces and provides renormalization group evolution for complex renormalization scales as well.

Program summary
Program Title: `REvolver`
CPC Library link to program files: https://doi.org/10.17632/m6cjfmzsxb.1
Developer's repository link: https://gitlab.com/REvolver-hep/REvolver
Code Ocean capsule: https://codeocean.com/capsule/6150064
Licensing provisions: GPLv3 or later
Programming language: `C++`, `Python`, `Wolfram Language`
Nature of problem: The strong coupling and the quark masses are fundamental parameters of QCD that are scheme and renormalization-scale dependent. The choice of scheme depends on the active number of flavors and the range of scales, and is dictated by the requirements to minimize the size of corrections and to sum large logarithmic corrections to all orders. For the strong coupling and the quark masses at high scales, the $\overline{\rm MS}$ scheme with logarithmic scale dependence is used. For quark masses at low scales, short-distance mass schemes with linear scale-dependence are used. The `REvolver` library provides conversions for the strong coupling and the most common quark mass schemes, with renormalization scale evolution implemented such that all types of large logarithmic terms are summed to all orders, accounting for flavor threshold effects and state-or-the-art correction terms. The pole mass, which is not a short-distance mass and contains a sizable renormalon ambiguity, is treated as a derived quantity.
Solution method: Renormalization group equations are solved for complex-valued scales to machine precision based on fast-converging iterative algorithms and analytic all-order expressions. Matching relations for the strong coupling at flavor thresholds are computed in a way that gives equal results for upward and downward evolution. `Core` objects allow to define an arbitrary number of physical scenarios for strong coupling values and quark mass spectra, where options for precision and matching scales can be set freely, and values for quark masses in all common schemes including the pole mass can be extracted. All `REvolver` routines are implemented entirely in `C++` and can be accessed through `Mathematica` and `Python` interfaces.

☆ The review of this paper was arranged by Prof. Z. Was.
☆☆ This paper and its associated computer program are available via the Computer Physics Communications homepage on ScienceDirect (http://www.sciencedirect.com/science/journal/00104655).
* Corresponding author.
E-mail addresses: andre.hoang@univie.ac.at (A.H. Hoang), christopher.lepenik@univie.ac.at (C. Lepenik), vmateu@usal.es (V. Mateu).

https://doi.org/10.1016/j.cpc.2021.108145

Contents

1. Introduction

Quark masses are fundamental parameters of quantum chromodynamics(QCD) and their precise determination in adequate schemes and at appropriate renormalization scales is of high interest for theoretical as well as experimental studies of many processes. These can be governed by energy scales ranging from a few GeV (e.g. for hadronic states) up to several hundred GeV and even TeV scales (e.g. for particle collisions that take place at the Large Hadron Collider). One needs to employ the renormalization group evolution equations to reliably relate the values of quark masses defined at such widely different energy scales. An interesting situation arises if the dynamical scale governing the quark mass dependence of an observable is much smaller than the quark mass itself. In this case, the common running $\overline{\rm MS}$ mass scheme, which obeys a renormalization group equation with logarithmic scale dependence, cannot be employed for high-precision applications, because it is only meaningful for scales of the order or larger than the mass. Rather, so-called low-scale short-distance masses must be used, which obey renormalization group equations with linear scale dependence. The numerical impact of the renormalization group evolution is particularly important for the top quark mass where, due to its large value, significant scale hierarchies can arise.

Here we present `REvolver`, a `C++` library with routines that provide renormalization-group resummed conversions between quark mass schemes defined at different renormalization scales, including scales much lower than the mass, where low-scale short-distance masses are employed, as well as above the mass value, where the $\overline{\rm MS}$ mass is used. The routines are based on the creation of so-called `Core` objects, each of which representing a certain physical scenario for the heavy quark masses (charm, bottom and top quarks, as well as hypothetical heavier flavors), the number of massless quarks and the strong coupling α_s. In a single session, an (in principle) arbitrary number of `Core` objects can be created and managed. Each `Core` object can then provide values for the quark masses in the most popular low-scale short-distance schemes as well as for the $\overline{\rm MS}$ mass and the strong coupling at any (real or complex-valued) renormalization scale and in any flavor number scheme, consistently accounting for flavor threshold effects and the resummation of large logarithms of all kinds. The basis of the quark mass evolution equations for scales below the respective mass is the renormalization group equation of the natural MSR mass (here simply called the MSR mass), which was provided in Refs. [1] together with a full treatment of flavor matching corrections when the evolution crosses the thresholds related to lighter massive quarks [2]. Furthermore, for each `Core` object, options can be set to specify the perturbative precision in the flavor matching and the renormalization group evolution. Using all available theoretical input in the literature, see Sec. 8 for a detailed listing, it is possible to relate the $\overline{\rm MS}$, MSR and most other low-scale short-distance quark masses with a theoretical precision of 10 to 20 MeV (neglecting any parametric uncertainties). Quark mass values in the pole scheme cannot be defined at the same level of precision due to the pole mass renormalon ambiguity which decreases the accuracy by an order of magnitude [3,2]. `REvolver` offers the possibility to set up `Core` objects using pole masses as an input or to extract pole mass values from a `Core` object, but it treats the pole mass as a derived quantity where the user has to specify the way in which the pole mass value is defined. Furthermore, `REvolver` provides various options to account for the asymptotic higher order corrections of the pole mass and the pole mass renormalon ambiguity. All `REvolver` routines are implemented entirely in `C++` and can be accessed through `Mathematica` and `Python` interfaces.

There is an existing `C++` library accompanied by a `Mathematica` package called `CRunDec` and `RunDec` [4,5], respectively, which already provide many functionalities included in the `REvolver` library. We have cross checked in detail that any theoretical (perturbative) input implemented in `CRunDec` and `RunDec` agrees with the corresponding one employed for `REvolver`. We have furthermore checked that the numerical output of the routines provided in `CRunDec`/`RunDec` is in agreement with the equivalent routines of `REvolver`. The `REvolver` library, however, exceeds `CRunDec`/`RunDec`

(i) by providing the `Core` concept that allows to automatically create, extend and manage an arbitrary number of scenarios for strong coupling values, mass spectra and theory settings, and to extract quark masses and the QCD coupling in all flavor number schemes and at all scales,
(ii) by accounting for the renormalization group resummation of large logarithms and lighter massive quark flavor thresholds when dealing with quark masses at renormalization scales smaller than the quark mass, as well as for low-scale short-distance masses,
(iii) by giving access to machine-precision numerical routines that provide quasi-exact solutions of the renormalization group equations for the running masses and the strong coupling at complex scales, and
(iv) by providing routines to determine the asymptotic series for the pole mass to an arbitrary order that allow to extract different pole mass definitions and to quantify the pole mass renormalon ambiguity with various methods.

The emphasis of all `REvolver` functionalities is to provide integrated and easy-to-use routines, while maintaining the possibility to deviate from default settings and specify all available options, useful for high-precision phenomenological and conceptual QCD studies aiming for uncertainties at the level of 10 to 20 MeV for short-distance masses.

This article is organized as follows: In Sec. 2 essential terminology used for the description of the `REvolver` package is explained. In Sec. 3 we succinctly review the MSR mass and the R-evolution concepts [1,6] which are essential for the resummation of the logarithms mentioned above in bullet point (ii). Section 4 provides general information concerning the `REvolver` installation and setting up the `C++`, `Mathematica` and `Python` interfaces. The philosophy of the `Core` concept is explained in Sec. 5, and Sec. 6 provides a structured introduction to all available `REvolver` routines. In Sec. 7 a sizable number of pedagogical examples for applications of `REvolver` routines are provided, partly using the routine's default settings, partly using alternative optional parameter setting, to demonstrate the versatility of `REvolver` for important phenomenological applications in the literature. It is recommended that the user consults the examples shown in this section, which are also collected in a `Mathematica` notebook, a Jupyter Notebook using the `Python` interface, and a `C++` source file provided with the `REvolver` package. In Sec. 8 important references are provided which were used as the source for the higher order corrections implemented for the strong coupling and the mass schemes supported by `REvolver`. Here, also a detailed citation recommendation for these higher order corrections is provided. Section 9 contains a summary. Finally, some details concerning the algorithms used for `Core` creation and the quasi-exact solution of renormalization group equations are given in Appendix A. In addition, a number of essential formulae for implementation-dependent quantities are provided which cannot be found in the literature in the form used in `REvolver`.

2. Terminology

This article employs a particular terminology when referring to renormalization-scale dependent mass schemes and the pole mass:

- *Running quark mass in the n_f-flavor scheme* $m_q^{(n_f)}(\mu)$: Refers to the $\overline{\rm MS}$ mass if the flavor number n_f includes this massive quark, and the MSR mass otherwise. For example, the running top quark mass at the scale μ in the 6-flavor scheme $m_t^{(6)}(\mu)$ refers to the $\overline{\rm MS}$ mass $\overline{m}_t^{(6)}(\mu)$, and the running top quark mass at the scale μ in the 4-flavor scheme $m_t^{(4)}(\mu)$ refers to the MSR mass $m_t^{{\rm MSR},(4)}(\mu)$.
- *Standard running mass* $\overline{m}_q$: Refers to the $\overline{\rm MS}$ mass in the flavor number scheme where all lighter quarks along with this quark are treated dynamically, evaluated at the scale of this mass. For example, the standard running top mass is the 6-flavor $\overline{\rm MS}$ quark mass evaluated at the scale of this top mass: $\overline{m}_t \equiv \overline{m}_t^{(6)}(\overline{m}_t^{(6)})$. The mass dependence of all flavor-threshold corrections is expressed in terms of the standard running mass.
- *Asymptotic pole mass*: Refers to the pole mass value obtained from the running mass defined by summing the perturbative series to the order of the minimal correction.
- *Order-dependent pole mass*: Refers to the pole mass value obtained from the running mass by truncating the perturbative series at a specified order.

3. The MSR mass and R-evolution

The natural MSR mass of a massive quark defined in Ref. [1] (and called just the MSR mass here) plays a central role in `REvolver` and is a renormalization scale and flavor-number-dependent low-scale short-distance mass. It is derived from the $\overline{\rm MS}$ mass and treated as the natural extension of the $\overline{\rm MS}$ mass for renormalization scales below the mass of the quark. This combination of the scale-dependent $\overline{\rm MS}$ and MSR masses extends the well known concept of flavor-number dependent renormalization group evolution and flavor threshold matching for scales above the quark mass (where the $\overline{\rm MS}$ mass scheme is appropriate) to lower scales. In contrast to usual logarithmic renormalization scale evolution (as known from the $\overline{\rm MS}$ masses or the strong coupling), the MSR mass renormalization group evolution is linear. This is consequence of the linear dynamical scaling that arises when the off-shell massive quark quantum fluctuations are integrated out in the nonrelativistic limit. Together with the flavor number dependent strong $\overline{\rm MS}$ coupling, the $\overline{\rm MS}$ and MSR masses form the basis of the core concept of REvolver and allow to also resum large logarithms involving low-scale short-distance mass schemes other than the MSR mass. This functionality is used by default in the REvolver routines (but can also be switched off by the user on demand). The MSR mass [1,2,6] has already been used in a number of applications, but we still find it warranted to briefly review its main concepts in this section. For simplicity, we consider the case in which all n_ℓ quarks lighter than q are massless. The reader is referred to Ref. [2] for the case with massive lighter quarks.

To define the MSR mass, one starts with the relation between the standard running mass and pole mass,

$$m_q^{\rm pole} - \overline{m}_q = \overline{m}_q \sum_{n=1}^{\infty} a_n^{\overline{\rm MS}}(n_\ell, n_h) \left[\frac{\alpha_s^{(n_\ell+n_h)}(\overline{m}_q)}{4\pi}\right]^n , \tag{1}$$

where $n_f = n_\ell + n_h$ is the number of active flavors, with n_ℓ being the number of massless quarks and $n_h = 1$ referring to the quark q. Since the MSR mass is employed for renormalization scales below m_q, one integrates out the virtual heavy quark loops by setting $n_h = 0$. This allows to define a renormalization scale R smaller than m_q and the corrections to the pole mass having a linear dependence on R to implement a consistent nonrelativistic scaling behavior. The MSR mass is thus defined by furthermore setting $\overline{m}_q \to R$:

$$m_q^{\rm pole} - m_q^{{\rm MSR},(n_\ell)}(R) = R \sum_{n=1}^{\infty} a_n^{\overline{\rm MS}}(n_\ell, 0) \left[\frac{\alpha_s^{(n_\ell)}(R)}{4\pi}\right]^n . \tag{2}$$

In contrast to the $\overline{\rm MS}$ mass, which has only logarithmic dependence on the scale μ, the MSR mass has an additional linear dependence on R. The $\overline{\rm MS}$ and MSR masses can be related perturbatively and unambiguously through Eqs. (1) and (2) because the pole mass in both equalities is identical.[1] The resulting perturbative series for the difference of two MSR masses at different renormalization scales R_1 and R_2 is renormalon free, as long as it is expressed in powers of the strong coupling at the same renormalization scale. As a result, for disparate values of R_1 and R_2 large logarithms will appear. These logarithms can be consistently summed up with the renormalization group equation

$$-\frac{\rm d}{{\rm d}R} m_q^{{\rm MSR},(n_\ell)}(R) = \gamma_R^M[\alpha_s^{(n_\ell)}(R)] = \sum_{n=0}^{\infty} \gamma_n^R(n_\ell) \left[\frac{\alpha_s^{(n_\ell)}(R)}{4\pi}\right]^{n+1} . \tag{3}$$

In contrast to the logarithmic renormalization group equations for the $\overline{\rm MS}$ mass and the strong coupling, it shows a *linear power scaling* and has therefore been dubbed as the R-evolution equation. The anomalous dimension coefficients $\gamma_n^R(n_\ell)$ can be calculated from the relation [see Eq. (6) for the definition of the QCD β-function coefficients β_i]

$$\gamma_n^R(n_\ell) = a_{n+1}^{\overline{\rm MS}}(n_\ell, 0) - 2\sum_{j=0}^{n-1} (n-j)\,\beta_j\, a_{n-j}^{\overline{\rm MS}}(n_\ell, 0) . \tag{4}$$

The coefficients of the R-evolution equation have the following explicit form:

$$\begin{aligned}
&\gamma_0^R(n_\ell) = \tfrac{16}{3} , \\
&\gamma_1^R(n_\ell) = 96.1039 - 9.55076\, n_\ell , \\
&\gamma_2^R(n_\ell) = 1595.75 - 269.953\, n_\ell - 2.65945\, n_\ell^2 , \\
&\gamma_3^R(n_\ell) = (12319. \pm 417.) - (9103. \pm 10.)\, n_\ell + 610.264\, n_\ell^2 - 6.515\, n_\ell^3 .
\end{aligned} \tag{5}$$

The uncertainties in the $\mathcal{O}(\alpha_s^4)$ coefficient arise from the numerical uncertainties in the relation between the $\overline{\rm MS}$ and the pole masses at this order. In A.4 we present an efficient algorithm to exactly integrate Eq. (3).

Adopting appropriate values for R and n_ℓ the MSR mass $m_q^{{\rm MSR},(n_\ell)}(R)$ can be related in a renormalon-free manner to any other low-scale short-distance mass without the appearance of large logarithms and can thus be used to also resum potentially large R-evolution logarithms in the relation of other low-scale short-distance mass schemes. In the presence of massive quarks with masses lighter than m_q, the MSR mass has an n_ℓ-dependent renormalization group evolution and flavor threshold corrections in close analogy to the renormalization group evolution of the strong coupling and the $\overline{\rm MS}$ mass. This allows for the resummation of large logarithms involving the masses of the lighter massive quarks. For details we refer to Ref. [2].

4. Setup

There are three ways to access the functionalities of the `REvolver` library:

- via the `C++` library directly, which might be most suitable for extensive automated tasks and to interface with other libraries and codes,
- via the Wolfram `Mathematica` [7] interface (using `WSTP`/`MathLink`), which is suitable for interactive tasks and for using in parallel with other `Mathematica` features,
- via the `Python` [8] interface (generated using `SWIG` [9]) for usage in scripts and interactive execution in Jupyter notebooks [10].

4.1. Installation

Note that slightly more detailed instructions for installing the code, including Windows-specific commands, are given in the `README.md` file provided with the source code. Here we only describe the installation procedure for Linux and MacOS, and only for `REvolver` itself (not for `CMake` and other auxiliaries).

For the compilation of `REvolver` a `C++11` compatible compiler is needed. The recommended (and tested) choices are `gcc` on Linux, Apple `Clang` on MacOS and `MinGW` on Windows. It is expected that `REvolver` compiles on other platforms and with different compilers as well, although this has not been tested and we do not provide any specific instructions.

[1] This is consistent since the two series on the RHS of Eqs. (1) and (2) have the same leading linear and mass-independent renormalon ambiguity.

We provide a CMake script with various options controlling which interfaces and demonstration codes are built. To use the script, at least version 3.1 of CMake is required.

If REvolver is to be used via Mathematica, Wolfram Mathematica is required in a version which supports WSTP or MathLink.

For the Python interface, at least version 3 of Python has to be installed, including the development packages. We note that the Python interface is currently supported only on Linux and MacOS.

After downloading the code to the local hard drive, open a command line interface, navigate to the directory code/ and run the commands

```
$ mkdir build
$ cd build/
```

In the next step, the CMake script will be executed. Depending on which interfaces are to be prepared, various flags can be set:

- wolfr determines if the Mathematica interface is prepared (default: OFF),
- py determines if the Python interface is prepared (default: OFF),
- cpp_demo determines if the C++ demo executable is built (default: ON).

The static REvolver C++ library is always compiled. Note that to compile the C++ demo executable the library Quadpack++ [11] is used. However, no additional steps are required by the user since the library is provided with REvolver. Note that the Quadpack++ library is only compiled if the flag cpp_demo is set to ON.

To execute the CMake script with default flags and compile the code, one has to run the terminal commands

```
$ cmake ..
$ make install
```

or in general

```
$ cmake [(-D <flag>={ON|OFF})...] ..
$ make install
```

where <flag> is a placeholder for one of the flags listed above. For example, to prepare the Mathematica interface, but not the compilation of the C++ demo code one would use

```
$ cmake -D wolfr=ON -D cpp_demo=OFF ..
$ make install
```

The directory code/build/ can be safely removed after the compiling is done. The resulting libraries and executables can be found at the following locations:

- the static C++ library file:
  code/lib/libREvolver.a
- the MathLink/WSTP executable, ready to be loaded in a Mathematica notebook:
  code/bin/REvolver
- the Python module file and dynamic library, ready to be imported in a Python script:
  code/pyREvolver/lib/pyREvolver.py
  code/pyREvolver/lib/_pyREvolver.so
- the C++ demo executable:
  code/bin/examples

4.2. General usage

C++ interface

To use the REvolver C++ static library, the respective header file has to be included which is done via

```
#include REvolver.h
```

and the library has to be properly linked when compiling the code. After including the header file, the implemented classes and routines are available in the namespace revo and accessible with the scope resolution prefix revo:: unless the instruction using namespace revo; has been invoked, such that the resolution prefix is not necessary.

For a demonstration, we refer to the source file code/examples/examples.cpp and the related executable code/bin/examples (if cpp_demo=ON was set).

Mathematica interface

To load the WSTP executable in a Mathematica notebook, execute

```
Install["<path to executable>/REvolver"]
```

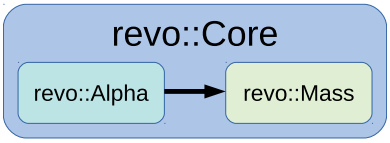

Fig. 1. Schematic structure of the class `revo::Core` in C++: the class contains an instance of the class `revo::Alpha` as a member providing functionalities related to the strong coupling such as running and matching, and an instance of the class `revo::Mass` providing functionalities related to the quark masses such as running, matching and conversion. `revo::Mass` uses `revo::Alpha` for coupling evolution, and `revo` is the namespace where all relevant `REvolver` classes are defined.

with `<path to executable>` referring to the directory path where the executable is located. For future convenience it might be useful to execute

```
CopyFile["<path to executable>/REvolver",
         $UserBaseDirectory <> "/Applications/REvolver"]
```

which copies the executable to the user base directory of `Mathematica`, making it possible to load the executable with the command

```
Install["REvolver"]
```

in the future.

For a demonstration of how to load `REvolver` in a `Mathematica` notebook and a general overview of the available functions, see the demonstration notebook `code/examples/examples.nb` provided with the package.

`Python` interface

The module can be loaded in a `Python` script or Jupyter notebook with the usual syntax

```
import pyREvolver
```

assuming that `pyREvolver.py` and the shared library file (`*.so`) are located in the same folder as the script or notebook, or have been added to the module search path with the following command

```
import sys
sys.path.append('<path to pyREvolver.py>')
```

For a demonstration of how to load and use the module, see the Jupyter notebook `code/examples/examples.ipynb` provided with the package.

5. `Core` structure

As described in the introduction, all functionalities of the library are centered around instances of the class `revo::Core` (simply called "`Core` objects" or "`Cores`" in the following) each representing a certain physical scenario for the quark mass spectrum and the strong coupling and from which numerical values for quark masses and the strong coupling in specified schemes and at specified scales can be extracted. In principle, the number of `Core` objects defined at the same time is only limited by the available memory, regardless of the interface used.

The schematic structure of the class `revo::Core` in C++ is depicted in Fig. 1: the class has objects of the classes `revo::Alpha` and `revo::Mass` as members. The class `revo::Alpha` has various member functions related to the strong coupling like running, matching and for obtaining the QCD scale $\Lambda_{\rm QCD}$. The class `revo::Mass` has member functions related to the evolution and matching of the running masses as well as the extraction of quark mass values in specified schemes. It uses an instance of the class `revo::Alpha` to obtain the necessary coupling values. The respective member objects of the `revo::Core` class can be accessed through the member functions `revo::Core::alpha()` and `revo::Core::masses()`, respectively. The class `revo::Core` itself represents the frame to access these member functions and provides additional functionalities related to setting up a physical coupling and quark mass spectrum scenario, and extending an existing scenario by adding additional heavier massive quarks.

Although in principle possible, helper classes such as `revo::Mass` and `revo::Alpha` are not meant to be used outside `Core` objects. All available functionalities can (and should) be accessed through `Core` objects.

When using the `Mathematica` interface, the specific structure of the classes are not relevant since the wrapper hides most details to fit into the Wolfram language syntax. To preserve the possibility to have multiple `Cores` defined at the same time in `Mathematica`, a unique name has to be specified for each `Core` instance, which is referred to when extracting mass and coupling values or when extending scenarios.

For concrete usage and examples we refer to Secs. 6 and 7.

6. Implemented functions

In the following descriptions and examples we will assume that the namespace `revo` has been introduced in the C++ code with the instruction

```
using namespace revo;
```

such that the scope resolution prefix `revo::` can be omitted, and that in `Python` the module was loaded with

```
from pyREvolver import *
```

to keep code snippets uncluttered.

The syntax and interface structure in `Python` is the same as in `C++`, with a few exceptions:

- If a constant of an `enum class` type has to be provided as an input, the scope resolution operator `::` has to be exchanged with `_`, e.g. the enumerator `MSbar` of type `MScheme` has to be provided using `MScheme_MSbar` instead of `MScheme::MSbar`.
- The `C++` function `Mass::mPole` allows for two optional pointer-type inputs to provide the possibility of accessing several output values (see Sec. 6.2.3). In `Python`, instead, within the class `Mass` the additional member function `mPoleDetailed` is provided which returns a tuple of values. In `Mathematica` the same functionality is provided by the function `MassPoleDetailed`.
- `C++` specific syntax cannot be used, e.g. initializing an `std::vector` with an initializer list.

We will treat the `C++` and `Mathematica` interfaces on an equal footing, always stating the `C++` function prototypes and definitions first with the `Mathematica` ones following. We will then briefly describe the inputs and outputs, and in most cases give short examples. If not stated otherwise, the related `Python` syntax is the same as in `C++`. Also, to focus on the essential functionalities first, we will present all commands without optional parameters at the beginning and describe additional options in a second step. Note that the given function prototypes do not always correspond exactly to the ones present in the source codes to make the descriptions more transparent, e.g. for template functions in `C++` or type restrictions in `Mathematica`.

For a more detailed and technical documentation of the full functionality and interface structure of the `C++` library, please consider reading the online doxygen documentation (see https://revolver-hep.gitlab.io/REvolver).

A detailed documentation of the functions accessible via the `Mathematica` interface is available through the `Mathematica` internal documentation.

6.1. Constructing a `Core` and accessing scenario parameters

In the following we describe how to construct `Core`s in the various interfaces and how to read out their scenario parameters. The scenario parameters of a `Core` uniquely reflect its physical scenario. They include the total flavor number, the flavor number scheme, value as well as scale of the strong coupling specified at `Core` creation, the running masses at reference scales, the flavor matching scales, and the parameters that specify the precision of the theoretical input and scheme choices. The latter include the perturbative orders of renormalization group equations and threshold matching relations, the lambda parameters setting variations in renormalization group equations, the variation related to the uncertainty of the perturbative 4-loop pole-$\overline{\text{MS}}$ mass coefficient, and the coefficients of the QCD β-function. All scenario parameters, except for coupling and quark mass values, acquire default values if not specified at `Core` creation.

6.1.1. *`C++` / `Python` only: `RunPar` and `RunParV`*

In the `C++` and `Python` interfaces, the `RunPar struct`

```
struct RunPar {
  int nf;
  double value;
  double scale;
};
```

is used to collect the parameters of the running coupling and masses. `RunPar structs` contain the active number of flavors `nf` specifying the flavor number scheme, the parameter (coupling or mass) value `value` and the respective renormalization scale `scale`. All numbers referring to quantities with dimensions of energy handled by REvolver (e.g. masses, renormalization scales or Λ_{QCD}) are understood in GeV units.

The related type `RunParV` is an alias for `std::vector<RunPar>`, i.e. a collection of `RunPar`s.

In the following `C++` example we define the `RunPar structs alphaPar` and `alphaPar2` specifying flavor number schemes, values and renormalization scales for the strong coupling, and the `RunParVs mPar` and `mPar2` containing three `RunPars` each, specifying values for running masses of charm, bottom and top quarks. `alphaPar` sets a realistic value for the strong coupling $\alpha_s^{(5)}(m_Z) = 0.1181$, while `alphaPar2` contains parameters to specify the strong coupling $\alpha_s^{(4)}(4.2\text{ GeV})$. `mPar` defines standard running masses with realistic values of charm, bottom and top quarks, namely $\overline{m}_c = 1.3$ GeV, $\overline{m}_b = 4.2$ GeV, and $\overline{m}_t = 163$ GeV, while `mPar2` defines values for different flavor number schemes and scales, specifically $m_c^{(6)}(163.0\text{ GeV}) = \overline{m}_c^{(6)}(163.0\text{ GeV})$, $m_b^{(4)}(4.2\text{ GeV}) = m_b^{\text{MSR},(4)}(4.2\text{ GeV})$, and $m_t^{(5)}(4.2\text{ GeV}) = m_t^{\text{MSR},(5)}(4.2\text{ GeV})$. In the `Python` example we only define `alphaPar` and `mPar` for brevity.

`C++` example

```
RunPar alphaPar = {5, 0.1181, 91.187};
RunPar alphaPar2 = {4, 0.22491680889566054, 4.2};

RunParV mPar;
mPar.push_back({4, 1.3, 1.3});
mPar.push_back({5, 4.2, 4.2});
mPar.push_back({6, 163.0, 163.0});
```

```
RunParV mPar2;
mPar2.push_back({6, 0.6173718176865822, 163.0});
mPar2.push_back({4, 4.20502733598667, 4.2});
mPar2.push_back({5, 172.37293079716443, 4.2});
```

Python example

```
alphaPar = RunPar(5, 0.1181, 91.187)

mPar = RunParV(3)
mPar[0] = RunPar(4, 1.3, 1.3)
mPar[1] = RunPar(5, 4.2, 4.2)
mPar[2] = RunPar(6, 163.0, 163.0)

mPar2 = RunParV(3)
mPar2[0] = RunPar(6, 0.6173718176865822, 163.0)
mPar2[1] = RunPar(4, 4.20502733598667, 4.2)
mPar2[2] = RunPar(5, 172.37293079716443, 4.2)
```

6.1.2. Constructing `Core` objects with masses

The prototypes for the functions constructing `Cores` in `C++` and `Mathematica`, respectively, are

```
Core::Core(int nTot, const RunPar& alphaPar,
           const RunParV& mPar);

CoreCreate[CoreName_String, nTot_Integer, alphaPar_List,
           mPar_List]
```

with the mandatory input `nTot`, specifying the total number of quark flavors in the scenario, as well as the input parameters for the strong coupling and the quark masses. In `C++`, the coupling and mass parameters are given by `RunPar structs` and `std::vectors RunParV`, respectively, which are described in Sec. 6.1.1, while in `Mathematica`, the parameter collections are given by lists and lists of lists, respectively. The argument `CoreName` in `Mathematica` specifies the user-defined unique name of the created `Core` instance. The given masses must be sorted in increasing order with respect to their standard running mass values starting with the lightest. The number of massless quarks in a `Core` is equal to `nTot` minus the number of elements in `mPar`. To construct a `Core` without massive quarks, see Sec. 6.1.3.

C++ example

The instructions

```
Core core1(6, alphaPar, mPar);
Core core2(6, alphaPar2, mPar2);
```

construct two `Core` objects named `core1` and `core2`, respectively, with a total flavor number of 6, and the parameters determining the strong coupling and masses contained in `alphaPar`, `alphaPar2`, `mPar` and `mPar2` as defined in the example of Sec. 6.1.1. These are the minimal set of parameters that have to be specified to create `Core` objects.

Mathematica example

To construct the same `Cores` in `Mathematica` one can use

```
alphaPar = {5, amZdef, mZdef};
mPar = {{4, 1.3, 1.3}, {5, 4.2, 4.2}, {6, 163.0, 163.0}};
CoreCreate["core1", 6, alphaPar, mPar]

alphaPar2 = {4, 0.22491680889566054, 4.2};
mPar2 = {{6, 0.6173718176865822, 163.0},
         {4, 4.20502733598667, 4.2},
         {5, 172.37293079716443, 4.2}};
CoreCreate["core2", 6, alphaPar2, mPar2]
```

using the predefined parameters `amZdef = 0.1181` for the strong coupling and `mZdef = 91.187` for the Z-boson mass.

Optional parameters

The `Core` constructor allows to set a number of optional parameters to control the flavor matching scales, the perturbative order of matching relations and renormalization group equations, to perform scale variation of the renormalization group equations, and to vary the 4-loop pole-$\overline{\text{MS}}$ mass coefficient within its error band. The values of these optional parameters are a defining property of the physical scenario represented by a `Core` object and respected by all functionalities related to numerical values of the strong coupling and the running masses.

The full `C++` constructor prototype is

```
Core::Core(int nTot, const RunPar& alphaPar,
           const RunParV& massPar,
           const doubleV& fMatch = doubleV(),
           int runAlpha = kMaxRunAlpha,
           double lambdaAlpha = 1.0,
           int orderAlpha = kMaxOrderAlpha,
           int runMSbar = kMaxRunMSbar,
           double lambdaMSbar = 1.0,
           int orderMSbar = kMaxOrderMSbar,
           int runMSR = kMaxRunMSR,
           double lambdaMSR = 1.0,
           int orderMSR = kMaxOrderMSR,
           double msBarDeltaError = 0.0);
```

with `doubleV` being an alias for `std::vector<double>` set by `REvolver`. If one of the optional parameters shown in the constructor above is explicitly specified, all parameters appearing prior in the argument list must be specified as well. The values `kMaxRunAlpha`, `kMaxOrderAlpha`, `kMaxRunMSR`, `kMaxOrderMSR`, `kMaxRunMSbar` and `kMaxOrderMSbar` are predefined constants representing the respective defaults. In the `Mathematica` interface, the optional parameters of the same name can be set individually via the options parameter syntax, i.e. by adding `opt->val` after the last regular function input, as shown in the examples below.

The meaning of the optional parameters is as follows:

- `fMatch`: a vector / list containing elements {`f1, f2, ...`}, where `fn` specifies that the flavor matching scale μ_n for the n-th lightest massive quark threshold is `fn` times the standard running mass: $\mu_n = \texttt{fn} \times \overline{m}_n$.
  Default: all `fn` are set to 1.0. (Note that the mass dependence of the flavor threshold corrections is expressed in terms of the standard running masses as well. The specification to use a different mass scheme to parameterize the flavor threshold corrections is not supported.)
- `runAlpha`: the loop order used for the running of the strong coupling. Default: highest available order which is 5.
- `lambdaAlpha`: a parameter probing the renormalization scale dependence of the QCD β-function. With respect to the perturbative series of the β-function truncated at the order set by `runAlpha` (used for the value 1.0), a (`runAlpha`+1) order term is estimated from renormalization scale variation (when a value different from 1.0 is specified): the estimate is obtained by expanding the original perturbative series $\beta[\alpha_s(\mu)]$ (truncated at order `runAlpha`) in terms of $\alpha_s(\texttt{lambdaAlpha}\times\mu)$, truncating at order `runAlpha`. The result is expanded in $\alpha_s(\mu)$ truncating again at order (`runAlpha`+1). A variation around 1.0 of $\mathcal{O}(\pm 10\%)$ leads to an adequate uncertainty estimation for the known lower orders of the β-function, so that variations exceeding this range should be avoided. Default: 1.0.
- `orderAlpha`: the loop order used for the strong coupling flavor threshold matching relations. The renormalization scale dependence of these matching relations is precise to loop order `orderAlpha` and independent of the value specified for `runAlpha`. Default: highest available order which is 4.
- `runMSbar`: loop order used for the $\overline{\text{MS}}$ mass running. Default: highest available order which is 5.
- `lambdaMSbar`: a parameter probing the renormalization scale dependence of the anomalous dimension γ of the $\overline{\text{MS}}$ mass in analogy to the parameter `lambdaAlpha`. The variation is performed by expanding the original series for $\gamma[\alpha_s(\mu)]$ (truncated at order `runMSbar`) in terms of $\alpha_s(\texttt{lambdaMSbar} \times \mu)$, truncating at order `runMSbar`. A variation around 1.0 of $\mathcal{O}(\pm 10\%)$ leads to an adequate uncertainty estimation for the known lower orders of γ, so that variations exceeding this range should be avoided. Default: 1.0.
- `orderMSbar`: loop order used for the flavor threshold matching relations of the $\overline{\text{MS}}$ masses. The renormalization scale dependence of these matching relations is precise to loop order `orderMSbar` and independent of the values specified for `runAlpha` and `orderAlpha`. Default: highest available order which is 4.
- `runMSR`: the loop order used for the MSR mass running. Default: highest available order which is 4.
- `lambdaMSR`: a parameter probing the renormalization scale dependence of the anomalous dimension γ^R of the MSR mass in analogy to the parameters `lambdaAlpha` and `lambdaMSbar`. The variation is performed by expanding the original $\gamma^R[\alpha_s(R)]$ series (truncated at order `runMSR`) in terms of $\alpha_s(\texttt{lambdaMSR} \times R)$, truncating at order `runMSR`. A variation around 1.0 by factors of around 0.5 and 2 leads to an adequate uncertainty estimation for the known lower orders of the γ^R, so that variations exceeding this range should be avoided. Default: 1.0.
- `orderMSR`: the loop order used for the flavor threshold matching relations of the MSR masses associated to the massive quark itself and all lighter massive quarks. The renormalization scale dependence of these matching relations is precise to loop order `orderMSR` and independent of the value specified for `runMSR`, `runAlpha` and `orderAlpha`. Default: highest available order which is 4.
- `msBarDeltaError`: controls the error of the 4-loop coefficient in the pole-$\overline{\text{MS}}$ mass relation. Should be varied between -1 and 1 to scan the standard deviation as quoted in Ref. [12]. Default: 0.0.
- `precisionGoal`: the parameter setting the relative precision of all convergent infinite sums and iterative algorithms. The input value is clipped to the range $[10^{-6}, 10^{-15}]$. Default: 10^{-15} which we refer to as *machine precision*. The default should be adequate for most applications, but a lower precision goal may be specified for improving speed.

The quark mass dependence of all flavor matching relations (for the strong coupling and the running masses) is expressed in terms of the corresponding standard running masses $\overline{m}_q$. Changing this to an arbitrary mass scheme is not supported in `REvolver`. This concerns flavor threshold matching as well as perturbative reexpansions of the strong coupling in other flavor number schemes. The resulting numerical differences are, however, tiny and smaller than the corresponding perturbative uncertainties.

C++ example
The instruction

```
Core core3(6, alphaPar, mPar, {2.0, 1.0, 1.0});
```

constructs a `Core` object named `core3` with a total flavor number of 6 and the parameters specifying the strong coupling and masses contained in `alphaPar` and `mPar`, respectively, as defined in the example of Sec. 6.1.1. The matching scale of the flavor threshold related to the lightest massive particle is $2 \times \overline{m}_c = 2.0 \times 1.3$ GeV.

Mathematica example
The command

```
CoreCreate["core3", 6, alphaPar, mPar,
           fMatch->{2.0, 1.0, 1.0}]
```

has the same effect as the analogous `C++` example, using the lists `alphaPar` and `mPar` defined in the previous example of this section.

6.1.3. Constructing `Core` objects without massive quarks
The functions with the prototypes

```
Core::Core(const RunPar& alphaPar);

CoreCreate[CoreName_String, alphaPar_List]
```

are used to construct a `Core` object with massless quarks only and without specifying any optional parameters. The parameters are analogous to the massive case described in Sec. 6.1.2.

Optional parameters
The full `C++` constructor prototype for a `Core` with only massless quarks is

```
Core::Core(const RunPar& alphaPar,
           int runAlpha = kMaxRunAlpha,
           double lambdaAlpha = 1.0,
           const doubleV& beta = doubleV());
```

where the optional variables `runAlpha` and `lambdaAlpha` are analogous to the massive case described in Sec. 6.1.2 and can be set in `Mathematica` using option parameters. With the optional input `beta` (which is a constant reference to a `std::vector<double>` of arbitrary length) one can specify an arbitrary number of custom β-function coefficients. Their default values are the common $\overline{\text{MS}}$ QCD β-function coefficients up to 5 loops with all higher order coefficients set to zero. These are defined based on the β-function form

$$\mu \frac{\mathrm{d}\alpha_s(\mu)}{\mathrm{d}\mu} = \frac{\mathrm{d}\alpha_s(\mu)}{\mathrm{d}\ln(\mu)} = \beta_{\text{QCD}}(\alpha_s(\mu)) = -2\alpha_s(\mu) \sum_{n=0}^{\infty} \beta_n \left[\frac{\alpha_s(\mu)}{4\pi}\right]^{n+1}, \tag{6}$$

where the elements of the `C++` container `beta` correspond to the ordered list of coefficients $\beta_0, \cdots, \beta_n$. Note that adding masses to `Core` objects with custom β-function coefficients is not supported and that, depending on the choice of `runAlpha` not all coefficients specified by the user may be used.

In `Mathematica` the functionality of custom QCD β-function coefficients can be used with

```
CoreCreate[CoreName_String, alphaPar_List, beta_List]
```

with `beta` being the list of β-function coefficients and the additional option parameters already explained before.

6.1.4. `Mathematica` only: listing and deleting `Core`s

```
CoreList[]
CoreDelete[CoreName_String]
CoreDelete[CoreNames_List]
CoreDeleteAll[]
```

These commands list the names of the `Core`s currently defined, and delete specific or all `Core`s, respectively. The argument of `CoreDelete` is a string referring to a `Core` name or a list containing several `Core` names.

Example

```
In[]:= CoreList[]
Out[]= {core1, core2, core3}

In[]:= CoreDelete["core3"]
       CoreList[]
Out[]= {core1, core2}
```

where the Core named core3 has been deleted from memory. We explicitly show In[] and Out[] to separate in- from out-put and assumed that definitions from previous examples are still valid.

6.1.5. Accessing Core parameters

A Core represents a certain physical scenario for the strong coupling and the quark mass spectrum that also depends on the theoretical approximations and conventions implemented (with optional/default parameters) specified at the time the Core was created. The scenario parameters of a Core (coupling, quark masses, theoretical approximations and conventions) unambiguously specify a given scenario and can be accessed by dedicated routines. Note that the scenario parameters of a Core for the strong coupling depend on the way how the strong coupling was specified when the Core has been created. Therefore it is possible to create two physically equivalent Cores with differing scenario parameters for the strong coupling.

While in C++ the scenario parameters of Core objects are returned from separate functions, some Mathematica commands print collections of them. The respective function prototypes in C++ are

```
int            Core::nTot() const;
const RunPar&  Alpha::defParams() const;
const doubleV& Core::standardMasses() const;
const doubleV& Core::fMatch() const;
int            Core::getOrder(OrderPar para) const;
double         Core::getLambda(LambdaPar para) const;
double         Core::msBarDeltaError() const;
const doubleV& Core::betaCoefs(int nf) const;
```

returning the total number of flavors, the defining RunPar related to the coupling, an std::vector of the standard running masses in increasing order, an std::vector with the fn factors specifying the flavor matching scales, the perturbative orders used for coupling and mass evolutions, the lambda scaling parameters set for coupling and mass evolution, the variation parameter of the 4-loop coefficient in the pole-$\overline{\rm MS}$ evolution, and the β-function coefficients in the nf-flavor number scheme.

The function inputs of the types defined as

```
enum class OrderPar {
  runAlpha,
  orderAlpha,
  runMSbar,
  runMSR,
  orderMSbar,
  orderMSR
};
```

and

```
enum class LambdaPar { lambdaAlpha, lambdaMSbar, lambdaMSR };
```

i.e. the enumerators of type OrderPar and LambdaPar, respectively, govern to which evolution (coupling, $\overline{\rm MS}$, MSR) or matching procedure the output of the functions getOrder and getLambda refers to.

In Mathematica, the parameters discussed above can be extracted using the functions

```
CoreParams[CoreName_String]
CoreParamsDetail[CoreName_String]
BetaCoefs[CoreName_String]
```

CoreParams returns from the specified Core a list containing the total number of flavors, the flavor number scheme, value and renormalization scale of the strong coupling specified at Core creation, and the standard running masses in increasing order. CoreParamsDetail returns the coupling and mass values at all flavor matching scales (in the flavor schemes above as well as below the corresponding threshold), the flavor number scheme, value as well as scale of the strong coupling specified at Core creation, and all optional parameters set by CoreCreate and described in the C++ description above. BetaCoefs returns the β-function coefficients in all relevant flavor number schemes with the normalization as given in Eq. (6).

In addition to just printing the parameters, CoreParamsDetail allows for an optional parameter to which the parameters are saved as a nested list. The corresponding function prototype is

```
CoreParamsDetail[CoreName_String, output_Symbol]
```

where output is the symbol in which the list is stored.

C++ example

The instructions

```
core1.nTot();
core1.getOrder(OrderPar::runAlpha);
```

return the total number of flavors and the perturbative order used in the running of the strong coupling, respectively, for the `Core` named `core1`. They correspond to the values `(int)6` and `(int)5`, respectively, given the definition of `core1` from the `C++` example of Sec. 6.1.2.

`Mathematica` example

In the following we show how the output of the functions `CoreParams` and `BetaCoefs` looks like for the `Core` named `core1` given in the `Mathematica` example of Sec. 6.1.2:

```
In[]:= CoreParams["core1"]
Out[]= {6, {5, 0.1181, 91.187}, 1.3, 4.2, 163.}
```

showing the list containing the total number of flavors, the flavor number scheme, value and renormalization scale of the strong coupling given at `Core` creation, and the standard running masses in increasing order; and

```
In[]:= BetaCoefs["core1"]
Out[]= nl = 3: {9.,64.,643.833,12090.4,130378.}
       nl = 4: {8.33333,51.3333,406.352,8035.19,58310.6}
       nl = 5: {7.66667,38.6667,180.907,4826.16,15470.6}
       nl = 6: {7.,26.,-32.5,2472.28,271.428}
```

showing the β-function coefficients in the relevant flavor number schemes.

The output of the function `CoreParamsDetail` is more extensive than that of `CoreParams`, giving

```
In[]:= CoreParamsDetail["core1"]
Out[]=
```

[core1, 6]	m1-threshold	m2-threshold	m3-threshold
aS-values	{0.385234, 0.383676}	{0.224917, 0.224684}	{0.108577, 0.108555}
m1-values	{1.30636, 1.3}	{0.947058, 0.945337}	{0.617575, 0.617372}
m2-values	{4.64086, 4.62912}	{4.20503, 4.2}	{2.7438, 2.7429}
m3-values	{172.819, 172.807}	{172.383, 172.373}	{163.032, 163.}

```
       aS input: {5,0.1181,91.187}
       Matching f-factors: {1.,1.,1.}
       runAlpha: 5
       lambdaAlpha: 1.
       orderAlpha: 4
       runMSbar: 5
       lambdaMSbar: 1.
       orderMSbar: 4
       runMSR: 4
       lambdaMSR: 1.
       orderMSR: 4
       msBarDeltaError: 0.
       precisionGoal: 1.*10^-15
```

for the `Core` named `core1`. The set of printed values represents the full physical content of a `Core`. Creating a new `Core` from this output in an arbitrary way leads to a physically equivalent core. So `Core`s are created in a self-consistent way. This is made possible because `REvolver`'s algorithm to solve the renormalization group evolution for the strong coupling provides (machine precision) exact solutions and because its algorithm for the flavor matching is self-consistent, see the routines described in Sec. 6.2.1. Therefore, all massive quarks consistently affect each others flavor number scheme dependent running values depending on the parameters specified at `Core` creation.

For a demonstration, consider the output of `CoreParamsDetail` of the `Core` named `core2`

```
In[]:= CoreParamsDetail["core2"]
Out[]=
```

[core2, 6]	m1-threshold	m2-threshold	m3-threshold
aS-values	{0.385234, 0.383676}	{0.224917, 0.224684}	{0.108577, 0.108555}
m1-values	{1.30636, 1.3}	{0.947058, 0.945337}	{0.617575, 0.617372}
m2-values	{4.64086, 4.62912}	{4.20503, 4.2}	{2.7438, 2.7429}
m3-values	{172.819, 172.807}	{172.383, 172.373}	{163.032, 163.}

```
       aS input: {4,0.224917,4.2}
       Matching f-factors: {1.,1.,1.}
       runAlpha: 5
```

```
lambdaAlpha: 1.
orderAlpha: 4
runMSbar: 5
lambdaMSbar: 1.
orderMSbar: 4
runMSR: 4
lambdaMSR: 1.
orderMSR: 4
msBarDeltaError: 0.
precisionGoal: 1.*10^-15
```

which is (apart from the `Core` name and the strong coupling specifications at `Core` creation) exactly the same. In fact, the numbers used to create `core2` in the examples of Sec. 6.1.2 have been taken from the output of `CoreParamDetails["core1"]`.

6.2. Extraction of masses and couplings

The following section presents the routines to extract the values for the strong coupling and the running quark masses in any flavor number scheme at any scale, as well as values in other quark mass schemes from a given `Core`.

6.2.1. Running masses and strong coupling

The functions with the prototypes

```
double Mass::mMS(int nfIn, double scale) const;
double Alpha::operator()(double scale) const;

MassMS[CoreName_String, nfIn_Integer, scale_Real]
AlphaQCD[CoreName_String, scale_Real]
```

are used to extract a running mass (i.e. the $\overline{\text{MS}}$ mass if the flavor number scheme includes this massive quark, the MSR mass otherwise) and strong coupling at a specific renormalization scale `scale` from a `Core` where the optional parameters valid in the creation of the `Core` are respected. The functions furthermore use an *automatic matching convention*, which means that the flavor number scheme of the output is deduced automatically from `scale`, with flavor threshold matching at $\mu_n = \texttt{fn} \times \overline{m}_n$, see Sec. 6.1.2. `nfIn` specifies for which quark the running mass is returned and refers to the number of dynamical flavors of the associated standard running mass.

In `C++`, as indicated by the scope resolution prefixes of `Mass::mMS` and `Alpha::operator()`, these functions are not by themselves members of the class `Core`, but members of the classes `Mass` and `Alpha` respectively. Consequently, in practice they are accessed through the `Core` member functions `Core::alpha` and `Core::masses` (see Sec. 5 the following examples).

Note that matching at flavor thresholds is *always* done from below to above the thresholds, meaning that matching between n_ℓ and $n_\ell + 1$ flavor schemes always uses the perturbative expansion in $\alpha_s^{(n_\ell)}$. If this is not possible directly, e.g. when $\alpha_s^{(n_\ell+1)}$ is given and $\alpha_s^{(n_\ell)}$ still needs to be determined, the solution is computed iteratively. This convention is strictly applied everywhere, and in particular for the determination of the `Core` parameters described in Sec. 6.1.5. For the computation of the renormalization group evolution equations (at any specified order) we use algorithms which are exact, i.e. they provide results with *machine precision*. This, in combination with the flavor matching convention, has the advantage that `Core`s are created in a self-consistent way. This means that a `Core` that is created from the coupling and the masses at any renormalization scales extracted from an existing core `Core` will lead to a `Core` that is physically equivalent within machine precision if all optional parameters are set to equivalent values.

Both functions above are also available in a version permitting complex-valued input for `scale`, resulting in a complex-valued output. The function prototypes in this case are

```
std::complex<double>
  Mass::mMS(int nfIn, std::complex<double> scale);
std::complex<double>
  Alpha::operator()(std::complex<double> scale);

MassMS[CoreName_String, nfIn_Integer, scale_Complex]
AlphaQCD[CoreName_String, scale_Complex]
```

and the flavor number scheme of the output is determined from the automatic matching conventions based on the absolute value of `scale`.

Note that for applications where negative real values of `scale` are expected, the user of the `C++` or `Python` interfaces should declare `scale` as complex-valued explicitly from the start so that the intrinsic `C++` function evaluations can be performed. Otherwise, in such a case `NaN` will be returned. Using the `Mathematica` interface, the complex-valued declaration is automatically employed if `scale` is negative real (or complex). In the way `C++` treats the branch cuts of complex-valued functions involved in the calculations, this corresponds to adding an infinitesimally small positive imaginary part to `scale`.

In case the input parameter `scale` is not provided when executing `Mass::mMS` and `MassMS`, the routines return the respective standard running mass.

C++ example

The instruction

```
core1.masses().mMS(6, 20.0);
```

returns the mass value of the heaviest of the six quarks defined in the `Core` named `core1`, referred to by the flavor number 6 of the corresponding standard running mass flavor scheme, at the scale 20.0 GeV with automatic flavor matching (performed at the standard running mass of the heaviest quark in `core1`). Referring to the corresponding quark mass as m_t, the returned value `(double)171.046` corresponds to $m_t^{\text{MSR},(5)}(20.0\text{ GeV})$.

The instruction

```
core1.alpha()(10.0);
```

returns the value of the strong coupling defined in the `Core` named `core1` at the scale 10.0 GeV. Due to automatic matching the returned value `(double)0.178468` refers to $\alpha_s^{(5)}(10.0\text{ GeV})$. Note that the `Core` member functions `Core::alpha` and `Core::masses` have been used to access member functions of the classes `Alpha` and `Mass`, see Sec. 5.

Mathematica example

The `Mathematica` command

```
In[]:= MassMS["core1", 5, 30.0]
Out[]= 3.199542552851507
```

returns the mass value of the next-to-heaviest of the six quarks defined in the `Core` named `core1`, referred to by the flavor number 5, at the scale 30.0 GeV. Referring to the corresponding quark mass as m_b, due to automatic matching, the shown output corresponds to the $\overline{\text{MS}}$ mass $\overline{m}_b^{(5)}(30.0\text{ GeV})$. The command

```
In[]:= AlphaQCD["core1", -10.0 + 0.1 I]
Out[]= 0.11619771241600231 - 0.08307724827828394 I
```

returns the value of the strong coupling defined in the `Core` named `core1` at the complex scale $\mu = (-10.0 + 0.1\,i)$ GeV. Due to the automatic matching convention, the flavor number scheme is automatically chosen to be 5 since $|\mu| = 10.0005$ GeV exceeds the standard running bottom mass in `core1`. Consequently the output refers to $\alpha_s^{(5)}((-10.0 + 0.1\,i)\text{ GeV})$.

Optional parameters

Automatic matching at the flavor thresholds can be overruled using the additional input `nfOut`, which specifies the flavor number scheme. The function prototypes are

```
double Mass::mMS(int nfIn, double scale,
                 int nfOut = kDefault) const;
double Alpha::operator()(double scale,
                         int nfOut = kDefault) const;

MassMS[CoreName_String, nfIn_Integer, scale_Real,
       nfOut_Integer:kDefault]
AlphaQCD[CoreName_String, scale_Real, nfOut_Integer:kDefault]
```

and analogously for complex-valued input. In `C++` as well as in `Mathematica`, the value `kDefault` is a predefined constant, internally set to -1, specifying that the respective default values will be used.

6.2.2. Other short-distance masses

From a given `Core`, the extraction of values of quark masses in a number of other short-distance quark mass schemes is supported. This includes the renormalization group invariant (`RGI`) scheme [13] and the following low-scale short-distance mass schemes: 1S (`1S`) [14–16], kinetic (`Kin`) [17], potential subtracted (`PS`) [18,19], and renormalon subtracted[2] (`RS`) [20]. Note that the optional parameters setting the loop orders of the conversion formulae used for the extraction of these masses are independent of the loop order parameters specified during `Core` creation (`runAlpha`, `orderAlpha`, `runMSbar`, `orderMSbar`, `runMSR`, `orderMSR`), see Sec. 6.1.2.

The functions with the prototypes

```
double Mass::mRGI(int nfIn) const;
double Mass::m1S(int nfIn) const;
double Mass::mKin(int nfIn, double scaleKin) const;
double Mass::mPS(int nfIn, double muF) const;
double Mass::mRS(int nfIn, double scaleRS) const;
```

[2] We implement only the "unprimed" version of the RS mass, which has a finite $\mathcal{O}(\alpha_s)$ term in its relation to the pole mass.

```
MassRGI[CoreName_String, nfIn_Integer]
Mass1S[CoreName_String, nfIn_Integer]
MassKin[CoreName_String, nfIn_Integer, scaleKin_Real]
MassPS[CoreName_String, nfIn_Integer, muf_Real]
MassRS[CoreName_String, nfIn_Integer, scaleRS_Real]
```

extract from a `Core` a quark mass value in the specified short-distance scheme. The variable `nfIn` is again the specifier for the massive quark, referring to the number of dynamical flavors of the associated standard running mass. The variables `scaleKin`,[3] `muF` and `scaleRS` specify the renormalization scales of the kinetic, potential subtracted and renormalon subtracted masses, respectively. Note that the `1S`, `Kin`, `PS` and `RS` masses are defined in (`nfIn`−1)-flavor schemes, while the `RGI` mass is defined in the `nfIn` flavor scheme.

In C++, all routines outlined above are member functions of the class `Mass`, as indicated by the scope resolution prefix `Mass::`, and are accessed through the `Core` member function `Core::masses` (see Sec. 5 and the following examples).

Without specifying any additional optional parameters, the extraction of the low-scale short-distance masses is done in the following default way: first, the running mass in the (`nfIn` − 1)-flavor scheme is determined at the *intrinsic scale* of the low-scale short-distance mass using R-evolution. The intrinsic scales of the `Kin`, `PS` and `RS` schemes are the respective values of 2×`scaleKin`, `muf` and `scaleRS`, while for the `1S` scheme it is the inverse Bohr radius $M_{q,B}$ determined with the routine `Mass::mBohr` described below with default setting. Subsequently, the running mass is converted to the low-scale short-distance mass using both masses' perturbative relation to the pole mass employing the strong coupling at the intrinsic scale, where the pole mass is then consistently eliminated to the corresponding order. The resulting relation is renormalon-free avoiding large logarithms. Whenever known, finite mass effects stemming from lighter massive quarks are taken into account in this relation, which is up to three loops for the pole mass relations of the `1S`, `PS` and `Kin`[4] schemes. For the `RS` mass, finite lighter quark mass effects have not been explicitly specified in the literature. Note that the lighter quark mass effects in the perturbative relation between the pole and running ($\overline{\rm MS}$ or MSR) masses are known to three loops. In the conversion between the running and the `RS` masses these lighter quark mass corrections are set to zero coherently everywhere to avoid upsetting the renormalon cancellation. Effective methods to simulate finite quark mass effects (e.g. by enforcing a change in the flavor number scheme of the strong coupling) are not implemented as regular `REvolver` functionalities, but can still be realized, as we show in the examples given in Sec. 7.

`REvolver` provides the routine `Mass::mBohr` to calculate the heavy quarkonium inverse Bohr radius $M_{q,B}$ for a massive quark q. In the default setting, $M_{q,B}$ is the root of the function $f(x) = C_F\alpha_s^{(n_\ell)}(x)m_q^{\rm MSR,(n_\ell)}(x) - x$, and determined using an algorithm based on a modified version of Dekker's method. The corresponding routine is a global function and always uses machine precision. The inverse Bohr radius for a massive quark q can be extracted from a given `Core` through the functions with the following prototypes

```
double Mass::mBohr(int nfIn, double nb = 1.0) const;

MBohr[CoreName_String, nfIn_Integer, nb_Real:1.0]
```

where `nfIn` is the specifier for the massive quark and `nb` refers to an optional rescaling factor such that the inverse Bohr radius is determined from the equality $M_{q,B}^{\rm nb} = {\rm nb}\, C_F\alpha_s^{(n_\ell)}(M_{q,B}^{\rm nb})m_q^{\rm MSR,(n_\ell)}(M_{q,B}^{\rm nb})$. This option is useful for scale variation e.g. in the context of higher excited heavy quarkonium states. For the computation of the intrinsic scale used for the `1S` mass scheme conversions, `nb` is used with the default setting `nb` =1.

C++ example

The instruction

```
core1.masses().m1S(6);
```

returns the mass value in GeV units of the heaviest of the six quarks defined in the `Core` named `core1`, referred to by the flavor number 6, in the 1S scheme, which is `(double)171.517`.

`Mathematica` example

The `Mathematica` command

```
In[]:= MassPS["core1", 5, 2.0]
Out[]= 4.521091787631138
```

returns the mass value of the next-to-heaviest of the six quarks defined in the `Core` named `core1`, referred to by the flavor number 5, in the potential subtracted scheme at the scale 2.0 GeV, i.e. $m_b^{\rm PS}(2\ {\rm GeV})$, referring to that quark mass as m_b.

Optional parameters

The functions responsible for extracting quark mass values in short-distance mass schemes other than the running mass allow for several optional parameters whose nature is tied to the respective schemes. The full prototypes are given by

[3] Following Refs. [21,22], the default value for the kinetic mass intrinsic scale (where the default log resummed conversion between the running and the kinetic masses is carried out, see below) is set to be twice its renormalization scale, 2×`scaleKin`.

[4] For the kinetic mass `REvolver` adopts the definition of lighter massive quark corrections given in Ref. [22] where these quark mass corrections are absent in the flavor number scheme below the corresponding threshold and exclusively come from the flavor number decoupling relations of the strong coupling above the threshold.

```
double Mass::mRGI(int nfIn,
                  int order = kMaxRunMSbar) const;
double Mass::m1S(int nfIn, int nfConv = kDefault,
                 double scale = kDefault,
                 Count1S counting = Count1S::Default,
                 double muA = kDefault,
                 int order = kMaxOrder1s) const;
double Mass::mKin(int nfIn, double scaleKin,
                  int nfConv = kDefault,
                  double scale = kDefault,
                  double muA = kDefault,
                  int order = kMaxOrderKinetic) const;
double Mass::mPS(int nfIn, double muF,
                 int nfConv = kDefault,
                 double scale = kDefault,
                 double muA = kDefault,
                 double rIR = 1,
                 int order = kMaxOrderPs) const;
double Mass::mRS(int nfIn, double scaleRS,
                 int nfConv = kDefault,
                 double scale = kDefault,
                 double muA = kDefault,
                 int order = kMaxRunMSR,
                 int nRS = kMaxRunAlpha - 1,
                 double N12 = kDefault) const;
```

```
MassRGI[CoreName_String, nfIn_Integer,
        order_Integer:kMaxRunMSbar]
Mass1S[CoreName_String, nfIn_Integer,
       nfConv_Integer:kDefault,
       scale_Real:kDefault,
       counting_String:"default",
       muA_Real:kDefault,
       order_Integer:kMaxOrder1s]
MassKin[CoreName_String, nfIn_Integer, scaleKin_Real,
        nfConv_Integer:kDefault,
        scale_Real:kDefault,
        muA_Real:kDefault,
        order_Integer:kMaxOrderKinetic]
MassPS[CoreName_String, nfIn_Integer, muF_Real,
       nfConv_Integer:kDefault,
       scale_Real:kDefault,
       muA_Real:kDefault,
       rIR_Real:1.0,
       order_Integer:kMaxOrderPs]
MassRS[CoreName_String, nfIn_Integer, scaleRS_Real,
       nfConv_Integer:kDefault,
       scale_Real:kDefault,
       muA_Real:kDefault,
       order_Integer:kMaxRunMSR,
       nRS_Integer:kMaxRunAlpha - 1,
       N12_Real:kDefault]
```

where the variables `kDefault`, `kMaxRunMSbar`, `kMaxRunMSR`, `kMaxOrder1s`, `kMaxOrderKinetic` and `kMaxOrderPs` as well as the values `"default"` and `Count1S::Default` in `Mathematica` and `C++`, respectively, are predefined constants representing the respective default values. In `C++` and `Mathematica`, if one of the optional parameters shown above is explicitly specified, all parameters appearing prior in the argument list must be specified as well.

In the following the meaning of the optional parameters is explained.

The extraction of the RGI mass has only one optional parameter, which is `order`, specifying the loop order of the β-function and $\overline{\text{MS}}$ mass anomalous dimensions (which are taken equal) entering the conversion formula from the standard running mass, see Eq. (A.19). The default value is the highest available order, which is 5.

Considering the functions extracting low-scale short-distance masses, there are some optional parameters affecting the formulae used for the conversion computations:

- `nfConv`: specifies the flavor number scheme of the running mass that is used in the conversion formula. For `nfConv = nfIn - 1` the MSR scheme is used; for `nfConv = nfIn` the $\overline{\rm MS}$ scheme is used. The strong coupling is always employed in the `nfIn - 1` flavor scheme. Default: `nfIn - 1`.
- `scale`: specifies the scale of the running mass from which the conversion is determined. Default: intrinsic scale of the low-scale mass.
- `muA`: specifies the scale of the strong coupling used for the conversion. Default: intrinsic scale of the low-scale mass.
- `order`: specifies how many perturbative orders are used in the conversion. Default: Highest available order for the low-scale mass.

Note that for very heavy quarks (such as the top quark) specifications of the parameters `nfConv`, `scale` and `muA` that differ from their defaults can lead to large logarithmic corrections in the conversions involving low-scale short-distance masses. On the other hand, for the case of lighter massive quarks (such as the bottom and especially the charm quark) the default settings may lead to unphysically low scales causing perturbative instabilities. The parameters `nfConv`, `scale` and `muA` should therefore be used with some care.

Furthermore, for some low-scale masses there are additional optional parameters related to their definition and specific properties:

- `counting`: specifies the order counting used for the conversion computation to extract the 1S mass. The available options are `Count1S::Nonrelativistic` and `Count1S::Relativistic` (enumerations of type `Count1S`) in `C++`, and `"nonrelativistic"` and `"relativistic"` in `Mathematica`. For non-relativistic counting it is assumed that `scale` is of the same order as the inverse Bohr radius, which is much smaller than the quark mass value and both are counted as $\mathcal{O}(m_n\alpha_s)$; for the relativistic counting it is assumed that `scale` is of the same order as the quark mass, and the inverse Bohr radius is counted as $\mathcal{O}(m_n)$, see Sec. 5.2 of Ref. [1]. If one chooses to convert from the $\overline{\rm MS}$ mass, only the relativistic counting is supported. Note that here the optional parameter `order` always specifies how many non-zero terms are taken into account in the conversion series, e.g. in the case of non-relativistic counting `order` $= 1$ refers to $\mathcal{O}(m_n\alpha_s^2)$, while it refers to $\mathcal{O}(m_n\alpha_s)$ in the relativistic counting. (So for `order` $= 1$ the conversion formula is the same in both counting schemes.) To simplify language, we refer to a perturbative term in the 1S-pole mass relation as n-loop, if it is combined with the n-loop coefficient in the relation between the running mass and the pole mass, independent of the employed counting. Default: `Count1S::Default` and `"default"` for `C++` and `Mathematica`, respectively, which corresponds to `"nonrelativistic"` for an MSR mass input and to `"relativistic"` for $\overline{\rm MS}$.
- `rIR`: specifies the ratio of the IR subtraction scale $\mu_{\rm IR}$ with respect to the scale `muF` employed in the 4-loop term of the pole-PS mass relation, `rIR` $= \mu_{\rm IR}/\mu_F$, see Secs. 4.5.3 and 5.1 of Ref. [1]. Default: 1.0, which corresponds to the definition given in Ref. [19].
- `nRS`: specifies the number of terms (used in the perturbative construction of the Borel function and the normalization `N12`) for the calculation of the coefficients of the pole-RS mass perturbation series, see Ref. [20]. Default: highest available order which is 4.
- `N12`: specifies the pole mass renormalon normalization constant employed in the pole-RS mass relation. Default: value computed by the sum rule formula employed by the routine `Mass::N12` (`C++`) or `N12` (`Mathematica`), see Sec 6.2.4, summing up `nRS` terms in the sum rule series using all available information on the QCD β-function and anomalous dimension of the MSR mass.

`C++` example

The instruction

```
core1.masses().mKin(5, 2.0, 4, 5.0, 3.0, 2);
```

returns the kinetic mass value of the next-to-heaviest of the six quarks defined in the `Core` named `core1`, referred to by the flavor number 5 of the corresponding standard running mass flavor scheme. The intrinsic kinetic mass scale is set to 2 GeV, the conversion formula is applied to the MSR mass in the 4 flavor scheme at 5 GeV and with the renormalization scale of the strong coupling set to 3 GeV. Terms up to $\mathcal{O}(\alpha_s^2)$ are included in the conversion formula. The returned value is `(double)4.3105`.

`Mathematica` example

The `Mathematica` command

```
In[]:= MassRS["core1", 6, 20.0, 6, 163.0, 60.0, 3]
Out[]= 170.48477730509723
```

returns the RS mass value of the heaviest of the six quarks defined in the `Core` named `core1`, referred to by the flavor number 6. The intrinsic scale of the RS mass is set to 20 GeV and the conversion formula is applied to the $\overline{\rm MS}$ mass in the 6 flavor scheme. The $\overline{\rm MS}$ mass renormalization scale is specified to be 163 GeV, while the renormalization scale of the strong coupling is set to 60 GeV. The last parameter shown above specifies that three perturbative orders are used in the conversion. For `nRS` and `N12` no inputs are specified, consequently the default setting is applied.

6.2.3. Pole mass

Quark mass values in the pole mass scheme can be extracted from a given `Core`. The pole mass scheme suffers from a renormalon ambiguity so that there are several options to quote a value. `REvolver` supports two ways of extracting pole quark mass values, accessible through the functions corresponding to the prototypes

```
double Mass::mPoleFO(int nfIn, int nfConv, double scale,
                     double muA, int order) const;
double Mass::mPole(int nfIn, double scale) const;

MassPoleFO[CoreName_String, nfIn_Integer, nfConv_Integer,
```

```
            scale_Real, muA_Real, order_Integer]
  MassPole[CoreName_String, nfIn_Integer, scale_Real]
```

All parameters shown have to be specified by the user. For both routines the variable `nfIn` is the specifier for the quark whose pole mass value is extracted, referring to the number of dynamical flavors of the associated standard running mass, while `scale` specifies the scale of the running mass for which the conversion formula to the pole mass is employed. Furthermore, the loop orders of the various components entering the conversion formula used in the computation of the pole mass value are provided by the settings of the loop order parameters specified during `Core` creation (`runAlpha`, `orderAlpha`, `runMSbar`, `orderMSbar`, `runMSR`, `orderMSR`), see Sec. 6.1.2. Here the parameters `runMSR` and `runAlpha` are particularly important because they also set the loop order of the exact coefficients accounted for in the perturbative series between the MSR and the pole masses, see Eq. (A.28) in Sec. A.5. Because in `REvolver` matching is always applied at flavor thresholds, the latter series are the only ones being affected by the renormalon.

The functions `Mass::PoleFO` and `MassPoleFO`, respectively, return the pole mass using the conversion formula up to the order set by `order` from the running mass in the flavor number scheme specified by `nfConf`. The input parameter `muA` specifies the renormalization scale of the strong coupling used in the conversion formula. The input `order` allows, in principle, an arbitrarily large integer. For $\texttt{order} \leq \min(\texttt{runMSR}, \texttt{runAlpha} - 1)$ the exact perturbative coefficients up to this order are utilized in the relation between MSR and pole mass. For $\texttt{order} > \min(\texttt{runMSR}, \texttt{runAlpha} - 1)$ a renormalon-based asymptotic formula for the coefficients of the asymptotic series is used, see Eq. (A.28) in Sec. A.5 for details.

The functions `Mass::Pole` and `MassPole`, respectively, return the value of the asymptotic pole mass, i.e. the conversion is done by summing the perturbative series for the conversion formula relating running and pole mass to the order of minimal correction, again potentially employing the already mentioned asymptotic formula if the order of minimal correction is larger than $\min(\texttt{runMSR}, \texttt{runAlpha} - 1)$. The asymptotic pole mass is always determined from the MSR mass in the flavor number scheme where all massive quarks are integrated out regardless of the value of `scale`. The method used for the calculation of the asymptotic value is the minimal correction method (`"min"`) described below.

C++ example

The instruction

```
core1.masses().mPole(5, 2.0);
```

returns the asymptotic pole mass of the next-to-heaviest of the six quarks defined in the `Core` named `core1` in GeV units, referred to by the flavor number 5, using the minimal correction method, which is `(double)4.91150`. The scale employed for the running mass at conversion is 2 GeV.

Mathematica example

The `Mathematica` command

```
In[]:= MassPoleFO["core1", 6, 5, 20.0, 20.0, 16]
Out[]= 1190.2576448418606
```

returns the order-dependent pole mass value of the heaviest of the six quarks defined in the `Core` named `core1`, referred to by the flavor number 6. The conversion formula is applied to the respective MSR mass with 5 active flavors at the scale 20 GeV, choosing the same scale for the renormalization scale of the strong coupling. The perturbative series terms are summed up to $\mathcal{O}(\alpha_s^{16})$.[5]

Optional parameters

The functions `Mass::mPoleFO` and `MassPoleFO` in `C++` and `Mathematica`, respectively, are completely general and do not support any additional optional parameters.

The full prototypes of the functions responsible for accessing the asymptotic pole mass are

```
double Mass::mPole(int nfIn, double scale,
                   double muA = kDefault,
                   PoleMethod method = PoleMethod::Default,
                   double f = 1.25,
                   double* ambiguity = nullptr,
                   int* nMin = nullptr) const;

MassPole[CoreName_String, nfIn_Integer, scale_Real,
         muA_Real:kDefault,
         method_String:"min",
         f_Real:1.25]
MassPoleDetailed[CoreName_String, nfIn_Integer, scale_Real,
                 muA_Real:kDefault,
                 method_String,
                 f_Real:1.25]
```

[5] The value obtained with this command is unphysically large due to the asymptotic (non-convergent) nature of the series that relate the pole mass and short-distance masses. This behavior is the origin of the ambiguity of the pole mass.

where MassPoleDetailed in Mathematica is a function returning a list, containing the asymptotic pole mass, the associated renormalon ambiguity and the order of the minimal correction term, providing the functionality corresponding to the C++ routine Mass::mPole (with specified optional pointer parameters ambiguity and nMin), see the descriptions below. In Python there is the analogous function Mass.MassPoleDetailed.

The meaning of the optional input parameters is as follows:

- muA: specifies the renormalization scale of the strong coupling in the conversion formula. The default is the value of scale.
- method: specifies the method used to obtain the asymptotic pole mass and the ambiguity. In C++ the available options are PoleMethod::Min for the minimal correction term method, PoleMethod::Range for the range method and PoleMethod::DRange for the corresponding discrete version, see the explanation below. In Mathematica these options correspond to the string inputs "min", "range" and "drange", respectively. The input method is optional if only the asymptotic pole mass is returned; the defaults in that case are PoleMethod::Min (C++) and "min" (Mathematica). The input method is *not* optional if the pole mass ambiguity is also returned, i.e. for MassPoleDetailed in Mathematica and when the optional pointer to ambiguity is given in C++.
- f: specifies a constant larger than unity multiplying the minimal correction for the methods "range" and "drange". Default: 1.25
- ambiguity: a pointer to double. If specified, the value of the pole mass ambiguity is saved in the variable pointed to (C++ only).
- nMin: a pointer to int. If specified, the order of the minimal correction term is saved in the variable pointed to (C++ only).

Note that for the Mathematica routine MassPoleDetailed the input variable method does not have a default and must always be specified (because it always returns a value for the pole mass). Calling the function with 4 arguments means that values are specified for the four input parameters CoreName, nfIn, scale, and method, while the variables muA and f are set to their default values.

The *minimal correction* method ("min") to obtain the asymptotic pole mass value and its ambiguity refers to the method suggested in Ref. [3] where the ambiguity is determined from the size of the minimal correction based on a quadratic function fitted to the smallest correction and the two neighboring corrections. However, in contrast to the procedure described in Ref. [3], REvolver accounts for the mass effects of lighter massive quarks by the exact expressions given in Ref. [2] instead of including them in an approximate way by flavor number scheme modifications of the strong coupling. Also, for coefficients of order higher than min(runMSR, runAlpha − 1) the asymptotic formula of Eq. (A.28) in Sec. A.5 is employed.

The *drange* ("discrete range", "drange") choice refers to the method suggested in Ref. [2], where the pole mass value and its ambiguity are computed from the range in orders around the minimal term where the corrections are smaller than f times the minimal correction. The method *range* ("range") refers to a continuous generalization which is analogous but provides smoother results. Here the order-dependent discrete-valued individual perturbative coefficients of the relation between the pole and running masses, as well as the related cumulant, are made continuous by a cubic interpolation. From these functions, the asymptotic pole mass value and the ambiguity are determined in analogy to the "drange" method. For all methods (including "range"), the returned order of the minimal correction term is an integer and refers to the original series without any interpolation.

C++ example

With the instructions

```
double ambiguity;
int nMin;
core1.masses().mPole(6, 10.0, 10.0, PoleMethod::Range, 1.25,
                     &ambiguity, &nMin);
```

first the variables nMin and ambiguity are initialized and pointers to them are passed in the call of the function Mass::mPole. The instruction returns the asymptotic pole mass value (double)173.107 for the heaviest of the 6 quarks of the Core named core1, obtained from the conversion formula for the running mass at the scale 10.0 GeV for 3 active flavors $[m_t^{\mathrm{MSR},(3)}(10,\mathrm{GeV})]$ using the *range* method. The values of the pole mass ambiguity (double)0.179811, and the order of the minimal correction term (int)4 are stored in the variables ambiguity and nMin, respectively.

Mathematica example

The Mathematica command

```
In[]:= MassPoleDetailed["core1", 6, 10.0, "min"]
Out[]= {173.09681693689498, 0.1307735468951421, 4}
```

corresponds to the previous commands given in C++, however, here the minimal correction method is used. muA is automatically set to default value which is 10.0 in this case. The output list entries correspond to the asymptotic pole mass value, the ambiguity and the order of the smallest correction term, respectively.

6.2.4. Norm of the pole mass renormalon ambiguity

The pole mass renormalon normalization constant can be accessed using the functions with the following prototypes

```
double Mass::N12(double lambda = 1.0) const;
double Mass::P12(double lambda = 1.0) const;

N12[CoreName_String, lambda_Real:1.0]
P12[CoreName_String, lambda_Real:1.0]
```

where the two functions correspond to the normalization conventions $P_{1/2}$ and $N_{1/2} = \Gamma(1+\hat{b}_1)\beta_0 P_{1/2}/(2\pi)$ as described in Ref. [1]. The routines employ the renormalon sum rule formula shown in Eq. (A.30) of App. A.6. The number of massless quarks for which the normalization is determined is tied to the `Core` used to extract the normalization. The optional input parameter `lambda` is a scaling parameter to estimate the uncertainty of the output (1.0 by default). The number of terms summed up in the sum rule formula is set by `runMSR` specified at `Core` construction. The QCD β-function coefficients entering the sum rule formula are used up to `runAlpha` loop order, all higher order coefficients are set to zero, so that $\hat{b}_1 = 0$ when `runAlpha` $= 1$.

6.2.5. Extracting $\Lambda_{\rm QCD}$

The functions corresponding to the prototypes

```
double Alpha::lambdaQCD(int nf) const;

LambdaQCD[CoreName_String, nf_Integer]
```

return from a given `Core` the QCD scale $\Lambda_{\rm QCD}^{(\texttt{nf})}$ in the $\overline{\rm MS}$ definition (see Ref. [23]) for the QCD coupling in the `nf` flavor scheme, utilizing the exponential formula given in Eq. (A.12) of App. A.2. The parameters `runAlpha` and `lambdaAlpha` specified at `Core` creation set the number of coefficients of the β-function used. The possible values for `nf` range from the number of massless quarks to the total number of quarks in the specified `Core`.

C++ example

The instruction

```
core1.alpha().lambdaQCD(3);
```

returns $\Lambda_{\rm QCD}^{(3)}$ in the $\overline{\rm MS}$ definition in GeV units from the scenario encoded in `core1`, corresponding to `(double)0.335547`

Optional parameters

The definition in which $\Lambda_{\rm QCD}$ is extracted can be chosen with an optional parameter. The full function prototypes are

```
double Alpha::lambdaQCD(
    int nf, LambdaConvention convention =
                LambdaConvention::MSbar) const;

LambdaQCD[CoreName_String, nf_Integer,
          convention_String:"MSbar"]
```

In addition to the conventional $\overline{\rm MS}$ definition according to the PDG 2020 [23], which is the default, the "t-scheme" is supported referring to the definition based on the t-variable notations of Ref. [1]. To choose the t-scheme the optional parameter `convention` has to be set to `LambdaConvention::tScheme` and `"tScheme"` in `C++` and `Mathematica` respectively. See App. A.2 for more details on the different conventions.

6.3. Adding masses to an existing `Core`

The following section presents routines to extend existing `Core` scenarios by adding one *heavier* massive quark. The mass value of the *additional* quark can be given as a running mass, in the pole mass scheme (order-dependent as well as asymptotic), or in any of the short-distance schemes described in Sec. 6.2.2, with the same obligatory and optional parameters. Unless the mass of the additional quark is already given in the running mass scheme, the quark mass value is first converted to the running mass (specified by the parameters). The value for the running mass is then added to the scenario. The optional parameter `fnQ` specifies the matching scale for the new threshold, analogous to the individual entries of `fMatch` at `Core` creation, see Sec. 6.1.2.

The routines employed for converting to the running mass are the *exact inverse* of those used for extracting mass values in the respective scheme. This is achieved by numerically inverting the respective relations with iterative algorithms.

The related function prototypes, including all relevant optional parameters are

```
void Core::addMsMass(int nf, double mass, double scale,
                     double fnQ = 1.0);
void Core::addPoleMass(double mPole, double scale,
                       double muA = kDefault,
                       PoleMethod method =
                         PoleMethod::Default,
                       double f = 1.25,
                       double fnQ = 1.0);
void Core::addPoleMassFO(double mPole, int nfConv,
                         double scale, double muA, int order,
                         double fnQ = 1.0);
void Core::addPSMass(double mPS, double muF,
```

```
                      int nfConv = kDefault,
                      double scale = kDefault,
                      double muA = kDefault,
                      double rIR = 1,
                      int order = kMaxOrderPs,
                      double fnQ = 1.0);
  void Core::add1SMass(double m1S,
                      int nfConv = kDefault,
                      double scale = kDefault,
                      Count1S counting = Count1S::Default,
                      double muA = kDefault,
                      int order = kMaxOrder1s,
                      double fnQ = 1.0);
  void Core::addRGIMass(double mRGI,
                       int order = kMaxRunMSbar,
                       double fnQ = 1.0);
  void Core::addRSMass(double mRS, double scaleRS,
                      int nfConv = kDefault,
                      double scale = kDefault,
                      double muA = kDefault,
                      int order = kMaxRunMSR,
                      int nRS = kMaxRunAlpha - 1,
                      double N12 = kDefault,
                      double fnQ = 1.0);
  void Core::addKinMass(double mKin, double scaleKin,
                       int nfConv = kDefault,
                       double scale = kDefault,
                       double muA = kDefault,
                       int order = kMaxOrderKinetic,
                       double fnQ = 1.0);
```

in C++ and

```
  AddMSMass[CoreName_String, NewCoreName_String, nf_Integer,
            mass_Real, scale_Real]
  AddPoleMass[CoreName_String, NewCoreName_String, mPole_Real,
              scale_Real,
              muA_Real:kDefault,
              method_String:"min",
              f_Real:1.25]
  AddPoleMassFO[CoreName_String, NewCoreName_String,
                mPole_Real, nfConv_Integer, scale_Real,
                muA_Real, order_Integer]
  AddPSMass[CoreName_String, NewCoreName_String, mPS_Real,
            muF_Real,
            nfConv_Integer:kDefault,
            scale_Real:kDefault,
            muA_Real:kDefault,
            rIR_Real:1,
            order_Integer:kMaxOrderPs]
  Add1SMass[CoreName_String, NewCoreName_String, m1S_Real,
            nfConv_Integer:kDefault,
            scale_Real:kDefault,
            counting_String:"default",
            muA_Real:kDefault,
            order_Integer:kMaxOrder1s]
  AddRGIMass[CoreName_String, NewCoreName_String, mRGI_Real,
             order_Integer:kMaxRunMSbar]
  AddRSMass[CoreName_String, NewCoreName_String, mRS_Real,
            scaleRS_Real,
            nfConv_Integer:kDefault,
            scale_Real:kDefault,
            muA_Real:kDefault,
            order_Integer:4,
            nRS_Integer:kMaxRunAlpha - 1,
            N12_Real:kDefault]
```

```
AddKinMass[CoreName_String, NewCoreName_String, mKin_Real,
           scaleKin_Real,
           nfConv_Integer:kDefault,
           scale_Real:kDefault,
           muA_Real:kDefault,
           order_Integer:kMaxOrderKinetic]
```

in Mathematica, where fnQ can be set by the option parameter syntax (fnQ -> <value>).

In Mathematica, adding a new heavier quark results in creating a new Core with a (not yet assigned) name specified in the obligatory input argument NewCoreName. This new Core is based on the Core with the name specified in CoreName containing only lighter massive quarks. The scenario parameters of the Core CoreName are passed on to the new Core named NewCoreName. If it turns out that the standard running mass associated to the mass to be added to a Core is not the heaviest one in the new configuration, an error is returned and the new Core is not created.

In C++ the new heavier quark is added directly to the Core from which the member function is called. This saves resources and copying the old Core can be easily done applying the assignment operator =, see the C++ example below.

C++ example

With the instructions

```
RunParV mPar4;
mPar4.push_back({4, 1.3, 1.3});
mPar4.push_back({5, 4.2, 4.2});
Core core4(5, alphaPar, mPar4);
Core core5 = core4;
core5.add1SMass(171.51726494075493);
```

in the first line, the std::vector<RunPar> mPar4 is declared, and subsequently filled in the next two lines according to Sec. 6.1.1 with information on two massive quarks. Together with alphaPar taken from the example in Sec. 6.1.1, it is the input for creating the Core named core4 in the third line, containing a total of 5 quark flavors. In the fifth line a copy of core4, named core5, is produced. In the last line a heavier quark with a mass value in the 1S scheme is added to core5 which contains a total number of 6 flavors. The input value for the 1S mass is taken from the C++ example of Sec. 6.2.2 where the 1S mass value was extracted from core1. Therefore core5 and core1 contain physically equivalent scenarios. core4 has not been modified by adding the additional heavier quark and consequently its scenario still contains 5 quark flavors.

Mathematica example

The command

```
In[]:= mPar4 = {{4, 1.3, 1.3}, {5, 4.2, 4.2})};
       CoreCreate["core4", 5, alphaPar, mPar4]
       Add1SMass["core4", "core5", 171.51726494075493]
```

has the same effect as the C++ example. First a list mPar4 is defined, containing the standard running masses of two quarks, which are used as an input for creating core4 with a total number of 5 flavors. In the next line the new Core named core5 is created, which is a copy of core4, to which a heavier quark is added with a mass value specified in the 1S scheme.

7. Applications and pedagogical examples

In this section we demonstrate some of the features provided by REvolver in a number of concrete examples as they may arise in practical applications. We give the examples in terms of Mathematica code since, due to its interactive nature, it is especially suitable for that purpose. We provide all examples given here as a Mathematica notebook, as Python code in form of a Jupyter Notebook as well as C++ code, together with the library. For sake of clarity, all digits of the Mathematica output are displayed.

7.1. Cores without massive quarks

7.1.1. Strong coupling evolution

Strong coupling from inclusive jet cross sections

In this first application we demonstrate one possible way to make use of the strong coupling evolution in REvolver by reproducing and analyzing some results of Ref. [24], where the CMS collaboration carried out a strong coupling measurement from inclusive jet cross sections in different p_T bins based on 8 TeV LHC data. In that publication, the evolution of the strong coupling from different values of Q (the average p_T in the bins) to m_Z was carried out with $n_f = 5$ active flavors and 2-loop accuracy. In the following, we focus on the result $\alpha_s^{(5)}(Q) = 0.0822^{+0.0034}_{-0.0031}$ for $Q = 1508.04$ GeV shown in Table 5 of that article.

In a first step the relevant values can be defined by

```
In[]:= {aQCentral, Q} = {0.0822, 1508.04};
       {aQMin, aQMax} = aQCentral + {-0.0031, 0.0034};
```

and the respective `Cores` for the central, upper and lower strong coupling values, setting the strong-coupling evolution to 2-loop order, can be created by

```
In[]:= CoreCreate["central2", {5, aQCentral, Q},
         runAlpha -> 2];
       CoreCreate["min2", {5, aQMin, Q}, runAlpha -> 2];
       CoreCreate["max2", {5, aQMax, Q}, runAlpha -> 2];
```

The central value of $\alpha_s^{(5)}(m_Z)$ can then be extracted by

```
In[]:= amZCentral2 = AlphaQCD["central2", mZdef]
Out[]= 0.11616452350227859
```

coinciding with $\alpha_s^{(5)}(m_Z) = 0.1162$, as given in Ref. [24]. Likewise the quoted uncertainties $^{+0.0070}_{-0.0062}$ are easily reproduced by executing

```
In[]:= (AlphaQCD[#, mZdef] & /@ {"max2","min2"}) - amZCentral2
Out[]= {0.007009865309335922, -0.006168760659529524}
```

Note that in the `Mathematica` interface the variable `mZdef` has the predefined value 91.187 GeV.

For comparison, we also employ 5-loop evolution for the strong coupling, resulting in equivalent numbers after rounding:

```
In[]:= CoreCreate["central5", {5, aQCentral, Q},
         runAlpha -> 5];
       CoreCreate["min5", {5, aQMin, Q}, runAlpha -> 5];
       CoreCreate["max5", {5, aQMax, Q}, runAlpha -> 5];

In[]:= amZCentral5 = AlphaQCD["central5", mZdef]
       AlphaQCD[#, mZdef] & /@ {"max5", "min5"} - amZCentral5
Out[]= 0.11624523920392597
Out[]= {0.007003095615252941, -0.006184136846029031}
```

Note that the specification of the running order `runAlpha -> 5` at `Core` creation is not mandatory since 5-loop running is the default. We show the specification to be explicit.

We now have a look at the perturbative uncertainty of these results. One approach to estimate the perturbative uncertainty of the given 2-loop result is to consider the difference of the values obtained by 2-loop and 1-loop evolution. This can be easily computed using `REvolver` by creating a new `Core` with specified 1-loop coupling evolution:

```
In[]:= CoreCreate["central1", {5, aQCentral, Q},
         runAlpha -> 1];
       amZCentral2 - AlphaQCD["central1", mZdef]
Out[]= 0.0017745561167654411
```

The obtained conservative perturbative error estimate is about 25% of the stated experimental error. For the highest available perturbative order for running, 5 loop, this proportion shrinks to 0.005%:

```
In[]:= CoreCreate["central4", {5, aQCentral, Q},
         runAlpha -> 4];
       amZCentral5 - AlphaQCD["central4", mZdef]
Out[]= 3.573226484421266*^-7
```

A different approach to estimate the perturbative error of $\alpha_s^{(5)}(m_Z)$ is to vary the β-function scaling parameter λ (controlled by the optional parameter `lambdaAlpha`) as described in Sec. 6.1.2. In Fig. 2 the value of $\alpha_s^{(5)}(m_Z)$ is shown, obtained by evolving the strong coupling down from $\alpha_s^{(5)}(1508.04\text{ GeV})$ with different loop orders in the evolution equation and with varying values of λ; the value of $\alpha_s^{(5)}(m_Z)$ obtained by including one more perturbative order in the evolution with $\lambda = 1$ (which corresponds to the standard form of the β-function) is subtracted. We observe that, to reproduce a value near to the one obtained with one more perturbative order included in the running, λ has to be varied by about 10% around 1, as already described in Sec. 6.1.2.

Assuming this to be also the appropriate range to estimate the perturbative uncertainty of the 5-loop result, the error can be estimated by scanning over λ values. Employing `REvolver` for this task, we first define a list of 20 logarithmically distributed values of λ in the appropriate range

```
In[]:= lamList = 1.1^Range[-1, 1, 2/19];
```

and create one `Core` for each value in λ. For convenience, the `Core` names are set to the associated λ values

```
In[]:= CoreCreate[ToString[#], {5, aQCentral, Q},
           lambdaAlpha -> #] & /@ lamList;
```

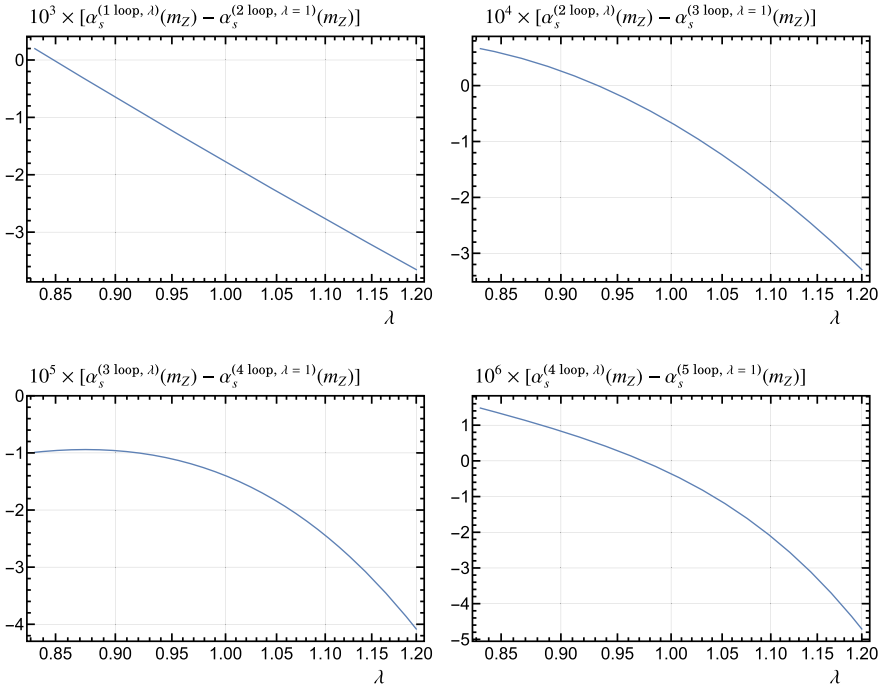

Fig. 2. Values of $\alpha_s^{(5)}(m_Z)$ over the β-function scaling parameter λ, obtained by evolving the strong coupling down from $\alpha_s^{(5)}(1508.04\text{ GeV})$ with different loop orders in the evolution equation. The value of $\alpha_s^{(5)}(m_Z)$ computed by including one more perturbative order in the evolution with $\lambda = 1$ is subtracted to highlight for which ranges of λ both results for $\alpha_s^{(5)}(m_Z)$ coincide or come close. The results indicate that a variation for λ of about 10% around 1 is a reasonable range to estimate the perturbative uncertainty.

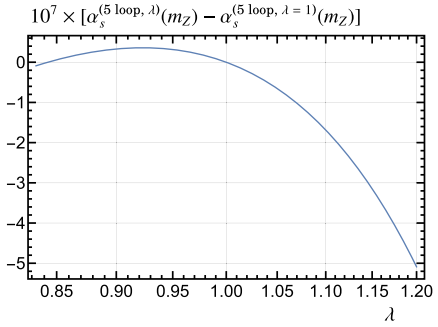

Fig. 3. Variation of $\alpha_s^{(5)}(m_Z)$ with λ, obtained by evolving the strong coupling down from $\alpha_s^{(5)}(1508.04\text{ GeV})$ with 5-loop accuracy. The value of $\alpha_s(m_Z)$ for $\lambda = 1$ is subtracted. Varying λ in a range of about 10% around 1 the value of $\alpha_s(m_Z)$ changes by 10^{-7}.

The span of values of $\alpha_s^{(5)}(m_Z)$ corresponding to the range in λ can then be obtained with

```
In[]:= aLamList = AlphaQCD[ToString[#], mZdef] & /@ lamList;
```

The central value of this range and the associated error are consequently given by

```
In[]:= (Max[aLamList] + {1, -1} * Min[aLamList])/2
Out[]= {0.11624517272452983, 1.0224197660724244*^-7}
```

giving the same order of magnitude as the conservative approach. The variation in λ of $\alpha_s^{(5)}(m_Z)$ when employing 5-loop running is also depicted in Fig. 3.

7.1.2. Complex renormalization scales

In this application we illustrate the `REvolver` functionality to determine the strong coupling $\alpha_s(\mu)$ at complex scales μ. To this end we consider the analyses in Refs. [25,26], where the perturbative QCD corrections $\delta^{(0)}$ to the inclusive τ hadronic width were considered in fixed-order perturbation theory (FOPT) as well as contour-improved perturbation theory (CIPT). In the second reference a scheme different

from the usual $\overline{\rm MS}$ definition is used for α_s. We exploit this fact to demonstrate the ability of `REvolver` to deal with user-defined β-function coefficients.

Hadronic τ decay

In CIPT, determining $\delta^{(0)}$ involves integrating over powers of the strong coupling $\alpha_s^{(3)}(\mu)$ multiplied with a kinematic weight function in the complex μ^2 plane along a circle with radius m_τ^2

$$\delta^{(0)}_{\rm CI} = \sum_{n=1}^{\infty} c_{n,1}\, J_n^a(m_\tau^2)\,,$$
$$J_n^a(m_\tau^2) = \frac{1}{2\pi i}\oint\limits_{|x|=1} \frac{{\rm d}x}{x}(1-x)^3(1+x)\left[\frac{\alpha_s^{(3)}(\sqrt{-m_\tau\, x})}{\pi}\right]^n, \tag{7}$$

where the coefficients $c_{n,1}$ are given in Eqs. (2.13), (2.15) and (3.10) of Ref. [25]. In that article, 4-loop running for the strong coupling was used, as well as the input value $\alpha_s^{(3)}(m_\tau) = 0.34$. To reproduce the numbers for $\delta^{(0)}_{\rm CI}$ given in Eq. (3.9) of Ref. [25] we first define variables accounting for the employed input values

```
In[]:= {nfa, aTau, mTau} = {3, 0.34, 1.77686};
       {c11, c21, c31, c41, c51} =
         {1, 1.640, 6.371, 49.076, 283};
```

and a function to compute $J_n^a(m_\tau^2)$

```
In[]:= Ja[n_, core_] := 1/(2 Pi)
          NIntegrate[(1 - E^(I phi))^3 (1 + E^(I phi))
            (AlphaQCD[core, Sqrt[-mTau^2 E^(I phi)]]/Pi)^n,
           {phi, 0, 2 Pi}];
```

where we change variables via $x = \exp(i\phi)$. Furthermore, we define a `Core` with 4-loop running for the coupling

```
In[]:= CoreCreate["CI4", {nfa, aTau, mTau}, runAlpha -> 4]
```

All requirements are now set to reproduce the numbers given in Eq. (3.9) of Ref. [25]

```
In[]:= Ja[1, "CI4"]*c11
       Ja[2, "CI4"]*c21
       Ja[3, "CI4"]*c31
       Ja[4, "CI4"]*c41
       Ja[5, "CI4"]*c51
Out[]= 0.14789839179248082 + 0. I
Out[]= 0.02968556861749222 - 1.3583618952083769*^-18 I
Out[]= 0.0121854520515486 + 4.947098114161149*^-18 I
Out[]= 0.008592183988059407 - 8.468364884304664*^-19 I
Out[]= 0.0037863076541974016` - 9.919281576456942*^-19 I
```

with full agreement.

We can now easily inspect the corrections induced by the 5-loop running of the strong coupling by creating an appropriate `Core`

```
In[]:= CoreCreate["CI5", {nfa, aTau, mTau}, runAlpha -> 5];
```

and evaluating

```
In[]:= Ja[1, "CI5"]*c11
       Ja[2, "CI5"]*c21
       Ja[3, "CI5"]*c31
       Ja[4, "CI5"]*c41
       Ja[5, "CI5"]*c51
Out[]= 0.14775354880331787 - 8.834874115176436*^-18 I
Out[]= 0.02960219692750483 - 1.811149193611169*^-18 I
Out[]= 0.012122455789576415 + 3.4080009230887917*^-18 I
Out[]= 0.008521503950040327 - 1.6936729768609328*^-18 I
Out[]= 0.0037376807938461127 - 1.5260433194549141*^-18 I
```

We observe a small negative $\mathcal{O}(1\%)$ shift in the individual coefficients. Note that the explicit specification of the running order `runAlpha -> 5` at `Core` creation is not mandatory since 5-loop running is the default. We included it to be explicit.

Hadronic τ decay with C-scheme strong coupling

We now turn to Ref. [26] for which we reproduce the value quoted for $\delta^{(0)}_{\rm CI}$ in Eq. (22). To obtain this number the 3-flavor strong coupling, the related β-function coefficients and the coefficients $c_{n,1}$ were converted to a class of schemes for the strong coupling where the β-function adopts the following exact all order form

$$\hat\beta(\hat\alpha_s) = -2\hat\alpha_s \frac{\frac{\hat\alpha_s}{4\pi}\beta_0}{1-\frac{\hat\alpha_s}{4\pi}\frac{\beta_1}{\beta_0}} = -2\hat\alpha_s \sum_{i=0} \hat\beta_i \left(\frac{\hat\alpha_s}{4\pi}\right)^{i+1}, \tag{8}$$

where $\hat\beta_i = \beta_0(\beta_1/\beta_0)^i$. Within that class of schemes one needs to fix a parameter C to uniquely specify the strong coupling. This parameter was set to $C = -1.246$ in Eq. (22) of Ref. [26] with the argument that the unknown 5-loop coefficient can then be neglected resulting in the value $\delta^{(0)}_{\rm CI}(\hat\alpha(m_\tau), C = -1.246) = 0.1840 \pm 0.0062$. The quoted uncertainty refers to the size of the 4-loop correction term. Solving Eq. (6) of the reference paper to convert the quoted value of the $\overline{\rm MS}$ strong coupling $\alpha_s^{(3)}(m_\tau) = 0.316$ to the scheme described above leads to $\hat\alpha_s(m_\tau, C = -1.246) = 0.477$. The transformed coefficients $c_{n,1}$ can be extracted from Eq. (12) therein. `REvolver` allows the order-by-order specification of user-defined β-functions, so we expand $\hat\beta(\hat\alpha_s)$ up to $\mathcal{O}(\hat\alpha_s^{11})$.

We define the relevant input values related to $\hat\alpha_s$, the coefficients $c_{n,1}$ and $\hat\beta_i$ for $n_f = 3$ with

```
In[]:= {nfa, aTau, mTau} = {3, 0.477, 1.77686};
       {c11, c21, c31, c41} =
         {1, 1.640 + 2.25 c, 7.682 + 11.38 c + 5.063 c^2,
           61.06 + 72.08 c + 47.4 c^2 + 11.39 c^3} /.
          c -> -1.246;
       betaHat = 9. * (64/9)^Range[0, 9];
```

and the related `Core`

```
In[]:= CoreCreate["Hat", {nfa, aTau, mTau}, betaHat]
```

Reusing the function `Ja[n_, core_]` as defined in the previous example we obtain

```
In[]:= Ja[1, "Hat"]*c11 + Ja[2, "Hat"]*c21 +
        Ja[3, "Hat"]*c31 + Ja[4, "Hat"]*c41
Out[]= 0.18403340012158337 - 1.0177988675705949*^-17 I
```

for $\delta^{(0)}_{\rm CI}(\hat\alpha(m_\tau), C = -1.246)$ and

```
In[]:= Ja[4, "Hat"]*c41
Out[]= 0.006222359703784199 - 2.951274747776552*^-19 I
```

for the last correction term. Both the central value and the size of the last correction term are in perfect agreement with Ref. [26].

Cauchy integral theorem for the strong coupling

It is worth mentioning that Cauchy's integral formula can be utilized to check the numerical quality of the coupling evolution routine implemented in `REvolver`. For example, valuating $\alpha_s^{(3)}(2\text{ GeV})$ directly as well as by employing Cauchy's integral formula with a radius of 1 GeV gives equivalent results up to machine precision

```
In[]:= mu0 = 2;
       aDirect = AlphaQCD["CI5", mu0]
       aResidue =
        1/(2 Pi) NIntegrate[AlphaQCD["CI5", mu0 + E^(I phi)],
          {phi, 0, 2 Pi}, PrecisionGoal -> 10]
       aResidue - aDirect
Out[]= 0.3169005366613899
Out[]= 0.31690053666139 + 1.1043592643970545*^-17 I
Out[]= 1.1102230246251565*^-16 + 1.1043592643970545*^-17 I
```

For all practical purposes the solution for the strong coupling evolution provided by `REvolver` based on a given QCD β-function can be considered as exact.

7.2. `Core`s with one massive quark

In the previous sample applications the impact of flavor thresholds was not considered. In the following we discuss examples where threshold effects associated to one massive quark are accounted for.

7.2.1. Strong coupling with a flavor threshold

Strong coupling from multijet events

We consider Ref. [27], where the strong coupling value was determined by the ATLAS collaboration from transverse energy-energy correlations in multijet events based on 8 TeV LHC data. The measurements were made for different values of the transverse momentum sum H_{T2} of the two leading jets. All values of H_{T2} considered in that analysis were much larger than the top quark mass, consequently the associated respective strong coupling values $\alpha_s^{(6)}(Q)$ are defined in the 6-flavor scheme. In Tabs. 2 and 3 of Ref. [27] values for $\alpha_s^{(6)}(Q)$ and the associated results for $\alpha_s^{(5)}(m_Z)$ are quoted. For the strong coupling running an approximate analytic 2-loop solution of the evolution equation was used accounting for continuous matching at the top quark mass (which is correct for 1-loop matching when the matching scale is at the top quark mass). In the following, we focus on the associated results $\alpha_s^{(5)}(m_Z) = 0.1186^{+0.0090}_{-0.0047}$ and $\alpha_s^{(6)}(810\text{ GeV}) = 0.0907^{+0.0052}_{-0.0026}$, where for simplicity, we added the respective upper and lower uncertainties in quadrature. We reproduce the asymmetric uncertainties for $\alpha_s^{(6)}(810\text{ GeV})$ for the given $\alpha_s^{(5)}(m_Z)$ range and start by defining the relevant parameters for the 5-flavor coupling $\alpha_s^{(5)}(m_Z)$, where we set the top quark standard running mass to $\overline{m}_t = 163$ GeV

```
In[]:= {amZCentral, Q, mtmt} = {0.1186, 810, 163};
       {amZMax, amZMin} = amZCentral + {0.0090, -0.0047};
```

Next we create the `Cores` for our evaluation (including a `CoreDeleteAll[]` to remove older cores)

```
In[]:= CoreDeleteAll[]
       CoreCreate["central2", 6, {5, amZCentral, mZdef},
        {{6, mtmt, mtmt}}, runAlpha -> 2]
       CoreCreate["max2", 6, {5, amZMax, mZdef},
        {{6, mtmt, mtmt}}, runAlpha -> 2]
       CoreCreate["min2", 6, {5, amZMin, mZdef},
        {{6, mtmt, mtmt}}, runAlpha -> 2]
```

To obtain the 6-flavor strong coupling values at $Q = 810$ GeV including the error range we simply evaluate

```
In[]:= aQCentral2 = AlphaQCD["central2", Q, 6]
       AlphaQCD[#, Q, 6] & /@ {"min2", "max2"} - aQCentral2
Out[]= 0.09079931707610696
Out[]= {-0.002757013433150532, 0.005129916277931454}
```

agreeing very well with the result given in Ref. [27].

We investigate this setup with two-loop evolution further by determining the uncertainty related to varying the matching scale accounting for the top threshold corrections at one loop. This is easily done using `REvolver` by creating a set of `Cores` with a range of `f`-parameters. To this end we first define a table containing 20 logarithmically scaled `f`-parameters in the range $[1/2, 2]$, which corresponds to matching scales between one half and twice the standard running top mass. Subsequently the table is used to create the corresponding set of `Cores`

```
In[]:= list2 = 2^Range[-1, 1, 2/19];
In[]:= CoreCreate[ToString[#] <> "run2", 6,
           {5, amZCentral, mZdef}, {{6, mtmt, mtmt}},
           runAlpha -> 2, orderAlpha -> 1,
           fMatch -> {#}] & /@ list2;
```

Finally, we can determine a list of the corresponding strong coupling values $\alpha_s^{(6)}(810\text{ GeV})$ and compute the central value as well as the error range

```
In[]:= aQList2 = AlphaQCD[ToString[#] <> "run2", Q, 6] & /@
          list2;
       (Max[aQList2] + {1, -1} * Min[aQList2])/2
Out[]= {0.09081555469961156, 0.00009936201139525841}
```

The perturbative uncertainties associated to the threshold corrections are about 3% of the quoted experimental error.

Employing 5-loop instead of 2-loop running for the strong coupling and 4-loop matching corrections we obtain

```
In[]:= CoreCreate["central5", 6, {5, amZCentral, mZdef},
        {{6, mtmt, mtmt}}, runAlpha -> 5]
       CoreCreate["max5", 6, {5, amZMax, mZdef},
        {{6, mtmt, mtmt}}, runAlpha -> 5]
       CoreCreate["min5", 6, {5, amZMin, mZdef},
        {{6, mtmt, mtmt}}, runAlpha -> 5]
In[]:= aQCentral5 = AlphaQCD["central5", Q, 6]
       AlphaQCD[#, Q, 6] & /@ {"min5", "max5"} - aQCentral5
Out[]= 0.09078701609518454
Out[]= {-0.002755235739243 55, 0.005125931453417 2346}
```

for $\alpha_s^{(6)}(810\text{ GeV})$ and its upper and lower uncertainty and

```
In[]:= CoreCreate[ToString[#] <> "run5", 6,
           {5, amZCentral, mZdef}, {{6, mtmt, mtmt}},
           runAlpha -> 5, fMatch -> {#}] & /@ list2;
In[]:= aQList5 = AlphaQCD[ToString[#] <> "run5", Q, 6] & /@
          list2;
       (Max[aQList5] + {1, -1} * Min[aQList5])/2
Out[]= {0.09078682756270738, 1.9445996186917558*^-7}
```

for the central value and error estimate derived from varying the matching scale. Within the experimental uncertainties as quoted in Ref. [27] using 2-loop evolution and continuous matching is perfectly adequate.

Strong coupling from inclusive jet cross sections

We return to the analysis of Ref. [24] and investigate the impact of a top quark threshold on the values given there, staying with 2-loop running as employed in that reference. In the following we create `Core`s with the given range of values of $\alpha_s^{(5)}(m_Z) = 0.1162^{+0.0070}_{-0.0062}$ and determine the strong coupling $\alpha_s^{(6)}(1508.04\text{ GeV})$ in the 6-flavor scheme instead of the 5-flavor coupling $\alpha_s^{(5)}(1508.04\text{ GeV})$ determined in Ref. [24]. After defining the parameters

```
In[]:= {amZCentral, Q, mtmt} = {0.1162, 1508.04, 163};
       {amZMax, amZMin} = amZCentral + {0.007, -0.0062};
```

and creating the respective `Core`s, accounting for the standard running top quark mass $\overline{m}_t = 163$ GeV and default 4-loop matching

```
In[]:= CoreCreate["central2", 6, {5, amZCentral, mZdef},
         {{6, mtmt, mtmt}}, runAlpha -> 2];
       CoreCreate["min2", 6, {5, amZMin, mZdef},
         {{6, mtmt, mtmt}}, runAlpha -> 2];
       CoreCreate["max2", 6, {5, amZMax, mZdef},
         {{6, mtmt, mtmt}}, runAlpha -> 2];
```

we obtain

```
In[]:= aQCentral2 = AlphaQCD["central2", Q, 6]
       (AlphaQCD[#, Q, 6] & /@ {"min2","max2"}) - aQCentral2
Out[]= 0.08406136347372324
Out[]= {-0.003262229612787812, 0.0035626775539831235}
```

for the central value and the upper and lower uncertainties, respectively. Comparing these values to $\alpha_s^{(5)}(1508.04\text{ GeV}) = 0.0822^{+0.0034}_{-0.0031}$, quoted in Ref. [24], we observe a positive shift of about 0.002 in the central value. This already amounts to about 60% of the given experimental error, illustrating that flavor-thresholds effects can lead to significant changes.

7.2.2. Asymptotic pole and low-scale MSR mass

To demonstrate the `REvolver` functionalities related to mass conversions accounting for flavor threshold effects, we investigate how much the asymptotic top quark pole mass m_t^{pole} as well as the top MSR mass at 2 GeV $m_t^{\text{MSR}}(2\,\text{GeV})$ would change if the strong coupling value quoted in Ref. [24] $\alpha_s(1508.04\,\text{GeV}) = 0.0822^{+0.0034}_{-0.0031}$ would be interpreted as a 6-flavor compared to a 5-flavor result. After defining the relevant constants and `Core`s (we keep using the values of `Q` and `mtmt` already defined in the previous section)

```
In[]:= aQ = 0.0822;
       CoreCreate["5", 6, {5, aQ, Q}, {{6, mtmt, mtmt}}];
       CoreCreate["6", 6, {6, aQ, Q}, {{6, mtmt, mtmt}}];
```

where we have employed default highest-order precision for coupling and mass evolution and flavor threshold matching, we first extract $m_t^{\text{MSR}}(2\text{ GeV})$ from both `Core`s and then determine their difference:

```
In[]:= mMSR25 = MassMS["5", 6, 2]
       mMSR26 = MassMS["6", 6, 2]
       mMSR25 - mMSR26
Out[]= 172.45858180514585
Out[]= 172.10074770514723
Out[]= 0.3578340999986267
```

For the asymptotic pole masses we obtain

```
In[]:= mPole5 = MassPole["5", 6, mtmt]
       mPole6 = MassPole["6", 6, mtmt]
```

```
        mPole5 - mPole6
Out[]= 172.8732843267365
Out[]= 172.4868549739421
Out[]= 0.3864293527944085
```

where we adopted $\overline{m}_t = 163$ GeV as the conversion scale for the asymptotic pole mass determination. The differences we obtain amount to 358 MeV and 386 MeV, both of which exceed the uncertainty of the current world average for direct top mass measurements [23].

7.2.3. Bottom and charm quark short-distance masses

Bottom $\overline{\rm MS}$ mass at high scales

In Ref. [28] the partonic cross section for Higgs production via bottom quark fusion was presented. This involves the bottom running mass at the Higgs scale $m_H = 125.09$ GeV, quoted to be $m_b^{(5)}(m_H) \equiv \overline{m}_b^{(5)}(m_H) = 2.79$ GeV using 4-loop $\overline{\rm MS}$-mass running, $\alpha_s^{(5)}(m_Z) = 0.118$ and the bottom quark standard running mass $\overline{m}_b = 4.18$ GeV, see Table 2 therein. We can reproduce this relation in `REvolver` by defining the relevant parameters

```
In[]:= {mH, amZ, mbmb} = {125.09, 0.118, 4.18};
```

and creating a corresponding `Core`

```
In[]:= CoreDeleteAll[]
       CoreCreate["b", 5, {5, amZ, mZdef}, {5, mbmb, mbmb},
          runMSbar -> 4]
```

The value of $m_b^{(5)}(m_H)$ can now be extracted with

```
In[]:= MassMS["b", 5, mH]
Out[]= 2.78854676339097
```

showing perfect agreement with Ref. [28].

Bottom quark PS and 1S masses

In Ref. [29] the conversion between the $\overline{\rm MS}$ and various low-scale short-distance masses was carried out with 4-loop fixed-order formulae. To illustrate the functionalities of `REvolver` for mass conversions we now consider the values of the PS and 1S bottom quark masses given in Table II of that article. We start defining the input parameters $\alpha_s^{(5)}(m_Z) = 0.1185$, $\overline{m}_b = 4.163$ GeV and $\mu_f = 2.0$ GeV for the strong coupling, the standard running bottom mass and the bottom PS mass renormalization scale, respectively, as specified in Ref. [29],

```
In[]:= {amZ, mbmb, mufB} = {0.1185, 4.163, 2.0};
```

and the related `Core`

```
In[]:= CoreCreate["b", 5, {5, amZ, mZdef},
         {{5, mbmb, mbmb}}, fMatch -> {2.0}]
```

Following Ref. [29] we set the bottom quark matching scale to twice the standard running bottom mass. Comparing the 4-loop value for the bottom PS mass $m_b^{\rm PS}(2\,{\rm GeV}) = 4.483$ GeV quoted in Ref. [29] and obtained by `REvolver` we obtain

```
In[]:= mbPSRef = 4.483;
       mbPSREvo = MassPS["b", 5, mufB, 5, mbmb, mbmb]
       mbPSREvo - mbPSRef
Out[]= 4.484037803646092
Out[]= 0.0010378036460920725
```

where, following Ref. [29], the conversion is carried out using the fixed-order relation between the standard running and PS masses using the standard running mass $\overline{m}_b$ as the renormalization scale for the strong coupling.

The small difference of about 1 MeV results from the fact that in `REvolver` *all conversions* between mass schemes are based on formulae starting from the value of the running mass, while in Ref. [29] the conversion was obtained the other way around, i.e. the running mass was computed starting from a value in the PS scheme. The difference is naturally covered by the perturbative uncertainty and not relevant for practical purposes.

In the previous example we have used `REvolver` to determine the PS from the standard running mass $\overline{m}_b$. The conversion in the opposite direction can be achieved using the `REvolver` functionality to add a heavier mass to an existing `Core`, see Sec. 6.3. To determine the standard running mass we first create a `Core` containing 4 massless flavors

```
In[]:= anf4mu3 = AlphaQCD["b", 3.0, 4];
       CoreCreate["O4", {4, anf4mu3, 3.0}]
```

which requires the 4-flavor strong coupling $\alpha_s^{(4)}(3\,\text{GeV})$ as an input, which here we obtain from the previously created `Core` named `b`.

We now create a new `Core` with name `b2` by adding the bottom PS mass $m_b^{\rm PS}(2\,\text{GeV}) = 4.483$ GeV to the `Core` named `O4`, reusing the parameters `mbPSRef` and `mufB` defined in the previous example as well as the matching scale factor 2.0, specified by the option parameter `fnQ`

```
In[]:= AddPSMass["O4", "b2", mbPSRef, mufB, 5, 4.2,
         4.2, fnQ -> 2.0]
```

Internally, first the 5-flavor running mass is determined and subsequently used to create the 5-flavor `Core` named `b2`. To match precisely the conversion method used in Ref. [29] we set the running mass scale and the renormalization scale of the strong coupling for that conversion to 4.2 GeV here.

Reading out the resulting bottom quark standard running mass results in

```
In[]:= MassMS["b2", 5]
Out[]= 4.1621220500397325
```

with the expected 1 MeV difference to the value $\overline{m}_b = 4.163$ GeV quoted in the reference paper. This difference arises here again because the numerical conversion formulae employed in `REvolver` are exactly invertible, i.e. they produce the same numerical mass differences regardless in which way the conversion is carried out.

Note that the default `REvolver` routines convert from the MSR mass to a low-scale short-distance mass at the *intrinsic scale* of the low-scale short-distance mass (see Sec. 6.2.2) to resum potentially large logarithms involving the ratio of the quark mass and the renormalization scale. In the example above, we have, however, explicitly set the input parameter `nfConv` of the function `MassPS` to 5 to enforce conversion at the scale of the $\overline{\rm MS}$ mass (which is the approach used in Ref. [29] and which does not resum these logarithms). The result including log-resummation via R-evolution differs by around 15 MeV and can be extracted by using the corresponding `REvolver` commands with default parameter settings. For example, converting from the standard running mass to the PS mass we obtain

```
In[]:= MassPS["b", 5, mufB]
Out[]= 4.468247788253957
```

where `nfConv` is automatically set to 4 and R as well as the renormalization scale of the strong coupling are set to `mufB`.

The corresponding (log-resummed) conversion from the PS mass to the standard running mass is achieved by adding to the `Core` named `O4` the bottom quark PS mass $m_b^{\rm PS}(2\,\text{GeV}) = 4.483$ GeV, specifying log resummation via R-evolution. The associated new `Core` named `b3` is created by

```
In[]:= AddPSMass["O4", "b3", mbPSRef, mufB, fnQ -> 2.0]
```

resulting in a bottom quark standard running mass of

```
In[]:= MassMS["b3", 5]
Out[]= 4.176206116625182
```

At this point it should be mentioned that for bottom quarks large scale hierarchies cannot arise, such that the log-resummed conversion is not superior and the difference between the fixed-order and the log-resummed conversions may be better considered as a scheme variation. To illustrate this we show, order by order, the bottom quark PS mass computed in the fixed-order expansion as well as by utilizing R-evolution:

```
In[]:= MassPS["b", 5, mufB, 5, mbmb, mbmb, 1.0, #] & /@
         {1, 2, 3, 4}
       MassPS["b", 5, mufB, 4, mufB, mufB, 1.0, #] & /@
         {1, 2, 3, 4}
Out[]= {4.371486051575019, 4.452182487749768,
        4.484416838176134, 4.484037803646092}
Out[]= {4.456398324160689, 4.487678320598545,
        4.494296775616467, 4.468247788253957}
```

Next, we consider the 1S scheme. Comparing the 1S bottom quark mass $m_b^{\rm 1S} = 4.670$ GeV quoted Ref. [29] and obtained in `REvolver` using the relativistic counting and conversion at the high scale $\overline{m}_b$ (which again agrees with the approach used in Ref. [29] and does not account for the resummation of logarithms involving the bottom mass and inverse Bohr radius) we obtain

```
In[]:= mb1SRef = 4.670;
       mb1SRevo = Mass1S["b", 5, 5, mbmb, "relativistic"]
       mb1SRevo - mb1SRef
Out[]= 4.671281708897272
Out[]= 0.0012817088972720825
```

Again, the 1 MeV discrepancy emerges from the perturbative difference between converting from or to the standard running mass. For comparison, we also present the corresponding 1S mass value accounting for log-resummation via R-evolution. This can be achieved

by calling the routine `Mass1S` without any optional parameters. This implies that the default setting is used, namely that the 1S mass is converted from the MSR mass at the inverse Bohr radius $M_{q,B}$ (the intrinsic scale of the 1S mass, see Sec. 6.2.2) and that non-relativistic counting is applied. The bottom 1S mass is, however, sensitive to the ultra-soft scale $M_{q,B}^2/m_b$, related to logarithms of the strong coupling. This entails that for the conversion from the MSR mass (at the inverse Bohr radius) a scale larger than $M_{q,B}$ may be adopted as the renormalization scale for the strong coupling to avoid perturbative instabilities.[6] Adopting $2M_{q,B}$ for the renormalization scale of the strong coupling, the 1S mass accounting for log-resummation is obtained by

```
In[]:= MbB = MBohr["b", 5]
       Mass1S["b", 5, 4, MbB, "nonrelativistic", 2*MbB]
Out[]= 1.8792648142678285
Out[]= 4.6676688462595175
```

The result differs by 4 MeV to the one using fixed-order conversion. As for the bottom PS mass, there is no conceptual improvement using log-resummation. This can again be seen from comparing the 1S mass values at lower orders. Order by order, the values of the bottom quark 1S mass, derived in fixed-order and with R-evolution, respectively, are given by

```
In[]:= Mass1S["b", 5, 5, mbmb, "relativistic", mbmb, #] & /@
        {1, 2, 3, 4}
       Mass1S["b", 5, 4, MbB, "nonrelativistic", 2*MbB,
        #] & /@ {1, 2, 3, 4}
Out[]= {4.516545706062886, 4.64055194539697,
        4.680062686477036, 4.671281708897272}
Out[]= {4.609340303152403, 4.666301702298438,
        4.6809114692112495, 4.6676688462595175}
```

Of course one can also convert from the 1S scheme to the standard running mass using the routine `Add1SMass`, shortly demonstrated in the following.

Reusing the `Core` named `O4`, which contains 4 massless quarks, we create a new `Core` with name `b4` by adding the bottom 1S mass using fixed-order conversion

```
In[]:= Add1SMass["O4", "b4", mb1SRef, 5, mbmb,
        "relativistic", mbmb, fnQ -> 2.0]
```

which results in the following bottom quark standard running mass:

```
In[]:= MassMS["b4", 5]
Out[]= 4.161807379452769
```

again with the expected 1 MeV difference to the value $\overline{m}_b = 4.163$ GeV quoted in Ref. [29], related to invertible numerical conversion algorithm employed in `REvolver`. The analogous procedure for converting the 1S mass to the standard running mass using R-evolution can be performed by executing

```
In[]:= Add1SMass["O4", "b5", mb1SRef, 4, MbB,
        "nonrelativistic", 2*MbB, fnQ -> 2.0]
In[]:= MassMS["b5", 5]
Out[]= 4.165169213761735
```

Charm and bottom quark RS masses

In Ref. [30] the charm quark RS mass $m_c^{\rm RS}(\nu_f) = 1.202$ GeV at the scale $\nu_f = 1$ GeV was extracted from charmonium bound states masses, given in Eq. (2.15) of that paper. The RS mass was converted to the standard running charm mass $\overline{m}_c = 1.217$ GeV with 4-loop fixed-order formulae for $\alpha_s^{(5)}(m_Z) = 0.1184$ and using $\mu_c = 1.27$ GeV as the charm threshold matching scale. The renormalization scale of the strong coupling was set to $\nu_c = 1.5$ GeV and the pole mass renormalon normalization constant for $n_f = 3$ active flavors was quoted to be $N_m = 0.5626$. This relation can be easily reproduced with `REvolver`. First, we set the relevant variables

```
In[]:= {amZ, Nm} = {0.1184, 0.5626};
       {mcmc, mcmcMatch, nufc, nuc} =
        {1.217, 1.27, 1.0, 1.5};
       {mbmb, mbmbMatch} = {4.185, 4.2};
```

and create the respective `Core`

```
In[]:= CoreDeleteAll[]
       CoreCreate["cb", 5, {5, amZ, mZdef},
        {{4, mcmc, mcmc}, {5, mbmb, mbmb}},
        fMatch -> {mcmcMatch/mcmc, mbmbMatch/mbmb}]
```

[6] This issue does not arise for the top quark due to is large mass value.

We include the standard running bottom mass $\overline{m}_b = 4.185$ GeV with the corresponding threshold matching scale $\mu_b = 4.2$ GeV to enable automatic matching of the strong coupling constant which is given at $\mu = m_Z$. The charm quark RS mass computed by `REvolver` and the difference to the value quoted in the reference paper are given by

```
In[]:= mcRSRef = 1.202;
       mcRSREvo = MassRS["cb", 4, nufc, 4, mcmc, nuc,
         4, 4, Nm]
       mcRSRef - mcRSREvo
Out[]= 1.201144351209422
Out[]= 0.0008556487905779786
```

showing agreement at the sub-MeV level.

In Ref. [30] also the bottom quark RS mass value $m_b^{\rm RS}(\nu_f) = 4.379$ GeV at the scale $\nu_f = 2$ GeV was extracted from bottomonium meson masses [see Eq. (2.3) of that paper] and subsequently converted to the standard running bottom mass $\overline{m}_b = 4.379$ GeV with 4-loop fixed-order formulae using $\mu_b = 4.2$ GeV as the bottom threshold matching scale and $\nu_b = 2.5$ GeV as the renormalization scale of the strong coupling. The charm mass corrections in the perturbative relation between the RS and the $\overline{\rm MS}$ mass have been implemented in an effective way by evaluating the conversion series that relates the $\overline{\rm MS}$ and the RS masses for the bottom quark and n_ℓ massless quarks for $n_\ell = 3$ dynamical flavors, but using the 3-flavor strong coupling $\alpha_s^{(3)}$ computed with the charm mass threshold properly accounted for. This treats the charm quark as a decoupled flavor. The `REvolver` RS mass routines do not directly provide this functionality, but in the following we show how this evaluation can still be carried out in `REvolver`. We first set the necessary parameters not yet defined before

```
In[]:= {nufb, nub} = {2.0, 2.5};
```

and compute the 3-flavor strong coupling $\alpha_s^{(3)}(\mu_c)$ at the charm matching scale $\mu_c = 1.27$ GeV, taking into account the bottom as well as charm quark thresholds in the usual way

```
In[]:= as3 = AlphaQCD["cb", mcmcMatch, 3];
```

Next, we define a `Core` with decoupled charm quarks by using the precomputed $n_f = 3$ strong coupling and specifying a total number of 4 flavors, including 3 massless flavors and the massive bottom quark as the 4-th flavor

```
In[]:= CoreCreate["b", 4, {3, as3, mcmcMatch},
         {4, mbmb, mbmb}, fMatch -> {mbmbMatch/mbmb}]
```

Setting all previously defined scales we get

```
In[]:= mbRSRef = 4.379;
       mbRSREvo = MassRS["b", 4, nufb, 4, mbmb, nub,
         4, 4, Nm]
       mbRSREvo - mbRSRef
Out[]= 4.379013026999629
Out[]= 0.00001302699962923981
```

for the bottom quark mass in the RS scheme with a negligible difference to the value quoted in the reference article.

We can also convert from the bottom RS to the standard running mass using the `REvolver` routine `AddRSMass`. To do that, we first create a `Core` containing the 3 massless non-decoupled flavors with

```
In[]:= CoreCreate["O3", {3, as3, mcmcMatch}]
```

and subsequently create a new `Core` with name `b2` by adding the bottom RS mass to the `Core` with name `O3` setting the various input parameters in analogy to the example above, i.e. using fixed-order conversion

```
In[]:= AddRSMass["O3", "b2", mbRSRef, nufb, 4, 4.2, nub, 4,
         4, Nm]
```

Internally, first the 5-flavor running mass is determined and subsequently used to create the `Core` named `b2`. We set the running mass scale for that conversion to 4.2 GeV.

Extracting the bottom quark standard running mass from the newly created `Core` results in

```
In[]:= MassMS["b2", 4]
Out[]= 4.184987620121892
```

Bottom quark kinetic masses

In Ref. [21] the 3-loop corrections to the perturbative relation between the pole and kinetic quark mass schemes have been determined for the case of one massive quark and n_ℓ massless quarks. Here we show how to employ `REvolver` to reproduce the values for the

bottom quark kinetic mass $m_b^{\rm kin}(\mu)$ at the scale $\mu = 1$ GeV given in Eq. (8) of that paper, obtained by converting from the standard running mass $\overline{m}_b = 4.163$ GeV.

The conversion from $\overline{m}_b$ to the bottom kinetic mass was considered using the perturbative series computed with the massive bottom quark and n_ℓ massless quarks for $n_\ell = 4$ (i.e. with the charm quark treated as massless) with the result $m_b^{\rm kin}(\mu) = 4.523$ GeV, as well as for $n_\ell = 3$ (i.e. with the charm quark treated as decoupled) with the result $m_b^{\rm kin}(\mu) = 4.521$ GeV. The first case can be reproduced in a straightforward way with `REvolver` as it corresponds to a realistic physical scenario.

First we define the relevant parameters

```
In[]:= {mbmb, amZ, muCutb} = {4.163, 0.1179, 1.0};
```

and create a `Core` in which the charm quark is treated as massless

```
In[]:= CoreDeleteAll[];
       CoreCreate["b4", 5, {5, amZ, mZdef},
        {{5, mbmb, mbmb}}]
```

The value obtained by `REvolver` and the difference to the value quoted in Ref. [21] is

```
In[]:= mKinb4Ref = 4.523;
       mKinb4REvo = MassKin["b4", 5, muCutb, 5, mbmb, mbmb]
       mKinb4REvo - mKinb4Ref
Out[]= 4.523457226246508
Out[]= 0.0004572262465085686
```

i.e. there is perfect agreement.

The second case is in close analogy to the treatment of the RS mass just discussed above and requires that the conversion series, which relates the $\overline{\rm MS}$ and the kinetic mass for the bottom quark and n_ℓ massless quarks, is evaluated for $n_\ell = 3$ dynamical flavors, but using the 3-flavor strong coupling $\alpha_s^{(3)}$ computed with the charm mass threshold properly accounted for. `REvolver` does not provide functionality to carry out this conversion directly, but in the following we show how this evaluation can still be performed.

To obtain the $n_f = 3$ strong coupling in the usual way, we first create a new `Core` involving a massive bottom as well as charm quark

```
In[]:= mcmc = 1.263;
       CoreCreate["bc", 5, {5, amZ, mZdef},
        {{4, mcmc, mcmc}, {5, mbmb, mbmb}}]
```

and extract $\alpha_s^{(3)}(\overline{m}_b)$

```
In[]:= a3mbmb = AlphaQCD["bc", mbmb, 3];
```

Next, we create the `Core` to be employed for the mass scheme conversion. We use the computed $n_f = 3$ strong coupling and specify a total number of 4 flavors with 3 massless flavors and the massive bottom quark

```
In[]:= CoreCreate["b3", 4, {3, a3mbmb, mbmb},
        {{4, mbmb, mbmb}}]
```

The value of the kinetic bottom quark mass computed by `REvolver` and the difference to the corresponding result quoted in Ref. [21] can now be obtained by

```
In[]:= mKinb3Ref = 4.521;
       mKinb3REvo = MassKin["b3", 4, muCutb, 4, mbmb, mbmb]
       mKinb3Ref - mKinb3REvo
Out[]= 4.520784332346221
Out[]= 0.00021566765377922792
```

The numbers are in perfect agreement.

In Ref. [22] the lighter flavor mass corrections to the relation between the pole and kinetic masses were computed explicitly up to $\mathcal{O}(\alpha_s^3)$. These corrections are implemented in `REvolver`. They have the property that they exclusively come from the flavor number decoupling relations of the strong coupling, and they are also referred to as "scheme B" in that reference. In Eq. (79) of that reference the bottom quark kinetic mass $m_b^{\rm kin}(1\text{ GeV}) = 4.526$ GeV was obtained using $\alpha_s^{(5)}(m_Z) = 0.1179$ for the strong coupling, the charm quark running mass $\overline{m}_c(2\text{ GeV}) = 0.993$ GeV and the bottom quark standard running mass $\overline{m}_b = 4.136$ GeV. For the calculation, fixed-order conversion was applied using the standard running bottom mass $\overline{m}_b$ as the renormalization scale of the strong coupling. To reproduce the result with `REvolver` we define the input values with

```
In[]:= {amZ, mc3, mbmb} = {0.1179, 0.993, 4.163};
```

and the related `Core` with

```
In[]:= CoreDelete["bc"]
       CoreCreate["bc", 5, {5, amZ, mZdef},
         {{4, mc3, 3}, {5, mbmb, mbmb}}]
```

The bottom quark kinetic mass extracted by `REvolver` and its difference to the reference value are returned by

```
In[]:= mbKinRef = 4.526;
       mbKinREvo = MassKin["bc", 5, 1.0, 5, mbmb, mbmb]
       mbKinRef - mbKinREvo
Out[]= 4.527084826155039
Out[]= -0.0010848261550391314
```

The small deviation of 1 MeV originates from the fact that in Ref. [22] the light massive flavor corrections related to the charm quark are parametrized in terms of $\overline{m}_c(3\,\text{GeV})$, while in `REvolver` they are parametrized in terms of the charm standard running mass $\overline{m}_c$.

Performing the same conversion with R-evolution to resum logarithms of the intrinsic physical scales of the mass schemes gives

```
In[]:= MassKin["bc", 5, 1.0]
Out[]= 4.53472077059131
```

i.e. the bottom quark kinetic mass with log-resummation is larger by about 7 MeV. We note that, following Ref. [22], the default value for the kinetic mass intrinsic scale (where the default log-resummed conversion between the running and the kinetic mass is carried out) is set to be twice its renormalization scale, that is, 2 GeV in the example above.

7.2.4. Top quark mass at low scales

We return to Ref. [29] and investigate the top quark mass conversion between the $\overline{\text{MS}}$ and various short-distance schemes with 4-loop accuracy. This concerns Table I of that article.

Following Ref. [29] we first define the values for the strong QCD coupling $\alpha_s^{(5)}(m_Z) = 0.1185$, the top quark standard running mass $\overline{m}_t = 163.643$ GeV and the renormalization scale of the PS mass $\mu_f = 20$ GeV

```
In[]:= {amZ, mtmt, mufT} = {0.1185, 163.643, 20.0};
```

and a `Core` with a top threshold matching scale of twice the top standard running mass

```
In[]:= CoreDeleteAll[]
       CoreCreate["t", 6, {5, amZ, mZdef}, {{6, mtmt, mtmt}},
        fMatch -> {2.0}]
```

In analogy to Sec. 7.2.3, we evaluate the PS and 1S top quark mass employing `REvolver` and determine the difference to the values $m_t^{1S} = 172.227$ GeV and $m_t^{PS}(20\,\text{GeV}) = 171.792$ GeV quoted in the reference paper by converting directly from the $\overline{\text{MS}}$ scheme, leading to

```
In[]:= mtPSRef = 171.792;
       mtPSRevo = MassPS["t", 6, mufT, 6, mtmt, mtmt]
       mtPSRevo - mtPSRef
Out[]= 171.7950829141975
Out[]= 0.0030829141975061702
```

for the PS scheme, and

```
In[]:= mt1SRef = 172.227;
       mt1SRevo = Mass1S["t", 6, 6, mtmt, "relativistic"]
       mt1SRevo - mt1SRef
Out[]= 172.2298841816133
Out[]= 0.0028841816132967324
```

for the 1S scheme, respectively.

As already described in Sec. 7.2.3, the small difference (of about 3 MeV) results from the fact that in `REvolver` conversion is based on formulae where the (standard) running mass is taken as the input, while in Ref. [29] the conversion was carried out starting from the PS and 1S masses.

We now investigate the influence of large logarithms of the ratio between the top quark mass and the intrinsic scale of the respective short-distance schemes. For the top quark the impact of the summation of these logarithms can be significant. To this end we consider the convergence of the perturbative series relating the standard running top mass $\overline{m}_t$ to the PS mass $m_t^{PS}(20\,\text{GeV})$, the 1S mass m_t^{1S} as well as the running mass $m_t^{(5)}(2\,\text{GeV})$.

Using fixed-order conversion (without log-resummation) from $\overline{m}_t$ and using $\overline{m}_t$ as the renormalization scale, the top PS mass at 4 loops, and the corresponding corrections of order $\mathcal{O}(\alpha_s^n)$ with $1 \le n \le 4$ amount to

```
In[]:= MassPS["t", 6, mufT, 6, mtmt, mtmt]
       Table[
```

```
         MassPS["t", 6, mufT, 6, mtmt, mtmt, 1.0, n] -
          MassPS["t", 6, mufT, 6, mtmt, mtmt, 1.0, n - 1],
         {n, 1, 4}]
Out[]= 171.7950829141975
Out[]= {6.636196514422409, 1.199280138792858,
         0.26779429813998945, 0.048811962842222556}
```

On the other hand, employing R-evolution to first evolve down to the PS mass renormalization scale $\mu_f = 20$ GeV and then converting to the PS mass at that scale, which is `REvolver`s default procedure, we obtain

```
In[]:= MassPS["t", 6, mufT]
       Table[
        MassPS["t", 6, mufT, 5, mufT, mufT, 1.0, n] -
         MassPS["t", 6, mufT, 5, mufT, mufT, 1.0, n - 1],
        {n, 1, 4}]
Out[]= 171.79912206134247
Out[]= {0., 0.06895809427228983,
         0.001838267705210228, -0.01976315025407871}
```

We observe that the corrections are considerably smaller when R-evolution is accounted for and that there is a difference of around 4 MeV in the final 4-loop converted values for the two approaches. The $\mathcal{O}(\alpha_s)$ correction term is zero in the case of the log-resummed conversion since the 1-loop perturbative coefficients of the PS and MSR masses coincide.

For the conversion to the 1S mass the observation regarding fixed-order versus log-resummed conversion is similar. In the fixed-order case we get

```
In[]:= Mass1S["t", 6, 6, mtmt, "relativistic", mtmt]
       Table[
        Mass1S["t", 6, 6, mtmt, "relativistic", mtmt, n] -
         Mass1S["t", 6, 6, mtmt, "relativistic",
          mtmt, n - 1], {n, 1, 4}]
Out[]= 172.2298841816133
Out[]= {7.129280949172028, 1.227243021981991,
         0.21914263057425387, 0.01121757988499894}
```

while the log-resummed evaluation gives again substantially smaller corrections:

```
In[]:= mBohr = MBohr["t", 6]
       Mass1S["t", 6, 5]
       Table[
        Mass1S["t", 6, 5, mBohr, "nonrelativistic",
          mBohr, n] - Mass1S["t", 6, 5, mBohr,
          "nonrelativistic", mBohr, n - 1], {n, 1, 4}]
Out[]= 32.11684612826197
Out[]= 172.20797480544945
Out[]= {1.1666583987086199, 0.18536848855083576,
         -0.047109547951663444, -0.010351024770614004}
```

where the inverse Bohr radius, i.e. the intrinsic scale of the 1S mass, is shown as the first output for completeness.

Finally, we investigate the effect of log-resummation on the computation of the top quark 5-flavor running mass at 2 GeV, $m_t^{(5)}(2\text{ GeV})$, when converting from $m_t^{(5)}(\overline{m}_t)$. For simplicity we create a new `Core` named `t`, this time where for the top threshold matching scale the default value, the top quark standard running mass, is adopted:

```
In[]:= CoreDelete["t"]
       CoreCreate["t", 6, {5, amZ, mZdef},
         {{6, mtmt, mtmt}}];
```

Now we extract the value of the 5-flavor MSR mass $m_t^{(5)}(\overline{m}_t)$ at the scale of the standard top running mass from this `Core` as a reference

```
In[]:= m5mt = MassMS["t", 6, mtmt, 5]
Out[]= 163.67571467667918
```

`REvolver` does not provide fixed-order conversions of the running masses between two different renormalization scales. It is, however, possible to access these fixed-order corrections through the pole mass routine `MassPoleFO`. Care has to be taken that the two calls of the `MassPoleFO` routines involve the same renormalization scale (which here is the standard running mass) to ensure that the pole mass renormalon is properly canceled:

```
In[]:= FOTab =
         MassMS["t", 6, 2.0, 5] -
           MassPoleFO["t", 6, 5, 2.0, mtmt, #] +
           MassPoleFO["t", 6, 5, mtmt, mtmt, #] & /@
          {0, 1, 2, 3, 4};
       FOTab[[5]]
       Table[FOTab[[n]] - FOTab[[n - 1]], {n, 2, 5}]
Out[]= 173.2337130005733
Out[]= {7.46778271952536, 1.5242807051151317,
        0.4246371655552821, 0.14129773369833742}
```

The difference of the two calls of the `MassPoleFO` routine removes the log-resummed corrections from the output of `MassMS` and replaces it by the corresponding fixed-order terms. As for the above examples, we first display the $m_t^{(5)}(2\text{ GeV})$ value at $\mathcal{O}(\alpha_s^4)$ and the fixed-order perturbative correction terms at order $\mathcal{O}(\alpha_s^n)$ with $1 \le n \le 4$.

For the investigation of the correction terms in the case of R-evolution we create four `Cores`, setting the respective loop order n of the R-evolution equation to $1 \le n \le 4$

```
In[]:= CoreCreate["t-R" <> ToString[#], 6, {5, amZ, mZdef},
           {{6, mtmt, mtmt}}, runMSR -> #] & /@ {1, 2, 3, 4};
```

The four `Cores` differ only by the loop order used for R-evolution, but employ the default 4-loop matching to determine $m_t^{(5)}(\overline{m}_t)$ from the standard running mass $\overline{m}_t$. The value of $m_t^{(5)}(2\text{ GeV})$ corresponding to 4-loop running and the corrections coming from the individual running orders can be extracted with

```
In[]:= MassMS["t-R4", 6, 2.0]
       RevoTab = MassMS["t-R" <> ToString[#], 6, 2.0] & /@
          {1, 2, 3, 4};
       RevoTab = Prepend[RevoTab, m5mt];
       Table[RevoTab[[n]] - RevoTab[[n - 1]], {n, 2, 5}]
Out[]= 173.36186564820926
Out[]= {8.841888795217045, 0.8531892592812653,
        0.035471795296302844, -0.044398878264530595}
```

where the first entry in the curly brackets is the difference between $m_t^{(5)}(\overline{m}_t)$ and $m_t^{(5)}(2\text{ GeV})$ obtained with 1-loop R-evolution, while the subsequent entries refer to the differences to the previous order in $m_t^{(5)}(2\text{ GeV})$ obtained when adding the 2-, 3- and 4-loop terms to the R-evolution anomalous dimension. Once again we observe that the convergence is much better when using R-evolution, and that the corresponding results are more precise than using fixed-order conversion. Using 4-loop R-evolution leads to a value for $m_t^{(5)}(2\text{ GeV})$ that is about 130 MeV higher than when using 4-loop fixed-order conversion. This difference is consistent with the size of the 4-loop fixed-order correction of 141 MeV, when adopting the latter as an uncertainty for the 4-loop fixed-order conversion.

We see that the higher order corrections to the R-evolution anomalous dimension lead to very small effects, so that one could worry that their size may not reflect the perturbative uncertainty at the corresponding loop order. A different way to estimate perturbative uncertainties is to perform λ-variation in the R-evolution equation, which we shortly demonstrate in the following.

We create a set of `Cores` with λ values in the range $1/2 \le \lambda \le 2$ and for various loop orders in the R-evolution equation. The `Cores` are created with

```
In[]:= list2 = 2^Range[-1, 1, 2/49];
       Outer[
         CoreCreate["t-l" <> ToString[#2] <> "-R" <>
            ToString[#1], 6, {5, amZ, mZdef},
           {{6, mtmt, mtmt}}, lambdaMSR -> #2,
           runMSR -> #1] &, {1, 2, 3, 4}, list2];
```

and the table containing the corresponding values of $m_t^{(5)}(2\text{ GeV})$ is generated by

```
In[]:= mListRevo =
         Outer[
          MassMS["t-l" <> ToString[#2] <> "-R" <>
             ToString[#1], 6, 2.0, 5] &, {1, 2, 3, 4},
          list2];
```

Order by order, the values of the λ variations divided by two are then given by

```
In[]:= Table[(Max[mListRevo[[n]]] - Min[mListRevo[[n]]])/2,
        {n, 1, 4}]
Out[]= {1.082493387031036, 0.2525991201191715,
        0.041115232629010734, 0.02465406235192802}
```

The values of λ variations are consistent with the size of the corrections to the R-evolution equation and substantially smaller than the size of the fixed-order corrections, illustrating that resumming logarithms via R-evolution leads to a more precise mass conversion than using fixed-order corrections.

7.2.5. Running masses for complex renormalization scales

`REvolver` provides the functionality to determine running masses at complex renormalization scales. In analogy to Sec. 7.1.2, we demonstrate the quality of the running mass evolution in the complex plane by showing numerical consistency for the high-scale ($\overline{\rm MS}$) running top quark mass concerning the Cauchy's integral formula, where we adopt `muMS` = 350 GeV for the central scale and 174 GeV for the radius of the Cauchy integral. We set up a `Core` with the top quark standard running mass $\overline{m}_t = 163$ GeV and subsequently determine the central running mass and the corresponding value using the residue theorem

```
In[]:= CoreCreate["O", 6, {5, amZdef, mZdef},
         {{6, 163, 163}}]
In[]:= {muMS, rMS} = {350, 174};
       mMSDirect = MassMS["O", 6, muMS, 6]
       mMSResidue =
        1/(2 Pi)
         NIntegrate[MassMS["O", 6, muMS + rMS E^(I phi), 6],
          {phi, 0, 2 Pi}, PrecisionGoal -> 10]
       mMSResidue - mMSDirect
Out[]= 154.072755231406
Out[]= 154.07275523140612 + 4.240739575284689*^-16 I
Out[]= -1.1368683772161603*^-13 - 4.240739575284689*^-16 I
```

Both results are in perfect agreement reflecting the high numerical precision of the evolution routines implemented in `REvolver`.

This high numerical precision is also maintained at much smaller renormalization scales (where perturbation theory in general is less reliable). We demonstrate this for the top quark running (MSR) mass at a central scale of 2 GeV and a radius of 1 GeV for the Cauchy integral:

```
In[]:= muR = 2;
       mRDirect = MassMS["O", 6, muR, 5]
       mRResidue =
        1/(2 Pi)
         NIntegrate[MassMS["O", 6, muR + E^(I phi), 5],
          {phi, 0, 2 Pi}, PrecisionGoal -> 10]
       mRResidue - mRDirect
Out[]= 172.64605095372784
Out[]= 172.64605095372804 + 4.417437057588218*^-18 I
Out[]= 1.9895196601282805*^-13 + 4.417437057588218*^-18 I
```

7.2.6. Top quark pole masses

The pole mass scheme suffers from an $\mathcal{O}(\Lambda_{\rm QCD})$ renormalon, which entails that its perturbative relation to a short-distance mass involves a factorially divergent perturbative series and an associated ambiguity in its value [31,32,3,1]. The pole mass (and its value) can either be treated as an order-dependent concept or one can assign its value to be in the region where the perturbative series reaches its minimal correction term (and the partial sum of the perturbative series increases linearly), sometimes called the asymptotic region. We call the latter value the "asymptotic pole mass". The associated ambiguity arises from the principle ignorance where precisely to truncate the partial sum within the asymptotic region. Different lines of reasoning have been proposed concerning the determination of the asymptotic value and the associated ambiguity, see Refs. [1,3] for recent analyses.

`REvolver` provides functionalities to extract the order-dependent as well as the asymptotic pole mass value from a `Core`. In case of the asymptotic value and the associated ambiguity, `REvolver` provides routines employing a number of different methods and allowing for various options as explained in Sec. 6.2.3. In the following we demonstrate some of these functionalities reproducing results quoted in Refs. [3] and [1] focusing on the scenario of the top quark with massless bottom and charm quarks. Scenarios with massive bottom and charm quarks are treated in Sec. 7.3.4.

Minimal correction approach for the pole mass ambiguity

First, we consider Ref. [3] where the top quark pole mass renormalon ambiguity quoted in Eq. (4.7) is determined from the perturbative series between the pole mass and the standard running mass for the case where the bottom and charm mass effects are ignored. To reproduce the result we define the top standard running mass value used in Ref. [3]

```
In[]:= mtmt = 163.508;
```

and create an associated `Core`

```
In[]:= CoreDeleteAll[]
       CoreCreate["t", 6, {5, amZdef, mZdef},
        {{6, mtmt, mtmt}}]
```

We execute the function `MassPoleDetailed` to extract the asymptotic pole mass value, the ambiguity, and the order of the smallest correction term. The method adopted in Ref. [3] to determine the pole mass ambiguity was associated to the size of the minimal correction and is accessed in `REvolver` specifying the `min` method:

```
In[]:= MassPoleDetailed["t", 6, mtmt, mtmt, "min"]
Out[]= {173.60839591880665, 0.06443134543422957, 8}
```

Furthermore the third and fourth arguments are set to the standard running top mass `mtmt` to mimic the choices adopted in Ref. [3]. The choice of arguments when calling the function `MassPoleDetailed` ensures that the analyzed series is the one for the difference between pole and the (5-flavor) MSR mass at the scale `mtmt` and that the renormalization scale for the strong coupling is `mtmt` as well. The values for the asymptotic pole mass and its ambiguity quoted in Eq. (4.8) in Ref. [3] are 173.608 GeV and 67 MeV, respectively. The asymptotic value is in perfect agreement. The small discrepancy of 3 MeV in the ambiguity is related to the fact that `REvolver` uses the perturbative series for the relation between the pole and the MSR mass for the routine `MassPoleDetailed` while in Ref. [3] the relation between the pole and the standard running mass was considered.

Asymptotic series for the pole-$\overline{\text{MS}}$ mass relation

The method of estimating higher order coefficients in the pole-$\overline{\text{MS}}$ relation employed by `REvolver` is described in Sec. 4.4 of Ref. [1] and relies on an asymptotic formula that can, depending on the specified options, reproduce the exactly known coefficients, see Eq. (A.28) in Sec. A.5.

The values of the asymptotic coefficients can be easily read out using the function `MassPoleFO`. For the orders 5–9 `REvolver` returns

```
In[]:= (MassPoleFO["t", 6, 5, mtmt, mtmt, #] -
            MassPoleFO["t", 6, 5, mtmt, mtmt, # - 1])/
          (mtmt * (AlphaQCD["t", mtmt, 5]/(4 Pi))^#) & /@
        Range[5, 9]
Out[]= {1.4248584469453057*^7, 1.1661884055877335*^9,
        1.1323781055413771*^11, 1.2729796430260885*^13,
        1.6260702903901682*^15}
```

for $a_n^{\text{MSR}\prime}$ (i.e. the series coefficients for the MSR and pole mass difference) and

```
In[]:= (MassPoleFO["t", 6, 6, mtmt, mtmt, #] -
            MassPoleFO["t", 6, 6, mtmt, mtmt, # - 1])/
          (mtmt * (AlphaQCD["t", mtmt, 6]/(4 Pi))^#) & /@
        Range[5, 9]
Out[]= {1.429074531848818*^7, 1.1687368433901165*^9,
        1.1344063409072752*^11, 1.2749318929376549`*^13,
        1.6282469370459092*^15}
```

for $a_n^{\overline{\text{MS}}\prime}$ (i.e. the series coefficients for the standard running and pole mass difference), agreeing well with Table 2 of Ref. [1] within errors. The deviation from the central values quoted in that table arises because in Ref. [1] the central values of asymmetric uncertainty intervals have been quoted.

Asymptotic series for the pole-$\overline{\text{MS}}$ mass relation and the asymptotic pole mass

Having access to the pole mass at in principle arbitrary order using conversion from $\overline{\text{MS}}$ and MSR masses at arbitrary renormalization scales, `REvolver` allows to easily reproduce the numbers utilized to produce Fig. 6 of Ref. [2], where the order-dependent top quark pole mass was shown. We create a new `Core` to switch to the top standard running mass value $\overline{m}_t = 163$ GeV in accordance with Ref. [2]

```
In[]:= mtmt = 163;
       CoreDeleteAll[]
       CoreCreate["t", 6, {5, amZdef, mZdef},
        {{6, mtmt, mtmt}}]
```

Converting directly from the $\overline{\text{MS}}$ mass at the scale $\overline{m}_t$, including scale variation in the range $\overline{m}_t/2 \le \mu \le 2\overline{m}_t$ the pole mass, order by order $0 \le n \le 12$, is given by

```
In[]:= Table[{{ord, MassPoleFO["t", 6, 6, mtmt, mtmt, ord]},
          {MassPoleFO["t", 6, 6, mtmt, mtmt/2, ord] -
            MassPoleFO["t", 6, 6, mtmt, mtmt, ord],
           MassPoleFO["t", 6, 6, mtmt, 2*mtmt, ord] -
            MassPoleFO["t", 6, 6, mtmt, mtmt, ord]}},
         {ord, 0, 12}]
Out[]= {{{0, 163.}, {0., 0.}},
        {{1, 170.5097731904309},
         {0.7122980457679375, -0.5972354956839183}},
```

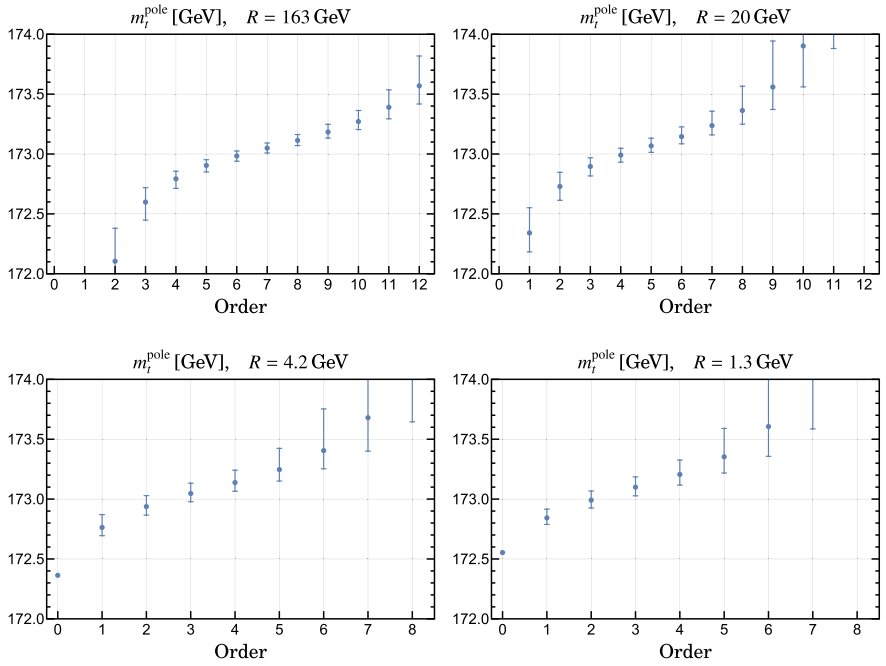

Fig. 4. Top quark pole mass $m_t^{\rm pole}$ as a function of the perturbative order for massless bottom and charm quarks, converted from the $\overline{\rm MS}$ mass (upper left panel) or the MSR mass (other panels) at different scales of R. The central dots are obtained for the default renormalization scales for the strong coupling, the error bars represent the scale variation. This corresponds to the black dots and error bars in Fig. 6 of Ref. [2].

```
{{2, 172.11277687226905},
 {0.27618516105792423, -0.3086769323029728}},
{{3, 172.6079790748946},
 {0.12091854036228256, -0.15116686757511388}},
{{4, 172.80297651883814},
 {0.06337072738099891, -0.08027361964516899}},
{{5, 172.9150350500228},
 {0.04822992022724293, -0.05421541398965246}},
{{6, 172.99420261176041},
 {0.04210709824803871, -0.043768064396573436}},
{{7, 173.06058298165766},
 {0.042838521236177485, -0.04090645714344987}},
{{8, 173.1250293570062},
 {0.04963473302441912, -0.04338206485874707}},
{{9, 173.19612979388887},
 {0.0644919645042421, -0.05147133915082236}},
{{10, 173.28398617671283},
 {0.09283257854019666, -0.06758882965976909}},
{{11, 173.40418238677069},
 {0.14657118914180955, -0.09737521610099975}},
{{12, 173.58454177427788},
 {0.2518136273276639, -0.1527834480848469}}}
```

Analogous commands can be used to extract the relevant values of the pole mass when converting from the MSR scheme at various scales of R. Utilizing these numbers it is now straightforward to reproduce Fig. 6 of Ref. [2] for vanishing bottom and charm mass (black dots in Ref. [2]), see Fig. 4.[7] The asymptotic value which can be assigned to the pole mass lies in the region where the series grows linearly, which is in Fig. 4, roughly in the region around 173 GeV. This is confirmed by the output of the command `MassPoleDetailed`, which gives

```
In[]:= MassPoleDetailed["t", 6, mtmt, mtmt, "min"]
Out[]= {173.07508395890844, 0.06445302708283407, 8}
```

[7] Note that the upper left panel of Fig. 4 (corresponding to the numbers given above) shows the conversion directly from the standard $\overline{\rm MS}$ mass instead of the MSR mass at the high scales.

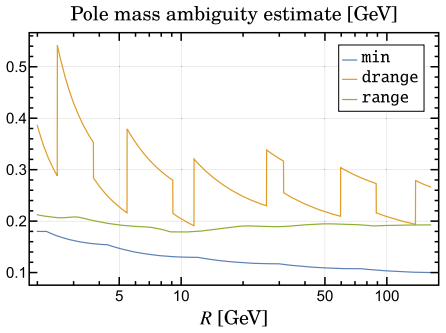

Fig. 5. Comparison of the pole mass ambiguity estimating strategies available in `REvolver` obtained from the series between the pole mass and the running mass $m_t^{(5)}(R) = m_t^{\rm MSR}(R)$ for the case that all quarks lighter than the top quark are considered to be massless. The figure shows the size of the ambiguity of the top quark pole mass in GeV as estimated by the `min` (blue lower curve), `drange` (orange upper curve) and `range` (green middle curve) strategies over the scale R. (For interpretation of the colors in the figure(s), the reader is referred to the web version of this article.)

```
In[]:= MassPoleDetailed["t", 6, mtmt, mtmt, "range"]
Out[]= {173.07976320487433, 0.12605058936964042, 8}

In[]:= MassPoleDetailed["t", 6, mtmt, mtmt, "drange"]
Out[]= {173.1081654841447, 0.16284602132711257, 8}
```

for the three methods to estimate the asymptotic pole mass supported by `REvolver` from the relation between the pole and the MSR mass $m_t^{(5)}(\overline{m}_t)$ at the scale 163 GeV. While the estimation of the ambiguity can vary by more than a factor of 2 depending on the employed strategy, the estimated asymptotic pole mass is fairly stable.

Fig. 5 shows a comparison of the three strategies of estimating the pole mass ambiguity implemented in `REvolver` from the perturbative series between the pole mass and the running (MSR) mass $m_t^{(5)}(R) = m_t^{\rm MSR}(R)$ at the scale R. The plot is produced with the command

```
In[]:= LogLinearPlot[
         {MassPoleDetailed["t", 6, R, "min"][[2]],
          MassPoleDetailed["t", 6, R, "drange"][[2]],
          MassPoleDetailed["t", 6, R, "range"][[2]]},
         {R, 2, mtmt}, PlotRange -> {0.05, 0.26}]
```

omitting all options related to plot styling and annotations for brevity.

The figure shows the size of the ambiguity of the top quark pole mass in GeV as estimated by the strategies over the scale R, specifying the scale in the perturbative relation between the pole and running mass. All quarks lighter than the top quark are considered to be massless. Due to its discrete nature, the `drange` method produces a discontinuous curve, while the continuous version `range` provides a very stable result. The `min` method leads to an ambiguity estimate that is logarithmically decreasing with R.

7.3. `Cores` with multiple massive quarks

7.3.1. Strong coupling and $\Lambda_{\rm QCD}$

Strong coupling evolution through multiple flavor thresholds

In Ref. [33] the 3-flavor strong coupling value $\alpha_s^{(3)}(m_\tau)$ was determined from hadronic e^+e^- R-ratio data for c.m. energies below the charm production threshold. For this determination, fixed-order (FO) as well as contour-improved (CI) perturbation theory were applied, and the corresponding values $\alpha_s^{(3)}(m_\tau)_{\rm FO} = 0.298$ and $\alpha_s^{(3)}(m_\tau)_{\rm CI} = 0.304$ were subsequently converted to $\alpha_s^{(5)}(m_Z)$ employing the 4-loop beta function as well as the 3-loop matching relations at the charm and bottom thresholds. The respective values for the strong coupling at the Z-scale were quoted in Eq. (4.7) of that reference as $\alpha_s^{(5)}(m_Z)_{\rm FO} = 0.1158$ and $\alpha_s^{(5)}(m_Z)_{\rm CI} = 0.1166$, respectively.

For the conversion, the values $\overline{m}_c = 1.28$ GeV and $\overline{m}_b = 4.2$ GeV were used for the charm and bottom standard running masses, respectively, and the charm and bottom threshold matching scales were set to $\mu_c = 2.0$ GeV and $\mu_b = 4.0$ GeV, respectively. To reproduce the conversion with `REvolver` we define these input values with

```
In[]:= mTau = 1.77686;
       {mcmc, mbmb} = {1.28, 4.2};
       matchList = {2.0/mcmc, 4.0/mbmb};
       {amTauFO, amTauCI} = {0.298, 0.304};
```

and define one `Core` for each value of $\alpha_s^{(3)}(m_\tau)$

```
In[]:= CoreCreate["FO", 5, {3, amTauFO, mTau},
```

```
        {{4, mcmc, mcmc}, {5, mbmb, mbmb}}, runAlpha -> 4,
        orderAlpha -> 3, fMatch -> matchList]
      CoreCreate["CI", 5, {3, amTauCI, mTau},
        {{4, mcmc, mcmc}, {5, mbmb, mbmb}}, runAlpha -> 4,
        orderAlpha -> 3, fMatch -> matchList]
```

where the parameters relevant for running and matching were set with the optional parameters `runAlpha`, `orderAlpha` and `fMatch`.

The values of $\alpha_s^{(5)}(m_Z)$ can now be easily extracted by

```
In[]:= AlphaQCD["FO", mZdef, 5]
       AlphaQCD["CI", mZdef, 5]
Out[]= 0.11581049250660494
Out[]= 0.11662117512902259
```

in full agreement with Eq. (4.7) of Ref. [33].

Similarly, in Ref. [34] $\alpha_s^{(3)}(m_\tau)$ was determined from τ decay data and converted to $\alpha_s^{(5)}(m_Z)$ employing 4-loop evolution and matching. We update the values for the standard running bottom and charm masses to the ones in the reference paper and define the value of $\alpha_s^{(3)}(m_\tau)$ as given in Eq. (19) therein as well as the associated `Core`

```
In[]:= {mcmc, mbmb} = {1.286, 4.164};
       amTau = 0.332;

In[]:= CoreDeleteAll[]
       CoreCreate["O", 5, {3, amTau, mTau},
        {{4, mcmc, mcmc}, {5, mbmb, mbmb}}, runAlpha -> 4]
```

where, following Ref. [34], the strong coupling evolution is set to 4-loop precision. We focus on the central value here for brevity. The value of $\alpha_s^{(5)}(m_Z)$ can now easily be extracted with

```
In[]:= AlphaQCD["O", mZdef, 5]
Out[]= 0.12019776978833413
```

agreeing with Eq. (20) of Ref. [34].

Flavor number dependence of the QCD scale $\Lambda_{\rm QCD}^{(n_f)}$

To demonstrate the capability of `REvolver` to extract $\Lambda_{\rm QCD}^{(n_f)}$ in various flavor number schemes we consider Ref. [35], where $\alpha_s^{(5)}(m_Z) = 0.1179$ has been determined by the ALPHA collaboration and values for $\Lambda_{\rm QCD}^{(nf)}$ with $3 \le n_f \le 5$ were determined, see Eqs. (4.14) as well as (5.3) and (5.4) of that reference.

To reproduce the $\Lambda_{\rm QCD}^{(n_f)}$ values with `REvolver` we create a `Core` with massive bottom and charm quarks (with standard running mass values taken from the PDG [23]) and define the value of $\alpha_s^{(5)}(m_Z)$ to be the one given in the reference paper

```
In[]:= {amZ, mcmc, mbmb} = {0.1179, 1.27, 4.18};

In[]:= CoreDeleteAll[]
       CoreCreate["O", 5, {5, amZ, mZdef},
        {{4, mcmc, mcmc}, {5, mbmb, mbmb}}]
```

We now extract $\Lambda_{\rm QCD}^{(n_f)}$ in the $n_f = 5, 4, 3$ flavor schemes in the so-called $\overline{\rm MS}$ scheme [see Eq. (A.13) in App. A.2] with

```
In[]:= LambdaQCD["O", 5]
       LambdaQCD["O", 4]
       LambdaQCD["O", 3]
Out[]= 0.20745573124097272
Out[]= 0.288991643859333
Out[]= 0.33153068987761314
```

The numbers are in exact agreement with the values shown in Ref. [35].

7.3.2. Top quark running mass at low scales

In Ref. [36] a calibration analysis was provided which suggested that the top quark running mass $m_t(1\text{ GeV})$ agrees within theoretical uncertainties with the MC top mass parameter $m_t^{\rm MC}$ of the `Pythia` event generator. Specifically, the authors quote a value of $m_t(1\text{ GeV}) = 172.82 \pm 0.19$ GeV for a calibration with $m_t^{\rm MC} = 173$ GeV, given in Table 1. That analysis was carried out in the approximation of massless bottom and charm quarks. Here we demonstrate how `REvolver` can be used to investigate how finite charm and bottom quark masses affect the value of the standard running mass $\overline{m}_t$ calculated from $m_t(1\text{ GeV})$. As an estimate of the uncertainties we quote the difference of the values computed using 4- and 3-loop R-evolution.

To this end we create six Cores: two with massless bottom and charm quarks, two with a massless charm quark and a massive bottom quark, and two with massive bottom and charm quarks, employing $\overline{m}_c = 1.27$ GeV and $\overline{m}_b = 4.18$ GeV for the standard running charm and bottom quark masses. Among the two respective Cores one employs 3-loop and the other 4-loop precision for the R-evolution equation:

```
In[]:= {mcmc, mbmb, mt1} = {1.27, 4.18, 172.82};

In[]:= CoreDeleteAll[]
       CoreCreate["t4", 6, {5, amZdef, mZdef}, {{5, mt1, 1}},
        runMSR -> 4]
       CoreCreate["t3", 6, {5, amZdef, mZdef}, {{5, mt1, 1}},
        runMSR -> 3]
       CoreCreate["bt4", 6, {5, amZdef, mZdef},
        {{5, mbmb, mbmb}, {4, mt1, 1}}, runMSR -> 4]
       CoreCreate["bt3", 6, {5, amZdef, mZdef},
        {{5, mbmb, mbmb}, {4, mt1, 1}}, runMSR -> 3]
       CoreCreate["cbt4", 6, {5, amZdef, mZdef},
        {{4, mcmc, mcmc}, {5, mbmb, mbmb}, {3, mt1, 1}},
        runMSR -> 4]
       CoreCreate["cbt3", 6, {5, amZdef, mZdef},
       {{4, mcmc, mcmc}, {5, mbmb, mbmb}, {3, mt1, 1}},
       runMSR -> 3]
```

The Core setups specify that $m_t^{\rm MSR}(1\,{\rm GeV}) = 172.82$ GeV is the running top quark mass in the scheme in which all massive flavors above the scale of 1 GeV are integrated out. It is easy to extract the top quark standard running masses and their uncertainties from the Cores above with

```
In[]:= MassMS["t4", 6]
       MassMS["t4", 6] - MassMS["t3", 6]
Out[]= 163.00308510782256
Out[]= 0.05105270648016358

In[]:= MassMS["bt4", 6]
       MassMS["bt4", 6] - MassMS["bt3", 6]
Out[]= 162.94352028117146
Out[]= 0.050962554040836494

In[]:= MassMS["cbt4", 6]
       MassMS["cbt4", 6] - MassMS["cbt3", 6]
Out[]= 162.92268002391415
Out[]= 0.049529435610025985
```

where the first numbers refer to the setup with massless bottom and charm quarks and the last ones to the one where bottom and charm quarks have mass.

We observe that the finite bottom mass lowers the standard top running mass by around 60 MeV and the finite charm mass decreases the standard top running mass by about another 20 MeV. The perturbative uncertainty of the conversion amounts to around 50 MeV in all cases. Together, the finite charm and bottom masses lower the standard running top mass by about 80 MeV, which is larger than the perturbative uncertainty.

7.3.3. Charm mass effects for the bottom quark mass

To demonstrate the effect of lighter massive flavors in conversions between short-distance mass schemes we consider Ref. [37], where effects of the finite charm quark mass on bottom quark mass determinations from Υ mesons were (calculated and) examined. In Eq. (99) of that paper the bottom standard running mass is computed from the 1S mass $m_b^{\rm 1S} = 4.7$ GeV with and without the contribution of the charm standard running quark mass $\overline{m}_c = 1.5$ GeV. The strong coupling value was set to $\alpha_s^{(4)}(m_b^{\rm 1S}) = 0.216$. We define these parameters with

```
In[]:= {mb1S, mcmc, amb1S} = {4.7, 1.5, 0.216};
```

and create two 4-flavor Cores, one with a massless charm quark and one with the charm mass given above

```
In[]:= CoreDeleteAll[]
       CoreCreate["c0", {4, amb1S, mb1S}]
       CoreCreate["cm", 4, {4, amb1S, mb1S},
        {{4, mcmc, mcmc}}]
```

We then create two additional Cores by adding the bottom quark 1S mass $m_b^{\rm 1S} = 4.7$ GeV to the existing Cores, where, following Ref. [37], the perturbative order of its relation to the standard running mass is $\mathcal{O}(\alpha_s^3)$ and the relativistic ("upsilon-expansion") counting scheme is adopted.

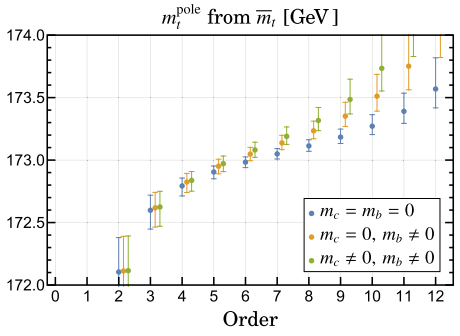

Fig. 6. Top quark pole mass $m_t^{\rm pole}$ as a function of the perturbative order with bottom and charm quark masses set to zero (left blue), massless charm quark (middle orange) and massive bottom and charm masses (right green). The conversion is performed from the $\overline{\rm MS}$ mass. The central dots are obtained for the default renormalization scales for the strong coupling $\mu = \overline{m}_t$, the error bars represent the scale variation $\overline{m}_t/2 \le \mu \le 2\overline{m}_t$. (For interpretation of the colors in the figure(s), the reader is referred to the web version of this article.)

```
In[]:= Add1SMass["c0", "bc0", mb1S, 5, mb1S, "relativistic",
         mb1S, 3]
       Add1SMass["cm", "bcm", mb1S, 5, mb1S, "relativistic",
         mb1S, 3]
```

We have furthermore set the running mass scale and the renormalization scale of the strong coupling to $m_b^{\rm 1S}$ and the parameter `nfConv` to 5 to specify direct conversion without R-evolution to be in accordance with the computation carried out in Ref. [37].

Extracting the standard mass from the massless charm `Core` gives

```
In[]:= MassMS["bc0", 5]
Out[]= 4.190311348710497
```

in perfect agreement with $\overline{m}_b = (4.7 - 0.382 - 0.098 - 0.030)$ GeV $= 4.190$ GeV as quoted in Ref. [37]. For the standard mass from the massive charm `Core` we get

```
In[]:= MassMS["bcm", 5]
Out[]= 4.178691644159289
```

with a sub-MeV difference to the reference value $\overline{m}_b = (4.7 - 0.382 - (0.098 + 0.0072) - (0.03 + 0.0049))$ GeV $= 4.178$ GeV.

7.3.4. Top quark pole masses

In the following we investigate the influence of massive bottom and charm quarks on the perturbative series relating the top quark standard running mass and the pole mass.

Pole-$\overline{\rm MS}$ mass series dependence on lighter massive quarks

In Ref. [2] the dependence of the high-order asymptotic series for the top quark pole-$\overline{\rm MS}$ mass relation on finite bottom and charm quark mass was examined and an algorithm to determine explicit analytic formulae (accounting for the semianalytical results given in Ref. [38]) were provided, which are implemented in `REvolver`. Explicit results for the asymptotic series coefficients beyond $\mathcal{O}(\alpha_s^4)$ were provided in Ref. [2] for the scenarios of massless bottom and charm quarks, massive bottom and massless charm quarks as well as massive bottom and charm quarks. To compare the results of `REvolver` to those of Ref. [2] we set the appropriate relevant parameters for the standard running charm, bottom and top quark masses as well as for the strong coupling and create the `Core`s for the three scenarios

```
In[]:= {mcmc, mbmb, mtmt} = {1.3, 4.2, 163};
       {amZ, mZ} = {0.118, 91.187};

In[]:= CoreDeleteAll[]
       CoreCreate["tbc", 6, {5, amZ, mZ},
        {{4, mcmc, mcmc}, {5, mbmb, mbmb}, {6, mtmt, mtmt}}]
       CoreCreate["tb", 6, {5, amZ, mZ},
        {{5, mbmb, mbmb}, {6, mtmt, mtmt}}]
       CoreCreate["t", 6, {5, amZ, mZ}, {{6, mtmt, mtmt}}]
```

The perturbative series relating the standard running mass and the pole mass can be generated as shown in Sec. 7.2.6 and depicted in the upper left panel of Fig. 4 for massless bottom and charm quarks. In Fig. 6 we show the result of repeating this procedure for each of the `Core`s created above. It is clearly visible that for each additional accounted massive quark flavor the series diverges faster and consequently the respective pole mass ambiguity increases.

In accordance with Ref. [2] we read out the value of the asymptotic top quark pole mass, the associated ambiguity and the order of the minimal correction term from each `Core` employing the `drange` approach, which is based on all series terms in the superasymptotic region, by executing

```
In[]:= MassPoleDetailed["t", 6, mtmt, "drange"]
       MassPoleDetailed["tb", 6, mtmt, "drange"]
       MassPoleDetailed["tbc", 6, mtmt, "drange"]
Out[]= {173.09649964256326, 0.16178589168021063, 8}
Out[]= {173.17525229067104, 0.2336983055654116, 7}
Out[]= {173.17973196293923, 0.26632540751468525, 7}
```

The three results agree with the numbers given in Table 5 of Ref. [2] within uncertainties.[8]

We now return to Ref. [3]. There, finite charm and bottom quark mass effects on the value of the top quark asymptotic pole mass were quantified by an approximate and heuristic method utilizing order-dependent light flavor decoupling in the strong coupling. A numerical value for the resulting ambiguity of the asymptotic pole mass was quoted in Eq. (5.1) of that paper using size of the minimal correction of the asymptotic series.

Fixing the value of the top, bottom and charm quark standard running masses to the values given in Ref. [3] and creating an associated `Core`

```
In[]:= {mtmt, mbmb, mcmc} = {163.508, 4.2, 1.3};

In[]:= CoreCreate["tbc2", 6, {5, amZdef, mZdef},
         {{4, mcmc, mcmc}, {5, mbmb, mbmb}, {6, mtmt, mtmt}}]
```

we obtain

```
In[]:= MassPoleDetailed["tbc2", 6, mtmt, mtmt, "min"]
Out[]= {173.61531203486197, 0.10050070355543994, 7}
```

where we employ the `min` method to match the approach used in Ref. [3]. The asymptotic pole mass value and the associated ambiguity are quoted as 173.667 GeV and 108 MeV, respectively, in that reference and differs by around 50 and 8 MeV, respectively, to the result provided by `REvolver`. The difference is mainly related to the exact treatment of light massive flavor corrections provided by `REvolver`.

Normalization of the pole mass renormalon

Finally, we demonstrate `REvolver`'s capability to compute the normalization $N_{1/2}^{(n_\ell)}$ of the pole mass renormalon for a given number n_ℓ of massless quark flavors. Reusing the `Core`s created in one of the previous examples, the value of the normalization for $n_\ell = 3, 4, 5$ can be extracted with

```
In[]:= N12[#] & /@ {"tbc","tb","t"}
Out[]= {0.5371120004494861, 0.5055628679671248,
        0.4612967890971816}
```

in excellent agreement with the corresponding values $N_{1/2}^{(n_\ell=3,4,5)} = \{0.5370 \pm 0.0011,\ 0.5056 \pm 0.0015,\ 0.4616 \pm 0.0020\}$ given for $\mu/\overline{m} = 1$ in Table 1 of Ref. [3].

In Eq. (2.21) of Ref. [2] the λ-parameter was varied in the range $1/2 \le \lambda \le 2$, and the associated central value and uncertainty of the renormalon normalization $N_{1/2}^{(n_\ell)}$ were determined. The corresponding values for $n_\ell = 3, 4, 5$ can be reproduced by `REvolver` with

```
In[]:= list2 = 2^Range[-1, 1, 2/19];

In[]:= N3Tab = N12["tbc", #] & /@ list2;
       (Max[N3Tab] + {1, -1} * Min[N3Tab])/2
Out[]= {0.5256087104548577, 0.011913515642471062}

In[]:= N4Tab = N12["tb", #] & /@ list2;
       (Max[N4Tab] + {1, -1} * Min[N4Tab])/2
Out[]= {0.4916415824077933, 0.016342715842279004}

In[]:= N5Tab = N12["t", #] & /@ list2;
       (Max[N5Tab] + {1, -1} * Min[N5Tab])/2
Out[]= {0.44606744334202203, 0.023867353429116556}
```

in perfect agreement with the values $N_{1/2}^{(n_\ell=3,4,5)} = \{0.526 \pm 0.012,\ 0.492 \pm 0.016,\ 0.446 \pm 0.024\}$, quoted in Eq. (2.21) of Ref. [2].

8. Theoretical input

The perturbative coefficients of the QCD β-function, that is the renormalization group equation of the $\overline{\text{MS}}$ strong coupling $\alpha_s^{(n_f)}(\mu)$ in a given n_f flavor number scheme, are known to five loops and can be found in Refs. [39–46]. If `REvolver` is used for scenarios with

[8] The 10 MeV discrepancy in the asymptotic pole mass value is because in Ref. [2], an additional λ variation was applied in the estimate of the asymptotic coefficients and the quoted coefficients were the central values of the obtained intervals. `REvolver` does not support this functionality.

massless quarks only, it is recommended to cite those references. The perturbative coefficients for the strong coupling flavor matching relation at the quark thresholds are known up to four loops and can be found in Refs. [47–50]. If `REvolver` is used for strong coupling evaluations in different flavor number schemes involving massive quark threshold matching, these references should be cited.

The perturbative coefficients of the relation between the $\overline{\rm MS}$ mass $\overline{m}_q^{(n_f)}(\mu)$, for the case where $n_f - 1$ is the number of flavors lighter than the massive quark q, and the pole mass $m_q^{\rm pole}$ for the case that all lighter quarks are massless, are known to four loops and can be found in Refs. [51–53,12]. If REvolver is used to compute relations between the $\overline{\rm MS}$ mass and the pole mass when all lighter quarks are massless, these references should be included. The two- and three-loop corrections coming from the masses of lighter massive quarks can be found in Refs. [52] and [38,54], respectively. It would be appropriate to also cite these references, if REvolver is used to compute lighter massive flavor effects in the relation between the $\overline{\rm MS}$ mass and the pole mass of a heavy quark. The perturbative coefficients of the $\overline{\rm MS}$ mass renormalization group equations (relevant for renormalization scales above the mass of quark q) are known to five loops and can be found in Refs. [55–58]. These references should be cited whenever the code is used to compute the running of the $\overline{\rm MS}$ mass in any flavor scheme that includes the heavy quark itself. The perturbative coefficients of the flavor matching relations needed when the running $\overline{\rm MS}$ mass evolves to scales beyond even heavier massive quarks are known up to four loops and can be found in Refs. [47,59]. These references should be included, if the $\overline{\rm MS}$ mass is evaluated in different flavor number schemes involving threshold matching associated to even heavier massive quarks.

The MSR mass $m_q^{{\rm MSR},(n_\ell)}(\mu)$ is derived from the perturbative relation between the pole mass and the standard running mass $\overline{m}_q$ by integrating out the quark flavor q, see Sec. 3. Thus, all perturbative properties of the MSR mass are derived from expressions known for the $\overline{\rm MS}$ scheme from the references mentioned in the previous paragraph. The MSR mass concept was first suggested in Ref. [6] and allows to consistently consider renormalization group evolution for scales μ below the quark mass m_q, called "R-evolution". The perturbative coefficients of (i) the relation between the MSR mass $m_q^{{\rm MSR},(n_\ell)}(\mu)$, where n_ℓ is smaller or equal to the number of flavors lighter than the massive quark q, and the pole mass $m_q^{\rm pole}$, (ii) the matching relation of the MSR mass to the $\overline{\rm MS}$ mass, and (iii) its n_ℓ flavor-number-dependent renormalization group equation for the case that all lighter quarks are massless (which are all known to four loops) can be found in Ref. [1]. The MSR mass scheme implemented in REvolver is called the "natural" MSR mass scheme in Ref. [1]. The two- and three-loop corrections coming from the masses of lighter massive quarks including the flavor matching relations, when the MSR mass evolution crosses a lighter massive quark threshold, can be found in Ref. [2]. The results for the lighter massive quark effects given in Ref. [2] involve a parametrization of the results provided in Ref. [38] (in terms of coefficients δ_2 and $\delta_{Q,n}^{(q,q',\ldots)}$) that accounts for theoretical interrelations of the different contributions not considered in Ref. [38], and allows for a straightforward generalization for the case of multiple lighter massive quark flavors. The parametrization is also fully compatible with the recent analytic updates on the three-loop corrections given Ref. [54] within a few MeV. The expression for δ_2 used in REvolver has been given in Ref. [2]. The concrete expressions for the other coefficients $\delta_{Q,n}^{(q,q',\ldots)}$ have been taken from Ref. [60]. If REvolver is used to calculate the MSR mass of a massive quark in the case that all lighter quarks are massless, Refs. [1,2] should be cited. If REvolver is used to calculate the MSR mass in different flavor number schemes involving flavor threshold matching as light massive quark thresholds Ref. [2] should be cited. The possibility to resum (large) logarithms in the relation between short-distance quark mass definitions involving scales below the quark mass scale (e.g. concerning the ratio of the heavy quark mass and a lighter quark mass) is currently only provided through the MSR mass, which is therefore the primary short-distance mass scheme for scales below the quark masses contained in the REvolver core objects. If REvolver is used to resum such logarithms in the relation of short-distance masses (even not involving the MSR directly), this MSR mass functionality is used as an intermediate step, and it is appropriate to cite Ref. [1,6].

The quark mass dependence of the formulae of the flavor threshold matching relations for the flavor-number-dependent strong coupling $\alpha_s^{(n_f)}(\mu)$, the $\overline{\rm MS}$ mass $\overline{m}_q^{(n_f)}(\mu)$ and the MSR mass $m_q^{{\rm MSR},(n_\ell)}(\mu)$ implemented in `REvolver` are expressed in terms of the standard running mass $\overline{m}_q$. Changing the scheme of the quark mass in these matching relations is not supported in `REvolver` because the corresponding numerical impact is tiny and negligible for practical applications where large logarithmic corrections are properly resummed.

The perturbative coefficients of the relation between the kinetic and pole mass, assuming lighter massive quarks to be massless, can be found in Refs. [17,21]. The 1S mass scheme was first suggested in Refs. [15,14]. The perturbative coefficients for the 1S mass scheme have been derived in Refs. [15,14,61,19,62–64]. The perturbative coefficient for the PS mass scheme, first suggested in Ref. [18], can be obtained from Refs. [18,19] using analytic results for the static potential as given in Refs. [65–71]. The relation connecting the RS and pole mass schemes is described in Refs. [30,20] and references therein. Whenever values for any of these masses are obtained through `REvolver`, the corresponding references should be mentioned. The lighter massive flavor corrections in the relation to the pole mass are known for the kinetic [22], 1S [72,73] and PS masses [74]. For the 1S mass `REvolver` currently only accounts for the fixed-order corrections in the relation to the pole mass. Therefore, if lighter quarks are considered massive, the appropriate references should be cited.

To compute the RGI mass [13] the standard formula is evaluated as described below Eq. (A.20).

9. Summary

In this article we have presented `REvolver`, a `C++` library for carrying out state-of-the-art renormalization group evolution and flavor matching for the QCD coupling and quark masses, and conversion between the most common quark mass renormalization schemes. For short-distance quark masses the achievable precision is at the level of 10 to 20 MeV. In addition to similar libraries that are already available `REvolver` offers the `Core` concept, that allows to define and manage different physical scenarios for coupling and quark mass values, and to carry out renormalization group summation of logarithms from scales above and below the quark masses. `REvolver` supports, in particular, the summation of logarithms described by the R-evolution equation, which describes the linear scale evolution characteristic to low-scale short-distance masses, and it accounts for the flavor threshold corrections that arise in this linear scale evolution. Furthermore, `REvolver` provides access to the asymptotic perturbative relations to the pole mass to in principle any perturbative order, and it provides quasi-exact solutions to the renormalization group equations (i.e. exact up to machine-precision) for complex renormalization scales. The `REvolver` library can be also accessed through `Mathematica` and `Python` interfaces. We have provided a large

number of examples for the most common applications, which are shipped along with the library in the form of `Mathematica` and Jupyter notebooks, as well as a `C++` program.

Declaration of competing interest

The authors declare that they have no known competing financial interests or personal relationships that could have appeared to influence the work reported in this paper.

Acknowledgements

This work was supported in part by FWF Austrian Science Fund under the Project No. P28535-N27, the Spanish MINECO Ramón y Cajal program (RYC-2014-16022), the MECD grants FPA2016-78645-P and PID2019-105439GB-C22, the IFT Centro de Excelencia Severo Ochoa Program under Grant SEV-2012-0249, the EU STRONG-2020 project under the program H2020-INFRAIA-2018-1, grant agreement No. 824093 and the COST Action CA16201 PARTICLEFACE. CL is supported by the FWF Doctoral Program "Particles and Interactions" No. W1252-N27. We thank D. Boito and M. Steinhauser for explanations concerning the content of their respective articles.

Appendix A. Algorithms to solve the differential equations

In this appendix some details on the algorithms used in `REvolver` are provided.

A.1. `Core` creation

For the creation of a `Core`, values for the strong coupling and the running masses of the n_q massive quarks at specified scales and in specified flavor-number schemes, as well as the total number of flavors n_T, are provided by the user.[9] Let us call the corresponding tuples $\{n_\alpha, \alpha_s^{(n_\alpha)}(\mu_\alpha),\ \mu_\alpha\}$ for the strong coupling and $\{k_n, m_{q_n}^{(k_n)}(R_n), R_n\}$, with $\max[k_n, n_\alpha] \le n_T$, $1 \le n \le n_q$, for the n_q massive quarks, where q_1 refers to the lightest and q_{n_q} to the heaviest massive quark. In a first step `REvolver` determines the values of the standard running masses $\overline{m}_{q_n}$. Subsequently, the following strong coupling and running mass values at each flavor threshold matching scale μ_n are obtained: $\alpha_s^{(n_T+n-1-n_q)}(\mu_n)$, $\alpha_s^{(n_T+n-n_q)}(\mu_n)$ and $m_n^{(n_T+n-1-n_q)}(\mu_n)$, $m_n^{(n_T+n-n_q)}(\mu_n)$. These numbers serve as the initial conditions to compute α_s and the running masses m_{q_n} at any renormalization scale and in any specified flavor-number scheme. We have implemented into our code a fast multi-dimensional recursive algorithm that solves the coupled system of equations to the specified precision.

The determination of the standard running masses $\overline{m}_{q_n}$ in the algorithm is particularly important since the flavor matching scales μ_n are specified as dimensionless coefficients times $\overline{m}_{q_n}$. If at the i-th iteration the standard running masses are $[\overline{m}_{q_n}]_i$, the numerical values $[\overline{m}_{q_n}]_{i+1}$ at step $(i+1)$ are computed evolving (and matching if necessary) the quark masses $m_{q_n}^{(k_n)}(R_n)$ from the user-specified $\mu = R_n$, for which the numerical value of the mass was provided, to $\mu = [\overline{m}_{q_n}]_i$. To do that, before running the masses, the program computes the values of α_s at the various thresholds μ_n using $[\overline{m}_{q_n}]_i$ as well. After each iteration is carried out, the new standard running masses are compared to the previous ones, and if their largest relative deviation is smaller than the required precision, the process stops. In the initial step it is assumed that $[\overline{m}_{q_n}]_{i=0} = m_{q_n}^{(k_n)}(R_n)$. We checked that the algorithm is very robust and converges quickly even for very extreme starting conditions such as a charm quark mass defined with $k_1 = 6$ active flavors taking for R_1 a very large scale, together with a top quark mass defined at $R_3 = 1$ GeV with $k_3 = 3$ active flavors. There is the possibility that the algorithm does not converge, if a particular sequence of $[\overline{m}_{q_n}]_i$-values repeats itself. This is avoided by adopting, after the 20-th iteration ($i \ge 21$) the linear combination $(1 - \texttt{damp})[\overline{m}_{q_n}]_i + \texttt{damp}[\overline{m}_{q_n}]_{i-1}$, with `damp` being a random number between 0 and 0.2, as the outcome of the i-th iteration.

To compute the strong coupling flavor matching `REvolver` takes as exact the upward relation (at the user-specified loop order)

$$\alpha_s^{(n_\ell+1)}(\mu_n) = \alpha_s^{(n_\ell)}(\mu_n)\left\{1 + \sum_{i=1}\left[\frac{\alpha_s^{(n_\ell)}(\mu_n)}{4\pi}\right]^i \xi_i(n_\ell)\right\}, \tag{A.1}$$

where ξ_i may depend on $\log(\overline{m}_{q_n}/\mu_n)$. This means that the values for $\alpha_s^{(n_\ell)}(\mu_n)$ and $\alpha_s^{(n_\ell+1)}(\mu_n)$ in `REvolver` always satisfy exactly Eq. (A.1). If $\alpha_s^{(n_\ell)}(\mu_n)$ is given, the value of $\alpha_s^{(n_\ell+1)}(\mu_n)$ is computed directly from Eq. (A.1). If, on the contrary, $\alpha_s^{(n_\ell+1)}(\mu_n)$ is given and $\alpha_s^{(n_\ell)}(\mu_n)$ shall be obtained, our program numerically inverts Eq. (A.1) in an iterative way as described in the following. For simplicity we omit the argument μ_n and write $[\alpha^{(n_\ell)}]_k$ for the k-th iteration value. The value at the $(k+1)$-th step the reads

$$[\alpha^{(n_\ell)}]_{k+1} = \frac{\alpha_s^{(n_\ell+1)}(\mu_n)}{1 + \sum_{i=1}\left(\frac{[\alpha^{(n_\ell)}]_k}{4\pi}\right)^i \xi_i(n_\ell)}, \tag{A.2}$$

where for the first iteration $[\alpha^{(n_\ell)}]_{k=0} = \alpha_s^{(n_\ell+1)}(\mu_n)$ is adopted. The algorithm converges very quickly, even for $\alpha_s^{(n_\ell+1)}(\mu_n)$ values as large as 0.69. For smaller values of the strong coupling, and specially if $\mu_n \simeq \overline{m}_{q_n}$, the RHS of Eq. (A.2) is very weakly depending on $\alpha_k^{(n_\ell)}$ (since the 1-loop term is very small or vanishing) and only a few iterations are necessary. If $\alpha_s^{(n_\ell+1)}(\mu_n)$ is larger than 0.69, there is no solution to Eq. (A.1) and the iterative procedure will fail. In those cases the program will return the leading order solution $\alpha_s^{(n_\ell)}(\mu_n) = \alpha_s^{(n_\ell+1)}(\mu_n)$. If the solution exists, the algorithm converges as well, because the slope of the left-hand-side is smaller than unity in absolute value.

[9] The `Core` contains $n_T - n_q$ massless quarks, and the standard running mass of the n-th massive quark is defined with $n_T + n - n_q$ active flavors. In the `Core` the strong coupling and the running masses can be evaluated in a n_f flavor number scheme with $n_T - n_q \le n_f \le n_T$, i.e. for $n_q + 1$ different flavor number schemes.

A.2. Strong coupling

For the QCD β-function at N-loop order (where N is the integer value specified in the variable `runAlpha`), see Eq. (6), the coefficients b_i are defined by

$$\beta^N_{\rm QCD}(\alpha_s) \equiv -\frac{\alpha_s^2}{2\pi}\beta_0\biggl[1+\sum_{i=1}^{N-1}\Bigl(\frac{\alpha_s}{4\pi}\Bigr)^i b_i\biggr], \qquad b_i \equiv \frac{\beta_i}{\beta_0}\,. \tag{A.3}$$

The algorithms implemented in `REvolver` provide solutions for the strong coupling differential equation based on the N-loop β-function that are numerically exact (within the specified precision) and do not involve any additional approximation related to N-loop precision. The associated coefficients c_n^N, which parametrize the associated inverse QCD β-function, are defined by

$$\frac{1}{\beta^N_{\rm QCD}(\alpha_s)} = -\frac{2\pi}{\beta_0}\frac{1}{\alpha_s^2}\biggl[1+\sum_{i=1} c_i^N\Bigl(\frac{\alpha_s}{4\pi}\Bigr)^i\biggr], \tag{A.4}$$

where, except for $N=1$, the sum extends to infinity[10] even though there is a finite limit N in the sum defining $\beta^N_{\rm QCD}$ (for $N=1$ one has $c_i^N=0$ for all $i\geq 1$). The (infinite set of) c_i^N coefficients can be computed in terms of $N-1$ coefficients $b_1,\ldots b_{N-1}$ using the recursive relation shown in Eq. (A.5). The convergence radius of the series is set by the distance from the origin to the nearest pole in the complex plane, which is equivalent to the smallest module of the β-function roots (excluding the double pole at the origin), which are in general complex numbers. Hence the convergence radius depends both on the number of flavors and the loop order N. It increases with the number of flavors and decreases with the loop order N, and in all cases is much larger than any physical value of α_s that may arise in phenomenological applications.

For convenience we define $b_0 = c_0^N = 1$, which allows to write

$$c_{n+1}^N = -\sum_{i=1}^{\min(N-1,n+1)} c_{n+1-i}^N\, b_i\,. \tag{A.5}$$

Many analytic formulae implemented in `REvolver` use the t-variable formalism [6,1] which is based on the definition

$$t = -\frac{2\pi}{\beta_0}\frac{1}{\alpha_s}\,, \tag{A.6}$$

which gives the relation

$$\mathrm{d}\ln(\mu) = -\hat{b}^N(t)\,\mathrm{d}t\,, \tag{A.7}$$

for the renormalization scale μ where

$$\hat{b}^N(t) = -\frac{2\pi}{\beta_0\, t^2\,\beta^N_{\rm QCD}\bigl(-\frac{2\pi}{\beta_0}\frac{1}{t}\bigr)} \equiv 1+\sum_{i=1}\hat{b}_i^N\, t^{-i}\,, \tag{A.8}$$

with $\hat{b}_n^N = (-1)^n c_n^N/(2\beta_0)^n$, which implies $\hat{b}_0^N = 1$.[11] The c_n^N and $\hat{b}_n^N$ coefficients are obtained numerically whenever needed and stored in a member vector (whose length is extended if necessary) such that they are not re-computed again when used later. For the integral of Eq. (A.7) it is useful to define the following polynomial in $1/t$ expressed in terms of $\hat{b}_i^N$:

$$\tilde{G}^N(t) \equiv \int\limits_{-\infty}^{t}\mathrm{d}t'\biggl[\hat{b}^N(t') - 1 - \frac{\hat{b}_1^N}{t'}\biggr] = -\sum_{n=1}\frac{\hat{b}_{n+1}^N}{n}\,t^{-n}\,. \tag{A.9}$$

For $N=1$ one has $\tilde{G}^N(t)=0$ while for $N\geq 2$ the sum in $\tilde{G}^N(t)$ always extends to infinity. The exponential of this expression defines the coefficients g_ℓ^N upon reexpansion in powers of $1/t$, $e^{\tilde{G}^N(t)} \equiv \sum_{\ell=0} g_\ell^N (-t)^{-\ell}$, which can be computed with the recursive relation

$$g_{n+1}^N = \frac{1}{n+1}\sum_{i=0}^{n}(-1)^i\,\hat{b}_{i+2}^N\, g_{n-i}^N\,, \tag{A.10}$$

where $g_0^N = 1$. It is also necessary to define the coefficients that result from expanding $e^{-\tilde{G}^N(t)} \equiv \sum_{\ell=0}\tilde{g}_\ell^N(-t)^{-\ell}$ in an analogous way. They can be computed with a very similar recursive algorithm

$$\tilde{g}_{n+1}^N = -\frac{1}{n+1}\sum_{i=0}^{n}(-1)^i\,\hat{b}_{i+2}^N\,\tilde{g}_{n-i}^N\,, \tag{A.11}$$

[10] The notation where the upper limit of the sum is omitted signifies that the `REvolver` algorithms employ the number of terms mandatory to reach numerical results that are exact within the specified precision. The analogous notation is used for other formulae shown below.

[11] The $\hat{b}_i^N$ should not be confused with the b_i coefficients defined in Eq. (A.3).

where $\tilde{g}_0^N = 1$. Once again one has $g_n^N = \tilde{g}_n^N = 0$ for $n \geq 1$ when $N = 1$. Both g and $\tilde{g}$ coefficients are computed when first needed and then are conveniently stored in member vectors for later use.

The QCD scale $\Lambda_{\rm QCD,t}$ in the t-scheme [1] is defined by

$$\Lambda^N_{\rm QCD,t} = \mu\, e^{G^N(-\frac{2\pi}{\beta_0}\frac{1}{\alpha_s(\mu)})}\,, \tag{A.12}$$

where $G^N(t) = t + \hat{b}_1^N \log(-t) + \tilde{G}^N(t)$ (where we recall that $\hat{b}^N_{i>0} = 0$ if $N = 1$). The summation for the function $\tilde{G}^N$ in Eq. (A.9) is terminated after the relative size of the last term compared to the associated partial sum is smaller than the specified precision. Since in the evaluation of Eq. (A.12) the exact solution of the strong coupling differential equation with N-loop β-function $\beta^N_{\rm QCD}$ (see next section) for $\alpha_s(\mu)$ is used, the numerical value of $\Lambda^N_{\rm QCD}$ does (within the specified precision) not depend on μ. For the evaluation in `REvolver` the value $\mu = 100$ GeV is always used. The values for the QCD scale are computed for each number of active flavors and stored as members of the class. For cases in which α_s is very large, the sum G^N may not converge within the specified precision after adding 200 terms and `REvolver` will return `NaN` (see below why the limit is set to 200). Again, this only happens for unphysical α_s values.

For the QCD scale in the $\overline{\rm MS}$ definition, $\Lambda_{\rm QCD,\overline{MS}}$ (following [23]), we use the formula

$$\Lambda^N_{\rm QCD,\overline{MS}} = 2^{\hat{b}_1^N}\, \Lambda^N_{\rm QCD,t}\,, \tag{A.13}$$

therefore both schemes coincide for $N = 1$.

The algorithm used by `REvolver` to solve the differential equation for the strong coupling is based on variable separation. Defining $\ell_\mu \equiv \log(\mu/\mu_0)$, $\alpha_\mu \equiv \alpha_s(\mu)$, $\alpha_0 \equiv \alpha_s(\mu_0)$ and $a \equiv \alpha_s/(4\pi)$ one can expand $1/\beta^N_{\rm QCD}$ as in Eq. (A.4) and integrate term by term. This gives

$$\ell_\mu = \int_{\alpha_0}^{\alpha_\mu} \frac{{\rm d}\alpha}{\beta^N_{\rm QCD}(\alpha)} = -\frac{1}{2\beta_0}\left[\frac{1}{a_0} - \frac{1}{a_\mu} + c_1^N \log\!\left(\frac{a_\mu}{a_0}\right) + \sum_{i=1} \frac{c^N_{i+1}}{i}(a_\mu^i - a_0^i)\right]. \tag{A.14}$$

where the sum on the RHS is carried out until the last term added is smaller than the specified precision.

We now describe the algorithm to determine a_μ from the algebraic equation (A.14). At leading-log (LL), i.e. using the 1-loop β-function ($N = 1$), one has $\beta_{n>0} = 0$ and the solution is $a_\mu^{\rm LL} = a_0/(1 + 2\beta_0 a_0 \ell_\mu)$. For $N \geq 2$ the LL solution is used to rewrite Eq. (A.14) in the form

$$\frac{1}{a_\mu} = \frac{1}{a_\mu^{\rm LL}} + c_1^N \log\!\left(\frac{a_\mu}{a_0}\right) + \sum_{i=1} \frac{c^N_{i+1}}{i}(a_\mu^i - a_0^i)\,, \tag{A.15}$$

which is solved recursively. In this iterative procedure, the $(n+1)$-th iteration value for the N-loop strong coupling is obtained from the n-th iteration one by the relation

$$[a_\mu]_{n+1} = \frac{1}{\frac{1}{a_\mu^{\rm LL}} + c_1^N \log\!\left(\frac{[a_\mu]_n}{a_0}\right) + \sum_{i=1} \frac{c^N_{i+1}}{i}[([a_\mu]_n)^i - a_0^i]}\,. \tag{A.16}$$

With the initial choice $[a_\mu]_0^N \equiv a_\mu^{\rm LL}$ it is ensured that the correct solution is obtained in all cases. The iterative method converges provided that (i) the solution exists and (ii) the (absolute value of the) slope of the right-hand-side function is smaller than 1. The second condition is always satisfied, and the former will be discussed later in this paragraph. Since $\beta_1 > 0$ we have that $a_\mu^{\rm LL} < a_\mu$, and the solution beyond 1-loop order is approached from below. The iterative procedure is carried out until the numerical value of a_μ does not change within the specified precision, with a maximum allowed number of 200 iterations.

The convergence radius for the infinite sum over c^N_{i+1} in Eq. (A.16) is the same as for the inverse β-function in Eq. (A.4). However, due to technical limitations related to double-precision floating numbers, `REvolver` cannot carry out the sum for α_s values arbitrarily close to the convergence radius within the specified precision. If after adding 200 terms this precision is not met, the recursive procedure to obtain α_s will stop and `NaN` will be returned. This happens for $\alpha_s \gtrsim 0.7$, hence outside the range of any physical application.

A.3. $\overline{\rm MS}$ and RGI masses

The K-loop renormalization group equation (where K is the integer value specified in the variable `runMSbar`) for the $\overline{\rm MS}$ quark mass $\overline{m}_q(\mu)$ has the form

$$\frac{{\rm d}\,\overline{m}_q(\mu)}{{\rm d}\ln(\mu)} = 2\overline{m}_q(\mu)\gamma_m^K(\alpha_s) = 2\overline{m}_q(\mu)\sum_{n=0}^{K-1}\gamma_n\left[\frac{\alpha_s(\mu)}{4\pi}\right]^{n+1}, \tag{A.17}$$

which implies logarithmic scale evolution. The `REvolver` algorithm provides (within the user specified precision) the exact solution of Eq. (A.17) employing the N-loop strong coupling described in Sec. A.2. Changing the integration variable from $\ln(\mu)$ to α_s followed by separation of variables, and using the mass $\overline{m}_q(\mu_0)$ at the scale μ_0 as the initial value, the analytic solution reads

$$\overline{m}_q(\mu) = \overline{m}_q(\mu_0)\exp\!\left[2\int_{\alpha_0}^{\alpha_\mu}{\rm d}\alpha\,\frac{\gamma_m^K(\alpha)}{\beta^N_{\rm QCD}(\alpha)}\right] \equiv \overline{m}_q(\mu_0)\exp\!\left[\tilde{\omega}^{(N,K)}(\mu_0,\mu)\right], \tag{A.18}$$

which defines the running kernel $\tilde{\omega}^{(N,K)}(\mu_0,\mu)$. The `REvolver` algorithm determines $\tilde{\omega}^{(N,K)}(\mu_0,\mu)$ from the Taylor series of the integrand in α where each term is integrated individually. The result can be written in the form [$a_i=\alpha_s(\mu_i)/(4\pi)$]

$$\tilde{\omega}^{(N,K)}(\mu_1,\mu_2)=-\frac{1}{\beta_0}\Bigg[\gamma_0\log\!\left(\frac{a_2}{a_1}\right)+(1-\delta_{N,1}\delta_{K,1})\sum_{n=1}(a_2^n-a_1^n)\,d_n^{(N,K)}\Bigg], \tag{A.19}$$

where the coefficients $d_n^{(N,K)}$, defined for $n>0$, are non-zero if either N or K are larger than 1. We also have $d_n^{(1,K)}=\gamma_n/\beta_0$ if $n<K$ and zero otherwise. They are given by the following expression

$$d_n^{(N,K)}\equiv\frac{1}{n}\sum_{i=0}^{\min(n,K-1)}c_{n-i}^N\,\gamma_i\,, \tag{A.20}$$

where the terms c_i^N arise in the expansion of the inverse β-function (A.4). `REvolver` carries out the sum in Eq. (A.19) until the relative size of the last computed term with respect to the associated partial sum is below the user specified precision. The convergence radius of the infinite sum is the same as for the inverse β-function in Eq. (A.4). In practice, if convergence is found when computing α_s, the sum for the computation of $\tilde{\omega}^{(N,K)}$ is going to be convergent as well. If no convergence is found, `NaN` is returned.

The RGI-mass $\hat{m}_q$ is obtained from the $\overline{\rm MS}$ mass $\overline{m}_q(\mu)$ by removing its scale-dependence writing $\tilde{\omega}^{(N,K)}(\mu_0,\mu)=\tilde{\omega}^{(N,K)}(\mu)-\tilde{\omega}^{(N,K)}(\mu_0)$ with

$$\tilde{\omega}^{(N,K)}(\mu)=-\frac{1}{\beta_0}\Bigg[\gamma_0\log\!\left(\frac{a_\mu}{\pi}\right)+(1-\delta_{N,1}\delta_{K,1})\sum_{n=1}d_n^{(N,K)}a_\mu^n\Bigg]. \tag{A.21}$$

This leads to the definition $\hat{m}_q\equiv\overline{m}_q(\mu)\exp[-\tilde{\omega}(\mu)]$. `REvolver` uses the N-loop exact solution for a_μ and the K-loop solution for $m_q(\mu)$, which ensures that the value obtained for the RGI-mass is μ-independent. In `REvolver` the computation of $\tilde{\omega}(\mu)$ is carried out in the same way as for the $\overline{\rm MS}$ mass explained above. For the numerical calculation μ is set to the standard running mass, $\mu=\overline{m}_q$.

A.4. MSR mass

The M-loop renormalization group equation for the MSR mass $m_q^{\rm MSR}(R)$ (where M is the integer value specified in the variable `runMSR`) has the form

$$\frac{{\rm d}m_q^{\rm MSR}(R)}{{\rm d}\ln(R)}=-R\,\gamma_R^M[\alpha_s(R)]=-R\sum_{n=0}^{M-1}\gamma_n^R\left[\frac{\alpha_s(R)}{4\pi}\right]^{n+1}, \tag{A.22}$$

and implies logarithmic and linear scale dependence. The coefficients γ_n^R are obtained from the series relating the pole and MSR masses using Eq. (3.2) of Ref. [1]. The `REvolver` algorithm provides (within the user specified precision) the exact solution of Eq. (A.22) employing the N-loop strong coupling described in Sec. A.2. In the following we provide details of the algorithm's mathematical derivation.

Switching to the t-variable formalism [6,1] one obtains re-scaled γ_R coefficients:

$$\gamma_R^M\!\left(-\frac{2\pi}{\beta_0}\frac{1}{t}\right)\equiv\sum_{n=0}^{M-1}\tilde{\gamma}_n^R(-t)^{-n-1},\qquad \tilde{\gamma}_n^R=\frac{\gamma_n^R}{(2\beta_0)^{n+1}}\,. \tag{A.23}$$

These can be used to define the series coefficients $S_j^{(N,M)}$ in the expansion of the product function $\gamma_R^M(-\frac{2\pi}{\beta_0}\frac{1}{t})\hat{b}^N(t)e^{-\tilde{G}^N(t)}\equiv\sum_{j=0}S_j^{(N,M)}(-t)^{-j-1}$ in powers of $1/t$, see Sec. A.2. The coefficients have the form

$$S_j^{(N,M)}=\sum_{k=0}^{\min(M-1,j)}\tilde{\gamma}_k^R\sum_{i=0}^{j-k}(-1)^i\,\tilde{b}_i^N\,\tilde{g}_{j-i-k}^N\,, \tag{A.24}$$

which implies that $S_k^{(1,M)}=\tilde{\gamma}_k^R$ for $k<M$ and $S_k^{(1,M)}=0$ for $k\geq M$. The difference of MSR masses at the renormalization scales R_1 and R_2, $\Delta_{\rm MSR}(R_2,R_1)\equiv m_q^{\rm MSR}(R_2)-m_q^{\rm MSR}(R_1)$, can be computed from Eq. (A.22) by integrating over α_s (or t) using the relation $R=\Lambda_{\rm QCD}^N e^{-G^N[-\frac{2\pi}{\beta_0}\frac{1}{\alpha_s^N(R)}]}$

$$\begin{aligned}\Delta_{\rm MSR}^{(M,N)}(R_2,R_1)&=-\Lambda_{\rm QCD}^N\int_{\alpha_1}^{\alpha_2}\frac{{\rm d}\alpha}{\beta^N(\alpha)}e^{-G^N[-\frac{2\pi}{\beta_0}\frac{1}{\alpha}]}\gamma_R^M(\alpha)\\&=\Lambda_{\rm QCD}^N\int_{t_1}^{t_2}{\rm d}t\,\hat{b}^N(t)e^{-\tilde{G}^N(t)}\gamma_R\!\left(-\frac{2\pi}{\beta_0}\frac{1}{t}\right)e^{-t}(-t)^{-\hat{b}_1^N}\\&=\Lambda_{\rm QCD}^N\sum_{j=0}S_j^{(N,M)}\int_{t_1}^{t_2}{\rm d}t\,e^{-t}(-t)^{-1-\hat{b}_1^N-j}\end{aligned} \tag{A.25}$$

$$\equiv \Lambda_{\rm QCD}^N \sum_{j=0} S_j^{(N,M)} [I(\hat{b}_1^N, j, t_2) - I(\hat{b}_1^N, j, t_1)] ,$$

where in the first line we have used $\beta^N(\alpha) \mathrm{d}R = \Lambda_{\rm QCD}^N e^{-G^N\left[-\frac{2\pi}{\beta_0}\frac{1}{\alpha_s^N(R)}\right]} \mathrm{d}\alpha$, in the second we have switched variables to t and in the third we used the definition of the coefficients in Eq. (A.24). Using integration by parts repeatedly one can write $I(\hat{b}_1^N, j, t)$ in terms of $I(\hat{b}_1^N, 0, t)$

$$I(\hat{b}_1^N, j, t) = \frac{1}{(1+\hat{b}_1^N)_j}\left[I(\hat{b}_1^N, 0, t) + e^{-t} \sum_{i=1}^{j} (1+\hat{b}_1^N)_{i-1} (-t)^{-i-\hat{b}_1^N} \right], \tag{A.26}$$

with $(a)_n = \Gamma(a+n)/\Gamma(a)$ being the Pochhammer symbol. The exponential contained in $I(\hat{b}_1^N, 0, t)$ can be expanded in powers of t (with infinite convergence radius) and each term can be integrated separately. In practice, the algorithm computes the difference

$$I(\hat{b}_1^N, 0, t_2) - I(\hat{b}_1^N, 0, t_1) = \sum_{i=0} \frac{1}{i!} \frac{(-t_2)^{i-\hat{b}_1^N} - (-t_1)^{i-\hat{b}_1^N}}{\hat{b}_1^N - i} , \tag{A.27}$$

terminating the infinite sum once the specified precision is achieved, and the result for this difference is saved, such that it needs to be computed only once for each computation of $\Delta_{\rm MSR}^{(M,N)}(R_2, R_1)$. In case $\hat{b}_1^N = 0$ the $i = 0$ term in Eq. (A.27) is replaced by $\ln(t_1/t_2)$. Furthermore, the values of the Pochhammer symbols in the formula Eq. (A.26) are computed only once in one `Core` object and stored for later use. Likewise, since the sum in Eq. (A.26) depends on j only through its upper limit, its value is stored and updated as j grows by one unit.

`REvolver` computes the (infinite) sum over j in Eq. (A.25) by truncating it once the desired precision is achieved. The convergence radius of the j sum coincides with that of the inverse β-function explained in Sec. A.2. So, if convergence is found for the evolution of the strong coupling α_s, the sum in Eq. (A.25) converges as well. If no convergence is found for the sum or for the strong coupling, `NaN` is returned. `REvolver` stores in a member vector the values of $S_j^{(M,N)}$ after they are computed the first time, such that their values can be recycled in later evaluations of R-evolution.

A.5. Asymptotic pole mass coefficients

For the asymptotic formulae for the $\mathcal{O}(\Lambda_{\rm QCD})$ renormalon-dominated perturbative coefficients of the relation between the MSR and pole masses (see Eqs. (2.1) and (2.3) in Ref. [1]), always defined in the flavor number scheme where all massive quarks are integrated out, we use the expression

$$a_n = (2\beta_0)^n \sum_{k=0}^{k_{\max}[n-1]} S_k^{(N,M)} \sum_{\ell=0}^{\ell_{\max}[n-1-k]} g_\ell^N (1+\hat{b}_1^N + k)_{n-1-\ell-k} , \tag{A.28}$$

where

$$\begin{aligned} k_{\max}[m] &= \min[m, M-1] , \\ \ell_{\max}[m] &= \max[\min(m, N-2), 0] . \end{aligned} \tag{A.29}$$

The integers N and M are explained in App. A.2 and A.4. The asymptotic formula (A.28) depends on the number of massless quarks (entering the expressions for the QCD β-function coefficients β_i and the coefficients $S_k^{(N,M)}$ and g_ℓ^N) and was derived in Ref. [1] [see Eq. (4.19) in that reference]. It has the property that it reproduces the exact coefficients a_n up to $\mathcal{O}(\alpha_s^{\min[M,N-1]})$. In contrast to the expression given in Ref. [1], Eq. (A.28) displays concrete truncation prescriptions for the sums as a function of the loop order variables.

A.6. Renormalon sum rule

To extract the pole mass renormalon normalization $N_{1/2}$ from a `Core`, the following formula is used:

$$N_{1/2} = \frac{\beta_0}{2\pi} \sum_{k=0}^{M} \frac{S_k^{(N,M)}}{(1+\hat{b}_1^N)_k} . \tag{A.30}$$

The formula was derived in Ref. [1], and Eq. (A.30) is adapted to account for the optional parameters used in `REvolver`. In analogy to Eq. (A.28), $N_{1/2}$ is always evaluated in the flavor number scheme where all massive quarks are integrated out. The expression for the coefficients $S_k^{(N,M)}$ is given in Eq. (A.24) while b_1^N has been defined in Eq. (A.8).

References

[1] A.H. Hoang, A. Jain, C. Lepenik, V. Mateu, M. Preisser, I. Scimemi, I.W. Stewart, J. High Energy Phys. 04 (2018) 003, https://doi.org/10.1007/JHEP04(2018)003, arXiv:1704.01580.
[2] A.H. Hoang, C. Lepenik, M. Preisser, J. High Energy Phys. 09 (2017) 099, https://doi.org/10.1007/JHEP09(2017)099, arXiv:1706.08526.
[3] M. Beneke, P. Marquard, P. Nason, M. Steinhauser, Phys. Lett. B 775 (2017) 63–70, https://doi.org/10.1016/j.physletb.2017.10.054, arXiv:1605.03609.
[4] K. Chetyrkin, J.H. Kuhn, M. Steinhauser, Comput. Phys. Commun. 133 (2000) 43–65, https://doi.org/10.1016/S0010-4655(00)00155-7, arXiv:hep-ph/0004189.
[5] F. Herren, M. Steinhauser, Comput. Phys. Commun. 224 (2018) 333–345, https://doi.org/10.1016/j.cpc.2017.11.014, arXiv:1703.03751.

[6] A.H. Hoang, A. Jain, I. Scimemi, I.W. Stewart, Phys. Rev. Lett. 101 (2008) 151602, https://doi.org/10.1103/PhysRevLett.101.151602, arXiv:0803.4214.
[7] Wolfram Mathematica, https://www.wolfram.com/mathematica/. (Accessed May 2020).
[8] G. Rossum, Python reference manual, Tech. rep., Amsterdam, The Netherlands, 1995.
[9] SWIG, http://swig.org/. (Accessed May 2020).
[10] T. Kluyver, B. Ragan-Kelley, F. Pérez, B. Granger, M. Bussonnier, J. Frederic, K. Kelley, J. Hamrick, J. Grout, S. Corlay, P. Ivanov, D. Avila, S. Abdalla, C. Willing, J. development team, in: F. Loizides, B. Scmidt (Eds.), Positioning and Power in Academic Publishing: Players, Agents and Agendas, IOS Press, 2016, pp. 87–90, https://eprints.soton.ac.uk/403913/.
[11] Quadpack++, https://github.com/drjerry/quadpackpp. (Accessed January 2021).
[12] P. Marquard, A.V. Smirnov, V.A. Smirnov, M. Steinhauser, D. Wellmann, Phys. Rev. D 94 (7) (2016) 074025, https://doi.org/10.1103/PhysRevD.94.074025, arXiv:1606.06754.
[13] E.G. Floratos, S. Narison, E. de Rafael, Nucl. Phys. B 155 (1979) 115–149, https://doi.org/10.1016/0550-3213(79)90359-6.
[14] A.H. Hoang, Z. Ligeti, A.V. Manohar, Phys. Rev. Lett. 82 (1999) 277–280, https://doi.org/10.1103/PhysRevLett.82.277, arXiv:hep-ph/9809423.
[15] A.H. Hoang, Z. Ligeti, A.V. Manohar, Phys. Rev. D 59 (1999) 074017, https://doi.org/10.1103/PhysRevD.59.074017, arXiv:hep-ph/9811239.
[16] A.H. Hoang, Phys. Rev. D 61 (2000) 034005, https://doi.org/10.1103/PhysRevD.61.034005, arXiv:hep-ph/9905550.
[17] A. Czarnecki, K. Melnikov, N. Uraltsev, Phys. Rev. Lett. 80 (1998) 3189–3192, https://doi.org/10.1103/PhysRevLett.80.3189, arXiv:hep-ph/9708372.
[18] M. Beneke, Phys. Lett. B 434 (1998) 115–125, https://doi.org/10.1016/S0370-2693(98)00741-2, arXiv:hep-ph/9804241.
[19] M. Beneke, Y. Kiyo, K. Schuller, Nucl. Phys. B 714 (2005) 67–90, https://doi.org/10.1016/j.nuclphysb.2005.02.028, arXiv:hep-ph/0501289.
[20] A. Pineda, J. High Energy Phys. 06 (2001) 022, https://doi.org/10.1088/1126-6708/2001/06/022, arXiv:hep-ph/0105008.
[21] M. Fael, K. Schönwald, M. Steinhauser, Phys. Rev. Lett. 125 (5) (2020) 052003, https://doi.org/10.1103/PhysRevLett.125.052003, arXiv:2005.06487.
[22] M. Fael, K. Schönwald, M. Steinhauser, Phys. Rev. D 103 (1) (2021) 014005, https://doi.org/10.1103/PhysRevD.103.014005, arXiv:2011.11655.
[23] P. Zyla, et al., Prog. Theor. Exp. Phys. 2020 (8) (2020) 083C01, https://doi.org/10.1093/ptep/ptaa104.
[24] V. Khachatryan, et al., J. High Energy Phys. 03 (2017) 156, https://doi.org/10.1007/JHEP03(2017)156, arXiv:1609.05331.
[25] M. Beneke, M. Jamin, J. High Energy Phys. 09 (2008) 044, https://doi.org/10.1088/1126-6708/2008/09/044, arXiv:0806.3156.
[26] D. Boito, M. Jamin, R. Miravitllas, Phys. Rev. Lett. 117 (15) (2016) 152001, https://doi.org/10.1103/PhysRevLett.117.152001, arXiv:1606.06175.
[27] M. Aaboud, et al., Eur. Phys. J. C 77 (12) (2017) 872, https://doi.org/10.1140/epjc/s10052-017-5442-0, arXiv:1707.02562.
[28] C. Duhr, F. Dulat, V. Hirschi, B. Mistlberger, J. High Energy Phys. 08 (08) (2020) 017, https://doi.org/10.1007/JHEP08(2020)017, arXiv:2004.04752.
[29] P. Marquard, A.V. Smirnov, V.A. Smirnov, M. Steinhauser, Phys. Rev. Lett. 114 (14) (2015) 142002, https://doi.org/10.1103/PhysRevLett.114.142002, arXiv:1502.01030.
[30] C. Peset, A. Pineda, J. Segovia, J. High Energy Phys. 09 (2018) 167, https://doi.org/10.1007/JHEP09(2018)167, arXiv:1806.05197.
[31] I.I.Y. Bigi, M.A. Shifman, N.G. Uraltsev, A.I. Vainshtein, Phys. Rev. D 50 (1994) 2234–2246, https://doi.org/10.1103/PhysRevD.50.2234, arXiv:hep-ph/9402360.
[32] M. Beneke, V.M. Braun, Nucl. Phys. B 426 (1994) 301–343, https://doi.org/10.1016/0550-3213(94)90314-X, arXiv:hep-ph/9402364.
[33] D. Boito, M. Golterman, A. Keshavarzi, K. Maltman, D. Nomura, S. Peris, T. Teubner, Phys. Rev. D 98 (7) (2018) 074030, https://doi.org/10.1103/PhysRevD.98.074030, arXiv:1805.08176.
[34] P.A. Baikov, K.G. Chetyrkin, J.H. Kuhn, Phys. Rev. Lett. 101 (2008) 012002, https://doi.org/10.1103/PhysRevLett.101.012002, arXiv:0801.1821.
[35] M. Bruno, M. Dalla Brida, P. Fritzsch, T. Korzec, A. Ramos, S. Schaefer, H. Simma, S. Sint, R. Sommer, PoS LATTICE2016 (2016) 197, https://doi.org/10.22323/1.256.0197, arXiv:1701.03075.
[36] M. Butenschoen, B. Dehnadi, A.H. Hoang, V. Mateu, M. Preisser, I.W. Stewart, Phys. Rev. Lett. 117 (23) (2016) 232001, https://doi.org/10.1103/PhysRevLett.117.232001, arXiv:1608.01318.
[37] A.H. Hoang, A.V. Manohar, Phys. Lett. B 483 (2000) 94–98, https://doi.org/10.1016/S0370-2693(00)00595-5, arXiv:hep-ph/9911461.
[38] S. Bekavac, A. Grozin, D. Seidel, M. Steinhauser, J. High Energy Phys. 10 (2007) 006, https://doi.org/10.1088/1126-6708/2007/10/006, arXiv:0708.1729.
[39] O.V. Tarasov, A.A. Vladimirov, A.Y. Zharkov, Phys. Lett. B 93 (1980) 429–432.
[40] S.A. Larin, J.A.M. Vermaseren, Phys. Lett. B 303 (1993) 334–336, arXiv:hep-ph/9302208.
[41] T. van Ritbergen, J.A.M. Vermaseren, S.A. Larin, Phys. Lett. B 400 (1997) 379–384, https://doi.org/10.1016/S0370-2693(97)00370-5, arXiv:hep-ph/9701390.
[42] M. Czakon, Nucl. Phys. B 710 (2005) 485–498, https://doi.org/10.1016/j.nuclphysb.2005.01.012, arXiv:hep-ph/0411261.
[43] P.A. Baikov, K.G. Chetyrkin, J.H. Kühn, Phys. Rev. Lett. 118 (8) (2017) 082002, https://doi.org/10.1103/PhysRevLett.118.082002, arXiv:1606.08659.
[44] K.G. Chetyrkin, G. Falcioni, F. Herzog, J.A.M. Vermaseren, J. High Energy Phys. 10 (2017) 179, https://doi.org/10.1007/JHEP10(2017)179, Addendum, J. High Energy Phys. 12 (2017) 006, arXiv:1709.08541.
[45] T. Luthe, A. Maier, P. Marquard, Y. Schröder, J. High Energy Phys. 10 (2017) 166, https://doi.org/10.1007/JHEP10(2017)166, arXiv:1709.07718.
[46] F. Herzog, B. Ruijl, T. Ueda, J.A.M. Vermaseren, A. Vogt, J. High Energy Phys. 02 (2017) 090, https://doi.org/10.1007/JHEP02(2017)090, arXiv:1701.01404.
[47] K.G. Chetyrkin, B.A. Kniehl, M. Steinhauser, Nucl. Phys. B 510 (1998) 61–87, https://doi.org/10.1016/S0550-3213(98)81004-3, arXiv:hep-ph/9708255.
[48] K.G. Chetyrkin, J.H. Kühn, C. Sturm, Nucl. Phys. B 744 (2006) 121–135, https://doi.org/10.1016/j.nuclphysb.2006.03.020, arXiv:hep-ph/0512060.
[49] Y. Schröder, M. Steinhauser, J. High Energy Phys. 01 (2006) 051, https://doi.org/10.1088/1126-6708/2006/01/051, arXiv:hep-ph/0512058.
[50] B.A. Kniehl, A.V. Kotikov, A.I. Onishchenko, O.L. Veretin, Phys. Rev. Lett. 97 (2006) 042001, https://doi.org/10.1103/PhysRevLett.97.042001, arXiv:hep-ph/0607202.
[51] R. Tarrach, Nucl. Phys. B 183 (1981) 384–396, https://doi.org/10.1016/0550-3213(81)90140-1.
[52] N. Gray, D.J. Broadhurst, W. Grafe, K. Schilcher, Z. Phys. C 48 (1990) 673–680, https://doi.org/10.1007/BF01614703.
[53] K. Melnikov, T.v. Ritbergen, Phys. Lett. B 482 (2000) 99–108, https://doi.org/10.1016/S0370-2693(00)00507-4, arXiv:hep-ph/9912391.
[54] M. Fael, K. Schönwald, M. Steinhauser, J. High Energy Phys. 10 (2020) 087, https://doi.org/10.1007/JHEP10(2020)087, arXiv:2008.01102.
[55] J.A.M. Vermaseren, S.A. Larin, T. van Ritbergen, Phys. Lett. B 405 (1997) 327–333, https://doi.org/10.1016/S0370-2693(97)00660-6, arXiv:hep-ph/9703284.
[56] K.G. Chetyrkin, Phys. Lett. B 404 (1997) 161–165, https://doi.org/10.1016/S0370-2693(97)00535-2, arXiv:hep-ph/9703278.
[57] P.A. Baikov, K.G. Chetyrkin, J.H. Kühn, J. High Energy Phys. 10 (2014) 076, https://doi.org/10.1007/JHEP10(2014)076, arXiv:1402.6611.
[58] T. Luthe, A. Maier, P. Marquard, Y. Schröder, J. High Energy Phys. 01 (2017) 081, https://doi.org/10.1007/JHEP01(2017)081, arXiv:1612.05512.
[59] T. Liu, M. Steinhauser, Phys. Lett. B 746 (2015) 330–334, https://doi.org/10.1016/j.physletb.2015.05.023, arXiv:1502.04719.
[60] V. Mateu, P.G. Ortega, J. High Energy Phys. 01 (2018) 122, https://doi.org/10.1007/JHEP01(2018)122, arXiv:1711.05755.
[61] Y. Kiyo, Y. Sumino, Nucl. Phys. B 889 (2014) 156–191, https://doi.org/10.1016/j.nuclphysb.2014.10.010, arXiv:1408.5590.
[62] N. Brambilla, Y. Sumino, A. Vairo, Phys. Rev. D 65 (2002) 034001, https://doi.org/10.1103/PhysRevD.65.034001, arXiv:hep-ph/0108084.
[63] A.A. Penin, M. Steinhauser, Phys. Lett. B 538 (2002) 335–345, https://doi.org/10.1016/S0370-2693(02)02040-3, arXiv:hep-ph/0204290.
[64] Y. Kiyo, Y. Sumino, Phys. Lett. B 730 (2014) 76–80, https://doi.org/10.1016/j.physletb.2014.01.030, arXiv:1309.6571.
[65] W. Fischler, Nucl. Phys. B 129 (1977) 157–174, https://doi.org/10.1016/0550-3213(77)90026-8.
[66] A. Billoire, Phys. Lett. B 92 (1980) 343–347, https://doi.org/10.1016/0370-2693(80)90279-8.
[67] Y. Schroder, Phys. Lett. B 447 (1999) 321–326, https://doi.org/10.1016/S0370-2693(99)00010-6, arXiv:hep-ph/9812205.
[68] A.V. Smirnov, V.A. Smirnov, M. Steinhauser, Phys. Lett. B 668 (2008) 293–298, https://doi.org/10.1016/j.physletb.2008.08.070, arXiv:0809.1927.
[69] A.V. Smirnov, V.A. Smirnov, M. Steinhauser, Phys. Rev. Lett. 104 (2010) 112002, https://doi.org/10.1103/PhysRevLett.104.112002, arXiv:0911.4742.
[70] C. Anzai, Y. Kiyo, Y. Sumino, Phys. Rev. Lett. 104 (2010) 112003, https://doi.org/10.1103/PhysRevLett.104.112003, arXiv:0911.4335.
[71] R.N. Lee, A.V. Smirnov, V.A. Smirnov, M. Steinhauser, Phys. Rev. D 94 (5) (2016) 054029, https://doi.org/10.1103/PhysRevD.94.054029, arXiv:1608.02603.
[72] D. Eiras, J. Soto, Phys. Lett. B 491 (2000) 101–110, https://doi.org/10.1016/S0370-2693(00)01004-2, arXiv:hep-ph/0005066.
[73] A.H. Hoang, Bottom quark mass from Upsilon mesons: Charm mass effects, arXiv:hep-ph/0008102, 2000.
[74] M. Beneke, A. Maier, J. Piclum, T. Rauh, Nucl. Phys. B 891 (2015) 42–72, https://doi.org/10.1016/j.nuclphysb.2014.12.001, arXiv:1411.3132.

Bibliography

[1] P. A. Dirac, *The quantum theory of the electron*, *Proc. Roy. Soc. Lond. A* **A117** (1928) 610–624.

[2] C. D. Anderson, *The Apparent Existence of Easily Deflectable Positives*, *Science* **76** (1932) 238–239.

[3] H. Yukawa, *On the Interaction of Elementary Particles I*, *Proc. Phys. Math. Soc. Jap.* **17** (1935) 48–57.

[4] C. Lattes, G. Occhialini and C. Powell, *Observations on the Tracks of Slow Mesons in Photographic Emulsions. 1*, *Nature* **160** (1947) 453–456.

[5] W. Pauli, *Dear radioactive ladies and gentlemen*, *Phys. Today* **31N9** (1978) 27.

[6] F. Reines and C. L. Cowan, *The neutrino*, *Nature* **178** (1956) 446–449.

[7] M. Gell-Mann, *A Schematic Model of Baryons and Mesons*, *Phys. Lett.* **8** (1964) 214–215.

[8] G. Zweig, *An SU(3) model for strong interaction symmetry and its breaking. Version 1*, .

[9] E. D. Bloom et al., *High-Energy Inelastic e p Scattering at 6-Degrees and 10-Degrees*, *Phys. Rev. Lett.* **23** (1969) 930–934.

[10] S. Weinberg, *A Model of Leptons*, *Phys. Rev. Lett.* **19** (1967) 1264–1266.

[11] UA1 collaboration, G. Arnison et al., *Experimental Observation of Lepton Pairs of Invariant Mass Around 95-GeV/c**2 at the CERN SPS Collider*, *Phys. Lett. B* **126** (1983) 398–410.

[12] ATLAS collaboration, G. Aad et al., *Observation of a new particle in the search for the Standard Model Higgs boson with the ATLAS detector at the LHC*, *Phys. Lett. B* **716** (2012) 1–29, [1207.7214].

[13] P. W. Higgs, *Broken Symmetries and the Masses of Gauge Bosons*, *Phys. Rev. Lett.* **13** (1964) 508–509.

[14] F. Englert and R. Brout, *Broken Symmetry and the Mass of Gauge Vector Mesons*, *Phys. Rev. Lett.* **13** (1964) 321–323.

[15] K. G. Chetyrkin and F. V. Tkachov, *Integration by Parts: The Algorithm to Calculate beta Functions in 4 Loops*, *Nucl. Phys.* **B192** (1981) 159–204.

[16] F. V. Tkachov, *A Theorem on Analytical Calculability of Four Loop Renormalization Group Functions*, *Phys. Lett.* **100B** (1981) 65–68.

[17] S. Laporta, *High precision calculation of multiloop Feynman integrals by difference equations*, *Int. J. Mod. Phys.* **A15** (2000) 5087–5159, [hep-ph/0102033].

[18] C. Anastasiou and A. Lazopoulos, *Automatic integral reduction for higher order perturbative calculations*, *JHEP* **07** (2004) 046, [hep-ph/0404258].

[19] A. Smirnov and F. Chuharev, *FIRE6: Feynman Integral REduction with Modular Arithmetic*, 1901.07808.

[20] J. Klappert, F. Lange, P. Maierhöfer and J. Usovitsch, *Integral Reduction with Kira 2.0 and Finite Field Methods*, 2008.06494.

[21] A. von Manteuffel and C. Studerus, *Reduze 2 - Distributed Feynman Integral Reduction*, 1201.4330.

[22] R. N. Lee, *LiteRed 1.4: a powerful tool for reduction of multiloop integrals*, *J. Phys. Conf. Ser.* **523** (2014) 012059, [1310.1145].

[23] V. A. Smirnov, *Analytic tools for Feynman integrals*, vol. 250. Springer, 2012, 10.1007/978-3-642-34886-0.

[24] H. Cheng and T. T. Wu, *Expanding protons: Scattering at high energies*. MIT Press, 1987.

[25] A. V. Kotikov, *Differential equations method: New technique for massive Feynman diagrams calculation*, *Phys. Lett.* **B254** (1991) 158–164.

[26] A. V. Kotikov, *Differential equations method: The Calculation of vertex type Feynman diagrams*, *Phys. Lett.* **B259** (1991) 314–322.

[27] A. V. Kotikov, *Differential equation method: The Calculation of N point Feynman diagrams*, *Phys. Lett.* **B267** (1991) 123–127.

[28] J. M. Henn, *Multiloop integrals in dimensional regularization made simple*, *Phys. Rev. Lett.* **110** (2013) 251601, [1304.1806].

[29] O. Gituliar and V. Magerya, *Fuchsia and master integrals for splitting functions from differential equations in QCD*, *PoS* **LL2016** (2016) 030, [1607.00759].

[30] O. Gituliar and V. Magerya, *Fuchsia: a tool for reducing differential equations for Feynman master integrals to epsilon form*, *Comput. Phys. Commun.* **219** (2017) 329–338, [1701.04269].

[31] M. Prausa, *epsilon: A tool to find a canonical basis of master integrals*, *Comput. Phys. Commun.* **219** (2017) 361–376, [1701.00725].

[32] J. M. Henn, *Lectures on differential equations for Feynman integrals*, *J. Phys. A* **48** (2015) 153001, [1412.2296].

[33] K. Hepp, *Proof of the Bogolyubov-Parasiuk theorem on renormalization*, *Commun. Math. Phys.* **2** (1966) 301–326.

[34] E. Speer, *Mass Singularities of Generic Feynman Amplitudes*, *Ann. Inst. H. Poincare Phys. Theor.* **26** (1977) 87–105.

[35] T. Binoth and G. Heinrich, *An automatized algorithm to compute infrared divergent multiloop integrals*, *Nucl. Phys.* **B585** (2000) 741–759, [hep-ph/0004013].

[36] A. V. Smirnov, *FIESTA4: Optimized Feynman integral calculations with GPU support*, *Comput. Phys. Commun.* **204** (2016) 189–199, [1511.03614].

[37] S. Borowka, G. Heinrich, S. Jahn, S. Jones, M. Kerner, J. Schlenk et al., *pySecDec: a toolbox for the numerical evaluation of multi-scale integrals*, *Comput. Phys. Commun.* **222** (2018) 313–326, [1703.09692].

[38] A. V. Manohar, *Introduction to Effective Field Theories*, in *Les Houches summer school: EFT in Particle Physics and Cosmology*, 4, 2018. 1804.05863.

[39] A. Pich, *Effective field theory: Course*, in *Les Houches Summer School in Theoretical Physics, Session 68: Probing the Standard Model of Particle Interactions*, pp. 949–1049, 6, 1998. hep-ph/9806303.

[40] M. Neubert, *Les Houches Lectures on Renormalization Theory and Effective Field Theories*, in *Les Houches summer school: EFT in Particle Physics and Cosmology*, 1, 2019. 1901.06573.

[41] S. Weinberg, *Phenomenological Lagrangians*, *Physica A* **96** (1979) 327–340.

[42] J. Gasser and H. Leutwyler, *Chiral Perturbation Theory: Expansions in the Mass of the Strange Quark*, *Nucl. Phys. B* **250** (1985) 465–516.

[43] W. Buchmuller and D. Wyler, *Effective Lagrangian Analysis of New Interactions and Flavor Conservation*, *Nucl. Phys. B* **268** (1986) 621–653.

[44] I. Brivio and M. Trott, *The Standard Model as an Effective Field Theory*, *Phys. Rept.* **793** (2019) 1–98, [1706.08945].

[45] T. Appelquist and J. Carazzone, *Infrared Singularities and Massive Fields*, *Phys. Rev. D* **11** (1975) 2856.

[46] H. Georgi, *Effective field theory*, *Ann. Rev. Nucl. Part. Sci.* **43** (1993) 209–252.

[47] R. Abbate, M. Fickinger, A. H. Hoang, V. Mateu and I. W. Stewart, *Thrust at N^3LL with Power Corrections and a Precision Global Fit for alphas(mZ)*, *Phys. Rev. D* **83** (2011) 074021, [1006.3080].

[48] Y.-T. Chien and M. D. Schwartz, *Resummation of heavy jet mass and comparison to LEP data*, *JHEP* **08** (2010) 058, [1005.1644].

[49] Particle Data Group collaboration, P. Zyla et al., *Review of Particle Physics*, *PTEP* **2020** (2020) 083C01.

[50] F. Bezrukov, M. Y. Kalmykov, B. A. Kniehl and M. Shaposhnikov, *Higgs Boson Mass and New Physics*, *JHEP* **10** (2012) 140, [1205.2893].

[51] G. Degrassi, S. Di Vita, J. Elias-Miro, J. R. Espinosa, G. F. Giudice, G. Isidori et al., *Higgs mass and vacuum stability in the Standard Model at NNLO*, *JHEP* **08** (2012) 098, [1205.6497].

[52] S. Alekhin, A. Djouadi and S. Moch, *The top quark and Higgs boson masses and the stability of the electroweak vacuum*, *Phys. Lett. B* **716** (2012) 214–219, [1207.0980].

[53] ALEPH, DELPHI, L3, OPAL, LEP Electroweak collaboration, S. Schael et al., *Electroweak Measurements in Electron-Positron Collisions at W-Boson-Pair Energies at LEP*, *Phys. Rept.* **532** (2013) 119–244, [1302.3415].

[54] M. Ciuchini, E. Franco, S. Mishima and L. Silvestrini, *Electroweak Precision Observables, New Physics and the Nature of a 126 GeV Higgs Boson*, *JHEP* **08** (2013) 106, [1306.4644].

[55] A. Manohar and H. Georgi, *Chiral Quarks and the Nonrelativistic Quark Model*, *Nucl. Phys. B* **234** (1984) 189–212.

[56] G. Colangelo, S. Lanz, H. Leutwyler and E. Passemar, *Dispersive analysis of $\eta \to 3\pi$*, *Eur. Phys. J. C* **78** (2018) 947, [1807.11937].

[57] Flavour Lattice Averaging Group collaboration, S. Aoki et al., *FLAG Review 2019: Flavour Lattice Averaging Group (FLAG)*, *Eur. Phys. J. C* **80** (2020) 113, [1902.08191].

[58] E. Braaten, S. Narison and A. Pich, *QCD analysis of the tau hadronic width*, *Nucl. Phys. B* **373** (1992) 581–612.

[59] N. Isgur and M. B. Wise, *Weak Decays of Heavy Mesons in the Static Quark Approximation*, *Phys. Lett. B* **232** (1989) 113–117.

[60] N. Isgur and M. B. Wise, *WEAK TRANSITION FORM-FACTORS BETWEEN HEAVY MESONS*, *Phys. Lett. B* **237** (1990) 527–530.

[61] G. T. Bodwin, E. Braaten and G. Lepage, *Rigorous QCD analysis of inclusive annihilation and production of heavy quarkonium*, *Phys. Rev. D* **51** (1995) 1125–1171, [hep-ph/9407339].

[62] B. Dehnadi, A. H. Hoang and V. Mateu, *Bottom and Charm Mass Determinations with a Convergence Test*, *JHEP* **08** (2015) 155, [1504.07638].

[63] W. E. Caswell and G. P. Lepage, *Effective Lagrangians for Bound State Problems in QED, QCD, and Other Field Theories*, *Phys. Lett. B* **167** (1986) 437–442.

[64] A. H. Hoang, Z. Ligeti and A. V. Manohar, *B decay and the Upsilon mass*, *Phys. Rev. Lett.* **82** (1999) 277–280, [hep-ph/9809423].

[65] A. H. Hoang, Z. Ligeti and A. V. Manohar, *B decays in the upsilon expansion*, *Phys. Rev. D* **59** (1999) 074017, [hep-ph/9811239].

[66] A. Hoang, *1S and MS-bar bottom quark masses from Upsilon sum rules*, *Phys. Rev. D* **61** (2000) 034005, [hep-ph/9905550].

[67] M. Beneke and V. M. Braun, *Heavy quark effective theory beyond perturbation theory: Renormalons, the pole mass and the residual mass term*, *Nucl. Phys. B* **426** (1994) 301–343, [hep-ph/9402364].

[68] A. Pineda, *Determination of the bottom quark mass from the Upsilon(1S) system*, *JHEP* **06** (2001) 022, [hep-ph/0105008].

[69] I. I. Bigi, M. A. Shifman, N. Uraltsev and A. I. Vainshtein, *High power n of m(b) in beauty widths and n=5 —¿ infinity limit*, *Phys. Rev. D* **56** (1997) 4017–4030, [hep-ph/9704245].

[70] M. Fael, K. Schönwald and M. Steinhauser, *The Kinetic Heavy Quark Mass to Three Loops*, *Phys. Rev. Lett.* **125** (2020) 052003, [2005.06487].

[71] A. H. Hoang, A. Jain, I. Scimemi and I. W. Stewart, *Infrared Renormalization Group Flow for Heavy Quark Masses*, *Phys. Rev. Lett.* **101** (2008) 151602, [0803.4214].

[72] A. H. Hoang, A. Jain, C. Lepenik, V. Mateu, M. Preisser, I. Scimemi et al., *The MSR mass and the $\mathcal{O}(\Lambda_{\rm QCD})$ renormalon sum rule*, *JHEP* **04** (2018) 003, [1704.01580].

[73] A. H. Hoang, C. Lepenik and M. Preisser, *On the Light Massive Flavor Dependence of the Large Order Asymptotic Behavior and the Ambiguity of the Pole Mass*, *JHEP* **09** (2017) 099, [1706.08526].

[74] I. I. Bigi, M. A. Shifman, N. Uraltsev and A. Vainshtein, *The Pole mass of the heavy quark. Perturbation theory and beyond*, *Phys. Rev. D* **50** (1994) 2234–2246, [hep-ph/9402360].

[75] M. Beneke, *Renormalons*, *Phys. Rept.* **317** (1999) 1–142, [hep-ph/9807443].

[76] R. Tarrach, *The Pole Mass in Perturbative QCD*, *Nucl. Phys. B* **183** (1981) 384–396.

[77] N. Gray, D. J. Broadhurst, W. Grafe and K. Schilcher, *Three Loop Relation of Quark (Modified) Ms and Pole Masses*, *Z. Phys. C* **48** (1990) 673–680.

[78] K. Chetyrkin and M. Steinhauser, *Short distance mass of a heavy quark at order α_s^3*, *Phys. Rev. Lett.* **83** (1999) 4001–4004, [hep-ph/9907509].

[79] K. Chetyrkin and M. Steinhauser, *The Relation between the MS-bar and the on-shell quark mass at order alpha(s)**3*, *Nucl. Phys. B* **573** (2000) 617–651, [hep-ph/9911434].

[80] K. Melnikov and T. v. Ritbergen, *The Three loop relation between the MS-bar and the pole quark masses*, *Phys. Lett. B* **482** (2000) 99–108, [hep-ph/9912391].

[81] P. Marquard, L. Mihaila, J. Piclum and M. Steinhauser, *Relation between the pole and the minimally subtracted mass in dimensional regularization and dimensional reduction to three-loop order*, *Nucl. Phys. B* **773** (2007) 1–18, [hep-ph/0702185].

[82] P. Marquard, A. V. Smirnov, V. A. Smirnov and M. Steinhauser, *Quark Mass Relations to Four-Loop Order in Perturbative QCD*, *Phys. Rev. Lett.* **114** (2015) 142002, [1502.01030].

[83] P. Marquard, A. V. Smirnov, V. A. Smirnov, M. Steinhauser and D. Wellmann, $\overline{\text{MS}}$*-on-shell quark mass relation up to four loops in QCD and a general $SU(N)$ gauge group*, *Phys. Rev. D* **94** (2016) 074025, [1606.06754].

[84] M. Dasgupta and G. P. Salam, *Event shapes in e+ e- annihilation and deep inelastic scattering*, *J. Phys. G* **30** (2004) R143, [hep-ph/0312283].

[85] S. Kluth, *Tests of Quantum Chromo Dynamics at e+ e- Colliders*, *Rept. Prog. Phys.* **69** (2006) 1771–1846, [hep-ex/0603011].

[86] A. Banfi, G. P. Salam and G. Zanderighi, *Resummed event shapes at hadron - hadron colliders*, *JHEP* **08** (2004) 062, [hep-ph/0407287].

[87] A. Banfi, G. P. Salam and G. Zanderighi, *Phenomenology of event shapes at hadron colliders*, *JHEP* **06** (2010) 038, [1001.4082].

[88] E. Farhi, *A QCD Test for Jets*, *Phys. Rev. Lett.* **39** (1977) 1587–1588.

[89] S. Brandt, C. Peyrou, R. Sosnowski and A. Wroblewski, *The Principal axis of jets. An Attempt to analyze high-energy collisions as two-body processes*, *Phys. Lett.* **12** (1964) 57–61.

[90] L. Clavelli, *Jet Invariant Mass in Quantum Chromodynamics*, *Phys. Lett. B* **85** (1979) 111–114.

[91] T. Chandramohan and L. Clavelli, *Consequences of Second Order QCD for Jet Structure in e^+e^- Annihilation*, *Nucl. Phys. B* **184** (1981) 365–380.

[92] L. Clavelli and D. Wyler, *Kinematical Bounds on Jet Variables and the Heavy Jet Mass Distribution*, *Phys. Lett. B* **103** (1981) 383–387.

[93] R. K. Ellis, D. A. Ross and A. E. Terrano, *The Perturbative Calculation of Jet Structure in e+ e- Annihilation*, *Nucl. Phys. B* **178** (1981) 421–456.

[94] P. E. L. Rakow and B. R. Webber, *Transverse Momentum Moments of Hadron Distributions in QCD Jets*, *Nucl. Phys. B* **191** (1981) 63–74.

[95] C. W. Bauer, S. Fleming, D. Pirjol and I. W. Stewart, *An Effective field theory for collinear and soft gluons: Heavy to light decays*, *Phys. Rev.* **D63** (2001) 114020, [hep-ph/0011336].

[96] C. W. Bauer, D. Pirjol and I. W. Stewart, *Soft collinear factorization in effective field theory*, *Phys. Rev.* **D65** (2002) 054022, [hep-ph/0109045].

[97] C. W. Bauer and I. W. Stewart, *Invariant operators in collinear effective theory*, *Phys. Lett.* **B516** (2001) 134–142, [hep-ph/0107001].

[98] S. Fleming, A. H. Hoang, S. Mantry and I. W. Stewart, *Jets from massive unstable particles: Top-mass determination*, *Phys. Rev.* **D77** (2008) 074010, [hep-ph/0703207].

[99] S. Fleming, A. H. Hoang, S. Mantry and I. W. Stewart, *Top Jets in the Peak Region: Factorization Analysis with NLL Resummation*, *Phys. Rev.* **D77** (2008) 114003, [0711.2079].

[100] M. A. G. Aivazis, J. C. Collins, F. I. Olness and W.-K. Tung, *Leptoproduction of heavy quarks. 2. A Unified QCD formulation of charged and neutral current processes from fixed target to collider energies*, *Phys. Rev. D* **50** (1994) 3102–3118, [hep-ph/9312319].

[101] M. A. G. Aivazis, F. I. Olness and W.-K. Tung, *Leptoproduction of heavy quarks. 1. General formalism and kinematics of charged current and neutral current production processes*, *Phys. Rev. D* **50** (1994) 3085–3101, [hep-ph/9312318].

[102] S. Gritschacher, A. H. Hoang, I. Jemos and P. Pietrulewicz, *Secondary Heavy Quark Production in Jets through Mass Modes*, *Phys. Rev.* **D88** (2013) 034021, [1302.4743].

[103] P. Pietrulewicz, S. Gritschacher, A. H. Hoang, I. Jemos and V. Mateu, *Variable Flavor Number Scheme for Final State Jets in Thrust*, *Phys. Rev.* **D90** (2014) 114001, [1405.4860].

[104] B. Dehnadi, *Heavy quark mass determinations with sum rules and jets*. PhD thesis, Vienna U., 2016. 10.25365/thesis.42936.

[105] P. Pietrulewicz, *Variable flavor scheme for final state jets*. PhD thesis, Vienna U., 2014. 10.25365/thesis.34439.

[106] P. Nason and C. Oleari, *Next-to-leading order corrections to the production of heavy flavor jets in e+ e- collisions*, *Nucl. Phys. B* **521** (1998) 237–273, [hep-ph/9709360].

[107] W. Bernreuther, A. Brandenburg and P. Uwer, *Next-to-leading order QCD corrections to three jet cross-sections with massive quarks*, *Phys. Rev. Lett.* **79** (1997) 189–192, [hep-ph/9703305].

[108] G. Rodrigo, M. S. Bilenky and A. Santamaria, *Quark mass effects for jet production in e+ e- collisions at the next-to-leading order: Results and applications*, *Nucl. Phys. B* **554** (1999) 257–297, [hep-ph/9905276].

[109] G. Salam and D. Wicke, *Hadron masses and power corrections to event shapes*, *JHEP* **05** (2001) 061, [hep-ph/0102343].

[110] V. Mateu, I. W. Stewart and J. Thaler, *Power Corrections to Event Shapes with Mass-Dependent Operators*, *Phys. Rev. D* **87** (2013) 014025, [1209.3781].

[111] M. Preisser, *Jet shapes with massive quarks for e^+e^--annihilation*. PhD thesis, Vienna U., 2018.

[112] A. Bris, V. Mateu and M. Preisser, *Massive event-shape distributions at N^2LL*, *JHEP* **09** (2020) 132, [2006.06383].

[113] E. Lunghi, D. Pirjol and D. Wyler, *Factorization in leptonic radiative $B \to \gamma e \nu$ decays*, *Nucl. Phys.* **B649** (2003) 349–364, [hep-ph/0210091].

[114] T. Becher and M. Neubert, *Toward a NNLO calculation of the $\bar{B} \to X_s\gamma$ decay rate with a cut on photon energy. II. Two-loop result for the jet function*, *Phys. Lett.* **B637** (2006) 251–259, [hep-ph/0603140].

[115] R. Brüser, Z. L. Liu and M. Stahlhofen, *Three-Loop Quark Jet Function*, *Phys. Rev. Lett.* **121** (2018) 072003, [1804.09722].

[116] A. Jain, I. Scimemi and I. W. Stewart, *Two-loop Jet-Function and Jet-Mass for Top Quarks*, *Phys. Rev.* **D77** (2008) 094008, [0801.0743].

[117] C. W. Bauer, F. J. Tackmann, J. R. Walsh and S. Zuberi, *Factorization and Resummation for Dijet Invariant Mass Spectra*, *Phys. Rev.* **D85** (2012) 074006, [1106.6047].

[118] M. Procura, W. J. Waalewijn and L. Zeune, *Resummation of Double-Differential Cross Sections and Fully-Unintegrated Parton Distribution Functions*, *JHEP* **02** (2015) 117, [1410.6483].

[119] A. V. Manohar and I. W. Stewart, *The Zero-Bin and Mode Factorization in Quantum Field Theory*, *Phys. Rev.* **D76** (2007) 074002, [hep-ph/0605001].

[120] A. H. Hoang, P. Pietrulewicz and D. Samitz, *Variable Flavor Number Scheme for Final State Jets in DIS*, *Phys. Rev.* **D93** (2016) 034034, [1508.04323].

[121] P. Pietrulewicz, D. Samitz, A. Spiering and F. J. Tackmann, *Factorization and Resummation for Massive Quark Effects in Exclusive Drell-Yan*, *JHEP* **08** (2017) 114, [1703.09702].

[122] J.-y. Chiu, A. Fuhrer, A. H. Hoang, R. Kelley and A. V. Manohar, *Soft-Collinear Factorization and Zero-Bin Subtractions*, *Phys. Rev.* **D79** (2009) 053007, [0901.1332].

[123] A. Grozin, *Integration by parts: An Introduction*, *Int. J. Mod. Phys. A* **26** (2011) 2807–2854, [1104.3993].

[124] E. Remiddi, *Differential equations for Feynman graph amplitudes*, *Nuovo Cim.* **A110** (1997) 1435–1452, [hep-th/9711188].

[125] T. Gehrmann and E. Remiddi, *Differential equations for two loop four point functions*, *Nucl. Phys.* **B580** (2000) 485–518, [hep-ph/9912329].

[126] G. Heinrich, *Sector Decomposition*, *Int. J. Mod. Phys.* **A23** (2008) 1457–1486, [0803.4177].

[127] J.-Y. Chiu, A. Jain, D. Neill and I. Z. Rothstein, *A Formalism for the Systematic Treatment of Rapidity Logarithms in Quantum Field Theory*, *JHEP* **05** (2012) 084, [1202.0814].

[128] A. H. Hoang, *The Top Mass: Interpretation and Theoretical Uncertainties*, in *7th International Workshop on Top Quark Physics*, 12, 2014. 1412.3649.

[129] P. Ball, M. Beneke and V. M. Braun, *Resummation of (beta0 alpha-s)**n corrections in QCD: Techniques and applications to the tau hadronic width and the heavy quark pole mass*, *Nucl. Phys. B* **452** (1995) 563–625, [hep-ph/9502300].

[130] M. Beneke, *A Quark mass definition adequate for threshold problems*, *Phys. Lett. B* **434** (1998) 115–125, [hep-ph/9804241].

[131] T. Lee, *Renormalons beyond one loop*, *Phys. Rev. D* **56** (1997) 1091–1100, [hep-th/9611010].

[132] G. S. Bali, C. Bauer, A. Pineda and C. Torrero, *Perturbative expansion of the energy of static sources at large orders in four-dimensional SU(3) gauge theory*, *Phys. Rev. D* **87** (2013) 094517, [1303.3279].

[133] M. Beneke, P. Marquard, P. Nason and M. Steinhauser, *On the ultimate uncertainty of the top quark pole mass*, *Phys. Lett. B* **775** (2017) 63–70, [1605.03609].

[134] M. Beneke, *More on ambiguities in the pole mass*, *Phys. Lett. B* **344** (1995) 341–347, [hep-ph/9408380].

[135] S. Bekavac, A. Grozin, D. Seidel and M. Steinhauser, *Light quark mass effects in the on-shell renormalization constants*, *JHEP* **10** (2007) 006, [0708.1729].

[136] V. Mateu and P. G. Ortega, *Bottom and Charm Mass determinations from global fits to $Q\bar{Q}$ bound states at N^3LO*, *JHEP* **01** (2018) 122, [1711.05755].

[137] Wolfram Research, Inc., "Mathematica."

[138] G. Van Rossum and F. L. Drake, *Python 3 Reference Manual*. CreateSpace, Scotts Valley, CA, 2009.

[139] A. Czarnecki, K. Melnikov and N. Uraltsev, *NonAbelian dipole radiation and the heavy quark expansion*, *Phys. Rev. Lett.* **80** (1998) 3189–3192, [hep-ph/9708372].

[140] M. Beneke, Y. Kiyo and K. Schuller, *Third-order Coulomb corrections to the S-wave Green function, energy levels and wave functions at the origin*, *Nucl. Phys. B* **714** (2005) 67–90, [hep-ph/0501289].

[141] E. G. Floratos, S. Narison and E. de Rafael, *Spectral Function Sum Rules in Quantum Chromodynamics. 1. Charged Currents Sector*, *Nucl. Phys. B* **155** (1979) 115–149.

[142] J.-y. Chiu, A. Jain, D. Neill and I. Z. Rothstein, *The Rapidity Renormalization Group*, *Phys. Rev. Lett.* **108** (2012) 151601, [1104.0881].

[143] C. collaboration et al., *Updates on projections of physics reach with the upgraded cms detector for high luminosity lhc*, *CMS Performance Note CMS DP-2016/064* (2016) .

[144] J. Aparisi et al., *Snowmass White Paper: prospects for measurements of the bottom quark mass*, 2203.16994.

[145] J. Aparisi et al., *mb at mH: The Running Bottom Quark Mass and the Higgs Boson*, *Phys. Rev. Lett.* **128** (2022) 122001, [2110.10202].

[146] A. H. Hoang and I. W. Stewart, *Top Mass Measurements from Jets and the Tevatron Top-Quark Mass*, *Nucl. Phys. B Proc. Suppl.* **185** (2008) 220–226, [0808.0222].

[147] P. Nason, *The Top Mass in Hadronic Collisions*, pp. 123–151. World Scientific, 2019. 1712.02796. 10.1142/9789813238053_0008.

[148] J. Kieseler, K. Lipka and S.-O. Moch, *Calibration of the Top-Quark Monte Carlo Mass*, *Phys. Rev. Lett.* **116** (2016) 162001, [1511.00841].

[149] M. Butenschoen, B. Dehnadi, A. H. Hoang, V. Mateu, M. Preisser and I. W. Stewart, *Top Quark Mass Calibration for Monte Carlo Event Generators*, *Phys. Rev. Lett.* **117** (2016) 232001, [1608.01318].

[150] A. H. Hoang, S. Plätzer and D. Samitz, *On the Cutoff Dependence of the Quark Mass Parameter in Angular Ordered Parton Showers*, *JHEP* **10** (2018) 200, [1807.06617].

[151] G. Cortiana, *Top-quark mass measurements: review and perspectives*, *Rev. Phys.* **1** (2016) 60–76, [1510.04483].

[152] C. Lepenik, *Heavy jet mass with massive quarks*, Master's thesis, University of Vienna, Vienna, 2016.